SCIENTIFIC SOCIETY OF MECHANICAL ENGINEERS (SSME/GTE)

PROCEEDINGS

OF THE

11TH INTERNATIONAL CONFERENCE ON

RAILWAY BOGIES AND RUNNING GEARS

Budapest, Hungary

9 - 12 September, 2019

Edited by

Prof. István Zobory

Department of Rolling Stock, SSME/GTE

PROCEEDINGS

OF THE

11TH INTERNATIONAL CONFERENCE ON

RAILWAY BOGIES AND RUNNING GEARS

Budapest, Hungary

9 - 12 September, 2019

Edited by:

Prof. István Zobory

Department of Rolling Stock, SSME/GTE

The Conference Organising Committee gratefully acknowledges the generosity of the following *Major Sponsors* and Sponsors:
KNORR-BREMSE RAILWAY VEHICLE SYSTEMS HUNGÁRIA Ltd. (H)
NIPPON STEEL CORPORATION (J),
STADLER TRAINS HUNGARY Ltd. (H),
GANZ MOTOR Ltd. (H)
SIEMENS Mobility Ltd. (H),
BME INTELLIGENT TRANSPORTATION AND VEHICLE SYSTEMS Co. (H),
HUNGARIAN ASSOCIATION OF TRANSPORT (H)
BKV RAILWAY VEHICLE REPAIR AND SERVICE Ltd. (H),
GRAMPET - DEBRECEN WAGON FACTORY (H)

Issued by the *Department of Rolling Stock* of the SSME, Budapest, 2020
ISBN 978-963-9058-42-2

Participants of BOGIE ’19 in front of the portal of Hotel Flamenco
where the Conference was held

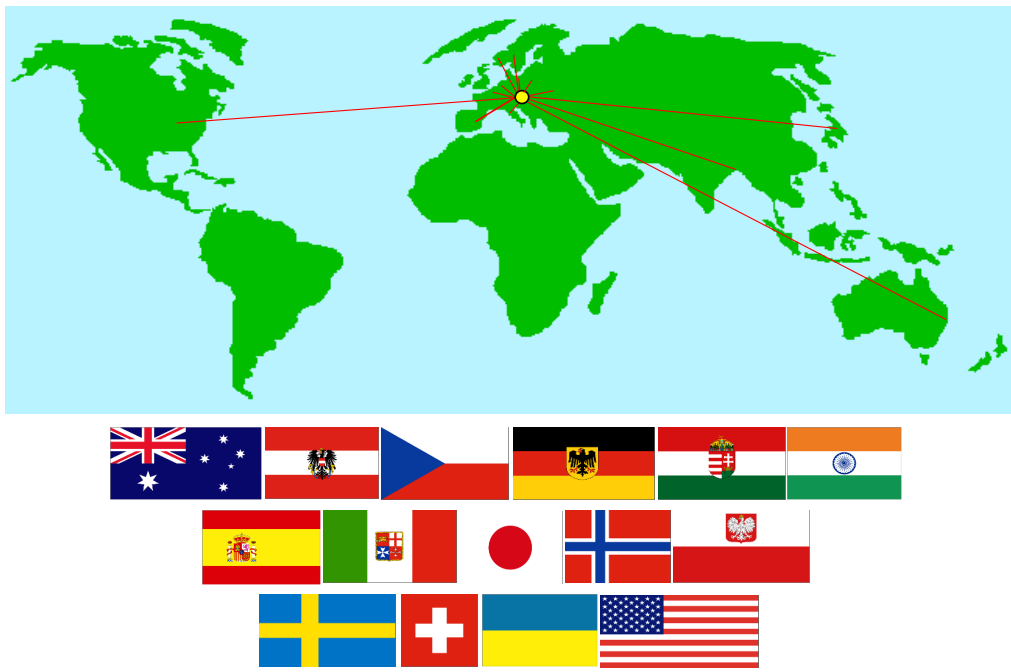

The 15 Countries interested in BOGIE ’19

Editor in Chief:
Prof. István Zobory

This volume was prepared using MS Word files submitted by the authors.
No scientific or linguistic revisions were provided by the Organising Committee.

CONTENTS

PREFACE

In the initial two decades of the 21st century railway transportation continues to expand and develop at an international level. The total length of high-speed railway lines in Europe and the Far East has grown, which means that the rail can capture a larger and larger share of passenger traffic from aviation, and contribute to reducing congestion on motorways. Increasing rail's share of surface freight volumes is an ongoing policy objective in several countries in Europe, America and the Far East. Accordingly, bogies and running gears for passenger carriages and electric multiple units require continuing development to ensure appropriate running stability, riding safety and comfort at higher speeds. In addition, the introduction of new running gear concepts in freight-cars can meet the requirements for increased operational reliability, lower wear of wheels and rails, and the possibility of using multi-purpose, modular car designs. Worldwide, over the past three years there has been no sign of decreasing interest by rail transportation companies and their suppliers in needing the continuous scientific support and relevant research results from our special field of *bogies and running gears*. It is accepted by the rail operators and vehicle manufacturers that new generation bogies and running gears represent very complex and integrated engineering systems, so the application of advances in the theory of vehicle dynamics, control and mechatronics is essential. Similarly, computer aided design and testing methods, as well as system reliability analyses, find broader application both in the design and manufacture of modern railway bogies and running gears. Advanced design concepts and the requirements for maximum operational reliability make thorough feasibility and risk analyses imperative in the field of bogie and running gear development to satisfy the requirements of the increasingly competitive market. Transport operators are interested in making maximum LCC-effective vehicle-investments.

The complex character of this special field was clearly reflected in the program of the ***11th International Conference on Railway Bogies and Running Gears*** (**BOGIE '19**) held in Budapest, Hungary on the 9 -12 of September 2019. The selection of papers presented at the Conference was helped by the *International Scientific Committee*. The *Conference Organising Committee* received numerous contributed papers due to considerable international interest in bogies and running gears. Each paper offered was thoroughly reviewed by the Organisers, and in the end 34 papers of superior scientific value from 13 different countries were selected to be included in the Conference Program for oral presentation. As some valuable papers which were offered had to be left out, an additional poster session was included, with 5 posters from 3 different countries.

There were a total of 105 participants at BOGIE '19 representing 15 different countries from all over the world. As usual, the professional atmosphere of the Conference was excellent, and provided an outstanding opportunity for the exchange of ideas between theorists, researchers and specialists. The Technical Visit on the third conference day to the *Knorr-Bremse Railway Systems, Budapest Ltd.* made first-hand observation of Hungarian railway brake system manufacturing practice possible. The evening social programs of the conference were pleasant occasions for the participants to get acquainted with each other and to discuss the possibility of both collegial and corporate international collaborations.

In this Proceedings Volume the full papers submitted for publication by the authors in electronically edited versions are included. This Volume gives an adequate review of the most recent results of research and development achieved in the past three years in the field of railway bogies and running gears.

Budapest, 10 December, 2019

Prof. István Zobory
Conference President
Head of Department of Rolling Stock

THE RAILWAY AND THE WEATHER IN CHANGING TIMES

Otmar KRETTEK

Krettek Separation GmbH
D-41749 Viersen, Andreasstraße 99

Received: September 9, 2019

ABSTRACT

The dramatic climate change holds us firmly in its grip since 1980. So the mean temperature had risen significantly since then and reached an unsurpassed level. One of the main reasons for this development is the clear rise of carbon dioxide by the increased use of fossil fuels. In the transport area the following international initiatives for climate protection arise: the reduction of the transport requirement, the use of more efficient means of transport and the increase of attractiveness of the traffic. The accompanying symptoms of the temperature rise are increasing weather extremes, if necessary with hail and thunderstorms. The consequences of heavy rain are severe for the rail. Scree that rolls off at mountain sections from the slopes to the rails has repeatedly led to derailments of trains in Germany as well as in the neighbouring countries. For climate protection in several cities the rail transport shall be expanded. Rechargeable battery buses as well as the fuel technology are since then gaining ground. In North Rhine-Westphalia one tries to lure 25000 drivers back to the rail with 7 lines of double-deck multiple-unit trains running at 10 minute intervals. In order to win new clients and to sweep the roads even emptier, the Swiss Railway puts great emphasis on the automatic coupling in the domestic traffic. The punctual delivery of the customers becomes thereby far more reliable on the part of the SBB Cargo.

Keywords: Derailment due climate change, faster regional railcar, fuel cell railcars, new logistic concept

1. IN 1960 THE WINTERS WERE STILL HARD, THE CAR WAS HOWEVER THE MOST POPULAR MEANS OF TRANSPORT

In wintry weather conditions it occurred often enough that a journey in business obligations ended with a skidding on the icy road or at worst in the ditch. Sometimes only a heap of scrap was left over that was the pride of the owner. The railway tried to encourage such contemporaries to use the train, understandably first and foremost in its own interest. In 1966 a poster was thereupon issued by the railway that emphasizes the independence of this means of transport from the elements.

Picture 1 Poster of the German Federal Railway of the year 1966 with the reference of the independence of the rail from wintry weather conditions in the cold seasons [1]

On the poster is shown an express train speeding through the snow, in addition the title:

„Everybody talks about the weather, we don´t!“ One or the other who had experienced an episode as the one described above did not need to be convinced, he went where it was possible in wintry weather conditions by railway.

2. WHAT STILL APPLIED IN 1960 IS NOW PAST, TODAY THE CLIMATE CHANGE HAS US FIRMLY IN ITS GRASP.

Cold winters with high snow conditions as they appeared still in the Sixties are today a thing of the past long since. The median temperature level has significantly increased since then (Picture 2). The consequences for the rail of this increase of temperature are enormous and charge the railway with thousands of euros.

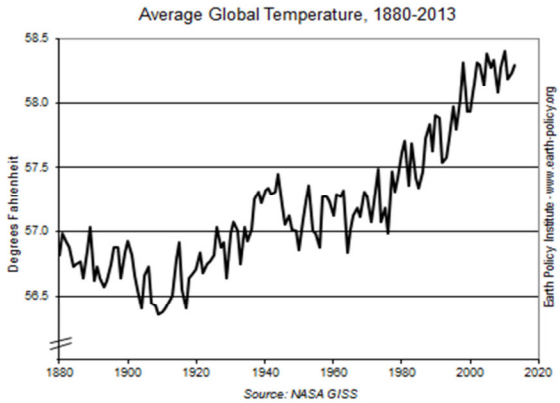

Picture 2 Near the ground in the years 1880 – 2013 [2]. The frightening thing of this situation is that the global warming is constantly continuing.

The solar radiation is not under consideration as a cause because of its constancy. The reason is rather, as today 97% of all climatologists evaluate unanimously, the greenhouse effect discovered by Jean Baptiste Joseph Fourier of which the responsible gases were partly identified by John Tyndall in 1862. Today we know that the deposits of carbon dioxide (CO2), methane and dinitrogen monoxide, but also water vapour are the crucial causes of this effect at the border of our atmosphere.

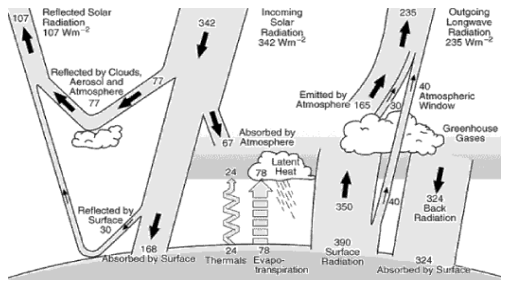

Picture 3 Explanatory models of the climate change with the balance of the shortwave solar radiation causing the phenomenon and the long wave heat reflection of the surfaces of the earth and of the water [3]

They impede, as demonstrates Picture 3, all of them the transmitting of the long-wave thermal radiation into the outer space that is emitted from the surface of the earth (whether ground or water) as a result of the heat of the sun. Instead, they are absorbed by the greenhouse gases and are subsequently reflected to the surface of the earth again.

This pitiless irrevocable reality determines the global warming and its consequences such as heavy rain, hail, storms, drought, melting of the polar caps, rise of the sea water and local limitation of the weather pattern (picture 4). The inevitable consequences are floodings, forest parts in the form of aisles and signal and rail switch failures caused by lightning. The fatal thing is that the global warming and therefore the climate change is exclusively due to human activities.

Picture 4 through drought dried soil [4]

No weather service is able to make locally limited weather forecasts. The screen widths of the available climate models that are determined by the size of the precipitation zones are not capable to provide this information. So for the railway nothing else remains but to let its trains roll blindly into bad weather zones. The localities of such events that cannot be inspected lets the rail without a chance,[5].

3. ACCIDENTS THAT ARE CAUSE FOR CONCERN

3.1. Obstructions by derailments

The derailments, irrespective of whether at the German railway or foreign rails, took place following a similar pattern: The train hit the obstacle – in the majority avalanches of soil and scree that had rolled off from the mountain slopes on the tracks, it was lifted off the tracks and lost its trace. The result was the same. The causes of the derailments are therefore not closely examined anymore. On the contrary, the following information is to give only the impediments and complications that such courses of events produce.

The beginning of the derailments was the incident on the sinistral part of the Rhine at St. Goar. It happened on 20 February 2002, thus on the threshold of the indicated climate change. The reason was a previously fallen heavy rain with a waterflood of 25l/m2. It flushed 10-15m3 of clay and scree on the rails. The IC 2315 had suffered the accident on its way to Stuttgart. The locomotive and four of the subsequent modern passenger carriages, equipped with bogies of the type Minden Deutz (VMAX 200

km/h) were lifted off the rails. Fortunately they did not fall over, but remained in inclined position. 10 passengers and the train conductor suffered injuries. The locomotive driver suffered a fracture of the leg. 300 assistants from the fire brigade, the technical relief organization, the rescue service and the police approached in a hurry to the accident site. The passengers of all wagons were, supported with the help of ladders, taken out of the wagons by the fire brigade and afterwards fetched down on the circa 4m deeper road, also by ladders leaned at three points at the supporting walls of the railway embankment. Also at the second descent to the road assistance had to be provided.

Picture 5 IC 2315, lifted off the tracks on its way to Stuttgart on 20 February 2002, as a consequence of 10-15m3 of clay and shale, flushed from the mountainsides on the tracks near St. Goar [6]

The passengers stranded in such a way were later taken to Mainz in buses. Two special recovery cranes were fetched from Cologne in order to rerail the locomotive and the wagons involved in the accident. They were taken to the nearest repair centre for a thorough examination.

Picture 6 Evacuation of the passengers out of the derailed IC wagon [7]

By the extremely high forces that the wheels of the locomotive and the wagons exerted in the last few metres on both track lines until the standstill of the train, the railway sleepers have been damaged on 300m and the track has been deformed. In the end a

work train had to arrive in order to replace the sleepers and to align the rails. In the regional traffic the rail had to provide a replacement bus service during the entire interruption of the route between Boppard and Oberwesel. By means of this description it becomes clear what financial burdens this spectacular accident entailed.

Picture 7 With an incredible swiveling from the track over the adjacent track the head vehicle of the regional express was thrown after its derailment on 25 June 2016 against the crash barrier of the adjacent main road B9 and bent it on the side of the road. Because of the early hour of the incident no secondary accident happened. [8]

Any further accidents that took place in a similar way are touched only briefly in the following. Thereby it is striking that as from 2016 the derailments occur at increaseingly short notice. In this context it should be noted that, according to the climatologists pursuant to the temperatures they gathered the years 2016-2018 were, by a clear margin, the four warmest ones since measurements began.

Another derailment took place accordingly only close to Barrach on 25 June 2016. The head vehicle of the four-part regional express RE 4251 was thrown off its track by the impact of the collision with a barrier of stone so that it swung out over the opposite track and ended up at the crash barrier of the main road 9 running along which it bent on the side facing the street. It was a really fortunate circumstance that the incident happened early in the morning at 5.30 a.m., there was not yet any traffic on the street and therefore no collision with a road vehicle followed.

The subsequent derailment took place on 19 May 2017 near Stadtroda.

Picture 8 Regional express RE1, derailed as a result of an avalanche of rock and sludge washed on the rails on 19 May 2017 during the journey from Glauchau (Saxony) to Göttingen [9]

In this case, too, the head vehicle of the regional express RE1 broke out off the tracks taking away the trailer document whereby the head vehicle came to a standstill in the middle of the bushes pushing away young trees and shrubs. The injured people received medical care by emergency doctors on duty.

In Lünen on 3 January 2018 the tradition unit train driving from the station towards Dortmund crashed against a tree which had fallen on the tracks and derailed. The passengers were transported to their destination by replacement buses.

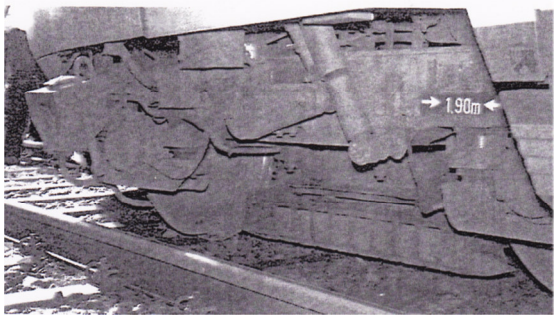

Picture 9 Crash of the local train RE 51 on its way to Dortmund against a tree which had fallen on the tracks during a violent storm [10]

Darkness reigned in the tunnel of Wilseck when the multiple unit train headed for the southern exit of the tunnel. The train driver only saw the near field being illuminated by his headlights. At the exit a rock fall was awaiting him, ranging over both tracks and broken out in the area of the forehead wall panelling. There the journey ended.

Picture 10 DB-regional railcar, crashed on a boulder avalanche that blocked the whole exit after an unexpected landslide at the south exit of the rail tunnel of Wilseck [11]

The list ends with an incident in Spain. Near Barcelona a local train drove into a rock pile that had rolled off from an incision of the route and derailed on 20 July 2019. The wagons swang out in zigzag, whereby the railway car-bodies were deformed in the transition areas. The bulges of the wall indicate the tremendous forces which caused

the dynamic of the derailment in the vehicle.

Picture 11: Regional railcar of the Renfe, derailed as a result of a landslide between the cities Terrasse and Manresa on3 January 2018. The bulges of the wagon walls indicate the incredible forces which acted upon the rail car. [12]

3.2 The malfunctions by lightning strikes [13]

The indicated climate change has not only multiplied the caprioles of heavy rain but also the frequency of thunderstorms that went off often accompanied by flogging rain and hail showers. Their occurrence is due to sultry air masses carried in greater heights by up winds whose vapour included in the air cells separates from the cells and freezes to ice crystals, due to the colder temperatures and thereby their sinking absorption capacity of water vapour. They become charged positively. The water droplets accumulated in the subjacent level of the cloud, however, become charged negatively. The circumstances which are essential for a thunderstorm, the voltage potential and the area of the heaviest rainfalls on the underside of the layer are therefore given. According to Prof. Michael Kunz of the Institute for Meteorology and Climate Research of the Institute for Technology of Karlsruhe, the potential of thunderstorms has significantly increased since the eighties. Thereby he refers to the dissertation of Susanna Mohr in which she proves that there is a certain correlation between occurrences of thunderstorm and of hail. The latter, however, has increased verifiably in the last decade.

Signal boxes are all naturally equipped with lightning conductors. So the question rises how lightnings can cause disruptions of the operation of the railway at all. The causes are diverse.

Lightning strikes can destroy the electric lines coming from the signal box as well as its building blocks and components. The most frequent reason for failures and standstills and damages of the system are lightning strikes in the overhead lines, the rails or the masts. If a lightning hits the soil, the overvoltage spreads over the cables or is coupled inductively and damages unprotected electronic assemblies. Interfacing units ready for connection are therefore examined before delivery in the laboratory of surge for their reaction to over-voltages and overflows in order to protect signals, low-voltage distributors and system cabinets. Potential sources of danger are, in this respect, even distant radio masts of GSM-R-systems which transmit the lightning currents and lightning surges to the signal box.

Point heatings and axle counters can also react similarly under the impact of lightning strikes.

Malfunctions in the rail traffic inevitably entail delays and high subsequent costs.

As the rail tries to handle the traffic with the help of few electronic signal boxes and consequently with the help of economical staffing, in case of disorders, especially in agglomerations, larger transport areas are generally affected from this. This, in turn, obliges us to examine a large number of security points after lightning strikes in the net.

A compilation is to provide a general overview on such disorders below.

The switching point Solingen was decommissioned for two and a half hours by a lightning strike on 27 September 2014. 27 trains in total could therefore not run on schedule anymore. The delays were 30 minutes on average.

A business interruption provoked in the same way brought traffic between Duisburg and Dortmund to a halt. As spare parts had necessarily to be provided for the control and the signal technology the disruption extended over 21 hours.

Shortly afterwards the suburban railway broke down between Mönchengladbach and Hagen because of a lightning. The railway organized taxis and buses.

A further lightning strike on the same day paralysed the traffic of the suburban railway between Köln and Essen.

A lightning strike in the signal box of Köln brought the rail the delay of nine long-distance trains and 23 trains of the local transport.

4. IN CITIES WITH A REALLY HIGH CARBON DIOXIDE AND FINE DUST POLLUTION AND A LIFE EXPECTANCY REDUCED BY DIESEL VEHICLES

In big cities frequently occur, due to the arterial roads that are heavily polluted by vehicles, asthma, cancerous diseases, heart failures, strokes, diabetes and dementia. As a result, the medical profession has sought dialogue with colleagues from specialized clinics because of the basic pattern of the symptoms that were detected in all four diseases, the constriction of vessels and bronchial tubes. In the course of this exchange of ideas and patient referrals to the addressed doctors it finally distilled that all of them are the consequences of an increased inhalation of carbon dioxide with fine substances. Related inquiries of the International Council on Clean Transportation (ICCT) have shown that in Germany 13 000 cases of death – that is approximately 16% - of the population are due to this cause. The respective investigations relate to the contaminations by cars, trucks, buses, agricultural vehicles and construction machines. With this rate Germany is in the vanguard of all European countries and exceeds the average by 50%. The top values in the pollutions are led by the cities Stuttgart, Köln and Berlin. The economic loss of the Federal Republic of Germany is estimated in this study at 89 000 000 euros, which is close to 3% of the gross national income.

In India 74 000 premature deaths were registered in 181 cities in the course of medical questioning. This number might be too low because of the rural population that was not taken into account. Other numbers indicate the number of the persons that died prematurely at 1 400 000.

China estimates 114 000 cases of death on the basis of three related registered cities. Also this number is incorrect, on the one hand because the multitude of the citizens that died prematurely in the numerous large cities was not captured by this number, and on the other hand it is ignored to what extent the heating of the houses is made with the pollutant coal. As a more credible information the number 1 600 000 is spooking in literature.

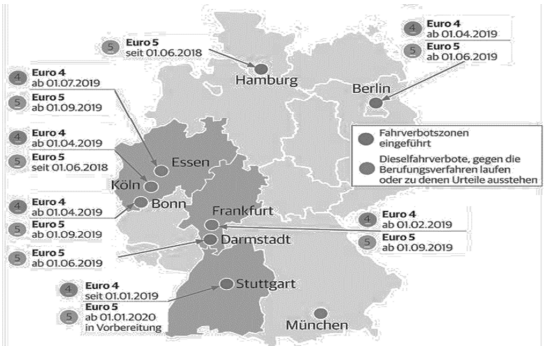

Picture 12 Closed cities due to particles of carbon dioxide and fine dust particles exceeding the limit values for the transit traffic on main streets for diesel vehicles [14]

Finally the in the ICCT-document mentioned number of people who died early in the USA shall be discussed furthermore. That would be no more than 22 000 citizens. Considering the size of the country and the tremendously big motor vehicles that the population uses in this country this number is also more than questionable.

Following their duty to care for their citizens a large number of cities has introduced a ban on diesel vehicles after the results of the findings if the levels of damage were seriously overstepped. The Ruhr area was particularly concerned by this exclusion of diesels in which even near medium size cities had to follow the driving ban. Long-standing professional drivers felt unable to reach their places of work at the edict of this order. Between 25 000 and 32 000 computers thereupon express that they wanted to make the journey to their placement by rail in the future (Picture 12).

5. COORDINATED CONCERTED ACTIONS OF RUHR CITIES AND RAIL

It is the heart of the DB-project arranged between the cities of the rail to provide an improved mobility offer in the most charged road section between Dortmund and Düsseldorf by modern vehicles travelling at precisely timed intervals. In order to keep to the timetables steadily the rail network between Dortmund and Duisburg is extended to four tracks. The lines in the edge regions of the Ruhr area are liberally ramified in order to connect also the commuters from the rural regions surrounding the Ruhr area. The trains Desiro HC, delivered by Siemens that will run in the Ruhr area under the name RRX, consist, due to the limited platform lengths, of respectively two one-storeyed head vehicles that bear the electrical equipment at the roof and two two-storey middle cars. They provide space for 800 passengers sitting. With their modern design they make the journey pleasant. The maximum speed of the trains is 160 km/h. The performance of their

axis of at least 4000 kW gives them an acceleration of 1,2m/s^2. So they are capable to be merged on the only double-track outside distances in spite of the larger number of intermediate stops within the interval of the long distance high-speed trains.

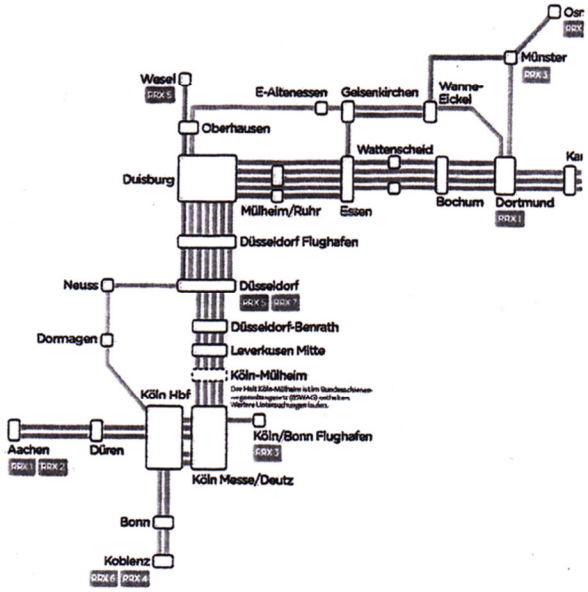

Picture 13: Target network of the RRX rapid transit [15]

Picture 14 Siemens Rhein Ruhr Xpress HC, V max = 160 km/h, power = 4.000 kW, number of seats: 400 [16]

6. OFFERS OF CITIES THAT ARE ALSO OBLIGED TO IMPOSE DRIVING BANS ON DIESEL VEHICLES OUTSIDE OF CONURBATIONS

The constraint to impose driving bans on diesels also applies to a larger number of German big cities, like for example Berlin, Dresden, Düsseldorf, Wiesbaden or Münster, to pick out only a few of them that are now also obliged to improve the public transport. Depending on the amount of the available investment resources the decision was made in favour of the development of the line of the suburban railway, the tram network or also only the use of battery-powered buses, as for example in Münster.

7. THE RAIL OF THE MODEL COUNTRY SWITZERLAND GIVES AN EXAMPLE OF A PUNCTUAL DELIVERY OF GOODS SATISFACTORY FOR THE CLIENTELE

The satisfaction of the customers cannot be better expressed than in the excellent modal-split value of the rail of 38%. These facts reflect already merely the burden of the German motorways in Switzerland. German motorways suffocate in heavy-duty traffic, partly with giga-liners (which are not authorized in Switzerland) and elephant racing on the right lane whereas on Swiss motorways things are moderate in this regard. While the State supported the Swiss railway with 3,47 billions of Swiss Francs in 2018, the German railway is compelled not only to gain profits since the rail reform but is furthermore asked to maintain the financial ability to act. Under these constraints it was obliged to reduce its route network from 40 395 km to 34 128 km. Alternative routes for freight trains are since then missing and the punctuality of delivery got broken. Components that had to be installed promptly to the casings, as a striking example, subsequently arrived often too late so that their connection with the so far finished casings could not be completed anymore in the remaining time. They could not be handed over to the customer on schedule. The consequence was a loss of reputation, at worst the demand for penalties. The anyhow low modal-split of the German railway was further impaired. It is currently at 16%.

The SBB-Cargo controlling the freight transport is meanwhile struggling not to lose this leading position in the modal-split but to expand it even further as far as possible. To stay on the pulse of the companies the employees of the Cargo-Customer sale Service, in other words the sales agents, visited regularly the directors of the companies working with the rail in order to question them about the reliability of the deliveries as well as about emerged problems and wishes.

The transport relations between the companies interlinked in the freight transport have traditionally increased. In order to intensify the rail traffic opposed to the truck transport in its competitiveness it is necessary to shorten the shunting processes and furthermore to increase the driving speeds and tensile loads. Under this aspect the management team of SBB-Cargo remembered the timid efforts of the OSShD and UIC in 1961 to create an automatic coupling by which the standing times of the vehicles should be reduced and the personnel costs be contained. Looking back to these activities this world of ideas was picked up again and inspired by the boost of innovation due to the automatic coupling by which the existing customers could be served more quickly by rail than by

truck. Of course this applied only for the rail transports of Central Switzerland. In joint meetings the savings of time were thereupon taken into account. It was recognized that the new couplings shorten the shunting process because a cable had to be pulled in order to separate the wagons, when coupling together the wagons and with the locomotive the couplings had only to be pushed together slowly.

At this also the compressed air lines of the brakes are interlinked. Both operations take place much faster than with the traditional screw coupling. SBB-Cargo thereupon opted for this pilot project.

The implementation of this technical improvement required however a logistic summary of the charging stations and unloading stations of the supplied companies. As such arose the stations Dottikon, Oensingen, Renens, the airport of Lausanne as a handling location between air and rail traffic and the terminals Cadenazzo, Lugano-Vedeggio, Biasca and Mendrisio. 100 freight wagons and 120 locomotives were converted before the introduction of the test traffic at the beginning of May 2019 at a cost of 15 000 000 (11 013 020) euros, 800 employees were previously schooled in the modified logistics concept.

As a centre of this new concept the shunting yard Dottikon arose. In it the trains that were running in were dismantled and the wagons/groups of wagons arrived in accordance with the shunting list from the shunting mountain into the respective tracks whereby the times of changing the points were between 0,6 and 0,8 seconds. By the introduction of the automatic coupling also the brake tests could be simplified. The control if the brakes applied and released properly can therefore be omitted. The introduced automatic system transmits since then by sensors the condition of the brake to the wagon on a tablet computer in the cabin of the locomotive. The brake test with a 500m train takes since then only still 10 minutes towards previously four times this length of time. Only the adjustment of the brake on position P (reacts quickly) and G (reacts slowly) has still to be positioned manually. Also the calculation of the brake evades the automatization. They are part of the further system extension, as is also the review of the condition of the wagon and the cargo with an employee who goes along the train. In the long term Switzerland is planning until 2030 to expand the infrastructure of the rail network in two stages taking particular account of the freight transport. This shall not only be faster but also be less affected by the quicker passenger transport. This measure is estimated at 12 billions of Swiss francs. By the planned high speed of the freight train of 120 km/h the ride between Lausanne and St Gallen, for instance, shall be reduced by 25%. At timetable intervals of 30 minutes a mutual obstruction of the freight trains that are integrated in the meantime is therefore excluded if the service runs on schedule after the network expansion. Furthermore, the aim is to encourage the neighbour rails with regard to the extension of the previous sole domestic traffic to join the pioneer project of SBB-Cargo. Also the concept of logistics in bringing the trains together to the common junction station Dottikon for decomposition and merger of the wagons to the respective exit tracks in accordance with their destination terminals was also handled according to the present pattern. The loading and unloading of the containers and semitrailers took place by means of gantry cranes overlapping the track (Picture 15).

Also nothing had changed with regard to the switching concept. The arriving trains were

pulled to the hump in sequence and set in motion. Thereby the couplings were separated and the train was pressurized in the slope. Automatically functioning rail brakes were also employed to secure the process operation, namely while the trains were rolling and before they were running in into the guide track. The first brake conveyed to the wagons or the whole train the permissible or rather necessary speed, according to their resistance to rolling and the distance to the previously lowered wagons. The wagons had to obtain this speed in order to come to a halt near the wagons that ended in the directional group. The calculation of the speeds took place thereby according to base equations calculated by a calculator for every time the train rolled in.

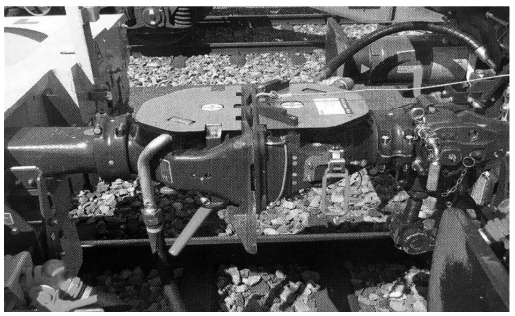

Picture 15 Cargo Flex coupling of the type Scharfenberg [17]

This procedure has also remained the same in principle. The acceleration of the manoeuvring procedure was aimed at only by the automatic couplings. Semi-automatic Cargo Flex couplings of type Scharfenberg were installed that close automatically while the wagons were brought together (picture 15).

For the practical trial 95 new pocket wagons were delivered with the new couplings and 25 locomotives were prepared for it. Together with an automated brake test that became thereby possible the last imponderables in the operating procedure could thus be eliminated.

Thanks to these measures not only the modal split increased by 2% but also the Swiss motorways remained empty of trucks compared with the German motorways (Picture 17). The decrease of the pollution of the atmosphere by the greenhouse gases produced in the traffic is obvious (Picture 16).

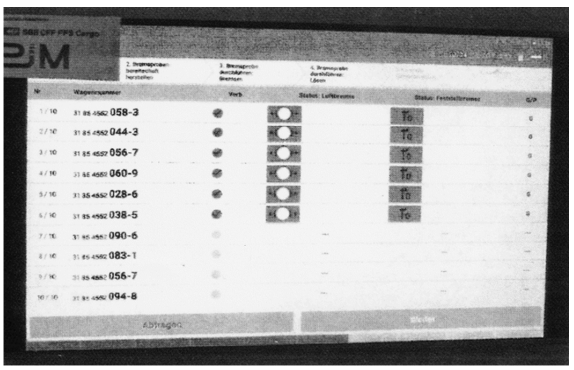

Picture 16 State of the brake test conveyed on the desk of the train driver by means of a tablet computer [18]

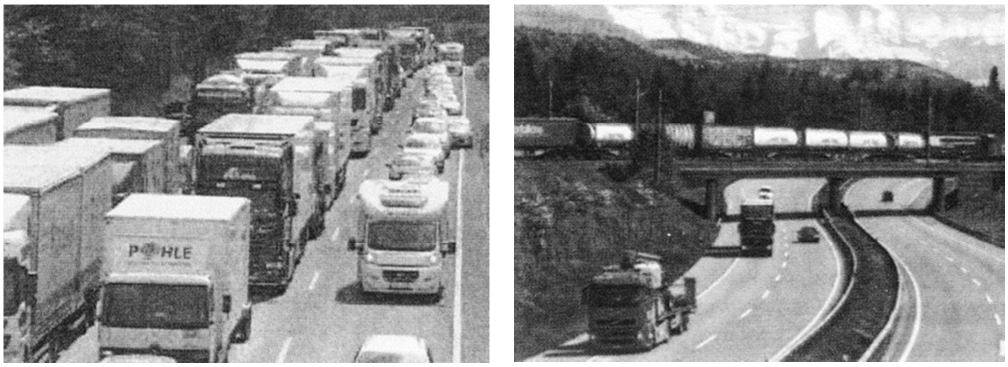

Picture 17 Trucks on motorways in Germany and Switzerland

8. FUEL-CELL DRIVE OR BATTERY-POWERED ENERGY SUPPLY [19], [20]

Both types of drive avoid detrimental gas emissions. And yet the battery-powered drive may prove to be the better one for the moment. The hydrogen fuel-cell drive namely requires the storage of the gas below 700-800 bar (so since 2011). This storage process consumed, however, 12% of the emittable energy. Subsequently hydrogen fuel-cell drives have, by hydrogen production via the electrolysis a total efficiency of no more than 30%, battery-driven vehicles, in contrast, 65%. Regarding the overall energy use that is why the battery-powered ones have to be classified as more climate-friendly. Such a vehicle is delivered in three parts under the name „FLIRT Akku“ by Stadler.

9. THE PREFERRED USE OF THE RAIL – ONE OF THE ARISING WAY OUT FROM THE MESS OF THE CLIMATE CHANGE

A blind race into the emerging climate catastrophe would seal permanently the end of mankind. Australian scientists outline the future of the human species as gloomy and pitch-black, as the atmosphere is polluted by people and thereby the concentration of carbon dioxide has risen the most rapidly since 800 000 years. Around the middle of the present century, according to their forecast, the consequences will have such disastrous effects that the civilization will experience its own decline. The upward spiral of the warming results - among other things - from the consistency of the reluctance to exhaust the arising opportunities of diminishing, the main reasons of the production of greenhouse gases. By this lack in the realisation of countermeasures there is a danger that certain tipping points are exceeded that block any way back out of the trend of the climatic happening. So if for example the permafrost soils dew, to take a closer look at such a tipping point, methane and carbon dioxide are released which virtually fire the heating gases.

The present development can only partly be stopped if the emission of greenhouse gases such as carbon dioxide from the coal combustion of power plants, diesel emissions from the traffic of motor vehicles and methane from the agriculture are significantly reduced. Our means of transport, the rail, has long since understood that the energy import of coal-fired power stations is precarious regarding the development of climate and feeds 57% of the traction current with renewable energies. In Switzerland where rail transport

is promoted the travel energy is even delivered from hydroelectric power stations by 90%. In Japan the air traffic between the giant cities along the Maglev-route Tokio Nagoya under construction on which 600 km/h shall be allowed, is cut in the long term. Moreover, in Germany the Deutsche Bahn AG is working on reducing drastically the energy demand by installing driver assistance systems. Related studies have shown that in doing so up to 15% of the energy consumption can be saved. Therefore the rail should be supported. These explanations shall encourage the participants of the conference to talk to politicians and responsible railwaymen and to stand up for an increase of the investments per head to improve the infrastructure of the rail in which in Europe the German rail comes third to last. The rail has to be the main mode of transport again in order to get out of the climate impasse.

10. REFERENCES

[1] Deutsche Bundesbahn, Plakat 1966 (In German)
[2] Earth Policy Institute, 2013 Marked the Thirty-seventh Consecutive Year of Above-Average Temperature
[3] IPCC 2001, Weltklimabericht WGI, Seite 90 (In German)
[4] dpa
[5] **Leuton, T.- Held, H. - Kriegler, E. - Hall, I. - Lucht, W. - Rahmstart, S. - Schelln, H.- Huber, I.**: Tipping elements in the Earth's climate system; Proceedings of the National Academy of Sciences 105 (208) p.1786 – 1793.
[6, 7] dpa
[8] dpa sab
[9] Schackow B./dpa
[10,11] dpa
[12] Anti-radar Catalunya/AP/dpa
[13] „Nach Blitzeinschlag war der Bahnverkehr stundenlang gestört", Westdeutsche Allgemeine Zeitung am 3. Juni 2019 unter der Rubrik „Unwetter" (In German)
[14] Dreher H., Ludwigsburger Kreiszeitung, 30. Januar 2019 (In German)
[15] Deutsche Bahn AG 2019, Linienkonzept des RRX, Der Bundesverkehrswegeplan (BVWP) 2030 (In German)
[16] Siemens Mobility GmbH, Desiro HC RRX, Elektrische Triebzüge und Instandhaltung für den Rhein-Ruhr-Express (In German)
[17,18] **Rellstab, M.:** Schweizer Eisenbahn-Revue 2019, SBB Cargo testet automatische Kupplung und weitere Innovationen. (In German)
[19] **Kirfel, A. - Mietzsch, O.:** Wasserstoff als Antriebstechnologie – Rechtliche und wirtschaftliche Rahmenbedingungen, Eisenbahnrevue International (2019), H.5, p. 273 (In German)
[20] **Schulz, T.:** Ohne Emmisionen, Regionalverkehr 125 (2019), H.4, p.30 – 31. (in German)

OPERATION OF A SINGLE AIR SPRING BOGIE

Frank SZANTO

Downer Rail
38 Delhi Rd,
North Ryde, NSW, 2113
Australia

Received: September 12, 2019

ABSTRACT

Downer developed a single air spring bogie for the new double deck trains which were introduced to the Sydney suburban rail network in 2002. These trains now make up about 60% of the Sydney suburban fleet. Downer has a long term contract to maintain these trains, and this paper describes the steps being taken to extend the overhaul interval, and problems encountered in achieving this goal.

Keywords: bogie construction, air-spring, stabilisator beam, axle-box, bearing

1. INTRODUCTION

The Sydney suburban rail network extends approximately 50km to the north, west and south, and is unique in Australia in that it is standard gauge, (the other capital cities have broad or narrow gauge), is served by a fleet of double deck EMUs (Electric Multiple Units), and has EMUs with single air spring bogies. More than half of the trains in the double deck EMU fleet have single air spring bogies, and were supplied by, and are maintained by Downer Rail.

The first of these were the Millennium trains, introduced in 2002. These 4 car sets, 35 in total, were designed and built in Australia, with Alstom traction equipment. These were followed by 78 Waratah trains, an improved design introduced in 2011. The Waratahs are 8 car sets with Hitachi traction equipment, and were largely built in China. A second tranche of 24 Waratah trains was delivered in 2018-2019, and another 17 sets are currently being manufactured in China for delivery in 2020.

A common feature of the Millennium and Waratah trains is the single air-spring bogie. The brainchild of engineers C.Butcher and K.Wiwatowski, its development is described in a paper presented at CORE 2002 [1].

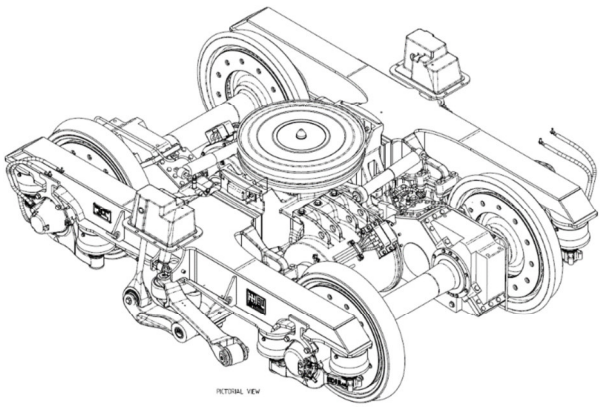

The single air spring sits directly between the underframe and the bogie transom. Bolsterless bogies with two air springs are common in Australia, but single air spring bogies are relatively uncommon in the world.

The single air spring design has a much lower resistance to yawing than the conventional, dual air spring bolsterless design, however it relies on an anti-roll bar for stability. A key reason for

choosing this arrangement was to give low wheel unloading on uneven track, even with deflated air springs.
Australian rail standards specify a twist test [2] with the wheels on one side of the car on a ramp with a slope of 1:350, plus a "dip" of 35mm. This represent the worst case of the change in superelelvation in a curve transition, combined with track defect. Wheel unloading must not exceed 60%, including for the condition of deflated air springs. Air springs become stiff vertically when deflated, but unlike the usual two air spring arrangement, with one central spring there is minimal increase in bogie to body torsional stiffness.
The anti-roll bars have links which are inclined towards the centre of the car, and end in pockets which are recessed into the underframe. When the bogie rotates in a curve, the links impose slight tilting of the body towards the inside of the curve.

The configuration of both EMUs is TC-MC-MC-TC (TC= trailer car, MC= motor car). The motor car bogies are largely identical to the trailer car bogies, other than having two frame-mounted traction motors. The two-stage gearboxes hang from the axles at one end, and have a gear-coupling to the motor.
The bogie frames are fabricated, however the central section of the transom is a casting which incorporates brackets for the lateral bump stops, the lateral dampers and an enlarged landing for the air spring. On the MC bogie this casting also incorporates brackets for mounting the traction motor. The bogie transom is designed as a pressure vessel, and acts as an auxiliary volume for the air spring.
Primary suspension is by two rubber cone springs on each axle box. Both motor and trailer bogies have wheel mounted disc brakes, with callipers mounted from the bogie transom. There are no dampers in the primary suspension, and no yaw dampers.
Currently the maximum operating speed is 115 km/h, but the trains are designed to run at 130 km/h and have been successfully tested at 10% overspeed, in readiness for an increase which may be allowed following signalling upgrades. The ride meets the specified indices and acceleration levels, and customer acceptance has been demonstrated by orders for additional sets.

2. MAINTENANCE TASK

Downer maintains both the Millennium and Waratah fleets, with a 30 year maintenance contract for the Warath. Currently the Millennium bogies are overhauled at around 800,000 km, while the Waratah bogies are overhauled at 1.2 Gm (1.2 million km). For reasons of cost and availability, there is a strong incentive to extend the overhaul interval, and the company has set a goal of reaching 1.6 Gm (1.6 million km) between overhauls, as this would eliminate one overhaul cycle in the life of the trains. The remainder of this paper focuses on the steps towards such an extension, and possible obstacles to this goal.

2.1 Overhaul Period

The Waratah trains average 200,000 km per year. After six years in service, nearly two thirds of the sets have now completed their first bogie overhaul. Wheels, axle bearings, elastomeric components, and hydraulic dampers are replaced, and the brake callipers and gearboxes are overhauled. The brake discs are being re-used, as wear is very low.

There is a program to assess the components which have been removed to see whether they could remain in service longer.
Achieving 1.2 Gm before overhaul on the Waratah trains was a step increase from the Millennium trains, where the brake discs are generally at their wear limit before 0.8 Gm. Brake pads on the Millennium train are typically replaced after 6 months, while on the Waratah they generally last until overhaul.
The reason for the very different brake wear rates is not yet clear. The brake discs on the Millennium trains are steel, while on the Waratah they are cast iron. The Waratah has higher dynamic brake effort with 126 kN per motor car (18% adhesion) up to 55 km/h (1.9MW), compared with 88 kN per motor car to 62 km/h (1.5 MW) on the Millennium. The effectiveness of slide control may also be a factor. Another possible factor is that the Waratah trains can apply pure electric braking, while in blended braking the Millennium trains always apply a small amount of brake cylinder pressure to close the gap between brake pad and disc, and this light drag may induce wear.

2.2 Wheel Life and RCF

Having easily achieved 1.2 Gm life with the friction brake components, wheel life is the next challenge. Both the Millennium and Waratah trains have AAR Class C wheels [3], with hardness typically around 350 BHN. The WPR2000 [4] tread profile used in New South Wales is a "worn wheel" profile. Conicity is 1/20 near the tread midline, but gradually increases towards the flange. Wear rates have been low, even though the Sydney system has many curves, with some having radius as low as 220 m. Note that track lubrication is used extensively on curves across the system, and flange wear is low even though on-board flange lubrication is not provided on the bogies.
When delivering the Waratah trains, Downer built a dedicated maintenance facility which includes an underfloor wheel lathe. This allows scheduled turning at regular intervals to restore the profile before tread hollowing reaches 2mm. However, this was not available prior to 2011. The Millennium train wheels showed very low wear, and, as a lathe at a shared facility owned by our customer had to be used, turning was on an irregular basis.
After about six years in service, one Millennium wheel was found to have a large circumferential crack, and a fleetwide inspection found two more wheels with evidence of shelling on the tread surface. One wheel had run for 586,000 km without being turned. The wheel with the visible crack had two turns before reaching 796,000 km, but these involved relatively shallow cuts. Examination revealed sub-surface cracks which were the result of rolling contact fatigue (RCF). It was therefore mandated that all wheels should be reprofiled at intervals less than 400,000 km. The wheels are 940 mm diameter new, and 860 mm fully worn. With a 12mm deep cut at 400,000 km intervals, the diameter is still 880 mm if the wheels are replaced at 1.2 Gm. A third turn is required to run to 1.6 Gm. A trial with a 7mm cut (plus depth of tread hollow) at each turn is being conducted, combined with ultrasonic testing for sub-surface cracks.

2.3 Wheel Roundness and Bainite

If the wheel diameter is reduced by 20 mm every 400,000km, 1.6 Gm life should be easily achieved, provided unscheduled wheel turns are not required. While wheel skids have been rare, a different problem emerged requiring early, corrective wheel turns.

The Sydney rail network has a number of WILD (Wheel Impact Load Detector) sites. After the Waratah trains entered service and run about 150,000 km, it was noted that many were showing wheel impacts in the Low range and increasing. Eventually the whole fleet required an early wheel turn. After this, nearly all wheels remained at the minimum level until first overhaul, which suggested that the operating conditions were not causing the increasing wheel impacts. However, the cause was never properly explained at the time.

After the first bogie overhaul, with new wheels fitted, the same problem is now recurring. Almost all the overhauled sets are showing increasing wheel impacts, while those with old wheels remain at low impact levels. We now believe that the cause is uneven wear due to the presence of bainite in the tread surface. Affected wheels have been found to be out-of-round by up to 0.4 mm.

The wheels are hardened by quenching, which can give a mixture of bainite and pearlite. While bainite has similar hardness to the pearlite, it has been found that it wears more quickly. The manufacturing process has now been changed to use a slightly oversize blank for the wheel forging, with more material removed when the tread profile is machined, which it is hoped will remove all the bainite.

2.4 Bearing Life

Both the Millennium and Waratah bogies use AAR "L" class taper-roller package unit axle bearings, which were originally rated for less than 1 Gm. Grease degradation was the major barrier to longer life. Timken and SKF have offered premium grade greases to extend life, and we are currently trialling SKF bearings to run to 1.6 Gm. However, there have been some unrelated bearing problems.

A most unexpected problem was the discovery of mixed rollers in some bearings. First discovered on the second last set to enter service, at around 175,000 km, when a bearing was investigated because of unusual noise, and was found to have a dislodged seal. When the bearing was sent to the manufacturer for investigation, it was found to contain both E class (correct) and D class rollers. Timken later identified that this was from a particular batch of 241 bearings assembled during one afternoon of production in 2014, which were tainted with the suspicion of having mixed rollers. Timken's procedures have subsequently been improved so this cannot happen again. Nevertheless, was almost impossible tell conclusively if a bearing was affected without removing it and dismantling it.

The fleet was monitored using RailBAM and hot-box detectors, with regular visual inspections for weeping grease or other unusual signs. A total of 106 bearings were identified as potentially affected and were removed, of which six were found to have mixed rollers, and these were all from two train sets. These bearings contain 24 rollers in each race, and of the six, one had only 1 undersize (D class) roller, while one had 18 undersize rollers. The D class rollers are 2.8 gram lighter.

Apart from the one displaced seal, no bearing actually failed in service. While this defect caused great anxiety, the problem was mainly in managing the many inspections, demonstrating that bearing failure was unlikely and ensuring that risks were reduced as far as was reasonably possible while keeping the fleet running.

It was thought that after bogie overhaul, all residual concerns about the bearings would be gone, and the focus would be on extended life. However, there have been an num-

ber bearings which have triggered lineside hot-box detectors, and one bearing collapsed while a set was being withdrawn from service. The failures have been confined to two sets which were among the first in the overhaul program and have since covered over 150,000 km.
On each occasion, all bearings were removed from the affected bogie and examined. The bearings with raised temperatures all show spalling in the cup at the top of the outer race. One bearing which was caught early shows patches of spalling directly under 6 rollers, and it appears that with time these patches grow into a continuous band. It appears the bearings may have suffered brinelling damage either while being fitted to the axles or during subsequent storage or transport of the wheelsets. This is still under investigation, and all aspects of the overhaul process are being considered.

3. CONCLUSION

The major challenges in extending the bogie maintenance interval from 1.2 Gm have largely been addressed, i.e. the life of wheels, brake discs and bearings. While it does appear that it will be possible to extend the overhaul interval, some serious problems have emerged which can lead to early failure. This has highlighted the need for rigour in all maintenance processes, and also shown the importance of condition monitoring. Currently, trackside monitoring such as WILD, RailBAM and hot box detectors are provided by the track owner, and we are evaluating various additional forms of monitoring which would be more directly accessible such as axle-box mounted accelerometers, and more non-destructive testing during scheduled maintenance.
Additional work is still being done to ensure the life of other components such as dampers, brake calipers and elastomeric components is acceptable.

4. REFERENCES

[1] **Baxter, M. – Kippist, D.:** 4th Generation Train Development, CORE 2002 Conference Paper, Rail Technical Society of Australia.
[2] **NSW Transport Asset Standards Authority T HR RS00200 ST** RSU 283 Static Twist Test
[3] **Association of American Railroads**, Manual of Standards and Recommended Practices Section G, Wheels and Axles. Specification M-107/M-208.
[4] **NSW Transport Asset Standards Authority T HR RS00870 ST** RSU Appendix G WPR2000 Wheel Profile

DESIGN BY ACCIDENT - ACCIDENT BY DESIGN

Wolfgang-D. RICHTER

Dipl.-Ing. Wolfgang-D. Richter - Wheel & Rail - Consulting
D-90610 Winkelhaid, Germany

Received: 9 September, 2019

ABSTRACT

It is a matter of course to investigate new systems intensely, by theoretical studies as well as by test research. An additional safety aspect is the transfer of proven solutions as far as applicable. But even failure-free operation over a nearly 100 years period may not prevent the occurrence of hidden system properties.
This was the case, when a Wuppertal Suspension Railway train hit a forgotten temporary end stop and derailed. Further investigations led to detection of unknown relationships in the system functionality.

Keywords: Safety aspects of system and detail design solutions, accident procedure reconstruction

1. INTRODUCTION

For decades the Wuppertal suspension system was well known for its inherent safety properties, preventing any danger of derailment by hardware design measures. But, even the inventor demonstrated foresight with regard to many aspects - some influence of the vehicle dynamic behavior was not realized.
Suddenly and unexpected, in the early morning on April 12 in 1999, the hidden property struck, when a Wuppertal Suspension Railway train hit a forgotten temporary end stop, left from just finished previous construction works. The leading bogie connection cracked, the train derailed and rushed down to the river, where five passengers lost their life and other 47 were injured.

Fig. 1 Incident situation [1]

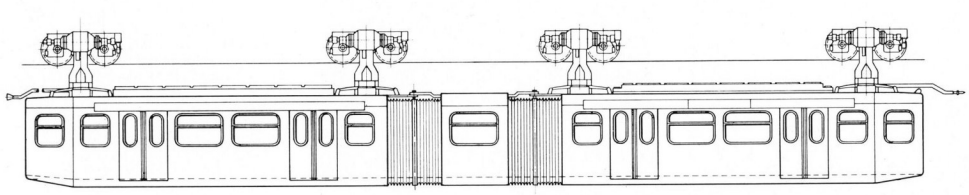

Fig. 2: Train configuration [2]

2. HISTORY OF TECHNICAL DEVELOPMENT

In 1893 Eugen Langen specified in his patent specification two different solutions for suspension railway systems, with a double rail and a hunting articulation between running gear and carbody support structure, and a single rail solution where an articulation was no longer applicable as its function was naturally given by the wheel-rail contact point.

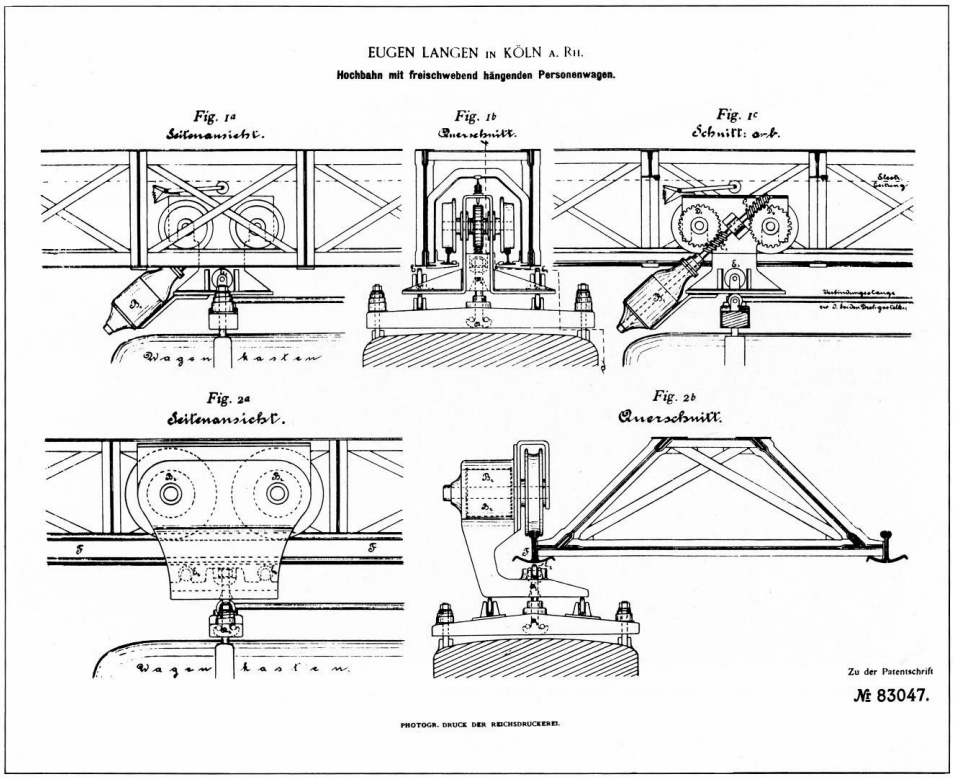

Fig. 3 Principal arrangement of suspension system versions as described by the inventor Eugen Langen [2]

After trial runs on an experimental track at Van der Zypen & Charlier workshop area, Langen decided to continue with the single rail solution only, as "the undefined wheel load changes due to lateral load influences may create wear and guidance problems" (nevertheless, other inventors went back to the dismissed solution decades later, reaping all the disadvantages predicted by Langen).

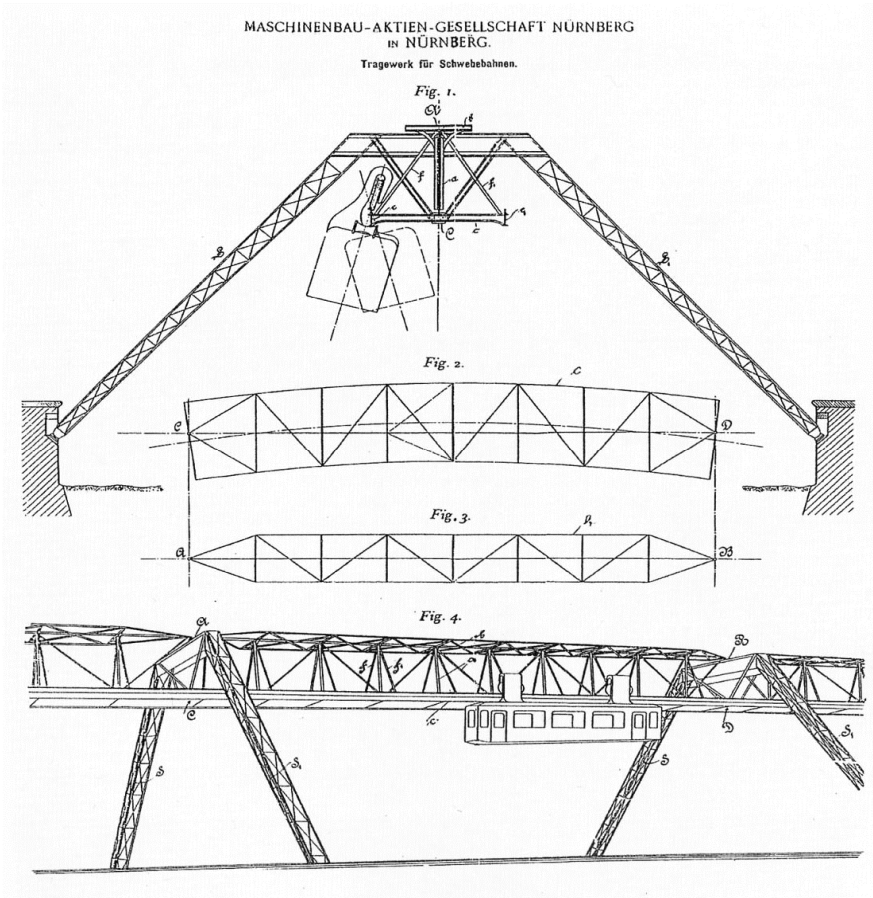

Fig. 4 Rail arrangement and track structure [2]

3. FURTHER INCIDENT INVESTIGATION REASONS

From the legal point of view the situation was clear - the construction company was responsible and only the participation of the transport authority in the release process was under discussion for a while.

From the technical point of view more than one open question remained. As the responsible chief of the criminal investigation realized that the end wall of the second vehicle showed severe traces of the river's gravel bed, it became clear that this part of the vehicle, which was never in contact with the temporary end stop, crashed first. Obviously additional influences caused an important impact in the incident results – especially the number of victims.

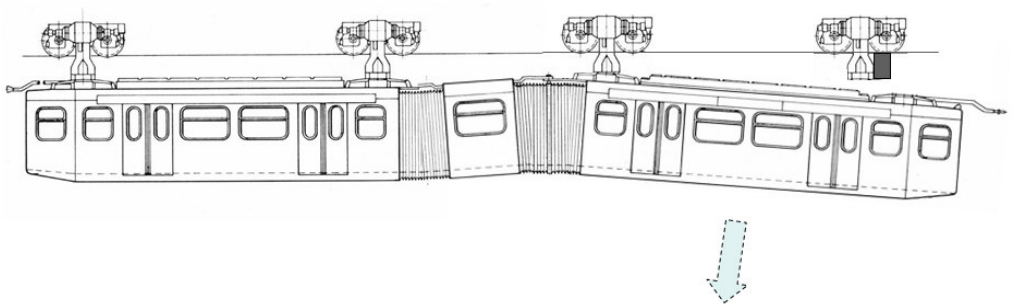

Fig. 5 Expected incident scenario

Consequently, further investigations were not only necessary for technical clarification; they became an official part of public prosecution. For deeper investigation of the incident steps sequence the Fraunhofer Institute at Freiburg i. Br. was called in.

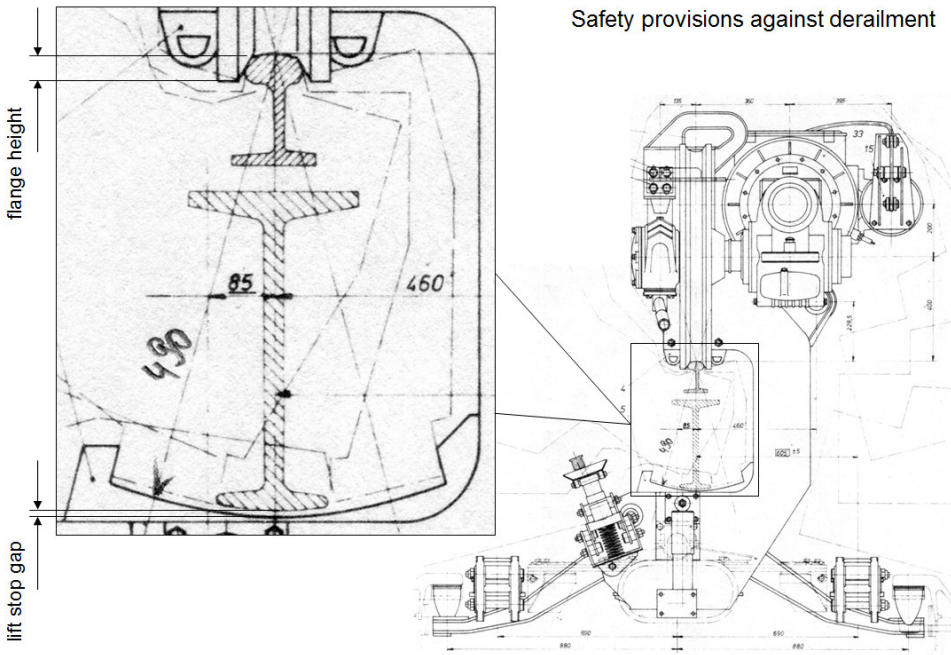

Fig. 6 Safety device arrangement [2]

4. INVESTIGATION RESULTS

Finally, two questions had to be answered: why did a train derail even though each bogie was equipped with an efficient lift stop, which prevents the flanges from climbing by half of the travel necessary? Why did the second half of the train derail first, sweeping the leading one away only after touching the river's bed itself first? Big questions and not a marginalia, cause insufficient answers could cast doubt on the whole system functionality.

In an independent technical investigation the circumstances of the accident and the sequences of the derailment process were analyzed and could be reconstructed in detail.

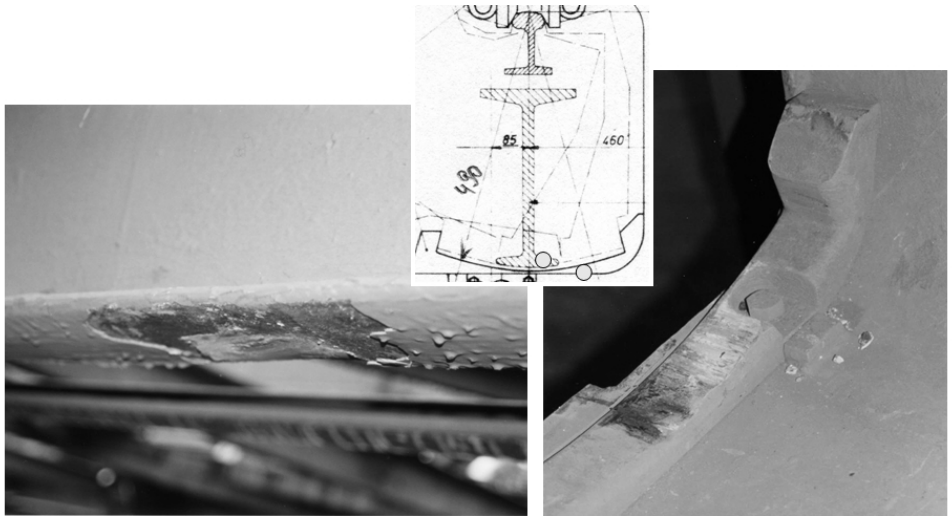

Fig. 8 Derailment traces at rail bottom and bogie frame safety device [3]

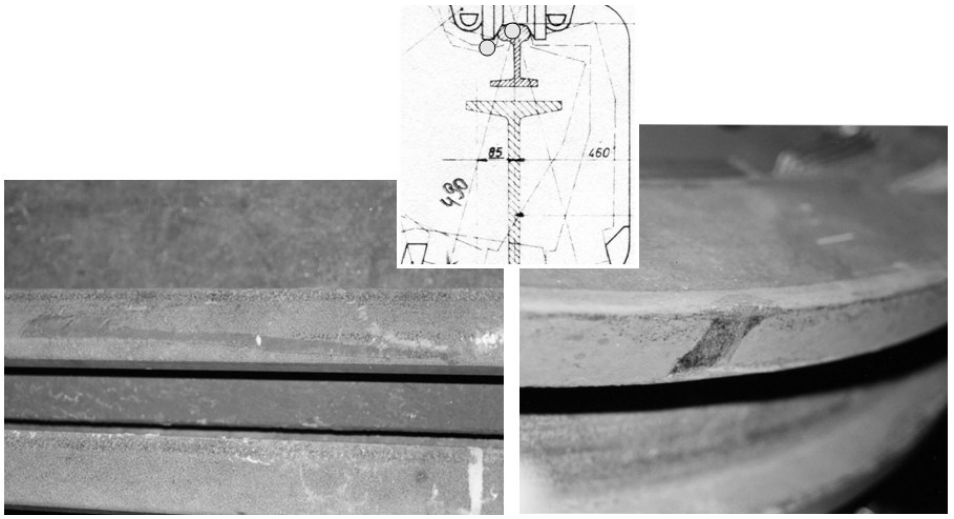

Fig. 9 Corresponding derailment traces at rail surface and wheel flange [3]

According to the traces found at rail upper and lower surface as well as at the corresponding surfaces at bogie frame end stop and wheel flange, the sequence of the incident became evident.

After the first bogie was disrupted, both bogies of the second car derailed at the same moment. Finally the remaining second bogie lost its connections due to overload.

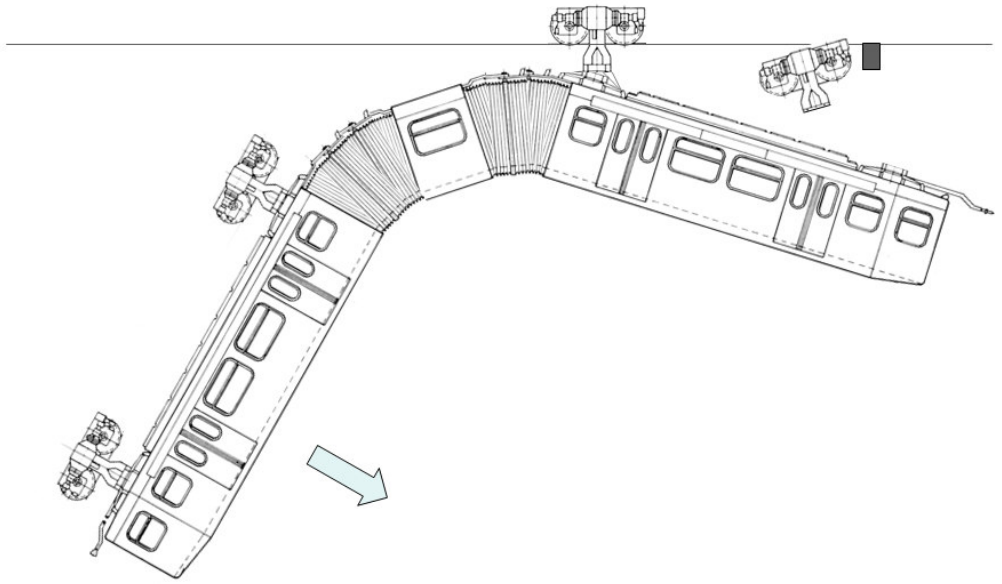

Fig. 10 Incident scenario as happened

It could be substantiated that the vehicle concept with its comparably short intermediate compartment was responsible for the opposite lateral turning of the two vehicle main elements. The resulting forces (see fig. 12) at the wheel-rail contact raised as far as the bogie frame and the flanges suffered mechanical deformation and the wheels overrode the limits given by the lift stops. [4]

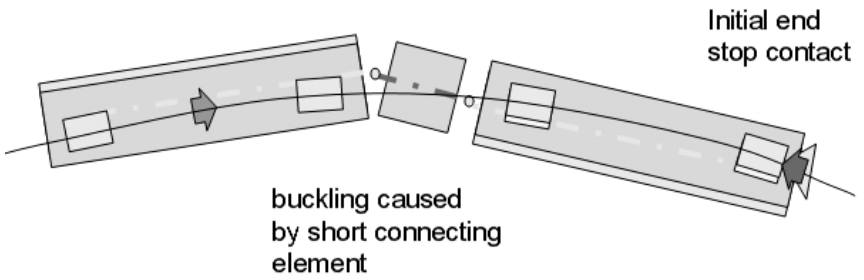

Fig. 11: Incident scenario at the very beginning

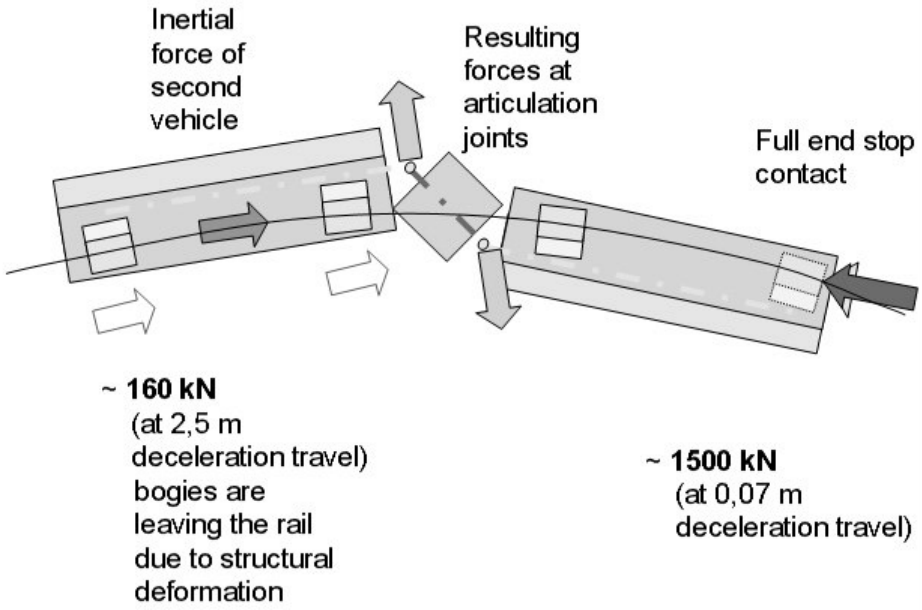

Fig. 12 Incident scenario at the moment of derailment

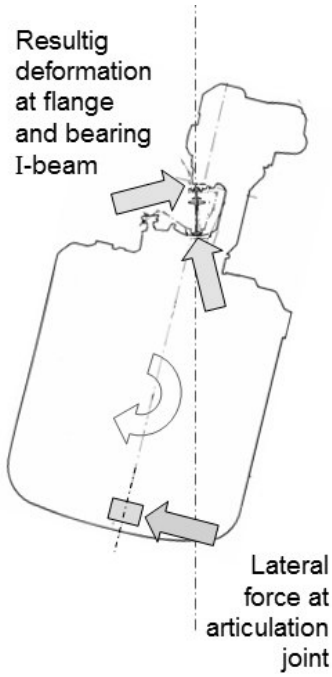

Fig. 13 Incident scenario at the cross section contact points

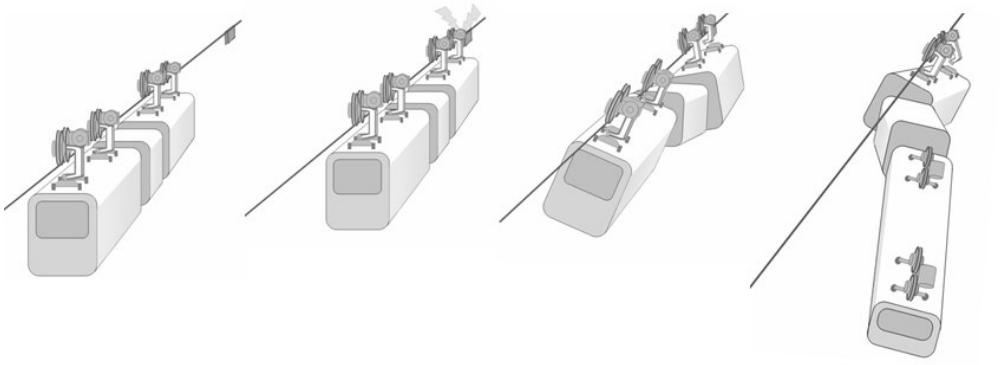

Fig. 14 Incident scenario sequences

A look back at the network history allows to discover another incident that happened in May 1917 - obviously following the same procedure, caused by the same relationships, when a train crashed into the trailer car of another one which was stopped by a system brake down. Records denote: „The cause never could be explained in detail finally“... - up to now.

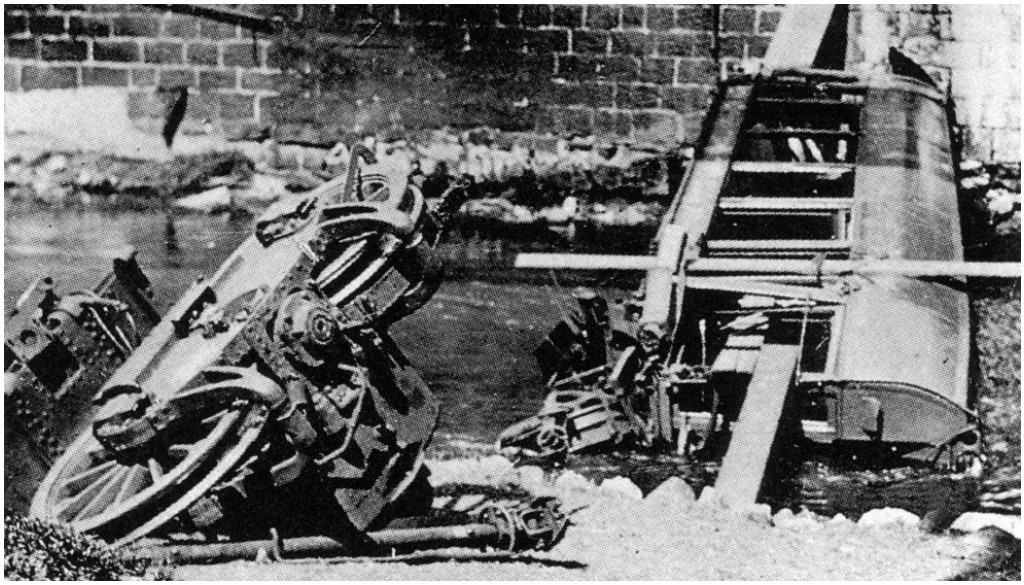

Fig. 15 Derailment scene of May 1917 [5]

Accordingly, April 1999 was not the "first case ever", but in the past it was missed to investigate the root cause and to define consequences for further developments. As history still reiterates sometimes, also in 1999 eyes were kept closed with regard to revise the requirements for future vehicle concepts - as far as potential alternatives were left.

5. AN ALTERNATIVE SOLUTION

As the short compartment between the two vehicle main sections is detected as the critical component, a design change is necessary at this very point. Using all the same dimensions and the same components of the same size, a shifting of the articulation sections only can lead to the safe solution required. As a spin-off, a better door and passenger distribution is given.

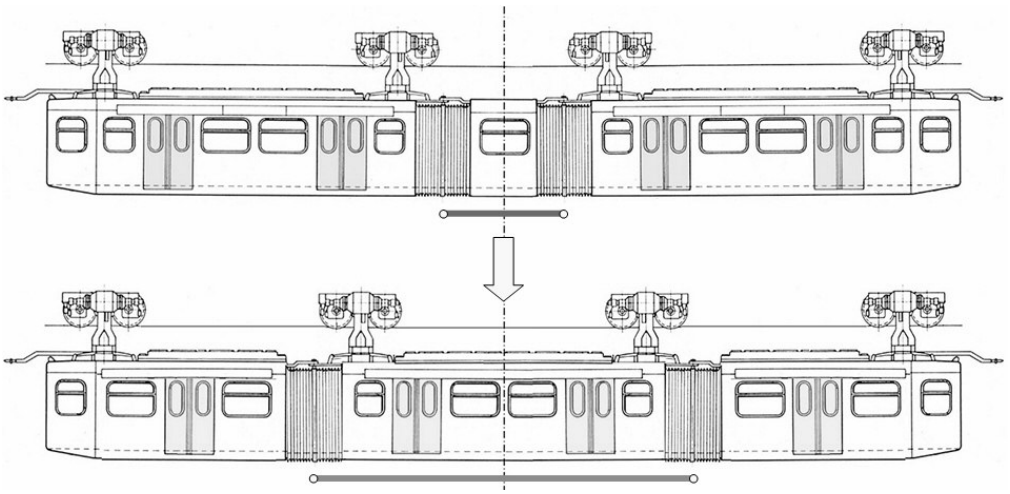

Fig. 16 Derailment safe vehicle concept

Further investigations demonstrate in addition that even the vehicle gauge requires less space restrictions - an all around satisfying solution for future application.

6. CONCLUSION

The application and combination of "well known" concepts and a statically safe mechanism alone turned out to be not sufficient even in case of typical accident situations like rear-end collisions. Feasible design measures applied - resilient or shock absorbing elements at the articulation, different position of bogies, stronger derailment stops - most of the consequences never had happened in the given case.
Since 2015 a new generation of 31 vehicles was introduced, but no findings of the year 1999 investigations have been considered, the conceptual design remained unchanged. Some enhanced imagination in the concept phase - up to a change of the bogie and articulation location - and a more broadly based analysis of vehicle and track interface characteristics beyond the specification requirements might have increased the total system performance remarkably, even saving passengers lives and integrity - but the chance was missed.

Fig. 17 The new generation of 2015 [6]

5. REFERENCES

[1] -.-: Schwebebahnunfall in Wuppertal 1999; last download at June 30, 2019 from: https://de.wikipedia.org/wiki/Schwebebahnunfall_in_Wuppertal_1999

[2] -.-: drawings and photographs from the MAN historical archive at the Nuremberg DB Museum

[3] **Richter, W-D.**: Wuppertaler Schwebebahn-Unfall vom 12.04.1999, Rekonstruktion des Entgleisungsvorgangs, Nürnberg 1999 (experts report, not published)

[4] **Zeller, R.**: Abschätzung der Kräfte beim Wuppertaler Schwebebahn-Unfall, Fraunhofer Institut, Freiburg i. Br. 1999 (experts report, not published)

[5] **Eschmann, J.**: Die Wuppertaler Schwebebahn, Wuppertal 1990

[6] -.-: schwebebahn; online presence of WSW mobil, Wuppertal; last download at January 12, 2020 from: https://www.schwebebahn.de/

NUMERICAL STUDY ON THE DYNAMICS OF A NOVEL, HIGH-SPEED PASSENGER BOGIE DESIGN WITHOUT A PRIMARY SUSPENSION SPRING

Paul SCHÖNHUBER, Erik ROLFF and Christian SCHINDLER

Institute for Rail Vehicles and Transport Systems (IFS)
Faculty of Mechanical Engineering
RWTH Aachen University
D-52074 Aachen, Germany

Received: June 16, 2019

EXTENDED ABSTRACT

1. INTRODUCTION

Due to track excitations or twisted tracks, bogies generally need a primary suspension. However, a design free of a primary suspension spring can offer significant benefits, especially in terms of design simplicity and weight saving. The key to this implementation lies in modifying the bogie frame design in such a way that it offers the necessary flexibility to compensate for the lack of the primary suspension spring. Possible solutions are a frame consisting of two halves offering an additional degree of freedom or a flexible bogie frame.

2. BOGIE DESIGN

This numerical study introduces a novel double-axle running gear with independent wheels and an analysis of its dynamic behavior. In contrast to standard wheelsets, this type of bogie does not show any hunting oscillation. Thus, an improved behavior concerning wear and ride comfort can be achieved.

2.1 Frederich Bogie Type

In the late 80s, Friedrich Frederich introduced a bogie design which consists of a bogie frame divided into two halves. Each half is a rigid construction that bears the wheels of one side and has a rotational degree of freedom about the lateral axis with respect to the other half. [1]

The design was track tested and was consequently proven to be able to run at speeds up to 507 km/h without experiencing hunting. The downside is a poor ride comfort and a rather high unsprung mass. As a result, the bogie did not go into commercial production.

In this study, this bogie type with the centrally pivoted frame is taken as a reference bogie.

2.2 Flexible Bogie Frame

These disadvantages could be overcome by using a flexible bogie frame made of glass-fibre reinforced plastic (GRP) [2]. The frame is flexible and light, thereby offering a significant reduction in the unsprung mass.

Each bogie (Fig. 1) consists of two pairs of independent wheels, which are mounted (using bearings) on axles at the front and rear. An H-shape GRP frame is placed between the axles, which bears the secondary springs and an anti-roll bar.

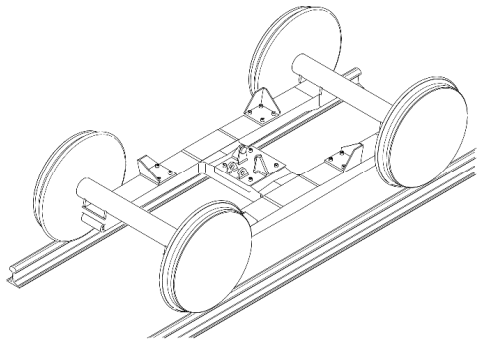

Fig. 1 Bogie design.

3. TRACK

A track was defined to analyze the dynamic behavior. In accordance with the high-speed application, the track was designed to include a high percentage of straight sections. The curved sections have a minimum radius of 5000 m.
The track design was complemented with synthetic excitations from the European Rail Research Institute (ERRI) B176 low definitions in vertical, lateral, roll and gauge direction [3][4]. The vehicle velocity was set to 300 km/h, the simulation time to 980 s.

4. RESULTS

The calculated forces and accelerations were evaluated according to the standards DIN EN 14363 [5] and DIN EN 12299 [6]. Initial results show that the novel bogie design is capable of improving the dynamic behaviour of the vehicle.
Fig. 2 shows the frequency distribution of the vertical wheel forces. It can be observed, that a reduction can be achieved.

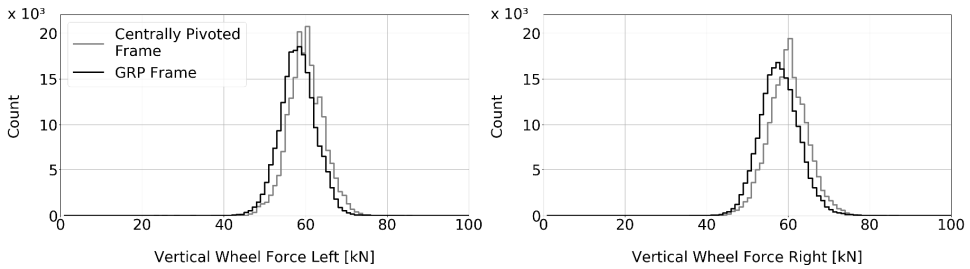

Fig. 2 Frequency distribution of the vertical wheel forces at the leading wheelset.

Regarding the ride comfort, a significant improvement is obtained in vertical direction. Fig. 3 compares the continuous comfort of the novel and the reference bogie.

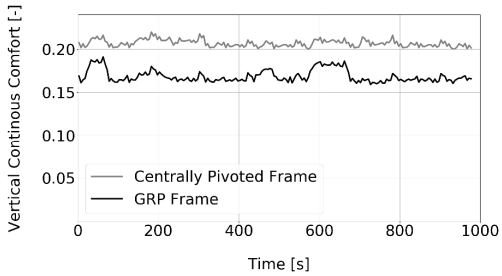

Fig. 3 Ride comfort.

5. CONCLUSION AND OUTLOOK

This numerical study points out the favorable dynamic behavior of a GRP bogie frame. It facilitates a lightweight design as well as the integration of the suspension spring function into the frame due to the high allowable elastic strain.

In the next steps, it is planned to conduct validation and optimization experiments using test beams. Especially the characterization of the damping properties can prove to be challenging.

Apart from the dynamic behavior, further studies concerning the structural integrity, fatigue and manufacturing need to be carried out in order to design a first prototype.

6. REFERENCES

[1] **Schraut, R.**: Das Einzelrad-Doppelfahrwerk - Konstruktive Ausführung und erste Versuchsergebnisse, ZEV + DET Glasers Annalen, Volume **115**(1-2), 1991, p.37-41.

[2] **Mayer, R.:** Reducing Maintenance of Tracks by a New Design of Environmentally Friendly Bogie. ZEVrail, Volume **140** (5), 2016, p.188-193.

[3] **Haigermoser, A. - Luber, B. - Rauh, J. - Gräfe, G.**: Road and track irregularities: Measurement, assessment and simulation. Vehicle System Dynamics, Volume **53**(7), 2015, p.78-957.

[4] **N. N.**: Simpack Documentation, Simpack Release 2018, Dassault Systèmes Simulia Corp, 2018.

[5] **DIN EN 14363**: Railway applications – Testing and Simulation for the acceptance of running characteristics of railway vehicles – Running Behaviour and stationary tests. Berlin: Beuth Verlag, 2016.

[6] **DIN EN 12299**: Railway applications – Ride comfort for passengers – Measurement and evaluation. Berlin: Beuth Verlag, 2009.

A REALLY INNOVATIVE FREIGHT BOGIE

Andrea BRACCIALI and Gianluca MEGNA

Department of Industrial Engineering, University of Florence, Italy
Via Santa Marta 3, I-50139, Florence, Italy

Received: September 9, 2019

ABSTRACT

A new bogie for freight wagons, named 4L (*"four legs"*) is introduced, aiming at fighting against Y25 in terms of cost, running dynamics behaviour, track friendliness and maintainability. Compatibility with exisiting vehicles was kept. Structural, dynamics and contact mechanics analyses are discussed, showing how the 4L bogie is definitely the winner of this battle.

Keywords: Y25 bogie, freight wagons, bogie frame, AIR Wheelset, running dynamics, contact mechanics, 4L bogie

1. INTRODUCTION

Even if the Y25 bogie has recently celebrated the 50th anniversary from its first development [1], it is still the most common freight bogie in Europe. The main reason can be found in the low manufacturing and maintenance costs, which have strongly reduced the possibility of the application of innovative solutions. However, the increase of the efficiency of goods transport by means of freight wagons is one of the main objectives for the next years and projects are dedicated to develop an innovative freight bogie with superior characteristics respect to current Y25 bogie [2] [4]. Several aspects have to be involved in this process, with special attention to wagon design, monitoring and maintenance. As lower noise, greater load capacity, lower downtime and better ride quality are requested today by railway companies, bogie designer have to face very challenging problems. This is confirmed by considering that the state of the art of freight bogies, composed by improved design of Y25 (like the GB25RS or the TVP2007) or advanced new design (like the RC25NT, the DRRS25LD or the TF25), is not able to completely replace the classic design of Y25, even if greater performances could be guaranteed in terms of safety, speed and reliability.

In this paper an innovative freight bogie, named 4L (*"four legs"*) for its peculiar structure, is described considering its impact on freight wagon market. Differently from other modern bogies, the 4L shows a better ride quality by means of its suspension arrangement and its lightweight design, without the need of rubber cushions or hydraulic dampers.

2. DESCRIPTION OF THE Y25, LEILA AND 4L BOGIE

Freight wagons are typically allowed to travel with a maximum cant deficiency of 92 mm (non-compensated acceleration a_{nc}=0.6 m/s^2), while they can stop in canted curves with a maximum cant excess of 160 mm (a_{nc}=-1.05 m/s^2). In any case, lateral forces are one order of magnitude lower than vertical forces, that are due to gravity (≅ 10 m/s^2).

To better understand the differences of the solutions compared in this chapter, Figure 1 shows the position of the applied vertical force (in the centre bowl) and the position of the bogie frame reactions in the Y25 bogie, in the Leila bogie and in the 4L bogie (described below). Obviously closer reaction points generate less bending and are easier to react.

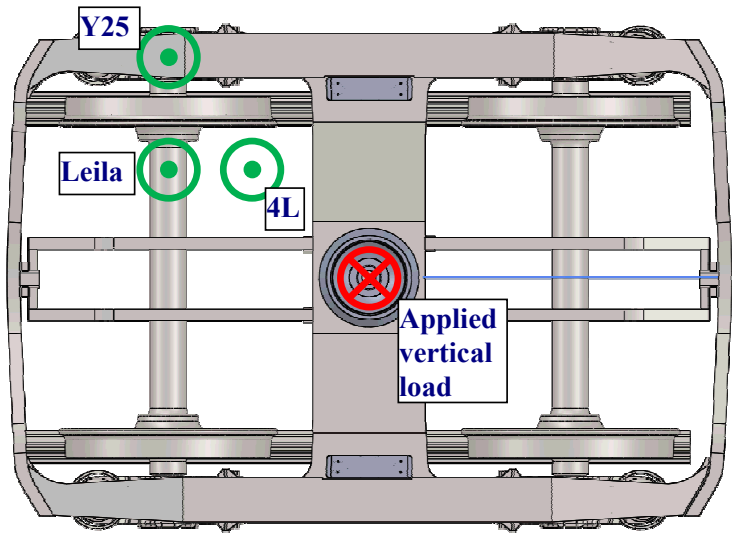

Fig. 1 Comparison of reaction forces on the bogie frame for three different bogie architectures. It can be seen that the Y25 bogie has the farthest reaction point while the 4L bogie has the closest reaction point.

Starting from the Y25 bogie frame and limiting the analysis to vertical loads, the flow of the forces is shown in Figure 2. As a general rule, it is known that every time a force is shifted laterally bending appears. The path followed by vertical load acting on the centre bowl shows that the elements of the Y25 bogie are subjected to bending, requiring a beam-like structure.

The second case considered relates to bogies with inside frame design (i.e. with inboard bearings wheelsets). The most famous bogie representative of this category is certainly the Leila bogie by Prof. Markus Hecht from TU Berlin (Figure 3), designed to replace the Y25 offering superior performances.

The Leila bogie frame has a shorter bolster beam, leaving the side beams nearly unaffected. However, one of the most important benefits of inboard bearings solutions is that the bending on the axle is reversed, and the overall stresses on the axle are relieved by curving forces. Regardless an extensive testing campaign and the presentation to Innotrans trade fair in 2004 and 2006, to the authors' knowledge the mass production of the Leila bogie did not start yet.

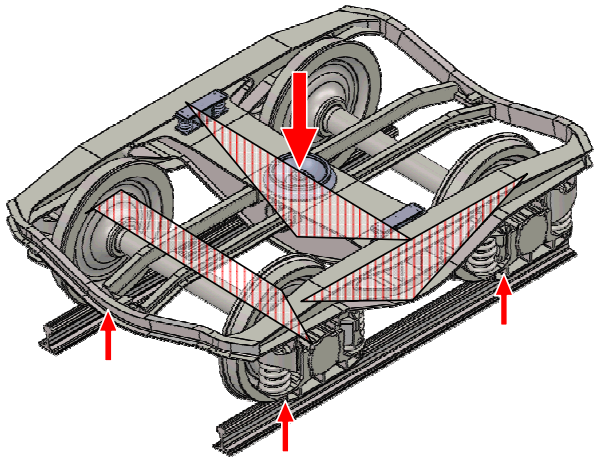

Fig. 2 Path of the vertical force in Y25 bogie. The bolster and the side beams are subject to bending. Axle bending is worsened in curves, where flange forces increase the stresses in this component

Before discussing the bogie introduced in this paper, it is worth observing the forces acting on a generic bogie. The vertical force, applied at the centre of the sphere of the centre bowl (z≅900 mm) is reacted by the forces at the wheel-rail contact, with Δx=1800 mm and Δy=1500 mm. The resulting almost right angle "pyramid", shown in Figure 4, cannot nevertheless be applied to real bogies with inboard bearings, as the wheelsets must be connected elastically to the bogie frame by using springs of any kind.

An architecture that can shorten the bogie frame is the one of the Wegmann-Kassel bogie (Figure 5), that was used quite extensively in the '60s and in the '70s especially for sleeping cars due to its good ride quality properties. It can be seen that in this case the bogie frame becomes much shorter than the similar conventional bogie (e.g. approximately 1900 mm vs. 3000 mm for a 2500 mm wheelbase bogie) as twice the length of the horizontal part of the swinging arm must be subtracted to the wheelbase.

The 4L bogie, introduced in this paper (Figure 6), is an inboard bearings bogie in which the primary suspension acts in longitudinal direction as done in the Wegmann-Kassel bogie, with the innovation that each spring connects the two swinging arms on one side and consequently the two wheelsets, replacing the eight springs used on each side of an Y25 bogie.

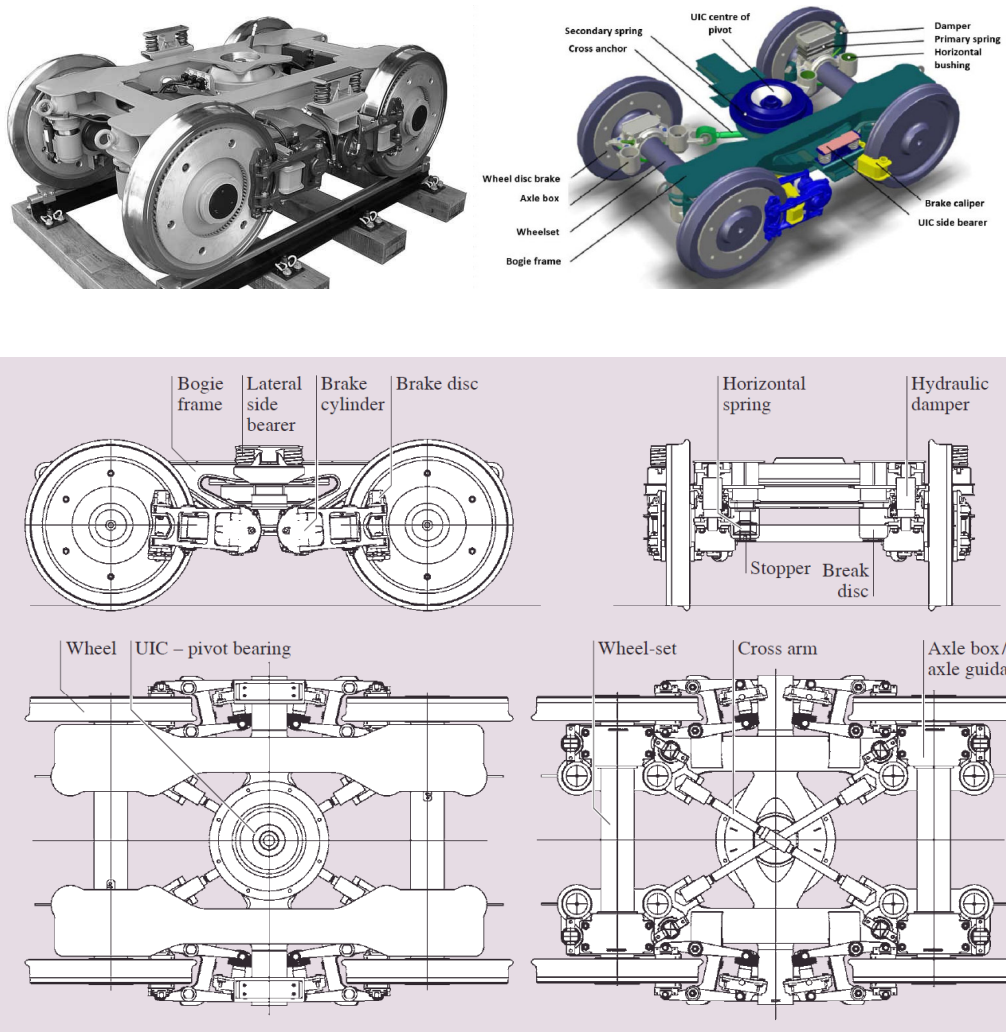

Fig. 3 The Leila bogie, with inboard bearings wheelsets, web-mounted disc brakes, Gigabox primary suspension, two levels of suspension and cross-bracing (lower figure from Grote Antonsson - Springer Handbook of Mechanical Engineering, ch. 13.3 Railway Systems – Railway Engineering)

Therefore, vertical movements of the wheelset and the bogie are transformed in horizontal movements by the swinging arm and energy is dissipated by friction (load dependent) in the cylindrical pin connection between the arm and the frame. The cylindrical pin is composed by wear resistance elements (manganese steel or wear-resistant austempered ductile iron).

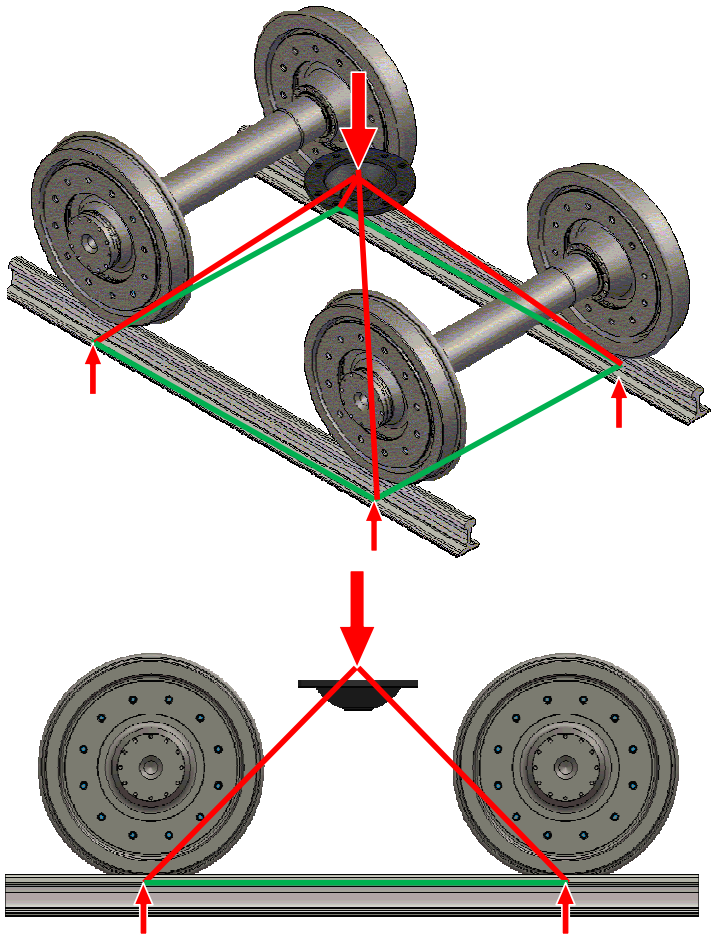

Fig. 4 Sketch of the reactions to the vertical force applied to the centre bowl of a freight wagon.

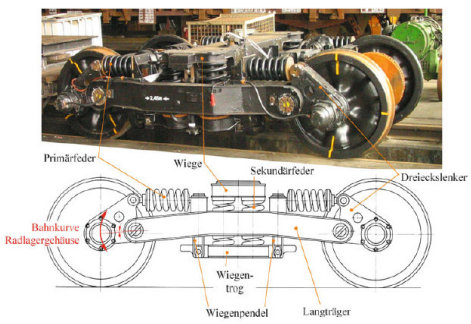

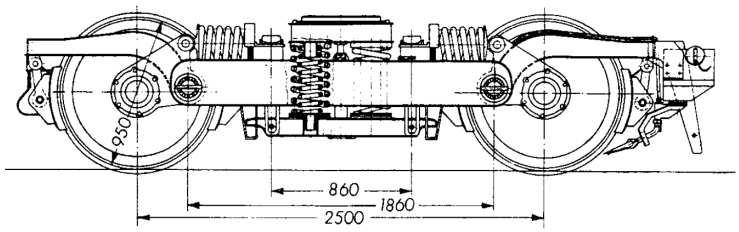

Fig. 5 Top: the Wegmann-Kassel (also know as the München-Kassel) bogie, with swinging arms and horizontal primary suspension (from J. Ihme – Schienenfahrzeug-technik - Springer Vieweg Verlag 2016, pp. 183-184). Bottom: drawing taken from K. Sachs – Elektrische Triebfahrzeuge, Springer Verlag, 1973.

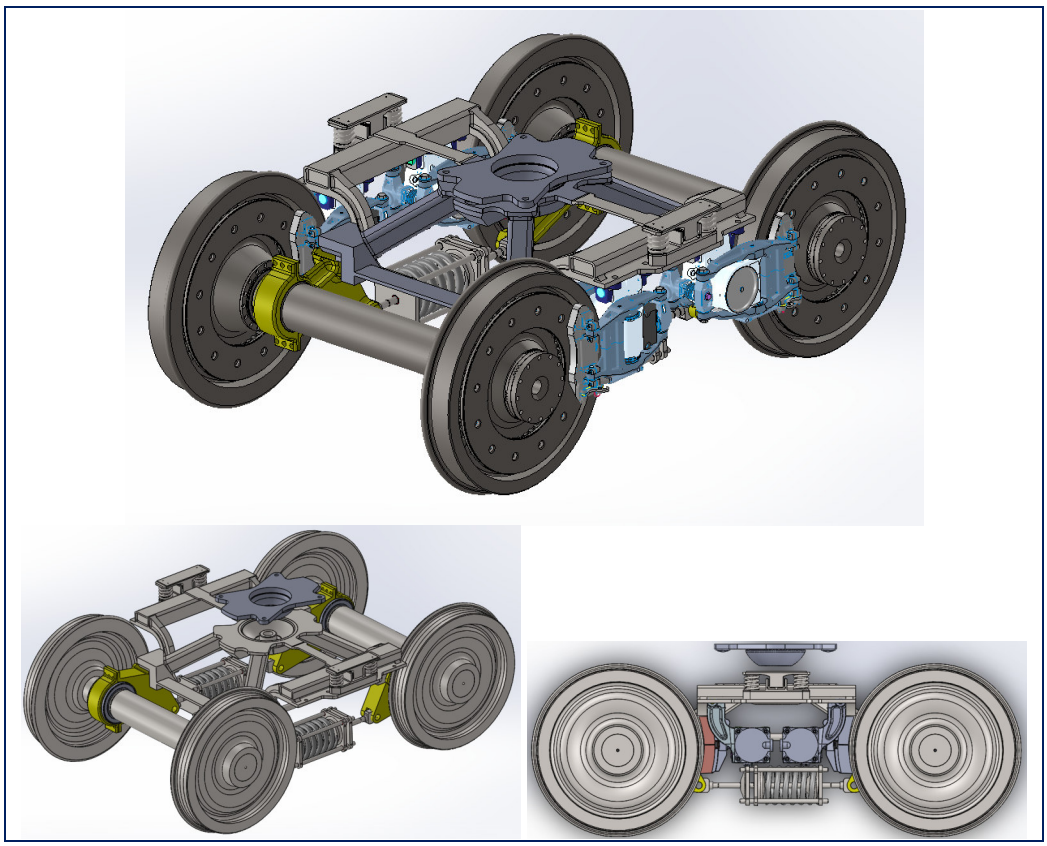

Fig. 6 Top: the 4L bogie with web-mounted brake discs and AIR Wheelsets (mass ≅ 4100 kg). Bottom: the 4L bogie with compact brake units acting on thermostable wheels and conventional inboard bearings wheelsets (mass ≅ 3700 kg).

This solution seemed very attractive especially for running dynamics reasons. As it will be shown below, the vertical static stiffness of the 4L bogie is identical to the Y25 bogie with the differences that the force-displacement curve is smooth, and a peculiar behaviour is obtained under certain conditions described below, resulting in a dynamic

equivalent stiffness lower than the static one. This leads to a superior behaviour about running dynamics properties of the 4L bogie compared to the Y25 under these circumstances. Moreover, the absence of components requiring specific maintenance (such as hydraulic dampers) is a distinct advantage of this solution that is made only of steel.

The greatest structural advantage of the 4L bogie is that the vertical force is transferred to the joints with a pyramidal structure made of "trusses", i.e. the eight elements of the bogie frame are four "legs" (from which the name of the bogie) in compression and four elements at the base in tension. The latter were made torsionally soft for reasons described below. The 4L bogie with the axlebridges of the AIR wheelsets [6] (with wheels removed) in shown in Figure 7.

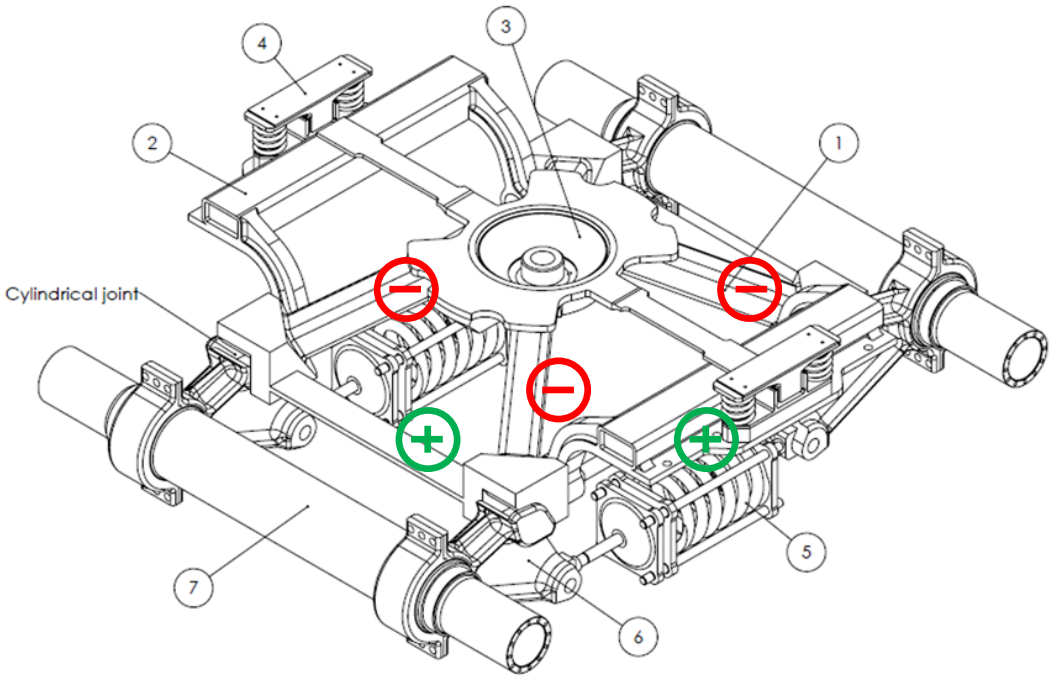

Fig. 7 Main components of the 4L bogie. 1: pyramidal frame; 2: supporting arm for side bearer and brake calipers for wheel web mounted discs (or compact tread braking units); 3: centre bowl; 4: side bearers; 5: horizontal coil springs with single-stage progressive stiffness; 6: swinging arm; 7: Inboard bearings axle. "Legs" are compressed (indicated with "-"), while the basis of the frame is in tension (indicated with "+")

It can be observed that the centre bowl has two appendices along the longitudinal axis to react the pitch movement that appears during braking. The new suspension mechanism, in fact, frees one degree of freedom around the lateral axis. This modification is deemed to be small and vehicles can be slightly modified to support the resulting forces.

The interface with the carbody remains the same as that of the Y25 bogie, i.e. it is composed of a centre bowl (or centre pivot) to support the vertical load and two side bearers that support the unbalance of the carbody when running with non-zero cant

deficiency/excess (e.g. when standing still on a canted track). The side bearers are connected to the bogie frame by the supporting frames, described below, with interesting manufacturing and maintenance solutions.

The overall design proves to be extremely efficient in terms of mass and moment of inertia, leading to low material purchasing and manufacturing costs. The key of the design was abandoning the classical architecture with beams subjected to bending and passing to trusses subjected to normal load.

3. DESIGN OF THE 4L BOGIE

While it will be shown afterwards that the 4L bogie exhibits distinct advantages in terms of maximum speed, running dynamics and track friendliness (especially on highly defective track), the main innovation consists in the extremely simple design that results in reduced manufacturing costs and, therefore, aggressive selling prices.

The number of components is reduced, and their role and properties may be summarized as follows:

- the bogie frame is made by mild steel welded parts, of the classical S355 grade, that include standard profiles, with a mass as low as around 320 kg;
- the centre bowl and the "knees" where arms hinge are located can be obtained either by forging or by casting and then welded to the frame, with equally low costs;
- the axlebox arms can be made of cast iron (typically GJS 400 grade) and can either house the bearings (if a standard inboard bearings are used) or clamp the axlebridge in case an AIR Wheelset [6] is used;
- hinges are made of easily replaceable wear-resistant components, and are designed in order to provide a friction damping proportional to axleload;
- the suspension springs are progressive and provide the correct stiffness to keep the vertical (bouncing) frequency of the wagon constant regardless of the axleload;
- the supporting arms, manufactured separately, are bolted to the bogie frame and can be replaced / repaired if needed without scrapping the entire frame.

3.1 Description of the 4L bogie frame design and numerical validation

As any other rigid bogie frame, it is particularly sensitive to track twists. While in the Y25 bogie, as in all the other conventional bogies, twists are managed by differential suspension movements, in the 4L bogie the axlebox arms are connected to the bogie frame with "rigid hinges" that allow rotations while contraining translations. The possibility of surviving the largest possible twists was therefore assigned to frame flexibility. This concept is somewhat similar to other existing conventional bogies equipped with stiff primary suspensions (Figure 8).

Designing a bogie frame strong enough to survive all exceptional and fatigue loads under a 22.5 t/axle load and flexible enough not to fail under exceptional and repeated track twists proved to be extremely challenging and required no less than the evaluation of at least 50 alternatives.

The details of the structural design of the bogie frame cannot be given here for space reasons. As an example, the validation under fatigue loads is shown in Figure 9. It is important to highlight that the structural analysis was possible only after a complete finite element simulation of the entire bogie, as the flexibility of all the components (axlebox arms, springs, wheelsets, etc.) has a large influence on the actual loads imparted on the frame.

A first coarse mesh model was therefore used to find out displacements under all loading combinations; these boundary conditions were therefore inserted in a finer model that allowed to validate the design according to EN 13749 standard. As some welds are not "conventional" joints ("T", butt, etc.), some joints were validated according to the "advanced" methods (such as the hot spot approach and the effective notch stress approach) described in the draft standard prEN 17149 (see Figure 10). The development of the design was stopped when the validation phase was passed successfully.

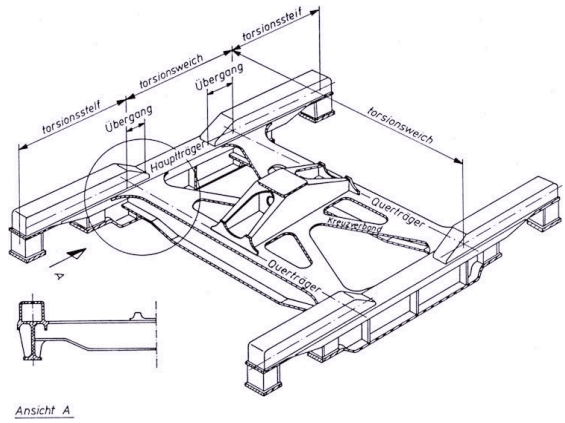

Fig. 8 Example of torsionally soft bogie frame used in bogies with particularly stiff primary suspension (from J. Ihme – Schienenfahrzeugtechnik - Springer Verlag 2016, p.196)

	Fzp = 392400 N	Fzp = 313920 N Fzsb = 78480 N	Fy = 88290 N	Fx = 22072,5 N	dz = 9 mm	Fb = 24615 N Fx = 16187 N	Fi_vert = 5592 N	Fi_lat = 4460 N	Fi_long = 2230 N
J	X (+30%)								
K	X (-30%)								
L	X			X	X				
M	X			X (-)	X				
N	X					X			
O	X					X (-)			
P		X	X		X				
Q		X (opp)	X (-)		X (-)				
R	X								
S		X	X		X				
T	X		X				X	X	X
U	X		X				X (-)	X (-)	X (-)

Fig. 9a Validation under fatigue loads of the frame of the 4L bogie according to EN13749. Load cases.

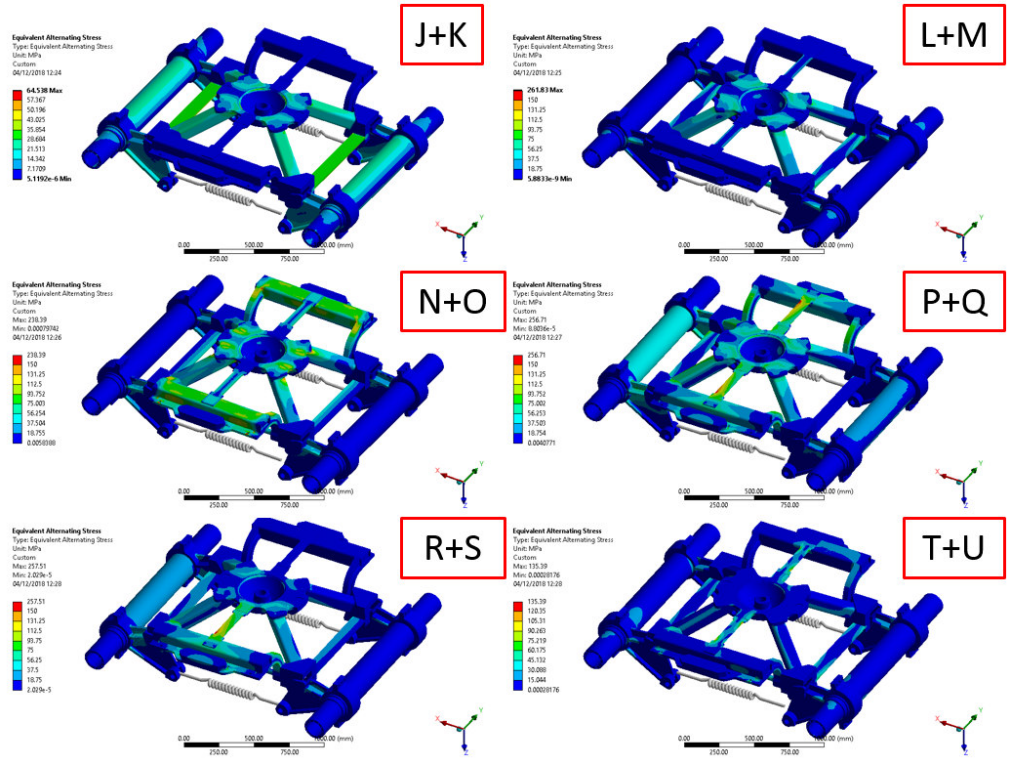

Fig. 9 Validation under fatigue loads of the frame of the 4L bogie according to EN13749. Alternate stress validation. All load cases were successfully validated.

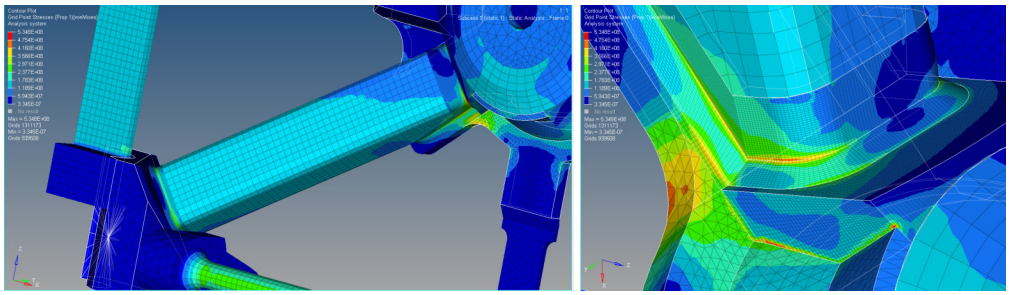

Fig. 10 Validation of the frame of the 4L bogie with the methods described in prEN 17149. Due to the extremely high number of elements, the analysis was applied only locally to weld seams ad adjacent areas as specified by the standard.

3.2 Suspension elements in the 4L bogie frame

Central in the design of the 4L bogie is the selection of the proper suspension element. Although no details can be given here, Figure 11 shows the non-linear stiffness of the helical springs used (one per side) that replace all the 16 springs on the Y25 bogie.

This component provides the correct dynamic response with several advanteges (only one component, easily inspectable, etc.), the most important of which is the absence of the "knee" in the stiffness curve of Y25 bogie due to the intervention of the inner spring at "intermediate" loads with the related uncertainties on dynamic behaviour.

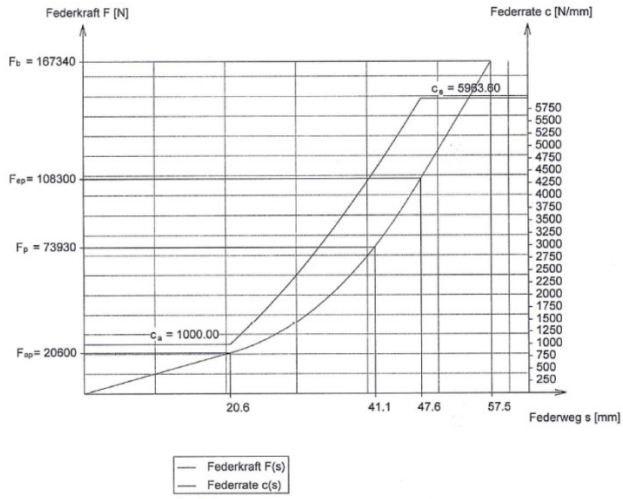

Fig. 11 Stiffness of the progressive spring used in the 4L bogie. Space and mass constraints, particularly stringent, were all satisfied by the contacted supplier.

To better understand the reason why the 4L has an extremely high track friendliness, the concept of the "short circuit" of the two swinging arms needs to be better explained.

In a Y25 bogie, the vertical load F_Z applied on the centre bowl is shared on the 4 wheels, each with a stiffnes K_{Y25} per axlebox. The resulting vertical displacement is $\Delta z_{Y25}=(F_Z/4) / K_{Y25}$. In the 4L bogie (Figure 12a), that has only two springs (one per side), let suppose for the sake of simplicity that the swinging arm has a geometry such that $\Delta x=\Delta z$, i.e. the horizontal elongation of each end of the spring is the same as the vertical displacement of the centre bowl, i.e. $\Delta x_{4L}=2\ \Delta z_{4L}$. This results in $\Delta z_{4L} = \Delta x_{4L}/2 = (F_Z/4) / 2\ K_{4L}$. To ensure the compatibility of the 4L bogie with existing vehicles, must be $\Delta z_{Y25}=\Delta z_{4L}$, i.e. $K_{4L}= K_{Y25}/2$. The 4L bogie springs were therefore designed to have a stiffness that is a half of the stiffness of Y25 *per axlebox*. This guarantees the same static displacements under the same vertical loads.

This suspension arrangement, that reminds somewhat the Munchen-Kassel bogie, has an interesting behaviour in case short defects are encountered. Let suppose (Figure 12b) that the vehicle finds a local irregularity the forces the first wheelset to lift up with by a quantity Δz_L. If the irregularity is short, i.e. if the bogie frame still did not start to rotate or displace yet, the total elongation of the spring i $\Delta x_L=\Delta z_L$ but, as long as the stiffness is $K_{4L}= K_{Y25}/2$, this implies that *the vertical stiffness observed during a*

transient vertical displacement of a wheelset of the 4L bogie is a half of the stiffness of the Y25 axlebox.

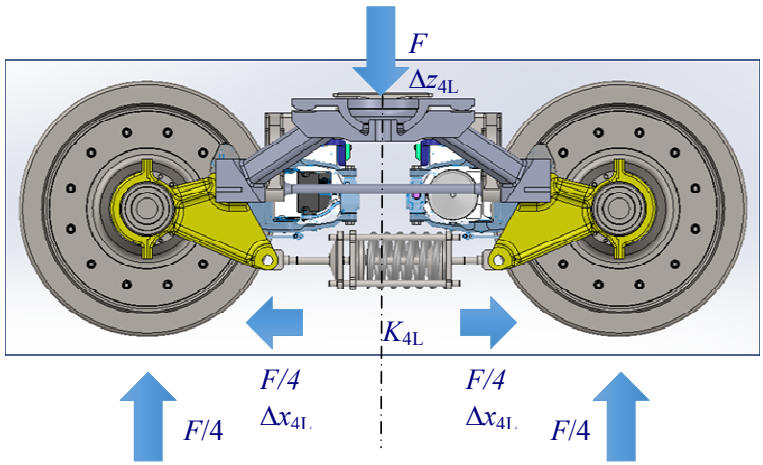

Fig. 12a Calculation of the stiffness of the progressive spring used in the 4L bogie.

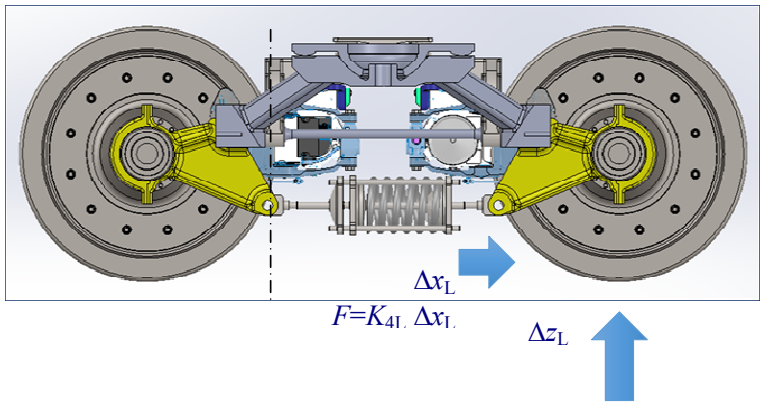

Fig. 12b Calculation of the stiffness seen by a wheelset in presence of a local vertical irregularity.

As an extreme case, consider now that the displacements applied at the wheel-rail contact points are opposite (Figure 12c). In this case the spring does not undergo any elongation. If the displacements are applied harmonically at a sufficiently high frequency, there are in practice no reaction forces on the bogie frame that remain neutral. This explains the exceptionally good behaviour of the 4L bogie in presence of some kinds of irregularities (see the relevant chapter below) that was called “short circuit effect”.

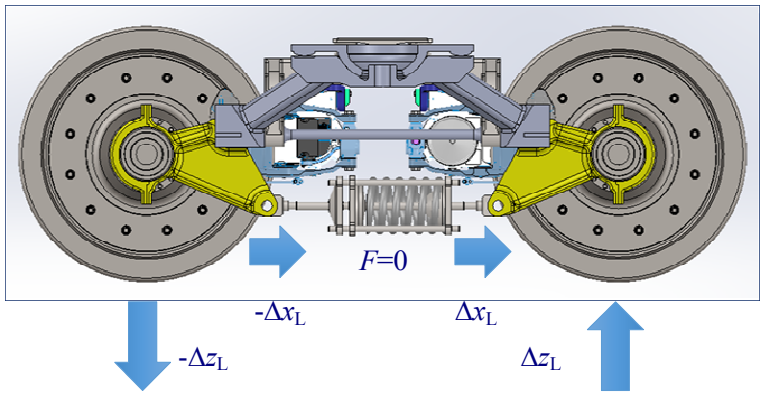

Fig. 12c Counterphase vertical irregularities effect on the 4L bogie.

3.3 Friction damping and hinges of the axlebox arms

Rubber elements and hydraulic damping system are not welcome in the freight wagons industry as they may give rise to aging or unexpected and early failures. The Y25 bogie only includes steel and consumable parts (Lenoir link) made of manganese steel. That's why the 4L bogie includes only manganese steel or ADI (Austempered Ductile Iron) consumable components, using the same friction damping mechanism of the Y25.

Long academic discussions could be made about the evident superiority of hydraulic (viscous) damping compared to friction damping, but the lack of success of more sophisticated bogies is indisputably due also to the presence of hydraulic dampers. Figure 13 shows a sketch of the joint, with the two cylindrical (around longitudinal and transversal axes) couplings in evidence. This particular design keeps the reactions inside the bearings of a conventional wheelset to the lowest levels.

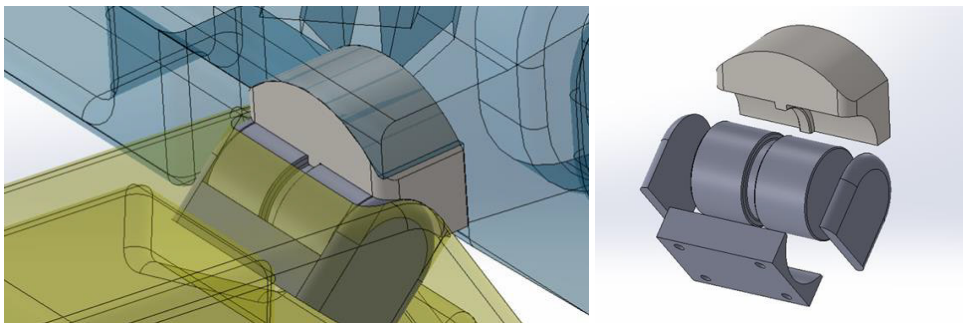

Fig. 13 Left: transparent view of the joint used in the 4L bogie. Right: exploded view of the consumables, made of a few components of low cost.

3.4 Axlebox (swinging) arms

This components do not require a specific description. Their size, shape and stresses are such that they should be casted in spheroidal graphite cast iron (austempered only if needed) and machined accordingly to the common practice. It is nevertheless important

to say that as long as no rubber elements (silent blocs) are included in the drawing, tolerances should be strictly respected.

3.5 Wheelsets and bearings

As already mentioned, the 4L bogie can be equipped with conventional inboard bearings wheelsets as well as the AIR Wheelset solution described in [6]. Due to its design, the current architecture of the 4L bogie is not compatible with axle-mounted brake discs, mainly because of the difficulty of housing the callipers. This is not deemed to be a serious drawback of the 4L bogie, as tread-braked thermostable wheels are gaining back the favour of the freight industry and web-mounted brake discs are spread in all the applications.

A final word should be said to discuss the use of inboard bearings, that are a central element to get the astonishing characteristics of the 4L bogie. It is not by chance that all modern bogies use this solution [6], and today, with digital monitoring and "smart vehicle" concepts spreading also into the world of freight wagons, monitoring of inboard bearings is not a problem anymore thanks to advanced and low-power diagnostic on-board devices.

4. RUNNING DYNAMICS AND CONTACT MECHANICS OF THE 4L BOGIE

Running dynamics of Y25 was often criticized because of the intrinsic non-linearity of the suspension (only piecewise linear) and for the presence of friction damping elements. It is a matter of fact, anyway, that the Y25 was extremely successful and that represent the benchmark for any other solution.

While approaching the design of the 4L bogie, several choices were made. First, it was readily acknowldeged that the higher speeds, in the order or in eccess of 160 km/h, cannot be achieved with a single suspension bogie. Discussing with experts in the freight wagon sector, a top speed of 140 km/h in empty conditions was set as a target. This may look unambitious, but it should be considered that current freight wagon travelling in "SS" regime run at 120 km/h when empty and 100 km/h when loaded.

The selection of this target speed was in line with the locomotives available for freitght trains (e.g. some locomotives of the TRAXX family by Bombardier have a maximum speed of 140 km/h, allowing a relevant simplification in the drive chain) and seems well suited for the distances and traffic on conventional routes

The validation of the 4L bogie from the running dynamics point of view was therefore performed, according to the prescription of the EN 14363 standard, by using the multibody code VI-Rail. Only some information extracted from paper [4], to which the reader is referred, will be shown in the following.

4.1 Lateral dynamics (stability)

Lateral dynamics simulation results are shown in Figure 14. Stability limits on straight track with "high level" track defects are reached for a speed of about 145 km/h for the empty wagon and for a speed of 180 km/h for the laden wagon. This means that the 140 km/h target is achieved.

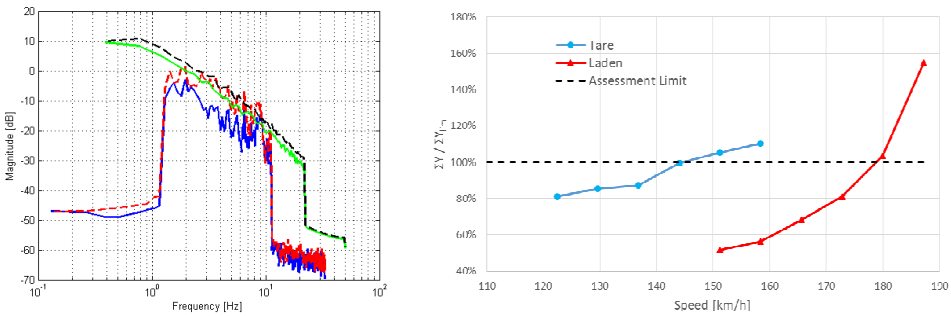

Fig. 14 Left: PSD distribution of lateral (alignment, solid blue) and vertical (longitudinal level, dashed red) for measured defects and the corresponding ERRI "High Level" irregularities lateral (solid green) and vertical (dashed black). Right: stability assessment according to EN 14363 in tare and laden conditions for the 4L bogie (from [4]).

4.2 Vertical damage and track access charges

The implication on track access charges in the UK according to the *Ride Force Count* method allowed to find the *Suspension Discount Factor*. The dynamics of 4L bogie and Y25 bogie was compared, showing that the average dynamic vertical force per unit of axle load are low for the new bogie even at higher speeds (Figure 15).

Vehicle		Mean value (tare)	Mean value (laden)
Y25 (120 km/h)		0.238	0.102
4L bogie	120 km/h	0.127	0.052
	145 km/h	0.162	0.072
	160 km/h	-	0.085

Fig. 15 Vertical force average dynamic component of Y25 and 4L bogies in different loading conditions (adapted from [4])

4.3 Running through curves – wheel and rail wear and RCF

A specific attention was devoted to the identification of the 4L bogie behaviour in curves. It is known, in fact, that the Y25 bogie has poor steering performances and one of the goals was to get $T\gamma$ values as low as possible. $T\gamma$, the wear number, is directly related to rail wear and crack growth, as shown in Figure 16.

Due to the roll angle of the wagon and the increase of the load of the external wheels, the suspension arrangement of the new bogie generates a better steering performance as it allows the wheelset to align radially when the vehicle runs with h_d>0 (a_{nc}>0). In such case the external suspension arms rotate more than the internal ones, generating an outer wheelbase greater than the inner one. For h_d=92 mm (a_{nc}=0.6 m/s^2), typical for freight trains, $T\gamma$ rapidly drops to zero, generating virtually no damage in the rails (Figure 9).

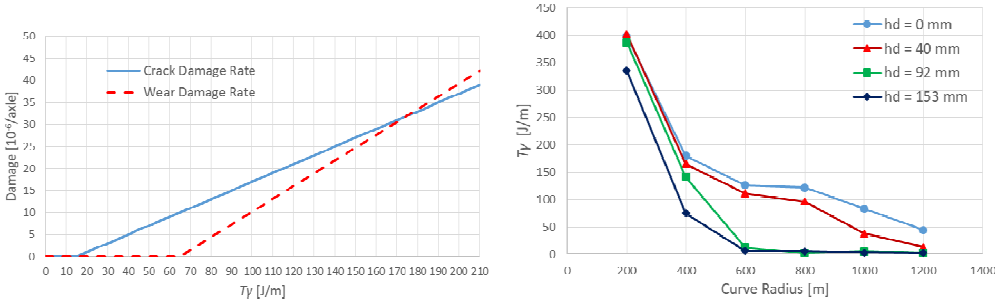

Fig. 16 Damage given by single axle (left). Tγ of the front axle a leading 4L bogie for different curve radii and cant deficiencies in laden condition (adapted from [4], right).

4.4 Safety against derailment

Derailment coefficient was evaluated considering method 2 of EN 14363, measuring the lateral force of the outer wheel on flat track with radius *R*=150 m and no transition and the minimum vertical force due to a twist of 0.42% applied during static tests [5].

Both 4L and Y25 bogies showed a maximum derailment ratio lower than the safety limit of 1.2 (1.06 for the Y25 and 1.01 for the 4L), obviously in empty conditions. Figure 17 shows the lateral forces of the outer leading wheels of the two bogies in empty conditions. While the stationary value for the Y25 is about 15 kN, the peak value at the beginning of the curve is almost double and it is higher than the 4L for about 20 m.

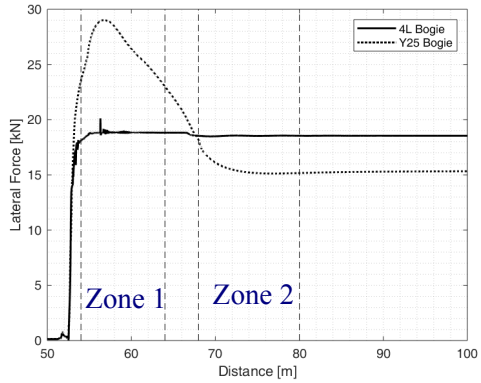

Fig. 17 Lateral force of outer leading wheel of both bogies in empty conditions. According to EN14363, the track is divided in zone 1 (only the first bogie is entered in the curve) and zone 2 (both bogies are entered in the curve).

4.5 Response to harmonic and isolated longitudinal level defects

Vertical track irregularities are usually statistically distributed as shown above. To highlight the superiority of the 4L suspension architecture, numerical tests were arranged with longitudinal level defect harmonically distributed from 1.2 m to 3.6 m, including 1.8 m (the wheelbase of both Y25 and 4L bogies).

When the harmonic defect moves the two wheels in counterphase, the "short-circuit effect" exists as expected and leads to dynamic contact forces very similar to the static ones (Figure 18). A direct comparison of the response to harmonic defects of the two investigated bogies show the superiority of 4L vs Y25. In the worst case, in fact, the 4L bogies exhibits vertical forces 25% lower than the Y25, while in the best cases this reduction reaches even 80%.

The behaviour in presence of isolated level defects was investigated by exciting the vehicle with a defect with spectral content up to 20 Hz [5]. While the response at the wheel-rail contact is only slightly lower for 4L compared to Y25 (depending mainly on *P1* force which depends on the mass of the wheelset, that in practice is the same for the two bogies), the acceleration (and therefore the inertia forces) on the centre bowl are much lower for the 4L bogie compared to Y25 bogie (Figure 19).

The forces on the centre bowl were then investigate in three different conditions: empty, partially laden and fully laden (respectively 5.5, 11 and 22.5 t/axle). The difference between the peak dynamic forces increases with the static load, as shown in Figure 20, resulting in a beneficial effect of the suspension, highlighting the superiority of 4L bogie when isolated defects are encountered.

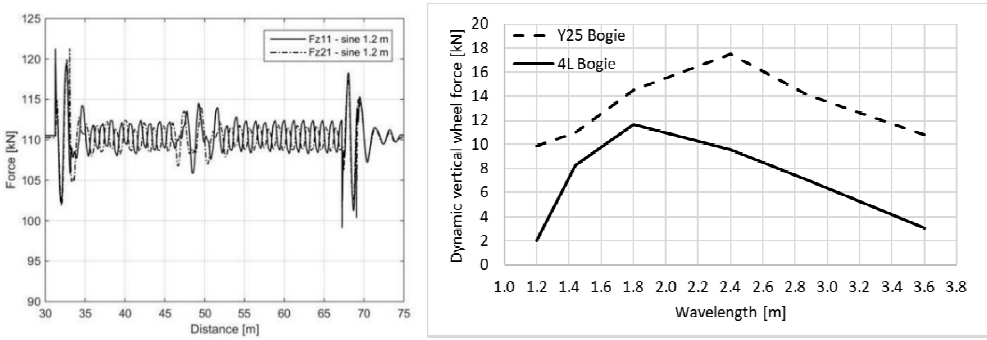

Fig. 18 Left: "short-circuit effect" of the 4L bogie for the 1.2 m wavelength case in laden condition. Right: comparison of dynamic vertical force for 4L and Y25 bogies as a function of longitudinal level harmonic defect wavelength in laden condition.

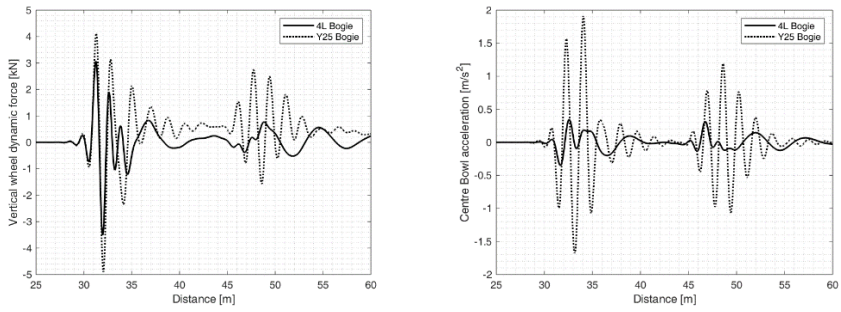

Fig. 19 Left: Vertical wheel-rail dynamic force. Right: Centre bowl acceleration. Signals are shown for the empty case.

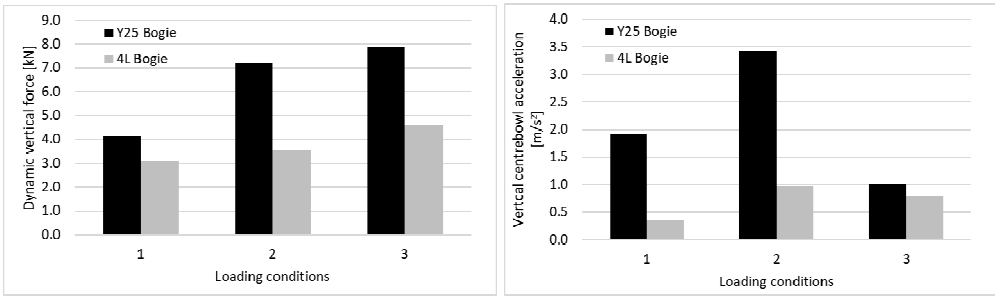

Fig. 20 Dynamic vertical force (left) and vertical centre bowl acceleration (right) in empty condition (1), partially laden condition (2), fully laden condition (3).

4.6 Running behaviour on switches and crossings

The running dynamics behaviour on S&C is a particularly complex subject that requires specific skills and experience to be correctly simulated. Figure 21 compares the behaviour of Y25 and 4L bogies when running on a switch in the through direction. It can be seen that the dynamic force generated by the 4L bogie is almost negligible when compared to that of the Y25 bogie.

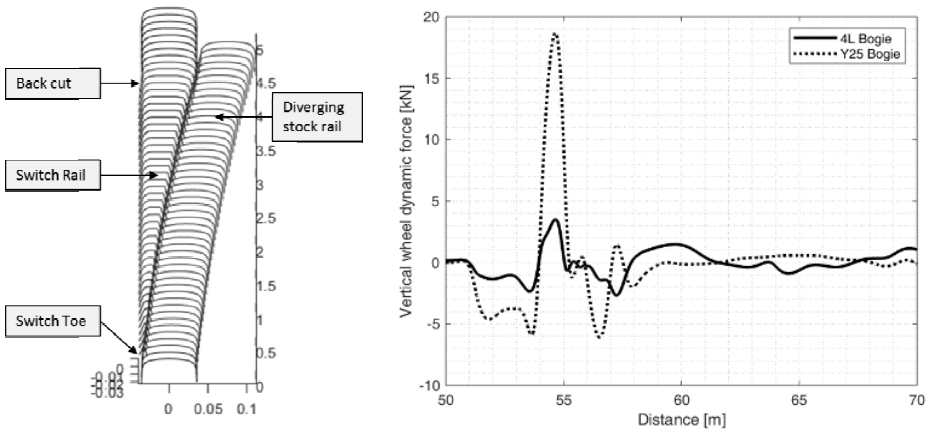

Figure 21. Comparison of the vertical dynamic forces in the laden case at 80 km/h in the through direction.

The evaluation was performed for the aforementioned three load cases, obtaining the results shown in Figure 16. For all the cases the vertical impact force given by the 4L bogie is only a fraction of the one given by the Y25.

The behaviour in the diverging direction is fundamental to forecast switch blades wear. An excerpt form [5] says:

The results in terms of wear number must be discussed according to the considered zone of the switch. The initial peak value at switch toe is practically the same for both bogies for the leading wheel, while the rear wheel of 4L bogie initially increases more rapidly than the Y25's but quickly comes back down. While negotiating the diverging

part of the switch, the Y25 shows a large increase of the wear number covering almost the entire lead length between toe and crossing nose. Significant wear will ensue, which is not the case for the 4L bogie. Beyond the lead length, the stationary value is about the same for both bogies but the mean value (calculated as the area under the wear number curve divided for the length of the curved part of the switch) is always favourable for the new bogie. In conclusion the new bogie would impose far less wear than current freight bogies in the initial transition areas of switch panels, where severe wear leads to increased maintenance and early switch rail replacement.

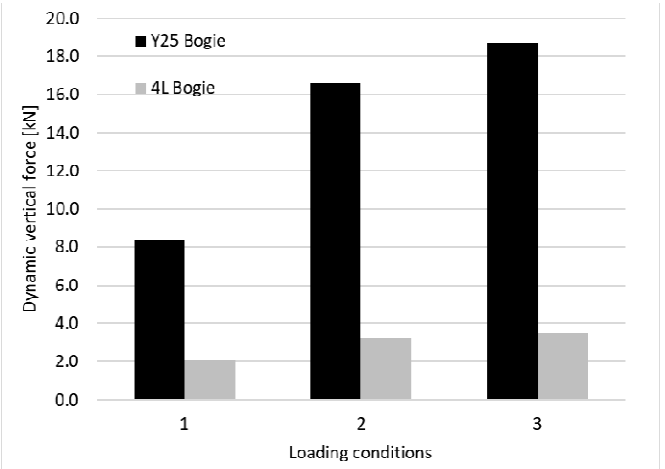

Figure 22. Vertical dynamic peak force in empty condition (1), partially laden condition (2), fully laden condition (3). Speed = 80 km/h in the through direction.

This confirms the huge superiority of the Y25 also in the negotiation of switches in the diverging direction (Figure 23).

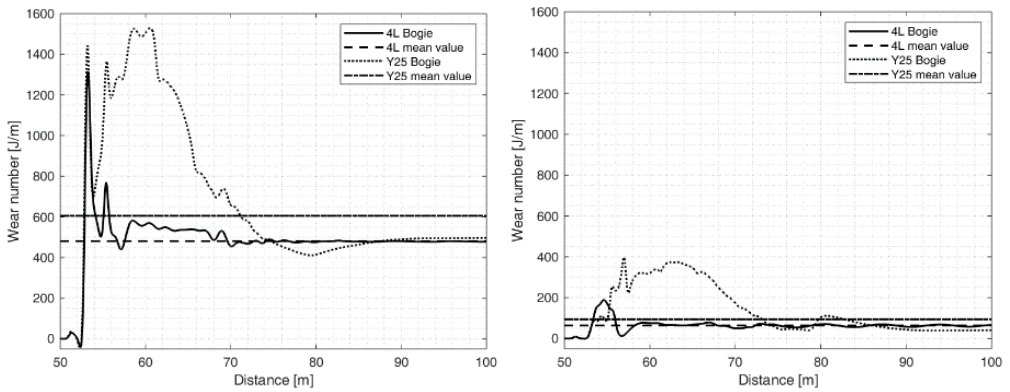

Figure 23. Comparison of wear numbers on the switch blade in the diverging direction for the front wheel (left) and the rear wheel (right) of 4L and Y25 bogies.

5. CONCLUSIONS

In this paper the innovative 4L bogie is described with special attention to manufacturing costs. Adopted solutions are simple and easily maintainable.

Structural issues were addressed rigorously and the straightforward applicability of the 4L bogie concept is ensured. Improvements on running dynamics and track friendliness are enormous, leading to a very low-cost and extremely track friendly bogie.

As the estimated cost of the frame is 20÷30 % lower than the Y25, the impact on the market could be relevant. Implementation times look short as all the main tasks were addressed and the bogie frame can be considered "virtually homologated" having passed all the phases requested by international standards.

6. REFERENCES

[1] **Csiba, J.**: Bogie Type Anniversary: the Bogie Type Y25 is over 50 Years. Proceedings. of the 10th International Conference on Railway Bogies and Running Gears: BOGIE '16 (Ed. by Prof. I. Zobory), SSME, Department of Rolling Stock, Budapest, 2017, p.253-262. ISBN 978-963-9058-38-5

[2] **SUSTRAIL Project**. Concluding Technical Report, available at www.sustrail.eu/

[3] IMG/pdf/sustrail_final_book_web.pdf (accessed 21.03.2019)

[4] **5L Project**. White Paper Innovative Rail Freight Wagon 2030, available at https://www.schienenfzg.tu-berlin.de (accessed 21.03.2019).

[5] **Bracciali ,A. – Megna, G**.: Track friendliness of an innovative freight bogie, In: Li Z., Nunez A. (eds.), 11th International Conference on Contact Mechanics and Wear of Rail/Wheel Systems (CM 2018), pp. 81-89, Delft, The Netherlands, September 24-27, 2018

[6] **Megna, G. – Magalhaes, H. – Bezin, Y. - Bracciali A.**: Running dynamics and contact mechanics comparison of two freight bogies running in plain line and through switches and crossings, Proc. of the 26th IAVSD Symposium on Dynamics of Vehicles on Roads and Tracks, Gothenburg, Sweden, from 12-16 August 2019.

[7] **Bracciali, A. – Megna, G**.: Inside Frame Bogies & Air Wheelset A Winning Marriage. Proceedings. of the 10th International Conference on Railway Bogies and Running Gears: BOGIE '16 (Ed. by Prof. I. Zobory), SSME, Department of Rolling Stock, Budapest, 2017, p.61-71. ISBN 978-963-9058-38-5

LOCOMOTIVE BOGIES FROM CZ LOKO PRODUCTION

Michal BENICKÝ, Lukáš HAUPT and Jan KOPAL

Research and Development Department,
Department of Mechanical Construction,
CZ LOKO, a.s.
Semanínská 580
CZ-560 02 Česká Třebová, Czech Republic

Received: September 9, 2019

ABSTRACT

CZ LOKO Company is now capable to build new two, four or six-axle whole new locomotive with its own design of running gear. Development of this design started in 2008 and it is still modified to improve its functionality in terms of railway track interaction, new standard requirements, as well as reliability and maintenance. In these days the prototype of three-axle bogie was built and one two-axle locomotive and ten four-axle locomotives is in usage in Czech Republic and Italy, and more than two dozens is in fabric for the Czech, Italian and Slovenian customers.

Keywords: CZ LOKO, bogies, running gear

1. INTRODUCTION

In recent years, the CZ LOKO company has evolved from locomotive repairer through its (initially lighter, then deep) modernization into a stable manufacturer of new shunting locomotives for European customers. Already during the delivery of the new locomotives with the old concept (709.4 series - the first Effishunter) between 2004 and 2008, the locomotive of the brand new concept began to be prepared in the CZ LOKO design offices. The work focused mainly on the running gear where the "weak" places of the original structure were replaced.

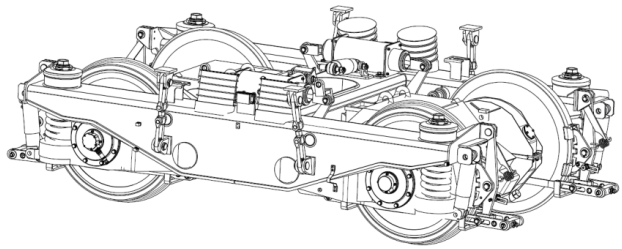

Fig. 1 Design of the old conception of the two-axle bogie from ČKD.

2. NEW DESIGN OF CZ LOKO RUNNING GEARS

The original wheelset guide by the swinging arm was replaced by longitudinal rods and the suspension was fitted with springs with the flexi-coil effect. The clasp brake as the source of the greatest noise in the running gear was replaced by a disc brake with disks in mono-block wheels. The nose suspended DC traction motor was replaced by an asynchronous motor. Of course, changes in the frame of the locomotive are needed according to the changes in running gear. The whole idea of the new running gear design was intended to its usage in two-axle locomotives and with minimal modifications also in the two-axle bogie of four-axle locomotives. At the same time, the requirement

to use both an asynchronous and a DC motor should be met. It was also supposed the various axle loads according to the weight of the locomotive.

The final conception of the running gear for diesel-electric locomotives is modular in terms of its use, both for two-axle locomotives, where a prototype of the 719.701 locomotive with a wheelbase of 5000 mm was implemented, and for two-axle bogies with a wheelbase of 2400 mm. Conceptually, the running gear is designed to allow the use and installation of various types of traction motors. One (yet unrealized) option is the DC motor TMD5003V1, or the (preferred) AC motor TAM1084C6, both of which are a product of the CZ LOKO company. The axle load for both types of traction motors is between 16 - 22.5 tons per axle. Different axle loads, resp. the total weight of the locomotive is determined by the different design of the locomotives (different lengths, used prime mover, various components, etc.). The running gear, which is installed in the two-axle locomotive, has a maximum speed of 80 kph. Use in bogie assumes a maximum locomotive speed of 120 kph.

3. RUNNING GEAR OF TWO-AXLE LOCOMOTIVE CLASS 719.7

The traction wheelset consists of a full axle from EA4T material, a helical toothed wheel and two 1100 mm diameter monoblock wheels from R8 material. Monoblock wheels and axles are manufactured by BONATRANS. FAIVELEY brake discs are mounted in the wheels. Also the SKF rolling bearings are installed on the axle to absorb radial and axial reaction forces from the gearing of the wheelset drive and at the same time serve as bearings for suspension tube, which mounting the nose suspension traction motor on the axle.

The traction motor is mounted on a suspension tube through screwed split housings. The other end of the traction motor is suspended by the rod on the main frame of the locomotive. On the traction motor is an flange for cooling air inlet from the fan. The connection of the ducts in the main frame of the locomotive and the traction motor is realized by flexible bellows.

Axle-boxes are designed as castings whose functional surfaces are machined to the appropriate size after normalization. The design of the axle-boxes is right and left according to the location on the wheelset. There are two single-row cylindrical FAG roller bearings in each axle-box. The bearing space seal is provided by a labyrinth seal and a set of lamella rings. The axle-box cover secures the outer bearing rings and is always adapted to the sensor used (anti-skid, speed sensor, etc.). On the axle-box is support places for the springs of the primary suspension. Due to the use of the disc brake in the wheels, the springs are placed eccentrically. Under one spring support, the guiding rod is mounted using the M30 screw. Below the second spring support there are brackets for screwing the vertical damper. At the top of the axle-box there is a mandrel serving as a vertical and transverse stop when the vehicle oscillates. The axle-box cover is provided with a retainer for vertical locking of the wheelset in the event of a vehicle lifting.

The primary suspension is provided by a set of coil springs. There are always two identical springs on each axle-box. In case of two-axle locomotive running gear, springs of length 525 mm (in the installed state) are used. Adjustment of wheel forces

is done by means of the adjusting screw on the top of the spring in the main frame of the locomotive.
The transmission of the traction forces between the wheelset and the main frame is realized by connecting (guiding) rods. The connecting rods have rubber bushing springs in their holes. The bushings are fitted with pins for connecting the rod to the main frame of the vehicle and to the axle-box with the M30 bolt. The two-axle locomotive uses a connecting rod with a distance of hole axis of 500 mm.
The torque from the traction motor shaft is transmitted through a single-stage gear transmission to the driving wheelset. This is a standard spur gearing with the teeth being 20 ° inclined. The pinion is mounted on the tapered end of the rotor shaft. The large gear is press-fitted directly onto the wheelset axle. The gear housing (cover) is welded from thin steel plates. It is split for the upper and lower portions, both of which are connected by a labyrinth seal in the split plane.
The mechanical part of the brake consists of a pneumatic disc brake, with braking discs placed on the mono-block wheels. The whole units are attached at three points and act on one wheel of the respective wheelset. In a two-axle locomotive, the brake units are attached to the main frame. One brake unit on each axle is equipped with a pneumatic cylinder with a spring brake. The second unit on the respective axle is without a spring brake. Each wheel has a cleaning pad of the running surface that operates in manual or automatic mode.
Dampers located inside the coil spring are used to dampen the vertical dynamic movements in the primary suspension. The vertical damping is done for the two-axle locomotive by the H8P 140.45.30 damper from STOS Oslavany. The locomotive 719.701 is equipped also with a transverse damper. Its location is on the body of the traction motor and the locomotive mainframe.
The flange lubrication is realized with a grease DELIMON Rail Jet, which is very resistant to mechanical damage and environmental influences. The lubricant is fed by the conditioned compressed air from the reservoir to the dosing pump and to the baffle nozzles located at the flanges. Flange nozzles are attached to the cleaning block holders. Depending on the direction of movement of the locomotive, only the flanges on the first wheelset are lubricated.

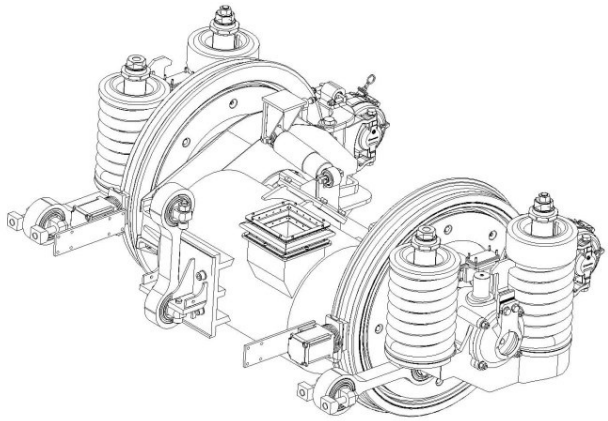

Fig. 2 Design of the running gear of the two-axle locomotive class 719.7.

4. RUNNING GEAR OF FOUR-AXLE LOCOMOTIVE CLASS 744.0

The 744.0 (B'oB'o) locomotive was successor of the two-axle locomotive. Experience from the two-axle locomotive - wheelset, its guidance, drive and braking - was applied in the bogie. Of course, that modifications were necessary due to the application running gear in the bogie.

The FAIVELEY brake units were replaced by DAKO units using the KOVIS brake discs, the traction motor was fitted with a chassis frame (rubber-metal silentblocks were used instead of the connecting rod). Significantly shorter springs (202 mm) are used in the primary suspension. Also, the bogies used shorter guiding rods of the wheelset (distance of hole axis 350 mm).

4.1 Bogie description

The basic part of the bogie is a frame consisting of two side beams, a cross beam and two front beams. The side beam has depressed centre due to the location of the secondary suspension. Beams consist of webs of sheet metal 12 mm thick and sheet flanges 15 mm thick. The spring seat is reinforced with sheet metal 15 mm thick for smooth load distribution from the vehicle body. There are several ribs inside the side beams to increase stiffness. On the lower part of the side beams are brackets for fixing the guiding rods of the wheelset. The side beams are connected in the middle part by a massive cross beam formed also by webs 12 mm thick and flanges 15 mm thick. The cross beam is reinforced in the middle part to reduce the stress flow especially in the middle area, where the pulling forces are transferred from the bogie frame to the main frame of the locomotive. The cross beam has a continuous oval hole in the central part for the central pivot. In this hole there is a rubber-metal support damping the shock between the bogie and the central pivot. The transverse stops are also in the area of the central pivot. At the ends of the frame, the side beams are interconnected by front beams. There are brackets for connecting the brake units. Traction motors are attached to the cross beam with cylindrical rubber-metal silent blocks.

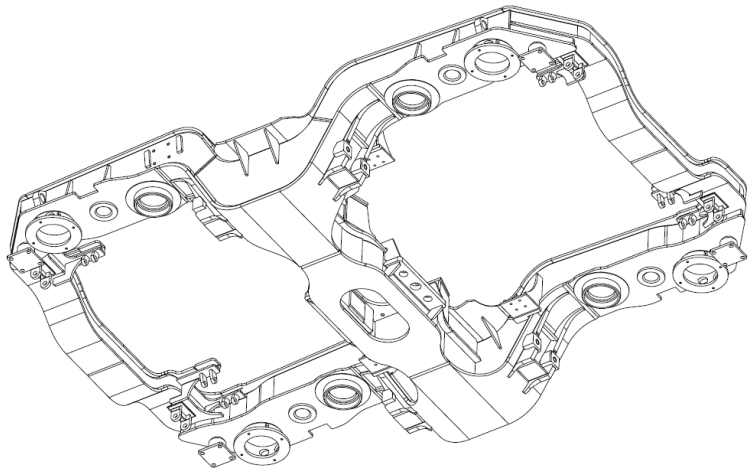

Fig. 3 Weldment of the bogie frame.

In the transverse direction, flexible stops are made on the bogie between the central pivot and the cross beam. The stops define the horizontal transverse movement of the bogie relative to the mainframe. The kinematic value of the run and stiffness of the stop is designed to optimally reinforce the overall stiffness of the transverse suspension between the mainframe and the bogie as optimally as possible. In addition, the design allows these values to be adapted very easily during the tests by means of a suitable arrangement of disc springs.
The transfer of traction forces from the main frame to the bogie frame is effected via a welded central pivot which is fixedly welded to the main frame of the locomotive. In the bogie, the pivot is passed through an hole in the cross beam that is equipped with buffers. The buffers are spring-loaded in order to mitigate the longitudinal impact, especially when the vehicle's high starting and braking forces are applied. The sliding surfaces are made of self-lubricating abrasion-resistant steel, alloyed primarily with manganese.
The secondary suspension, by means of which the main frame of the locomotive lies on the bogie frame, consists of two pairs of coiled steel springs, which are transverse to the vehicle axis. The lower ends of the springs are supported on rubber-metal washers, which soften the lower anchoring of the springs and reduce the bogies resistance against turning, which is particularly important in curves of small radii. The springs are designed and mounted between the main frame and the bogie frame so that the flexi-coil effect is used. This has a beneficial effect on the stability of the locomotive driving in the straight track and greatly simplifies the construction of the entire secondary suspension. On the upper side of the springs there is a regulating screw, which can be used to roughly adjust the size of the wheel forces between the bogies. Vertical damping of the vehicle is provided by a set of hydraulic dampers, one on each side of the bogie. The transverse vibration of the vehicle is damped by a pair of hydraulic dampers.
The locomotive was tested after production and after approval it was included in the CZ LOKO POOL (locomotive rental), where it was used by various operators in various operating modes during several years. This gave us feedback for the construction series of locomotives type 744.1.

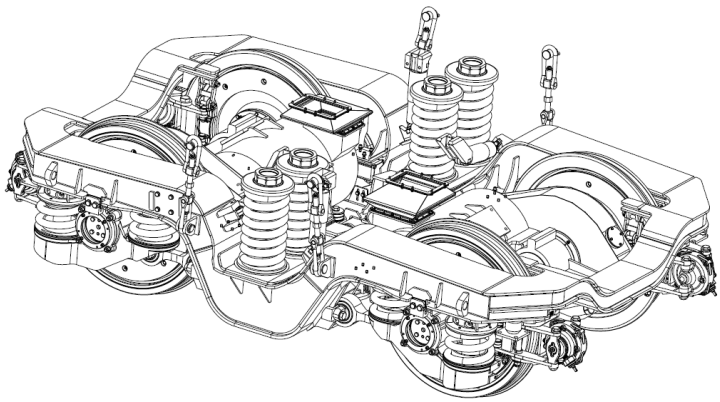

Fig. 4 Two-axle bogie of the four-axle locomotive class 744.0.

5. RUNNING GEAR OF FOUR-AXLE LOCOMOTIVE CLASS 744.1

This new locomotive differs to a certain extent from the 2012 prototype, mainly due to the requirements of the TSI [4], which necessitated some structural changes in the bogies as well, but also due to our own experience with the prototype.
Two single-row cylindrical FAG roller bearings had been replaced by the axle bearings with SKF's CTBU due to the requirement of EN 12082 [5], which, among other things, have brought the modification of axle, axle box and covers. Advantage of this solution (except that standard requirements were met) is better reliability and maintenance because there is no re-lubricating needed.

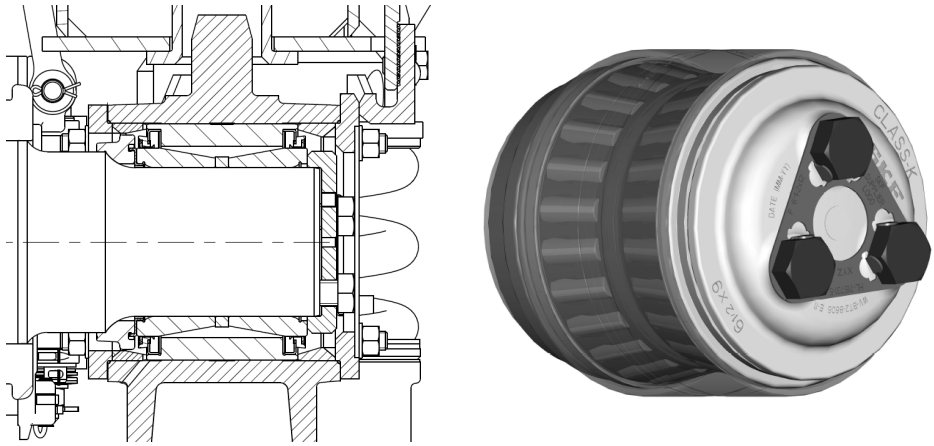

Fig. 5 Mounting of CTBU in bogie of the four-axle locomotive class 744.1.

Other modification was realized in secondary suspension. At the prototype bogie was used four right-handed flexi-coil springs. As the during evaluation of measurements from the driving tests was found that the resistance against bogie rotation is asymmetric (although the difference is not large) the two left- and two right-handed springs are used for the symmetric resistance.
During the trial operation of the prototype locomotive, deficiencies were found in terms of lubrication of the gear transmission between the traction engine and the wheelset. The gearing was originally stored in a metal cover and lubricated with a commonly used grease. Due to insufficient lubrication, the toothing was damaged and noise was increased. For this reason, after testing at WIKOV, a new grease from KLUEBER was selected. As it was a lubricant with a lower viscosity, it was necessary to adjust the gear cover. The greatest sealing problem occurred in the area of the gear wheel, which rotates with respect to the cover. The original labyrinth solution did not work, so SKF split washer was used for testing. Unfortunately, neither this new cover nor the newly used lubricant proved to work. There was still excessive wear of the toothing and the cover had a large leak of lubricant due to leakages. It was necessary to create a new, sealed cover so that it was able to meet the requirements for oil lubrication. A very precisely machined weldment was created, the rotary joint was sealed using a screwed several-part labyrinth, all dividing planes and potentially hazardous areas sealed with liquid rubber. The cover was provided with a soundproof coating.

This cover is now installed on new locomotives and, on the basis of the inspections, the new solution seems to be successful so far.

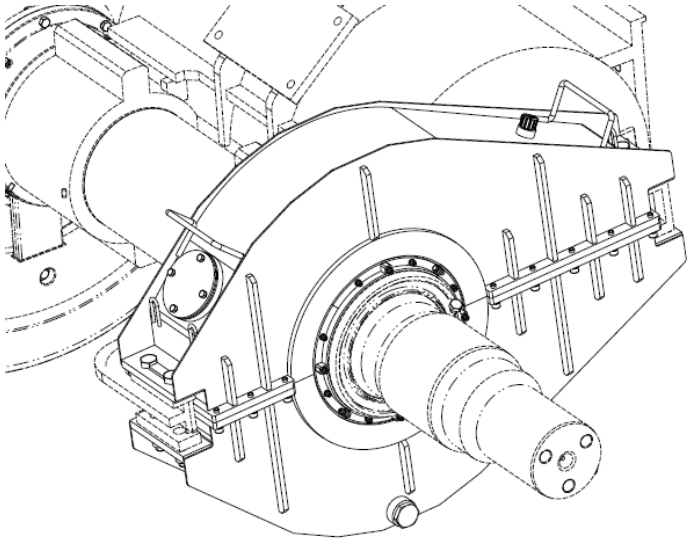

Fig. 6 New design of gear cover

Due to TSI [4] requirements the lifeguard must be added on the bogie. It was designed also as a sanding nozzle holder and holder of the sensor of the Italian safety system. For that reason the lifeguards is on the both side of the bogie (lifeguard as such is needed only on the outer side).

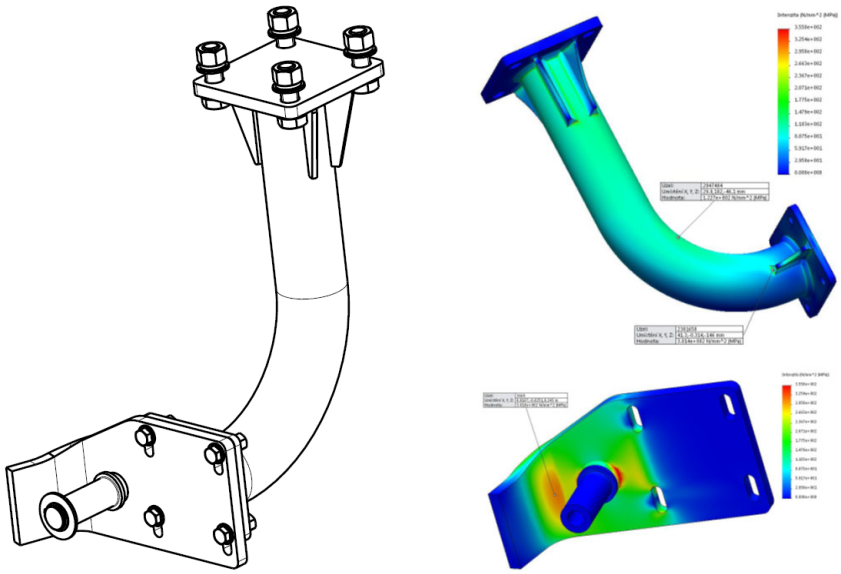

Fig. 7 Lifeguard on the bogie and its stress diagram

The bogie frame was tested at dynamic testing bench in VÚŽ in Cerhenice. The whole construction passed the test except the brake holder. Little crack was shown after 6 millions cycles on one console of that holder. As a result, calculations, modifications to the drawing documentation had to be performed, technology of welding was changed, and the affected node was repaired according to the new documentation, properly tested and thus passed the tests without any problems.

Fig. 8 Bogie frame of the locomotive class 744.1 mounted in the testing bench.

All of the above mentioned modifications and tests (not only the frame on the bench, but also driving with measuring wheelsets and others) were successfully concluded with the final approval of the locomotive for operation in the Czech Republic. After that the first series of five loco was sell to the Italy in 2016. This first series was followed by orders to more than 30 pieces of loco for various customers in Europe. First pieces from this series will be delivered this year.

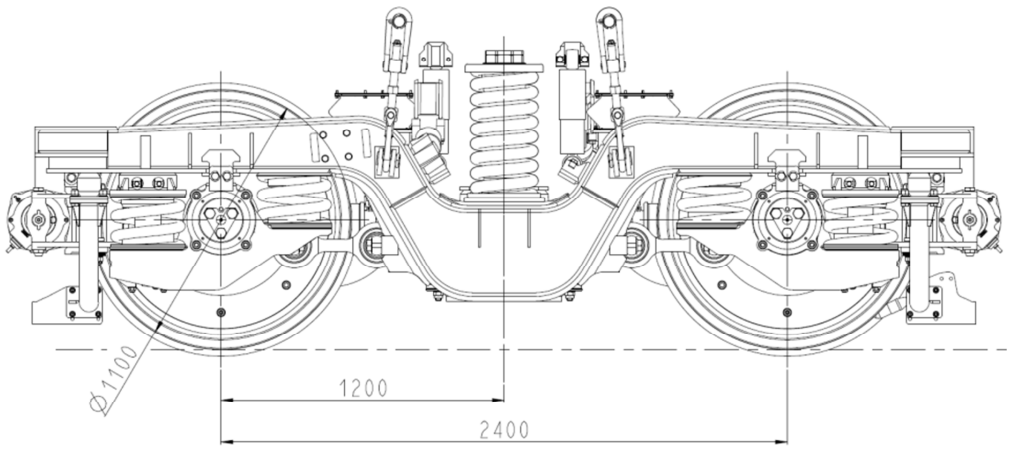

Fig. 9 Design of the two-axle bogie for the locomotive class 744.1.

5. THREE-AXLE BOGIE

In years 2015 to 2017 was developed new three-axle bogie to complement the CZ LOKO series of running gear. The bogie was developed in cooperation of the company CZ LOKO, a.s., and the Faculty of Transport Engineering of the University of Pardubice in framework of the R&D project No. TH0101045 of the Technology Agency of the Czech Republic. The aim of this project was development of a new three-axle bogie intended for o six-axle diesel-electric locomotive for the track gauge 1520 mm including manufacturing of a bogie prototype (see [2]).

New bogie based on unified components of the company CZ LOKO (mainly with components of the locomotives class 719.7, 744.0 and 744.1). Generally, a well-known problem of three-axle bogies is a high level of lateral force inter-action of the vehicle on the track in curves. Therefore, a special attention was paid to the design solution of secondary suspension and connection between the bogie and the vehicle body. We have applied some new components for us. In secondary suspension, under the flexi-coil springs were installed the tilting rubber-metal pads (specially oriented). Alternatively, the bogie can be equipped with a laterally situated active element for bogie steering in small-radius curves on the front beam of the bogie frame. This active element can also serve as a bogie yaw damper at run of the vehicle in straight track. [3] The results of calculations and multi-body simulations are interesting. Lateral force inter-action of the vehicle on the track in curves has been reduced, mechanical stress in the spring material at the horizontal deformation of the spring/pad assembly, i.e. especially at the rotation of the bogie relatively to the vehicle body if the flexi-coil effect is used has been reduced too. The finally design of the three-axle bogie can be seen in Fig. 10.

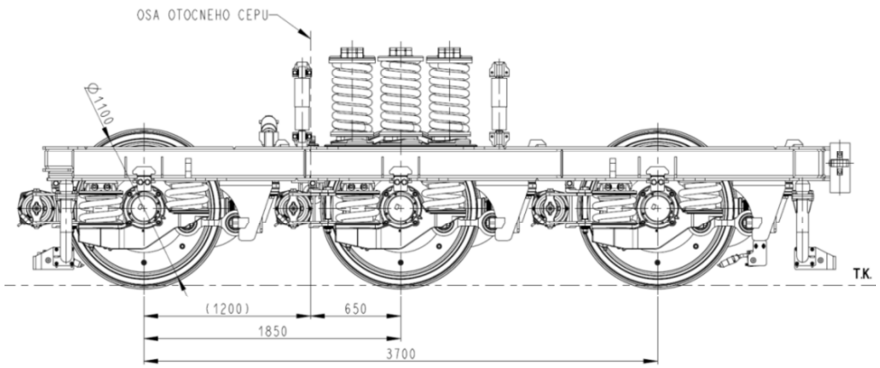

Fig. 10 Finally design of the three-axle bogie.

8. CONCLUSIONS

We can say that after many years of development, we have a functional design for running gear for 2, 4 or 6-axle shunting locomotives with good driving characteristics, track interaction and maintenance. However, we certainly cannot say that our work is done. In these days, we are currently focusing on modifying the two-axle bogies for mainline locomotive, for that we must develop new traction motor with “mainline” characteristics. Also we are finding the solution how implement the complete brake equipment (disc, brake unit and brake pads) from Knorr-Bremse to our bogies.

9. REFERENCES

[1] **Kopal, J**.: Running gear of CZ LOKO locomotives, Proceedings of the 19th conference with international participation Current Problems in Rail Vehicles 2009, Česká Třebová, University of Pardubice, Faculty of Transport Engineering, 2009, p.1-6.

[2] **Haupt, L. – Kopal, J. – Michálek, T. – Štěpánek, J. – Benický, M. – Staněk, P. – Čejka, T. – Liberová, S**.: Development of a three-axle bogie for diesel-electric locomotive, Proceedings of the 23rd conference with international participation Current Problems in Rail Vehicles 2017, Česká Třebová, University of Pardubice, Faculty of Transport Engineering, 2017, p.141–150.

[3] **Michálek, T., Haupt, L., Zelenka, J., Kohout, M., Liberová, S.**: Lateral force effects of three-axle locomotive bogie on track. In: Applied and Computational Mechanics, Vol. 12, No. 1 (2018), p.33–44. ISSN 1802-680X.

[4] REGULATION (EU) No 1302/2014 of 18 November 2014 concerning a technical specification for interoperability relating to the 'rolling stock — locomotives and passenger rolling stock' subsystem of the rail system in the European Union.

[5] EN 12082 – *1. Railway applications - Axleboxes - Performance testing.* Brussels: CEN2010

CONCEPTUAL DESIGN OF AN ACTIVE CENTRE PLATE

José A. ROMERO NAVARRETE and Frank OTREMBA

Federal Institute for Materials Research and Testing (BAM),
Unter den Eichen 44-46,
D-12203 Berlin, Germany.

Received: September 9, 2019

ABSTRACT

The efficiency and safety of railway transportation depend both on numerous factors linked to the vehicle, the infrastructure, the operator and the environment. Curved tracks are subjected to demanding situations due to elevated stress levels, as a function of the operating conditions and vehicle/infrastructure design. In such segments, steering forces are superimposed to lateral load transfers. The steering forces depend on the condition and the design of the centre plate and bogies´ suspensions design. While the friction at the centre plate provides the needed damping to mitigate the hunting vibration of the bogie in straight track segments, such yaw resistance originates high steering forces and rail damage on curved tracks. A centre plate with low friction at turns and high friction at straight track segments would thus be highly advantageous. In this paper, a centre plate design is proposed which provides a yaw-rotation resistance torque that depends on the bogie-car relative position. Two different designs are considered for that purpose, one that combines a spring-acted centring mechanism with a lower pair kinematics, while the other one involves higher kinematic pairs which should incorporate lateral damping elements. As a result of using an engineering design approach, the higher kinematic pairs–based design is recommended however, the validation of such operational principles, including the introduction of the needed damping, should be configured on the basis of experimental models.

Keywords: steering torques, railway transportation, bogie design, conceptual design, engineering design, transport externalities

1. INTRODUCTION

The efficiency and safety of the railway transportation depends on many interacting factors and operating conditions, associated to the vehicle, the infrastructure, the operator and the environment [1]. From the vehicle-infrastructure interaction perspective, some factors influencing the deterioration of the rail, depend on the dynamics of such interaction, especially when the vehicle operates on curved tracks. During such changes of direction, the vehicle dynamically responds to the lateral perturbation, producing a lateral load transfer that represents an increase in the magnitude of the wheel forces on one side of the track, as a function of the train operating conditions and track design, including track´s turning radius and over-elevation, and vehicle´s operating speed. In this context, such lateral load transfer superimposes to tangential steering forces, which are developed when the vehicle enters the curved track and stabilize when a steady state is reached along the curve (for constant track radius and vehicle speed). The magnitude of such tangential forces depends on a variety of factors, including the yaw stiffness of the bogie and the friction at the centre plate. The stiffness property being mostly dependent on the individual stiffness of the bogie´s suspensions, while the friction at the centre plate depends on the condition of the mating surfaces (rough or polished), and on the level and type of lubrication (dry, grease or oil).
While the friction at the centre plate generates higher tangential forces on the track and a consequential greater rail wearing, such a friction is also crucial to reduce the phenomenon of hunting when the vehicle travels along tangents. In this respect, it should be noted that such increased forces also generate some loss of locomotive energy.

In this paper, a mechanically active centre plate is proposed, which increases the friction torque at the centre plate when the vehicle travels along tangents and reduce such a torque when the vehicle negotiates curved tracks. The conceptual design of such a plate comprises the definition of the principles of operation of its critical parts, which should be validated through a preliminary experimental model in order to assess the potential benefits and the feasibility of such design. Additionally, such a testing should be used for complementing the definition of other operational principles of the equipment, especially the needed damping.

1.1 Design methodology

Manufacturing a prototype represents the final stage of an engineering process that initiates with the definition and clarification of the product´s needs, which eventually will configure out an engineering problem [2]. Once that needs are clarified, different interacting modules are to be identified, which are outlined in terms of the operative functions expected from the product [3]. While every stage of this design process is relevant in producing a useful detailed design and eventually a prototype, it is fundamental to describe, as the basement of the process and as accurately as possible, the needs that are expected to be fulfilled with the so developed device. These needs should be defined in terms of qualitative and quantitative dimensions, in such a way that could be considered such needs as design goals within the whole design process. In developing this process, attention should be paid also to any restrictions, which should be validated in order to avoid any false or unnecessary limitations. It should be noted that restrictions can emerge from different domains, including timing, economy, and environment. In developing products for the transport in general, and railway transport in particular, it results critical to pay attention to environmental and economic restrictions, in order to improve the economic and environmental competences of this mode of transport with respect to other transport modes, especially trucking.

Clarifying the needs while explicitly describing the influential restrictions for the development of any equipment, provide the basic elements to shape the design as an engineering problem, in order to identify further the resources and potential engineering tools to solve it. As a function of the problem at hand, the solutions can come from different areas in the engineering realm. In the case of a problem in the transportation area, it could involve a combination of disciplines, including materials, design and manufacturing. In the long term, however, in this area the maintainability of any new artifact becomes crucial.

The solution of the so-established engineering problem derives from a methodic reasoning embodying the assumed tools, methods and operational principles that eventually will provide the hypothetical solution of the so defined problem. This stage of the process keeps a parallel with the scientific method, as it involves the hypothesis description, which should be further validated. It is in this stage where the engineering problem is split into specialized modules that describe the different interacting components or systems of the equipment. In this respect, such different modules can or cannot have a direct interaction with the proposed component or equipment but can have a strong interaction with another module which strongly interacts with the module describing the specific equipment. For example, the environment can affect the centre plate (CP) design, but its influence is set through

other potential interacting modules, such as the car or the bogie. In the case of railway transportation, the environment has a strong influence on the performance of the vehicles. Railway cars can travel under drastically different climate conditions, linked to Nordic freezing temperatures that further combine with humidity, or to tropical – dry weathers. Such circumstance poses special engineering demands, especially from the materials perspective. However, the entire conceptual design phase should be developed under an interacting three-dimensional approach, involving materials, design and manufacturing [3]. On the other hand, it is worth noting that this stage is the most creative part of the engineering design process. Moreover, the needs for further re-conceptualization of the component should also be considered as part of the engineering design process [4]. The main output of the conceptual design stage of the whole design process, consists of a document defining the modules influencing the operation of the proposed equipment. For each of the so-defined modules, the corresponding principles of operation of such modules should be explicitly described. However, within this stage, the proposed principles of operation should be validated through experimental or analytical methods. It is noted that such principles of operation and the modules themselves, can be inspired or based upon existing equipment.
The next step in the design process entails the manufacturing/building of a prototype, in order to validate/assess both the whole design process as well as the final product. As it was already mentioned, and as a consequence of the assessment planned at this stage, the prototype can go further in the process of setting its volume manufacturing, or it can go back to previous stages of the design process, even into the needs definition and/or problem statement stage.

1.2 Transport externalities

The context associated to the development of the equipment proposed herein, is characterized by environmental concerns about the negative externalities of the transportation activities in general, and those attached to the railway transportation in particular. In this regard, about 30% of the total consumed energy concerns transport activities [5], while the corresponding greenhouse emissions of this sector represent 14% of the total human activities-related greenhouse emissions [6]. Railway transportation could represent a big difference if some of the payload shifts from trucking into railway, ever since the trucking transportation takes 55% of the total energy involved in the transport sector [5].

2. CONCEPTUAL DESIGN

The different elements for creating the conceptual design are described in this section: description of the needs, identification of the interacting modules and principles of operation, and the final CP configuration.

2.1 Needs description

The needs for this device should be as much as possible defined in terms of precise physical and numerical characteristics. Such needs are described in terms of the friction torque between the car and the bogie, which should be minimum in turns and maximum on straight track segments. In this regard, the context surrounding what is needed from the device, occurs in a relatively narrow angular dimension. That is, under special circumstances, the steering angle between the bogie and the car can be 5 de-

grees, but for normal infrastructure design, this angle is lower than one degree. In this matter, Figure 1 illustrates two infrastructure geometrical designs and the corresponding steering angles. While part (a) of this figure illustrates a tight turn that would correspond to yard maneuvering, with a maximum steering angle of 5 degrees, part (b) describes a smooth geometry track, for which part (c) depicts the resultant steering angles, which were obtained using the methodology described in [7]. According to these data, very small angular displacements are found in normal operating conditions for the railway system, and the proposed variable friction system must operate in such small angular displacement range, thus representing the operation of a highly accurate positioning-depending system.

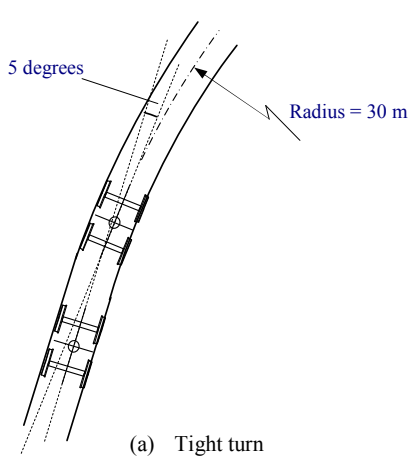

(a) Tight turn

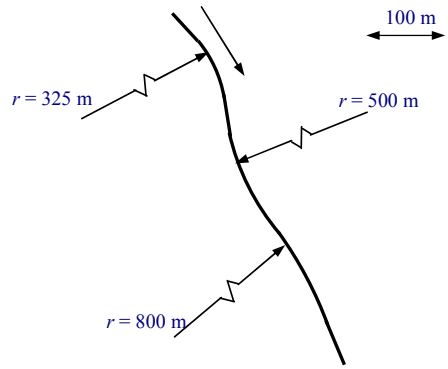

(b) Long radius turns

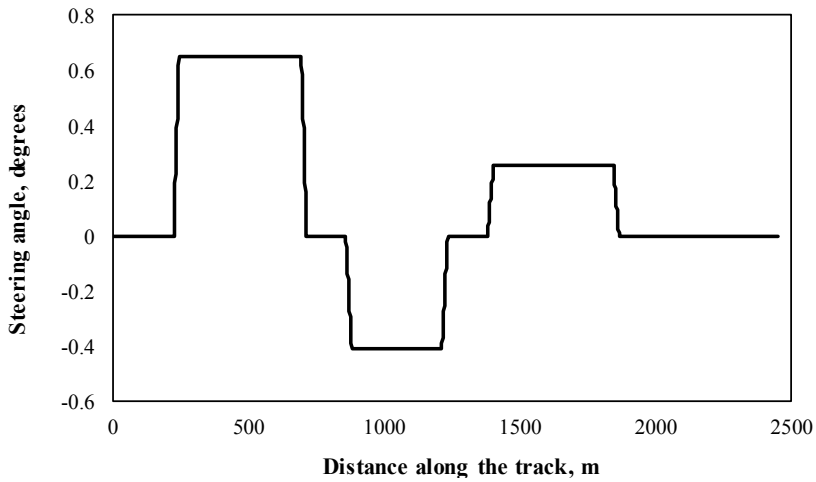

(c) Steering radius for the long radius turns track described in (b)

Fig. 1 (a) and (b) Different track horizontal geometries, and (c) steering angles for the smooth geometry track in (b)

In order to provide the necessary advantages regarding the damaging effects of the cars on the railway, a significant reduction of the yaw torque is needed. However, it is important to set a functional goal for such reduction in the friction torque linked to the proposed CP operation. That is, it cannot be physically reduced to zero. Consequently, an acceptable reduction in such a torque should be set in advance. In this context, a goal for reducing in 30% such a friction yaw torque would be acceptable.

Other requirements for the variable friction CP are related with the level of "fitting" of such device into the railway industry environment. That is, the proposed CP should be compatible with the design criteria used for any other rolling stock equipment. Such concepts are summarized in one term: "life cycle cost"(LCC), which integrates the following characteristics [8]: reliability, availability, maintainability and safety (RAMS). However, many other attributes can be identified from these demanding characteristics for the rolling stock. From this short list of needs, the following specific engineering demands can be listed:

CP´s mass. This is a basic criterium that is indirectly linked to the RAMS criteria, but that strongly influences the energy performance of any vehicle. While any additional tare mass can affect the operational efficiency of the vehicle, in the case of the railway industry such a criterium seems to be well behind the prominent criteria. That is, new regulations regarding DOT-111, implied thicker shells for the road tankers, in order to increase their puncture resistance (Standard DOT-117), from 7/16 inch to 9/16 inch [9], which means an increase of 28% in the tare weight of the vessel, which leads to conclude that safety is the most crucial criteria for designing any rolling stock. So, it is good to increase the tare mass of the vehicle, if its safety is upgraded in a certain degree. Such a compulsory increase in vehicle tare mass could be considered also as heading in the opposite direction of that of reducing the level of combined stresses in the rails in turns, as such heavier vehicles would increase the probability for having a failed rail in such curved segments. However, any effort to reduce the level of stress in such curved track segments is suitable, as broken rails have been identified as causing derailments, specifically in curved track segments [10] [11].

Because of what has been above-mentioned, there would not be any restriction for the proposed equipment concerning its weight. However, a moderate increase of tare mass in the order of 1% could be acceptable for the purpose of this development. The several criteria that thus apply for the proposed equipment thus consist of reliability, availability, maintainability and safety. On the basis of these criteria, the following specific requirements can be listed:

i) The equipment should not alter the reliability, availability and safety of the whole vehicle under current circumstances. In this respect, the equipment should not jeopardize the performance of any other vehicle´s component concerning such criteria. In particular, the operation of the proposed CP design should not represent extraordinary extra loads on other components.

ii) The maintainability of the equipment should be comparable to the one exhibited by some other elements in the vehicle. One of the main issues in this respect, has to do

with the potential lubrication of the centre plate. In this regard, the current practices for this device include from non-lubrication to full lubrication situations. Introducing lubrication based upon molybdenum sulfide has proven to have a short life, on the order of 30000 kms, with friction coefficients from 0.1 to 0.3, while for the dry friction counterpart situation, a friction coefficient of 0.5 would be expected, in such a way that a 10% to 15% reductions in the yaw resistance can be expected for lubricated CPs [12]. For the design proposed herein, it is assumed that the benefits in reduced yaw resistance are superior to the costs and maintenance issues regarding the lubrication of the centre plate. Especially, because of a central lubrication system could be required.

2.2 Modularization and principles of operation

Some modules are defined in the conceptual design, which will interact with each other through different actions, including forces and moments, while involving the relative positions of such modules with respect to the proposed component. The following modules and their identification are defined as follows: centre plate (*CP*), railway car (*RC*), bogie (*BO*), track (*TR*), cargo (*CA*), environment (*EN*) and auxiliary systems, including lubrication (*AU*). The boundaries and interactions of each of these modules are described in Figure 2, where it can be observed that such interactions relate the forces, moments and relative positions of the different components.

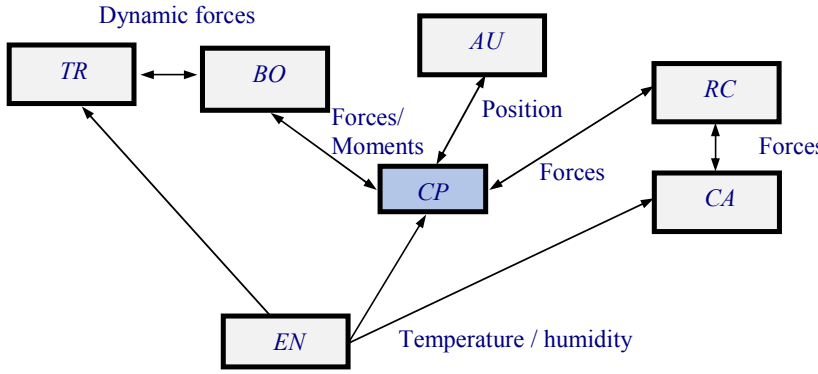

Fig. 2 Interacting modules defining the conceptual design of an active centre plate

Centre plate (CP). In the current designs, this part of the railway car constitutes a lower kinematic pair involving a surface contact between the car and the bogie [13]. The function of this part is to provide support and drive to the car. Standard CP designs include a flat circular centre plate, which is equipped with a central pivot to provide restrain in extreme cases [14]. Such a design thus provides support and driving to the car in all directions and is preferred for three-piece freight bogies. Inconveniences of this design, however, include the small contact surface that results from the roll motion of the bogie, especially during the vehicle´s turning. In order to avoid such concentration of damage in the CP, a spherical support has been considered in some designs [14]. Improvements to these two designs include the incorporation of lateral supports, to avoid the overloading of the centre plate. The pivot type of CP is another design that is usually used for passenger cars and consists of a central pivot and additional sup-

ports that provide high rotational friction to the bogie. These standard CP designs thus provide to the bogie a yaw resistance that does not depend on its relative position with respect to the railway car. Consequently, turning maneuvers could involve high bogie´s friction resistance torques, thus representing big forces on the railway infrastructure during such manoeuvres.

According to what has been described, the CP is a critical part for the railway system, as the friction phenomenon that takes place in it affects the amount of potential damage that is caused on the rails in curved portions of the track. In this respect, the contribution of the lateral supports can also be considered, further increasing the unfriendliness of the bogies towards the railway infrastructure. As noted earlier, a centre plate with minimum friction at curves, and maximum at tangents, is what is necessary to improve the energy efficiency of the railway car while not reducing its hunting stability performance. Such dual operating condition relates to a situation, according to which, the centre plate must provide a selective high rotation resistance for the car´s journal around the centre plate. For that purpose, there could be a series of operating mechanisms that are specifically designed to provide this position-dependent restraining force.

Figure 3 illustrates two of the potential mechanisms to perform such a position-dependent function. The upper part of this figure illustrates a modified car´s journal, on which a notch has been machined, into which penetrates the leaf spring that is inserted into the bogie´s counterpart. For this design, an efficient lubrication is considered, to develop small friction torques during turning. The bottom part of this figure illustrates a totally different mechanism for the CP, which substitutes the CP´s standard lower conical contact pair by four higher contact pairs and includes a centering mechanism based upon four compression springs. It should be stressed, however, that both conceptual designs, must provide additional viscous damping, whose design should take into account the relatively small rotational speeds of the components during the normal operation of the system, as it would involve large turning radiuses. In this regard, such damping forces could be incorporated through rubber elements. The characteristics of such energy-absorbing elements must be set as an output of experimental tests, which can be of scaled-down nature. However, such design is beyond the scope of this paper. The next step in the design process, consists in assessing the proposed designs, in the light of the expected outputs from the mechanism, in order to get elements to continue with the next design phase, which consists of fabricating an experimental model/prototype. A preliminary test, however, should be developed to validate the operational principles. For assessing the two different proposed mechanisms, three criteria are described in Table 1, based upon the needs that were described at the beginning of the conceptual design process. Assessments are rated from 1 (poor) to 10 (optimum).

The different rates given to the respective mechanisms are based upon estimations of their expected performance, always under a comparative basis. The reliability is better in the case of the CPNLS design due to the lower number of components with potential failure. However, the other design offers better safety to transport due to diminished rail stresses. The maintainability of the 4PCPSRM is better due to a less concentrated wearing.

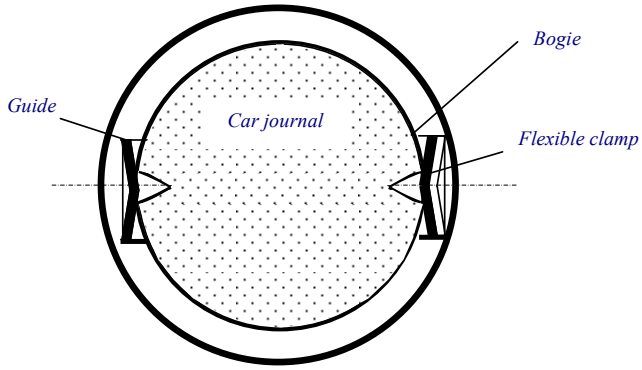

(a) Lubricated lower pair CP with notches and locking springs (CPNLS)

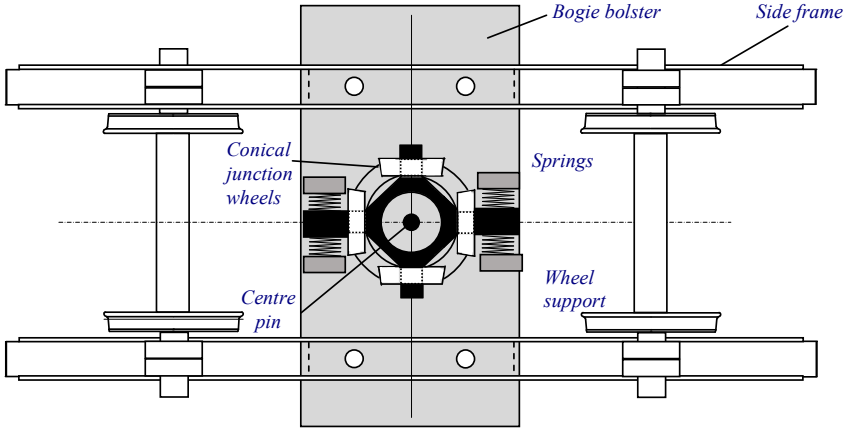

(b) Four higher-pair CP with spring return-to-the-center mechanism (4PCPSRM)

Fig. 3 Potential configurations for the active CP

Table 1 Comparative assessment matrix

	Assessment criteria		
Mechanism	**Reliabilty**	**Safety**	**Maintenability**
CPNLS	8	7	6
4PCPSRM	6	9	8

As it has been mentioned above, there is a need to evaluate the performance of the respective designs on the basis of experimental outputs that involve the introduction of viscous damping in both designs.

3. DISCUSSION

While neither of the two conceptual designs described earlier in this paper, represents an actual active center plate configuration, they do convey an idea of simple mechanisms that could provide, under ideal conditions, a restriction for the yaw motion of the vehicle when travelling along straight track segments, and very small friction torques when the vehicle is negotiating a turn. One of these designs substitutes the surface contact between the railway car and the bogie, with the line contact of rolling cylindrical elements. Several other mechanical configurations could be considered in this design process, on the basis of substituting surface to line or point contact between the parts. In addition to this, however, the validation of such operational principles should be the next step in the design process. On the other hand, it is noteworthy that the current priorities for the design of rolling stock equipment do not include the environmental friendliness of such equipment. That is probably due to the comparatively high environmental friendliness of the railway transportation, especially when compared with trucking. However, it should be recognized that the competitiveness and environmental friendliness of this mode of transport, could be improved even more with the introduction of new components, further gaining competitiveness in the sector. Apart from this, improving the rail friendliness of the vehicles could also mean to reduce the stresses on the bogie parts, further increasing their long-term performance.

4. CONCLUDING REMARKS

In this paper, the first stages of the design of an active centre plate have been described. Such design involves the core component of a mechanism that would fulfill the need for a variable friction centre plate that provides a high steering resistance on straight tracks, and a minimum one when the vehicle negotiates turns. Two potential designs are proposed and evaluated on the basis of some of the relevant criteria, including reliability, maintainability and safety. While some basic ideas have been arranged in this paper, other centre plate components need to be integrated, while its potential configuration should be validated through experimental testing. Considering the whole design process, the conceptual design methodology has proven to be useful in identifying the operational principles of the critical components of the proposed device.

5. REFERENCES

[1] **Lemmer, K.:** Research for future railway systems. Institute of Transportation Systems DLR. 2012. TS-Bahnsysteme-E-09/12.

[2] **Pahl, G. – Beitz, W. – Feldhusen, J. – Grote, K.**: Engineering Design A Systematic Approach. Springer-Vieweg, 2007. 610 pp.

[3] **Dieter, G.E.:** Engineering design, McGraw Hill Higher Education, 4th Edition, 1989.

[4] **Katz, R:** Information Management in Engineering design, Springer-Verlag, Heilderberg, Tokio. 2012. 90 pp.

[5] **DIW**.: Energy Balance (Energiebilanzen) Deutsches Institut für Wirtschaftsforschung. Recovered from https://www.ag-energiebilanzen.de/ on February 5, 2020.

[6] **EPA**.: Greenhouse Gas Emissions. Environmental Protection Agency. Recover on February 5, 2020, from https://www.epa.gov/ghgemissions/global-greenhouse-gas-emissions-data

[7] **Romero Navarrete J.A. – Otremba F.:** A variable friction centre plate. In: Uhl T. (eds) Advances in Mechanism and Machine Science. IFToMM WC 2019. Mechanisms and Machine Science, Springer, Cham, Vol. 73, p.3611-3620.

[8] **Murashov, A. – Ivanova, N. – Stavrova, E.:** Life cycle cost (LCC) as a basis for price calculation of railway equipment. Railway Equipment. Special issue for InnoTrans 2010, p.68-73.

[9] **Reschovsky, C. – Flowers, M. – Smallen, D.:** Fleet Composition of Rail Tank Cars Carrying Flammable Liquids: 2018 Report. US Department of Transportation.

[10] **Jiao, H.:** Failure of a low rail in curved railway track subject to log term rail-wheel interactive wear. Proceedings, ACMSM23, Australia 9-12 December 2014, p.595-600.

[11] **Magel, E. – Mutton, P. – Ekberg, A. – Kapoor, A.:** Rolling contact fatigue, wear and broken rail derailments. Wear: 366-367, 2016, p.249-257.

[12] **Wu, H. – Robeda J.:** Effects of bogie centre plate lubrication on vehicle curving and lateral stability. 2004. Vehicle System Dynamics Supplement 42: p.292-301.

[13] **Angeles, J.:** Generalities on Lower-Pair Kinematic Chains. In: Spatial Kinematic Chains. Springer, Berlin, Heidelberg, 1982.

[14] **Iwnicki, S. (ed):** Handbook of Railway Vehicle Dynamics. Taylor and Francis, London, 2006.

BOGIE FOR FREIGHT WAGON

Petr BAUER, Jan ČAPEK, Tomáš FRIDRICHOVSKÝ, Pavel KRULICH, Zdeněk MALKOVSKÝ, Jan MUSIL and Tomáš ZÍSKAL

VÚKV a.s.
Bucharova 1314/8, Stodůlky, Prague 5,
CZ-158 00, Czech Republic

Received: September 8, 2019

ABSTRACT

This paper deals with development of a new bogie for freight vehicles. The bogie concept is based on primary and secondary rubber suspension, wheelset guiding by swing arms, equilibrium mechanism in secondary suspension and UIC bogie interface. The advantage should be included in a small hysteresis in wheelset guiding which improves the wheelset steering in sharp curves and optimised friction damping system improving the dynamic impact on the track. The bogie envelope is minimised. Prototypes of bogie rubber suspension and friction damper were tested on test bench.

Keywords: freight wagon bogie/truck, double suspended with rubber springs, track friendly, low noise, small bogie envelop, suspension and damper prototype test.

1. INTRODUCTION

There are in principle three basic freight car bogie concepts widespread in the world, which are standardized and proved by a long time of operation – three piece bogie, bogie with leaf springs and suspension links, and Y25 bogie. These concepts are fundamentally different in their design and properties. Each concept brings another advantage while losing some of desired parameters.

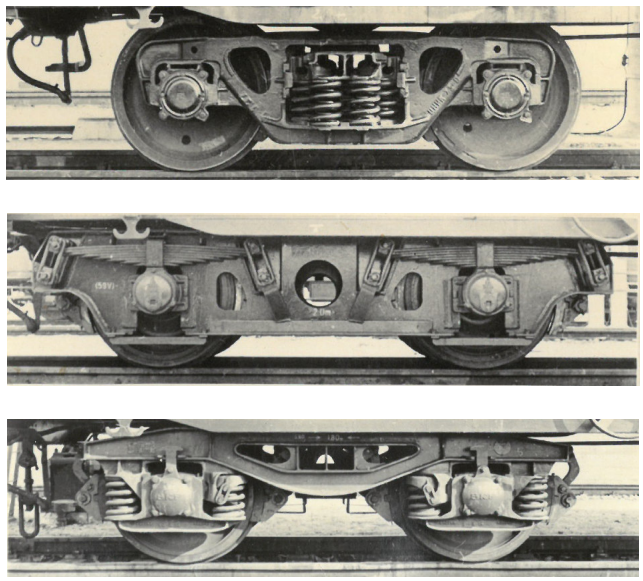

Fig. 1 Standardised freight car bogies – three piece-, leaf spring- and Y25 bogie

Combining advantages of all different concepts in one bogie, under the condition of a simple functional design, does not seem to be feasible. Some new innovated freight car bogies were introduced in the last 30 years in order to reduce wheel and rail wear and noise pollution. To bring a significant benefit in comparison to standardized bogies, under the condition not to increase weight, to stay at a reliable, simple and robust design while keeping the price and life cycle costs seems to be an unachievable goal. Except for suspension link, a simple and light self-steering wheelset system, with a stable response on a track with mixed operation, is not in wide operation yet.

2. NEW BOGIE DEVELOPEMENT

2.1 Requirements on freight car bogies

The requirements on the freight car bogies are stricter comparing to the requirements on the bogies for passenger vehicles. The principle requirements are:

- low price and LCC,
- easy and quick homologation of new vehicles,
- high reliability in a long term maintenance interval,
- low bogie weight – for higher vehicle carry load capacity.

The impact on the rails is not usually scope of natural operator interest. They are from this point of view concentrated on the wheelset lifetime. Only on the track with "train-path prising system" depending on the character of wheel-rail interaction, eventually also on noise pollution, are the operators interested in a bogie optimization to push down the prices for these fees. An expansion of this new, wheel-rail interaction depending payment system, is expected in the Europe.

2.2 Goals

The new bogie is intended especially for European railway infrastructure. The standard Y25 bogie with block brake is considered as a reference bogie, which is the most spread bogie in Europe. The new bogie development goals are:

- generally better dynamic and quasi-static interaction between wheel and rail to get lower wear of wheel and rails,
- better suspension functionality at empty vehicles on a track of a good quality (to avoid blocking of suspension at lower or common excitation),
- lower vehicle noise pollution,
- increase of a bogie price and LCC under an acceptable limit.

2.3 Operation conditions

The operation conditions were classified in two levels

- level 1: bogie for existing standard European operation – 120 km/h and 22,5 t/per axle,
- level 2: high speed freight bogie – up to 160 km/h combined with axle load 16 t.

The following boundary conditions were set for the new bogie development within the framework given by level 1:

- "standard" wheelset – axle acc. to the UIC 510-1,
- interchangeability with Y25 bogie:

  - "standard" bogie – car body interface acc. to the UIC 510-1,
  - not to exceed the parameters relevant for the loading gauge calculation,
  - bogie envelope
- maintenance intervals coherent to VPI rules,
- damping proportional to the vehicle load - without hydraulic dampers.

For bogie design within the framework given by level 2:

- larger lateral play in comparison to level 1
- lateral suspension stiffness proportional to the vehicle load.

2.4 New bogie concept search

Standardised and existing innovative solutions were researched on the project start [1]. Many multi body simulations (MBS) were made to find an appropriate conception for the new bogie. The MBS have followed to find an appropriate wheelset guiding and bogie suspension parameters to keep a good compromise between the vehicle stable run and wheelset radial steering in curves. Two bogie principles have been studied:

- bogie conception with suspension between wheelset and bogie frame (e.g. Y25 or DB665),
- bogie conception with suspension between the bolster and bogie frame (three-piece bogie).

The first conception has been chosen to be worked up. The three-piece bogie concept has been left for the following reasons:

- high un-sprung masses or high first suspended masses on a relatively stiff suspension (in case of wheelset anchorage – e.g. Scheffel bogie),
- difficulty to keep the interchangeability with Y25 bogie, when primary suspension is complemented (lateral play and resulting loading gauge),
- to prevent a bogie warping the bogie needs an additional mechanism or parts:
  - which partly remove the bogie torsional flexibility,
  - which suffer from wear,
  - whose functionality strong depends on absence of clearance and on a high stiffness in mechanism joints,
  - which represent an additional weight,
  - which needs interfaces on bogie parts.

Also based on the mentioned study and calculations the next decision followed – to resign on a wheelset anchorage combined with the standard wheelset (outer bearing). The wheelset anchorage seems to be effective to minimize the three-piece bogies warping. The benefits of wheelset anchorage for the radial steering are disputable for vehicles operating on the present continental European infrastructure, taking into account the anchorage reliability and functional parameters stability, higher LCC and higher bogie weight.

Based on this research the bogie conception has been determined – a bogie with suspension between the wheelsets and bogie frame to minimize the unsprung masses, bogie with an equalizing mechanism in suspension in order to decrease the wheel force changes on elevation ramps and bogie with a simple stiff wheelset guidance, but allowing particular radial steering in sharp curves. The suspension shall contain:

- a rubber parts to minimize a noise pollution,
- a rubber parts to utilize the naturally rubber progressivity to improve the suspension characteristics – mainly for operation of empty vehicles and vehicles loaded near to the so called "switch point" in suspension characteristic of reference bogie,
- friction damping proportional to vehicle load.

The bogie concept shall also allow to rebuild the lateral suspension to meet a requirements relevant for level 2 – i.e. optimally to complement a bolster – hanging on swing hangers – into the bogie.

2.5 Bogie description

The bogie has in base a classic arrangement – with a rigid bogie frame and two wheelsets. Wheelset guidance is performed via swing arms.

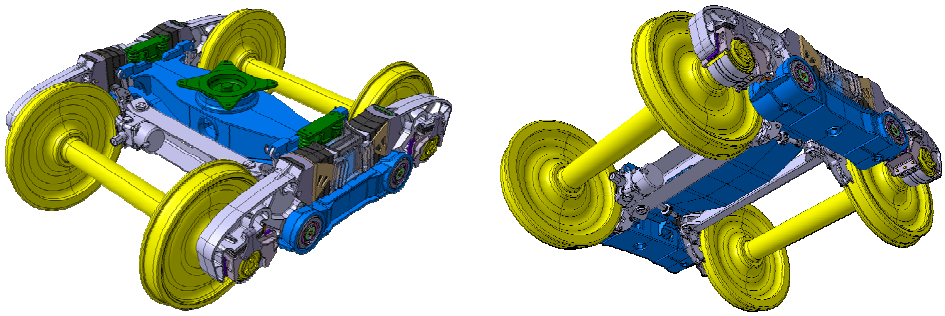

Fig. 2 New bogie

Primary springs are between wheelset bearing adapter and swing arms. The primary springs are arranged in an oblique position. This arrangement leads to vertical spring force decomposition producing a permanent longitudinal load stabilizing the wheelset rotation around the axis "z" in the bogie. The stabilizing load level is set to ensure a stable ride in straight track and simultaneously to allow a steering effect in sharp curves.

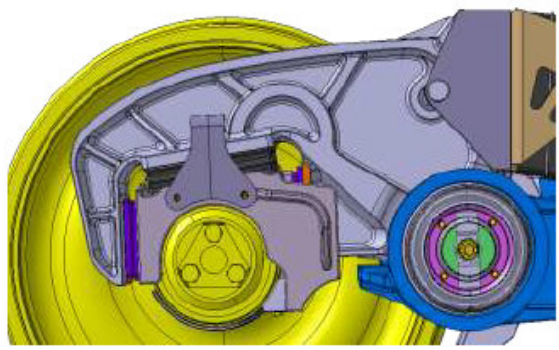

Fig. 3 New bogie – wheelset guiding with adapter and primary spring

The passive resistance in longitudinal wheelset guiding is minimised which improves the wheelset steering start and wheelset return in a “base” position after passing curve. Rubber bushings assemble the swing arms and the bogie frame.

Fig. 4 Wheelset stabilizing force – new and reference bogie

Secondary springs are arranged between the swing arms and the bogie frame. Direction of secondary spring deflection is nearly horizontal. The secondary springs are supported by brackets arranged directly on the bogie frame on one side of the bogie. On the other side of the bogie, the secondary springs are supported by each other with help of support which is movable in longitudinal direction. This support is arranged on a separate rubber spring. The support position is stabilized by a force component derived from force in secondary suspension – so the support bearing is friction less, which effect improves the wheel force balancing. In each secondary spring assembly is arranged a friction damper. The damper is arranged series-parallel to the system of secondary spring assembly. This solution allows optimization of the damping at the empty or low loaded vehicles – the suspension is not blocked by damper hysteresis in this case. Wedges in the damper are pushed by secondary springs on the friction leaf, which ensures damping proportional to the vehicle load.

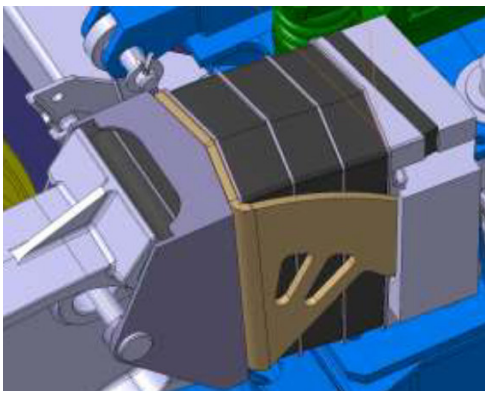

Fig. 5 Secondary suspension with friction damper

The secondary spring arrangement allows to achieve the suspension characteristics near to the optimum – constant frequency curve (see fig. 6).

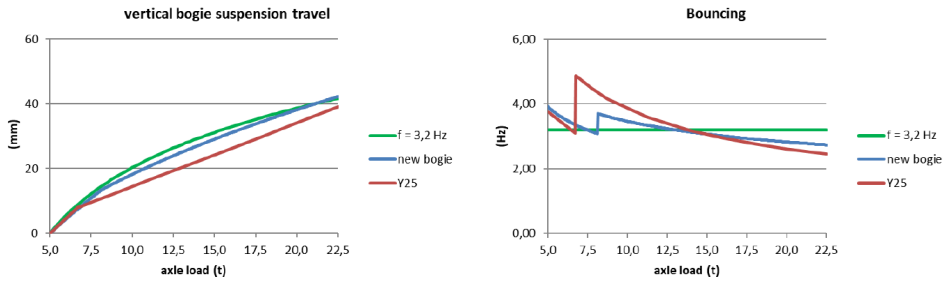

Fig. 6 Suspension characteristics

The bogie frame has an innovated arrangement – the cross beam is arranged over the longitudinal beams and all the beams are connected via Huck-Bolts® (see fig. 7)

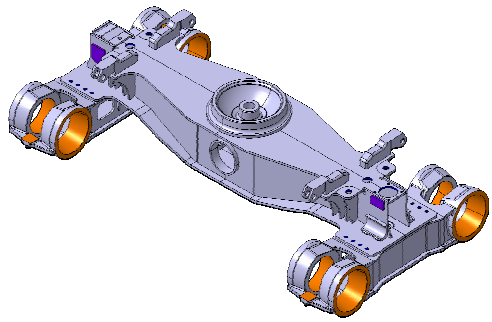

Fig. 7 Bogie frame

2.6 MBS results

The running behaviour was evaluated from the results of MBS calculations. Two MBS models were built in order to compare running characteristics of the reference bogie and new bogie. For this comparison were used quantities based on the EN14363.

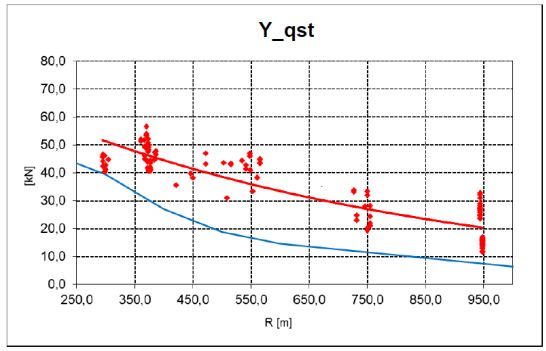

Fig. 8 Y forces (new bogie (MBS) – blue, reference bogie (measured) – red)

Also a known measuring result obtained at the vehicles equipped with reference bogies has been taken into account. The results show a potential of the new bogie to reduce the undesirable consequences of the wheel-rail contact (see fig. 8). The promising MBS results are necessary to validate by running tests.

2.7 Experiment

In order to validate the suspension calculations was necessary to perform an experiment. Various spring arrangements have been tested on the test rig.

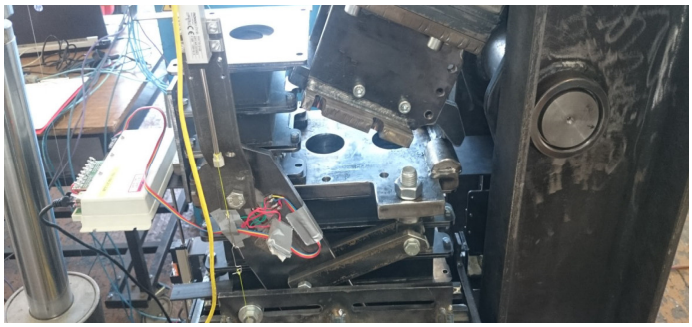

Fig. 9 Experiments on the test rig – secondary suspension and damper prototype

The measured quantities were set to obtain a complete information about suspension quasi-static behaviour (displacements, inclinations, forces). Also the new friction damper has been tested in various design variations. The measurements (displacement and damping forces) confirmed the intended damper functionalities. The performed experiments helped to set up the spring arrangement and damper design.

3. CONCLUDING REMARKS

The new bogie for freight vehicles was designed to meet the expected requirements on railway freight cars. The suspension functionality was tested on the test rig. Next stage in the development should be a test with bogie prototype.

Acknowledgment - this contribution has been published with the support of the project TE01020038 „Competence Centre of Rail Vehicles“ from the Technological Agency from the Czech Republic. The project is a part of the program supporting a long-term cooperation between the public and private sectors in development, research and innovations.

4. REFERENCES

[1] **Jönsson, P.A.:** *Freight wagon running gear – a review*. Division of Railway Technology, Department of Vehicle Engineering, Royal Institute of Technology (KTH), Stockholm, 2002

D-DART CONCEPT – A WAY TO HIGHER CAPACITY

Jan PLOMER (jun.)
JP-design, Ondříčkova 482/18,
CZ-360 01 Karlovy Vary, Czechia
jplomer@seznam.cz Phone: +420 606 774 178

Received: September 9, 2019

ABSTRACT

Single deck vehicles cannot offer more capacity without decreasing passenger comfort. Usually used 4-axle DD vehicles can offer more capacity by using two levels, but the use of two levels is limited to the area between bogies, and then the capacity increase is by approx. 40% only. There are also DD trainsets using 2-axle common bogies, which eliminate the SD ends of DD vehicles and provide slightly higher capacity, but the length which cannot be used for 2 levels is due to number of bogies still large. The number of bogies or car body length is limited by gauging and permitted axle load. To solve these two limitations and increase the capacity is the aim for development of concept D-DART. Its bogie functional design is based on two different concepts, which have been developed separately in the 20th century in UK and Eastern Germany. The common bogie of the D-DART concept is characterized by using 3 radial steered axles and situating of secondary suspensions at the ends of the bogie frame. This design allows using of 24 m long car bodies with high ratio of double-level section. It gives 15% greater capacity and 10% less weight in the comparison of the 100 m long 4-car D-DART EMU and the classic 100 m long 4-car DD EMU, but its potential use is much wider. EMUs, PUSH-PULLs, n-car blocks as a part conventional rakes etc.

Keywords: double-deck EMU, articulated train, capacity, radial steering

1. INTRODUCTION

The reason, why the double-deck passenger vehicles exist, is evident – higher capacity. The higher capacity is required to achieve better economy of the operation of those vehicles, but is also needed on many suburban railway networks, where the line capacity is shared with other segments of transportation and platform length is also limited.

How much bigger capacity can be achieved by double deck vehicles? In fact, there are three types of double-deck vehicles today:

1.1 Four-axle double-deck coaches

4-axle double-deck coaches are mostly used concept. This concept can be used as a separated coach or as a part of multiple units (push-pulls, EMUs). Coach like this is in european conditions characterized with following dimensions: length 26,4-26,8 m, width 2,78-2,82 m and bogie base 19-20 m. The bogie base dimension cannot be increased, because it would cause significant width reduction due to the loading gauge in a curve. The length of double-deck part is usually about 4,5 m shorter than bogie base. The coach of 26,4 m length, 2,80 m width and 19,5 m bogie base has then the double-deck part approx. 15 m long, which gives a potential to reach 146 seats while seat pitch is 875/1750 mm (airplane style/vis á vis), as is shown in Fig. 1.

1.2 Articulated double-deck units with common two-axle bogies

The length of a section of an articulated unit is equal to the bogie base. Therefore is the section length limited by the same rules as bogie base by 4-axle coaches. E.g. for the width of 2,80 m is the max. allowed bogie base 19,5 m.

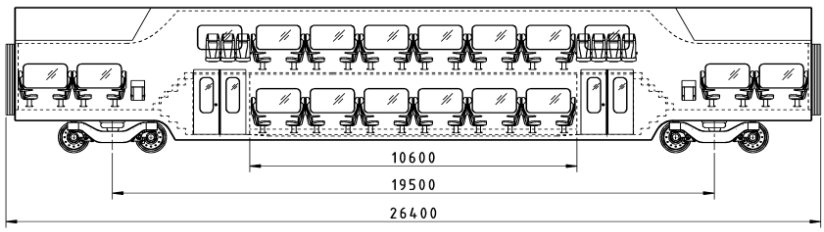

Fig. 1 Basic layout of 4-axle double-deck coach and a representative interior arrangement for the comparison

Moreover the section length is limited in order not to exceed the maximal axle-load. This relation is significantly influenced by the amount of payload caused by the vehicle operational rules. Due to this relation is possible to achieve the length 18,7 m with axle-load of 17 t on long-distance TGV Duplex train, while in case of suburban, regional and inter-regional trains with significantly higher specific payload must be the length decreased down to ca. 16 m for achieving axle-load 20 t (own weight 26,5+payload ca. 13,4 t). The section of this length provides capacity of 82 seats by the same rules of interior arrangement as is shown in Fig. 2.

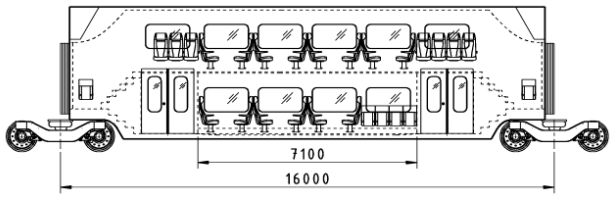

Fig. 2 Basic layout of an intermediate section based on 2-axle common bogies

1.3 Articulated double-deck units with common three-axle bogies

The length limitation caused by loading limits has been solved decades ago by designing the common bogies with 3-axles. That turned the situation around. The length limitation by loading limit has been increased by 50 % (to bogie base ca. 24 m at 20 t per axle), however the length limitation due to carbody width ca 2,8 m stayed at 19-20 m. The 19,5 m long section based on common 3-axle bogie has a potential to provide capacity of 106 seats as it's shown in Fig. 3.

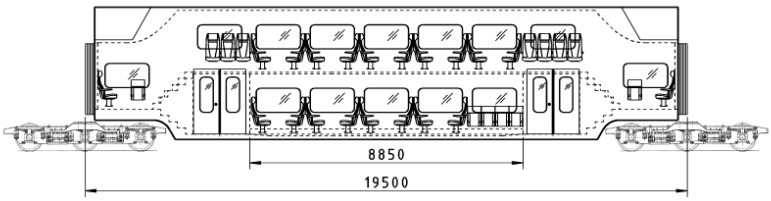

Fig. 3 Basic layout of an intermediate section based on 3-axle common bogies

2. THE D-DART CONCEPT

The aim of the D-DART concept is to harmonize the three limitations:

- Length limitation due to maximal axle-load for 3-axle common bogie (≤ 24 m)
- Length limitation due to carbody width reduction by loading gauge to maintain the width ≥ 2 800 mm (≤ 19,5 m)
- Length limitation due to max. distance of following wheelsets set by TSI CCS standard (≤ 20 m)

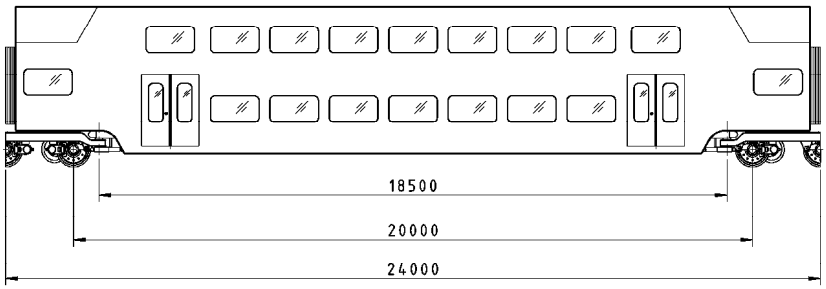

Fig. 4 Basic dimensions of the D-DART concept intermediate section

2.1 Bogie of the D-DART concept

The common 3-axle bogie is designed to improve the kinematic of the carbodies while negotiating the curve (simple and S-shaped). The design is based on formerly used and tested solutions. For allowing the better kinematic there is used analogous design as on the APT-P units (BR class 370) of British Railways in 60‘s. The pivoting points are pulled out of the bogie center. Therefore the section length can increase. Radial steering of wheelsets is inspired by the FEBA bogie (NSB class 72). In Fig. 5 the genesis of the D-DART bogie is ilustratively described.

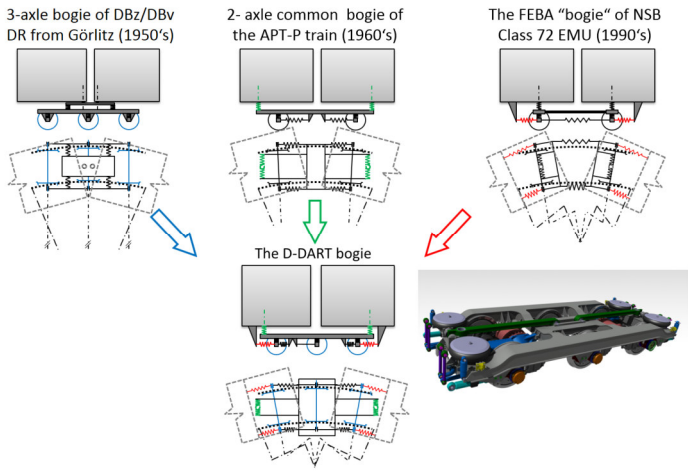

Fig. 5 Genesis of the D-DART bogie

The D-DART bogie is based on using 3-axles. These are guided by swinging arm. The horizontal stiffness is given by axial and radial stiffness of the rubber elements joining the swinging arm to the bogie frame. These elements are different for intermediate and

outer wheelsets. The intermediate is axially (latetally) relatively softer, while radially is stiffer. The rubber elements of the outer wheelset swinging arms is radially softer and axially stiffer. These properties allow easier radial steering. It's also possible to equip the wheelset guidance with a hydraulic or eventually mechanical cross-linkage.
The primary suspension is designed as a steel coil spring with additional rubber pad underneath and a parallel rubber bump stop, which is acting in case of exceptional load.
On the primary suspension is based the bogie frame. The bogie frame is a welded part made of metal sheets and also cast steel parts for complex nodes as the pockets in the longitudinal beam for the primary suspension.
The bogie frame is composed of two main longitudinal beams and two main cross beams at the end of the frame. In the central part is the bogie frame complemented by a structure for transmission of longitudinal forces.
On each end of the bogie frame is placed the secondary suspension for each car body. It is composed of two air-spring systems with a lateral base of 1500 mm. The secondary suspension is also equipped with a anti-roll stabilizer and also vertical and lateral dampers.
Transmission of the longitudinal forces between each carbody and the bogie is realized by a push-pull coupling rod. Each rod is connected to the carbody through a spherical joint in the area between the air spring of the secondary suspension and attached to the bogie frame in the central part. The rod is designed as a deformation element in case the longitudinal force exceeds the limit.
The three-axle bogie is equipped with a really simple radial steering device. It is formed of four longitudinally oriented, flexible elements with own damping, which are directly connecting the swinging arm of the outer wheelsets and the carbody. Position of each element is under the frame, under the secondary suspension. This position and orientation allows to not to connect other relative movements, but the radial steering.
The concept design of the D-DART bogie is shown in Fig. 6.

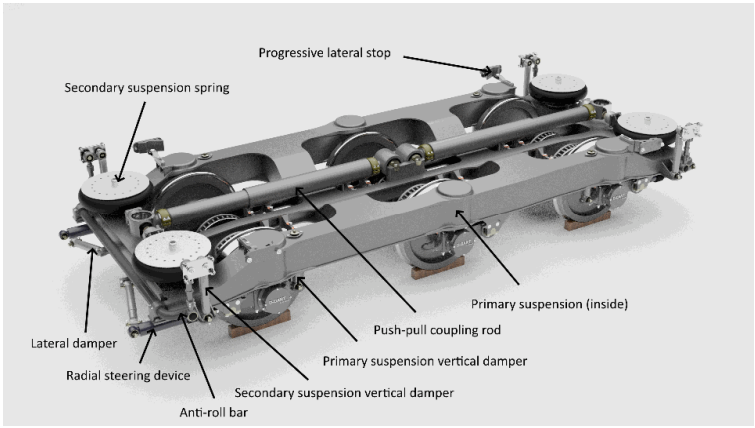

Fig. 6 The design concept of the D-DART bogie

2.2 Development works already executed on the bogie

It's been assembled the dynamic model of the 3-car unit with two 2-axle bogies at each end and two D-DART bogies. This consist has been tested in a multi-body simulation software acc. to the standard EN 14 363.
This way was tested:

- Quasistatic safety against derailment (method 2)
- Running safety (in all testing areas)
- Running behavior
- Sway coefficient

The concept passed all the limits required by the standard.
During the simulations has been tracked also the wear number (Nm/m) of both types of bogies. The comparison of the wear number of different types of bogies is shown in Fig. 7.

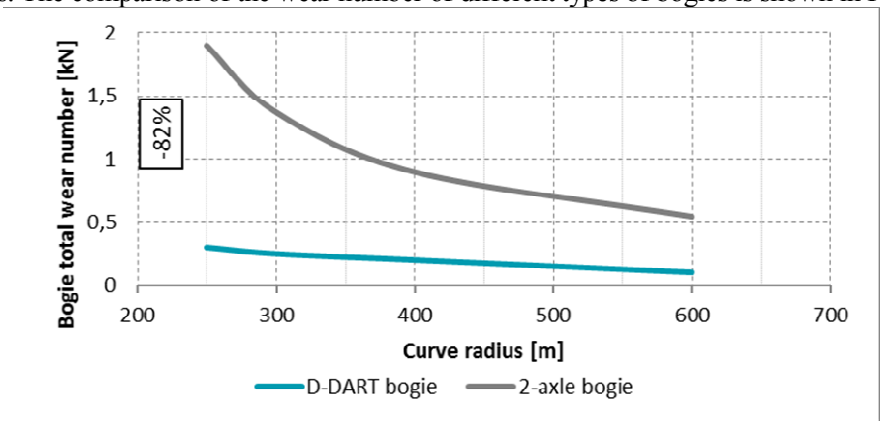

Fig. 7 The comparison of the wear number of different types of bogies within the tested unit.

A crucial topic for this bogie arrangement seems to be also the dynamic behavior in the carbody above the bogie. It's been also checked and compared between the two types of the bogies. In Figs. 8 - 11 you can see 4 diagrams representing the max. and rms values of acceleration above the secondary suspension in vertical and lateral direction.

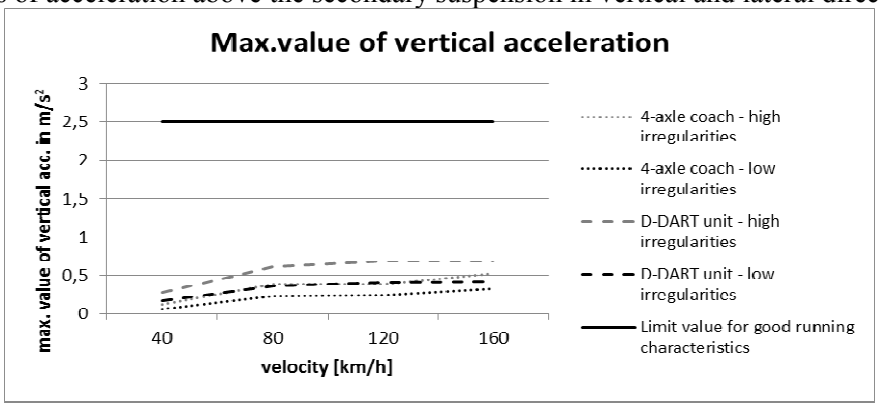

Fig. 8 Max. value of vertical acceleration - comparison D-DART bogie vs. 2-axle bogie

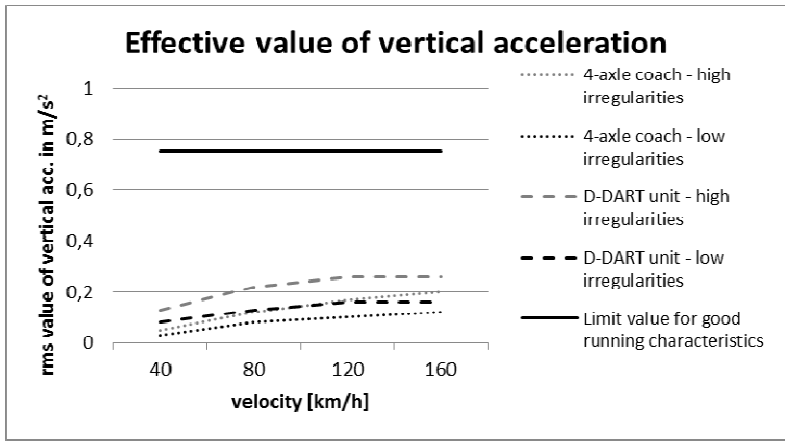

Fig. 9 Rms value of vertical acceleration - comparison D-DART bogie vs 2-axle bogie

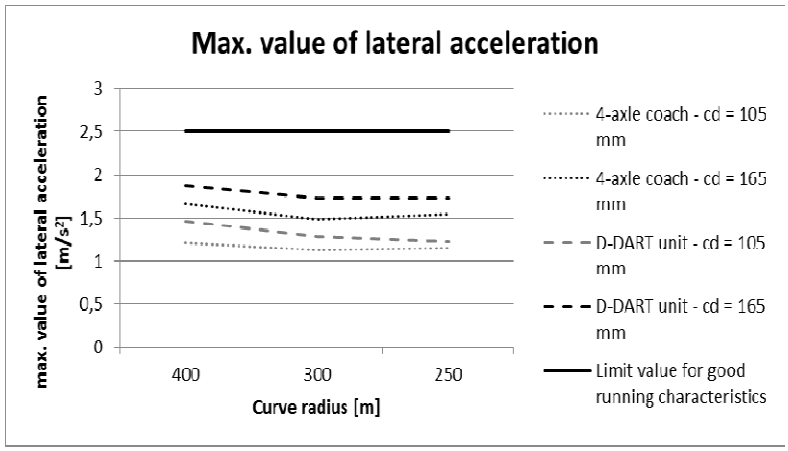

Fig. 10 Max. value of lateral acceleration - comparison D-DART bogie vs 2-axle bogie

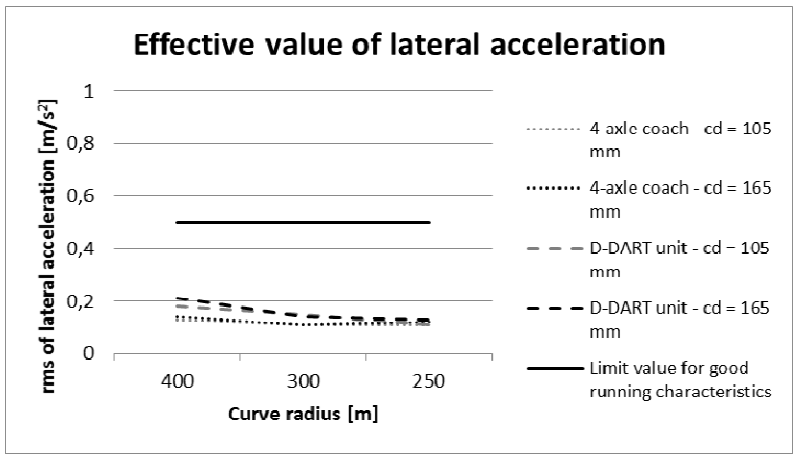

Fig. 11 RMS value of lateral acceleration - comparison D-DART bogie vs 2-axle bogie

2.3 Intermediate section of the D-DART concept

The intermediate section of the D-DART concept is 24 m long, 2,8 m wide. Its weight is ca. 39,1 t (incl. bogie). The section of this length provides capacity of 142 seats by the same rules of interior arrangement. The sketch of this arrangement is shown in Fig. 12.

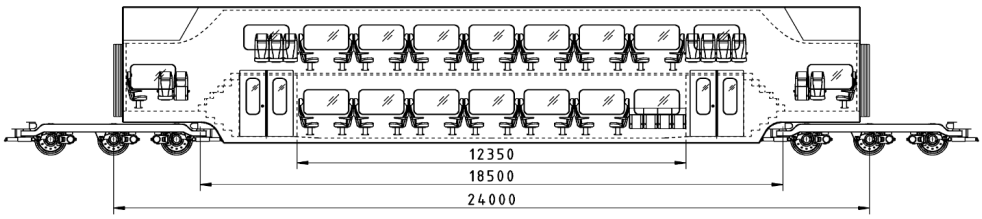

Fig. 12 The intermediate section of the D-DART concept.

3. COMPARISON

3.1 Comparison of intermediate sections

For comparison of single concepts their basic parameters have been calculated according to the following rules:

- Carbody (equipped) mass: 1,2 t/m
- Bogie mass: 2-axle: 8 t, 3-axle: 10 t, D-DART bogie:11 t
- Passenger weight: 70 kg
- Maximum standing density: 6 persons/m^2

Results of this comparison you can see and read in Figs. 13 and 14.

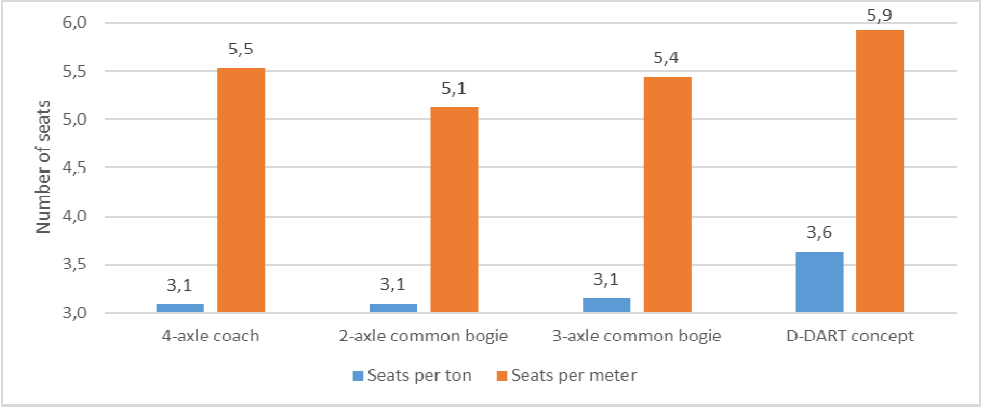

Fig. 13 Comparison of economical indicators of different double-deck intermediate sections

3.2 Comparison of double-deck "D-DART" twins for long-distance loco-hauled trains

The bogie concept also allow to design two- or more-sectional passenger double-deck coaches, which can operate as a high capacity modules in loco-hauled trains.

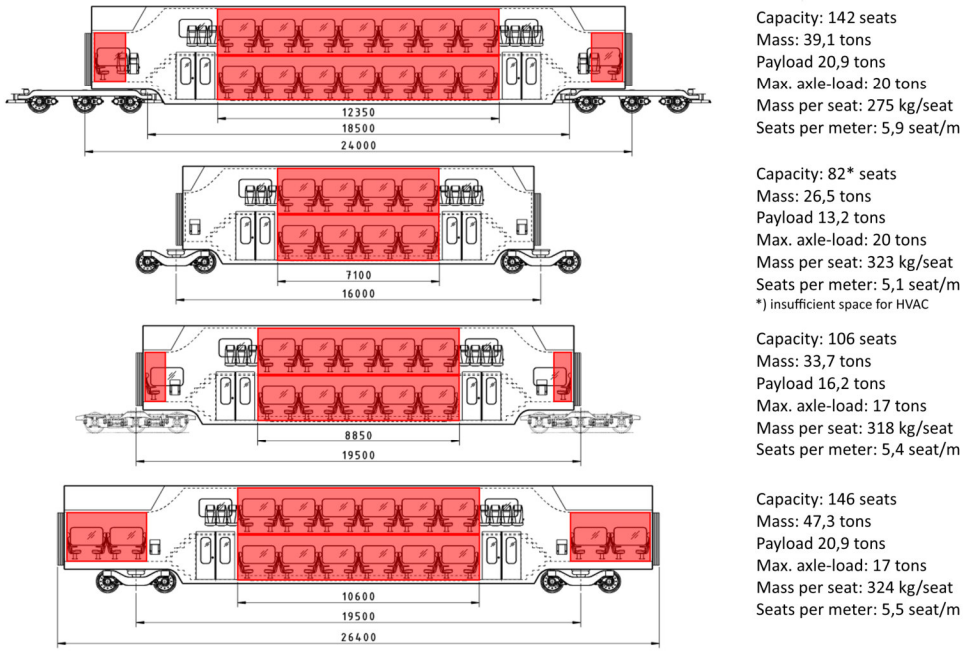

Fig. 14 Comparison of the usefull space of different double-deck intermediate section.

For comparison of their's parameters and benefits was choosed the simple example of czech commercial operator, which operates loco-hauled long distance trains.
In Fig. 15 is shown the evaluation of the parameters and also the economical part of the operation from the rolling stock point of view.

Consist	Length	Own weight	Capacity *	Price **	Price per seat	Traction power	Specific power	adhesion ratio	Daily run	Energy consumption costs for 30 years ***	Train path charges for 30 years ****	Total cost (INVEST+ +ENE+ +charges)	Total cost per seat	Total cost per seat per km
	[m]	[t]	[ks]	[€]	[Kč]	[MW]	[kW/t]	[%]	[km]	[€]	[€]	[€]	[€]	[€]
														
Traxx + 10xASTRA	283	535	800	14,7 M	18 400	5,6	10	16	1400	21,3 M	18,9 M	54,9 M	68 600	0,0045
														
Traxx + 7xDBz	207	449	784	15,3 M	19 500	5,6	12	19	1400	18,2 M	16,6 M	50,0 M	63 800	0,0042
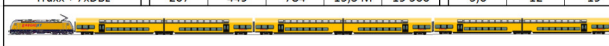														
Traxx + 3xD-DART IC	178	325	810	15,5 M	19 100	5,6	17	26	1400	13,8 M	13,3 M	42,6 M	52 600	0,0034

*) Seat pitch ca 1800 mm + comparable volume of luggare racks.
**) Price of the Traxx locomotive 3,9 M €, coach Astra 1,1 M €, DD coach DBz DBz 1,6 M €, double-deck D-DART NT IC 3,9 M €
***) Energy costs 0,093 €/kWh, consumption 25kWh/1000hrtkm
****) - Train path charge acc. to SŽDC rules 2016 [€] = (7,81+44,77*weight[t]/1000)/25,80

Fig. 15 Comparison of technical parameters and operational costs of different long-distance formations.

3.3 Comparison of double-deck EMUs concepts

It's been designed also the the whole DD EMUs based on the bogie concept. In the first case (4th line below) it's 104 m long EMU which is created of two halves based on

the bogie concept. The second case (6th line below) is whole 98m long EMU based on the bogies.

In Fig. 16 you can see a relation of technical parameters between these concepts and other DD EMUs which are suitable for Prague suburban operation (platform length 200 m).

Platform	Specification	Length	Mass	Capacity I	Comparable capacity II	Initial cost assumption	Price per seat III	Max. power	Specific power	Acceleration at 140 km/h IV	Adhesion ratio assumption	Required adhesion coef. for 1m/s²	Daily run	Cost of the energy for 30 year period VI	Usage charge for 30 year period V	Sum of in. cost, energy cost, us. charge	Sum of in. cost, energy cost, us. charge per seat	Price of 60 units project
		[m]	[t]	[pcs]	[pcs]	[EUR]	[EUR]	[MW]	[kW/t]	[m/s²]	[%]	[-]	[km]	[EUR]	[EUR]	[EUR]	[EUR]	[EUR]
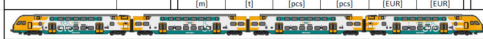																		
Fully DD EMU	Germany	106	215	424	442	11,7 M	26 500	3	14	0,36	29	0,34	420	4,2 M	3,1 M	19,0 M	44 900	1,14 bn
		2x = 212		2x = 848	2x = 884			6					5 m/30 y					
																		
Partially DD EMU	Germany	105	201	400	412	11,7 M	28 400	4	20	0,51	60	0,16	420	3,9 M	3,0 M	18,6 M	46 600	1,12 bn
		2x = 210		2x = 800	2x = 824			8					5 m/30 y					
								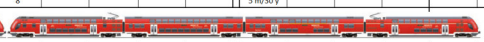										
Fully DD EMU	Germany	106	232	425	446	11,7 M	26 200	4,6	20	0,51	57	0,17	420	4,5 M	3,3 M	19,5 M	45 800	1,17 bn
		2x = 211		2x = 850	2x = 892			9,2					5 m/30 y					
																		
D-DART	2x2-car	104	195	498	498	11,7 M	23 500	4	21	0,53	70	0,14	420	3,9 M	3,0 M	18,6 M	37 300	1,12 bn
		2x = 208		2x = 996	2x = 996			8					5 m/30 y					
																		
Fully DD EMU	Switzerland	100	212	388	390	11,7 M	30 000	6	28	>1,2	57	0,18	420	4,1 M	3,1 M	18,9 M	48 700	1,13 bn
		2x = 201		2x = 776	2x = 780			12					5 m/30 y					
																		
D-DART	4-car	98	191	480	480	11,7 M	24 400	4,5	24	0,61	47	0,21	420	3,8 M	2,9 M	18,5 M	38 500	1,11 bn
		2x = 196		2x = 960	2x = 960			9					5 m/30 y					

200m length

200m length

I) - Acording the specification
II) - For comparability is the capacity standardised. Interior of each unit is full of seats with a seat pitch of >=1750 mm minus 18 seats for two standard and one universal toilet.
III) - Initial cost per seat and other specific values are related to the comparable capacity.
IV) - Acceleration represents here an influence of specific power. It doesn't calculate with forces against movement (resistance and rotating masses). The real acceleration would be about 30% lower.
V) - Usage charge calculated acording the SŽDC regulation (2016). Cost per km: [EUR] = (7,81+44,77*brutto weight[t]/1000)/25,80
VI) - Cost of the energy 0,093 €/kWh, Consumption 40kWh/1000 ton-kilometer brutto

Fig. 16 Comparison of DD EMUs suitable for Prague suburban operation

4. CONCLUSION

The D-DART bogie concept has a potential to increase the benefits of double-deck arranged passenger coaches and EMUs. The vehicles based on the D-DART concept are about 15% lighter per seat and also the specific capacity (seating density) is about 15% higher than standard solutions, while the seat pitch was not decreased.

DEVELOPMENT OF STEERING MECHANISM AND CONTROL METHOD FOR ACTIVE-STEERING BOGIE

Hisako NEGISHI[*1], Hiroyuki YAMADA[*1], Ken IWANAMI[*1], Ryohei SHIMAMUNE[*1], Daisuke SHINAGAWA[*2] and Manabu MIMURA[*2]

*1: Advance Railway System Development Center , Research and Develop Center of JR East , East Japan Railway Company
2-479, Nisshin-cho, Kita-ku, Saitama-shi, Saitama-pref 331-8513 Japan
*2: No.1 Railway Designing Department, Railway Bogie Division, Railway, Automotive & Machinery Parts Unit, Osaka Steel Works, NIPPON STEEL CORPORATION
5-1-109, Shimaya, Konohana-ku, Osaka City, Osaka 554-0024 Japan

Received: September 8, 2019

ABSTRACT

We developed an active bogie-steering truck with the aim of achieving compatibility between high-speed running stability required along Shinkansen sections and curving performance required along conventional line sections. The basic development concept is a bogie with two parallel yaw dampers on one side for through-service Shinkansen trains also running on conventional lines. The developed active-steering bogie is composed of a control device, a steering actuator, and a damping force switching yaw damper. In the running test, we confirmed lateral force reduction at the head-end outer-rail wheel by active-steering bogie.*Keywords:* active-steering bogie, high speed running stability, curving performance, lateral force, attack angle

Keywords: steering mechanism, control method, active steering

1. INTRODUCTION

JR East is working on development of next-generation Shinkansen to increase the maximum travel speed of the Shinkansen to 360 km/h, pursue higher levels of safety and stability, improve travelling comfort and environmental performance, and implement more innovative maintenance. Maintaining stable running and operation at increased speeds is an important component to fulfill that vision.

Vehicles running on the Akita and Yamagata Shinkansens are Shinkansen-dedicated vehicles, operating directly along both Shinkansen line and conventional line sections. Unlike the Shinkansen sections, conventional line sections include many small-curve radii along their routes. The bogie for through-operation between Shinkansen and conventional lines is required to have both high-speed running stability for the Shinkansen section and curve-passing performance for the conventional line section. However, high-speed running stability and curve-passing performance are in a contradictory relationship, and thus improving performance of one tends to lower that of the other. Therefore, their coexistence is key when raising maximum operating speed.

In anticipation of high speeds on Shinkansen sections, we developed an active-steering bogie with both running stability and curve-passing performance suitable for the sections of both Shinkansen and conventional lines.

In this report, we describe the development of the mechanism and control of theactive-steering bogie and and results of the running test.

2. DEVELOPMENT BACKGROUND AND POLICY

2.1 Background of active-steering bogie development

Various developments have been carried out to achieve both running stability and curve-passing performance on the Shinkansen and conventional route sections. However, in the case of seeking a happy medium for high-speed running stability and curve

performance, there is a limit as to what can be done by merely adjusting the distance between axes or incorporating a damping-force switching yaw damper, which have been some conventional solutions. Therefore, we focused on the steering bogie as a way to improve curve performance while at the same time improving high-speed running stability.

As a railcar passes a curve, the angle of attack causes lateral force. The “attack angle” is the angle of the wheel tangential to the rail. Lateral force increases as the attack angle increases. The steering bogie changes the direction of the wheel axis so that the wheel follows the curve when passing through it, thereby reducing the angle of attack and reducing lateral force.

A steering bogie can be broadly divided into “wheel steering” and “bogie angle steering.” Wheel steering is a method of steering the wheel shaft relative to the bogie frame. This feature involves a complicated structure and an increased number of parts due to alterations in the wheel shaft tightening mechanism, and requires a different type of maintenance compared to a conventional bogie. In addition, in the unlikely event that the bogie frame has difficulty in supporting the wheel shaft, there are concerns of meandering during high-speed operation.

On the other hand, an active-steering bogie turns the bogie frame relative to the vehicle body. This feature makes it possible to improve curve performance by arranging one actuator on each side between the car body and the bogie without the need for a wheel shaft steering link. Therefore, although this involves the added maintenance of the actuator and the control device, bogie maintenance can be performed in the same way as a conventional bogie. Further, when running at high speed on a Shinkansen section, running stability can be ensured by the yaw damper mounted parallel to the actuator.

Taking these characteristics into consideration, we decided to proceed with the development of an active-steering bogie,from the viewpoint of ease in construction, maintenance, and handling failure safely.

2.2 Development policy of active-steering bogie

The basic policy for the development of the bogie steering system was defined as follows:

(1) To be installed on bogies for Shinkansen through-operation with conventional lines and equipped with a steering actuator and a yaw damper at the yaw damper mounting position on a conventional bogie (Fig. 1).
(2) To sufficiently guarantee stability in high-speed operation as a bogie configuration (passive system) excluding the steering actuator.
(3) To have a yaw damper of a damping force switching type, with the damping force switched between the Shinkansen section and the conventional section.
(4) To have steering that reduces the steady lateral force of a conventional line (component due to attack angle = turning lateral force).
(5) To have highly reliable fail-safe functions such as reverse-steering prevention measures.
(6) To detect curves based on a position-detection type with rolling stock information.
(7) To comply with rolling stock specifications based on type E6; the current Akita Shinkansen railcars.

We conducted simulations and prototype production to develop an active bogie steering system that satisfies these basic policies, and we worked on a prototype running test on a current Akita Shinkansen railcar, described below.

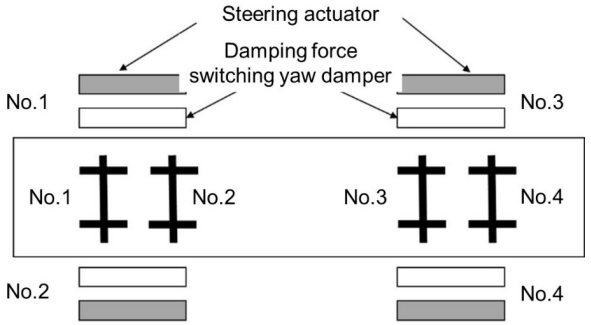

Fig. 1 Arrangement of steering actuator and damping force switching yaw damper

3. SIMULATION

3.1 Simulation verifies lateral force reduction effect

Using curve data from a section of the Tazawako line along the Akita Shinkansen route, curve simulation was performed for the specifications of an active-steering bogie with increased stiffness of primary suspension for high-speed operation in the Shinkansen section.3.2 Actuator thrust and effectiveness of lateral force reduction

Curve simulation was performed by changing the thrust of the steering actuator. Fig. 2 shows simulation results on the side of the front shaft outer rail where lateral force is greatest. Lateral force generated is shown when passing through a curve when the thrust of the actuator was changed from 5 kN / line to 20 kN / line with and without steering. It was observed that, as the thrust of the actuator is increased, the effectiveness of reducing lateral force on the outer shaft side also increases.

On the other hand, as shown in Fig. 3, lateral force of the rear shaft increased due to steering. This is thought to be from steering in the direction in which the wheel on the outer-rail side of the rear shaft is pressed against the rail. In addition, when the lateral force is at the same point and the thrust of the actuator is 15 kN/bar or more is compared between the outer side of the front shaft and outer side of the rear shaft, the lateral force on the rear axis outer side exceeds the lateral force of the front axis. From this, it was found that oversteering occurs with excessive actuator thrust.

From the above results, it was decided to set the upper limit of thrust of the actuator to a prototype of to 10 kN/piece in order to obtain maximum lateral force reduction effect while preventing such excessive steering.

3.3 Effect of reverse steering

Next, the thrust of the steering actuator was changed and a curve simulation was performed to verify the effect of reverse steering. As shown in Fig. 4, the lateral force on the outer side of the front shaft increased as the actuator thrust increased in reverse steering.

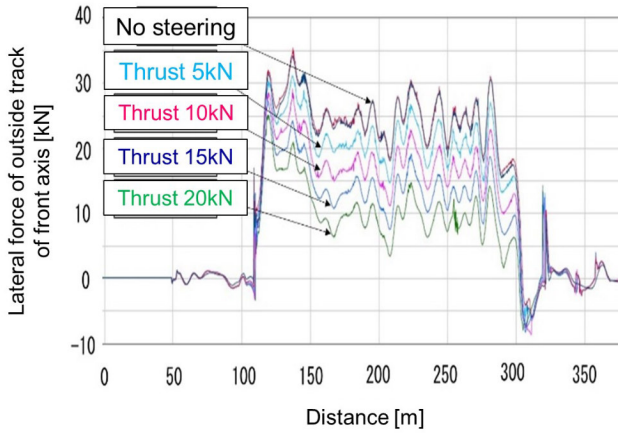

Fig. 2 Lateral force of outside track of front axis (In case of R250, 70km/h)

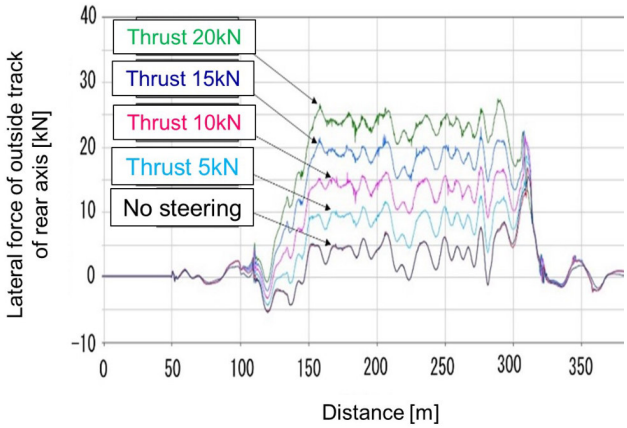

Fig. 3 Lateral force of outside track of rear axis (In case of R250, 70km/h)

Curve with tight radius (R250) tend to increase lateral force. However, even when the actuator thrust is 20 kN/piece at maximum, lateral force is about 65% of the reference value in the simulation results.

4. DEVELOPMENT OF PROTOTYPE

The prototype was produced based on the policy and simulation described in Sections 2 and 3. The prototype was produced for one car, consisting of a control device (1 unit), an electric actuator for steering (4 units), and a 2-stage switchable yaw damper (4 units).

4.1 Control device

When running speed exceeds a certain speed and a steering curve is detected, the steering command turns on. The controller has curve data and presets the maximum thrust output for each curve. In addition, the steering command is output only when the direction and the magnitude of the yaw rate measured by the gyro-sensor installed in the car body co-

incide with the thrust command direction in the curve data in the controller. This is to prevent reverse steering or wrong steering when travelling forward.
In addition, when an abnormality is detected by the control device, it shifts to "stop" mode. The actuator outputs all turn to zero, and it falls into a non-steering state.

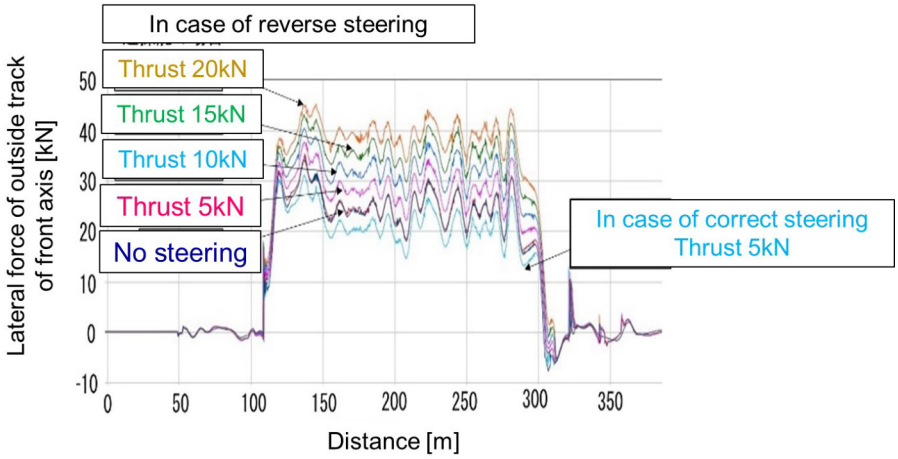

Fig. 4 Lateral force of outside track of front axis
(In case of R250, 70km/h, reverse steering)

4.2 Steering actuator

The actuator is an electric actuator that converts the rotation of the electric motor into linear motion with a ball screw. The maximum thrust of the actuator was 5 kN/bar.

4.3 Damping force switching yaw damper

A two-stage switching type yaw damper is used. The damping coefficient is C2500 for Shinkansen sections that require high-speed running stability, and C400 for conventional line sections that require curve performance, based on the performance in E5 and E6 series of current vehicles.

5. TESTING EFFECTIVENESS ON CARS IN ACTUAL USE

5.1 Running test on the Akita Shinkansen

In the running test, we attached this system to the 17th car of E6 series Shinkansen (Fig. 5, Fig. 6). E6 series Shinkansen is a commercial train operating on both Shinkansen and conventional lines in JR East. We tested this system with curves of radii less than 600m between Tazawako and Kakunodate stations.

The steering actuator has a maximum thrust of 5 kN/bar so that it would not affect the track even if it failed.

5.2 Running test results

Fig. 7 shows test results when running at a speed of 70 km/h at a right-turning curve of R300 as one example of the main line running test. Fig. 8 shows the tendencies of lateral force change for each wheel.

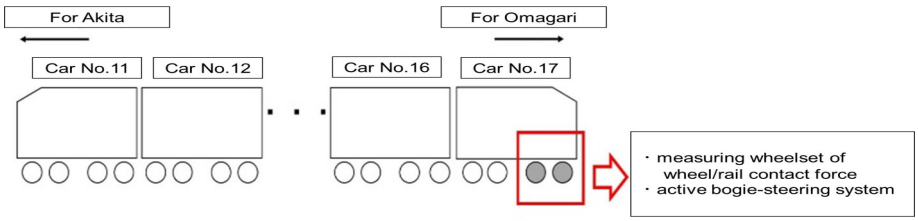

Fig. 5 Vehicle overview during running test

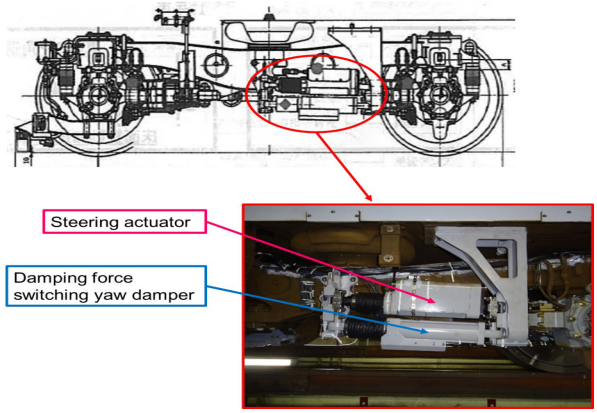

Fig. 6 Appearance of active-steering bogie

It can be seen from Fig. 7 that average lateral force is reduced by about 8 kN on the outside track leading-shaft where lateral force is greatest. In addition, reduction was also confirmed for fluctuating lateral forcecaused by rail joints. The reduction in lateral force averaged 3-8 kN throughout measurement. In addition, as shown in Fig. 8, there was no change on the inner rail side of the front shaft, a slight increase on the outer rail side of the rear shaft, and a slight decrease on the inner rail side of the rear shaft.

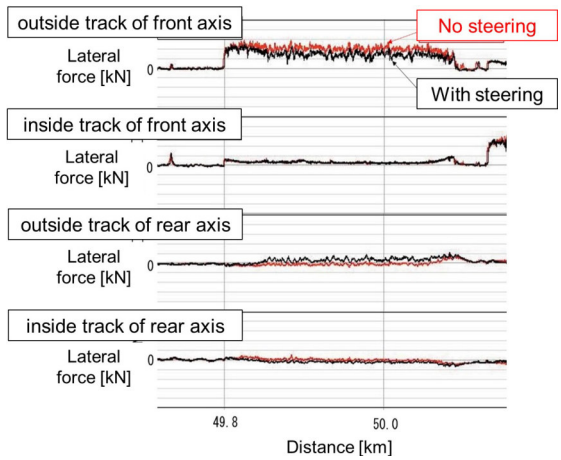

Fig. 7 Example of lateral force change with and without steering in running test (In case of R300, 70km/h)

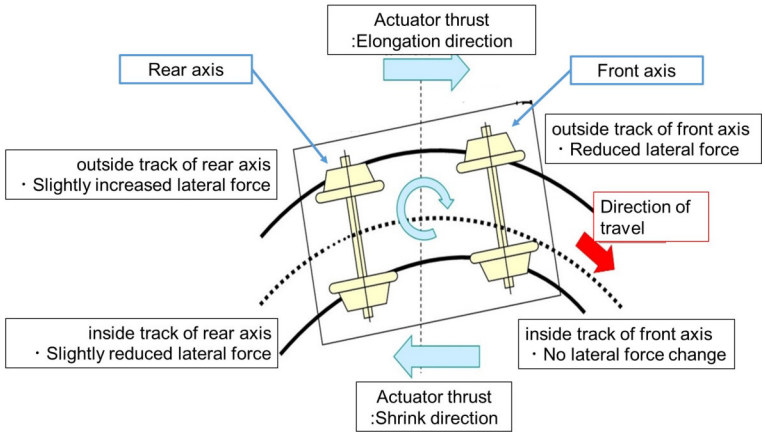

Fig. 8 Trend of lateral force change of each wheel in running test

The results of the running test confirmed that lateral force reduction of the active-steering bogie occurred in actual operation as well. It was also confirmed that the track is not affected by excessive steering with actuator thrust at 5kN/bar.

5.3 Failure Behavior

Failure behavior was confirmed under the following conditions.

(1) Thrust step on/off

Failure was hypothesized in which steering operation started or stopped in a curve. In the transition state between thrust on/off, it was found that no problem occurred, such as a sudden change in lateral force.

(2) Deviation of curve position (front 15m, 30m / delay 15m, 30m)

A case of was hypothesized in which a curve was misperceived. The further from the actual position of the curve, lateral force tended to increase, but it did not worsen over a an event of non-steering. This is because the output restriction based on the yaw angular velocity works to prevent steering operation before or after the curve.

(3) Stoping along a curve

It was confirmed that when a railcar stopped along a curve, output restriction by running speed activated and steering operations were stopped along with the railcar. As a result, there was no sudden change in lateral force, and it was confirmed that it was not a problem.

(4) In the case of damper damping force (C2500), with or without steering

A failure was hypothesized in which the switching yaw damper switching did not work. When the damping coefficient of the yaw damper was increased, there was a tendency for the lateral force on the outer shaft side to increase with or without steering. Even when steering with high damping force (C2500) for the Shinkansen section set this time, lateral force did not increase until it exceeded the reference value.

5.4 Concerns about rear steering

In the running test, a rear-steering test was also conducted in which the bogie was steered from the rear. Lateral force on the outer side decreased by about 6 kN on each curve, as when steeringfrom the front.

There was a situation in which a curve with front-axis inner-side lateral force larger than the outer-side lateral force. Since the rail surface at this time was wet, it is presumed that oversteering occurred due to a small friction coefficient. When a simulation was performed, with a normal friction coefficient, there was no significant increase in lateral force on the inner-gauge side. However, where the friction coefficient is small (i.e., wet), the inner-side lateral force on the front axis increased more than that in the case of non-steering, confirming the same event as in the running test.

When comparing the yaw angle between the normal state and the wet state, it was found that the yaw angle of the rear bogie fluctuated greatly due to steering in a wet state, resulting in an oversteering (Fig.9). From this, it is considered that the inner-side flange of the front axis at the rear bogie touched the rail, and the inner-side lateral force increased.

From the above, the rear bogie may have been in an oversteering state due to rail surface condition, and problems such as inner rail wear and resulting noise can be anticipated. For this reason, it is desirable not to conduct steering with the rear bogie, or to reduce actuator thrust.

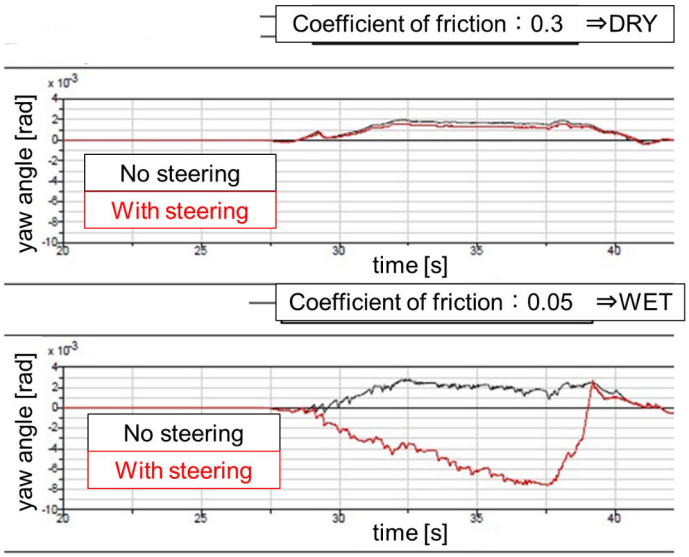

Fig. 9 Comparison of rear bogie angle (dry/wet)

6. CONCLUDING REMARKS

We worked on the development of an active-steering bogie with the aim of ensuring both stability in high-speed running as required for Shinkansen sections and the curve performance as required for conventional line sections. Through this development, we made the following findings:

- From the viewpoint of ease of construction, maintenance, and handling failures safely, we selected an active-steering bogie that turns the bogie frame relative to the railcar body.

- We have developed an active bogie-steering system consisting of a controller, steering actuators, and two-stage switchable yaw dampers for the bogies of cars running on Shinkansen that operate through-service with conventional line sections.
- We confirmed the effect of reducing lateral force and lateral force in cases of failure by simulation. It was found that when the thrust of the steering actuator was too large, the wheelset was oversteered and lateral force on the outer side of the rear axis was greater than the lateral force on the outer side of the front axis.
- The prototype was mounted on a Series E6 railcar, and a main line running test was conducted. As a result, it was confirmed that average lateral force and fluctuating lateral force on the leading-shaft outside track are reduced. This was consistent with the simulation.
- In the running test, the effect of reducing lateral force on the outer side of the front axis was 3 to 8 kN in terms of average lateral force.

In the future, we will continue to develop and miniaturize the active-steering bogie system, study its most effective placement, and develop a more accurate curve detection method.

7. REFERENCES

[1] **Matsumoto, A. et al.**: Multibody dynamics simulation and experimental evaluation for active-bogie-steering bogie, STECH2006, p.103-107.

[2] **Matsumoto, A. et al.**: Curving performance evaluation for active-bogie-steering bogie with multibody dynamics simulation and experiment on test stand, Vehicle System Dynamics, Vol. 46, Supplement, 2008, p.191-199.

[3] **Tanifuji, K. et al.**: Fundamental study on curve passing of railway vehicles by active steering, Transactions of the Japan Society of Mechanical Engineers (C), 66, 642, 2000, p.246-253.

[4] **Iwanami, K. et al.**: Design of Yaw Damper Equipment for Bogies for of vehicles that run through-operation the Shinkansen section and the conventional section, TRANSLOG, p.57-60.

EXPLORATION INTO THE APPLICABILITY OF RUNNING DYNAMICS OF CONVENTIONAL-FORM NON-POWERED BOGIES WITH VERY SMALL WHEELS

Shiping DONGFANG

Chair of Rail Vehicles
Institute of Land and See Transport Systems
Faculty V, Technical University of Berlin
Office SG 14, Room SG 202,
Salzufer 17-19, D-10587 Berlin, Germany

Received: September 9, 2019

ABSTRACT

This ongoing research explores the possibility of using unconventionally small wheels within a conventional two-axle singular-framed bogie in terms of running dynamics. The investigation is done as multibody-simulation-based theoretical case studies of a freight wagon with Y25 bogies with various nominal wheel radii (140mm – 500mm) in different running scenarios. The simulations will quantify the theoretically predictable changes in running stability, curve negotiability and wheel-rail contact wear behaviour as the wheels' nominal rolling diameter decreases. Further, it will be tested whether wheel-radius-dependent tread profile modifications and radial steering mechanisms can compensate for the decline in dynamical performance so that the reference vehicle retains conformity to the standardized acceptance requirements on running dynamics.

Keywords: small wheels, multibody simulation, wheel profile, radial steering

1. MOTIVATION

For both freight wagons and passenger coaches, a low-floor design brings about certain advantages. As the floor must transcend the entire bogie, application of smaller wheels for rail vehicles makes a low floor setting possible throughout the entire wagon. Demotivated by complicated authentication and marginal market profitability, small-wheeled vehicles are underdeveloped and their behaviour rarely researched.

1.1 Freight transport

For the transport of voluminous goods, a maximization of interior space for freight wagons is of benefit. The floor height has an abundant variation freedom and can be set much lower without loading gauge violation or operational difficulties, liberating more vertical interior space for loading cargo. For wagons transporting automobiles, loading and unloading can be greatly simplified if the automobiles to be loaded can be driven through the full length of the train. This requires the floor to have a near-uniform height throughout. For transporting taller payloads or loading on more than one deck, a lower floor is necessary. This calls for smaller wheel sizes so that the floor can be desirably low while still reaching over the running gears.

Fig. 1 Rollende Landstrasse automobile transport wagon bogie

Possibly the only design available on the European market is the Rollende Landstrasse wagons for loading entire tractor-trailers up to 4m tall and 2.6m wide [1], fully using up the 4.32m tall, 2.73m wide upper profile of the GB2 rolling stock loading gauge [2]. This is enabled with its 4-axle bogies with multilevel suspension using wheels with 360mm (new) / 335mm (worn to limit) diameters, see Fig. 1 [3].

1.2 Passenger transport

Double-deck coaches can accommodate up to double the number of passengers per unit vehicle length in the double-deck sections. At the car's ends, the bogies' height forces the floor to raise locally, leaving insufficient vertical space to arrange two decks over a large length of the wagon. This restricts passenger capacity and thoroughfare between wagons for passengers with reduced mobility. The state of art of cabin layout in 1984 presented in [4] as seen in Fig. 2 is still retained today to a great extent.

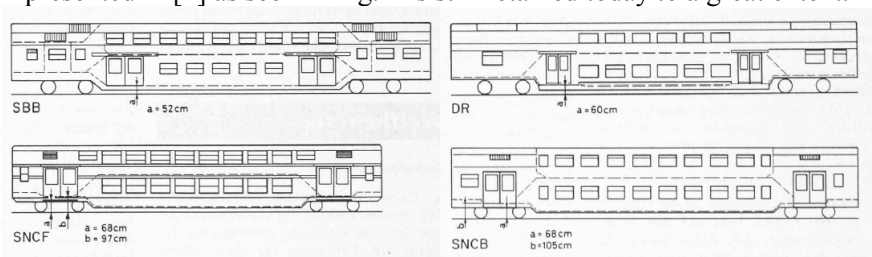

Fig. 2 Entrance area floor height of European coaches, excerpted from [4]

A full-length floor leading to gangways on the upper deck has already been realized with the TGV Duplex, see photos taken by the author in Fig. 3. Should compacter bogies with much smaller wheels be applied, it may become possible to have end-to-end floors on both decks each with their own gangways, thus providing a solution to both the capacity and the thoroughfare issues mentioned above.

Fig. 3 Gangway area of a TGV Duplex EMU viewed respectively from the upper-deck gangway towards the cabin, the entrance towards the gangway, and the outside

2. PURPOSES AND APPROACH

2.1 Quantifying the questionable dynamical behaviour

Klingel's equation for the hunting wavelength of a free-rolling conical wheelset $l = 2\pi(re/2\gamma)^{1/2}$ suggests that wheelsets with smaller wheel radii have shorter hunting wavelengths and thus more frequent and more violent oscillations [5]. This destabilizes the

vehicle at lower speeds, rendering it unfit for operation. The curving behaviour of a vehicle, which usually requires opposite vehicle design parameter settings to those required by stability, may on the other hand benefit. The lower unsuspended mass due to the wheels becoming smaller in volume also hypothetically reduces excessive wheel-rail interaction during guidance. The question is to what rate these conflicting performances are affected by wheel size reduction, and which effect dominates. This is essential for understanding the key target when proposing countermeasures.

2.2 Proposing countermeasures against extreme performance decline

In order to curb the hypothetically foreseeable deterioration in dynamical performance, it is proposed to combine the use of small wheels with accordingly modified wheel profiles or within a radial steering bogie. This work also assesses the effectiveness of each countermeasure as well as both measures combined.

2.3 Choice of research approach

This research has so far no industrial support and does not have physical testing possibilities. The work is thus done purely theoretically, namely as a simulation-based case study with parameter variation. A full-vehicle multibody system dynamics model with varying wheel radius is tested for stability, curve negotiation as well as wear behaviour and wheel-rail contact geometry through numerical time integration. Dynamical behaviour indices obtained from the simulation are related to the wheel radius. Subsequently, the proposed countermeasures are applied to the running gear. The same simulation assessments are carried out again to compare their effectiveness.

In this research, all modelling and simulation are conducted in the MBS software Simpack. The parameter variation, model setup in each studied case and the execution of the huge number of simulation and assessment processes must be automated for feasibility, which is also done in Simpack entirely with its own scripting functionality.

3. MULTIBODY SYSTEM DYNAMICS SIMULATION SETUP

3.1 Vehicle model

The reference vehicle is a freight wagon with Y25 standard bogies involved in a prior TU Berlin research project. The modelling data is taken from the project report [6]. Fig.4 shows the vehicle model with the reference frame in which it is set.

Fig. 4 Full vehicle model with reference frame axis directions

The model allows switching the carbody's mass and inertia between tare and laden states (Table 1). The Simpack-8-based Y25 bogie model from the original project is reconstructed in Simpack 2019x for compatibility and enabling parameter variation.

The model has been validated in the previous project, which has a similar application background as this research. It is thus no longer necessary to validate the model in this project.

Table 1 Carbody mass properties of the original reference vehicle

Load state	Tare	Laden
Mass m / t	16.6	79.8
Moment of inertia about x-axis I_{xx} / kg·m^2	24 200	102 000
Moment of inertia about y-axis I_{yy} / kg·m^2	295 000	1 030 000
Moment of inertia about z-axis I_{zz} / kg·m^2	291 000	992 000
Centre of gravity height (above rail level) / m	1.82	2.36

The nominal wheel radius r_0 varies in the range [140mm, 500mm] with increment 20mm, which covers the original radius 460mm and all radii to which UIC 510-2 applies (165mm-500mm). Its variation directly affects the height of all bodies above the wheelset-axlebox assembly as well as the wheelsets' own mass and inertial properties. The model is set up to automatically adapt to these dependencies. The inertial properties of the wheelset for each tested radius is acquired through an extra 3D geometry modelling of the wheelset in Inventor, see Fig. 5.

(a)

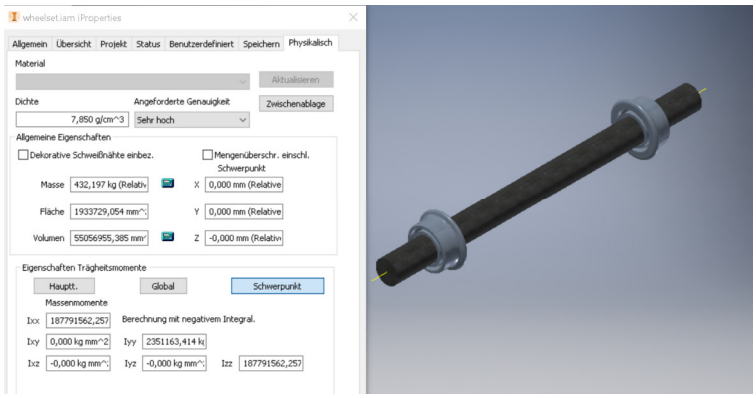

(b)

Wheel radius	m	Ixx	Iyy	Izz	Wheel radius	m	Ixx	Iyy	Izz
0.5	1200.233	675.1910594	122.9587884	675.1910594	0.3	678.846	333.1969537	19.40678031	333.1969537
0.48	1137.441	631.5473391	105.6270803	631.5473391	0.28	639.729	309.4195796	15.33640414	309.4195796
0.46	1077.016	590.1824561	90.20591093	590.1824561	0.26	602.979	287.3237886	11.982058	287.3237886
0.44	1018.958	551.0239005	76.55026026	551.0239005	0.24	568.597	266.8654807	9.255542089	266.8654807
0.42	963.268	514.0020034	64.52079044	514.0020034	0.22	536.582	248.0033971	7.074338608	248.0033971
0.4	909.946	479.0499367	53.98384558	479.0499367	0.2	506.934	230.6991198	5.361611771	230.6991198
0.38	858.991	446.1037137	44.81145179	446.1037137	0.18	479.654	214.917072	4.046207804	214.917072
0.36	810.404	415.1021883	36.88131723	415.1021883	0.16	454.742	200.6245178	3.06265493	200.6245178
0.34	764.184	385.9870556	30.07683202	385.9870556	0.14	432.197	187.7915623	2.351163414	187.7915623
0.32	720.331	358.7028517	24.28706833	358.7028517					

Fig. 5 Simplified 3D geometry model for the determination of wheelset mass and inertia properties with different wheel radii
(a) Inventor model (b) obtained values for all wheel radii (in SI units)

3.2 Track setup

The stability assessment requires a straight track with no track irregularities except the excitation to the vehicle required to induce hunting, which is given as a lateral track irregularity described by $y=9\sin(0.2\pi s)$, $s\in$ [25, 50] (s: distance along track in meters; y: lateral track offset in millimeters). It is placed 25m from the beginning of the track, clearing the whole vehicle at simulation start, to avoid causing unwanted wheel-rail penetration during model initialization.

For curve negotiation, wear and wheel-rail contact geometry assessments, an S-curve laid out with consideration for requirements stated in EN 13803:2017 [7] is used. Curves of two radius levels are separately modelled. The radii are chosen from the vehicle acceptance EN 14363:2016 [8]. Table 2 shows parameters of the track layout. The curves are sufficiently long to ensure a good observation of the quasistatic curve passing phase. No track irregularity inputs are given to ensure that all responses of the vehicle are induced only by the curves themselves.

The track gauge and rail cant is variable for both track models to enable switching between the different cases studied. The cases are introduced in Section 4.

Table 2 S-curve track layout

Parameter	Large-radius curve	Small-radius curve	Reference to standards
Radius in round curve / m	750	250	EN 14363:2016 §7.3.1, test categories 2 and 4
Superelevation in round curve / mm	100	133	EN 13803:2017 §6.2
Transition curve length / m	75	58	EN 13803:2017 §6.6

4. CASES STUDIED

To consider track setting variations found in European railways, track gauges are set to vary among values 1435mm, 1432mm and 1430mm (1437mm also planned) and rail cant between no cant and 1:40 for all simulation tests. Furthermore, cases specific to test purposes are considered and introduced below.

4.1 Running on straight track (stability)

The non-linear critical speed of the vehicle specific to the current vehicle-track system with each tested wheel radius of interest is sought. Only the vehicle in the tare condition is considered, as the critical speed is lower for a lighter vehicle whose eigenfrequency is higher. The assessment method used is consistent as is introduced by Polach in [9]. Among the two methods introduced, the method “with single excitation” shown in Figure 6 (a) allows for a readout of the critical speed and is thus primarily used for all test cases. The speeds used for the test range within [50km/h, 120km/h] at an 2km/h interval. The method “without excitation” shown in Fig. 6 (b) is optionally conducted as a rough visualization of the critical speed’s vicinity. This method is not used in the assessment, as no critical speed can be unambiguously determined.

4.2 Running on S-curve (curve negotiability, wear, contact geometry)

As mentioned in Section 3.2, two curve radii are chosen as simulation cases; specifically, they are chosen from Section 7.3.1 of EN 14363:2016, representing "test category 2: large curve radius" and "test category 4: very small curve radius" under vehicle acceptance tests for dynamic behaviour. This choice of radius is meant to provide the investigation with a stronger connection to reality.

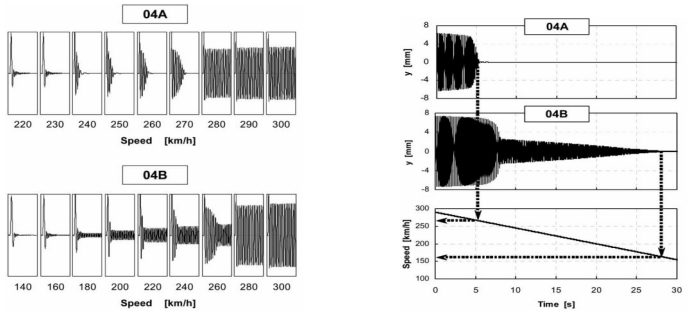

(a) (b)

Fig. 6 Stability assessment methods introduced by Polach
(a) with constant speeds (b) with decreasing speed

Likewise purposed, simulation cases are set up with the vehicle passing each curve with 3 constant speeds that cause the vehicle to have an unbalanced centrifugal acceleration around -0.5m/s^2, 0m/s^2 and 1m/s^2. The three cases represent a negative, a zero and a positive value of superelevation deficiency[1]. Table 3 shows all six combinations of curve radius and centrifugal acceleration.

Table 3 Case settings with different passing speeds for both curves

Scenario description	Parameter	Category 2 curve (750m radius)	Category 4 curve (250m radius)
Slow pass; superelevation excessive	Vehicle speed / (km/h)	38.5	34.75
	Unbalanced centrifugal acceleration / (m/s^2)	-0.5015	-0.4993
	Superelevation deficiency / mm	-76.68	-76.34
Quasi-equilibrium	Vehicle speed / (km/h)	79.75	53.25
	Unbalanced centrifugal acceleration / (m/s^2)	0.0003	0.0032
	Superelevation deficiency / mm	0.07	0.51
Fast pass; superelevation insufficient	Vehicle speed / (km/h)	100	77
	Unbalanced centrifugal acceleration / (m/s^2)	0.9634	0.9579
	Superelevation deficiency / mm	147.33	146.52

Each curve negotiation scenario is assessed with the maximum values of wheel-rail lateral force, track shift force ("sum of lateral forces" in Simpack), and derailment coefficient among all wheelsets of the wagon. Their time history, both filtered with a

[1] Most commonly referred to as "cant deficiency"; here intentionally altered to avoid confusion with "rail cant".

sliding mean filter over 2m windows as required by [8] and unfiltered, as well as the wheelset or wheel at which the maximum occurs are also recorded.
Since the curving simulation settings are more diverse, the wear evaluation is done based on the curving test results for a wider coverage. The T-γ based wear number and the total wear work of the vehicle during the entire curve passing process obtained by summing the integral of each wheel's wear number over their rolling distances.
The curve simulations are also used to assess the geometry of the wheel-rail contact, since the contact point shifts across a much wider region on the wheel during the S-curve passing. This evaluation takes the contact point position, contact patch area and rolling radius difference (abbreviated RRD) of each curve passing case into account.

5. OBSERVED DYNAMICAL BEHAVIOUR IN WHEELS OF VARIOUS RADII

Simulation results obtained so far are already able to indicate that the stability of smaller wheels is significantly worse than larger wheels, as hypothesized. As seen in Fig. 7, with 1435mm gauge and 1:40 rail cant, an original Y25 bogie gives the reference vehicle a critical speed of 88km/h under the current simulation conditions. The critical speed drops 12km/h for every 100mm decreased wheel radius.

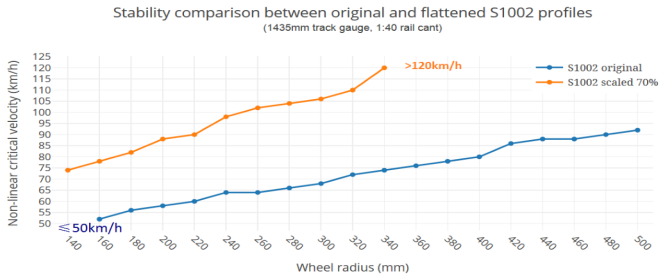

Fig. 7 Non-linear critical speeds observed with different wheel radii

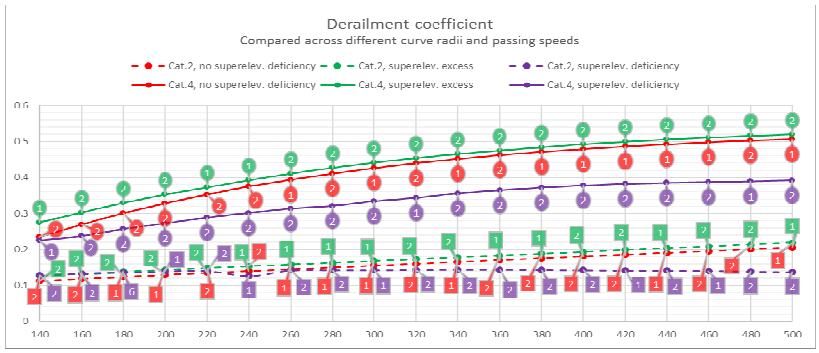

Fig. 8 Observed maximum derailment coefficient as function of wheel radius in all cases involving 1435mm track gauge and 1:40 rail cant. Annotations to data dots indicate which wheel exhibits the largest peak value

Fig. 8 shows the vehicle's derailment coefficient in the S-curve with all 6 cases of curve configuration and passing speed setting combination. The track gauge and rail cant involved remain as above in the stability assessment. Since curve negotiation and stable running on straight track usually have opposite requirements for running gear parameters, the smaller wheels which result in worse stability should perform better in curve negotiation. This is observed with 5 of the 6 simulation cases; however, the difference in derailment coefficient across the tested wheel radius range is not greatly significant and does not cause an excess of the limit for acceptable curving behaviour derived from Nadal's flange climbing criterion, which is 0.8 in normal cases and 1.2 in exceptional cases. The derailment risk is not even observed to consistently reduce with decreasing wheel size in the case of a fast passing of a broad curve (category 2 curve).
When the simulation results for all track gauge and rail cant cases become available, the quantification of dynamical performance decline for reduced wheel sizes will be complete. So far it can be inferred from results with 1435mm track gauge and 1:40 rail cant that the wheel size reduction primarily affects stability and has a less critical effect on curving.

6. COUNTERMEASURES AGAINST PERFORMANCE DECLINE

As a preliminary attempt against the low stability occurring with very small wheels, a profile created by scaling the radial dimension (z-coordinates) of the standard S1002 profile's tread by 70% is given to the reference bogie and simulated along with the S1002 profile for all test scenarios and purposes mentioned above. The flange is not scaled and the transitional gauge corner region is scaled with a factor quadratically transitioning from 1 (unaltered) at the flange end to 70% at the tread end. The stability assessment shown in Fig. 7 already includes results generated with this tread profile. The flatter profile significantly improves the wagon's stability, gaining the critical speed achieved with a 460mm-radius wheel with the standard profile (88km/h) with a much smaller 200mm-radius wheel under the same track settings. The curving derailment risk comparison in Fig. 9 indicates that the tread flattening makes the curving behaviour more sensitive to wheel size reduction to the favour of smaller wheels, whereas the derailment coefficient quickly drops as the wheel radius reduces.

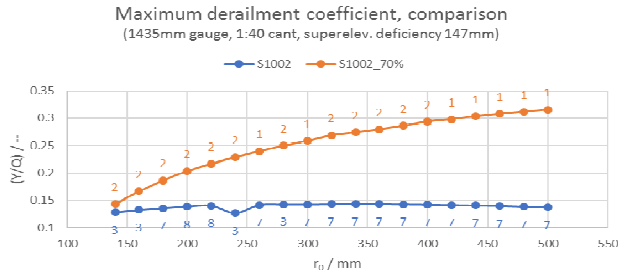

Fig. 9 Comparison of derailment coefficient on 1435mm gauge, 1:40 rail cant track achieved with standard and downscaled tread profiles

This finding infers that smaller wheels benefit more from a flatter tread in terms of both stability and curve negotiability, whereas larger wheels gain a better stability-

curving balance with more slanted profiles. Thus, radius-dependent profile dimension scaling factors are tested. First, the scaling factor is set as the ratio between the current wheel radius and the standard Y25 bogie's wheel radius 460mm. Figure 10 shows these profile forms in comparison. The choice of introducing the positive correlation between scaling factor and wheel radius is thus likely to maintain better consistency in performance across different wheel sizes. Subsequently, as an extreme comparison case, the matching order between the wheel radii and scaling factors are reversed; for instance, the smallest tested wheel with 140mm radius is given a wheel profile with the radial dimension scaled by 500/460 on the tread, originally paired with the largest tested wheel with 500mm radius. The same set of straight-track and S-curve simulations are repeated with both new wheel radius-tread scaling factor matchings.

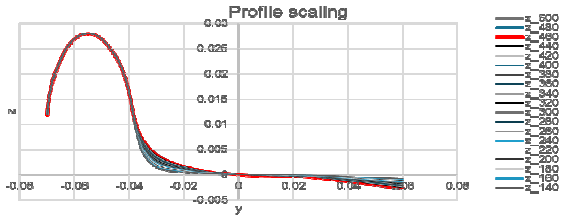

Fig. 10 Wheel profiles scaled from S1002 with radius-dependent factors

Stability simulation results (Fig. 11) show that the profile scaling factor, ultimately the tread conicity, has a greater influence on the stability than wheel radius. A flatter profile results in high critical speed regardless whether a large or small wheel radius is paired with it. On curves, a positive tread scaling factor to wheel radius correlation causes an equalization of maximum derailment coefficient for wheels with radii below 400mm. The derailment risk increases overall, especially for the smallest wheel radii, meanwhile maintaining well below the applicability limit 0.8.

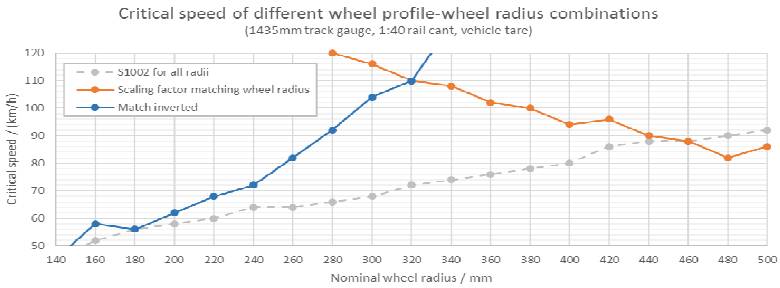

Fig. 11 Simulation results on stability with wheel-radius-dependent tread scaling

Another countermeasure, namely the introduction of a radial steering mechanism, was proposed and is currently undergoing simulation. The Y25 bogie model is simply given cross braces between diagonally located axle-boxes similar to the concept of TVP radial steering bogie series. The whole set of simulations on straight and curved tracks, with all track gauge, rail cant, curve passing speed and wheel profile-wheel radius combinations mentioned above, are repeated with the radial steering bogie model.

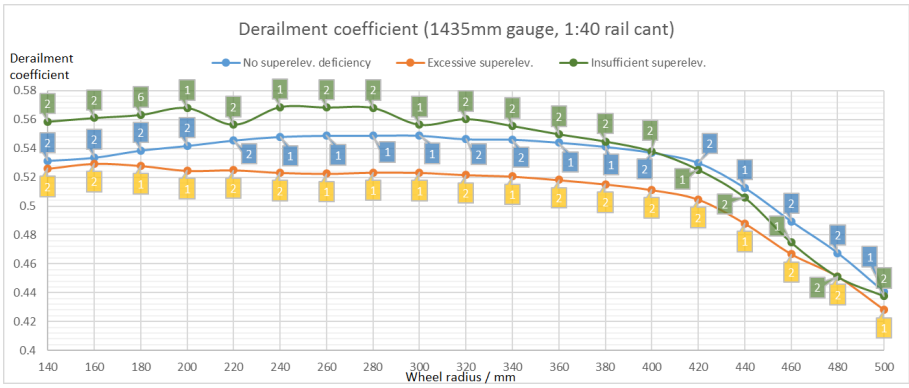

Fig. 12 Derailment coefficient results with wheel-radius-dependent tread scaling, scaling factor and wheel radius positively matched, simulated on category 2 curves

7. CURRENT CONCLUSIONS

- The decrease of wheel radius has a significant worsening effect on stability but a minor improving effect on curve negotiation
- A reduction in tread conicity increases the sensitivity of both stability and curve negotiability indices to wheel radius change
- Proper choice of a reduced tread conicity increases the performance of wheels with very small radii, which has a positive effect for their applicability

8. IMPORTANT PENDING TASKS AND FURTHER VISION

So far among the planned tasks within the scope of this research, wheel-rail contact geometry results for all cases simulated on the S-curve have been generated and are pending evaluation. The total wear work analysis method as described in Section 4.2 fails to consider the different lengths for curves of categories 2 and 4 and causes the results to be incomparable across categories; an alternative evaluation criterion is being considered. The comparison of performance indices with their acceptable limits given in standards is also to be completed in the time to come.

This research can be supplemented with a running dynamics behaviour analysis on tracks with measured irregularities, on-track tests for result confirmation, as well as a better formulated wheel profile design and optimization process.

9. REFERENCES

[1] **Rail Cargo Operator** (2019): Rollende Landstraße 2019. https://rola.railcargo.com/file_source/railcargo/rola/Downloads/ROLA-Brosch uere.pdf

[2] **EN 15273-2:2013**: Railway applications - Gauges - Part 2: Rolling stock gauge.

[3] Page “Rollende Landstraße”. In: Wikipedia (German version). URL: https://de.wikipedia.org/w/index.php?title=Rollende_Landstra%C3%9Fe&oldid=190627900 (accessed September 5, 2019).
[4] **B.P.** (1984): Doppelstockwagen der Zürcher S-Bahn: Stand der Vorarbeiten. In Schweizer Ingenieur und Architekt 102 (23). DOI: 10.5169/SEALS-75476.
[5] **Klingel, J**: Ueber den Lauf der Eisenbahnwagen auf gerader Bahn. In Organ für die Fortschritte des Eisenbahnwesens in technischer Beziehung 20 (4), 16, 1883, p.14-123.
[6] **Hecht, M**. - **Schelle, H**.: Simulation von Kesselwagen mit Y25-Drehgestellen bei Gleislagefehlern (16/2010), 2000
[7] **EN 13803:2017**: Railway applications - Tracks - Track alignment design parameters – Track gauges 1435 mm and wider.
[8] **EN 14363-2016:** Railway applications - Testing and simulation for the acceptance of running characteristics of railway vehicles - Running behaviour and stationary tests.
[9] **Polach, O**.: On non-linear methods of bogie stability assessment using computer simulations. In Proc.IMechE Vol. 220, Part F: J. Rail and Rapid Transit, p.13-27.

DEVELOPMENT OF THE LINKAGE TYPE STEERING BOGIE FOR THE LINEAR METRO

Teruhiko TANIMINE*, Tomofumi TOIDE*, Kazunori IWATO* and Yoshiyuki SHIMOKAWA*

* Railway Bogie Division, Nippon Steel Corporation,
Konohana-ku, Osaka, 554-0024, JAPAN

Received: September 9, 2019

ABSTRACT

The subway has many technical problems through curve negotiation. And a low cost subway in accordance with the transport demand is required. The Linear Metro was developed in Japan as a system of a linear motor driven system. In order to improve curve passing performance, we install a linkage type double-axis steering bogie to actual use for the new train series 2000 for The Linear Metro of Transportation Bureau City of Sendai Tozai Line.

Keywords: railway, vehicle dynamics, steering bogie, lateral force, squeal noise

1. INTRODUCTION

The subway is an important system of public transportation in the city. The subway has many technical problems through curve negotiation because it has a lot of sharp curve sections for reasons of construction. To solve these problems, we developed a single-axis steering bogie with the aim of improving curving performance, and it is adapted as a new vehicles bogie for 3 subway lines and a commuter line in Tokyo, Japan [1,2 and 3].
The subway construction requires large costs and long-term planning. A low cost subway in accordance with the transport demand is required. It was developed as a system of a linear motor driven system, called "Linear Metro" in Japan. The Linear Metro is operated on routes that take advantage of its ability to respond to small tunnel sections and sharp curves. However there are many problems in sharp curve negotiation such as large lateral force and squeal noises.
We had been involved in the development of Linear Metro. Therefore, in order to solve these problems, we install a linkage type double-axis steering bogie SC102 to actual use for the new train series 2000 for Linear Metro of Transportation Bureau City of Sendai Tozai Line (Fig.1, 2). In addition, as the result of field test, it was improved the running safety and reduced the noise than the conventional bogie[4].
In this paper, the previous work with the design concept of the steering bogie, and the outline of linkage type steering bogie for Linear Metro are described.

Fig. 1 Series 2000 for Transportation Bureau City of Sendai Tozai Line

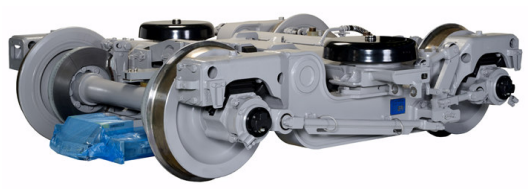

Fig. 2 Double-axis steering bogie SC102

2. DESIGN CONSEPT OF STEERING BOGIE

Fig.3 shows the problems and solutions through curve negotiation. In a sharp curve, increasing lateral force causes various problems such as vibration, squeaking noise, flange noise, wheel flange wear and rail wear. To prevent these problems, lubrication control is applied to the outer and inner rail. And the application of friction modifiers is also effective.

However, lubrication control is difficult to manage because it is easily affected by the external environment such as the weather. Therefore, we started the development of a steering bogie as a comprehensive measure against problems in sharp curve negotiation. And we designed single-axis steering bogie SC101 for the Series 1000 for Tokyo Metro Ginza-Line.

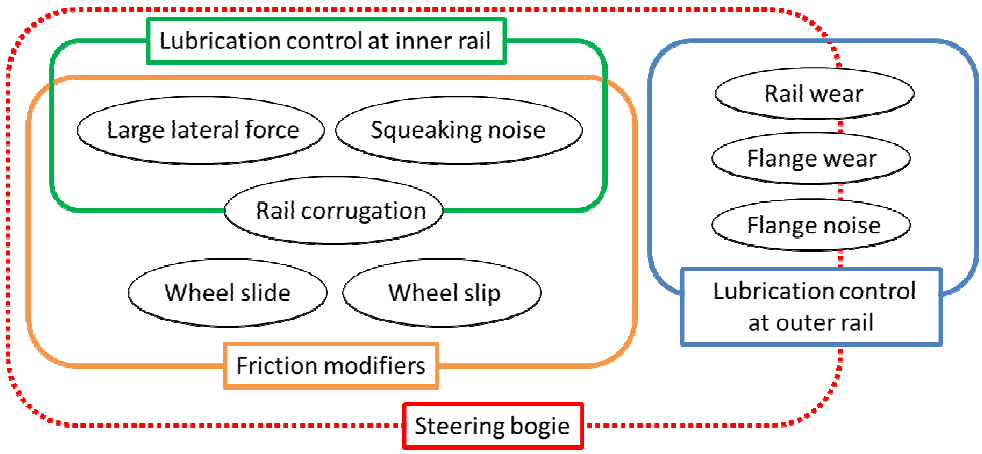

Fig. 3 problems and solutions through curve negotiation

3. OUTLINE OF SINGLE-AXIS STEERING BOGIE SC101

SC101 steers a rear wheelset in a front bogie and a front wheelset in a rear bogie as shown in Fig.4. On the other hand, a front wheelset in a front bogie and a rear wheelset in a rear bogie are non-steering. Fig.5 shows the exterior of SC101.

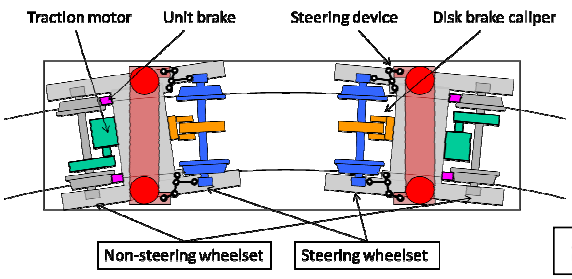

Fig. 4 Arrangement of steering wheelsets

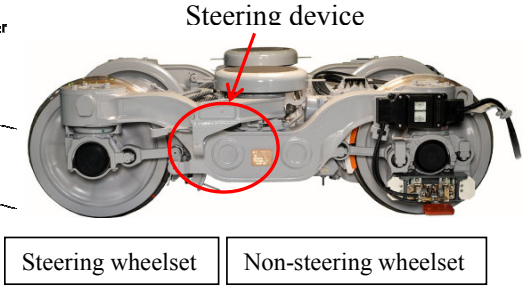

Fig. 5 Exterior of SC101

The behavior of non-steering bogie in curve is shown in Fig.6. Because the posture is under-steer in sharp curve, a front wheelset has a certain level of attack angle. That

generates lateral creep force directed to outer side of a curve at interface between front axle wheels and rail. Moreover, because a rear wheelset locates near the center of bogie, the difference of diameter is insufficient. That generates longitudinal creep force at interface between rear axle wheels and rail. And that force exert as anti-steering moment. Therefore high lateral force is produced at interface between an outer wheel flange of a front wheelset and rail (see Fig.4).

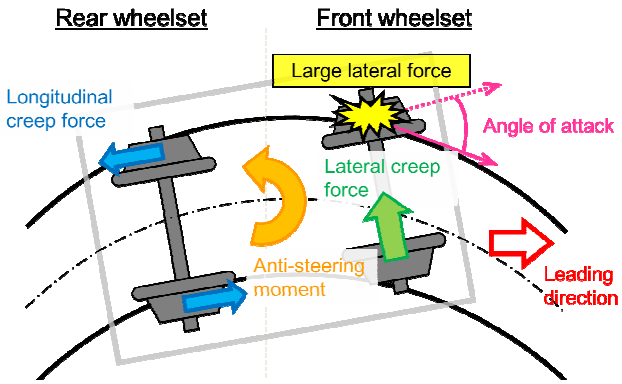

Fig. 6 Behaviour of non-steering bogie in sharp curve

In a front bogie, a rear wheelset is steered to outer side of a curve as shown in Fig.7. That means an attack angle of a rear wheelset increase. This causes the increase of lateral creep force at rear axle wheels and rail. And a rear wheelset moves to outer direction. Therefore, the longitudinal creep force at a rear wheelset reduce because difference of wheel diameter increase. In addition, the movement of rear wheelset to outer direction leads the increase of a bogie angle, and bogie position transitioned understeer to radial-steer. The improvement of bogie position decreases the attack angle at front wheelset that is not directly steered. In the result, both the lateral creep force at front wheelset and the longitudinal creep force at rear wheelset reduce. That leads the decrease of lateral force at the outer wheel of front axle.

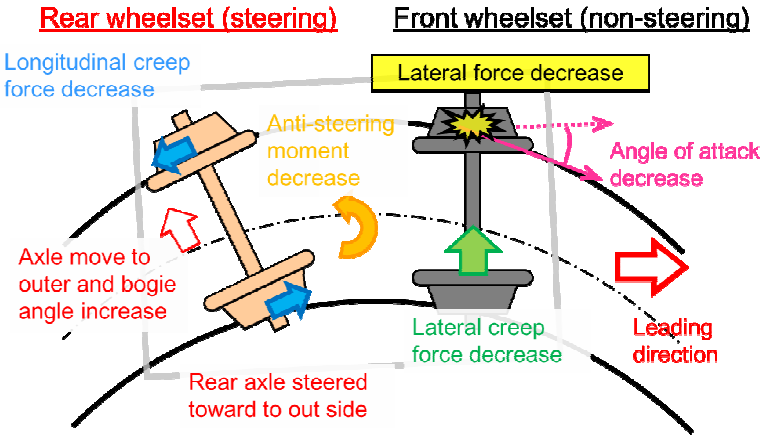

Fig. 7 Behaviour of single-axis steering bogie in front side of a vehicle in sharp curve

In a rear bogie, a front wheelset is steered to inner side of a curve as shown in Fig.8. That means an attack angle of a front wheelset is decreased. This causes the decrease

of lateral creep force at front wheelset. Therefore, the lateral force at outer wheel is reduced.

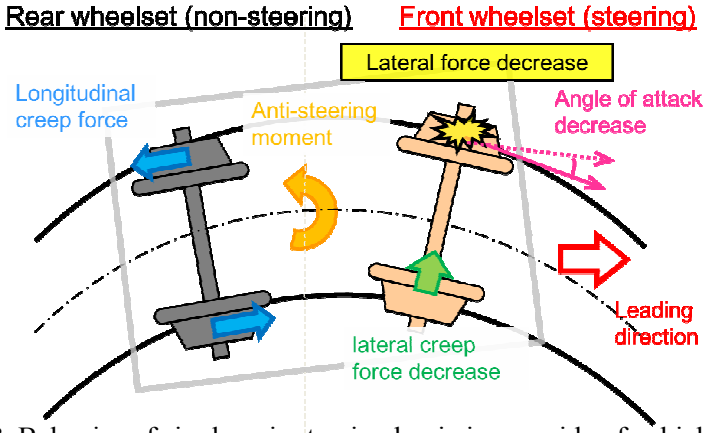

Fig. 8 Behavior of single-axis steering bogie in rear side of vehicle in sharp curve

4. OUTLINE OF STEERING BOGIE FOR LINEAR METRO

4.1 About Linear Metro

The Linear Metro started in 1990 with the opening of Japan's first Linear Metro line on Tsurumi-ryokuchi Line of Osaka Metro, and then opened in five cities. Unlike the conventional rotary motor, the linear motor, as its name implies, produces tractions and brakes through linear motion rather than rotary motion. The conventional motor drives a vehicle forward using the rotational force of the wheel via a gear and the appropriate friction between the wheel tread and the rail. On the other hand, linear metro is driven by the interaction of magnetic force between flat linear motors directly mounted to the bogies and the reaction plates laid in the center of rails and attached to the sleepers (see Figs.9, 10).

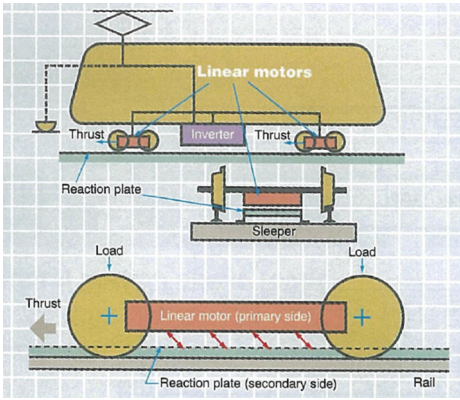

Fig. 9 Drive system of Linear Metro

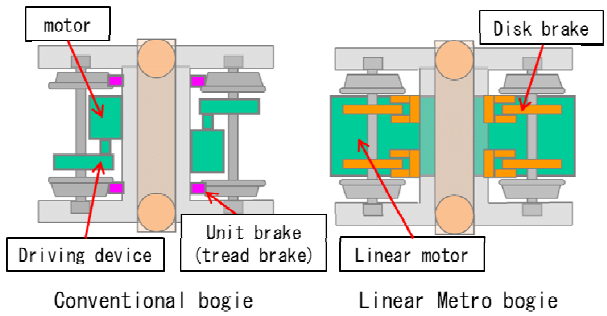

Fig. 10 Comparison of bogie configuration

Therefore, the floor height of vehicles can be lowerd relatively compared to the conventional bogie. Accordingly, the tunnel cross section area and the cost of tunnel construction can be reduced as shown in Fig. 11 [5,6 and 7].

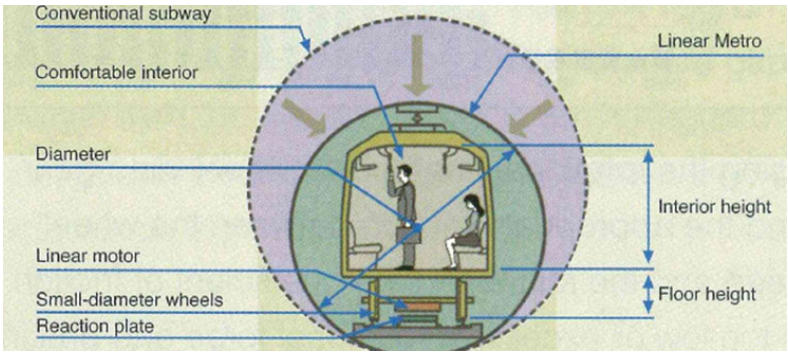

Fig. 11 Comparison of tunnel cross section area

4.2 Outline of double-axis steering bogie SC102

As previously described, the bogie for Linear Metro is driven by linear motor instead of a motor and driving device. This device configuration is not easily affected by each wheelset displacement. Therefore, the steering bogie for Linear Metro can be equipped with a steering devise on each wheelset s.

SC102 steers rear and front wheelset in each bogie as shown in Fig.12. Fig.13 shows the exterior of SC102. The steering device is comparatively small, low cost, and simple maintenance. For example, mass of steering device in SC102 is less than 150kg.

The bogie angle linked steering system is adopted to SC102 as shown in Fig.14. The steering device connects between a bogie frame, a bolster and an axle box by mechanical linkage. It can steer an wheelset in proportion to a bogie angle. Basically, the wheelset s are steered only when a vehicle runs a curve. And the direction of steering is mechanically determined by the yawing direction of bogie. Therefore, the possibility of opposite steering or miss steering is practically naught.

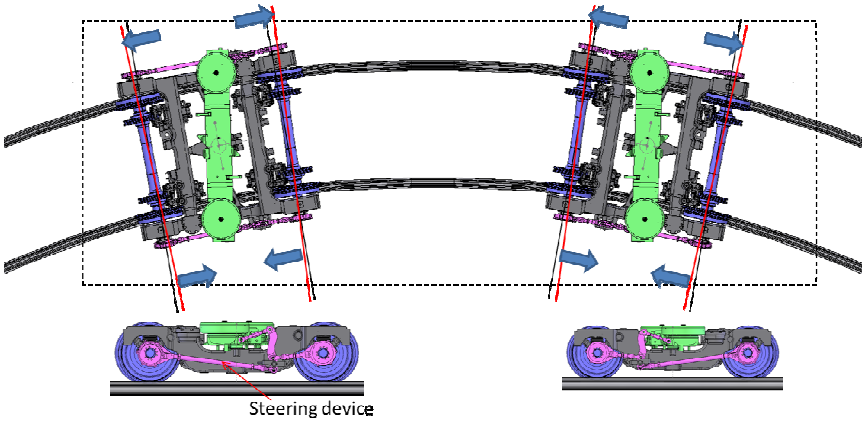

Fig. 12 Steering wheelset movement in curve

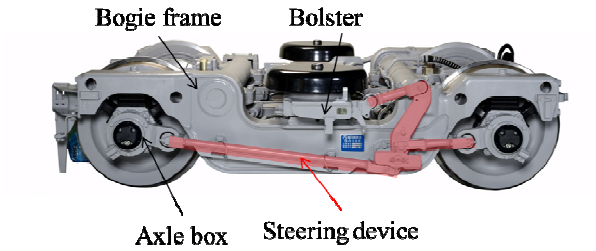

Fig. 13 Exterior of SC102

4.3 Outline of the behavior of double-axis steering bogie

The behavior of double-axis steering bogie in curve is shown in Fig.14. In addition to steering of rear wheelset shown in Fig.7, the front wheelset is steered along a curve. Therefore, the attack angle of the front wheelset is further decreased. In this result, the lateral creep force at front wheelset reduce, and the anti-steering moment is further decreased. That leads the decrease of the lateral force at the outer wheel of the front axle decreases.

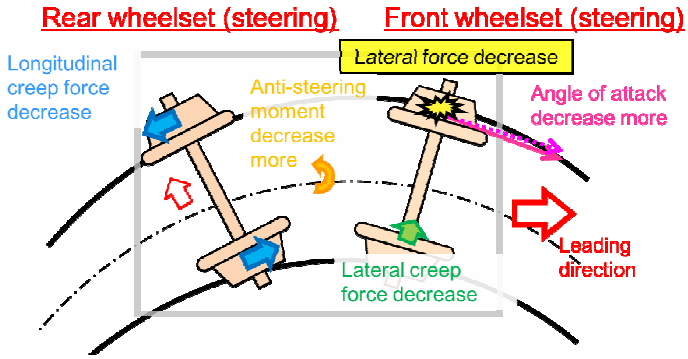

Fig. 14 Behaviour of double-axis steering bogie in sharp curve

5. EVALUATION OF CURVING PERFORMANCE OF DOUBLE-AXIS STEERING BOGIE

5.1 Field test condition

To confirm the running safety and noise reduction effect by linkage type steering bogie for The Linear Metro, the field test was done on Tozai line of Transportation Bureau City of Sendai from February to August 2015. In addition, to evaluate effectiveness of steering system, the test was done in the case that the linkage type steering bogie was converted to non-linkage conventional one (Fig.15).

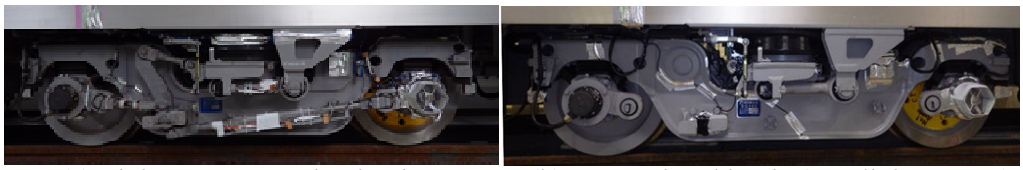

(a) Linkage type steering bogie (b) conventional bogie (non-linkage type)

Fig. 15 Exterior of test bogie

5.2 Test results

Lateral force at a front wheelset in a front bogie in the curve with radius 165 meter is shown in Fig.16. Compared to conventional bogie, steering bogie shows lower lateral force while runnning circular curve area. The decrease ratio is about 50 percent at circular curve.

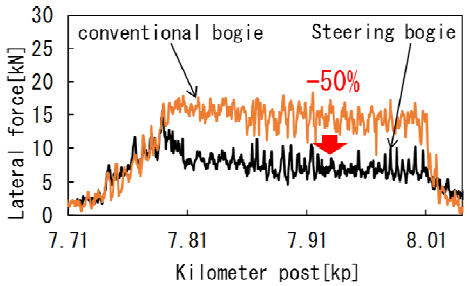

Fig. 16 Lateral force at outer wheel of front axle in front bogie (R=165m)

Lateral force at front wheelset in both front and rear bogie in a number of curves that have various radiuses is shown in Fig.17. This shows that the steering system can reduce a lateral force regardless of a radius of curve.

The attack angle of the front wheelset is shown in Fig.18. This shows that the attack angle is less than 10mrad even while running sharp curve with radius 105m. And, compared to conventional bogie, steering bogie shows lower attack angle. The yaw angle of the bogie is shown in Fig.19. Compared to conventional bogie, steering bogie shows lower yaw angle.

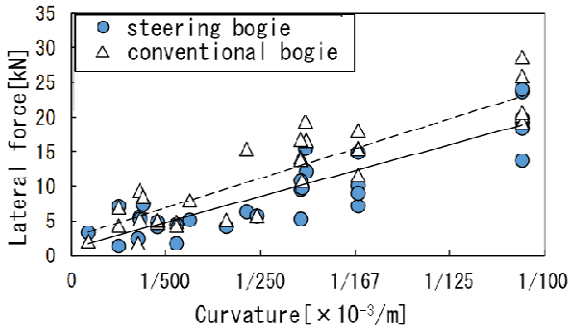

Fig. 17 Comparison of lateral force at outer wheel of front axle in front bogie

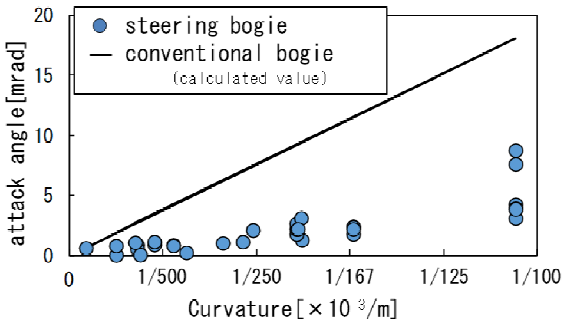

Fig. 18 Comparison of attack angle of the front wheelset

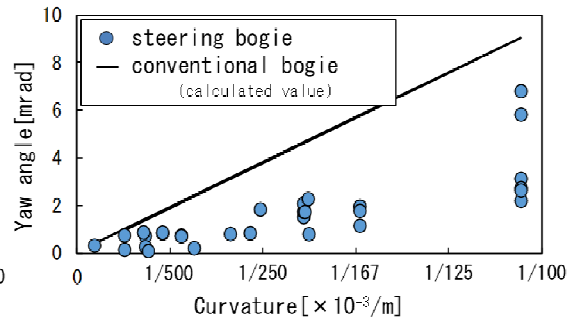

Fig. 19 Comparison of yaw angle of the bogie

This means that the bogie position of the steering bogie is improved to radial-steer. From these results, it is confirmed that the steering bogie reduces lateral force by the mechanism described in Section 4.3.

The in-vehicle noise measurement result while runnning sharp curve is shown in Fig.20. The noise level of any bogie is less than 60 dB at 3,000 Hz and higher, but there is a noticeable difference below 2000 Hz. And, the noise level reduction of more than 20 dB is confirmed by the linkage type steering bogie.

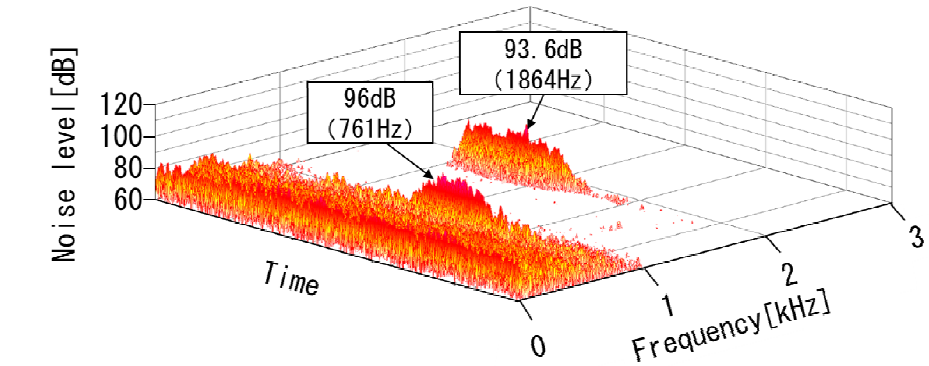

(a) Conventional bogie

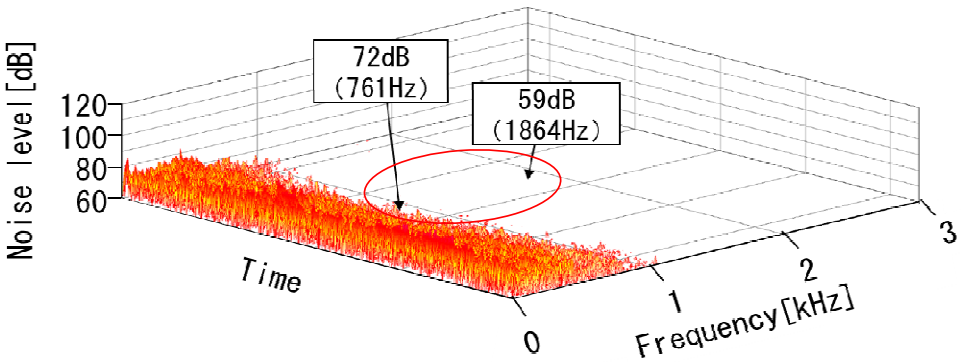

(b) Steering bogie

Fig. 20 Frequency analysis of in-vehicle noise

6. CONCLUSIONS

In order to solve various problems in sharp curve negotiation , we install a linkage type double-axis steering bogie to actual use for The Linear Metro of Transportation Bureau City of Sendai Tozai Line. In addition, as the result of field test, it was improved the running safety and reduced the noise than the conventional bogie. Based on these results, The Linear Metro of Transportation Bureau City of Sendai Tozai Line was opened on December 6, 2015, and it has been operated now. Hereafter, we will investigate rail and wheel wear suppression and energy saving effects by long-term use, and promote the actual use of linkage type steering bogie for The Linear Metro.

7. REFERENCES

[1] **Iwamoto, A. - Umehara, Y. - Shimomura, Y. - Ogino, T. - Shikata, K. - Mizuno, M. - Kikko, S. - Shimokawa, Y. - Nakai, T.**: Development of the new concept steering truck, Proc. the J-Rail 2010, 2010, p.191-194.

[2] **Togami, A. - Goto, Y. - Ogino, T. - Toide, T. - Mizuno, M. - Shimokawa, Y.**: Development of the new concept steering truck, Proc. the J-Rail 2012, 2012, p.73-76.

[3] **Togami, Y. - Goto, R. - Ogino, T. - Shikata, K. - Hagio, Y. - Toide, T. - Mizuno, M. Kikko, S.**: Development of the new type steering bogie. Proc. of the 9th International Conference on Railway Bogies and Running Gears, (Ed. by Prof. I. Zobory) BME Department of Railway Vehicles, Aircraft and Ships, Budapest, 2014, p.57-63.

[4] **Toide, T.- Iwato**, **K**.: Development of the linkage type steering bogie for The Linear Metro of Transportation Bureau City of Sendai Tozai Line. Rolling Stock and Technology, Rail & Tech. Publishing Co. Ltd., No.232, 2015. (p.2-6)

[5] **Japan Subway Association.**: Linear Metro System, 2004.

[6] **Japan Subway Association.**: Smart Linear Metro (New Linear Motor Railway System), 2014.

[7] **Japan Overseas Railway System Association.**: Series 2000 Linear Metro Trains for Sendai Subway Tozai Line. Japanese Railway, 2013.

VIBRATION OF FRICTION BRAKE SYSTEMS – MODELLING AND ATTENUATION

István NÉMETH

Department of Railway Vehicles, Aeronautics and Naval Arcitecture
Faculty of Transportation Engineering and Vehicle Engineering
Budapest University of Technology and Economics
H-1521 Budapest, Hungary
inemeth@vrht.bme.hu

Received: September 12, 2019

ABSTRACT

In this article simplistic mechanical models of the frictional brake system are set up by considering only a few degree of freedom of the system, but incorporating non-linear effects such as the friction characteristics and the inclination angle of the suspension link. Brake vibrations generate structural vibrations, as well as air-born noise and thereby affect ride comfort of passengers, wear and durability of the brake components, and not least have a contribution to the noise emission of the vehicle. From this follows that it is essential to avoid or more realistically at least attenuate railway brake noise and vibration. Many publications demonstrate that the vibration and noise of frictional brake systems is basically a self-induced vibration, which can be described as an instability of the equilibrium state of the system. The instability of the system is generally explained by the falling characteristic of the friction coefficient vs sliding velocity. The approach of this investigation is to keep the model degree of freedom small, but reproduce some nonlinear effects, such as inclined hanger iron and clearances of the suspension link in order to gain better understanding of the emergence of brake vibration, and develop strategies for its avoidance. The influences of stiffness, damping, and non-linear effects are examined.

Keywords: friction, brake vibration, stability criteria, clearance

1. INTRODUCTION

Brake vibrations generate structural vibrations, as well as air-born noise and thereby affect ride comfort of passengers, wear and durability of the brake components, and not least have a contribution to the noise emission of the vehicle. From this follows that it is essential to understand the brake vibration mechanism to be able to avoid or more realistically at least attenuate railway brake noise and vibration.

Several publications demonstrate that the vibration and noise of frictional brake systems is basically a self-induced vibration, which can be described as an instability of the equilibrium state of the system [1], [2]. The instability of the system is generally explained by the falling characteristic of the friction coefficient vs sliding velocity. In a previous preliminary work the vibration of a bogie with disk brake system was investigated [3], including parameter studies on some bogie parameters, like bogie frame inertia, primary and secondary suspension stiffness and damping, and so on. Experiments and everyday observations show, however, that sometimes brake vibration of in service vehicles appear and disappear seemingly in a random way during operation, therefore the phenomenon is supposed to be more complex and nonlinear.

The approach of the investigation is to keep the model degree of freedom small, but reproduce some nonlinear effects, in order to gain better understanding of the emergence of brake vibration, and develop strategies for its avoidance. The influences of stiffness, damping, and non-linear effects are examined.

2. THE OBJECT OF THE INVESTIGATION

The object of this study is the block brake system commonly used in freight wagons, see Fig. 1. The traditional standard material of the brake blocks is the so called P10 or P14 cast iron with a phosphor content of 1%, respectively 1.4%.

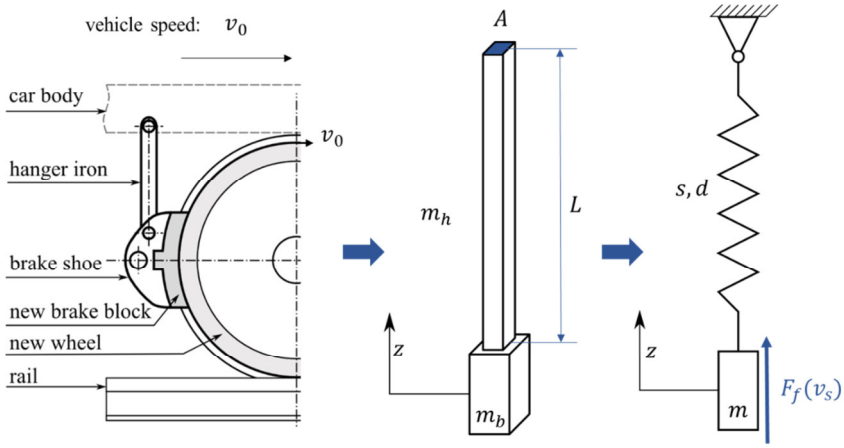

Fig. 1 Block brake system and its one degree of freedom model

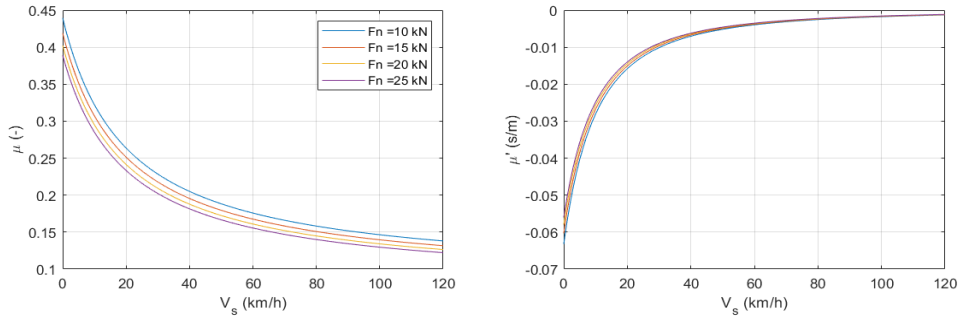

Fig. 2 Friction coefficient and the derivative of the friction coefficient by the sliding velocity vs. sliding velocity for P10/P14 phosphorous cast iron brake blocks at four different F_n normal force values

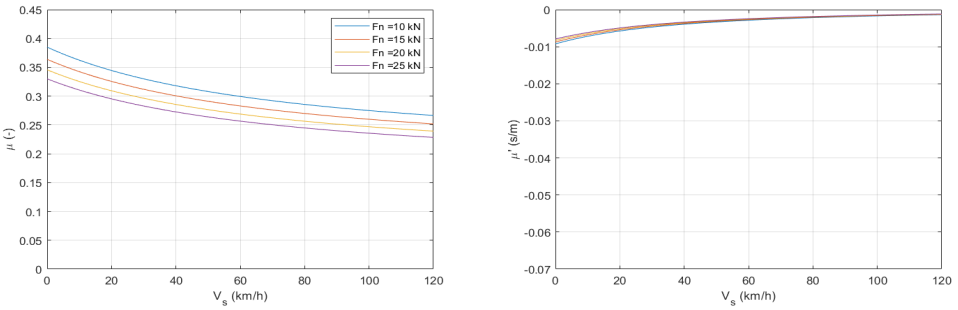

Fig. 3 Friction coefficient and the derivative of the friction coefficient by the sliding velocity vs. sliding velocity for a typical composite brake block material

The friction characteristics of cast iron brake blocks, i.e. $\mu(v_s)$ friction coefficient and its $\mu'(v_s)$ derivative by the v_s sliding velocity are described by Karwatzki's empirical law, which also accounts for the dependence on normal force F_n, see Fig. 2. For comparison, Fig. 3 shows the friction characteristics of a typical composite material.

3. FRICTION INDUCED VIBRATION OF THE BLOCK BRAKE

The equation of motion of the simplified one degree of freedom model shown on the right hand side of Fig. 1 is $m\,\ddot{z} + d\,\dot{z} + s\,z = F_f(v_s)$, where $v_s = v_0 - \dot{z}$ is the sliding velocity between brake block and running surface of wheel, and $F_f(v_s)$ is the friction force between them, Furthermore, m is the equivalent mass of suspension link, brake shoe and brake block, and s and d denote stiffness and damping of the suspension link, respectivelly. By linearizing the model at the $\bar{z}$ equilibrium displacement, and introducing the new $q = z - \bar{z}$ variable for small displacement around the stationary point the equation of motion reads as

$$m\,\ddot{q} + \underbrace{\left(d + \frac{\partial F_f(v_s)}{\partial v_s}\Big|_{\dot{q}=0}\right)}_{\eta}\dot{q} + s\,q = 0 \tag{1}$$

The linear system shows stable behaviour only if total damping $\eta = d + F_f'(v_0)$ is positive, othervise it is unstable, i.e. if the total damping is negative, then even small disturbances can cause an excessive vibration. Negative total damping results from negative slope of the friction coefficient, hence the stability criterion can be formulated as follows: the system is stable if the damping of the suspension link

$$d > F_f'(v_0) = -F_n \cdot \mu'(v_0) \tag{2}$$

Material damping is usually considered by the D damping ratio (or Lehr's damping), which expresses the level of system damping relative to the d_{crit} critical damping. The suspension link – as a first approach – can be modelled simply by steel bar, see Fig. 1 above. The damping ratio of the steel suspension bar is set to $D = 0.3\%$ in this investigation, although literature date vary to some extent. It is demonstrated, that the model parameters m, s and d are not independent in this particular system, because setting the cross sectional area A and length L of the steel bar determins all three model parameters. The available vertical space is generally determined by the construction, therefore the length of the suspension link is set to the arbitrary value of $L = 500\,mm$, hence there remains only one free *„design parameter"*, which is choosen to be the s stiffness instead of the cross sectional area. It means that functional relationships are established between the three model parameters, since m mass and d damping can be expressed as a function of s stiffness, see detailed data and derivation in the box of Fig. 4.

Now the question is: how to chose the design parameter s stiffness to ensure a stable system behaviour? Equation (2) gives us the criterion for the required damping, hence the expression for damping in Fig. 4 must be inverted to answer the question. In this way we get a new practical stability criterion regarding the required suspension stiffness:

$$s > \frac{-m_b + \sqrt{m_b^2 + \frac{1}{3}\left(\frac{L F_n \mu'(v_S)}{c D}\right)^2}}{\frac{2}{3}\left(\frac{L}{c}\right)^2} \tag{3}$$

where $c = \sqrt{\frac{E}{\rho}}$ is the wave propagation speed in steel. Numerical results for cast iron brake block is plotted in Fig. 5.

Suspension link (hanger iron) data:

Density: $\rho = 7850 \frac{kg}{m^3}$

Young-modulus: $E = 210\ GPa$

Damping ratio: $D = 0.003$

Length: $L = 500\ mm$

Stiffness: $s = \frac{A\,E}{L}$: design parameter

Cross sectional area: $A = \frac{L}{E} \cdot s$

Suspension link mass: $m_h = \rho A L = \frac{\rho}{E} \cdot L^2 \cdot s$

Eigenfrequency of the longitudinal vibrations:

$$\omega_0 \approx \sqrt{\frac{s}{m_b + \frac{m_h}{3}}} = \sqrt{\frac{s}{m}}$$

Modell mass:

$$m = m_b + \frac{m_h}{3} = m_b + \frac{1}{3}\frac{\rho}{E} L^2 s$$

Damping:

$$d = D \cdot d_{crit} = D \cdot 2 \cdot \sqrt{m\,s}$$

$$d = 2D \cdot \sqrt{m_b\, s + \frac{1}{3}\frac{\rho}{E} L^2 s^2}$$

Fig. 4 Establishing relationship between the model parameters *m*, *d* and *s*

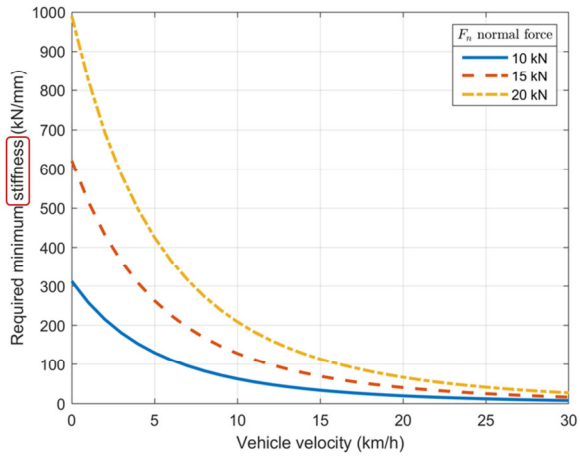

Fig. 5 Required minimum stiffness of the suspension link in case of cast iron brake blocks

4. EFFECT OF INCLINED SUSPENSION LINK

In this section the inclination angle of the hanger iron on the stability of the vibrating system is investigated. Even if the hanger iron of the block brake system is tipically vertically aligned in a 'design state', i.e. when new brake block is paired with new wheel, the orientation of the hanger iron gets inclined as the wear of the friction parts evolvs, see Fig. 1.

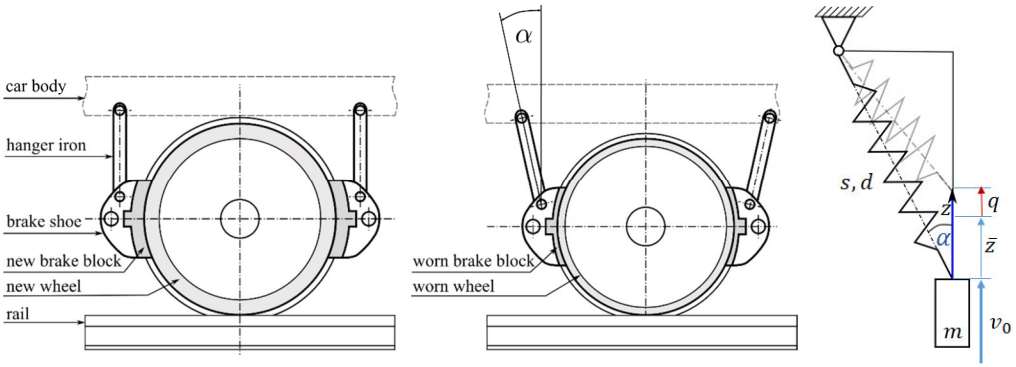

Fig. 6 Block brake with new and worn friction parts and its model

In some cases the hanger iron has a non-zero initial inclination angle in the 'design state', as well. The L length of the hanger iron is usually in the range of 200 to 600 mm, constrained mainly by the wheel diameter. The wear allowance of the brake block is about 50 mm, and that of the wheel radius is ca. 40 mm, hence the wear caused horizontal displacement of the lower pin of the hanger iron is ca. 90 mm, which in extreme case produces an α inclination angle up to 25°. If we consider some initial inclination angle, the theoretically interested range of angle α stretches up to 45°.

The vertical displacement z of the brake block is the only degrre of freedom of the model. At first, the stiffness characteristics from vertical displacement to vertical and to horizontal forces are considered by employing the $s_{zz} = s \cdot \cos^2 \alpha$ and $s_{xz} = s \cdot \cos \alpha \cdot \sin \alpha$ equations respectively, where s is still the spring stiffness of the hanger iron along its axis. Damping is modelled in a similar way, and coupled parallel to the spring. After that, the equation of motion of the system is set up:

$$m\,\ddot{z} = (F_c + s_{xz}\,z + d_{xz}\,\dot{z})\mu(v_s) - s_{zz}\,z - d_{zz}\,\dot{z}, \tag{4}$$

where F_c is the normal force actated by the pneumatic cylinder on the brake block. A cross coupling between frictional force and resultant normal force due to the alignment of the hanger iron can already be seen from eq. 4. The following step is the linearization of the system around the equilibrium point $\bar{z} = \frac{F_c}{s} \cdot \frac{\mu}{\cos^2 \alpha \cdot (1 - \mu \tan \alpha)}$, where the equilibrium friction force is $\bar{F_f} = \frac{\mu}{1 - \mu \tan \alpha} F_n$, with μ friction characteristics depending on vehicle velocity, normal force, etc. After linearizing the eq. (3) at the stationary point $\bar{z}$ we get

$$m\,\ddot{q} + [d_{zz} - d_{xz}\mu(v_0) + (F_c + s_{xz}\,\bar{z})\mu'(v_0)]\,\dot{q} + [s_{zz} - s_{xz}\,\mu(v_0)]\,q = 0$$

or by substituting the expressions depending on α inclination angle into the differential equation

$$m\,\ddot{q} + \eta\,\dot{q} + \gamma\,q = 0\ ,$$

where the system damping is

$$\eta = \underbrace{(\cos^2\alpha - \cos\alpha\ \sin\alpha\ \mu(v_0))}_{f_1}\,d\ + \underbrace{\frac{1}{1-\tan\alpha\ \mu(v_0)}}_{f_2} F_c\,\mu'(v_0)\ ,$$

and the system stiffness is

$$\gamma = (cos^2\,\alpha - cos\,\alpha\,sin\,\alpha\,\mu(v_0))\,s\ .$$

The dynamic system is stable if the system damping is positive, i.e.:

$$\eta = f_1 d + f_2\,F_c\,\mu'(v_0) > 0\ ,$$

or by rearranging the above inequality, the stability criterion for the required damping reads as follows

$$\boxed{d > -\frac{f_2}{f_1}\,F_c\,\mu'(v_0)} \tag{5}$$

Fig. 7 shows the $\frac{f_2}{f_1}$ gain of the required damping depending on the α inclination angle relative to the vertically aligned suspension link. It can be seen, that at $\alpha = 25°$ the required damping is almost *doubled*.

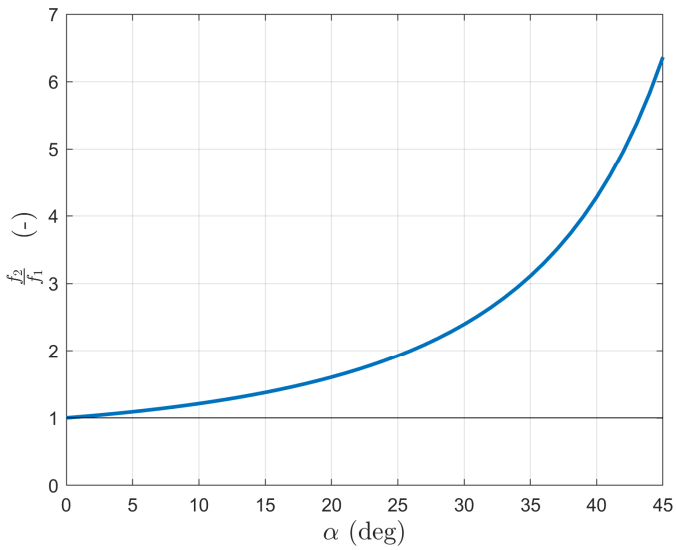

Fig. 7 Gain of the required damping vs. inclination angle of the suspension link

5. EFFECT OF BACKLASH IN THE SUSPENSION

In a further step the clearances (or backlash) in the suspension system, such as those between hanger iron, pins and sleeves are modelled as a single clearance according to Fig. 8. The non-linear visco-elastic force characteristics of the clearance model is plotted on the left hand side of Fig. 8, where the excitation was a symmetric periodic triangle-shaped displacement signal.

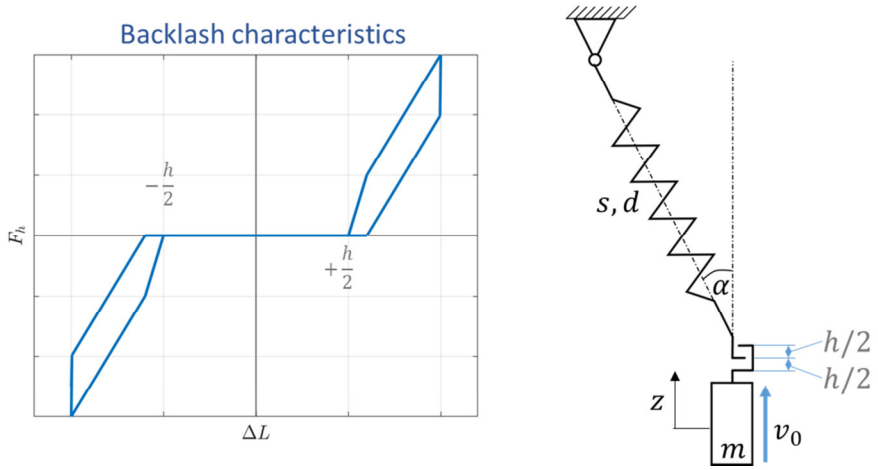

Fig. 8 Characteristics and arrangement of the modelled clearance

By the aid of the non-linear model a parametric study was carried out in order to analyse the influence of vehicle speed v_0, inclination angle α and clearance h on the system stability. The parameters were varied in the following ranges: $v_0 = 10 \ldots 60$ km/h, $\alpha = 0° \ldots 30°$ and $h = 0 \ldots 1$ mm. Fig. 9 a) and b) illustrate *phase portraits* of the model at lower and at higher vehicle speeds, respectively. The *Poincaré map* techniquie is adopted at maximum positive velocity of the brake block in steady state as depicted by the cutting plane in Fig. 9 b). Fig. 10 shows the summary of the parametric study, where it is to be noticed that a so called *'pitchfork bifurcations'* arise at non-zero clearances. The larger the clearance, the more significant the *'pitchfork bifurcation'*. The joint influence of α inclination angle is not so obvious, but in fine, the bifurcation can arise at all angles, including zero degree.

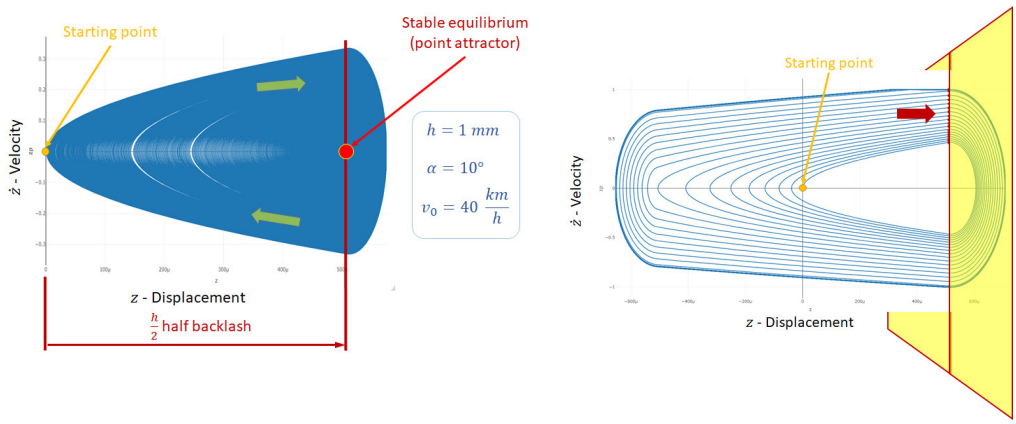

a) Point attractor at higher vehicle speed b) Limit cycle at lower vehicle speed

Fig. 9 Phase portraits of the model

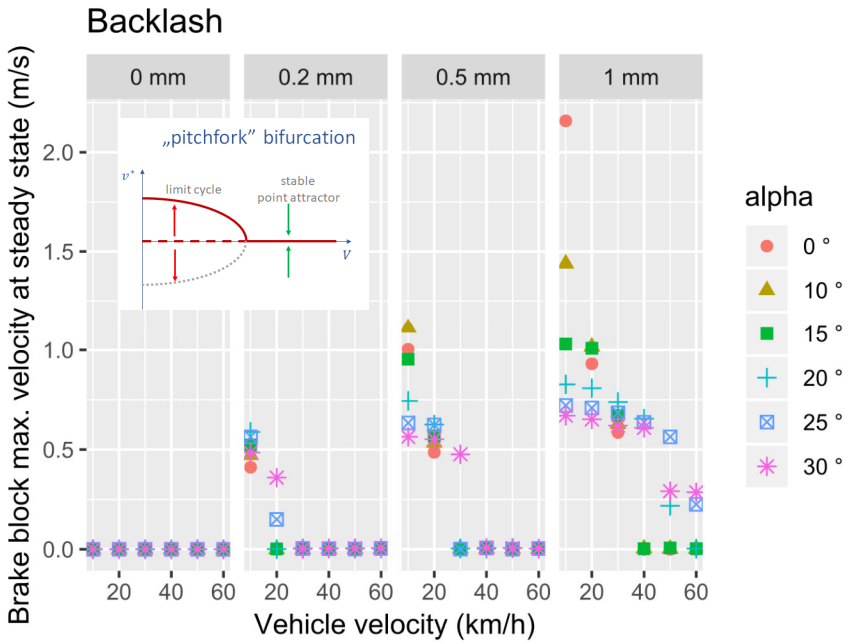

Fig. 10 Overview of the parametric study exhibiting 'pitchfork bifurcation'

8. CONCLUDING REMARKS

On the basis of the theoretical investigations and numerical simulations, the following conclusions can be drawn:

- By applying enough positive *damping*, the friction induced vibration could be eliminated;
- Stability criterion based on the *stiffnes* of suspension link is established;
- Positive *α inclination angle* of the suspension link increases the amount of negative damping;
- Inclined suspension link can generate an unstable behaviour, even if the brake system is stable with vertically aligned suspension link;
- *Backlash* between brake block and suspension link can lead to limit cycle, i.e. to a steady state vibration, even if the brake system is stable without backlash.

9. REFERENCES

[1] **Zobory, I.:** Investigation into the vibration phenomena of the disc-brake system of a railway bogie, Technical Report, Technical University of Budapest, Faculty of Transportation Engineering, Department of Railway Vehicles, 1997. (in Hungarian)

[2] **Papinniemi, A. – Lai, J.C.S. – Zhao, J. – Loader, L.:** Brake squeal: a literature review. Applied Acoustics 63, 2002, p.391–400.

[3] **Németh, I.:** How to avoid dynamical instability in disc-brake systems by using additional linear damping. Proceedings of the 16th MINI Conference on Vehicle System Dynamics, Identification and Anomalies, VSDIA 2018. (Ed. By Prof. I. Zobory). BME ITS nonprofit Co., Budapest 2020. p.131-142.

TRACK QUALIFICATION METHOD USING SYSTEM DYNAMICS BASED PARAMETER IDENTIFICATION PROCEDURE

Zoltán ZÁBORI and **István ZOBORY**

Group of Railway Vehicles and Vehicle System Analysis
Faculty of Transportation Engineering and Vehicle Engineering
Budapest University of Technology and Economics
H-1521 Budapest, Hungary

Received: September 10, 2018

ABSTRACT

A Track Qualifying Vehicle using a system dynamics based measurement evaluation method has been developed at the Department of Railway Vehicles at the Budapest University of Technology and Economics (BME). The measured vertical and the lateral accelerations of the measuring wheelset-carrier-frame contain higher frequency components due to the vibrations of the elastic vehicle components. This paper presents a simulation based identification procedure for determining the inhomogeneities in the vertical track stiffness along the track. The necessary smoothing of the measured acceleration signals is also dealt with. The measuring wheelset together with its close environment is modelled as a lateral in-plane dynamical system supported by the right- and left rails where the rails are modelled as an Euler-Bernoulli beam supported by non-homogeneous Winkler foundation subjected to moving time dependent load. Time-domain technique is applied by using the *Galerkin* method to find the numerical solution of the governing partial differential equation describing the vertical the rail motion. The dynamical system model of the complete measuring system consists of discrete and continuous sub-systems. The *Galerkin* method enables the discrete-continuous system to be managed in a unified way. The effect of foundation parameters such as, stiffness and damping modulus on dynamic deflection and bending moment responses were also investigated for the case of a moving measuring wheel-set of constant load at constant speed. The parameter identification has been traced back to the minimisation in *Sobolyev*-norm of the deviation of the measured and simulated accelerations on the measuring frame over the axle boxes of the measuring wheel-set. Numerical results obtained from the study are presented and discussed. The method described contributes to the reliable estimation of the inhomogeneity in the ballast stiffness and damping parameters along the track, thus the necessary track maintenance actions can be reliably planned.

Keywords: Railway track qualification, system dynamics, parameter identification, *Sobolyev*-norm

1. INTRODUCTION

A railway track qualifying vehicle using a system dynamics based measurement evaluation method was developed at the BME over the last decade.

- The measured signals of the vertical and the *lateral accelerations* of the measuring wheelset-carrier-frame *contain* higher frequency *disturbance components* due to the vibrations of the elastic vehicle components [1]
- This paper presents a simulation based identification procedure for determining the variations of the vertical track stiffness under the rails along the track [4]. The necessary smoothing of the measured acceleration signals is also dealt with. The right- and left rails are modelled as *Euler-Bernoulli beams* supported by a *non-homogeneous Winkler foundation* subjected to a moving, time dependent load. Time-domain technique is applied by using *Galerkin*'s method for finding the numerical solution of the governing set of partial differential equations [7].
- The dynamical system consists of *discrete and continuous sub-systems*. The *Galerkin* method makes it possible to manage the discrete-continuous system as a *unified finite dimensional system*.
- The effects of longitudinal variation in the vertical stiffness and damping of the track foundation on the dynamic deflection and bending moment responses were

also investigated for the case of loads moving at constant speed. Numerical results obtained from the study are presented and discussed [4].

- The method described contributes to the reliable prediction of the inhomogeneity in the underlying stiffness and damping parameters along the track.

2. DYNAMICAL MODEL OF THE MEASURING SYSTEM

In Fig. 1 the independently supported measuring wheelset and measuring frame can be seen. Air springs connected to the chassis of the vehicle apply a constant force [5] on the measuring wheelset.

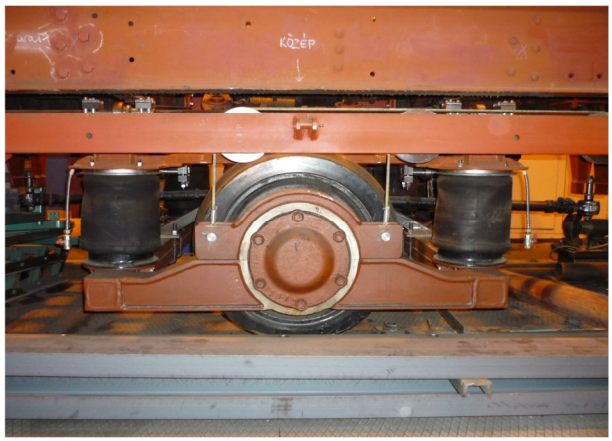

Fig. 1 The measuring wheel-set with the compressed air operated actuators

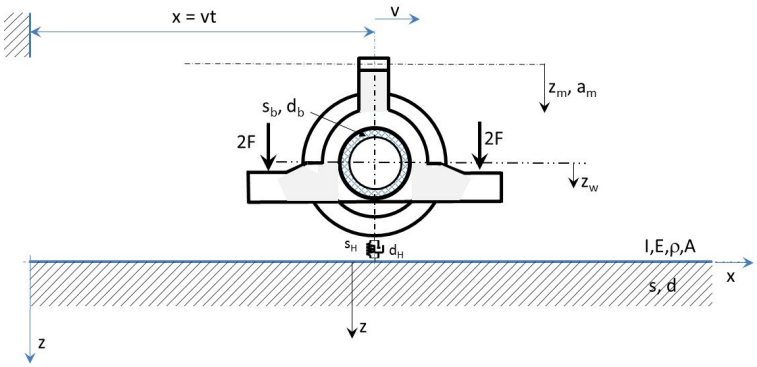

Fig. 2 Side elevation of the vertical dynamical model of the measuring wheel-set and the measuring frame connected with it

Fig. 2 presents the side elevation of the vertical dynamical model of the measuring wheel-set. The vertical accelerations of the measuring frame are measured at two points at lateral distance *a* from each other in which the *inhomogeneity of the variation in vertical stiffness of the elastic half planes under the rails are reflected when running along the track at a constant velocity v* [1], [4].

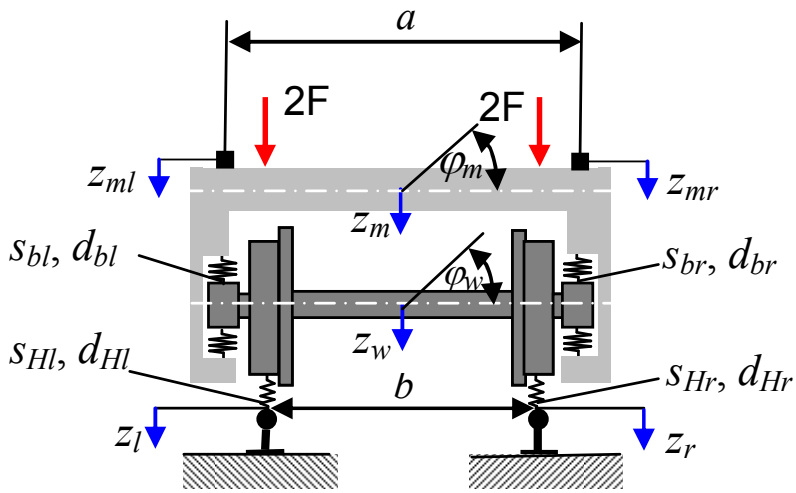

Fig. 3 Front elevation of the vertical dynamical model of the measuring wheel-set and the measuring frame

The motion equations of the measuring wheel-set and the measuring frame take the form of a system of ordinary second order differential equations, as follows:

$$\ddot{z}_w(t) = F_w(z_w(t),\dot{z}_w(t),\varphi_w(t),\dot{\varphi}_w(t),z_m(t),\dot{z}_m(t),\varphi_m(t),\dot{\varphi}_m(t),z_r(x,t),\frac{d}{dt}z_r(x,t),z_l(x,t),\frac{d}{dt}z_l(x,t))$$

$$\ddot{z}_m(t) = F_m(z_w(t),\dot{z}_w(t),\varphi_w(t),\dot{\varphi}_w(t),z_m(t),\dot{z}_m(t),\varphi_m(t),\dot{\varphi}_m(t))$$

$$\ddot{\varphi}_w(t) = G_w(z_w(t),\dot{z}_w(t),\varphi_w(t),\dot{\varphi}_w(t),z_m(t),\dot{z}_m(t),\varphi_m(t),\dot{\varphi}_m(t),z_r(x,t),\frac{d}{dt}z_r(x,t),z_l(x,t),\frac{d}{dt}z_l(x,t))$$

$$\ddot{\varphi}_m(t) = G_m(z_w(t),\dot{z}_w(t),\varphi_w(t),\dot{\varphi}_w(t),z_m(t),\dot{z}_m(t),\varphi_m(t),\dot{\varphi}_m(t))$$

The vertical motion equations of the rails as prismatic beams supported by Winkler-foundations have been extended by also taking into consideration the existing dynamical interaction with the measuring wheel-set, using linearized *Hertzian* springs and dampers to give the elastic/dissipative connection between the rails and the wheel-treads The extended motion equation of the right hand side reads [2], [6], [8]:

$$IE\frac{\partial^4 z_r(x,t)}{\partial x^4} + \rho A\frac{\partial^2 z_r(x,t)}{\partial t^2} + d_r\frac{\partial z_r(x,t)}{\partial t} + s_r(x)z_r(x,t) =$$

$$= \delta(x-vt)\left[s_{Hr}(z_w(t)-(b/2)\varphi_w(t)) - z_r(x,t)) + d_{Hr}(\dot{z}_w(t)-(b/2)\dot{\varphi}_w(t) - \frac{d}{dt}(z_r(x,t))\right]$$

Similarly, the motion equation of the left hand side rail takes the following form:

$$IE\frac{\partial^4 z_l(x,t)}{\partial x^4} + \rho A\frac{\partial^2 z_l(x,t)}{\partial t^2} + d_r\frac{\partial z_l(x,t)}{\partial t} + s_r(x)z_l(x,t) =$$

$$= \delta(x-vt)\left[s_{Hl}(z_w(t)+(b/2)\varphi_w(t)) - z_l(x,t)) + d_{Hl}(\dot{z}_w(t)+(b/2)\dot{\varphi}_w(t) - \frac{d}{dt}(z_l(x,t))\right],$$

where for the solution functions the following boundary conditions must be fulfilled:

$$\lim_{n\to\pm\infty} z_r(x,t) = 0 \quad és \quad \lim_{n\to\pm\infty} z_l(x,t) = 0\,.$$

3. THE MAIN PROBLEM TO BE SOLVED

Let's suppose that the measuring system has an operator $\boldsymbol{J}$, which transfers the *unknown vertical track stiffness function* $\boldsymbol{s}(x)$ via the whole signal transfer properties of the track and the measuring system into the measured acceleration $\boldsymbol{a}_{\mathrm{m}}(x)$ of the rubber sprung measuring frame over the axle boxes of the measuring wheel-set. In formula [3], [4]:

$$\boldsymbol{a}_m(x) = \boldsymbol{J}\boldsymbol{s}(x).$$

The task is to identify the unknown vertical track stiffness function $\boldsymbol{s}(x)$ in form of a finite parameter approximating function structure designated by $\boldsymbol{s}_a(x,\boldsymbol{p})$ which can ensure an appropriate framework for explaining the measured acceleration response straight over the axle box of the measuring wheel-set by appropriate (in a given sense optimum) selection of parameter vector $\boldsymbol{p}$. If the structure of the $\boldsymbol{p}$ parameter vector dependent stiffness function $\boldsymbol{s}_a(x,\boldsymbol{p})$ were *exactly correct*, such that $\boldsymbol{s}(x) = \boldsymbol{s}_a(x,\boldsymbol{p})$, then the measured acceleration function $\boldsymbol{a}_m(x)$ would result as the effect of system operator $\boldsymbol{J}$ on the assumed "exact" stiffness function $\boldsymbol{s}_a(x,\boldsymbol{p})$, in formula:

$$\boldsymbol{a}_m(x) = \boldsymbol{J}\,\boldsymbol{s}_a(x,\boldsymbol{p}).$$

Unfortunately, the signal transfer properties realised by the measuring system operator $\boldsymbol{J}$ are unknown. The authors therefore built up a detailed, combined hybrid dynamical model of the railway track and the loaded measuring wheel-set, embedded into a vertically loaded measuring frame through a linearly elastic and dissipative connection with the axle boxes of the measuring wheel-set. This hybrid dynamical model of the track/measuring wheel-set and measuring frame system model appears as a hybrid differential equation system, consisting of the two *Euler-Bernoulli* beams (modelling the rails) continuously supported by the right and left stiffness functions $s_{\mathrm{r}}(x,\boldsymbol{p})$ and $s_{\mathrm{l}}(x,\boldsymbol{p})$, and a finite dimensional lumped parameter dynamical sub-system, modelling the vertical and rolling motions of the measuring wheel-set and the measuring frame. It is useful to treat the above two track stiffness inhomogeneity functions together by the vector $\boldsymbol{s}_a(x,\boldsymbol{p}) = [s_{\mathrm{r}}(x,\boldsymbol{p}),s_{\mathrm{l}}(x,\boldsymbol{p})]^{\mathrm{T}}$. Furthermore, it is to be emphasized, that the vertical force between the rail-heads and the wheel-treads is transferred by *Hertzian* springs and dampers, i.e. the linearized version of the *Hertzian* contact law, around the static mean wheel-load values. Accelerometers are mounted on the measuring frame (connected to the axle boxes with rubber springs) just over the centres of the right and left axle-boxes of the measuring wheel-set.

If the hybrid dynamical system depicted above is considered, then one can characterise the signal transfer from the parameter dependent approximating vector valued stiffness function $\boldsymbol{s}_a(x,\boldsymbol{p})$ into the vector valued numerical simulation generated acceleration function by the symbolic mapping

$$\boldsymbol{a}_s(x,\boldsymbol{p}) = \boldsymbol{J}_m\,\boldsymbol{s}_a(x,\boldsymbol{p}),$$

where operator $\boldsymbol{J}_m$ stands for the combined simulation procedure, carried out by solving

the *hybrid differential equation system* of the track/measuring system, taking into consideration the longitudinal motion of the wheel-set/measuring frame system of speed *v* along the track.

In the course of the practical simulation procedure it is convenient to include the *parameter dependent* track stiffness inhomogeneity functions from which the track irregularity function can be composed in the form of a linear combination using shift, contraction or dilatation and multiplier transformations on a properly normalised *Gaussian bell-curve* shown in Fig 4. This function can be called a *basic* function for generating the parameter dependent track stiffness inhomogeneity function components (right and left) [3].

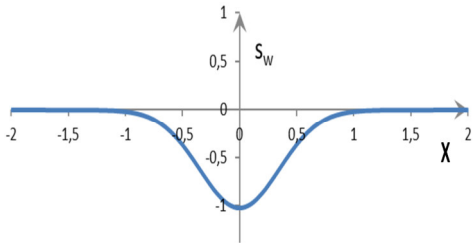

Fig. 4 Basic function for generating track stiffness inhomogeneity function

The functional relationship for the introduced basic function mentioned, is as follows [4]:

$$s_w(x) = -\exp\left\{-\frac{(3x)^2}{2}\right\}.$$

The vertical stiffness inhomogeneity functions under the two rails are composed by using the sum (linear combination) of appropriately transformed versions above basic function in form:

$$s_r(x) \approx s_{ra}(x) = \overline{s}_{ra} + \sum_{i=1}^{n} b_{ri} \cdot s_w(e_{ri} \cdot (x - c_{ri}))$$

$$s_l(x) \approx s_{la}(x) = \overline{s}_{la} + \sum_{i=1}^{n} b_{li} \cdot s_w(e_{li} \cdot (x - c_{li}))$$

The constants entered the formulas are included in four characteristic multidimensional vectors as follows:

$\overline{\boldsymbol{s}} = [\overline{s}_{ra}, \overline{s}_{la}]^T$ mean stiffness vector

$\mathbf{b} = [\mathbf{b}_r, \mathbf{b}_l]^{\mathrm{T}} = [b_{r1}, b_{r2}, \ldots, b_{rn}, b_{l1}, b_{l2}, \ldots, b_{ln}]^{\mathrm{T}}$ multiplication coefficient vector

$\mathbf{c} = [\mathbf{c}_r, \mathbf{c}_l]^{\mathrm{T}} = [c_{r1}, c_{r2}, \ldots, c_{rn}, c_{l1}, c_{l2}, \ldots, c_{ln}]^{\mathrm{T}}$ shift constant vector

$\mathbf{e} = [\mathbf{e}_r, \mathbf{e}_l]^{\mathrm{T}} = [e_{r1}, e_{r2}, \ldots, e_{rn}, e_{l1}, e_{l2}, \ldots, e_{ln}]^{\mathrm{T}}$ dilatation factor vector

In accordance with the formerly used designations, the parameter vector of the vector valued stiffness inhomogeneity approximating function $\boldsymbol{s}_a(x, \boldsymbol{p})$ gets a detailed meaning, using the unified parameter vector $\boldsymbol{p} = [\overline{\boldsymbol{s}}, \boldsymbol{b}, \boldsymbol{c}, \boldsymbol{e}]^T$. The approximating vector valued track stiffness representing inhomogeneity function takes the following detailed form:

$$\boldsymbol{s}_a(x,\boldsymbol{p}) = \boldsymbol{s}_a(x,[\overline{\boldsymbol{S}},\boldsymbol{b},\boldsymbol{c},\boldsymbol{e}]^T) = \begin{bmatrix} s_{ra}(x,[\overline{\boldsymbol{S}},\boldsymbol{b},\boldsymbol{c},\boldsymbol{e}]^T) \\ s_{la}(x,[\overline{\boldsymbol{S}},\boldsymbol{b},\boldsymbol{c},\boldsymbol{e}]^T) \end{bmatrix}.$$

The above vector valued assembly of the multivariable track stiffness describing functions
ensures the optimum fitting of the simulated vertical acceleration functions $\boldsymbol{a}_s(x,\boldsymbol{p})$ to the measured $\boldsymbol{a}_m(x,\boldsymbol{p})$accelerating functions. The approximate model-based operator $\boldsymbol{J}_m$ will now be used to represent operator $\boldsymbol{J}$. The former consists of the pair of fourth order linear partial differential equations representing the track, while the measuring system being in connection with the track system through the *Hertzian* spring/damper elements modelling the vertical contact of the track/wheel-set is described by a set of ordinary differential equations constructed for the vertical and rolling motion characterisation of the measuring wheel-set and the measuring frame.
The set of fourth order partial differential equations of variable coefficients describing the motion of the track is solved numerically by using *Galerkin's* approximation method, which seeks for the solution in form of the following expressions [7]:

$$z_r(\xi,t) = \sum_{j=0}^{n} \varphi_j(\xi) T_{rj}(t) \ , \ \ z_l(\xi,t) = \sum_{j=0}^{n} \varphi_j(\xi) T_{lj}(t).$$

Here variable ξ is in relation with the original position co-ordinate *x* as follows:

$$\xi = x - vt \ .$$

In the sum, functions $\varphi_j(\xi)$; j = 0,1,2,…,n are orthonormal, at least *n*-times continuously differentiable functions over the whole real line. This system of basic functions satisfy the prescribed boundary conditions with respect to their behaviour at limit transition$\xi \to \pm\infty$. The latter steps described meant that the examination transformed into a moving reference frame. The assumed solution function should be substituted into the two partial differential equations. If the function pair $z_r(\xi,t)$ and $z_l(\xi,t)$ were exact solutions to the set of equations, the two sides of the differential equations would be identically equal for every pair (ξ,t). In this case one must multiply the both sides of the equations in the sense of scalar product by any function $\varphi_j(\xi)$; j = 0,1,2,…,n and the balance of the equations would not change. Due to the orthonormal property [9] of the basic function used, it turns out that the resultant products at both sides depend only on the time t. This time dependence comes from the functions T_{rj}(t) and T_{lj}(t) and their first and second time derivatives. Omitting the details, one can get two sets of variable coefficient linear inhomogeneous ordinary differential equation systems for determining the unknown functions $T_{rj}(t)$ and $T_{lj}(t)$; j = 0,1,2,…,n. It is practical to include vector valued time functions formed from the unknown time dependent functions, which leads to the two set of ordinary differential equations below:

$$\mathbf{A}_r \underline{\ddot{T}}_r(t) + \mathbf{B}_r \underline{\dot{T}}_r(t) + \mathbf{C}_r(t) \underline{T}_r(t) = \underline{F}_r \ ,$$
$$\mathbf{A}_l \underline{\ddot{T}}_l(t) + \mathbf{B}_l \underline{\dot{T}}_l(t) + \mathbf{C}_l(t) \underline{T}_l(t) = \underline{F}_l \ ,$$

where the vector valued forces at the right hand side can be expressed by the following formulae:

$$\underline{F_r} = \left[s_{Hr}\left(\left(z_w(t) - \left(\frac{b}{2}\right)\varphi_w(t)\right) - \underline{\varphi}(0)\cdot\underline{T_r}(t)\right) + d_{Hr}\left(\left(\dot{z}_w(t) - \left(\frac{b}{2}\right)\dot{\varphi}_w(t)\right) - \left(\underline{\varphi}'(0)\cdot v\cdot\underline{T_r}(t) + \underline{\varphi}(0)\cdot\dot{\underline{T}}_r(t)\right)\right)\right] \cdot \underline{\varphi}(0)$$

$$\underline{F_l} = \left[s_{Hl}\left(\left(z_w(t) + \left(\frac{b}{2}\right)\varphi_w(t)\right) - \underline{\varphi}(0)\cdot\underline{T_l}(t)\right) + d_{Hl}\left(\left(\dot{z}_w(t) + \left(\frac{b}{2}\right)\dot{\varphi}_w(t)\right) - \left(\underline{\varphi}'(0)\cdot v\cdot\underline{T_l}(t) + \underline{\varphi}(0)\cdot\dot{\underline{T}}_l(t)\right)\right)\right]\cdot\underline{\varphi}(0)$$

Here designation

$$\underline{\varphi}(0) = [\varphi_0(0), \varphi_1(0), \dots, \varphi_n(0)\,]^T$$

has been introduced, which represents a constant $n+1$ dimensional vector, containing the substitution values of the basic functions at $\xi = 0$, in other form at $x=vt$.

It is to be mentioned, that the vector character of $\underline{F_r}(t)$ and $\underline{F_l}(t)$ originates from the vector character of $\underline{\varphi}(0)$, in other words the coefficients in bracket are identical time functions in any row of vectors $\underline{F_r}(t)$ and $\underline{F_l}(t)$,respectively.

The above mentioned identical time dependence of the expressions in bracket can be introduced in the following forms by using appropriate rearrangements:

$$F_r(t) = s_{Hr}\left(\left(z_w(t) - \left(\frac{b}{2}\right)\varphi_w(t)\right) - \underline{\varphi}(0)\cdot\underline{T_r}(t)\right) + d_{Hr}\left(\left(\dot{z}_w(t) - \left(\frac{b}{2}\right)\dot{\varphi}_w(t)\right) - \left(\underline{v\cdot\varphi}'(0)\cdot T_r(t) + \underline{\varphi}(0)\cdot\dot{\underline{T}}_r(t)\right)\right)$$

$$= s_{Hr}\left(\left(z_w(t) - \left(\frac{b}{2}\right)\varphi_w(t)\right)\right) + d_{Hr}\left(\left(\dot{z}_w(t) - \left(\frac{b}{2}\right)\dot{\varphi}_w(t)\right)\right) - s_{Hr}\cdot\underline{\varphi}(0)\cdot\underline{T_r}(t) - d_{Hr}\left(v\cdot\underline{\varphi}'(0)\cdot\underline{T_r}(t) + \underline{\varphi}(0)\cdot\dot{\underline{T}}_r(t)\right)$$

and

$$F_l(t) = s_{Hl}\left(\left(z_w(t) + \left(\frac{b}{2}\right)\varphi_w(t)\right) - \underline{\varphi}(0)\cdot\underline{T_l}(t)\right) + d_{Hl}\left(\left(\dot{z}_w(t) + \left(\frac{b}{2}\right)\dot{\varphi}_w(t)\right) - \left(v\cdot\underline{\varphi}'(0)\cdot\underline{T_l}(t) + \underline{\varphi}(0)\cdot\dot{\underline{T}}_l(t)\right)\right)$$

$$= s_{Hl}\left(\left(z_w(t) + \left(\frac{b}{2}\right)\varphi_w(t)\right)\right) + d_{Hl}\left(\left(\dot{z}_w(t) + \left(\frac{b}{2}\right)\dot{\varphi}_w(t)\right)\right) - s_{Hl}\underline{\varphi}(0)\cdot\underline{T_l}(t) - d_{Hl}\left(v\cdot\underline{\varphi}'(0)\cdot\underline{T_l}(t) + \underline{\varphi}(0)\cdot\dot{\underline{T}}_l(t)\right)$$

After recognising that the third and fourth members in the above final expressions for $F_r(t)$ and $F_l(t)$ depend on the components of vectors $\cdot\ \underline{T_r}(t)$ and $\dot{\underline{T}}_r(t)$, and vectors $\cdot\ \underline{T_l}(t)$ and $\dot{\underline{T}}_l(t)$, it becomes clear that after appropriate rearrangements the following two second order ordinary set of differential equations are yielded:

$$\mathbf{A}_r'\ddot{\underline{T}}_r(t) + \mathbf{B}_r'\dot{\underline{T}}_r(t) + \mathbf{C}_r'(t)\underline{T_r}(t) = \left[s_{Hr}\left(z_w(t) - \left(\frac{b}{2}\right)\varphi_w(t)\right) + d_{Hr}\left(\dot{z}_w(t) - \left(\frac{b}{2}\right)\dot{\varphi}_w(t)\right)\right]\cdot\underline{\varphi}(0),$$

$$\mathbf{A}_l''\ddot{\underline{T}}_l(t) + \mathbf{B}_l''\dot{\underline{T}}_l(t) + \mathbf{C}_l''(t)\underline{T_l}(t) = \left[s_{Hl}\left(z_w(t) + \left(\frac{b}{2}\right)\varphi_w(t)\right) + d_{Hl}\left(\dot{z}_w(t) + \left(\frac{b}{2}\right)\dot{\varphi}_w(t)\right)\right]\cdot\underline{\varphi}(0).$$

In the two new sets of differential equations the coefficient matrices are different from, thus the following matrix-triples are deduced:

$$\mathbf{A}_r', \mathbf{B}_r', \mathbf{C}_r'(t)\ ,\ \mathbf{A}_l'', \mathbf{B}_l'', \mathbf{C}_l''(t).$$

At this point of the discussion one should take into consideration that the measuring frame is in elastic and dissipative connection with the wheel-set and is loaded by constant, vertical pneumatic forces F applied at four symmetrically located points on the measuring frame.

Due to the above, the introduction of further motion equations is necessary, namely for the vertical motions and rolling motions of the measuring wheel-set and the measuring frame. Knowing the magnitudes of the time dependent vertical wheel/rail contact forces $F_r(t)$ and $F_l(t)$ transmitted onto the wheel-set by the *Hertzian* springs and damp-

ers treated above, the following two linear sets of second order ordinary differential-equations are yielded:

$$m_w\ddot{z}_w(t) = -F_r - F_l + s_{br}\left[\left(z_m(t) - \left(\frac{a}{2}\right)\varphi_m(t)\right) - \left(z_w(t) - \left(\frac{a}{2}\right)\varphi_w(t)\right)\right] + d_{br}\left[\left(\dot{z}_m(t) - \left(\frac{a}{2}\right)\dot{\varphi}_m(t)\right) - \left(\dot{z}_w(t) - \left(\frac{a}{2}\right)\dot{\varphi}_w(t)\right)\right] + s_{bl}\left[\left(z_m(t) + \left(\frac{a}{2}\right)\varphi_m(t)\right) - \left(z_w(t) + \left(\frac{a}{2}\right)\varphi_w(t)\right)\right] + d_{bl}\left[\left(\dot{z}_m(t) + \left(\frac{a}{2}\right)\dot{\varphi}_m(t)\right) - \left(\dot{z}_w(t) + \left(\frac{a}{2}\right)\dot{\varphi}_w(t)\right)\right];$$

$$m_m\ddot{z}_m(t) = 2F - s_{br}\left[\left(z_m(t) - \left(\frac{a}{2}\right)\varphi_m(t)\right) - \left(z_w(t) - \left(\frac{a}{2}\right)\varphi_w(t)\right)\right] - d_{br}\left[\left(\dot{z}_m(t) - \left(\frac{a}{2}\right)\dot{\varphi}_m(t)\right) - \left(\dot{z}_w(t) - \left(\frac{a}{2}\right)\dot{\varphi}_w(t)\right)\right] - s_{bl}\left[\left(z_m(t) + \left(\frac{a}{2}\right)\varphi_m(t)\right) - \left(z_w(t) + \left(\frac{a}{2}\right)\varphi_w(t)\right)\right] - d_{bl}\left[\left(\dot{z}_m(t) + \left(\frac{a}{2}\right)\dot{\varphi}_m(t)\right) - \left(\dot{z}_w(t) + \left(\frac{a}{2}\right)\dot{\varphi}_w(t)\right)\right];$$

Similarly, for the rolling motion of the measuring wheel-set and the measuring frame the following two linear sets of second order ordinary differential-equations are in force:

$$\begin{aligned}\Theta_w\ddot{\varphi}_w(t) = {} & F_r(t)\left(\frac{b}{2}\right) - F_l(t)\left(\frac{b}{2}\right) + s_{br}\left(\left(z_m(t) - \left(\frac{a}{2}\right)\varphi_m(t)\right) - \left(z_w(t) - \left(\frac{a}{2}\right)\varphi_w(t)\right)\right)\left(\frac{a}{2}\right) \\ & + d_{br}\left(\left(\dot{z}_m(t) - \left(\frac{a}{2}\right)\dot{\varphi}_m(t)\right) - \left(\dot{z}_w(t) - \left(\frac{a}{2}\right)\dot{\varphi}_w(t)\right)\right)\left(\frac{a}{2}\right) s_{bl}\left(\left(z_m(t) + \left(\frac{a}{2}\right)\varphi_m(t)\right)\right. \\ & \left. - \left(z_w(t) + \left(\frac{a}{2}\right)\varphi_w(t)\right)\right)\left(\frac{a}{2}\right) - d_{bl}\left(\left(\dot{z}_m(t) + \left(\frac{a}{2}\right)\dot{\varphi}_m(t)\right) - \left(\dot{z}_w(t) + \left(\frac{a}{2}\right)\dot{\varphi}_w(t)\right)\right)\left(\frac{a}{2}\right)\end{aligned}$$

$$\begin{aligned}\Theta_m\ddot{\varphi}_m(t) = {} & - s_{br}\left(\left(z_m(t) - \left(\frac{a}{2}\right)\varphi_m(t)\right) - \left(z_w(t) - \left(\frac{a}{2}\right)\varphi_w(t)\right)\right)\left(\frac{a}{2}\right) \\ & - d_{br}\left(\left(\dot{z}_m(t) - \left(\frac{a}{2}\right)\dot{\varphi}_m(t)\right) - \left(\dot{z}_w(t) - \left(\frac{a}{2}\right)\dot{\varphi}_w(t)\right)\right)\left(\frac{a}{2}\right) \\ & + s_{bl}\left(\left(z_m(t) + \left(\frac{a}{2}\right)\varphi_m(t)\right) - \left(z_w(t) + \left(\frac{a}{2}\right)\varphi_w(t)\right)\right)\left(\frac{a}{2}\right) \\ & + d_{bl}\left(\left(\dot{z}_m(t) + \left(\frac{a}{2}\right)\dot{\varphi}_m(t)\right) - \left(\dot{z}_w(t) + \left(\frac{a}{2}\right)\dot{\varphi}_w(t)\right)\right)\left(\frac{a}{2}\right)\end{aligned}$$

The above set of second order differential equations with respect to the unknown function vector of dimension *2n+6*:

$$\underline{Z}(t)=[\underline{T}_r(t), \underline{T}_l(t), z_w(t), z_m(t), \varphi_w(t), \varphi_m(t)]^T$$

can be written into the following concise form:

$$\mathbf{M}\ddot{\underline{Z}}(t)+ \mathbf{D}\dot{\underline{Z}}(t)+ \mathbf{S}(t)\underline{Z}(t) = \underline{0},$$

with given initial time t_0 and initial conditions $\underline{Z}(t_0) = \underline{Z}_0$ and $\dot{\underline{Z}}(t_0) = \dot{\underline{Z}}_0$ ordered to the former. For the numerical solution it is reasonable to introduce a state-vector in form $\underline{X}(t) = [\dot{\underline{Z}}(t),\underline{Z}(t)]^T$, in other words the treatment is continued in the framework of the state-space method. In the end a *first order linear homogeneous variable coefficient* set of ordinary differential equations is yielded, more exactly an initial value problem of the following form:

$$\dot{\underline{X}}(t)=\mathbf{A}(t,\mathbf{p})\,\underline{X}(t)$$
$$\underline{X}(t_0) = \underline{X}_0$$

At this point, the proper selection of the components of the initial value vector $\underline{X}_0$ arises. On the one hand the time dependent factor functions $\underline{T}_r(t)$ and $\underline{T}_l(t)$ in the *Galerkin* approximation of the vertical profile $z_r(\xi,t,\mathbf{p})$ and $z_l(\xi,t,\mathbf{p})$ of the right and left rails at time t_0 can be determined with the ξ-dependent orthonormal shape-function system used in the *Galerkin* approximation. In other words the shapes of the rails are considered under the static-load from the measuring wheel-set through the right and left *Hertzian* springs. For the sake of convenient treatment the initial time derivatives of time dependent factor functions $\underline{T}_r(t)$ and $\underline{T}_l(t)$ at t_0 can be taken as zero vectors. On the other hand initial displacements $z_w(t_0)$, $z_m(t_0)$, and angular displacements $\varphi_w(t_0)$, $\varphi_m(t_0)$ of the measuring wheel-set and the measuring frame can be determined by taking into account the static equilibrium under gravity, the static constant load acting on the measuring frame and the rail reaction forces. As for the initial time derivatives at t_0 of functions $z_w(t_0)$, $z_m(t_0)$, and angular displacements $\varphi_w(t_0)$, $\varphi_m(t_0)$ can be considered to be approximately zero.

With the application of the initial condition $\underline{X}_0$ the initial value problem formulated for the unknown vector function $\underline{X}(t)$ can be solved numerically by using a proper ODE code, and in this way the vector-valued solution manifold $\underline{X}(t,\underline{X}_0,\mathbf{p})$ becomes principally known for any parameter vector $\mathbf{p}$.

Knowing vector function manifold $\underline{X}(t,\underline{X}_0,\mathbf{p})$, the vertical shape of the right and left rails $z_r(\xi,t,\mathbf{p})$ and $z_l(\xi,t,\mathbf{p})$ can be determined by the linear combination of the *Galerkin* approximation since the orthonormal shape function system is known per definition. In our problem treatment the rail shape functions mentioned are interesting characteristics, but our attention is directed primarily to the variation of the supporting stiffness with track arc length under the right and left rails, which stiffness functions depend upon the parameter vector $\mathbf{p}$. The question is the determination of such a parameter vector $\mathbf{p}^*$ the coordinates of which ensure such linear combinations of the basic stiffness shape function in Fig. 4 for the right and left stiffness functions that they lead such simulated vertical acceleration vector $\boldsymbol{a}_s = \boldsymbol{a}_s(x,\mathbf{p}^*)$ for the measuring frame points over the axle-boxes of the measuring wheel-set, that the differences from the measured acceleration vector $\boldsymbol{a}_m(x)$ with respect to the *Sobolyev*-norm of second order should be *minimum* by using the objective function $\Psi(\boldsymbol{p})$ to be specified given in the following section.

3.2 Identification of the track stiffness inhomogeneities

The simulation backed identification method is based on minimising the second order *Sobolyev* norm of the deviation between the measured accelerations on the measuring frame over the axle boxes and the numerically generated parametrised response func-

tions of the complex track and measuring system model, the response functions of which are also determined on the measuring frame over the axle-boxes of the measuring wheel-set. In accordance with the above, the functional to be minimalized is formulated by the integral expression below:

$$\Psi(\boldsymbol{p}) = \Psi(\bar{s}, \mathbf{b}, \mathbf{e}, \mathbf{c}) =$$
$$\int_X \left\{ \left| \boldsymbol{J}_m \begin{bmatrix} \bar{s}_{ra} + \sum_{j=1}^{n} b_{rj} \cdot s_w\left(e_{rj}(x - c_{rj})\right) \\ \bar{s}_{la} + \sum_{j=1}^{n} b_{lj} \cdot s_w\left(e_{lj}(x - c_{lj})\right) \end{bmatrix} - \boldsymbol{a}_m(x) \right|^2 + \left| \frac{d}{dx} \boldsymbol{J}_m \begin{bmatrix} \bar{s}_{ra} + \sum_{j=1}^{n} b_{rj} \cdot s_w(e_{rj}(x - c_{rj})) \\ \bar{s}_{la} + \sum_{j=1}^{n} b_{lj} \cdot s_w(e_{llj}(x c_{lj})) \end{bmatrix} - \frac{d}{dx} \boldsymbol{a}_m(x) \right|^2 \right\} dx$$
$$= min!$$

As it is obvious, operator $\boldsymbol{J}_\mathrm{m}$ *is a mapping* from the parametrized set of the possible rail supporting stiffness irregularity functions $\{\boldsymbol{s}_a(x, \boldsymbol{p})\}$ into the set $\{\boldsymbol{a}_s(x, \boldsymbol{p})\}$of the *simulated acceleration functions* valid of the measuring frame over the axle boxes of the measuring wheel-set. In the integral expression, the square of the absolute values of the deviations in the parameter vector-dependent *simulated accelerations* $\{\boldsymbol{a}_s(x, \boldsymbol{p})\}$ and *acceleration derivatives* $\frac{d}{dx}[\boldsymbol{a}_s(x, \boldsymbol{p})]$ (*jerk*) from the measured (real) $\boldsymbol{a}_m(x)$ and $\frac{d}{dx}\boldsymbol{a}_m(x)$ acceleration jerk characteristics emerges. The action-parameters of the minimization of the integral expression are included into a parameter vector $\mathbf{p} \in \{\mathbf{p}\}$.Here $\{\mathbf{p}\}=\{[\ \bar{s}, \mathbf{b}, \mathbf{e}, \mathbf{c}\ ]^\mathrm{T}\} \subset R^{6n+2}$ is the set of *6n+2* dimensions of the possible parameters determining the two rail supporting stiffness functions $s_\mathrm{r}(x)$ and $s_\mathrm{l}(x)$.

It is to be emphasized that by introducing the second order *Sobolyev*-norm, the *quadratic deviation* between the measured and simulated vertical *measuring frame accelerations and vertical jerks* over the axle boxes are included in the evaluating functional $\Psi(\mathbf{p})$. Thus, by minimising $\Psi(\mathbf{p})$ the possibly high conformity in the shape of the simulated and measured measuring frame acceleration functions over the measuring wheel-set axle boxes can be ensured.

3.3 Numerical minimization of $\Psi(\mathbf{p})$

The numerical minimization of the integral expression generated **p**–dependent objective function $\Psi(\mathbf{p})$ is carried out by the gradient-method formulated by the sequence $\{\mathbf{p}_\mathrm{k}\}$ of the approximating parameter vectors below:

$$\mathbf{p}_{k+1} = \mathbf{p}_k - \frac{\mathbf{grad}\,\psi(\mathbf{p}_k)}{\left|\mathbf{grad}\,\psi(\mathbf{p}_k)\right|} \cdot \tau\,,$$

where τ is a non-negative small scalar increment, *k* is the number of iteration steps. The minimizing process can be started by selecting a proper initial vector $\mathbf{p}_0$, and the numerical process comes to an end if the difference in absolute value between two neighbouring steps remains under a sufficiently small bound ε, formulating the accuracy demand:

$$|\Psi(\mathbf{p}_{k+1}) - \Psi(\mathbf{p}_k)| < \varepsilon\,.$$

In the course of the numerical procedure, the co-ordinate-wise entering partial derivatives of the gradient vector of the objective function $\Psi(\mathbf{p})$ are approximated by the natural difference quotients taken by applying small increments in the co-ordinates of parameter vector **p.**

4. NUMERICAL RESULTS

To test the applicability of the developed identification method we set out from a known pair of simple artificial track stiffness inhomogeneity functions which had one wavelet term on both sides of the track. We carried out the dynamical simulation of the motion process of the track-measuring wheelset-measuring frame system when the wheelset passes through the known track stiffness inhomogeneities. The acceleration functions received at the positions of the acceleration transducers placed on the carrier frame above the axle-boxes, as well as their versions smoothed by known method for both sides of the track are stored in appropriate files.

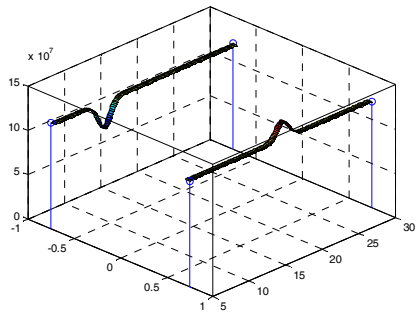

Fig.5 Track stiffness inhomogeneity on the right and left side rail

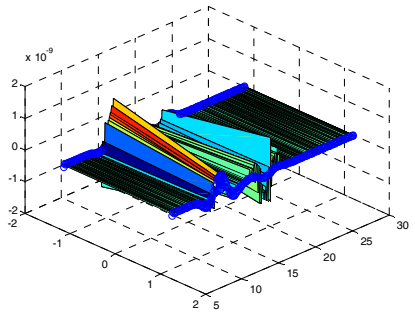

Fig.6 The smoothed and simulated acceleration of the measuring frame over the right and left side axle-box computed by the dynamical model

Fig. 5 represents the track stiffness inhomogeneity at the left and right side rails, while Fig. 6 shows the acceleration of the in-space model, and the thick lines show the smoothed curve of the vertical acceleration on the measuring frame over the axle-boxes of the measuring wheel-set.

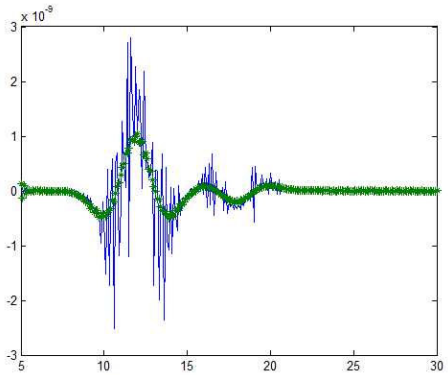

Fig.7 The simulated and smoothed acceleration of the left rail

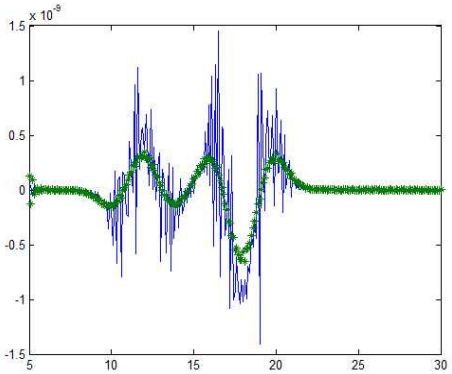

Fig.8 The simulated and smoothed acceleration of the right rail

Fig. 7 and Fig. 8 show the side-view of the simulated and smoothed accelerations. By using the described gradient method, the optimum estimations of the parameter **p**, as well as the identified track stiffness functions have been determined. In Fig. 9 and 10 the initial and the identified track stiffness functions are shown in common diagrams. The deviation between the real and the identified functions is less than the margin of error.

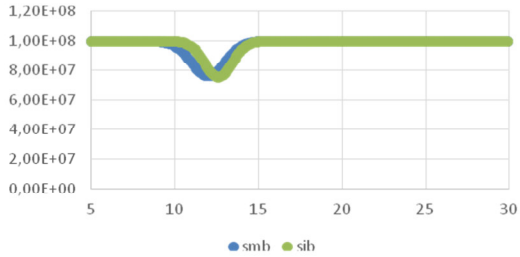

Fig. 9 Original (input) track stiffness inhomogeneity and the identified stiffness inhomogeneity along the left rail

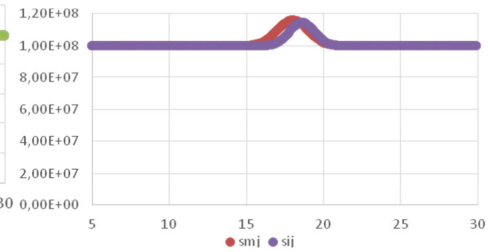

Fig.10 Original (input) track stiffness inhomogeneity and the identified stiffness inhomogeneity along the right rail

5. CONCLUDING REMARKS

- A simulation procedure has been elaborated for the determination of the elastic and dissipative supporting parameters present under the rails along the track by applying acceleration signals measured on the carrier-frame over the two axle boxes of the measuring wheel-set [1], [5].
- The variation in the elastic- and dissipative parameters of the track are included in the model, containing homogeneous beams representing the rails supported on inhomogeneous *Winkler*-foundation [2], [6]. The beams (the rails) are loaded by the moving measuring wheelset, which is connected to the carrier-frame of the measuring wheel-set receiving practically constant vertical load from four pneumatic actuators [3].
- The dynamical behaviour of the measuring wheel-set and the carrier-frame is described by a set of ordinary differential equations which is joint to the variable coefficient partial differential equation system describing the motion of the rails via the contact springs (*Hertzian*-springs) modelling the elastic and dissipative vertical wheel/rail connection [4].
- The received hybrid differential equation system can be solved by a numerical approximation method so that the manifold of the unknown motion state describing length-dependence are obtained by applying *Galerkin's* method [7], [8]. Each numerical solution has a given parameter vector specifying the track supporting stiffness and damping inhomogeneity functions assumed to be in force in the simulation step. Using this set of numerical solutions of the rail motion characteristics, the parameters of the unknown track supporting stiffness and damping functions can be approximated by applying the minimizing procedure for the sequence of differences in *Sobolyev*-norm of second order between the measured signals and the simulated approximations.
- The minimizing procedure is implemented by a version of the gradient method, where the partial derivatives of the objective function with respect to the coordinates of the parameter vector have been taken into account [3], [4].
- Further research is necessary to refine the identification method for in-space models and to take into account the statistical characteristics of the measurement errors, as well.
- It is of great practical importance in track qualification to develop considerably faster numerical procedures for full scale (on line) applications.

6. REFERENCES

[1] **Destek, M**.: Investigation of the Interaction of Track/Vehicle System in Approach of System Theory. Közlekedéstudományi Szemle, Budapest, 1974. No. 6, p.271-276. (In Hungarian)

[2] **Zobory, I. - Zoller, V. - Zábori, Z**.: Time Domain Analysis of a Railway Vehicle Running on a Discretely Supported Continuous Rail Model at a Constant Velocity, Z. angew. Math. Mech. 76, S4 (1996), p.169-172.

[3] **Zobory, I. - Zábori, Z.**:Track Qualification Method and Its Realisation Based on System Dynamics, Proceedings of the 5th Mini Conferenceon Vehicle System Dynamics, Identification and Anomalies, VSDIA 1996, (Ed. by Prof. I. Zobory). BME Department of RailwayVehicles, Budapest, 1997, p.173-181.

[4] **Zobory, I. – Békefi, E. - Zábori, Z.**: Simulation Backed Identification of Vertical Track Stiffness Functions by Using Wavelets, Proceedings of the 6th Mini Conferenceon Vehicle System Dynamics, Identification and Anomalies, VSDIA 1998, (Ed. by Prof. I. Zobory). BME Department of RailwayVehicles, Budapest, 1998, p.151-159.(ISBN: 963 420 6352)

[5] **Zobory, I.**:A vasúti pálya-jármű rendszer dinamikája - mérése- minősítése. In: Futástechnikai Konferencia. Konferencia helye, ideje: Harkányfürdő, Magyarország, 2007.07.27-2007.07.29. Proceedings of the Conference on Running Technique. p.1-12. (In Hungarian)

[6] **Zoller, V. –Zobory, I.**: On the Dynamics of the RailwayTrack/Vehicle System in the Presence of Inhomogeneous Rail Supporting Parameters. Proceedings of the 10th Mini ConferenceonVehicle System Dynamics, Identification and Anomalies VSDIA 2006. (Ed. by Prof. I. Zobory). BME Department of RailwayVehicles, Budapest, 2007, p.117-122. (ISBN: 9789634209683)

[7] **Kisilowski, J. - Sowinski, B.**: Problems of Simulating Vehicle Motion by Mathematical Models. In: *Advanced Railway Vehicle System Dynamics*, (Ed. by Prof. J.Kisilowski and Prof. K. Knothe), Wydawnictwa Naukowo-Techniczne, Warsaw, 1991, p.93-139.

[8] **Zábori, Z.**: Analysis of the in Plane Model of a Railway Track Measuring Car. Studies in the Sphere of Topics of Railway Vehicles and Vehicle System Analysis. *Remembrance-Book for the 70th Birth Day of Prof.Dr. István Zobory*. Öt Évszak Kft. Budapest, 2014. (In Hungarian)

[9] https://hu.wikipedia.org/wiki/Hermite-polinomok

RAIL VEHICLE MODEL POSSIBILITY OF SAFE MOTION ANALYSIS IN THE OVERCRITICAL VELOCITY RANGE

Miroslaw DUSZA

Warsaw University of Technology, Faculty of Transport
Department of Fundamentals of Transport Equipment Construction
Pl-00-662 Warsaw, Koszykowa str. 75, Poland

Received: September 12, 2019

ABSTRACT

An attempt to determine the maximum vehicle safe velocity (without any damage) is the subject of many theoretical studies of the rail vehicle-track system. The self-exciting vibrations appear in classical (so-called rigid) wheelset-track system. This well-known phenomenon is one of the reasons of safe vehicle motion velocity limitation. But the phenomenon can also be a measure of the system dynamic properties and make possibility to determine the permissible motion parameters according to the adopted criteria. Four axle rail vehicle-track model was created with use of VI-Rail software. In the range of velocity of stable vehicle-track model solutions existence the wheelset-track lateral forces are considered. Values of the calculated lateral forces are referred to the so-called track criterion.

Keywords: rail vehicle, critical velocity, numerical simulations, stability of motion

1. INTRODUCTION

The rail vehicle – track affect and mutual interaction is the subject of numerous experimental and theoretical studies since the beginning of the rail transport [6]. Under normal operating conditions, vehicles influence the track with the force of vertical pressure resulting from the vehicle weight and longitudinal and lateral forces resulting from several reasons. The vertical forces permissible values are strictly determined by regulations. Meeting the recommendations set out in the regulations does not cause problems, because control of these forces can be carrying out in static conditions. Permissible values of lateral forces are also specified in the regulations [1, 7, 8, 9]. However, their measurement and control cause a number of problems. They mainly results from the dynamic nature of these forces. Extreme values of lateral forces appear in motion conditions at a velocity close to or greater than the permissible value on a given track section. They may be an effect of a few reasons, but one of them is self-exciting vibrations in the vehicle track system appearance [2, 6, 11]. Undesirable high lateral forces (wheelsets guiding forces) arise in this case. Some effects of these forces acting, increase the risk of undesirable phenomena and may be manifested in:

- high wheel climbing on the rail head (wheel flange contact);
- the rail side bending and track gauge increase as a result;
- pull out of the rail from sleepers fastening and turn around the rail foot edge;
- some parts of track lateral displacements (rails and slippers against the ballast).

Each of these situation occurrences is an immediate threat to safety motion or permanent vehicle or track damage. Practical research of such events on real objects are involved in high implementation costs due to destructive tests character. The simulation methods involvement in research significantly reduces costs and implementation time [4, 10].

The simulation researches of self–exciting vibrations in vehicle-track system are the Author's interest for many years [2, 3, 11, 12]. The appearance and existence of self-

exciting vibrations results from reaching or exciding the critical vehicle velocity. This phenomenon, known as a „hunting motion", is inextricably linked to a conventional rigid wheelset and track system [4]. The wheelset lateral displacements and accompanying yaw motion become suddenly noticeably large when critical velocity v_n is achieved. The critical velocity v_n is a characteristic parameter of particular vehicle and track construction. Real vehicle velocity (operating one) cannot exceed the critical value, so v_n determine the maximum permissible velocity of modelled vehicle.

However, reaching or exceeding a v_n does not necessarily mean that there is no possibility of vehicle motion. Vehicle main motion (along the track) can be continued although the undesired self-exciting vibrations exist. Vehicle velocity can be increased in the over critical velocity range until the second characteristic velocity value v_s is achieved. Velocity v_s is the maximum possible velocity value from the theoretical (simulation method) point of view. It is the highest velocity value for which stable solution of the modelled vehicle-track system exists. Possible from theoretical point of view vehicle motion in the velocity range from v_n to v_s is strictly involved in undesirable motions resulting from self-exciting vibrations (hunting motion). The observations are concentrated on wheelset motions here. Wheelset lateral displacements y_p and yaw motions ψ around vertical axis are the undesirable motions associated with main wheelset motion. The lateral and yaw wheelset motions depend on each other, transmit to bogie frame and result in a strong transverse impact between wheelsets and track. In consequence each of the above mentioned threat of safe motion are possible to occur. The author's simulation studies show that almost all parameters of the vehicle-track system affect the velocity v_n and v_s values [2-3, 11, 12].

The researches presented in article are devoted to check the possibility of safe vehicle motion in the overcritical velocity range (between v_n and v_s). The assessment is being made from the point of view of the last aforementioned undesirable events, namely permanent track lateral deformation. Both wheelsets of first bogie lateral forces (guiding forces) in straight track and curves were determined for the tested 4-axle vehicle model. The calculated force values have been referred to the commonly used track criteria [7]. The criteria determine the permissible maximum values of wheelset-track force.

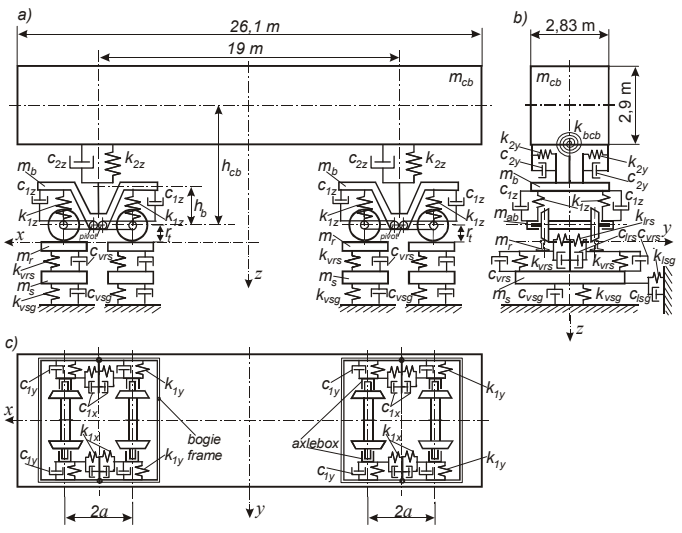

Fig. 1 Vehicle – track nominal model structure: *a*) side view, *b*) front view, *c*) top view

2. THE MODEL

The Multi Body System was build up with the engineering software VI-Rail (ADAMS/Rail formerly). The simulation model being tested in the paper consists of vehicle and track. Typical 4-axle passenger vehicle model is employed in the simulations (Fig. 1). Vehicle model corresponds to the 127A passenger car of Polish rolling stock. Bogies of the vehicle have 25AN designation in Polish terminology. The model consists of fifteen rigid bodies representing: car-body, two bogies with two solid wheelsets and eight axle-boxes. Each wheelset is attached to axle-boxes by joint attachment of a revolute type. So rotation of the wheelsets around the lateral axis with respect to axle-boxes is possible only. Arm of each axle-box is attached to bogie frame by pin joint (bush type element). They are laterally, longitudinally and rotary flexible elements. The linear and bi-linear characteristics of the primary and secondary suspension are included in the model. They represent metal (screw) springs and hydraulic dampers of primary and secondary suspension. In addition torsion springs (k_{bcb}) are mounted between car body and bogie frames. To restrict car body – bogie frame lateral displacements, bump-stops with 0.03 m clearance were applied (not visible in Fig. 1). A new S1002 wheel and UIC60 rail pairs of profiles are considered. Non-linear geometry of wheel - rail contact description is assumed. Contact area and other contact parameters are calculated with use of RSGEO subprogram (implemented into VI-Rail). To calculate wheel-rail contact forces, results obtained from RSGEO are utilized. In order to calculate tangential contact forces between wheel and rail, so called non-linear simplified theory of the rolling contact by J.J. Kalker is applied. It is implemented in the computer code FASTSIM [5] used worldwide.

Discrete, two level, vertically and laterally flexible track models were assumed. But models of track flexibility are simplified. For low frequency analysis (less than 50 Hz) simplified track model is accepted when dynamics of vehicle motion is considered [4]. Rails and sleepers are treated as a lumped masses (m_r, m_s) of the corresponding rigid bodies. No track irregularities are taken into account. Periodic support of the rails in real track is neglected in the model too. So, the non-inertial type of the moving load is adopted here. Linear elastic springs and dampers connect the track parts (rigid bodies) to each other. Similar approach is allowed in the works in vehicle dynamics where just low frequency deformations of the track are of interest [4].

The track has got 1.435 m gauge and 1:40 rail inclination. Each wheelset is supported by a separate track section consisting of two rail sections and sleepers that correspond to 1m length of typical ballasted real track. Every wheelset – track subsystem has homogenous properties and is independent from the remaining ones. Each route of curved track model is composed of short section of straight track, transition curve and regular arc. Constant value of superelevation depending on curve radius value is applied for each curved track route (Table 1). The predictor-corrector Gear's algorithm is applied to integrate equations of motion. Complete system has 82 kinematic degrees of freedom. More detailed information about the model can be found in [12].

Table 1
Curve radii tested and track superelevations corresponding to them

Curve radius R [m]	3000	4000	6000	∞
Superelevation h [m]	0.110	0.077	0.051	0

3. THE METHOD OF RESEARCH

Determination of velocity ranges, for which stable solutions of the model exists is the first stage of analysis. The stable model solutions are identifying with possibility of modelled (real) vehicle motion. The method is based on the creation and analysis of bifurcation diagrams, which depicts behaviour of the selected model parameter as a function of the bifurcation parameter [2, 3, 11, 12]. The first wheelset lateral displacements y_p were selected as an observed parameter. Vehicle velocity v is the bifurcation parameter here. Constant value of v is applied in each simulation process. Other model parameters also remain constant. Any exterior factor upset the system. Thus, each observed phenomena are characteristic features of the tested model under specific motion conditions. The phenomenon used in the research method base on the generation of self-excited vibrations observed in real vehicle–track systems [6]. Whelset-track vibrations appear when vehicle velocity achieves or exceed some critical value v_n [11]. This is the velocity corresponding to the saddle-node bifurcation point (Fig. 2). In simulation research, exceeding the critical value of a bifurcation parameter may mean a transition from stable stationary solutions (one solution value) to stable periodic solutions of limit cycle character. Ability to maintain such character of solutions in the supercritical range of bifurcation parameter value is characteristic feature of the nonlinear systems. Increasing velocity of motion in subsequent simulations leads to the next bifurcation point. The solutions may bifurcate to unstable one (non-stationary and non-periodic) or to stable stationary one. The maximum vehicle velocity value for which stable solutions occur (stationary or periodic) is called the loss of stability or numerical derailment velocity and denoted v_s. However, this velocity should not be identify with the possibility of real vehicle derailment.

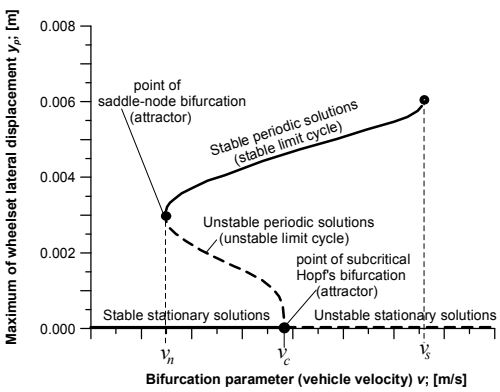

Fig. 2 Hypothetical diagram of vehicle-track model

The chart of the method of bifurcation diagrams creation is presented in figure 3. First wheelset lateral displacements y_p as a function of time (or distance) depicted in the form of diagrams **c** and **d** are the simulation of motion results. Stable stationary solutions exist for vehicle velocity lower than the critical value v_n (one value of the solutions, Fig. 3**c**). If the vehicle velocity is equal or bigger than the critical value v_n, stable periodic solutions may appear (limit cycle, Fig. 3**d**). Maximum values of wheelset lateral displacements absolute value $|y_p|max$ are recorded from each diagram $y_p=f(t)$ (of

3**d** shape). The $|y_p|max$ values presented versus vehicle velocity create the 3**a** diagram. Furthermore the peak-to-peak values of y_p are recorded too. The peak-to-peak values of y_p expressed versus velocity, form the 3**b** diagram. Pair of diagrams 3**a** and **b** prepared for a few curves, constitute the so-called stability map and was adopted as a form of results presentation. The wheelset lateral displacements presented in Figures 3**c** and **d** were obtained from simulation of motion along track consisting of straight section, transition curve and circular arc with radius of R = 2000 m. The need to use a combined route resulted from the fact, that the model created in the VI-Rail program does not start with calculations on the curve directly. The calculations can only be initiated on straight track. Therefore, to observe solutions on the curve, transition curve must be applied. The transition curve negotiation is also the way to put on initial conditions for curve solutions (all wheelsets are shifted laterally in track as a result of transition curve negotiation). To put on the initial conditions is necessary to initiate periodic solutions (self-excited vibrations in the real system) for systems with so-called hard excitation, to which the examined here model belongs. Non-zero wheelset lateral displacements on regular arc are observed (Fig. 3**c**). It is result the lack of balance between lateral forces acting on vehicle in curve. The component of centrifugal force and the component of gravitational force resulting from the applied track superelevation, acting in the track plane are not equal (the values of superelevations applied are shown in Table 1).
Low velocity value (about 10 m/s) is applied at the beginning of each simulation process. Stable stationary solutions occur then only, which means that at constant velocity y_p = const. (and peak-to-peak values are equal zero, p-t-p = 0). The research is concentrated on the critical velocity v_n determination and model properties (character and value of solutions) identification in the overcritical velocity range. The smallest value of the tested model critical velocity appeared at 61.7 m/s. Thus the bifurcation diagrams omit low velocity ranges and in these studies show results above 40 m/s.

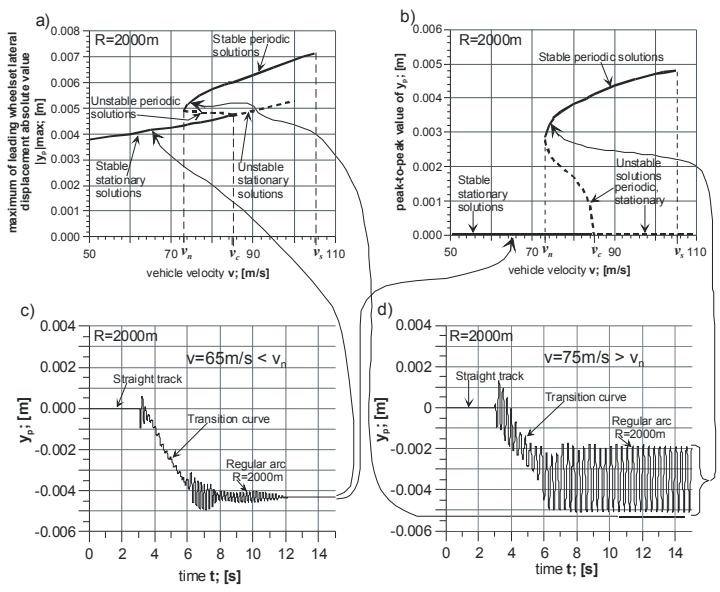

Fig. 3 The bifurcation diagrams creation method

4. THE SCOPE OF RESEARCH

Stable model solutions (stationary and periodic) mean possibility of real vehicle motion from theoretical point of view. The aim of these researches is to check whether, in the overcritical velocity range, when periodic solutions exists (limit cycle – self-exciting vibrations in real system) is possibility of motion determined by criterion other than the stable periodic solution existence. Several criteria are used in railway technology to determine stable and safety vehicle motion. One of the criterion was chosen – so-called ,,track criterion" [7, 8, 9]. This criterion describes the resistance of the track structure to permanent lateral deformation. Visible form of these deformations is the rail and sleepers lateral shift versus ballast [6] (Fig. 4).

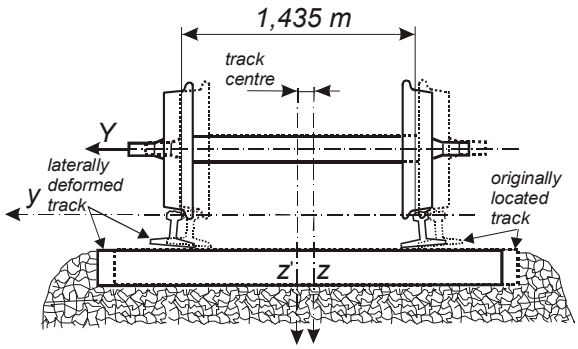

Fig. 4 Lateral track deformation as a result of *Y* force acting

The empirically determined criterion is defined as the permissible value sum of the wheelset guiding forces that is wheelset lateral force acting on track (1).

$$\lim \sum Y_{(2m)} \le K\left(10+\frac{2Q}{3}\right) \quad [kN] \tag{1}$$

where:

K – coefficient depending on the sleepers type, ballast type and its concentration;

2Q – wheelset static pressure on track in [kN].

The lower index of the lateral force sum (*2m*) informs that it is the average value analysed on 2 meters long track section at least. It is recommended to take the coefficient $K = 0.85$ for the track with wooden sleepers and non-compacted ballast. Higher values of factor K are allowed to accept for concrete sleepers and compacted ballast, when higher track resistance to displacements are observed. A similar relation to (1) has the so-called the Prud'homme criterion defining the permissible value of lateral force acting on the wheelset bearing [9].

The 127A type wagon, whose model is tested in a loaded condition, weights approximately 44400 kg. Dividing this mass evenly into four wheelsets, it can be estimated that each wheelset press the track with a mass approximately 11100 kg, i.e. the *2Q* pressure is approx. 111 kN. Substituting the above value for the formula (1) and the least favourable value of the coefficient $K = 0.85$ we get:

$$\lim \sum Y_{(2m)} \le 0{,}85\left(10+\frac{111}{3}\right) = 39{,}95 \quad [kN]$$

So, total lateral force acting on the track at a distance of at least 2 m should not exceed 39.95 kN. It is a force value determining the track resistance to permanent lateral deformation for the concrete model being tested here.
A series simulations of motion were performed on a straight track and curved track with radii R = 6000 m, 4000 m and 3000 m. Both wheelsets of the first bogie were observed. Each simulation was a source of information on the values of guiding forces, which wheelsets exert on the track. Plots showing the dependence of guiding forces versus vehicle velocity of motion were prepared. Vehicle velocity ranges cover the below and above critical velocity values, for which stable model solutions exist.

5. THE RESULTS

The so-called „*stability map*" in a wide range of curves were created at the initial stage of current researches. The map is presented in Figure 5. It is pair of diagrams showing maximum of the first wheelset lateral displacements absolute value $|y_p|max$ and the peak-to-peak values *p-t-p* versus vehicle velocity. One can notice a clear separation between stable stationary solutions (p-t-p = 0) and the area of stable periodic solutions (p-t-p > 0) in each curves except for curve of R = 1200 m. Stable stationary solutions exist only in these curve and for R < 1200 m. The transition from stable stationary to stable periodic solutions takes place at a certain vehicle velocity characteristic for each curve. These velocities are called critical velocities v_n and values are collected in Table 2.

Table 2
Critical velocities and loose of stability velocities for particular curve radius

Curve radius $\boldsymbol{R}$; [m]	2000	3000	4000	6000	∞
Critical velocity $\boldsymbol{v_n}$; [m/s]	62	71.5	67	63.2	61.7
Loos of stability velocity $\boldsymbol{v_s}$; [m/s]	88	109	120	142	130

Stable periodic solutions remain until the maximum vehicle velocity for which stable solutions exist in straight track only. In curves transitions from stable periodic to stable stationary solutions are observed. The maximum vehicle velocity for which stable solutions exist (stationary or periodic) is called the loose of stability velocity and marked v_s. The velocity is characteristic for each curve and particular values for tested curve radii are collected in Table 2.

First bogie wheelsets lateral forces (guiding forces), which acts on the track in lateral direction were also recorded from each simulation of motion made to create the above stability map. Examples of their forms at velocity 70 m/s are presented in Fig. 6.

The diagrams show variation of guiding forces during 1 second of motion (between 12 and 13 seconds from a 15 second simulation time). Horizontal dashed lines indicate the limit value of lateral forces $\Sigma Y_{(2m)}$ = ± 39950 N. Positive or negative force value means the direction of its action and direction of possible track displacement.

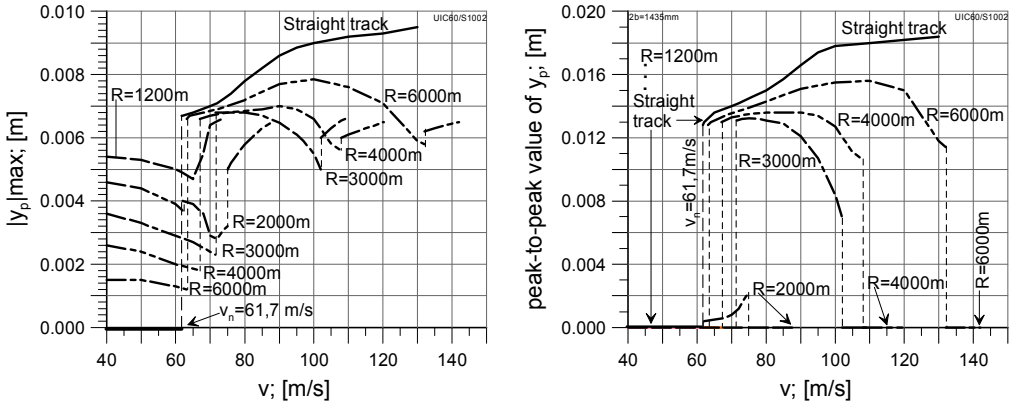

Fig. 5 The tested vehicle model stability map

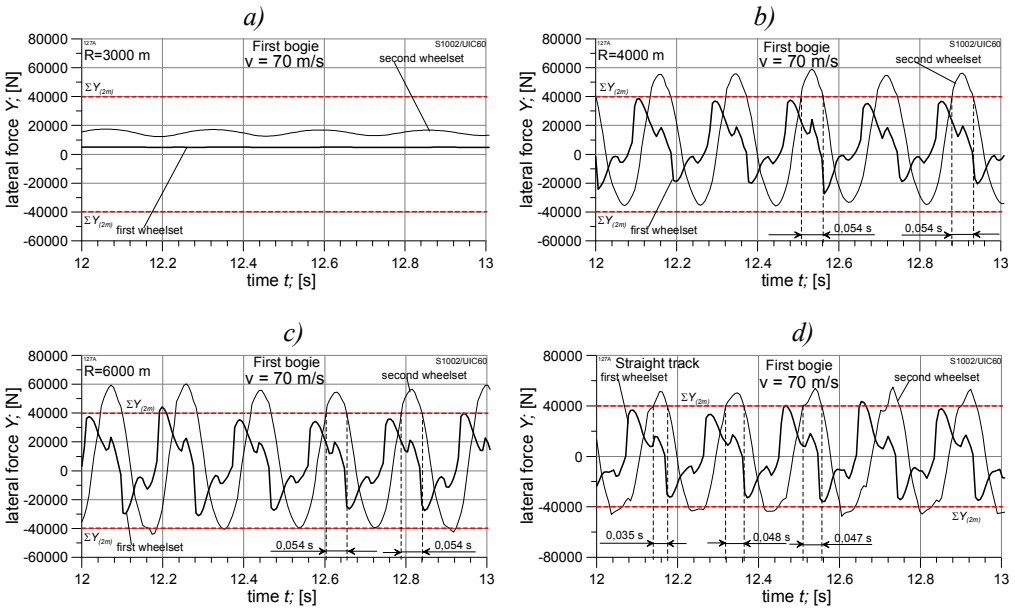

Fig. 6 The first bogie wheelsets lateral (guiding) forces at velocity 70 m/s in curves of radii R: *a*) 3000 m, *b*) 4000 m, *c*) 6000 m, *d*) ∞

Velocity value of 70 m/s is greater than the critical value on all curves except the curve of radius R = 3000 m. It can be noticed that only in this case lateral forces are significantly less than the permissible values. One of the wheelsets at least reaches or exceeds the limit value in other cases.

The researches of first bogie's wheelsets–track lateral interaction were conducted in wide range of vehicle velocity. Diagrams of the form visible in Fig. 6 were created for results obtained from each simulation process. Both wheelsets lateral forces maximum values were recorded. The results for curve radius R = 3000, 4000, 6000 and ∞ are shown in Figure 7.

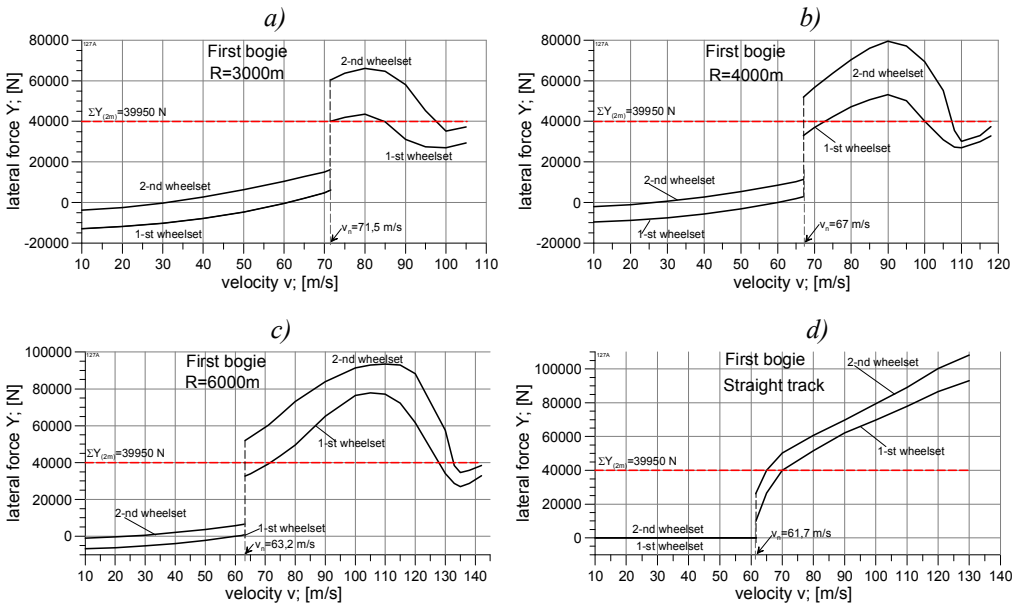

Fig. 7 The first bogie wheelsets lateral (guiding) forces affecting track in the range of stable model solutions in curves of radii: *a*) 3000 m, *b*) 4000 m, *c*) 6000 m, *d*) ∞

It can be noticed that in the scope of stable stationary solutions, both wheelsets lateral forces are significantly smaller than the permissible value $\Sigma Y_{(2m)} = \pm 39950$ N. Achieving the critical velocity (transition from stable stationary to stable periodic solutions) means a step increase of lateral forces coming from both wheelsets. The lateral force from one wheelset only exceeds the limit value already at the critical velocity v_n in curves. But in straight track the lateral forces from both wheelsets are smaller than the $\Sigma Y_{(2m)}$ at velocity v_n. Lateral force increase according to vehicle velocity increase for all curve radii applied. The growing character of solutions remains until the end of stable solutions existence in straight track (up to velocity of about 130 m/s). In curved tracks, lateral forces increase in the initial range of overcritical velocities, reach the maximum and then decrease to values smaller than $\Sigma Y_{(2m)}$. This is due to the centrifugal forces action, which increases according to vehicle motion velocity increase. The centrifugal forces acting on wheelsets, ,,dumps" the self-exciting vibrations generated in wheelset-track system and finally follow to transition from stable periodic to stable stationary solutions at the final velocity range of stable solutions existence (see Figure 5). Significant influence of curve radius on maximum values of wheelset-track lateral forces is noticeable.

6. CONCLUDING REMARKS

Achieving or exceeding the critical velocity v_n means several times increase of wheelset-track lateral forces impact compared to the forces operating below the v_n. The permissible value of lateral force is exceeded directly when v_n is achieved in curves. It

means a real possibility of permanent track damage through its lateral displacements. Curve radius influence on the lateral forces is noticeable and surprising. Maximum lateral forces increase according to curve radius increase. It is known that the centrifugal force decreases as the curve radius increase ($F_r = mv^2/R$). However, in the conditions of self-exciting vibrations existence, wheelsets perform larger lateral displacements in curves with larger radii (Fig. 5) and dynamical forces resulting from wheelsets oscillatory motion dominate over the small centrifugal force.

7. REFERENCES

[1] **Bałuch, H.**: *Diagnostyka nawierzchni kolejowej*, *Railway diagnostics*, WKŁ, Warsaw, 2003. (In Polish).

[2] **Dusza, M. – Zboiński, K**.: *Bifurcation approach to the stability analysis of rail vehicle models in a curved track*. The Archives of Transport, volume XXI, Issue 1-2, Warsaw 2009, p.147-160.

[3] **Dusza, M**.: *The wheel-rail contact friction influence on high speed vehicle model stability*. Transport Problems, Volume 10, Issue 3, Gliwice 2015, p.73-86.

[4] **Iwnicki, S**. (editor): *Handbook of railway vehicle dynamics*. CRC Press Inc., 2006.

[5] **Kalker, J.J**.: *A fast algorithm for the simplified theory of rolling contact*. Vehicle System Dynamics 11, 1982, p.1-13.

[6] **Knothe, K. – Bohm, F**.: *History of Stability of Railway and Road Vehicles*. Vehicle System Dynamics, 31, 1999, p.283-323.

[7] Norm: UIC CODE 518, Testing and approval of railway vehicle from the point of view of their dynamic behaviour – Safety – Track fatigue – Ride quality.

[8] **Sysak, J**.: *Drogi Kolejowe* (in polish). *Railways,* PWN, Warsaw 1986.

[9] **Towpik, K**.: *Infrastruktura drogi kolejowej, obciążenia i trwałość nawierzchni* (in polish). *Railway infrastructure, loads and surface durability.* Wydawnictwo Instytutu Technologii Eksploatacji – PIB Warsaw-Radom 2006.

[10] **Wilson, N**. **– Fires, R**. **– Witte, M**. **– Haigermoser, A**. **– Wrang, M**. **– Evans, J**. **– Orlova, A**.: *Assessment of safety against derailment using simulations and vehicle acceptance test: a worldwide comparison of state-of-the-art assessment methods*, Vehicle System Dynamics, Vol. 49, No. 7, July 2011, p.1113-1157.

[11] **Zboiński, K. – Dusza, M**.: *Self-exciting vibrations and Hopf's bifurcation in nonlinear stability analysis of rail vehicles in curved track*. European Journal of Mechanics, Part A/Solids, Volume 29, No. 2, 2010, p.190-203.

[12] **Zboiński, K. – Dusza, M**.: *Bifurcation analysis of 4-axle rail vehicle models in a curved track*, Nonlinear Dynamics, July 2017, Volume 89, Issue 2, DOI 10.1007/s11071-017-3489-y, ISSN 0924-090X, p.863-885.

ESTIMATING METHOD OF WHEEL-RAIL FRICTION CONDITION BY USING *PQ* MONITORING BOGIE

Itsuro ARAI[1], Masuhisa TANIMOTO[1], Shinichi WATANABE[1], Takuya MATSUDA[1], Akira MATSUMOTO[2] and Yohei MICHITSUJI[3]

[1]Tokyo Metro Co., Ltd. 3-19-6 Higashi-ueno, Taito-ku, Tokyo, 110-8614, Japan
[2]Nihon University, 1-2-1 Izumi-cho, Narashino, Chiba 275-8575, Japan
[3]Ibaraki University, 4-12-1 Nakanarusawa-cho, Hitachi, Ibaraki 316-8511, Japan

Received: September 12, 2019

ABSTRACT

When vehicles are passing sharp curves, both wheel flange and outer rail side are worn. The wear of wheels and rails is caused by high friction coefficient which will increase a risk of derailment. On the other hand, low friction coefficient will be a trigger for wheel slip. Despite this critical problem, there are few former researches on the wear of contact area. Therefore, authors developed an estimating method of identification for the friction condition of the wheels and rails by using PQ monitoring bogie. That bogie can measure lateral force, vertical force and tangential force on the contact area while running on commercial line. Furthermore, authors propose the method to predict wheel flange wear and rail side wear by using this estimating way of identifying the friction condition.

Keywords: flange wear, rail side wear, monitoring, friction coefficient

1. INTRODUCTION

Authors developed an estimating method of identification for the friction condition of the wheels and rails by using PQ monitoring bogie. The condition was estimated by the forces between wheel and rail monitored by this bogie.
Frist, a bench test was conducted to investigate whether a friction could be estimated. Then, a friction condition was estimated by monitored tangential force and vertical force. Second, we developed the estimating method for the wear of wheels and rails by using PQ monitoring bogie. In this method, the wear amount was calculated from the friction condition estimated by monitored tangential force and vertical force. Finally, verification of this method was confirmed by measured rail side wear and wear of flange.

1.1 Time-based maintenance

To maintain both wheels and rails, we used to conduct a time-based maintenance as following cycle.

(1) Measuring rail side wear and wheel flange wear at timing of measurement.
(2) Identify curves with high friction coefficient.
(3) Changing lubrication condition of outer rail by rail lubricators.

However, in this cycle, we couldn't identify curves with high friction coefficient immediately because this cycle is based on measurement timing once a half year. This time-based maintenance is a breakdown maintenance. Therefore, the purpose of our research is to develop estimating method of identification for the friction condition of the wheels and rails to realize a preventive maintenance.

1.2 Measurement of wear

An amount of rail side wear is measured by track inspection car once a half year. Fig.1 shows the example of measured rail side wear. In Fig.1, sometimes rail side wear

decreased, it means that rail renewal was conducted. And an amount of wheel flange wear is measured once a half year at timing of wheel turning at depot.

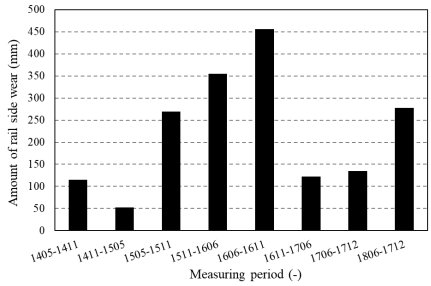

Fig. 1 Example of measured rail side wear

Graphs in Fig.2 are the comparison of outer rail side wear and wheel flange wear. Each wheel of trains touches outer rail side in different curves. It depends on both curve direction and train direction. Therefore, to consider each types of contact situation, we can compare wear of wheels and rails. From these graphs, outer rail side wear and wheel flange wear are correlated. However, there are some other factors that have an influence on the friction condition of the contact area like lubrication condition.

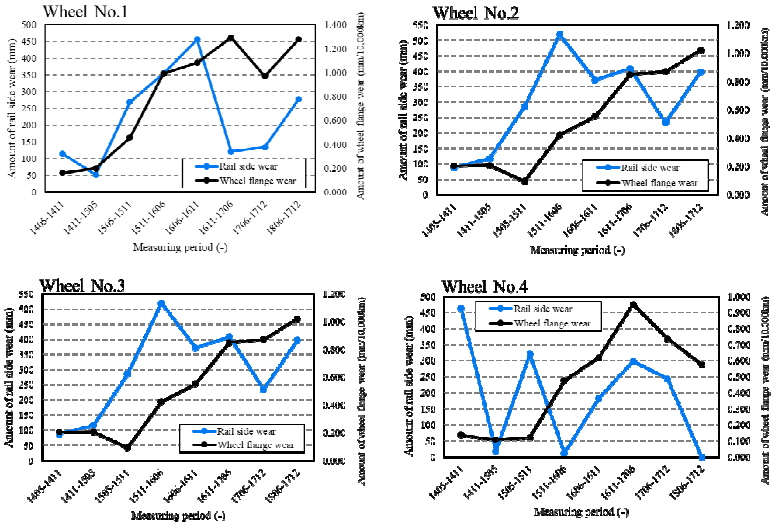

Fig. 2 Comparison of outer rail side wear and wheel flange wear

2. PRECONDITION OF RESEARCH

2.1 PQ monitoring bogie

PQ monitoring bogie can measure vertical force, lateral force and tangential force on the contact area while running on a commercial line. In this paper, P means the vertical force and Q means the lateral force. The bogie has three sensors to measure these

values (Fig.3). Vertical force sensor is measuring an axle spring deflection by magnetic strain gauge. Lateral force sensor is measuring a wheel plate deformation by eddy-current displacement gauge. Tangential force sensor is measuring the load on a single link by strain gauge. Trains with PQ monitoring bogie has data transmission device under the seats. Therefore, measured data by PQ monitoring bogie can be transmitted to office immediately.

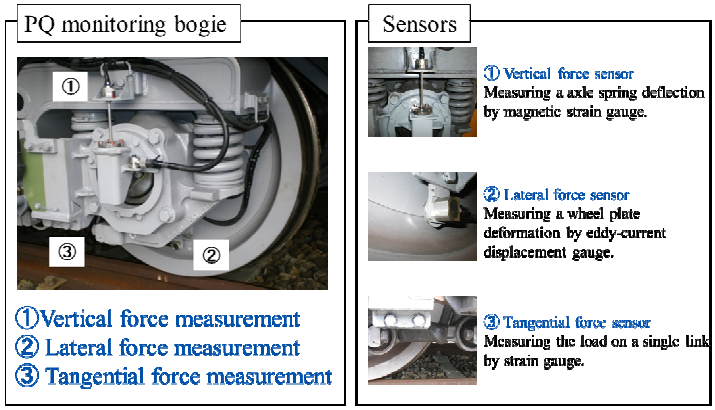

Fig. 3 Sensors of PQ monitoring bogie

2.2 Rail lubricator

Rail lubricators are installed at the beginning of transition curve (Fig.4). Outer rail lubricators are installed to prevent rail side wear. On the other hand, inner rail lubricators are installed to prevent rail corrugation and squeal noise.

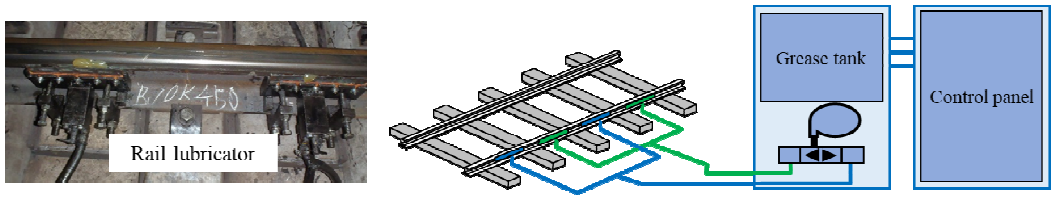

Fig. 4 Outline of rail lubricator

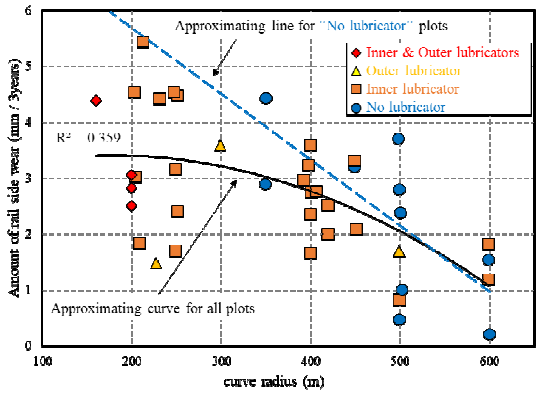

Fig. 5 Relationship between rail side wear and curve radius

Fig. 5 shows the relationship between rail side wear and curve radius. Plots in the Figure shows the effect of rail lubricators. Inner lubricators are installed to prevent corrugation, but lubrication for inner wheel effects its reaction, lateral force of outer wheel.
Therefore, inner lubricators also have a certain effect to the rail side wear. A low correlation coefficient in the figure is the reason why we change settings of rail lubricator for each curve. From this figure, it is considered that if there were no lubricators on sharp curves, more and more rail side wear would be observed on the curves.

3. STAND TEST BY ROLLER RIG

A stand test by roller rig was conducted to investigate whether a friction condition between wheels and rails could be estimated.

3.1 Test condition

The stand test by roller rig (Fig.6) reproduced bogie curving by installing a rotational speed of difference between outside and inside wheels and an angle of attack. This bogie used PQ monitoring wheelset to measure vertical force and tangential force. In addition, a friction coefficient could be changed easily by applying grease. Table.1 shows testing lubrication conditions. In Table.1, “oil” means low friction coefficient by the grease.

Fig. 6 Stand test by roller rig

Table. 1 Lubrication conditions

Condition	Leading axle	
	Outer	Inner
No.1	Dry	Dry
No.2	Oil	Dry
No.3	Oil	Oil
No.4	Dry	Oil

For example, condition No.2 is outer “oil” and inner “dry”, so it means that we applied grease only outer wheel of leading axle in this case. Condition No. 4 is outer “dry” and inner “oil”, so we applied grease only inner wheel of leading axle. Both condition No.2 and No.4 are shown in Fig. 7.

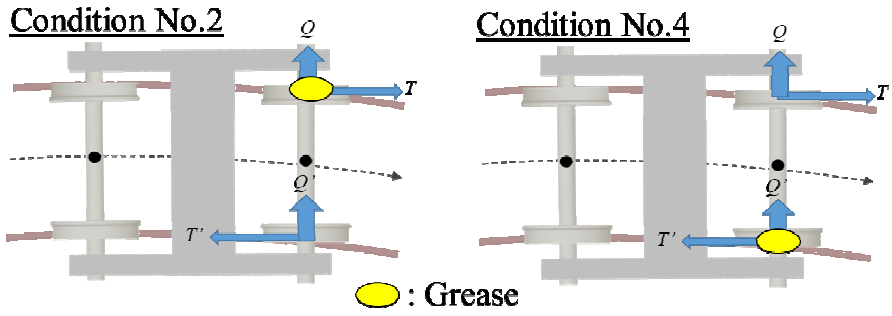

Fig. 7 Lubrication condition No.2 and No.4

In addition, as shown in this figure, lateral force (Q, Q') and tangential force (T, T') effects different direction.
Furthermore, wheel flange wear was measured by collecting worn powder on gluing kent paper in this stand test.

3.2 Test result

The occupation of scattered worn powder on gluing kent paper was calculated by special microscope. From Fig.8, in the case of high friction coefficient, worn powder was increased with an increase of curvature. However, we couldn't gather all of powder. Few powders were scattered out of the paper. So, this is a qualitative data to understand the tendency.

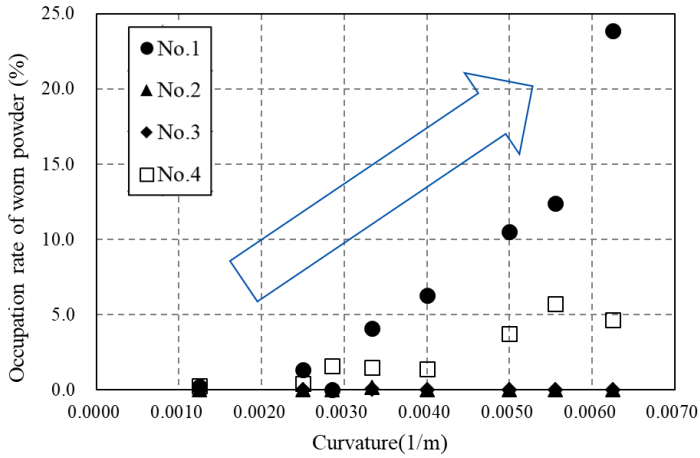

Fig. 8 Wheel flange wear in various lubrication conditions

The lubrication condition was estimated by lateral force divided by vertical force (κ) and tangential force divided by vertical force (T/P). Fig.9 shows the result of each lubrication conditions. From this figure, test results were plotted on 3 areas (Area A to C).

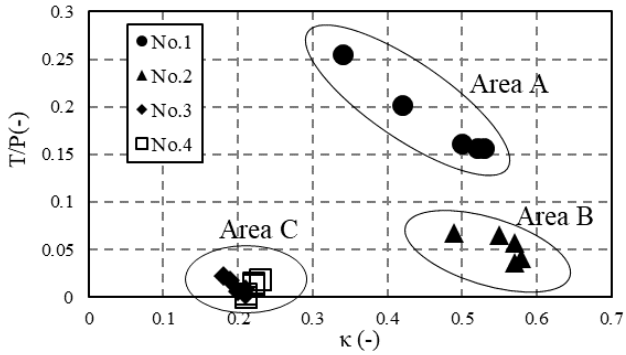

Fig. 9 Test results under different lubrication conditions

It was known that a wheel flange wear and outer rail side wear occurred under dry condition like Area A in Fig.9. Therefore, the result of the test showed that the lubrication condition could be estimated by κ and T/P measured by PQ monitoring bogie.
The relationship between these results in terms of T/P, κ and wheel flange wear in each lubrication condition was inspected.
The results of lubrication condition No.1 were plotted on area A. In addition, deep wheel flange wear was measured on the area (Fig. 8). Therefore, this result shows that the high friction coefficient generates deeper wheel flange wear.
The results of lubrication condition No.2 were plotted on area B. In this area, no wheel flange wear was measured (Fig. 8). No.2 condition was outer "oil" and inner "dry", so, low friction coefficient on wheel flange generates the wheel flange wear.
The results of lubrication condition No.3 were plotted on area C. In this area, we couldn't measure wheel flange wear (Fig. 8). We applied grease both outer and inner wheel. Therefore, friction coefficient of No.3 was very low.
At last, the results of lubrication condition No.4 were plotted on area C. Very few wheel flange wear was measured on the area (Fig.8).
Therefore, the lubrication condition could be estimated by "friction condition figure" like Fig. 9. From these results, authors created the estimating method of friction condition by the concept of this figure.

4. ESTIMATING METHOD FOR RAIL SIDE WEAR

Based on the result of the stand test by roller rig, an estimating method for rail side wear by measured values from PQ monitoring bogie was developed.

4.1 Estimating steps

The rail side wear was calculated by following 3 steps.

Step1: Create the lubrication condition figure for one month running on certain curve on a commercial line.

Step2: Calculate a ratio of the values in step1 that plotted in Area A in Fig.9. The ratio was γ_i , and it was defined as the ratio of high friction coefficient condition.

Step3: Calculate the sum of γ_i for some months.

Fig.10 shows the example of friction condition figure on a certain curve. The ratio of high friction coefficient was determined by threshold depends on each curvature (Table.2).

Table. 2 Threshold in each curvature

Curvature	Threshold	
	κ	T/P
0.0033	0.32	0.19
0.0040	0.35	0.16
0.0050	0.37	0.13
0.0056	0.38	0.12
0.0063	0.39	0.12

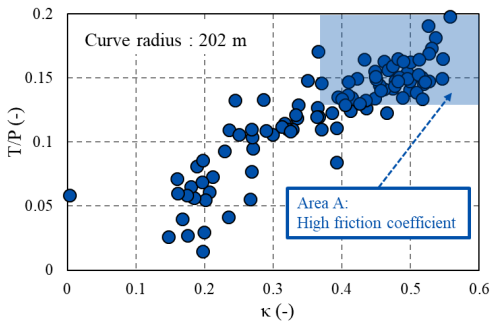

Fig. 10 Example of friction condition figure

A rail side wear measurement vehicle runs commercial line once every 6 months. Therefore, in the Step3, authors calculated $\Sigma\gamma_6$ to compare the estimated values and the measured values.

4.2 Result of the comparison

Fig.11 shows the result of the comparison. The deviation between the estimated values and the measured values was slight. The grease of rail lubricator was decreased in November 2016, and this result could grasp that change of lubrication condition.

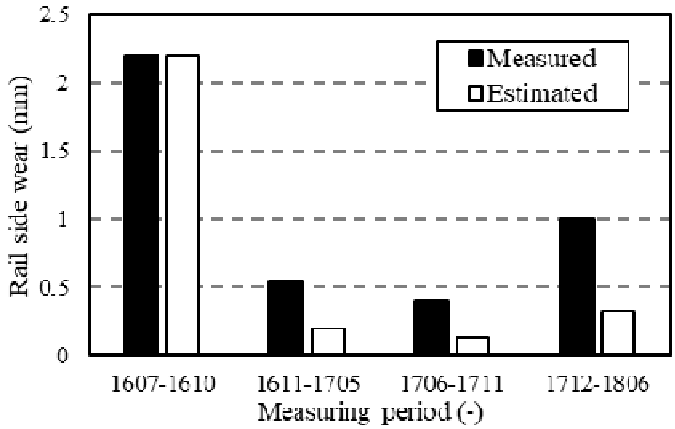

Fig. 11 Comparison between estimated rail side wear and measured values

5. ESTIMATING METHOD FOR WHEEL FLANGE WEAR

An estimating method for wheel flange wear by measured values from PQ monitoring bogie was developed.

5.1 Estimating steps

The wheel flange wear was calculated by following 5 steps. Step1 and Step2 were same as the case of rail side wear estimation.

Step1: Create the lubrication condition figure for one month running on certain curve on a commercial line.

Step2: Calculate a ratio of the values in step1 that plotted in Area A in Fig.9. The ratio was γ_i , and it was defined as the ratio of high friction coefficient condition.

Step3: The ratio γ_i was multiplied by the length of circular curve (L_i). The value was defined $\gamma_i \times L_i$.

Step4: Calculate the sum of $\gamma_i \times L_i$ in the case of curves that the wheel became outside of the leading axle.

Step5: Calculate the sum of $\gamma_i \times L_i$ for some months.

In this case, authors calculated $\Sigma\gamma_1$ to compare the estimated values and the measured values. Wheel flange wear of each wheel is measured once a half year at timing of wheel turning at depot, but authors could calculate the amount of wear for a month from the data of each wheel.

5.2 Result of the comparison

From the result shown in Fig.12, Same as the result of estimation for the rail side wear, our method could grasp a tendency of wheel flange wear. The deviation between the estimated values and the measured values was slight. Based on these estimated values, the curve with high coefficient where becomes the cause of wheel flange wear could be identified.

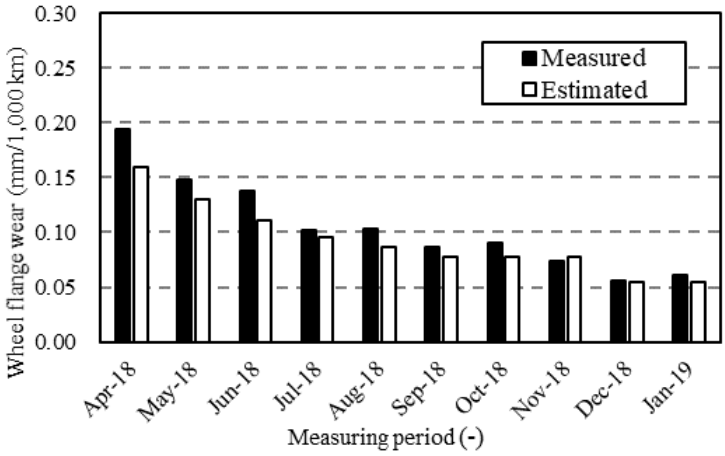

Fig. 12 Comparison between estimated wheel flange wear and measured values

6. CONDITION BASED MAINTENANCE

From the comparison results, an accuracy of our method in terms of wheel-rail wear was confirmed. The deviation was slight in both cases. Therefore, based on the estimating method of wheel-rail friction condition by using PQ monitoring bogie, the curve with high friction coefficient could be identified. By using the estimating method, we can decide lubrication priority to prevent the wear of both wheels and rails. For example, the grease of outer lubricator on a sharp curve with high friction coefficient will be increased to prevent wear of wheels and rails.

Unlike conventional time-based maintenance, condition based maintenance cycle as following was installed. It could be realized by the estimating method of this research.

(1) Measuring vertical force, lateral force and tangential force by PQ monitoring bogie.

(2) Create the friction condition figure for each curve.

(3) Estimating rail side wear and wheel flange wear.

(4) Decide lubrication priority.

This condition based maintenance cycle needs only several weeks. Because of this cycle, a lifetime of rails and wheels will be extended.

7. CONCLUSIONS

Authors developed an estimating method of identification for the friction condition of the wheels and rails by using PQ monitoring bogie. The deviation between the estimated values and the measured values was slight. Therefore, our method could identify the curve with high friction coefficient. That data could be updated quickly by using PQ monitoring bogie, and it applied to decide lubrication priority to prevent the wear of both wheels and rails. We believe that our method is highly effective to realize condition based maintenance on the prevention of wheel-rail wear.

In the future, we must verify the effect of our method on commercial lines. For example, to investigate costs and efficiency of the condition based maintenance, and the relationship between lubrication condition and wheel slip.

8. REFERENCES

[1] **Michitsuji, Ishii, Nagasawa, Matsumoto, Ohno, Sato, Ogata, Tanimoto, Iwamoto, Fukushima and Shinagawa**: Transactions of the JSME, Vol.83, No. 856, 2017.

[2] **Matsuda, T. - Fukushima, T. - Tanimoto, M. - Watanabe, S. - Arai, I. - Yonehara, Y.:** The relationship between rail side wear and flange wear. J-Rail 2018: JSCM10-2, 2018.

[3] **Matsuda, T. - Ogino, T. - Watanabe, S. - Arai, I. - Yonehara, Y. - Tanimoto, M. - Matsumoto, A. - Michitsuji, Y. - Ichiyanagi, Y. - Sato, Y. - Ohno, H.**: Estimation method of the curve where flange wear occurs by utilizing continuous data through the PQ monitoring bogie on Tokyo Metro's commercial line. Transactions of the JSME (Under review).

THE *LIBERTY WHEEL*

Andrea BRACCIALI and Gianluca MEGNA

Department of Industrial Engineering, University of Florence, Italy
Via Santa Marta 3,
I-50139, Florence, Italy

Received: September 10, 2019

ABSTRACT

A new concept for tyred wheels is introduced in the paper, allowing cost reduction, mass reduction and shorter supply times. The project is based on a deep and critical review of the current practice in wheel maintenance and the current supply chain, finding and solving the criticalities that led to the current monopoly of monobloc wheels. It will be shown that the new tyred wheel, named *Liberty Wheel*, keeps its promises, allowing seamless rolling stock operation thanks to simple and inexpensive maintenance operations possible in nearly all current maintenance shops. It is a revolution for vehicles running up to at least 160 km/h without "strong" tread braking (trams, metros, light rail, commuter trains, regional trains, locos for freight trains, etc.)

Keywords: tyred wheels, tyres, machining, dovetail coupling, thermal stresses, ADI cast iron.

1. INTRODUCTION

1.1 Why *Liberty Wheels*?

Liberty means freedom in an even higher acceptation. Franklin D. Roosevelt, in the State of the Union Address to the Congress, January 6, 1941, proposed four fundamental freedoms that people "everywhere in the world" ought to enjoy: *Freedom of speech, Freedom of worship, Freedom from want, Freedom from fear*.

Such freedoms can not all and always be available in the purchasing process of wheels. Wheelset manufacturers managed to drive the market to monobloc wheels solution, claiming it's safer, cheaper, lighter, in a word "better". This was embraced enthusiastically in a historical phase when many state-owned railway administration fell down or downsized dramatically. Outsourcing wheelset maintenance was often a no-alternatives decision, as internal workshops were closing, old workforce retiring and fixed costs reduction became an obsession.

Nowadays, almost all smaller railway enterprises sign "full service" contract with vehicle suppliers or, in the worst case, with external workshops to keep their wheelsets in good shape and to safely operate their fleets. Only larger railway enterprises still have their own "second level workshops", where wheels are replaced, axles are machined and checked and so on.

We have forgotten that the two basic components of a wheelset – the axle and the wheels – are designed for *infinite life*, i.e. they do not fail if properly operated in service whatever long they serve under a vehicle. This statement falls like a house of cards when considering wheel tread wear.

Wheel tread wear is the inevitable result of the interaction between the wheel tread and the rail. Both wheels and rails suffer of many kinds of defects whose description lies outside the scope of this paper. However, due to flange wear, hollow tread wear or both the nominal wheel tread profile must be periodically restored machining it by

means of underfloor lathe. This “reprofiling” process can be applied a limited number of times, until the wheel tread must be changed with a new one.

But, incidentally, tread is only a minor part of a monobloc wheel, that must be *entirely scrapped*, despite the fact that, as said, it was designed for infinite life. Moreover, the monobloc wheels replacing process may damage, and in many case *it damages*, the wheel seats, i.e. those portions of the axles that interface (with interference) with the wheels. As a consequence, axles need to be machined. After a few cycles, the axles need to be replaced, and this once again contradicts the assumption that axles should last forever.

All this nightmare, that makes wheelset manufacturers incredibly rich, was already existing before the “progress” of the last decades: the tyred wheel. Changing the (steel) tyres in a railway vehicle has the same effect of changing the (rubber) tyres in a car: the service may restart immediately without limitation. One could ask himself why tyred wheels went out of fashion: we’ll give our interpretation of the story, based on workshop practice, on workforce cost and on the distortion of a legislation that, at least in Europe, played a determinant role in forgetting what the founders of railways individuated as the best way to perform maintenance.

1.2 Technical and legislation reasons for tyred wheels death

Once all rail vehicles had tyred wheels. Since the braking was exclusively with blocks acting on the wheel tread, the only wear elements were, of course, brake blocks and wheel rims. There are steam locomotives and, subsequently, electric locomotives, which have been traveling for over 50 years without replacing the wheel centers and in many cases not even the axles, changing only the tyres.

Analyzing the reason of the rise of monobloc wheels, we must first mention the most serious problem of the tyred wheels, that is the risk of tyre loosening. This risk became certainty in the case of drag braking of freight wagons on long alpine descents, seriously affecting safety. From the 1960s onwards it was therefore understood that for freight traffic tyred wheels were unsuitable for guaranteeing the desired level of safety and monobloc wheels with low residual stresses, specific for the tread braking, began to develop.

The second reason for the gradual abandonment of the tyred wheels is to be found in European legislation. In 2002, in fact, the first Technical Specifications for Interoperability (TSIs) of the European High Speed system were published. As known, the TSIs are "supported" by the EN standards which must comply with the essential requirements of the Railway Safety Directing. Dealing with high speed, tyred wheels were considered as centrifugal actions at 300 km/h may loosen the tyres. When the TSIs for the "conventional railway" were published in 2007, the regulator "forgot" to reconsider tyred wheels. It is worth to remember that participation in standardization groups is voluntary and unpaid, and that no producer of railway wheels (obviously monobloc) had any interest in reintroducing a solution that made them earn less. But the third and final reason is linked to maintenance costs and will be discussed in the paper.

2. THE DESIGN OF TYRED WHEELS: SHRINK FIT STRESSES

Recent literature on the design of tyred wheels is simply non-existent. One of the few references providing information on stresses and strains in the wheel centre and in the

wheel tyre is the old book by K. Sachs, “Elektrische Triebfahrzeuge”, published in 1973. A sketch comparing monobloc and tyred wheels is shown for convenience in Figure 1.

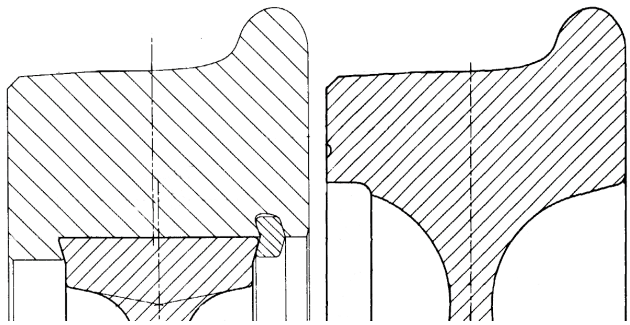

Fig. 1 Drawings of a tyred (420 kg, left) and monobloc (340 kg, right) wheel with the same external diameter of 940 mm. Tyres are fitted with a typical interference of 1.3‰ of the coupling diameter in mm.

We observed that almost all wheel centres had “curves” in the cross-section. Apparently, this was due to the need of ensuring some radial elasticity to compensate for the expansion and the contraction of the tyre during long drag brakings.

We developed a FEM model able to predict what happens when a tyre is applied by shrink fitting to four different types of wheel centre considering also the wheel centre fitting on the axle and we published the reults in paper [1]. The original results from prof. Sachs’s book that we used as a reference are shown in Figure 2.

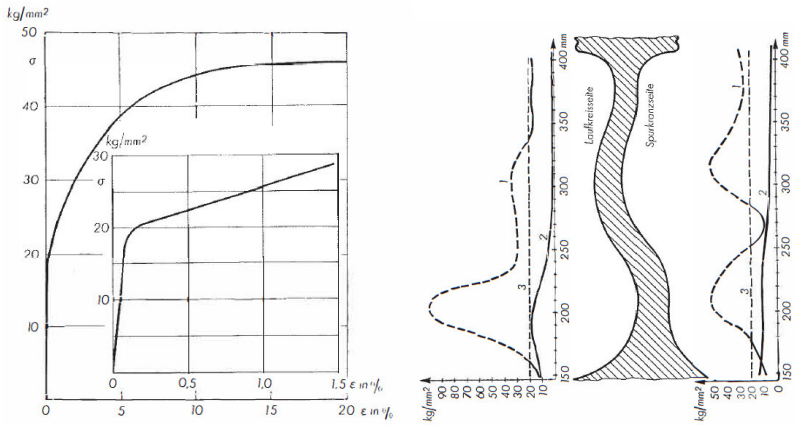

Fig. 2 Left: tensile strength curve for the wheel centre steel, with a focus on the yield point. Right: comparison of the von Mises equivalent stresses with the yield stress (3), for the axle + tyre fitting (1) and for the axle fitting only (2).

During the analyses, it readily emerged that in most cases the elastic limit of the material in the wheel centre is exceeded. A purely linear model of the material behaviour is therefore not sufficient and an ideal elasto-plastic material model was used. Resulting von Mises stresses from our simulations are shown in Figure 3.

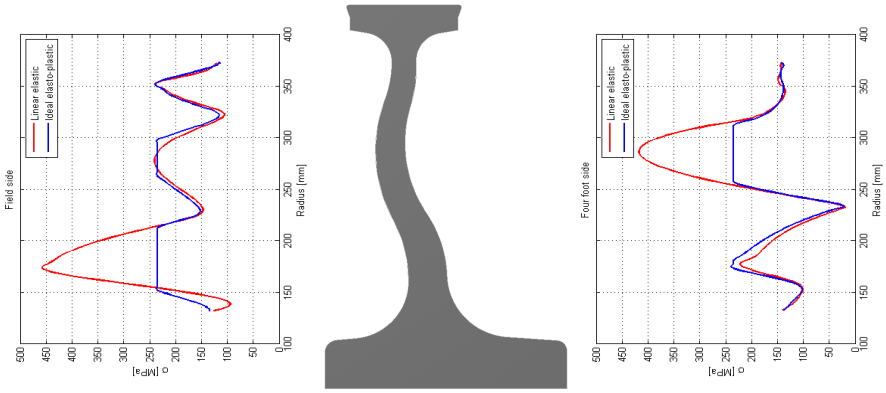

Fig. 3 von Mises stresses for a linear elastic material model and an ideal elasto-plastic material model.

Plastic strains can not be neglected and can bring to permanent shape modifications in the wheel centre geometry and may influence wheelset geometric tolerances. We learned therefore that the design of older wheel centre was probably performed before the computer era on the basis of (unknown) empirical calculations. We found in fact large variations in the radial stiffness (from 56 to 119 MPa/mm applying 1 MPa on the mating surface of linear models representing the four wheels analysed) and this means that a guideline or a general design rule was missing.

We discovered moreover that the pressure at the tyre/wheel centre interface was extremely variable, in one case from around 70 MPa just over the wheel web to around 28 at the ends of the contact (Figure 4). This looks like a design mistake, but we should never forget that in the XIX Century there were no the sophisticated resources that are available today.

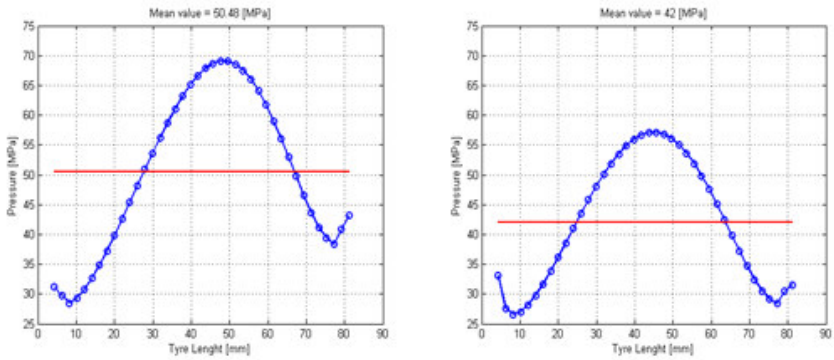

Fig. 4 Pressure at the wheel/tyre interface with the maximum interference and new tyre for two different axisymmetric wheels.

Thanks to the experience gained with these simulations, we are now able to analyse any existing wheel centre and evaluate its elasto-plastic behaviour, its radial stiffness and, even more important, lateral deviations arising from the tyre cooling process that may impair the correct geometry (Figure 5). The application of the *Liberty Wheel* con-

cept to existing wheel centre passes inevitably through this crucial phase that must be conducted carefully.

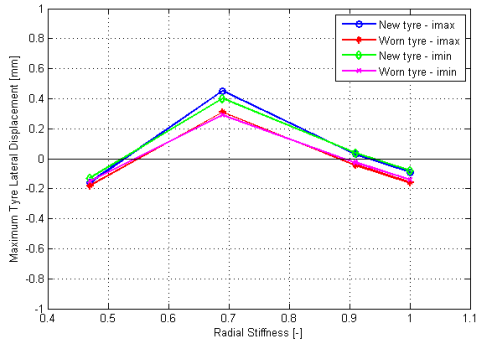

Fig. 5 Lateral displacement of the tyre after the shrink fitting as a function of radial stiffness (normalized to the stiffest wheel = 119 MPa/mm).

3. THE DESIGN OF TYRED WHEELS: IS TYRE THICKNESS CORRECT?

New tyre thickness is normally 70÷75 mm and the worn thickness is 35÷40 mm. This is due to the need of transmitting the maximum torque in all braking (hot) conditions also in fully worn conditions. As a consequence, tyred wheels are much heavier than monobloc wheels.

It should be remembered that the inequacy of tyred wheels to withstand drag braking was investigated and clarified in the '60s of the last century. As an example (see [2] for more details), tyres can be considered as "loosened" after a 15 minutes brake with a tread braking power of 20 kW, values that are much lower than those required by the standards simulating the Gotthard line slope. As a result, freight wagons are going to be equipped by 2020 only with monobloc wheels.

If the thermal input is largely decreased, as in modern EMU that use tread braking only marginally, or completely eliminated, as in all vehicles braked with brake discs, the tyre-wheel centre pressure needed is lower.

We performed a thorough analysis, published in [2], where we compared the torque transmitted at the wheel-rail contact (and therefore at the tyre-wheel centre interface) for light DMUs, a 20 t/axle diesel locomotive, a 17.2 t/axle electric locomotive and a 21 t/axle locomotive with different wheel and transmission arrangements, considering a maximum wheel-rail friction coefficient of μ=0.8. Also self-excited vibrations of kinematic transmission chain and traction motor short circuits were considered. A suitable model was set up and we found the the average pressure needed at the tyre-wheel centre interface was, in the worst case, lower than 1 MPa.

As we said before that the pressure at the tyre-wheel centre interface ranges from 25 MPa to nearly 70 MPa, it is evident that there are large margins of improvement to reduce tyre thickness and/or interference. Without any thermal input, in fact, the torque transmissible by the current (old) tyred wheels is more than ten times the traction motor short circuit situation.

We have developed all the tools needed to evaluate local slip that may happen at the tyre-wheel centre coupling in case the pressure is reduced. This analysis is central to avoid the appearance of a classical and certainly undesired phenomenon potentially present in interference fit couplings, i.e. *fretting corrosion*.

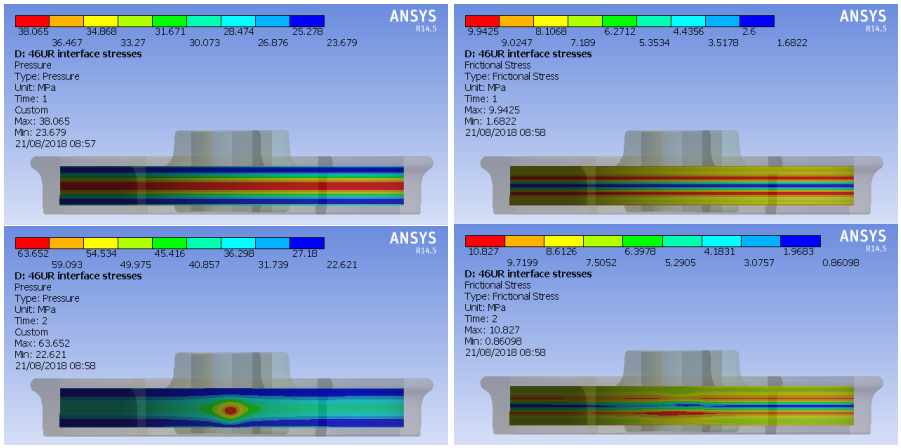

Fig. 6 Top: pressure at the wheel centre-tyre interface (left) and frictional stresses (right) for μ_{tw} =0.3 for a freight wagon wheel with the tyred fitted at maximum interference (1.106 mm). Bottom: the same with vertical load (100 kN) and maximum torque (14795 Nm)

Figure 6 gives an example of the degree of detail and accuracy that we have reached in simulating the combined effect of preload (tyre shrink fit), applied torque and applied vertical load.

Referring to the title of this chapter, we can say that the tyre thickness used in the past for heavily-tread braked vehicle is not correct, being to large. We can investigate the effect on pressure, loosening and fretting phenomena on vehicles of any kind, reducing the mass of existing tyres by nearly 50%.

4. TYRED WHEELS MAINTENANCE: ANALYSIS AND IMPROVEMENTS

Tyred wheels were not abandoned for mass reasons or for thermal reasons. There are in fact a number of applications in which they are undoubtedly winners vs. monobloc wheels. The main reason was the completely wrong maintenance cycle.

In the “worst case”, the following operations are traditionally performed, starting from the wheelset already removed from the bogie:

1. the wheelset is moved to a “wheelset lathe” where the retaining rings are machined and removed;
2. the wheelset is moved to the tyre cutting station, typically an alternating saw one;
3. the wheelset is moved to the tyre removal station, where the (nearly fully) cut tyres are pulled away from the wheel centre;
4. the wheelset is moved to the “wheelset lathe” where the wheel centres are machined to a new (smaller) diameter;

5. new tyres are moved to a vertical lathe and machined to the matching diameter to ensure the right interference;
6. new tyres are moved to the heating station;
7. both hot tyres and the wheelset are moved to the assembly station, where they are assembled with a manual procedure ("upside down");
8. retaining rings are installed manually;
9. after cooling, the completed wheelset is moved to a "wheelset lathe" where the wheels are reprofiled to the wanted profile and dimensions.

We discovered that different operators apply this sequence differently, proving that each operator works independently and that in the last decades there has not been any exchange of information among operators using tyred wheels.

There is no need to be top ranking economists to realize that this maintenance procedure totally vanishes any advantage of tyred wheels, as the maintenance cycle of a monobloc wheel (machining of the bore and press-fit) easily wins the competition.

We believe that the weakest points of the traditional mounting procedure are related to the presence of the retaining ring and the fact that the tyre bore diameter is adjusted every time on the wheel centre diameter after its machining, often needed as tyre removal damages the wheel centre mating surface.

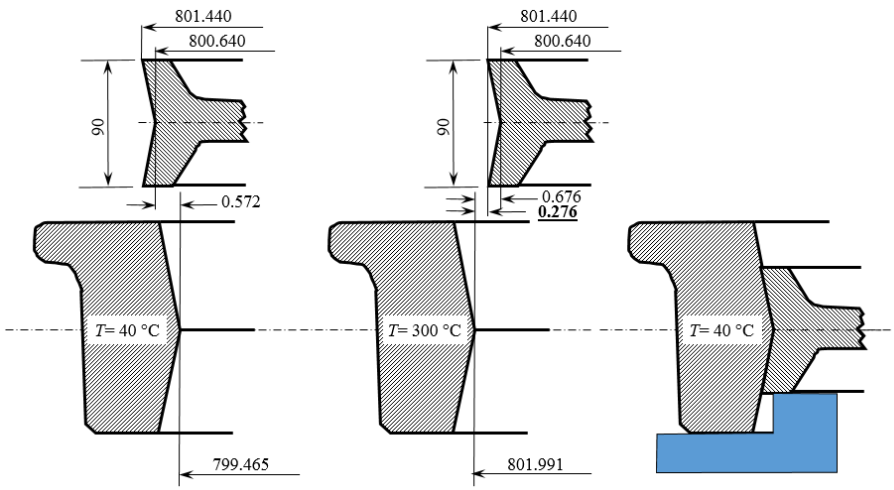

Fig. 7 Relative position of coaxial wheel centre and tyre with 800 t7/S8 coupling in cold (right) and hot (centre) conditions. A sufficient radial play for mounting of 0.276 mm is obtained even with the maximum radial interference of 0.572 mm. Right: simple tool to guarantee the respect of geometrical tolerances after fitting (from [3]).

Both the limitations were removed by recalling one of the basic principles of mechanics, i.e. interchangeability of components thanks to proper tolerancing. We initially thought about a "dovetail coupling", removing the need for the retaining ring, once structural calculations proved that the coupling is safe (Figure 7).

This solution appeared to be easy to machine and positively affecting the maintenance cycle. With this new technology, in fact, all was needed is a device to remove the tyre by heat without damaging the wheel centre (e.g. with an induction heater or propane burners) and a similar device to heat the new tyre up before installation.

The entire process makes sense only if fully machined tyres can be installed on machined wheel centres without needing any machine tool (e.g. the "wheelset lathe") and if both radial and lateral run-outs of the assembled wheelset with new tyres remain within the tolerances prescribed by the International Standards after assembly (Figure 8).

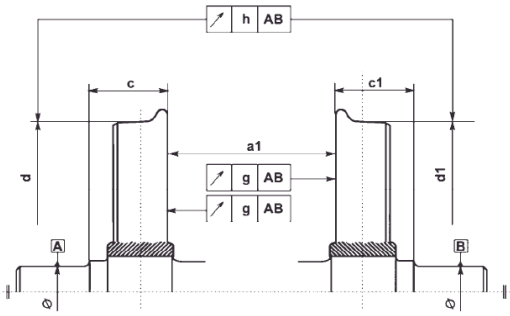

Dimensions in mm

Description	Symbol	Category 2		Category 1
		a	b	
Distance between the internal wheel faces[a]	a_1	$+2^{b}_{0}$		$+2^{b}_{0}$
Difference in distances between the internal face of each wheel and the plane on the journal side defining the corresponding collar bearing surface	$c - c_1$ or $c_1 - c$	≤ 1		≤ 1
Difference in tread circle diameter	$d - d_1$ or $d_1 - d$	≤ 0,5	≤ 0,3	≤ 0,3
Radial run-out in tread circle	h	≤ 0,5	≤ 0,3	≤ 0,3
Axial run-out of the internal wheel face[a]	g	≤ 0,8	≤ 0,5	≤ 0,3

[a] Measurement at 60 mm beneath the top of the flange

[b] The tolerances may be changed for special designs of wheelsets

Fig. 8 Tolerances and maximum errors after wheelset mounting (excerpt from EN 13260).

Extensive workshop activities were performed eventually leading to line tests on a DMU vehicle in November 2018 (Figure 9). The results were fully positive and all the expected targets were achieved. It must be said that the original dovetail coupling was modified to bring the contact of mating surfaces in the area where the wheel centre is stiffer. For further details the reader is referred to [7].

About safety, Common Safety Methods defined by European Union Regulation 402/2013 applies in this context because the evaluation of the impact on safety is obviously applicable to wheelsets. In general, if the proposed modification is considered "not significant" on the basis of a set of well defined criteria, "keeping adequate documentation to justify the decision shall be sufficient".

The application of CSM to the present case looks straightforward and painless. Removal of safety conditions based on friction (use of mechanical abutments), elimination of tread braking (no tyre loosening possible) and correct machining and mounting

procedures are sufficient to implement the modification without any real impact on safety, which results improved by the our design.
Summarizing, we defined and tested a new (and safer) approach to tyre changing that can be performed in any workshop, even the most remote, as it does not involve machine tools or any other specific "complex" operation. The wheelset maintenance cycle simplifies dramatically and it consists only in tyre removal by heat, cleaning of the surface, installation of a new (fully machined) hot tyre and tyre cool down. Our design proved to be simple, easy to machine and even easier to apply.

Thanks to this experience, we can implement the process (including the tools) in any practical situation involving tyred wheels.

Fig. 9 Left: lowering a trailed wheelset on a hot tyre resting on the specifically designed mounting jig with calibrated shims. Right: the ALn668.1036 vehicle before the tests on the roundtable in Iseo, Italy, 21st November 2018.

5. THE *LIBERTY WHEEL* TAKES SHAPE

5.1 Development of the idea and material selection

When discussing with potential customers we realized that what was needed is not only a way to improve maintenance but a comprehensive approach to tyred wheels in general.

As we have shown above, wheel centres are old and poorly designed, tyre thickness is wrong, maintenance operations are a nightmare. Tyre-wheel centre pressure was badly distributed, the retaining ring is a source of further problems, mass is too high.

There was, clearly, the need to rethink from the start to a modern, light, well designed, reliable and low cost tyred wheel.

We collected all the experience gained in the aforementioned studies and we decided to develop a brand new concept for a tyred wheel that we named *Liberty Wheel* for reasons that will be clear soon.

First of all we opted for a larger and (radially) stiffer area on the wheel centre in order to better distribute pressure on the tyre-wheel centre surface and to increase the safety linked to potential lateral movements of the tyre. We soon realized that one web was not sufficient to achieve such goal, then we were forced to abandon the classical forged and rolled wheel centre.

Having to make recourse to a casted solution, we discarded soon the steel option as an interesting alternative appeared at the horizon: "modern" cast iron. Cast iron has fan-

tastic pouring characteristics ("*cast irons are nature's gift to foundrymen*") but is traditionally considered brittle and with generally low mechanical properties, much lower than those of cast steel.

This frame changed completely in the '70s, when technologies to produce spheroidal graphite cast iron (developed in 1943) and austempering thermal treatment (known since the '30s) where first combined to get the first Austempered Ductile Iron (ADI). One of the most complete description of the ADI cast iron says:

What material offers the design engineer the best combination of low cost, design flexibility, good machinability, high strength-to-weight ratio and good toughness, wear resistance and fatigue strength? Austempered Ductile Iron (ADI) may be the answer to that question. ADI offers this superior combination of properties because it can be cast like any other member of the Ductile Iron family, thus offering all the production advantages of a conventional Ductile Iron casting. Subsequently it is subjected to the austempering process to produce mechanical properties that are superior to conventional ductile iron, cast and forged aluminum and many cast and forged steels. (from https://www.ductile.org/didata/Section4/4intro.htm).

The description of mechanical properties of the ADI grade we decided to use (ADI 800 according to ISO 17804, EN 1564 and ASTM A897) lies outside of the scope of this paper, but we can simply say that it competes with quenched and tempered alloyed steels such as 42CrMo4, showing therefore extremely interesting mechanical properties.

While the use of ADI is not new in the railway wheels field, quite recently Siemens developed a monobloc wheel made of this material (see K. Strommer, F.J. Weber, *Austempered Ductile Iron Spoke Wheel*, Proceedings of the XIX International Wheelset Congress, Venice, 16-20 giugno 2019) within the frame of a Shift2Rail European project. As the wheels interface with the rails, for clear compatibility reasons this wheel will be tested only in a metro, in which the consequences of RCF and wear problems are lower that on a conventional rail network. We discarded this option from the beginning, as a monobloc wheel, even if made of ADI, has the intrinsic limitation of a "disposable" product when the tyre is worn, which goes against the philosophy of our project.

We decided therefore to design a wheel centre with two spoked webs and a conventional steel tyre, opening the applicability to all vehicles running in the "conventional rail" environment. ADI was perfect: easy to purchase from a large number of suppliers and castable in nearly every shape without big headaches from the quality point of view.

The absence (or the strong reduction of thermal inputs) led to non-necessity of ondulated webs. Spokes were therefore conceived straight and nearly parallel for the specific vehicle, that was a DMU with 12 tonnes axleload. We started the FEM development of the wheel centre keeping the alternate stress very low (±89 MPa) under the loads described by the EN 13979 standard to take into account typical surface foundry defects. After some iterations, we were able to design a wheel centre easily castable and 50 kg lighter than the original one (Figure 10).

We also change the drawing of the tyre-wheel tread positive coupling. The surface became in fact a single taper (1:75) with a small abutment. This change was suggested by the the workshop as the presence of the abutment allows mounting with the axis horizontal, while its absence forces the mounting only with the axis vertical (Figure 10).

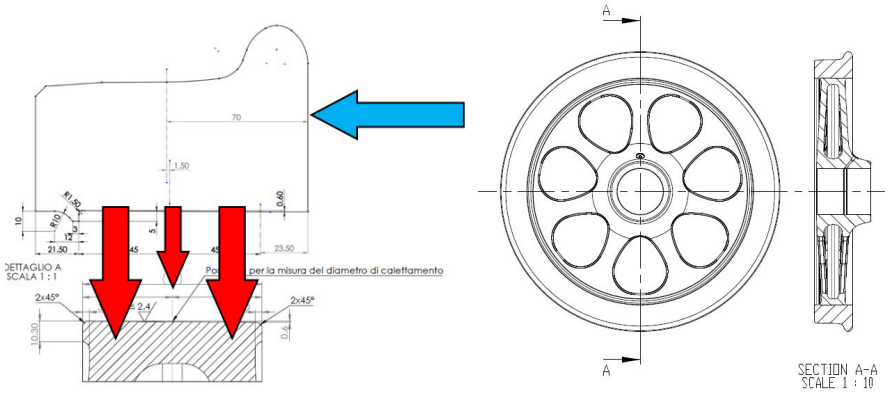

Fig. 10 Left: reaction to a lateral force distributed on the two rank of spokes of the *Liberty Wheel*. Right: final drawing of the *Liberty Wheel* with the tyre installed.

5.2 *Liberty Wheel* manufacturing and testing

The selected foundry performed castability validation (pouring, solidification, voids, etc.) starting from 3-D CAD drawings, preparing also models and moulds. First wheel centres were casted on 31.01.2019 (Figure 11, Figure 12).

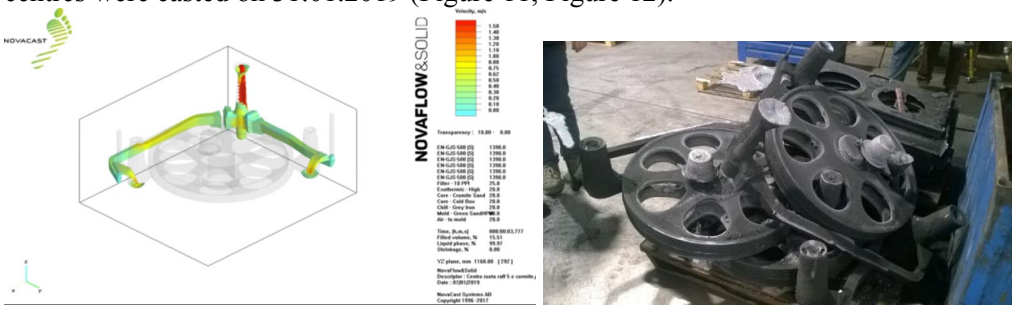

Fig. 11 Left: simulation of velocity during liquid cast iron pouring. Right: the first three *Liberty Wheels* (31.01.2019) before feeders are cut off.

Fig. 12 The first *Liberty Wheel* cut to get samples for mechanical properties tests (31.01.2019).

The first wheel centre was RT, while all wheel centres were UT 100%. After sand blasting, castings were heat treated, sand blasted again and machined (Figure 13, Figure 14). It is worth reporting that all the wheelsets assembled from machined wheels resulted to be naturally balanced (<75 gm), making the wheelset suitable for operation up to 200 km/h.

Fig. 13 Left: first mounting on an axle. Mid: CMM dimensional check. Right: first *Liberty Wheel* assembly with the tyre.

Fig. 14 Top: the very first wheelset with *Liberty Wheels* (16.04.2019). Bottom: comparison of the *Liberty Wheel* with the original wheel centre

A *Liberty Wheel* was tested on a full-scale test bench (Figure 15). Stresses in the spokes were first measured during tyre installation, then a 10^6 cycles test was performed with an alternate stress of ±300 MPa without any failure. This result was possible thanks to the pre-stress (compression) of the spokes such that they never go in the positive (tension) field. Cracks cannot therefore propagate. More detailed information on stress analysis can be found in [6].

5.3 Line tests with the *Liberty Wheels*

A complete set of wheelset for the selected DMU was tested in May 2019, making sure that the two bogies (one equipped with *Liberty Wheels*) and the other one with the original

solution have the same tread roughness to get valid noise data during the pass-by measurements (Figure 16).

Fig. 15 Measuring the strains in the spokes by means of ER strain gaugues during cooling of the tyre (left). The *Liberty Wheel* under test mounted in the full-scale facility (right).

5.3 Line tests with the *Liberty Wheels*

A complete set of wheelset for the selected DMU was tested in May 2019, making sure that the two bogies (one equipped with *Liberty Wheels*) and the other one with the original solution have the same tread roughness to get valid noise data during the pass-by measurements (Figure 16). Noise measurements, including all needed ancillary measurements (rail roughness, wheel roughness, track decay rate) are not reported here for brevity. Noise of the *Liberty Wheels* was more than 1.5 dB lower than the original wheels.

Fig. 16 *Liberty wheels* tested on the DMU vehicle ALn668.1053 (14.05.2019, Iseo, Brescia, Italy).

5. CONCLUSIONS

For a number of reasons, discussed in the paper, tyred wheels nearly disappeared from the railway world. We have seen how the maintenance cycle of a wheelset with tyred wheels was the most important reason for the decay of this product.

Tyred wheels maintenance requires at least one standard machine tool (a front lathe or a medium-sized vertical lathe) and often a special machine tool (a "wheelset lathe"). Machine tools are complex, require highly specialized workers and are large, heavy and expensive. This implies that maintenance of existing tyred wheels cannot be performed in any workshop but only in some specialized centers.

One might wonder why tyred wheels did not benefit from any technological progress. The market analysis easily explains this "lack of updating":

- no modern vehicle is equipped with tyred wheels, so maintenance cycles, submitted to the competent bodies for approval, were optimized only for the monobloc wheels;
- having neither development nor future, and with increasingly smaller fleets destined to local or secondary services, railway enterprises did not invest in either training of personnel or equipment / machinery, risking in some cases the paradox of stopping vehicles because "the good old mechanical turner" retired;
- neither the national regulatory bodies, always less influential, nor European standardization bodies ever considered tyred wheels, thus lacking a regulatory support that may also address maintenance practices;
- the various "historic" railway administrations, which have by now almost disappeared as a result of EU directives, stopped issuing “standards” in the field of wheelsets, so the only rules that can be found today on the maintenance of tyred wheels are never updated 20 or 30 years old "technical instructions" (and after all it would have made no sense).

As a result, the few workshops that today maintain tyred wheels are often characterized by manual machine tools, highly-skilled staff, manual measuring instruments and very low productivity. They ofter repair a mix of very different wheels, making the slightest automation of the maintenance process simply impossible. Wheelsets ofter arrive in "desperate" conditions resulting from a decades-long operation that makes them completely different from their design standards. In short, tyred wheels maintenance shops look more like a tailor-made atelier than an industrial process.

A quite simple idea – the introduction of the *dovetail coupling*, i.e. the replacement of the conventional cylindrical tyre/wheel centre mating with a positive coupling removing at the same time the retaining ring – triggered a deeper reconsideration on the future of tyred wheels. Although the absence of literature, and on the basis of just a few sources of data, the design of the wheel centres, of the tyres were criticized and a deep review of the maintenance process was performed.

We realized that what was perfect for our predecessors, in a world in which labour costs were affordable and time had a different value, became unacceptable to modern railways. What was good in the concept of tyred wheels was therefore discarded and

wasted in favour on monobloc wheels, a solution with *apparently* shorter overhaul times and lower costs.

With this work, we have demonstrated that tyred wheels may have a future again. The possibility of changing the tyres nearly everywhere and in real time opens new possibilities to railway enterprises operating certain classes of vehicles. But we understood that modifying an existing wheel was not enough: customers may need a complete solution with a shorter supply chain, involving new actors, saving considerable time and money. That's we developed the *Liberty Wheel*.

The *Liberty Wheel* is not just a design: it is a product. We designed it, we manufactured it, we tested it. It is a low cost way to be free of the current market necklace, unleashing the possibility of purchasing tyred wheels at a fraction of monobloc wheels and, even more important, to perform *real time maintenance* nearly for free. So, whatever you trust in, you should not fear asking for new wheels in reasonable time, at reasonable cost, with your own design and without fearing the possibility of the lack of a "plan B" in case relationships with wheelset manufacturers go wrong for whatever reason.

This paper described how we developed the *Liberty Wheel*, what we did, what we did not (and why), what we got and what you can get if you believe in this new (old!) technology.

6. REFERENCES

[1] **Bracciali, A. – Megna, G.:** Stresses and strains in tyred wheels during tyre fitting process, Proceedings of The Fourth International Conference on Railway Technolgy, Railways 2018, 3-7 September 2018, Sitges, Barcelona, Spain.

[2] **Bracciali, A. – Megna, G.:** Tyred wheels without braking: structural optimization, Proceedings of The Fourth International Conference on Railway Technolgy, Railways 2018, 3-7 September 2018, Sitges, Barcelona, Spain.

[3] **Bracciali, A. – Megna, G.:** Re-design of tyred wheels to optimize maintenance, Proceedings of The Fourth International Conference on Railway Technolgy, Railways 2018, 3-7 September 2018, Sitges, Barcelona, Spain.

[4] **Bracciali, A. – Caianiello, G. – Megna, G.:** Moderni sviluppi nella manutenzione delle sale ferroviarie, in Atti dell'8° Convegno Nazionale sul Sistema TRAM, Roma, Italy, May 29-30, 2019 (In Italian).

[5] **Bocciolini, L. – Bovì, R. –Bracciali, A. – Caianiello, G. – Megna, G. – Rota, L. – Temporin, E. – Veneri, E.:** Manufacturing and testing of a tyred wheel with casted ADI wheel centre, Proceedings of the XIX International Wheelset Congress, Venice, Italy, June 16-20, 2019

[6] **Bracciali, A. – Masaggia, S. – Megna, G. – Veneri, E.:** Quiet and light spoked wheel centres made of Austempered Ductile Iron, Proceedings of the XIX International Wheelset Congress, Venice, Italy, June 16-20, 2019.

[7] **Bracciali, A. – Caianiello, G. – Megna, G. – Petreschi, P. – Rota, L.:** Dovetail Tyred Wheels – Application to a DMU, Proceedings of the XIX International Wheelset Congress, Venice, Italy, June 16-20, 2019.

NEW SAFETY INDEX AGAINST FLANGE-CLIMB DERAILMENTS IN CURVING

Akira MATSUMOTO[1], Yohei MICHITSUJI[2], Yosuke ICHIYANAGI[2], Masuhisa TANIMOTO[3], Takuji NAKAI[4] and Yasuhiro SATO[5]

[1] Nihon University, 1-2-1 Izumi-cho, Narashino, Chiba 275-8575, Japan
[2] Ibaraki University, 4-12-1 Nakanarusawa-cho, Hitachi, Ibaraki 316-8511, Japan
[3] Tokyo Metro Co., Ltd. 3-19-6 Higashi-ueno, Taito-ku, Tokyo, 110-8614, Japan
[4] Nippon Steel Corporation, 5-1-109 Shimaya, Konohana-ku, Osaka, 554-0024, Japan
[5]National Traffic Safety & Environment Laboratory, 7-42-27 Jindaiji-higashi-machi, Chofu, Tokyo, 182-0012, Japan

Received: September 10, 2019

ABSTRACT

The safety against flange-climb derailments has been estimated by the value of "Q/P", or "Y/Q"; the ratio of lateral vs. vertical contact force at wheel/rail contact point. This index is very useful and has been used generally for safety evaluation in the world, but the actual friction condition has been not considered. The authors propose a new safety index "FCI (Flange Climb Index)", which can indicate the safety margin against derailments considering the friction condition. By using FCI, the safety margin against flange-climb derailments can be indicated quantitatively on every curve, and the monitoring-base maintenance on curved tracks can be realized.

Keywords: wheel-rail contact, flange-climb derailment, railway bogie, curving, Nadal's formula, MBS, lookup table

1. INTRODUCTION

The safety against flange-climb derailments has been estimated by the value of "Q/P". "Q/P" is the ratio of the lateral contact force against the vertical contact force at wheel/rail contact point (see Fig.1), which is described as "Y/Q" or "L/V" in western countries and calculated by following Nadal's formula.

$$\left(\frac{Q}{P}\right)=\left(\frac{Y}{Q}\right)=\left(\frac{L}{V}\right)=\frac{\tan\alpha-\mu}{1+\mu\tan\alpha} \tag{1}$$

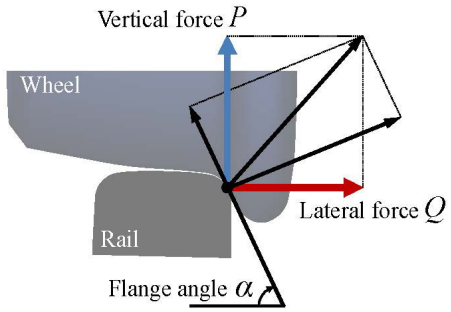

Fig. 1 Contact forces at wheel/rail contact point [4]

This index is very useful and has been used generally for safety evaluation of curving safety in the world [1-3], but it has a problem. In the calculation of the "critical value of Q/P" for safety evaluation, it is necessary to grasp the value of the friction coefficient "μ" between wheel-flange and rail. The measurement of the friction coefficient

μ of the wheel/rail contact point is very difficult and the real value cannot be measured by the conventional methods. Normally the average value μ=0.3 is used in the calculation, but by using such value it is impossible to grasp the real safety margin against flange-climb derailments quantitatively.
The authors developed the method to estimate the value of friction coefficient μ from the contact forces of the other wheels in the same bogie, which can be measured. And by using the estimated value of friction coefficient μ, the authors propose a new safety index "FCI (Flange Climb Index)", which can indicate the safety margin against flange-climb derailments quantitatively.

2. RESEARCHES ON WHEEL-RAIL CONTACT IN CURVING

The authors have carried out following researches to prevent undesirable phenomena, as well as flange-climb derailments, in curving.

2.1 Full-scale curving tests on roller rig [4]

The authors developed a full-scale bogie test roller rig in NTSEL (National Traffic Safety & Environment Laboratory), which can simulate curving conditions, in order to grasp various characteristics of bogie, wheel and rail in curved sections. Curving parameters, such as angle of attack, running path difference between inside/outside rails, the lateral force produced by unbalanced centrifugal force, can be given corresponding to the parameters of curves. The test bogie set on the rig (Fig.2(a)), and the contact states of each wheel can be observed in the screen (Fig.2(b)).

Various running tests have been carried out on the rig, and the authors got many information for improvement of curving performance.

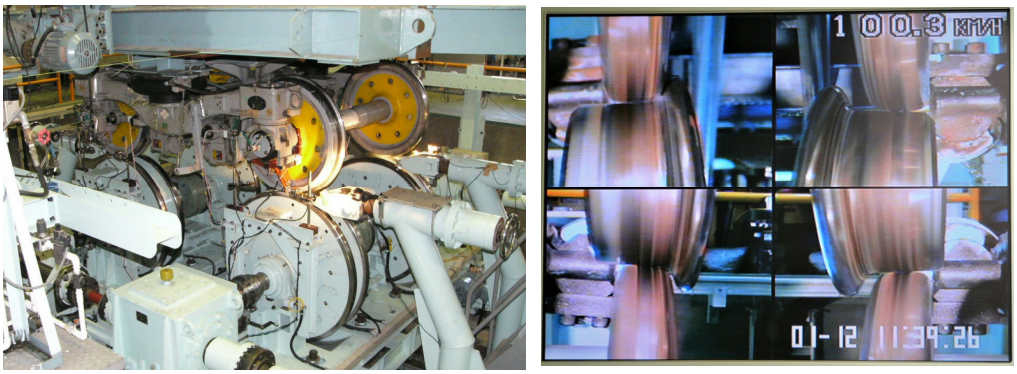

(a) Outline of roller-rig (b) Observation of contact-points of 4 wheels

Fig. 2 Full-scale bogie roller rig for curving in NTSEL

2.2 Development of PQ monitoring bogie [5]

The information about actual states of curving is very important, and especially the measurement of contact forces between wheels and rails is required. But such measurement is difficult because the wheels are rolling and moving on the rail at high speed

and the contact point is changed in every second. The conventional methods in the world use strain gauges attached on wheels for measuring contact forces and slip rings or telemeters for data transmitting from rotating wheels. These methods have insufficient durability and are hard for handling, so continuous measuring, such as monitoring by in-service trains every day, is impossible. On the contrary the states of wheel-rail contact change every time, so the new method which can observe the states from in-service trains is desired.

So, the authors developed the new measurement systems of wheel-rail contact forces by in-service trains. The newly developed system is called "PQ monitoring bogie", which can measure the contact forces not using strain gauges on the rotating wheels. Fig. 3 shows the image of the comparison of the newly developed PQ monitoring system and the conventional system. In the new system the contact lateral force is measured by the deformation of the wheel, which is measured by non-contact gap sensors attached on the bogie flame. The sensors are attached on the bogie flame, which is not rotating, so, slip ring and telemeters are not necessary.

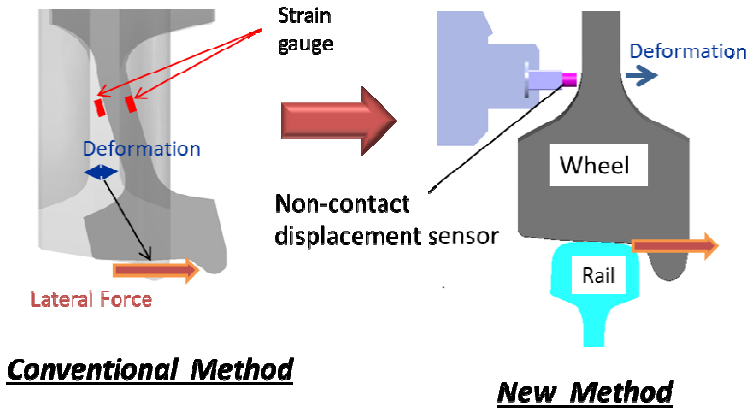

Fig. 3 Comparison of new method and conventional method

The measuring principle is rather simple, but accurate measurement is not easy because very small deformation is necessary to measure by the non-contact gap sensor. The force of 10kN produces the deformation of 0.08mm, and the resolution of the gap sensor is 0.001mm, so, the lateral force can be measured by this method. In order to realize practical use, various improvements, such as introduction of 2 more sensors for compensation of lateral movement of wheelset, fine machining of wheel plate surface. After various tests of the proto-type test bogie on roller rig and on commercial lines, the bogie for practical use was successfully achieved.

Fig. 4 shows one of the PQ monitoring bogies attached on the in-service train (Chiyoda-line; G=1,067mm). PQ monitoring bogies have been introduced to 3 lines of Tokyo Metro (Marunouchi, Tozai, Chiyoda), and covered the commercial lines of 82.2km length, which is 42.1% of whole Tokyo Metro line (195.1km). And it will be introduced to all lines in the future, and other railways lines.

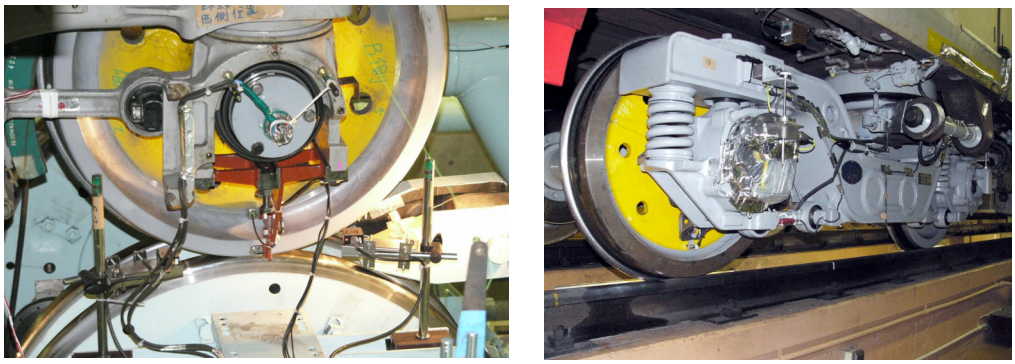

(a) Running tests on roller rig

(b) Running tests on a commercial line Marunouchi-line (G=1,435mm)

Fig. 3 Tests of proto-type PQ monitoring bogie

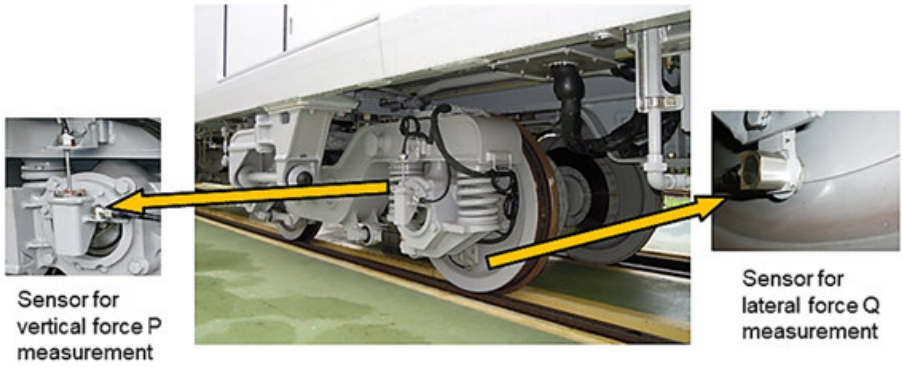

Fig. 4 PQ monitoring bogie for practical use attached on the in-service train [5]

Fig.5 is an example of measured data by PQ monitoring bogie through a sharp curve of 160m radius (cant= 125mm) [6]. This figure shows measured value of positional changes of outside Q/P from the beginning of the transition curve to the end of transition curve. Each wavy line shows the value for each train pass. Q/P value is changing in every running, depend upon track conditions, positions, hours, etc. Generally, Q/P values increase at the beginning of exit-side transition curve. In this way the actual state of wheel/rail contact can be well understood by PQ monitoring bogie through commercial running in every day.

PQ monitoring bogie is the world first system which can observe wheel/rail conditions quantitatively in every hour.

2.3 Different contact conditions between 4 wheels in a same curving bogie [7]

By using the information gathered by PQ monitoring bogies and the results of MBS simulation with SIMPACK, the authors found that the friction conditions of 4 wheels in a bogie are much different during curving.

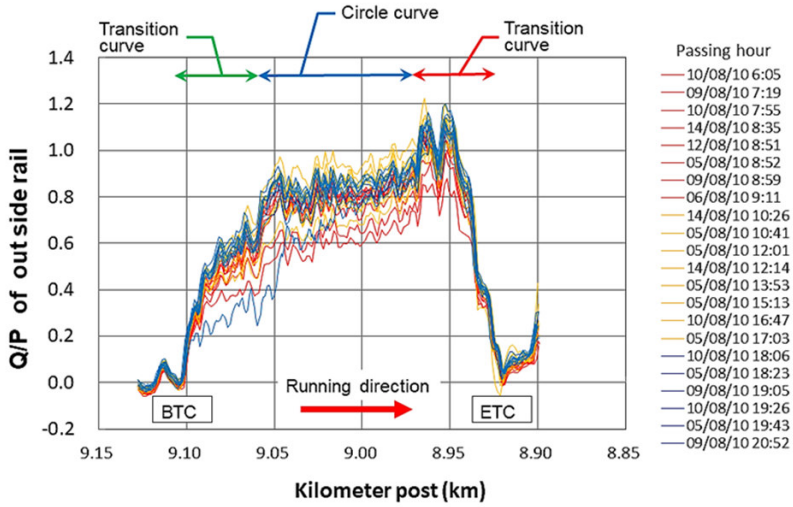

Fig. 5 Example of measured data by PQ monitoring bogie from in-service trains [6]

These characteristics are produced by the difference of contact points between wheels and rails, and the lubrication of wheels and/or rails, as shown in Fig. 6. That is, generally in the leading wheelset the outside wheel contacts with rail at flange and the inside wheel contact with rail at tread (anti-flange side). On the contrary in the trailing wheelset both wheels contact with rail at their tread.

In urban railways, where many sharp curves exist, lubrication to wheels and/or rails are generally applied for prevention of undesirable phenomena, such as wear, noise, derailment, etc. The application methods and positions of lubricant are different according to the purpose. For example;

1) On-board lubrication
2) Wayside lubrication
3) Lubrication to wheel-flange or/and rail-gauge-corner
4) Lubrication to wheel-tread or/and rail-head

Difference of lubrication positions and difference of wheel/rail contact points produces the difference of friction conditions of wheel/rail contact surface.

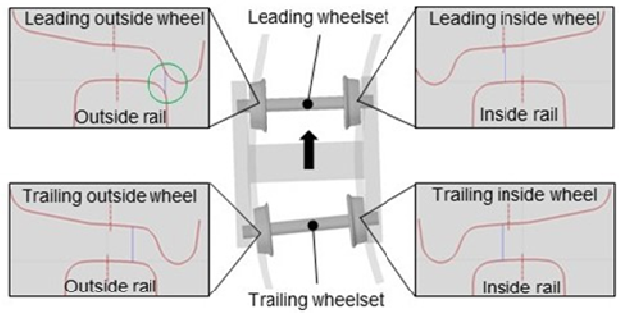

Fig. 6 Difference of contact points between 4 wheels in a same bogie during curving – an example of curving simulation on 160m-radius curve by SIMPACK [8]

3. FRICTION COEFFICIENT AND Q/P VALUE

The limit value of Q/P against flange-climb derailments are changed according to the friction coefficient between wheel-flange and rail-head. As shown in Fig. 7, the critical value of Q/P, which may be the limit of flange-climb possibility, decreases according to the increase of friction coefficient, i.e. flange-climbs may easily occur in the case of high friction conditions. When the friction coefficient is low (0.2), the critical value of Q/P is high (1.8), so Q/P value of 1.0 is safe enough against flange-climb, on the contrary when the friction coefficient is high (0.6), the critical value of Q/P is decreased to 0.7 and Q/P value of 1.0 becomes to exceed the limit value of Q/P. Therefore, it is important to consider the ratio of the measured Q/P against the calculated critical value of Q/P, not the absolute value of Q/P.

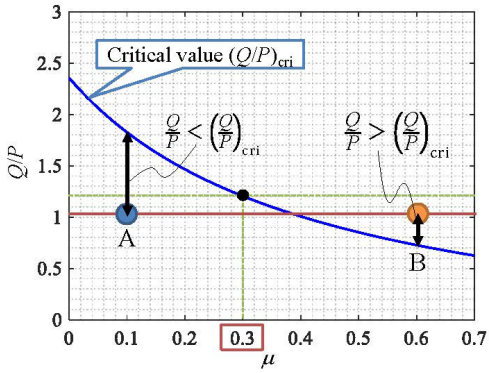

Fig. 7 Relationship between friction coefficient and Q/P value [8]

4. NEW SAFETY INDEX "FLANGE CLIMB INDEX" FCI

As the reason mentioned above, the authors propose a new safety index "FCI (Flange Climb Index)", which is the ratio of "measured Q/P" against "the critical value of Q/P" calculated by the value of μ.

$$FCI = \frac{(Q/P)_{\text{measure}}}{(Q/P)_{\text{cri}}} \tag{1}$$

Fig.8 shows one of the simulation results of MBD simulations for running vehicles through sharp curves. In this figure flange climb heights during curving are shown in the high friction condition (μ=0.65) and low friction condition (μ=0.35). When μ is 0.35 FCI is calculated about 0.5, and when μ is 0.65 FCI exceeds 1.0 at the beginning of exit-side transition curve section, and flange-climb of 3.3 mm occurred at this section. Thus, the flange-climb is possible to occur when FCI value exceeds 1.0.

In this way by using FCI, the safety margin against flange-climb derailments can be examined quantitatively. But the measurement of the friction coefficient μ between wheel-flange and rail-head is very difficult and we cannot grasp real value of it. So, the authors try to grasp such value by the estimation method described in next chapter.

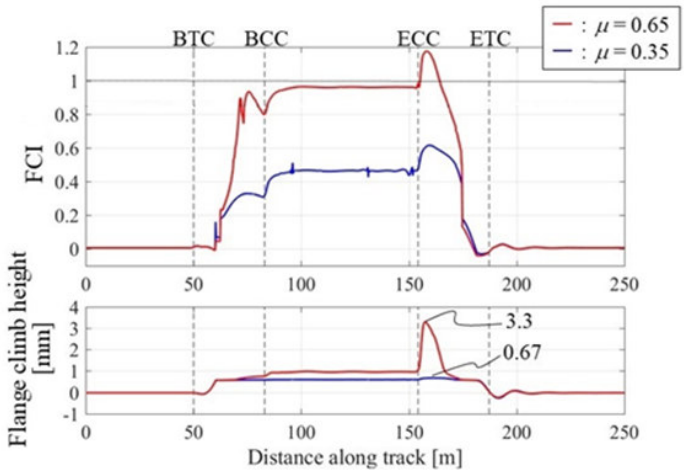

(a) Change of FCI value and flange-climb height along a curve (160mR)
Difference in the case of low μ and high μ

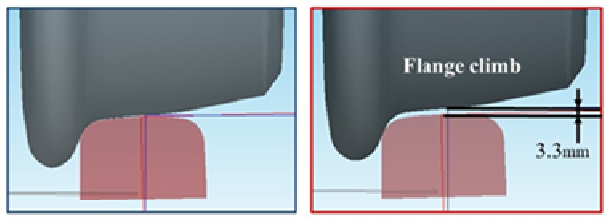

(b)Flange-climb occurrence in the case of high FCI value

Fig. 8 Relationship between FCI and flange-climb occurrence [8]

5. ESTIMATION OF FRICTION COEFFICIENT OF WHEEL/RAIL CONTACT

5.1 Estimation methods of friction coefficient

The authors developed the method to estimate the value of friction coefficient μ between the flange of leading-outside wheel and outside-rail-head from the contact forces of other wheels in the same bogie, which can be measured. Fig. 9 shows the method for estimation of the friction coefficient. As shown in the upper figure of Fig. 9, previously the parameters concerning wheel/rail contact, such as κ, T_1/P_{1in}, T_2/P_{2in}, were calculated using "bogie/rail system models" by MBD simulations with SIMPACK, and lookup-tables were made by the results of the simulations [8][9]. And then the friction coefficient μ_{1out} is obtained as inversive problem by using look-up tables (regression model) shown as the lower figure of Fig. 9.

By using this method, the friction coefficient of the leading-outside wheel μ_{1out} can be estimated from the parameters of the other wheels, which can be measured, and FCI value of the leading-outside wheel can be obtained. Thus, the safety margin against flange-climb derailment for the leading-outside wheel can be evaluated quantitatively from measured Q/P values.

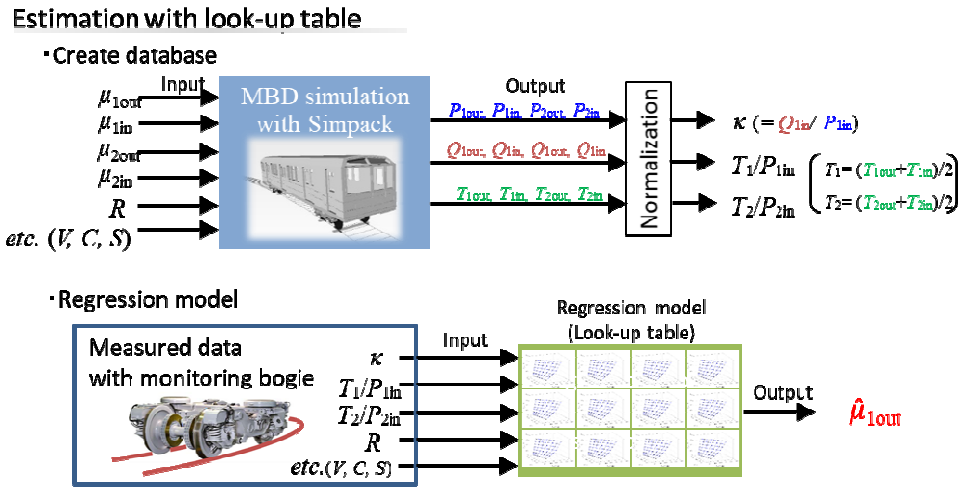

Fig. 9 Estimation method of friction coefficient of wheel flange by using look-up tables [9]

5.2 Example of safety evaluation by using FCI values in various lubrication conditions

The followings are simulation results of Q/P value of the leading-outside wheel during passing through a sharp curve of 160m-radius in various friction conditions, which are caused by the difference of lubrication positions.

1) 4 wheels dry; i.e. No lubrication to wheels and rails. μ=0.5 in all wheels.
   ***Q/P=0.52**, critical value of Q/P is calculated 0.86.
2) Only leading-outside wheel-flange lubricated: i.e. Flange lubrication of the leading-outside wheel-flange is applied from on-board or/and wayside.
   μ_{1out}=0.1, μ=0.5 in the other wheels.
   ***Q/P=0.65**, critical value of Q/P is calculated 1.84.
3) 2 inside wheels lubricated: i.e. Inside wheel treads and/or inside rail-head lubrications are applied. μ_{out}=0.5, μ_{in}=0.1 in 2 inside wheels.
   ***Q/P=0.19**, critical value of Q/P is calculated 0.86.
4) Leading-outside and 2 inside wheels lubricated: i.e. case 2) + case 3),
   μ_{1out} = μ_{1in} = μ_{2in}=0.1, μ_{2out}=0.5.
   ***Q/P=0.22**, critical value of Q/P is calculated 1.84.

In each case, the values of FCI are calculated as follows;

1) 4 wheels dry;
   ***FCI=0.60**
2) Only leading-outside wheel-flange lubricated:
   ***FCI=0.35**
3) 2 inside wheels lubricated:
   ***FCI=0.22**
4) Leading-outside and 2 inside wheels lubricated:
   ***FCI=0.12**

The maximum value of Q/P is 0.65 in case 2 (i.e. leading-outside wheel lubrication), which is higher than Q/P=0.52 in case 1 (i.e. 4 wheels dry), but FCI value is 0.35 in case 2, which is much lower than 0.60 in case 1. This means the safety margin against flange-climb derailments increases in this condition, although Q/P value increases. This is because the critical value of Q/P increases up to 1.82 from 0.86. The lubrication to the leading-outside wheel flange leads the increase of Q/P value in appearance, but the possibility of flange-climb derailments decreases.
The value of Q/P in case 3 is 0.19, which is lowest among 4 cases, on the other hand, FCI is lowest in case 4 (i.e. Leading-outside and 2 inside wheels lubricated). This means case 4 is most safe condition among 4 cases.
In this way FCI can indicate the safety margin against flange-climb derailments quantitatively, and the safety evaluation method using FCI can be effective and useful.

6. CONCLUSIONS

The authors developed the method to estimate the value of friction coefficient μ_{lout} of the leading-outside wheel from the contact forces of other wheels in a curving bogie, which can be measured, by using the lookup-tables made by the results of MBD simulation with SIMPACK.
In addition, the authors propose a new safety index "FCI (Flange Climb Index)", which is the ratio of "measured Q/P" against "the critical value of Q/P" calculated by the estimated value of μ_{lout} . By using FCI, the safety margin against flange-climb derailments can be examined quantitatively. In next stage the authors will try to examine the effect of FCI by running tests on the roller rig and commercial lines using real bogies and vehicles for further studies.

7. REFERENCES

[1] **Elkins J. A., Carter A.:** Testing and Analysis Techniques for Safety Assessment of Rail Vehicles: The State-of-the-Art, Vehicle System Dynamics 22(3-4), 1993, p185-208

[2] **CEN (European Committee for Standardization): European standard EN 14363:** Railway applications: Testing for the acceptance of running characteristics of railway vehicles; Testing of running behaviour and stationary tests (2005)

[3] **Wu H., Wilson N.**, Railway Vehicle Derailment and Prevention, Handbook of Railway Vehicle Dynamics (2006), Chapter 8, p.209-237, CRC Press.

[4] Matsumoto A., Sato Y., Ohno H., Mizuma T., Suda Y., Tanimoto M. & Oka Y.: Study on curving performance of railway bogies by using full-scale stand test, Vehicle System Dynamics, Vol.44 (supplement 1), 2006, p862-873

[5] **A. Matsumoto, Y. Sato, H. Ohno, M. Tomeoka, K. Matsumoto, M. Tanimoto, Y. Sato**: A new measuring method of wheel -rail contact forces and related considerations, Wear, 265(9-10), 2008, p1518-1525

[6] **A. Matsumoto, Y. Sato, H. Ohno, M. Shimizu, J. Kurihara, T. Saitou, Y. Michitsuji, R. Matsui, M. Tanimoto, M. Mizuno**: Actual states of wheel/rail contact forc-

es and friction on sharp curves -Continuous monitoring from in-service trains and numerical simulations, Wear, 314, 2013, p189-197

[7] **Y. Michitsuji, K. Ishii, K. Nagasawa, A. Matsumoto, Y. Sato, M. Tanimoto, A. Iwamoto et al**: Analysis on running safety considering the difference of coefficients of friction in a railway bogie（Comparison between experiment and numerical simulation of the roller-rig test）, Transaction of JSME, 83(856), 2017, 17-00283

[8] **Matsumoto A., Michitsuji Y., Ichiyanagi Y., Sato Y., Ohno H., Tanimoto M., Iwamoto A., Nakai T.**: Safety measures against flange-climb derailment in sharp curve - considering friction coefficient between wheel and rail. Wear, 432-433 (2019) 202931: ELSEVIER

[9] **Y. Ichiyanagi, Y. Michitsuji, A. Matsumoto, Y. Sato, H. Ohno, D. Yamaguchi, M. Tanimoto, T. Matsuda and T.**: Estimation of friction coefficient between outside wheel flange and rail considering influence of wheel/rail wear, 26th International symposium on dynamics of vehicles on roads and tracks (IAVSD 2019), Gothenburg, 2019

ESTIMATION OF RAIL WHEEL FORCES FROM VEHICLE ACCELERATION DATA USING ARTIFICIAL NEURAL NETWORKS

Nalinaksh S VYAS, Manoj NAYANI and Rohit Kumar SINGH

Department of Mechanical Engineering
Indian Institute of Technology Kanpur,
Kanpur 208016, India

Received: September 12, 2016

ABSTRACT

A technique to predict rail-wheel forces from vehicle accelerations using Artificial Neural Networks (ANN) is presented. The objective is to find a function *f* in the relationship $y = f(x)$, where x are the accelerations and y are the rail-wheel forces. An Indian railway passenger coach is considered. Initially, the forward problem is solved to simulate training data for the ANN. Multi body dynamics software ADAMS is used. Components and suspension properties of the vehicle are specified. Non-linear friction damping due to the friction wedge of the BOXN wagon is modeled and compared with experimental values. Static and modal analyses are performed on the vehicle. Worn out rail and wheel profiles are generated and utilized for analysis. Dynamic analysis is performed for a tangent track with measured track irregularities and using Indian track flexibility data. Acceleration and forces are obtained from the analysis. This acceleration data is then fed as input to the designed ANN architecture to train it for force prediction. The network is validated with accelerations from an untrained section of the track and the network output is compared with corresponding forces from the dynamic analysis.

Keywords: rail-wheel force estimation, Artificial Neural Networks (ANN), Passenger Coach, ADAMS

1. INTRODUCTION

Knowledge of lateral and vertical forces is critical for rail operations. The L-V ratio determines the derailment quotient. It also influences important phenomenon like wear. Reference can be made to Kalker [1] and Dukkipati et al [2] for contact mechanics and rail vehicle dynamics. ANNs have been used to predict lateral and vertical forces from track irregularities by Iwnicki et al. [4]. Nefti [5] used wavelets to compress the large data to neural network to predict derailment.

Estimation of rail-wheel forces is generally carried out through multi-body dynamics simulation, with wheel and rail profile data as inputs. However, vehicle accelerations are easier to measure than the track irregularity, which determines rail-wheel forces. In the present study an ANN is designed and trained to address the inverse problem of predicting the lateral and vertical forces acting on the wheel with vehicle accelerations as inputs. The vehicle is modelled as a system with several degrees of freedom by specifying the components and suspension properties of the vehicle. The response is obtained in terms of acceleration measurable at suitable points on the vehicle.

2. VEHICLE SIMULATION

To construct the inverse problem, initially the forward problem is solved to simulate training data for the ANN. Multi body dynamics software ADAMS is used. An Indian passenger coach is considered (Figs. 1, 2 and Tables 1-2: Source-RDSO, Lucknow). The complete vehicle is modeled as an assembly of different subsystems in ADAMS/Rail. Details of the coach and its components are given in subsequent Tables (Source-RDSO, Lucknow). Initially, the bogie template is created which consists of all the components

including the suspension elements. The front and the rear subsystems of the bogie are created corresponding to the front and rear bogies of the vehicle. The car body subsystem is created using the car body template. The three subsystems are assembled to compose the complete coach.

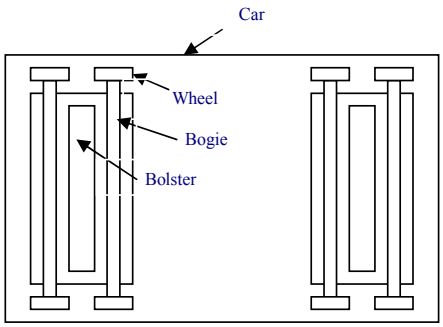

Fig. 1 Top view of the coach

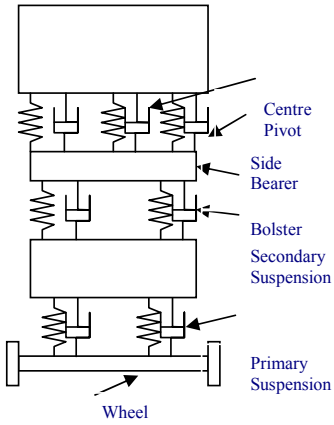

Fig. 2 Front view of the coach.

Table 1. Mass and inertia values of coach components about their C.G.s.

	No. of parts	Mass (kg)	I_x (kgm^2)	I_y (kgm^2)	I_z (kgm^2)
Car body	1	41240	69470	1597800	1600800
Bolster	2	638	490	35	536
Bogie	2	2498	1646	3080	4576
Wheel Set	4	1507	1197	110	1197

Table 2. Locations wrt C.G of first wheel set

Component	X-position (m)	Y-position (m)	Z-position (m)
Wheel set -1	0.0	0	0.457
Front bogie	1.448	0	0.666
Front bolster	1.448	0	0.809
Wheel set-2	2.896	0	0.457
Car body	8.840	0	2.079
Wheel set-3	14.783	0	0.457
Rear bogie	16.231	0	0.666
Rear bolster	16.231	0	0.810
Wheel set-4	17.679	0	0.457

Table 3. Static loads on the coach

Element	Vertical Preload (kN)
Primary suspension	58.24
Secondary suspension	104.29
Single wheel	65.72

The static vertical loads are given in the Table 3. Position of various suspension elements and their stiffness are given in Tables 4 and 5 (Nayani [6]).

Table 4. Position of different suspension elements in the coach

Suspension	X-position (m)	Y-position (m)	Z-position (m)
Front centre pivot	1.448	0	0.680
Rear centre pivot	16.231	0	0.680
Front side bearer left/right	1.448	-0.8/0.8	0.803
Rear side bearer left/right	16.231	-0.8/0.8	0.803
Front secondary suspension left/right	1.448	-1.127/1.127	0.471
Rear secondary suspension left/right	16.231	-1.127/1.127	0.471
Primary suspension at wheel set 1 left/right	0	-1.079/1.079	0.525
Primary suspension at wheel set 2 left/right	2.896	-1.079/1.079	0.525
Primary suspension at wheel set 3 left/right	14.783	-1.079/1.079	0.525
Primary suspension at wheel set 4 left/right	17.679	-1.079/1.079	0.525

Table 5. Stiffness and damping properties of suspension elements

Suspension	Stiffness (kN/m)	Damping (kNs/m)
Secondary vertical	936	58
Primary vertical	544	41
Centre Pivot vertical	35000	35
Secondary lateral	510	frictional force, 6.4 kN
Primary lateral	532	frictional force, 1.15 kN
Primary Longitudinal	575	0
Secondary Longitudinal	5039	0
Side bearer vertical	35000	35
Side bearer longitudinal	0	frictional force, 8.5 kN

'FASTSIM' is used to generate the wheel-rail contact mechanics. Measured irregularities as specified in the Section 2.5.1 are used. Young's modulus of the track is considered to be 210 GPa while Poisson ratio is taken as 0.27. Track flexibility is considered with the following values for each rail [10] - Lateral stiffness -1.75E7 N/m; Lateral damping - 1.75E6N-sec/m; Vertical stiffness - 1.06E7 N/m, Vertical damping - 0.54E5 N-sec/m. Track irregularity data, recorded at an interval of 0.305m, Figs. 3(a)-(b), is obtained from RDSO. The response for a vehicle speed of 5 m/sec, in terms of acceleration at (i) the front centre pivot (ii) C.G of the front bogie and (iii) left front axle box, is typically shown in Figs. 4 (a)-(c). Similar data is obtained for the lateral direction.

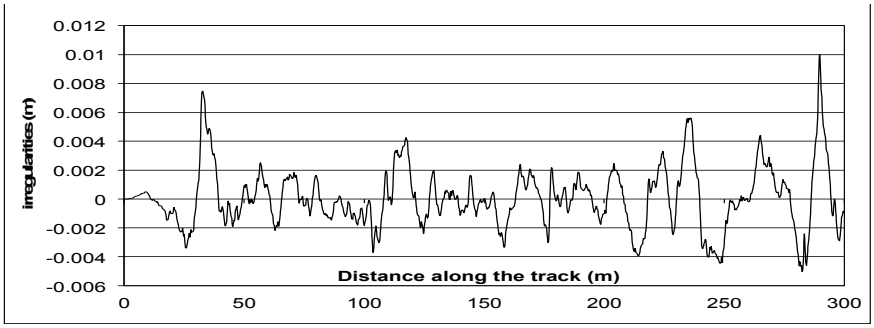

Fig. 3(a). Lateral irregularities- left rail

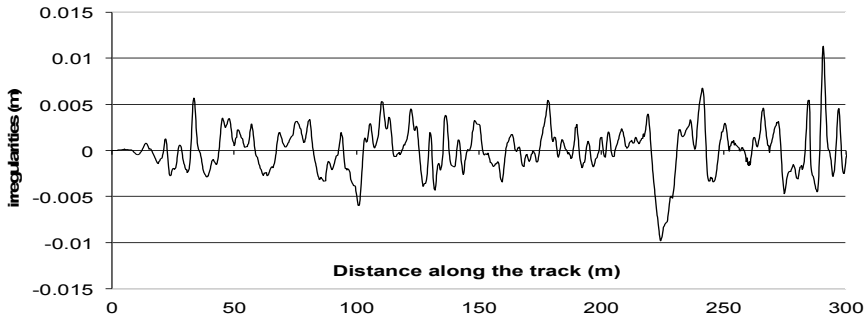

Fig. 3(b). Vertical irregularities-left rail.

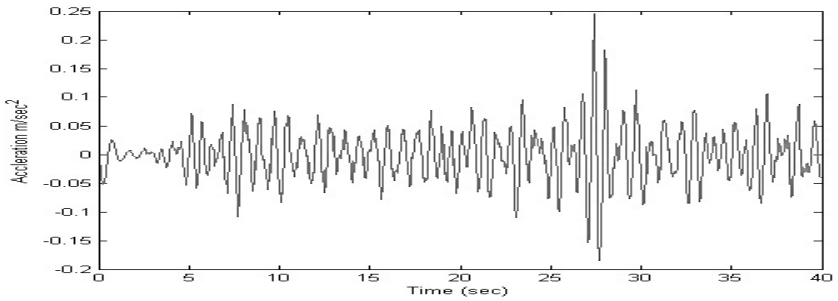

Fig. 4 (a) Vertical accln-front centre pivot

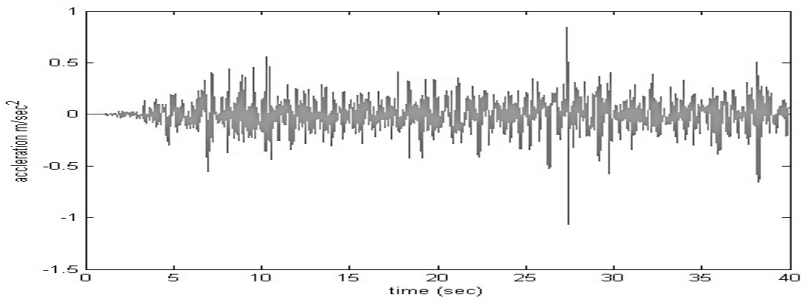

Fig. 4 (b) Vertical accln-axle box

This acceleration data is fed as training input to the ANN architecture for force prediction.

3. ANN ARCHITECTURE, TRAINING AND VALIDATION

ANN is designed with Resilient Back Propagation algorithm in MATLAB, with two hidden layers of 250 and 200 neurons, respectively. The output layer has a single neuron to give the force value. The target vector are the forces on the wheel. Non-linear activation functions 'logsig' and 'purelin' are used for hidden and output layers, respectively, with a network learning rate of 0.5. All the above network parameters have been decided after doing multiple iterations and studying their effects. The network output, along with the target, is shown in Fig. 5(a), (b). Network testing is done for input data which have not been used for training. Test results are given in Figs. 6 (a), (b).

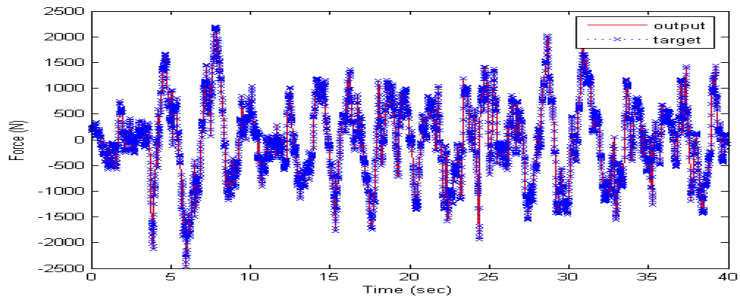

Fig. 5 (a) Training for Vertical force

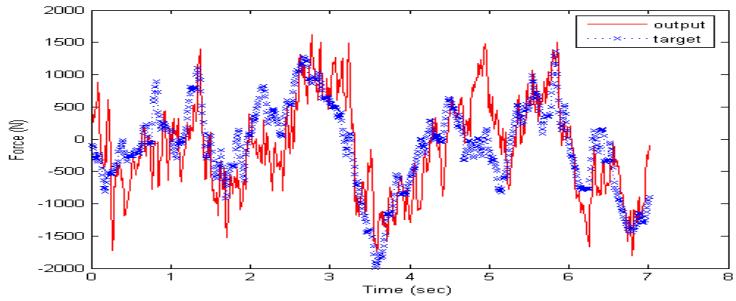

Fig. 6(a) Testing for vertical force

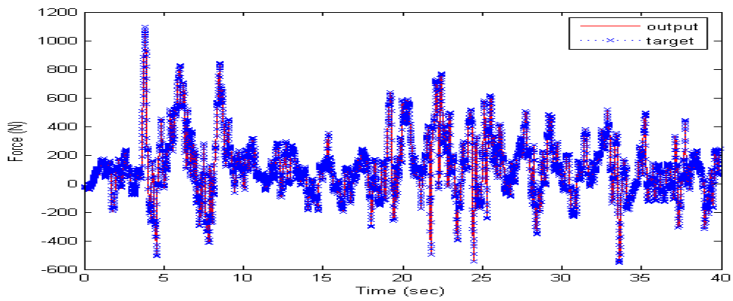

Fig. 5 (b) Training for Lateral force

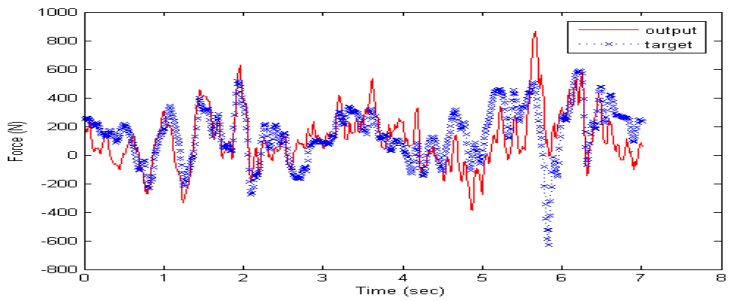

Fig. 6(b): Testing for lateral force

8. CONCLUSION

A technique to predict the rail forces online from accelerations of the vehicle using Artificial Neural Network is presented. Accelerations at different locations in the vehicle are considered as inputs and the forces on the wheel as the target for training the network. 'TRAINRP' a back propagation algorithm is used for training the network. Inclusion of previous time history of the accelerations in the training vector improves the convergence of the network. Testing of the network is done by providing accelerations that have not been used for the training process and comparing the output of the Neural Network with the wheel forces generated in ADAMS. It is observed that the network *is able to predict the wheel forces satisfactorily*. Multiple iterations are performed to study the effect of different network parameters.

9. REFERENCES

[1] **Kalker, J. J:** Three-Dimensional Elastic Bodies in Rolling Contact, Kluwer Acad. Publ., London.

[2] **Dukkipati, R. V. – Garg, V. K.:** 1984 Dynamics of Railway Vehicle Systems Acad. Press, Canada.

[3] **Iwnicki, S. – Parkinson, H. – Stow, J.:** Assessing railway vehicle derailment potential using Neural Networks, Rail Technology unit, Manchester Metropolitan Univ.

[4] **Nefti, S. – Oussaiah, M.:** Neural Network approach for Railway Saftey Prediction, IEEE International Conference on systems, Man and Cybernetics, 2004.

[5] **Nayani, M.:** Modeling and Analysis of Rail Vehicle Dynamics**,** M. Tech. thesis, IIT Kanpur, 2006.

DESIGN METHOD FOR SUPPRESSING HUNTING OSCILLATION FOCUSING ON ITS DAMPING RATIO

Hideki SAKAI

Kindai University
1 Takaya-Umenobe, Higashihiroshima,
Hiroshima 739-2116, Japan

Received: September 12, 2016

ABSTRACT

In order to further speed up high-speed trains, it is necessary to increase the speed at which bogie hunting occurs. The conventional design method to increase the vehicle speed where bogie hunting occurs is to make its wavelength longer. However, bogie hunting is self-oscillation. Since self-oscillation is caused by the negative damping ratio, a design method focusing on the increase of the negative damping ratio should be more effective than the increase of the wavelength. Therefore, this paper proposes a design method that focuses on the negative damping ratio of the wheelset hunting in order to increase the speed at which bogie hunting occurs. Therefore, in the first half of this paper, the symbolic solution of the negative damping ratio of wheelset hunting is derived by assuming the creep coefficient and the yaw radius of inertia of the wheelset. Interpreting this symbolic solution, this paper obtains insights of the influence of each design parameters on the negative damping ratio. Based on these insights, in the second half, this paper proposes two design methods to increase the speed at which bogie hunting occurs as follows. First, this paper proposes the reduction of mass of the wheelset because the damping ratio increases as the creep factor / wheelset mass increases. Secondly, this paper propose an increase in the wheel radius because the damping ratio increases as the wheel radius increases. Finally, this paper verifies that these measures increase the speed at which bogie hunting occurs.

Keywords: wheelset hunting, self-oscillation, formula of damping

1. INTRODUCTION

At high speeds, the hunting oscillation of the wheelset may occur. Because this hunting oscillation is a kind of self-oscillation, its damping ratio is negative. By increasing this negative damping ratio, self-oscillation seems to be less likely to occur. This paper formulates a damping ratio of the hunching oscillation. Further, by examining this formula, I will consider how to increase damping.

2. PREVIOUS STUDIES

2.1 Model

The model of the wheelset shown in Fig. 1 is used. Further, let m be the mass of the wheelset, i be the radius of wheelset inertia, κ_{11} be the longitudinal creep coefficient and κ_{22} be the transverse creep coefficient.

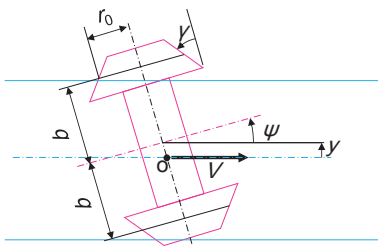

Fig. 1 The model of the wheelset

2.2 Equations of motion

The model of the wheelset shown in Figure 1 is used. Further, let m be the mass of the wheelset, i be the radius of wheelset inertia, κ_{11} be the longitudinal creep coefficient and κ_{22} be the transverse creep coefficient. The equations of motion of this model are described below (JSME,1999).

$$m\ddot{y} = -\frac{2\kappa_{22}}{V}\dot{y} + 2\kappa_{22}\psi \tag{1}$$

$$mi^2\ddot{\psi} = -\frac{2\kappa_{11}b^2}{V}\dot{\psi} - \frac{2\kappa_{11}b\gamma}{r_0}y \tag{2}$$

2.3 Static behaviour

The characteristic equation of this model is expressed by the following equation.

$$s^4 + \frac{2\left(b^2\kappa_{11} + i^2\kappa_{22}\right)}{i^2mV}s^3 + \frac{4b^2\kappa_{11}\kappa_{22}}{i^2m^2V^2}s^2 + \frac{4b\kappa_{11}\kappa_{22}\gamma}{i^2m^2r_0} = 0 \tag{3}$$

Substituting $m \rightarrow 0$ into eq. (3), we obtain

$$\frac{b}{V^2}s^2 + \frac{\gamma}{r_0} = 0 \tag{4}.$$

The natural frequency ω_{st} of eq. (4) is expressed by the following equation.

$$\omega_{st} = \sqrt{\frac{V^2\gamma}{br_0}} \tag{5}$$

The wavelength of ω_{st} is expressed below.

$$S_1 = 2\pi\frac{V}{\omega_{st}} = 2\pi\sqrt{\frac{br_0}{\gamma}} \tag{6}$$

The above is the previous studies. Because the damping ratio is zero in equation (4), the damping ratio cannot be considered.

3. FORMULA OF DAMPING RATIO

3.1 Characteristic equation

Assume $\kappa_{11}=\kappa_{22}=\kappa$ and $i = b$, the characteristic equation of this model is expressed by the following equation.

$$s^4 + 2\left(\frac{2\kappa}{mV}\right)s^3 + \left(\frac{2\kappa}{mV}\right)^2 s^2 + \frac{\gamma V^2}{r_0 b}\left(\frac{2\kappa}{mV}\right)^2 = 0 \tag{7}$$

3.2 Reduced characteristic equation

To simplify the notation, we use K_{mV} shown below.

$$K_{mV} \equiv \frac{2\kappa}{mV} \tag{8}$$

Using K_{mV}, eq. (7) is reduced below.

$$s^4 + 2K_{mV}s^3 + {K_{mV}}^2 s^2 + {\omega_{st}}^2 {K_{mV}}^2 = 0 \tag{9}$$

Further, instead of s, we introduce a new symbol s' defined below.

$$s' = s + \frac{K_{mV}}{2} \tag{10}$$

Substituting $s = s' - K_{mV}/2$ into s in equation (1) gives the following equation.

$$s'^4 - \frac{{K_{mV}}^2}{2} s'^2 + \left({\omega_{st}}^2 {K_{mV}}^2 + \frac{{K_{mV}}^2}{16} \right) = 0 \tag{11}$$

This is a quadratic function of s'^2. Thus we can solve eq. (11). These roots is below.

$$s' = \pm \frac{K_{mV}}{2} \sqrt{1 \pm 4 \frac{\omega_{st}}{K_{mV}} j} \tag{12}$$

3.3 Separation of imaginary part and real part

This section separates the real part and the imaginary part of eq. (16). For this purpose, s' in eq. (12) are identified as follows.

$$s'_1 = + \frac{K_{mV}}{2} \sqrt{1 + 4 \frac{\omega_{st}}{K_{mV}} j} \tag{13}$$

$$s'_2 = + \frac{K_{mV}}{2} \sqrt{1 - 4 \frac{\omega_{st}}{K_{mV}} j} \tag{14}$$

$$s'_3 = - \frac{K_{mV}}{2} \sqrt{1 + 4 \frac{\omega_{st}}{K_{mV}} j} \tag{15}$$

$$s'_4 = - \frac{K_{mV}}{2} \sqrt{1 - 4 \frac{\omega_{st}}{K_{mV}} j} \tag{16}$$

Since s'_1 and s'_2 have positive real parts, they constitute a conjugate complex root. The equation having s'_1 and s'_2 as roots is expressed by the following equation.

$$(s' - s'_1)(s' - s'_2) = 0 \tag{17}$$

Expanding eq. (17) yields the following equation.

$$s'^2 - (s'_1 + s'_2) s' + s'_1 s'_2 = 0 \tag{18}$$

Paying attention to that the real parts of s'_1 and s'_2 are both positive, eq. (18) can be transformed as follows.

$$s'^2 - \sqrt{(s'_1 + s'_2)^2}\, s' + s'_1 s'_2 = 0 \tag{19}$$

Substituting equations (13) and (14) into eq. (19) yields the following equation.

$$s'^2 - \frac{K_{mV}}{\sqrt{2}} \sqrt{1 + \sqrt{1 + 16 \frac{{\omega_{st}}^2}{{K_{mV}}^2}}}\, s' + \frac{{K_{mV}}^2}{4} \sqrt{1 + 16 \frac{{\omega_{st}}^2}{{K_{mV}}^2}} = 0 \tag{20}$$

When equation (20) is solved using the quadratic formula, the following equation is obtained.

$$s' = \frac{K_{mV}}{2\sqrt{2}}\sqrt{1+\sqrt{1+16\frac{\omega_{st}{}^2}{K_{mV}{}^2}}} \pm \frac{K_{mV}}{2\sqrt{2}}\sqrt{\sqrt{1+16\frac{\omega_{st}{}^2}{K_{mV}{}^2}}-1}\ j \tag{21}$$

Since the inside of all radical signs eq. (21) is positive, the first term on the right side of eq. (21) is a real number and the second term is a pure imaginary number. Therefore, eq. (21) is an expression obtained by separating the real part and the imaginary part of the eq. (12).

3.4 Formulation of the characteristic roots

Substituting eq. (10) into s' in eq. (21) yields the following equation.

$$s = \left(\frac{K_{mV}}{2\sqrt{2}}\sqrt{1+\sqrt{1+16\frac{\omega_{st}{}^2}{K_{mV}{}^2}}} - \frac{K_{mV}}{2}\right) \pm \left(\frac{K_{mV}}{2\sqrt{2}}\sqrt{\sqrt{1+16\frac{\omega_{st}{}^2}{K_{mV}{}^2}}-1}\right)j \tag{22}$$

By multiplying real part of eq. (22) by -1, the following equation is obtained.

$$\zeta\omega_n = -\frac{K_{mV}}{2}\left(\sqrt{\frac{1+\sqrt{1+16\frac{\omega_{st}{}^2}{K_{mV}{}^2}}}{2}}-1\right) = -\frac{\kappa}{mV}\left(\sqrt{\frac{1+\sqrt{1+4\frac{m^2}{\kappa^2}\frac{\gamma}{br_0}V^4}}{2}}-1\right) < 0 \tag{23}$$

where ω_n = natural frequency and ζ = damping ratio.

When $\zeta\omega_n$ is negative, $\zeta\omega_n$ represents the speed of divergence. On the other hand, since the imaginary part of eq. (22) represents the damped natural frequency ω_d, ω_d is expressed by the following equation.

$$\omega_d = \frac{K_{mV}}{2\sqrt{2}}\sqrt{\sqrt{1+16\frac{\omega_{st}{}^2}{K_{mV}{}^2}}-1} = \frac{\kappa}{\sqrt{2}mV}\sqrt{\sqrt{1+4\frac{m^2}{\kappa^2}\frac{\gamma}{br_0}V^4}-1} \tag{24}$$

When ω is converted into wavelength S_1, it is expressed by the following equation.

$$S_1 = 2\pi\frac{V}{\omega_d} = 2\pi\frac{\sqrt{2}mV^2}{k\sqrt{\sqrt{1+4\frac{m^2}{\kappa^2}\frac{\gamma}{br_0}V^4}-1}} \tag{25}$$

As in eqs. (20) through (24), the real part and the imaginary part of the characteristic roots of s'_3 and s'_4 are obtained below.

$$\zeta\omega_n = \frac{K_{mV}}{2}\left(\sqrt{\frac{1+\sqrt{1+16\frac{\omega_{st}{}^2}{K_{mV}{}^2}}}{2}}+1\right) = \frac{\kappa}{mV}\left(\sqrt{\frac{1+\sqrt{1+4\frac{m^2}{\kappa^2}\frac{\gamma}{br_0}V^4}}{2}}+1\right) > 0 \tag{26}$$

$$\omega_d = \frac{K_{mV}}{2\sqrt{2}}\sqrt{\sqrt{1+16\frac{\omega_{st}^{\ 2}}{K_{mV}^{\ 2}}}-1} = \frac{\kappa}{\sqrt{2}mV}\sqrt{\sqrt{1+4\frac{m^2}{\kappa^2}\frac{\gamma}{br_0}V^4}-1} \tag{27}$$

Since the value of eq. (26) is positive, it is the stable root to be derived from s'_3 and s'_4. Eq. (27) is equivalent to eq. (24).

By solving this quadratic equation for s'^2 and reconverting this solution into s, we obtain symbolic solution of its dominant root. The product of natural frequency ω_n and its damping ratio ζ is described below.

$$\zeta\omega_n = -\frac{K_{mV}}{2}\left(\sqrt{\frac{1+\sqrt{1+16\frac{\omega_{st}^{\ 2}}{K_{mV}^{\ 2}}}}{2}}-1\right) = -\frac{\kappa}{mV}\left(\sqrt{\frac{1+\sqrt{1+4\frac{m^2}{\kappa^2}\frac{\gamma}{br_0}V^4}}{2}}-1\right) < 0 \tag{28}$$

This value is negative. Therefore, wheelsets are unstable.

4. SCOPE OF APPLICATION

We assumed $\kappa_{11}=\kappa_{22}=\kappa$ and $i = b$. Effects of these assumption are shown in figure 2 and 3. From these figures, the author considers that the effects of these assumptions are negligible small. Therefore, the author judged that equation (28) can be applied to a common wheelset.

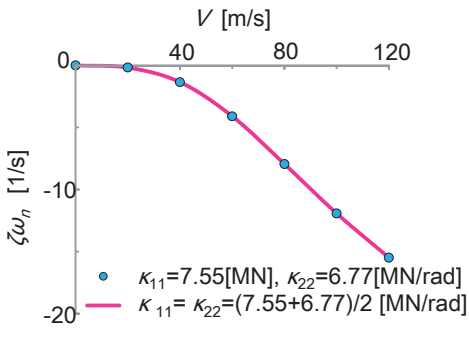

Fig. 2 Effect of κ assumption

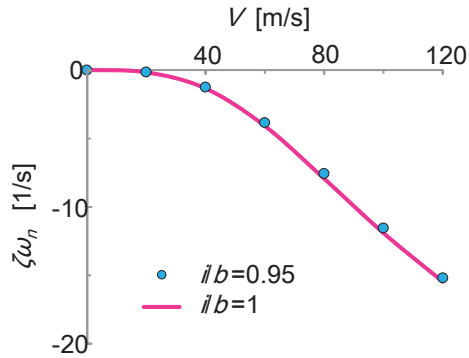

Fig. 3 Effect of i assumption

5. DISCUSSION

5.1 Global properties of characteristic roots

Consider the global property of ζωn for V. First, in order to consider the basic property around $V \fallingdotseq 0$, the following equation can be obtained by applying the Macrolin expansion of equation (28) to V.

$$\zeta\omega_n = -\frac{1}{2}\left(\frac{m}{k}\right)\left(\frac{\gamma}{br_0}\right)V^3 + O(V)^7 \tag{29}$$

Hence, eq. (28) is concave down around V=0. On the other hand, in order to consider the basic properties of the region where V is sufficiently large, if $V \rightarrow$ infinity, the following equation is obtained.

$$\lim_{V\to\infty}\zeta\omega_n = -\sqrt[4]{\left(\frac{\kappa}{m}\right)^2\left(\frac{\gamma}{br_0}\right)} \tag{30}$$

Thus, $\zeta\omega_n$ converges to a constant value. Thus, above a certain V, equation (28) is concave up. It is considered that the inflection point in the vicinity of $V \fallingdotseq 85$ [m / s] in figs. 2 (A) to 4 (A) cancels out the influence of concave up and down.

Now consider the global nature of S_1 for V. The following equation holds around V=0 for S_1.

$$S_1 = 2\pi\frac{V}{\omega_d} \approx 2\pi\left[1+\frac{1}{2}\left(\frac{m}{k}\right)^2 V^4\right]\sqrt{\frac{br_0}{\gamma}} \tag{31}$$

Thereby, S_1 is concave up. On the other hand, since $V\rightarrow$Infinity, the following equation holds.

$$\lim_{V\to\infty}\omega_d = \sqrt[4]{\left(\frac{\kappa}{m}\right)^2\frac{\gamma}{br_0}} \tag{32}$$

Therefore S_1 is concave down. Since figs. 2 (B) to 4 (B) are concave up, they are considered to correspond to the region of equation (31).

5.2 Increase of damping due to increase of wavelength of geometrical hunting

Equations (29) to (32) are made up of two terms, κ/m and γ/br_0, excluding V. Hence this section treats γ/br_0. The square root of γ/br_0 multiplied by 2π is the wavelength of the geometrical hunting. Therefore, this section focuses on the wavelength of geometrical hunting. The critical railway forward velocity at which the wheelset elastically supported from the stationary system becomes unstable is proportional to the wavelength of geometrical hunting of the wheelset itself (JSME 1999). On the other hand, from eq. (28), $\zeta\omega_n$ increases as γ/br_0 decreases. Thus, the increase in the critical velocity due to the increase in the wavelength of the geometrical hunting seems to be due to the increase in $\zeta\omega_n$ due to the reduction of γ/br_0. Therefore, this consideration is confirmed by Fig. 4.

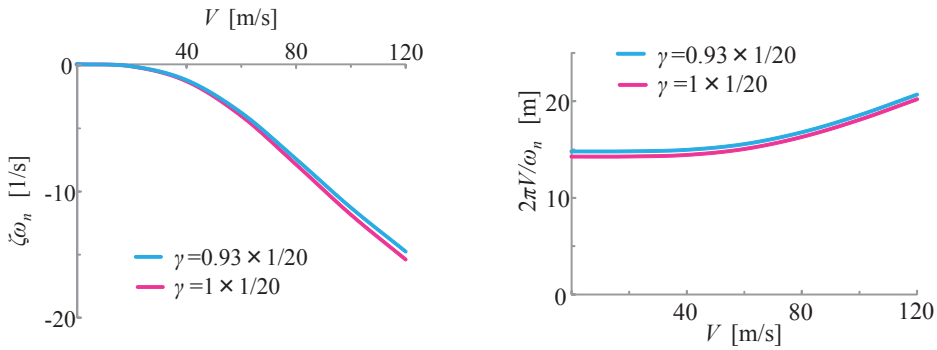

(A) Damping (B) Wavelength

Fig. 4 Influence of the gradient of wheel tread γ: This calculation is conducted with the values described in fig.2 except γ. When the mass of wheelset decrease, $\zeta\omega_n$ increases at this V.

Here, the wavelength of the geometrical hunting was increased as shown in Fig. 4 (B) by decreasing γ. As a result, it can be seen from Fig. 4 (A) that damping increased as expected. From this consideration, the reason why the critical railway forward velocity of the hunting of the elastically supported wheelset is increased by lengthening the wave length of the geometrical hunting seems to be due to an increase in the damping of the wheelset alone.

5.3 Increase of damping by mass of wheelset

This section examines increase of the damping due to mass reduction of the wheelset. As m changes, its wheel load changes and κ also changes. Thus, it is assumed that κ is proportional to the wheel load 2/3 power (Yokose 1971). Therefore, κ is defined as follows.

$$\kappa = q(m+M)^{\frac{2}{3}} \tag{33}$$

where M is defined so that $(M+m)g$=wheel load, g=gravitational acceleration, q=constant and q is set to satisfy the reference specifications.

When m is increased, $\zeta\omega_n$ decreases at a lower speed side than a certain V, and $\zeta\omega_n$ increases on the high speed side. Therefore, I describe a V as a metrics of the influence of m on $\zeta\omega_n$. Even if m is slightly changed, V that does not change $\zeta\omega_n$ is

$$V \approx \sqrt[4]{\left(2+\sqrt{5}\right)\left(1+\frac{M}{m}\right)\frac{br_0}{\gamma}\left(\frac{\kappa}{m}\right)^2} \tag{34}$$

From eq. (34), as M/m decreases (i.e. as m increases), this V moves to the low speed side. Substituting the reference specifications into the eq. (34), it yields V = 144.6 [m/s]. Therefore, fig. 5 shows the calculation result when κ/m is increased (i.e. m reduction) in order to increase $\zeta\omega_n$ on the lower speed side than this V. In fig.5, $\zeta\omega_n$ increased at least in the range of $0 \leqq V \leqq 120$ [m/s].

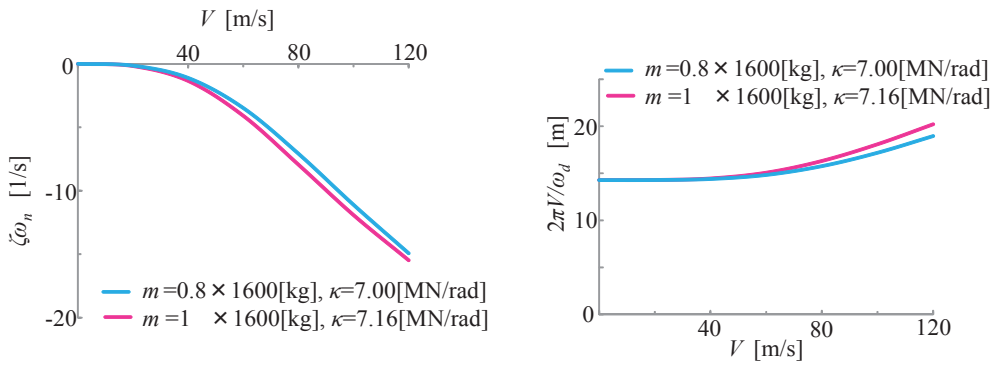

(A) Damping (B) Wavelength

Figure 5 Influence of the mass of wheelset m: This calculation was conducted with the values described in fig.2 except m and κ. κ is determined by eq. (17). Further m is assumed 4150[kg]. Reduction of m increases $\zeta\omega_n$.

5.4 Increase of damping due to wheel radius increase

Section 5.1 showed that $\zeta\omega_n$ can be increased by increasing the wavelength of geometrical hunting. When increasing the wavelength by increasing r_0, m may also increase. As m changes, $\zeta\omega_n$ also changes as described in section 5.2. Therefore, in this

section, the influence of r_0 on $\zeta\omega_n$ is considered under the assumption that m increases as r_0 increases. For the sake of simplicity, it is assumed that m is proportional to the wheel area seen from the sleeper direction. Therefore, m can be described as follows.

$$m = pr_0^{\,2} \tag{35}$$

where p=constant, p is chosen to satisfy the relationship between r_0 and m in the reference specifications.

When r_0 is increased, $\zeta\omega_n$ decreases at a lower speed side than another certain V, and $\zeta\omega_n$ increases on the high speed side. Therefore, as a metrics of the influence of r_0 on $\zeta\omega_n$, V that does not change $\zeta\omega_n$ is obtained even if r_0 is slightly changed. However, it is difficult to obtain the symbolic solution of this V under the assumption of eq. (33). Hence, when obtaining this V, κ is assumed to be constant even if m changes. Thus, substituting only the eq. (35) into the eq. (28), the following equation is obtained.

$$\zeta\omega_n = -\frac{\kappa}{pr_0^{\,2}V}\left(\sqrt{\frac{1+\sqrt{1+4\dfrac{pr_0^{\,2}}{\kappa^2}\dfrac{\gamma}{br_0}V^4}}{2}}-1\right) \tag{36}$$

Further, as a metrics of the influence of r_0 on $\zeta\omega_n$, even if r_0 is slightly changed, V that does not change $\zeta\omega_n$ described eq. (36) is

$$V \approx \frac{\sqrt{2}}{5}\sqrt[4]{\left(47+9\sqrt{89}\right)\left(\frac{\kappa}{pr_0^{\,2}}\right)^2\frac{b}{\gamma r_0}} \tag{37}$$

On the lower speed side than this V, the damping increases with smaller r_0. On the higher speed side than this V, the damping increases as r_0 is larger. This V is 96.6 [m/s] in the reference specifications. Therefore, for the purpose of increasing the damping on the higher speed side than this V, the influence when r_0 is multiplied by 1.2 of the reference parameter is shown in fig. 6. As shown in fig. 6, $\zeta\omega_n$ increased on the high speed side of V≈87 [m/s]. Therefore, reduction of damping due to increase in r_0 in this specification was effective even in consideration of m and κ.

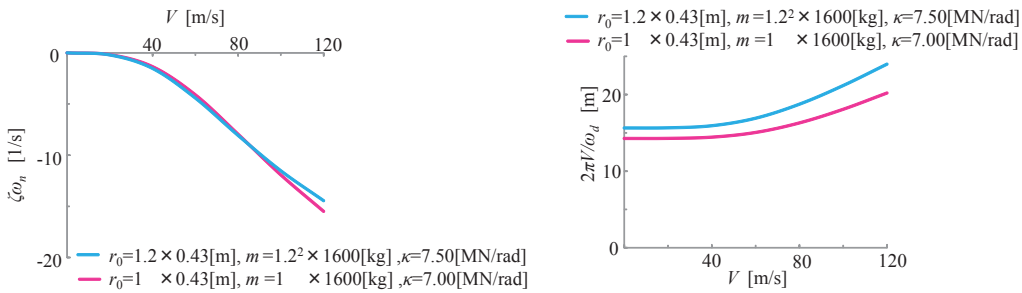

(A) Damping (B) Wavelength

Figure 6 Influence of the radius of wheel r_0 related mass of the wheelset m (κ is defined as a function of m): This calculation is conducted with the values described in

fig.2 except r_0 and m and κ. κ is determined by eq. (33). An increase in r_0 increased $\zeta\omega_n$ at V>87[m/s].

6. CONCLUSIONS

I obtained the character expressions of the exact solution of the natural frequency and its damping ratios of the hunting of the wheelset, and clarified its valid range under certain assumptions about its inertia radius and its creep coefficients of wheelset.

The damping formula consists of creep coefficient/mass of wheelset and natural frequency of geometrical wheelset hunting.

As a result of examining the character expression, it was effective to reduction of the mass of wheelset for increasing the damping of the hunting at V <140[m/s].

Assuming that the mass of the wheelset is proportional to the square of the radius of the wheel, the larger the wheel radius, the larger the damping at V >100[m/s].

7. REFERENCES

[1] **JSME, 1999**.: Dynamics and control of vehicle systems, Tokyo: Yokendo:126-133.
[2] **Yokose, K**.: Sharin to rairu no suberi gensho ni tsuite, Transaction of JSME 37(304): 2407-2422 . 86, 1971, p.112-125.

CONTRIBUTION OF ACTIVE ELEMENTS IN LOCOMOTIVE RUNNING GEAR TO REDUCTION OF GUIDING FORCES

Tomáš MICHÁLEK and Jaromír ZELENKA

Department of Transport Means and Diagnostics, Section of Rail Vehicles
Faculty of Transport Engineering
University of Pardubice
CZ-53210 Pardubice, Czech Republic

Received: September 12, 2019

ABSTRACT

This paper is focused on a potential contribution of active elements in a locomotive running gear to reduction of guiding forces during the run of a four-axle locomotive through curves. Two different applications are discussed – a system of active elements for bogie steering and a system of active elements for radial wheelset steering. The effectivity of both systems is assessed with using of results of multi-body simulations, performed by means of the simulation tool "SJKV". The attention is paid especially to the influence of parameters of the active systems (maximum force and stroke of individual elements) as well as to their limitations.

Keywords: system of active elements, bogie steering, radial wheelset steering, locomotive running gear, guiding forces, multi-body simulations

1. INTRODUCTION

One of the most significant compromises, which must be done in the design stage of new railway vehicles, is a determination of the right values of relevant parameters of their running gear (e.g. stiffness of wheelset guiding in longitudinal as well as lateral direction, bogie yaw resistance, damping etc.) to ensure a stable run of the vehicle at its maximum (test) speed and minimize its guiding forces in curves on the other hand. In case of railway vehicles intended for higher speeds (the high speed vehicles), the requirements on running stability usually lead to such technical solutions of running gears (a very stiff wheelset guiding, efficient yaw dampers etc.) which are not "track-friendly" in conditions of curved track sections, especially in the small-radius curves. Therefore, these vehicles show a higher level of the guiding forces as well as a higher level of wear of wheels and rails in curves. An important consequence of the higher intensity of wheel/rail wear is a higher level of maintenance costs which are related to a shorter lifetime of wheels (on side of the vehicle keeper/operator) and rails (on side of the infrastructure manager).

Possibilities for minimization of the guiding forces and wheel/rail wear by means of conventional passive systems can be represented e.g. by (mechanical or hydraulic) bogie couplings [1], interconnected wheelsets [2] or a concept of hydraulic wheelset guiding "HALL" [3]. Although the contribution of these solutions can be significant, it will always be limited because of the passive principle of their function. Therefore, an application of active elements into the running gear seems to be an effective way how to reach further improvement of the guiding behaviour of railway vehicles. In order to reduce the guiding forces in (small-radius) curves as well as the related wear of wheels and rails, the systems of active elements can be technically applied:

- into the secondary suspension stage, where they can support radial steering of the whole bogies,

- or into the primary suspension stage (wheelset guiding), where they can be used for radial steering of individual wheelsets.

In this paper, there is performed an assessment of potential effect of relevant active systems applied into the running gear of a modern four-axle electric locomotive. The attention is paid especially to the influence of parameters of the active systems (i.e. the maximum force and stroke of individual elements); limitations of contribution of the active systems are also discussed. The assessment was performed with using of multi-body simulation results; all relevant simulations were realized by means of the original simulation tool "SJKV" which was modified for purposes of modelling of the systems of active elements (a more detailed description of the basic academic version of the "SJKV" software can be found in [4]).

2. SYSTEM OF ACTIVE ELEMENTS FOR RADIAL STEERING OF BOGIES

The radial steering of the whole bogies in curves can be supported by *active yaw dampers*. Such a system – known as "ADD" (in German: *Aktive Drehdämpfer*) [5] – is commonly used e.g. in the bogies of some Siemens' Vectron locomotives (Class 1293 ÖBB), nowadays. Another application of the active yaw dampers is proposed as an optional equipment of the new three-axle bogie CZ Loko – see e.g. [6].

Technically, the actuators are integrated into the yaw dampers. The forces, exerted by these (electrohydraulic) actuators on relevant arm, act as a rotational moment on individual bogies (see Fig. 1) and support their rotation into the radial position during the vehicle run through a curve. The main difference between this active system and the passive system of bogie coupling lies in the fact, that the effect of bogie coupling is derived from a difference of yaw angles of both bogies (the bogie showing the bigger yaw angle – i.e. usually the rear bogie – helps to steer the second one). If the system of active yaw dampers is used, its function need not be limited by the difference of bogie yaw angles. Theoretically, individual (independent) steering of the front and the rear bogie is also possible with using of the actuators (and it cannot be applied in case of the bogie couplings).

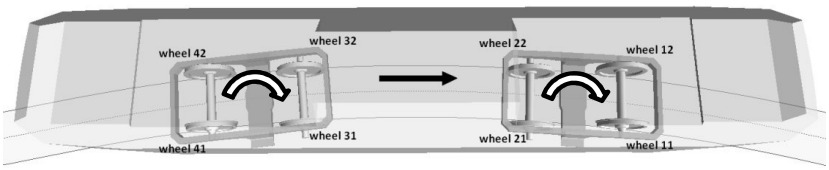

Fig. 1 Moments of active elements helping to steer the bogies in a curve

The system of active elements for bogie steering can be controlled on the basis of information about the bogie yaw angle. Relevant data can be gained with using of integrated yaw damper deformation sensors. A dependency of the damper deformation on curve radius can be determined for a specific vehicle (defined by its dimensional parameters) and for specific conditions (unbalanced lateral acceleration). If the system recognizes a curve (the bogie yaw angle exceeds a defined value), individual actuators start to exert a defined (push or pull) force and therefore they help to steer the bogies into a radial position, decreasing the angle of attack of the bogies.

2.1 Assessment of contribution to improvement of guiding behaviour

At the Faculty of Transport Engineering of the University of Pardubice, a possible contribution of the system of active yaw dampers to minimization of guiding forces of an electric locomotive in curves was investigated. In order to estimate the influence of a maximum force in the actuators on the guiding behaviour of the locomotive in small-radius curves, a set of simulations was performed and reached values of the quasistatic guiding force acting on individual wheels were observed. A detailed description of this stage of research of possibilities of active element systems can be found e.g. in [7]. An example of relevant results is presented in Fig. 2 in form of quasistatic values of the guiding forces reached on individual wheels of a multi-body model of the investigated locomotive (marking of the wheels corresponds to the scheme in Fig. 1) during its run through a right-hand curve with a radius of 300 m at the speed corresponding to the cant deficiency of 165 mm and under the condition of friction coefficient in wheel/rail contact of 0.4 (representing dry rails).

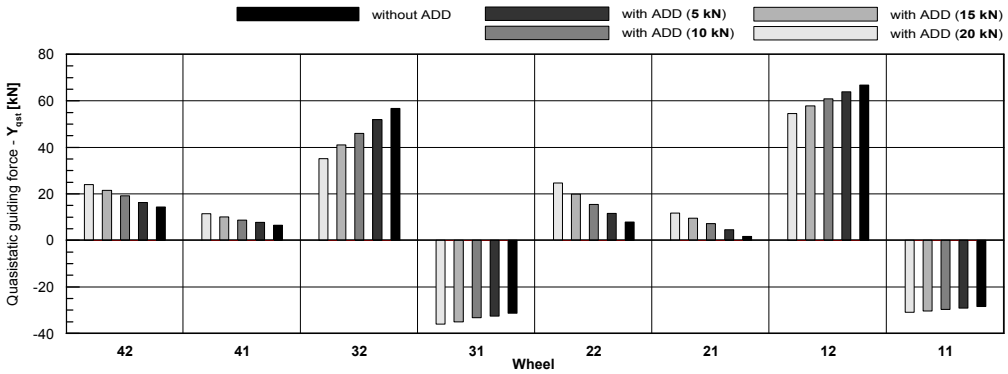

Fig. 2 Influence of maximum force in actuators on quasistatic guiding forces acting on individual wheels of an electric locomotive at its run through a right-hand 300-m curve under the conditions of cant deficiency of 165 mm and friction coefficient in wheel/rail contact of 0.4

The results show that the system of active yaw dampers can significantly reduce the quasistatic guiding forces acting on guiding wheels in both bogies (i.e. on the wheels No. 12 and 32 in the presented example) during the run of the vehicle through a curve. Because the sum of all quasistatic guiding forces must be equal to the total unbalanced lateral force acting on the vehicle (force equilibrium of the system vehicle/track in lateral direction), the observed reduction of guiding forces on the guiding wheels has to be compensated by means of an increase of the guiding forces on the other wheels, especially on the outer wheels of the non-leading wheelsets (i.e. on the wheels No. 22 and 42 in the presented example). It means that the distribution of the lateral (guiding) forces between the individual wheels can be more even.

An important fact, which is evident from the Fig. 2, is a different steepness of the reduction of the quasistatic guiding force at increasing force (moment) of the actuators on the wheels No. 12 and 32. In case of the wheel No. 12, each kilonewton of the force exerting by the actuators leads to a decrease of the guiding force, on average, about

0.6 kN (i.e. 0.9 % in comparison with the locomotive without the system of active yaw dampers) under the considered conditions (curve radius, speed/cant deficiency, friction coefficient etc.). In case of the wheel 32, this steepness reaches, on average, a value of approximately 1.0 kN/kN (i.e. 1.8 %/kN in comparison with the locomotive without the system of active elements). E.g., two actuators per bogie (situated on the position of the longitudinal yaw dampers) exerting the force of 15 kN decrease the quasistatic guiding force on the wheel 12 about ca. 9 kN and about ca. 15 kN on the wheel 32 in the investigated case. This effect can be explained by means of the influence of a bogie yaw resistance on individual bogies. Because of opposite signs of yaw angles of both bogies (their orientation relatively to the vehicle body) in curve, the system of active elements has to negotiate the bogie yaw resistance moment on the front bogie in order to steer the bogie into the radial position. However, the bogie yaw resistance moment acting on the rear bogie helps to reduce the angle of attack of this bogie, and therefore, its effects is superposed to the effect of the actuators.

2.2 Limitations of the active system

As described above, the system of active yaw dampers applied into the locomotive running gear can contribute to a relatively significant reduction of quasistatic guiding forces acting on outer wheels of leading wheelsets in both bogies during the run of the vehicle through small-radius curves. Therefore, this system can help to fulfill relevant requirements (TSI, EN 14363, UIC 518) on permitted lateral force effects between the vehicle and the track. However, this system shows some limitations, as well.

The first limitation is related to the maximum force (moment) which can be exerted by the active elements. As demonstrated in Fig. 2, higher forces can contributed to a very significant reduction of the problematic values of quasistatic guiding forces on the guiding wheels. However, the function of the active system must not endanger the operational safety. Therefore, it is necessary to prove the safety of the vehicle in all relevant situations, including incorrect function of the system. And this task does not have to be very simple in case that higher level of forces of actuators is applied.

The second limiting aspect is related to operational conditions. As described above, the system of active yaw dampers can help to redistribute in curves the magnitudes of guiding forces especially from the outer wheel of leading wheelset to the outer wheel of non-leading wheelset in framework of individual bogies of the vehicle. However, the distribution of quasistatic guiding forces between individual wheels of a specific railway vehicle is dependent, among others, on the curve radius, vehicle speed (cant deficiency) and friction conditions in wheel/rail contact. It means that a certain setup of parameters of the active system can lead – under certain conditions (i.e. especially a larger radius of curves and a lower friction coefficient in the wheel/rail contact) – to a situation that the maximum values of quasistatic guiding forces are observed on the outer wheels of non-leading wheelsets and the original target (i.e. the minimization of guiding forces) need not be fulfilled. Therefore, the parameters of the system (i.e. the force of individual actuators) have to be defined in order to ensure an optimal effect of the active system in the widest range of possible operational conditions. This question is also closely related to characteristics of the secondary suspension stage, i.e. to the bogie yaw resistance, which can be strongly influenced (“non-linearized”) especially by means of application of various types of spring pads – see e.g. [8].

And the last but not least limitation lies in guiding behaviour of a vehicle equipped with the system of active yaw dampers in switches and S-shape curves. The simulation results indicate that the system of active yaw dampers – controlled on basis of yaw damper deformation – can worsen the lateral force effects of the vehicle on the track in that conditions. The main reason for that is a delayed reaction of the system because it is not possible to identify the entrance of the 1st wheelset into the curve in time from the information characterizing the yaw damper deformation. Because the switches are usually designed without transition curves, the consequential need of a fast yawing of the bogie at its entrance into the switch (i.e. curve) usually leads to a high peak of the guiding force acting on the guiding wheel. Technically, it is not a simple task to ensure a sufficiently fast reaction of the active system in these situations.

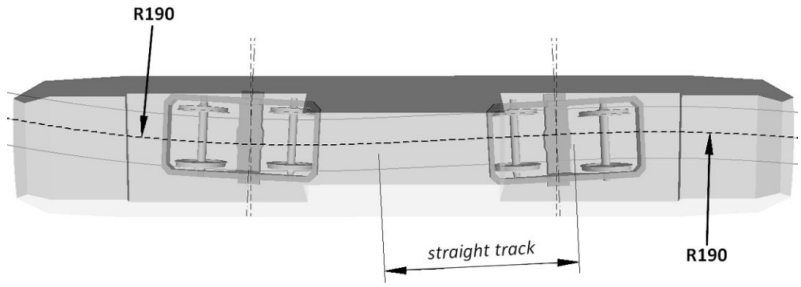

Fig. 3 Situations of the vehicle at its run through an S-shape curve

Besides to that, the reaction of the system in the S-shape curve can even be contrary if the length of an intermediate straight track section between the two curves is shorter than the relevant dimensional parameter of the vehicle (i.e. the distance between bogie pivots). This situation is demonstrated in Fig. 3. In this case, it is not possible to ensure the required reaction of the active elements in the front bogie on the entrance of this bogie into the second curve because the system – controlled on basis of yaw damper deformation – "does not know" that the vehicle enters this curve (the yaw angle of the 1st bogie still has an opposite sign).

3. SYSTEM OF ACTIVE ELEMENTS FOR RADIAL WHEELSET STEERING

The systems of active elements for radial wheelset steering represent the second possibility how the guiding behaviour of a railway vehicle can be improved by means of application of the active systems. Because of the direct influence of the system on the angle of attack of individual wheelsets, a more significant reduction of the wear of wheels and rails as well as the guiding forces in curves can be theoretically reached (in comparison with the active systems for steering of the whole bogies – see chapter 2). An application of such system is represented e.g. by the system "ARS" (in German: *Aktive Radsatzsteuerung*) which can be optionally installed into the Bombardier's bogie type Görlitz IX – see e.g. [9].

In framework of solving the R&D project "*Competence Centre of Rail Vehicles*" at the Faculty of Transport Engineering of the University of Pardubice in 2017–2019, a study of possible application of system of active elements for radial wheelset steering in a locomotive running gear was elaborated. The study is based on results of multi-body

simulations performed with modified computational model of a modern four-axle electric locomotive Škoda in the simulation software "SJKV", again. In this case, two actuators per bogie were considered, i.e. one active element for radial steering of each wheelset – see Fig. 4. The attention was paid especially to a possible contribution of the active elements to improvement of guiding behaviour of the vehicle in small-radius curves with respect to the influence of parameters of the actuators (maximum stroke and velocity) as well as to their control (control strategy, identification of entrance of the vehicle into the curve and related inaccuracy).

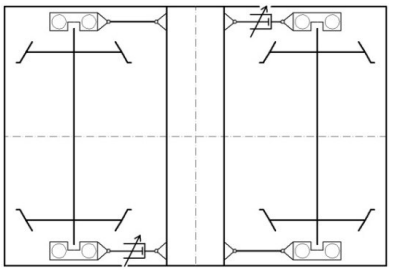

Fig. 4 Considered arrangement of active elements in the bogie of the investigated computational model of electric locomotive

3.1 Assessment of contribution to improvement of guiding behaviour

In Fig. 5 and 6, there is presented an example of simulation results demonstrating the potential improvement of guiding behaviour of the locomotive in a small-radius curve at various considered values of maximum stroke of individual active elements. In this case, the following strategy of the active system control was applied. In the first stage, dependencies of the angle of attack of individual wheelsets of the investigated vehicle (without the active system) on the curve radius and the cant deficiency were determined on basis of relevant analysis. Then, a relation to the deformation of bogie yaw dampers was estimated in order to allow the regulation of the system for active radial wheelset steering on basis of the information about bogie yaw angle (i.e. on basis of signals from the yaw damper deformation sensors). During the simulation of run of the vehicle on defined track, a required value of the active element stroke is continuously calculated for both bogies with respect to these signals. The developed algorithm covering estimation of the required stroke of active elements as well as the corresponding reaction of the active system is implemented into the multi-body model. In the presented example, the maximum stroke is limited in a range from 0 up to 12.5 mm. In Fig. 5, an influence of the maximum actuator stroke on the angle of attack of individual wheelsets in a 250-m is presented. It is evident that the angle of attack of leading wheelsets in both bogies (i.e. the wheelsets No. 1 and 3) can be reduced in the considered case by approximately 50 % if the stroke of 5 mm is used. And the value of active element stroke of ca. 12 mm even allows a total elimination of the angle of attack of the leading wheelset. (Note: In case of the rear bogie, the applied algorithm of calculation of the required active element stroke does not allow to use the values greater than approximately 8 mm in the discussed situation. Therefore, the results for the two highest considered values of the stroke are affected by this fact on this bogie.)

In Fig. 6, there are presented corresponding values of the quasistatic guiding forces acting on individual wheels (marking of the wheels corresponds to the scheme in Fig. 1, again) for the discussed situation (run of the locomotive through a right-hand 250-m curve at the speed corresponding to a cant deficiency of 150 mm under the condition of dry rails). These simulation results indicate that a very significant decrease of the quasistatic guiding force can be theoretically reached if the active systems for radial wheelset steering are applied. In case that the active element stroke of 10 mm is used, the quasistatic guiding forces on all wheels of the vehicle are lower than 40 kN in the discussed situation; on the leading wheel of the front bogie (i.e. the wheel No. 12), it represents a reduction about approximately 40 % in comparison with the locomotive model without the active elements.

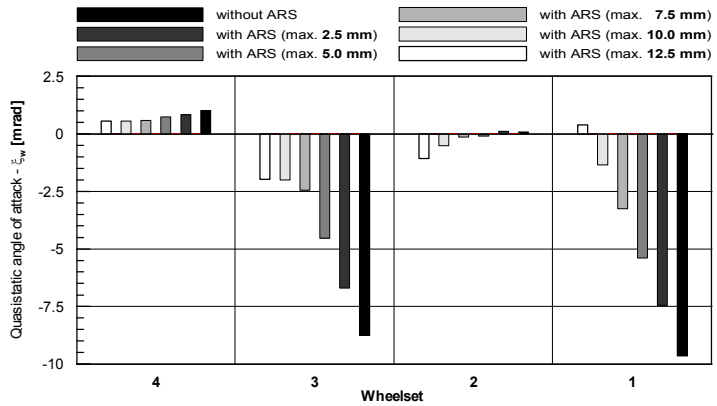

Fig. 5 Influence of maximum stroke of actuators on angle of attack of individual wheelsets of an electric locomotive at its run through a right-hand 250-m curve under the conditions of cant deficiency of 150 mm and friction coefficient in wheel/rail contact of 0.4

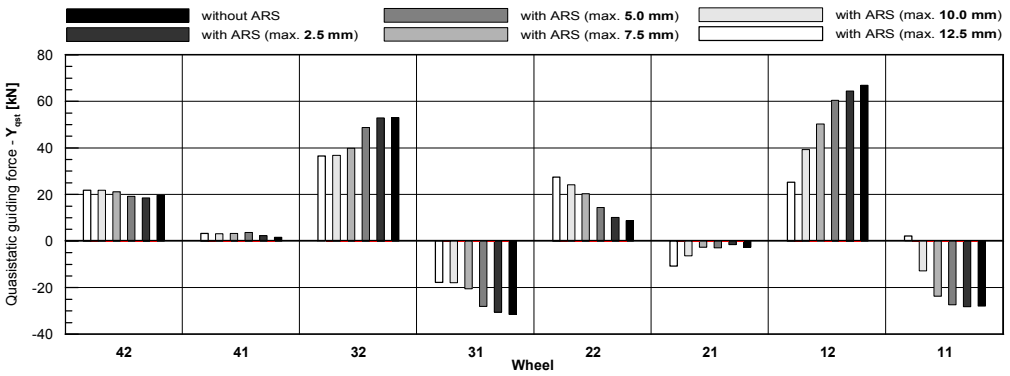

Fig. 6 Influence of maximum stroke of actuators on quasistatic guiding forces acting on individual wheels of an electric locomotive at its run through a right-hand 250-m curve under the conditions of cant deficiency of 150 mm and friction coefficient in wheel/rail contact of 0.4

3.2 Limitations of the active system

Besides the requirements resulting from solving questions concerning operational safety of the vehicle at a potential incorrect function of the system of active elements (see also chapter 2.2), which are highly relevant in this case, the limitations of the systems for active radial wheelset steering are connected especially with the velocity and accuracy of reaction of the system. In case that the vehicle runs through common curves on the track, the requirements on the reaction of the active system are not too strict. The time, which is necessary for the system reaction, corresponds to the time of run of the vehicle through the transition curves. Therefore, the required velocity of stroke of the individual actuators ranges in order of ones millimeters per second in these situations. However, in the switches and S-shape curves, a sufficiently fast and accurate reaction of the system creates an essential precondition for achievement of reduction of the lateral force effects of the vehicle on the track as well as the level of wear in wheel/rail contact. The reason is that the most intensive lateral force effects (the peak of guiding forces on guiding wheels) act immediately after the entrance of the vehicle into the curve.

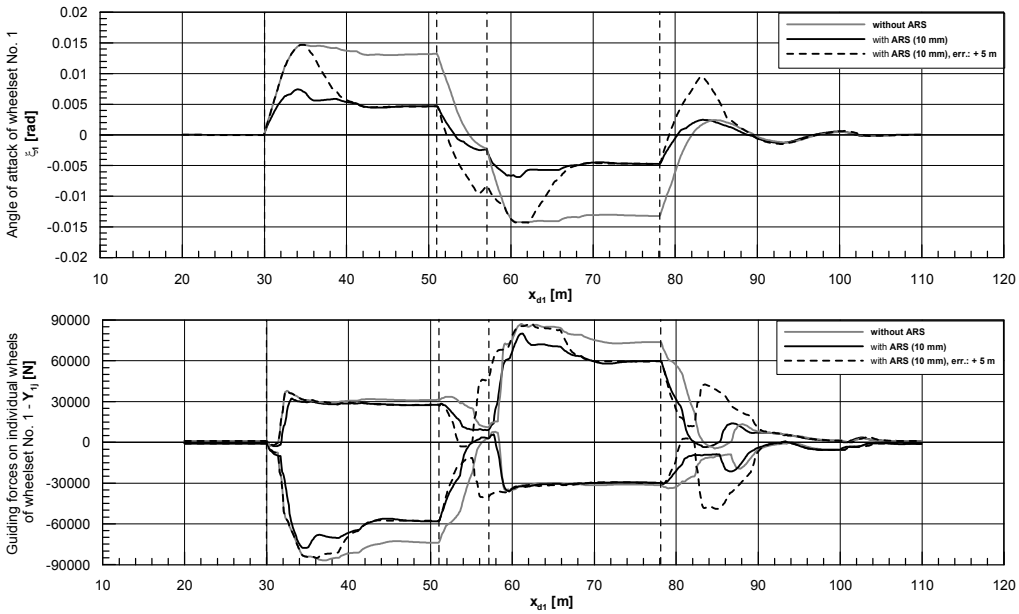

Fig. 7 Influence of inaccurate reaction of the active system on angle of attack of the 1st wheelset (upper graph) and on guiding forces acting on wheels of the 1st wheelset (bottom graph) at simulation of run of an electric locomotive through an S-shape curve 2 x 190 m with a 6 m long intermediate straight track section under the conditions of speed of 40 km/h and friction coefficient in wheel/rail contact of 0.4

The problem of the accurate reaction of the system is related with the possibility of recognition of the entrance of the 1st wheelset in the diverging part of the switch – i.e. the curve without transition part. Similarly to the active systems for bogie steering (see chapter 2.2), the recognition of the entrance into the curve in time is not a simple task if the information used for control of the active system is derived from the bogie yaw

angle (e.g. from the signals of yaw damper deformation sensors). And in specific cases of run of the vehicle through S-shape curves with a short intermediate straight track section (in comparison with the basic dimensional parameters of vehicle), a timeous recognition of the entrance of the vehicle into the second curve from these signals is totally impossible, again. (The reason is the same as in case of the active systems for bogie steering and it is demonstrated in Fig. 3.) Besides to that, a very fast change of the sign of the stroke of the actuators is necessary in the S-shape curves. Therefore, the required velocity of stroke ranges in order of tens millimeters per second.
In Fig. 7, there is presented an example of simulation results representing run of the investigated model of locomotive through an S-shape curve with radius of 2 x 190 m and with a 6 m long intermediate straight section. The upper graph in Fig. 7 shows the time history of angle of attack of the 1st wheelset; the bottom graph shows the guiding forces acting on both wheels of this wheelset. The results for a locomotive without the active system for radial wheelset steering is depicted by the grey line; the black lines represent the results of locomotive equipped with the active system with a maximum stroke of the actuators of 10 mm. The full black lines in the graphs correspond to an accurate (theoretical) reaction of the system. In comparison with the results obtained with the model of locomotive without the active elements, a very significant reduction of the angle of attack (about more than 50 %) as well as the guiding force acting on the leading wheel (about ca. 10 up to 15 kN) can be observed. However, this contribution of the system of active elements is seriously degraded in case that the reaction of the system is delayed. In order to demonstrate this fact, the dashed-line-depicted results present a behaviour of locomotive which shows delayed reaction of the active system about 5 m (at the considered speed of 40 km/h, it corresponds to a time delay of only 0.45 s). In this case, the most problematic aspect of the interaction vehicle/track in the S-shape curves (i.e. the peaks of guiding forces immediately after the entrance of the vehicle into the individual curves) cannot be eliminated by means of the active system for radial wheelset steering.

4. CONCLUSIONS

Application of the active systems into the running gear of rail vehicles opens a wide range of possibilities for optimization of guiding behaviour of the vehicles in curves. The systems of active steering of whole bogies are not so complicated and nowadays, they are really used in running gears of some types of locomotives (especially in form of the system “ADD” on the Siemens’ Vectron locomotives). In case of the systems for active radial wheelset steering, the wheel/rail wear level as well as the quasistatic guiding force level can be reduced more significantly, at least theoretically. However, the question of reliable and sufficiently accurate control of these innovative systems becomes highly relevant to ensure the expected benefits in a safe way. The results of the performed simulations also show that it is very problematic (or even impossible) to ensure a timeous reaction of the active systems in conditions of switches and S-shape curves if these systems are regulated on basis of on-board monitoring of the bogie yaw angles. Therefore, the possibilities of reliable uses of another information sources (e.g. data from systems GPS, ETCS or ATO) represent a next field of research.

5. ACKNOWLEDGEMENTS

This work was supported by R&D project No. TE01020038 "*Competence Centre of Rail Vehicles*" of the Technology Agency of the Czech Republic.

6. REFERENCES

[1] **Zelenka, J. – Špalek, P.**: Simulační výpočty vodicích vlastností lokomotivy ř. 380, posuzování vlivu mezipodvozkové vazby. In: *XIX. konference s mezinár. účastí Současné problémy v kolejových vozidlech 2009, Sborník přednášek*. 2009, p.195-198.

[2] **Polách, O.**: Curving and stability optimisation of locomotive bogies using inter-connected wheelsets. In: *Vehicle System Dynamics Supplement* 41, 2004, p.53-62.

[3] **Biber, R. – Gürtler, D. – Marzillier, W. – Schwab, P.**: Achslenkerlager. European patent No. EP1457706A1.

[4] SIMULACE JÍZDY KOLEJOVÉHO VOZIDLA. Available from the website: https://dfjp.upce.cz/dfjp/kdpd/kolejova-vozidla#collapse159900 [cit. 2019-09-04].

[5] **Breuer, W.**: Der Aktive Drehdämpfer (ADD) – Ein innovatives Dämpferkon-zept im Betriebseinsatz. In: *Eisenbahntechnische Rundschau* 4, 2007, p.186-189.

[6] **Michálek, T. – Haupt, L. – Zelenka, J. – Kohout, M. – Liberová, S.**: Lateral force effects of three-axle locomotive bogie on track. In: *Applied and Computational Mechanics* 12, 2018, p.33-44.

[7] **Michálek, T. – Zelenka, J.**: Reduction of lateral forces between the railway vehicle and the track in small-radius curves by means of active elements. In: *Applied and Computational Mechanics* 5, 2011, p.187-196.

[8] **Michálek, T. – Zelenka, J.**: The effect of spring pads in the secondary suspension of railway vehicles on bogie yaw resistance. In: *Vehicle System Dynamics* 53, 2015, p.1952-1964.

[9] **Kraft, D. – Grossenbacher, T.**: Erprobung von Prototypdrehgestellen für die Fernverkehrsdoppelstockzüge der SBB. In: *Eisenbahn-Revue International* 2, 2011, p.68-71.

FAULT DETECTION AND ISOLATION METHOD FOR VEHICLE RUNNING INSTABILITY FROM VEHICLE DYNAMICS RESPONSE USING MACHINE LEARNING

Rohan KULKARNI, Alireza QAZIZADEH, Mats BERG and Sebastian STICHEL

Department of Aeronautical and Vehicle Engineering,
KTH Royal Institute of Technology
Stockholm, Sweden

Received: September 12, 2019

ABSTRACT

In this paper, a Fault Detection and Isolation (FDI) method is proposed for monitoring the vehicle running stability in a high-speed railway bogie. The objective is to detect and isolate the different faults of bogie components which are critical to vehicle stability, especially degraded yaw dampers and high equivalent conicity caused by wheel wear. The proposed method has two steps; firstly, signal features sensitive to the characteristics of running instability are extracted based on frequency domain and time domain analysis of lateral accelerations of bogie frame and axlebox; then these features along with vehicle speed are fed into machine learning based fault classifiers. The supervised machine learning based fault classifier are trained to identify the cause of observed running instability among yaw damper degradation and wheel-rail profile pair with high equivalent conicity. The Support Vector Machine (SVM) classifier with Linear and Gaussian kernels is trained by k-fold crossvalidation method and the hyperparameters are optimized with a bayesian optimization algorithm to minimize the classification error. These fault classifiers are trained and tested with an extensive database generated from numerical experiments performed by multibody simulation (MBS) software. The performance of Linear and Gaussian SVM fault classifiers is compared with each other to identify the best performing classifier. The results underline the ability of machine learning based fault classifiers to be used for FDI of vehicle running instability and outline the possibility of detecting and isolating bogie faults critical to the vehicle stability based on onboard measurement of vehicle dynamic response.

Keywords: fault-detection, running instability, dynamical process, machine learning

1. INTRODUCTION

Vehicle hunting motion (running instability) is a classical issue in vehicle-track dynamic interaction. Typically, running instability appears at a fairly high vehicle speed and on straight track or in large-radius curves. The running instability is a vehicle system property which is dependent on the design and health of the vehicle subsystems. The foremost causes of running instability are poor vehicle yaw dampers, too soft primary suspension in the horizontal plane or poor wheel-rail interface. Vehicle running instability can be categorised into bogie hunting and carbody hunting. In January 2016, vehicle running instability was detected on many vehicles irrespective of their types, while running in the Hallandås tunnel located in southern Sweden [1]. The vehicle running instability resulted in poor ride comfort for passengers. The bogie hunting caused by high equivalent conicity was the cause behind the running instability which was identified by performing analyses in compliance with European standards. However, root cause identification could have been done more efficiently, if a fault detection and isolation (FDI) system was installed onboard every vehicle. However, the present methods are not capable of identifying the root cause of running instability from onboard measurements performed with help of accelerometers. In view of the above, there is a necessity to develop FDI methods for vehicle running instability to ensure

safety and maintain good ride comfort. In this way, FDI methods can be used for monitoring the status of bogie components.

The FDI methods can be categorised into model-based and signal-based methods. Model-based FDI approaches, identify and isolate the root cause of the fault condition based on analysis of the mathematical relationship between the input and the output of the dynamic system. However, model-based estimation techniques are not accurate enough to address the nonlinearities present at the wheel-rail interfaces and uncertainties associated with parameters of vehicle components [2]. Signal-based FDI techniques identify and isolate the root cause of the fault condition based on advanced signal processing in time, frequency or time-frequency domains. The crux of signal-based method is in the identification of the unique feature/pattern in the output signal which is associated with a unique fault condition. A huge database of unique feature/pattern paired with unique fault condition is generated and features extracted from an output signal are matched with features stored in the database to identify the root cause of the fault condition.

In recent years, signal-based approaches have incorporated machine learning (ML) based fault classifiers which are beneficial for identifying the faulty conditions of complex mechanical systems such as rail vehicles. ML classification algorithms are very effective fault classifiers, and in the railway field they are mainly used to detect defective conditions of railway vehicles. In [3], the authors propose a multisensory data fusion framework to detect small amplitude hunting before the lateral instability of high-speed trains occurs. The method proposes a combination of Empirical Mode Decomposition (EMD) and Sample Entropy (SE) methods to extract features associated with small amplitude hunting and incorporates Support Vector Machine (SVM) classifier as fault identifier. In [4], Random Decrement Technique (RDT) was applied to extract the signal-based features from lateral bogie accelerations, which were then fed into k Nearest Neighbour (kNN) and Artificial Neural Network (ANN) fault classifiers to diagnose the reason behind the observed vehicle running instability. The fault classifiers were trained to detect different faults that may occur in bogie components critical to vehicle stability.

In this paper, a signal-based FDI method in combination with data driven fault classifier is proposed to identify the root cause of running instability. A method is developed to detect and isolate bogie faults such as degraded yaw damper and high equivalent conicity at wheel-rail interface. The schematic of proposed FDI method is shown in Fig. 1. This introductory section is followed by a summarized description of the theoretical background, methodology and results of fault classification along with concluding remarks.

2. THEORETICAL BACKGROUND

2.1 Vehicle Running Instability

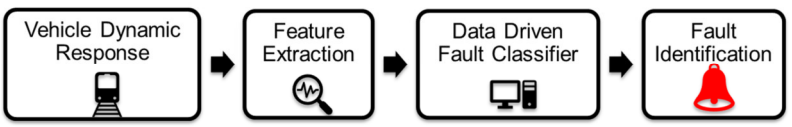

Fig. 1 Schematic of proposed FDI method

Railway wheelsets have a natural tendency to perform sinusoidal oscillations (hunting motion/lateral instability) on straight/large radius track. This intrinsic behaviour is attributed to the conical shape of the wheels which are rigidly connected with each other. The sustained sinusoidal oscillations of wheelsets lead to bogie/carbody hunting. The hunting behavior of the vehicle is generally observed at frequencies lower than 12 Hz (i.e. 0.4-12 Hz) [5]. The bogie hunting is critical to the operational safety of the vehicle and the vehicle is designed to avoid hunting during operation. The hunting behavior is a system level behavior and depends on multiple parameters of the vehicle-track system such as track irregularities, wheel-rail interface, vehicle suspension and vehicle speed. A fault associated with any of the above parameters can cause the hunting motion in the high-speed vehicle. The foremost causes of running instability are poor vehicle yaw dampers and high equivalent conicity at the wheel-rail interfaces. The instability of the vehicle is tested in compliance with EN 14343:2016 [6], where the vehicle is excited with stochastic track irregularities and the lateral acceleration of the bogie frame is monitored. The stability of the vehicle is evaluated based on the stability criterion related to the bogie mass. In this work, the faults associated with the wheel-rail interfaces and yaw dampers are diagnosed and isolated based on the dynamic response of the vehicle.

2.2 Data Driven Fault Classifiers

Supervised Machine Learning (ML) is the task of developing (learning) a function that maps an input to an output based on labelled input-output pairs provided in the training phase [7]. The trained model is then used to classify the test observations where the values of the features are known, but the value of the class label is unknown. ML algorithms are powerful in capturing the knowledge in data and finding (hidden) patterns which facilitate efficient and accurate decision-making. The most popular supervised ML technique is the SVM, where the fundamental concept is the generation of 'margin' on both sides of a hyperplane that separates two data classes. In the training phase the algorithm tunes hyperparameters to maximize the margin, which then creates the margin with the largest possible distance between the separating hyperplane and the instances [7]. Most problems in the real world are non-separable; there does not exist the optimal separating hyperplane. In this case, the training observations are transformed into a higher dimension design space by applying a kernel operation with the aim of converting non-separable data into linearly separable data. The same kernel function is applied for converting the hyperplane of a higher dimension space into a feature space to generate a decision hyperplane. The kernel trick makes SVM a unique classification technique which gives the possibility of transformation to higher dimensions. The SVM classifiers are robust and not very sensitive to changes in the training datasets. On the other hand, SVM classifiers are very difficult to interpret and the handling of the model parameters is difficult; especially if the feature space has more than three dimensions. In this work, Linear and Gaussian kernel functions are used to generate SVM fault classifiers.

3. METHODOLOGY

3.1 Numerical Simulations

A comprehensive study is conducted to investigate the relation between bogie faults and vehicle running instability. To facilitate such a study, multibody dynamics simula-

tions (MBS) of vehicle-track interaction are performed in the GENSYS software. A vehicle similar to a Swedish X2000 coach is selected as a reference vehicle as well as wheel and rail profiles and track geometry data of the Swedish railway network. The nonlinearities associated with the wheel-rail contact geometry and bogie yaw dampers are included in the vehicle model. The dynamic behavior of the vehicle is simulated at a constant speed on a 2 km tangent track section with stochastic longitudinal, lateral and cross-level track geometry irregularities expect gauge irregularities. Nonlinear time domain simulations in accordance with the EN 14363:2016 [6] standard are performed, but along with a few simplifications which simplified the relation between bogie faults and vehicle running instability. The most major simplification is that the track section is kept at a constant gauge of 1435 mm with the purpose of investigating the relation between equivalent conicity (λ_{3mm}) and vehicle running instability. Occasionally, bogie can exhibit small amplitude hunting behavior [3], where the bogie has sinusoidal oscillations but amplitude does not exceeds instability criterion defined in EN 14363:2016. These small amplitude hunting oscillations reduces the ride comfort; and should be detected by proposed FDI method. The objective is achieved by considering all cases even though lateral bogie frame acceleration does not exceed running instability criteria. The time domain simulations are performed for vehicle running speeds of 200 ± 10% km/h to capture the effect of operating speed on the vehicle running instability. The numerical simulations at discrete operating speed from 180 km/h to 220 km/h with 5 km/h increment are performed. The dynamic response of the vehicle is recorded with signals measured on the bogie frame and axlebox. Each acceleration response is bandpass filtered according to the simplified measurement scheme specified in EN 14363:2016.

A database of different conditions of wheel-rail profile and yaw damper is defined numerically in the vehicle model. A single measured rail profile which represents mildly worn condition of the tangent track is used in combination with 9 measured wheel profiles to generate a database of representative operational conditions of wheel-rail interface. These wheel profiles correspond to different combinations of

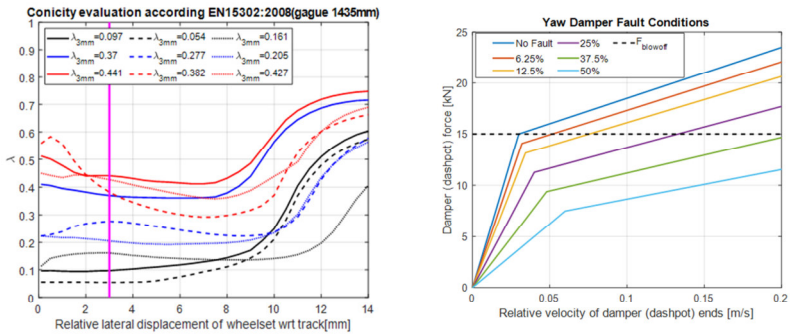

Fig. 2 Wheel-rail profile and yaw damper fault conditions

wheel tread and flange wear conditions. An equivalent conicity function corresponding to each pair of wheel & rail profile is calculated in accordance with EN15302:2008 [8] with the kpf program in GENSYS for 1435 mm track gauge. It is observed that the

obtained equivalent conicity functions are different from each other with respect to the variation of conicity with relative lateral displacement of wheelset on track (the left half of Fig. 2) and λ_{3mm} varies from 0.054 to 0.441; where 0.054 presents mildly worn wheel and 0.441 heavily worn wheel profile. The various performance conditions of yaw dampers are simulated by scaling down damping coefficients and blow-off force in the damper characteristic curve. These parameters model different degradation levels of the yaw damper. In this work, six performance conditions corresponding to 0% to 50% loss of damper performance are considered (the right half of Fig. 2). The database is built by considering each and every combination of yaw damper condition and wheel-rail interface.

3.2 Feature Extraction

Signal features sensitive to the characteristics of running instability are extracted based on frequency domain and time domain analysis of vehicle acceleration. The features used in this work are dominating frequency (f_c) along with corresponding relative damping coefficient (ζ), root mean square (RMS) of lateral bogie frame acceleration ($mean(\ddot{y}^{+}_{j,\ rms})$) and mean ratio of axlebox acceleration ($\ddot{y}_{j,\ rms}$) and bogie frame acceleration ($\ddot{y}^{+}_{j,\ rms}$). The dominating frequency in the lateral bogie frame acceleration is identified with Power Spectral Density (PSD) where dominating frequency corresponds to the highest peak in PSD. The relative damping coefficient corresponding to the dominating frequency is calculated by the half-power bandwidth method. These two features are sensitive to changes at the wheel-rail interface; mover over the relation between dominating frequency and λ_{3mm} complies with Klingel's equation [5]. The PSD graphs of lateral bogie frame acceleration corresponding to two different cases of the wheel-rail interface are shown in the left half of Fig. 4 where the distinct difference between dominating frequency and associated relative damping coefficient is noticeable. Two features are extracted from RMS of lateral bogie frame and axlebox acceleration which are calculated over 100 m moving window with 5 m steps. A mean of RMS lateral acceleration of bogie frame over 2 km track is selected as the third feature. Finally, the mean ratio of lateral accelerations of axlebox and bogie frame is chosen as the fourth feature. The RMS signals of lateral bogie frame acceleration corresponding to two different cases of yaw damper performance but with the same wheel profile are shown in the right half of Fig. 4 and the effect of poor yaw damper is noticed in the mean of RMS signal.

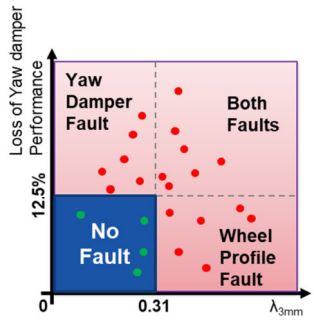

Fig. 3 Fault labelling strategy

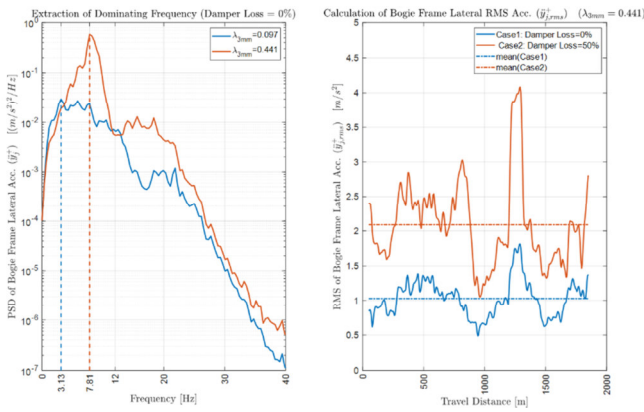

Fig. 4 Extraction of features from lateral acceleration of bogie frame

3.3 Formulation of Fault Classifiers

In this work, an extensive database is generated from the numerical simulations, where 486 simulation cases are formulated, which corresponds to each running speed and all combinations of wheel-rail pair and yaw damper performance conditions. All these cases are labelled based on their respective yaw damper performance condition and λ_{3mm} value. The wheel-rail pair having λ_{3mm} more than 0.31 is designated as faulty pair, whereas a yaw damper with more than 12.5% of loss of damping performance is categorized as faulty yaw damper. Hence, four fault categories are defined which represent No Fault (NF), Yaw Damper Fault (YDF), Wheel Profile Fault (WPF) and Both Faults (BF). The observations which has unfaulty yaw damper and unfaulty wheel-rail pair belongs to NF category. YDF category represents observations which has only faulty yaw damper, whereas observations which have only faulty wheel-rail pair belongs to WPF category. The observations which have a faulty yaw damper and a faulty wheel-rail pair are categories as BF. A graphical representation of a labelling strategy is shown in Fig. 3.

The formulated fault classification problem is well a posed multi-fault classification problem and a supervised machine learning based fault classifier is trained to identify the cause of observed running instability on the labelled database. The database is split into a training and testing dataset by following the 80:20 rule [9]. The signal features namely, dominating frequency, relative damping coefficient at dominating frequency, mean RMS of lateral bogie frame acceleration, mean ratio of lateral accelerations RMS of axlebox and bogie frame along with vehicle speed are selected as features. The fault classifier is trained to identify the type of fault condition based on the values of the features. The block diagram of the fault classifier is shown in Fig. 5.

In this work, Support Vector Machine (SVM) classifiers with Linear and Gaussian kernel are trained with the k-fold crossvalidation method because the process generates a more generalized classification model [9]. The hyperparameters are also optimized with a Bayesian optimization algorithm to minimize the crossvalidation error. The kernel scale and slack are the optimizing variables and the crossvalidation error is the objective function. The trained fault classifiers are tested with the test dataset and performance of each fault classifier is evaluated with a Confusion Matrix (CM) and with corresponding performance measures namely; accuracy, precision and recall rate [9]. The results obtained in the training and testing phases of both fault classifier are presented in the next section.

4. PERFORMANCE OF FAULT CLASSIFIERS

The fault classifiers are trained to generate a decision hyperplane during the training phase and then, the decision hyperplane classifies observations based on their respec-

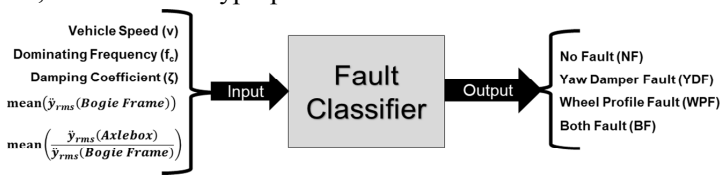

Fig. 5 Block diagram of fault classifier

tive feature values. The SVM classifiers generate the decision hyperplane as a linear

combination of feature values corresponding to support vectors. The Linear SVM classifier uses a linear kernel function which results in a linear decision hyperplane whereas the Gaussian SVM classifier uses a gaussian kernel function which results in a non-linear decision hyperplane. The graphical visualization of the decision hyperplane is challenging, considering the fact that the fault classification problem has more than three features, hence the dataset has more than three dimensions.

The Linear SVM fault classifier correctly classifies 97.2% of NF cases whereas 93.5%, 98.9% and 88.4% observations belonging to YDF, WPF and BF fault categories respectively during the training phase (Fig. 6a). The Gaussian SVM fault classifier is trained for correctly detecting of every observation of NF, YDF and WPF fault categories and 98.8% observations of BF fault categories (Fig. 6c). The Linear and Gaussian SVM fault classifiers have 94.6% and 99.7% overall accuracy for training dataset, whereas 94.5% and 99.8% overall precision and 94.5% and 99.7% recall rates respectively. The results of training phase are summarized in Table 1.

The Linear SVM fault classifier correctly classifies 96.3% of NF cases whereas 81.5%, 100% and 86.4% observations belonging to YDF, WPF and BF fault categories respectively during the testing phase (Fig. 6b). The Gaussian SVM fault classifier identifies 96.3% of NF cases whereas 92.6%, 100% and 81.8% observations belonging to YDF, WPF and BF fault categories respectively during the testing phase (Fig. 6d). The Linear and Gaussian SVM fault classifiers have 90.7% and 92.8% overall accuracy in testing phase which means that fault categories of more than 90% observations are correctly identified by both fault classifiers. The overall average precision rates are 90.6% and 92.9% for the Linear and Gaussian SVM fault classifier respectively. At the same time, overall average recall rates are 91.0% and 92.7% for the Linear and Gaussian SVM fault classifier respectively on test dataset. The results of testing phase are summarized in Table 1.

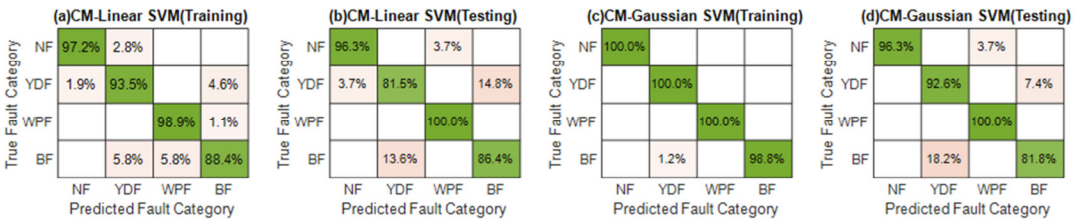

Fig. 6 Performance of fault classifiers in training and testing Phase

Table 1 Overall FDI performance of Linear and Gaussian SVM fault classifiers

Phase	Fault Classifier	Accuracy	Precision	Recall
Training	**Linear SVM**	94.6 %	94.5 %	94.5 %
	Gaussian SVM	99.7 %	99.8 %	99.7 %
Testing	**Linear SVM**	90.7 %	90.6 %	91.0 %
	Gaussian SVM	92.8 %	92.9 %	92.7 %

5. CONCLUSIONS AND FUTURE WORK

In this paper, a data-driven Fault Detection and Isolation (FDI) method is proposed for monitoring the vehicle running stability in a high-speed railway vehicle. Linear and

Gaussian SVM fault classifiers are trained and tested with an extensive database generated with numerical experiments and both fault classifiers identify the bogie faults among faulty yaw damper and wheel-rail profile pair with more than 90% accuracy. The Gaussian SVM fault classifier performs slightly better in the training and testing phase, but with a higher risk of overfitting to the current dataset. There are certain drawbacks of data driven fault classifying techniques and considerable attention should be given to them while combining data driven fault classifier in FDI method. The decision hyperplane may not be meaningful with respect to the vehicle dynamics. Nevertheless, the results presented in this work underline the capability of the machine learning based fault classifiers for the purpose of FDI of vehicle running instability.
There is considerable scope to improve the proposed methodology which will be the focus of future work. The features fed to the fault classifiers should be made independent of the track geometry irregularities and the sensitivity of features to the considered bogie faults should be investigated further. The running instability of the vehicle is strongly dependent on the track gauge irregularities and the same should be included in further analyses while training and testing data-driven fault classifiers. Advanced statistical techniques should be adopted to generate a diverse dataset for the purpose of training of fault classifiers which should be followed by testing with measurements and the same is part of future work of this research.

6. REFERENCES

[1] **Jönsson, L-O. - Asplund, M. - Li, M.:**Vehicle vibrations at the Hallandsås tunnel : Collaborative investigation and results. Proc. 25th Int. Symp. Dyn. Veh. Roads Tracks (IAVSD 2017). Rockhampton, Australia; 2018. p.1059–1063.
[2] **Li, C. - Luo, S. - Cole, C. et al.:** An overview: modern techniques for railway vehicle on-board health monitoring systems. Veh. Syst. Dyn. 2017; 55:1045–1070.
[3] **Ning, J. - Liu, Q. - Ouyang, H. et al.:** A multi-sensor fusion framework for detecting small amplitude hunting of high-speed trains. J. Vib. Control. 2018; 3797–3808.
[4] **Gasparetto, L. - Alfi. S. - Bruni, S.:** Data-driven condition-based monitoring of high-speed railway bogies. Int. J. Rail Transp. 2013;1:42–56.
[5] **Andersson, E. - Berg, M. - Stichel, S.:** Rail Vehicles Dynamics. Stockholm, Sweden: KTH Royal Institute of Technology; 2014.
[6] **EN 14363:2016+A1** - Railway applications – Testing and simulation for the acceptance of running characteristics of railway vehicles – Running behaviour and stationary tests. 2019.
[7] **Kotsiantis, SB.:** Supervised machine learning: A review of classification techniques. Informatica. 2007;31:3--24.
[8] EN 15302:2008+A1:2010 - Railway applications – Method for determining the equivalent conicity. 2010.
[9] **Hastie, T. - Tibshirani, R. - Friedman, J.:** The Elements of Statistical Learning. 2nd ed. Springer Ser. Stat. New York, NY: Springer New York; 2009.

EVALUATION OF PASSIVE AND MECHATRONIC STEERING SYSTEMS FOR THREE-AXLE LOCOMOTIVE BOGIES BY MEANS OF MULTIBODY SIMULATIONS

Márton PÀLINKÒ*[1], Stefano BRUNI[2], Egidio di GIALLEONARDO[2], Binbin LIU[2], Visakh V KRISHNA[3] and Jesus MUNOZ[4]

*[1]Chair of Rail Vehicles, Technical University of Berlin
Salzufer 17-19, SG14, 10587 Berlin, Germany
[2]Politecnico di Milano, Italy,
[3]Royal Institute of Technology, Sweden,
[4]Stadler Rail Valencia, Spain

Received: September 23, 2019

ABSTRACT

In a recent study, concepts were identified and examined that allow heavy-haul locomotive bogies to reduce various wheel and track deterioration in operation. The behaviour of a CoCo Locomotive with passive and active radial steering bogies was evaluated using multibody simulations and compared with the original existing vehicle with rigid axles. The chosen concepts were the following: passive steering using mechanical linkages (EMD), passive hydraulic steering (PHS), active steering using Secondary Yaw Control (SYC), active hydraulic steering (AHS) and self-steering secondary yaw control (SS-SYC). In this analysis, many running conditions were considered, straight track and curves down to 250 m radius with track irregularities according to the standard DIN EN 14363 [1]. Various non-compensated lateral accelerations and presumed friction levels were chosen as input parameters to cover a wide range of operating conditions in order to estimate the benefits of these solutions over the life cycle of the vehicle. As it is a locomotive, traction was also included in some simulation scenarios.
A comparative assessment of the track-friendliness was performed, considering a variety of track layouts (represented by diverse mixes of straight track sections and curved track sections with different curvatures) and operation scenarios. Track loading was assessed considering four performance indexes: track component fatigue, track settlement, rail/wheel wear and RCF accumulation. The investigation evinced significant reduction of wheel/rail wear especially for the EMD, AHS and SS-SYC concepts. Due to reduced primary suspension stiffness, the EMD, PHS and SS-SYC solutions provide lower track component fatigue. The presence of traction increases wear and RCF, but the EMD, AHS and SS-SYC bogies still provide significant benefits compared to the original locomotive.

Keywords: 3-axle bogie, vehicle dynamics, track-friendliness

1. INTRODUCTION

Today, the use of six-axle locomotives is not prevalent in Europe, even though it could represent the future of freight traffic in railways. In praxis, two coupled four-axle locomotives drive heavy freight trains across the continent. Using one locomotive with six axles could offer an alternative to this solution, as even though it is a marginally more expensive investment than a normal locomotive, it can spare significant amount of money in operation, as it would make the second locomotive obsolete. Therefore, in a recent project called “Dynafreight” [2], the possibilities of the new generation running gear consisting of three axles was examined. One aspect was the running dynamics of such a system, particularly the wheel/rail forces and wear.
As the distance between the first and last axles is around 3.5-4 m for three-axle bogies, these constructions give rise to higher wear between wheel and rail. To reduce this, steering systems have been developed in the last decades that make the end-axles steer into the curve. This can be solved via passive systems, where the axles steer each other, or via mechatronic (active) steering, where actuators force the axles into the

curve. To avoid getting stuck in the curve, the middle axle has either a wheel profile with modified flange or significantly reduced lateral suspension, which allows lateral shift of the axle. This project looked into both passive and active systems with the latter mid-axle solution.

2. MODELLING OF RADIAL STEERING BOGIES

As a first step, the existing solutions in operation were examined and their advantages and disadvantages analysed. Two-axle bogies were also included, as these solution could be modified for three-axle bogies as well. Five solutions were selected for the evaluation:

- EMD – Solution with mechanical linkages (see Fig. 1)
- PHS – Passive hydraulic steering (see Fig. 1)
- SYC – Secondary yaw control (see Fig. 1)
- AHS – Active hydraulic steering
- SS-SYC – Self-steering secondary yaw control

It has to be said that the SYC is not a real steering bogie in the sense that the actuator steers the bogie frame with respect to the carbody. Nevertheless, it was included in this project, as it is relatively easy to implement.

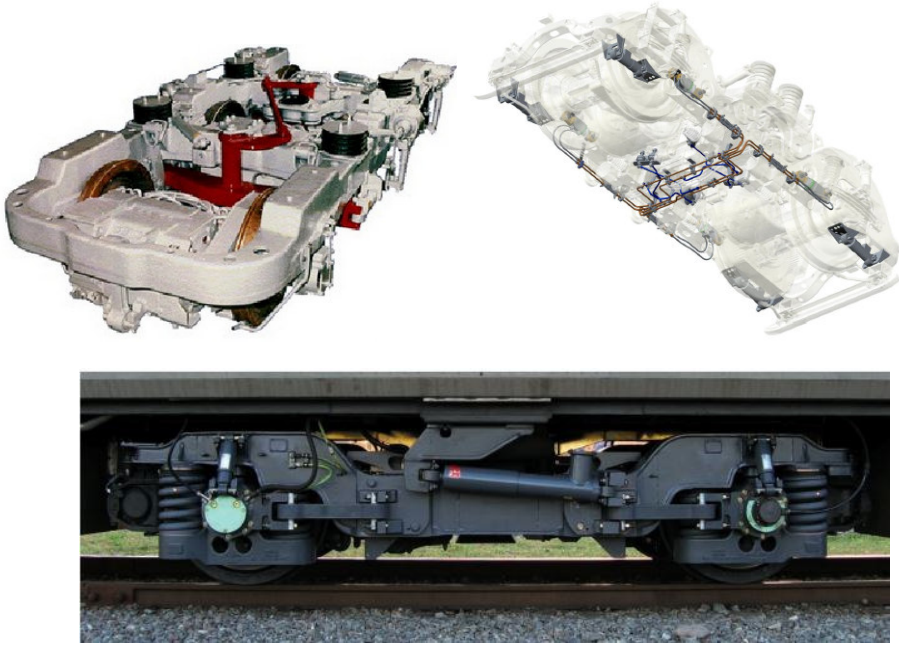

Fig. 1 The EMD [3], PHS [4] and SYC [5] solutions (from left to right and top to bottom)

The concepts were modelled and evaluated using the multibody simulation software Simpack. First, a baseline locomotive, using an existing locomotive, was defined for comparison. Then, this initial model was modified to accommodate the different steering arrangments.

The locomotive was built up symmetrically, with the two bogies mirrored to the centre of the locomotive. The motors are on the inner side of each axle. There are primary- and secondary springs in all three directions in the locomotive. The motors are attached to the axles with a bearing, and they are connected to the bogie frame via a vertical spring. The layout of the baseline locomotive can be seen in Fig. 2, its main parameters are listed in Table 1.

Table 1 Parameters of the locomotive

Mass	126 t
Wheel base (first and third wheel)	3.7 m
Pivot distance	14 m

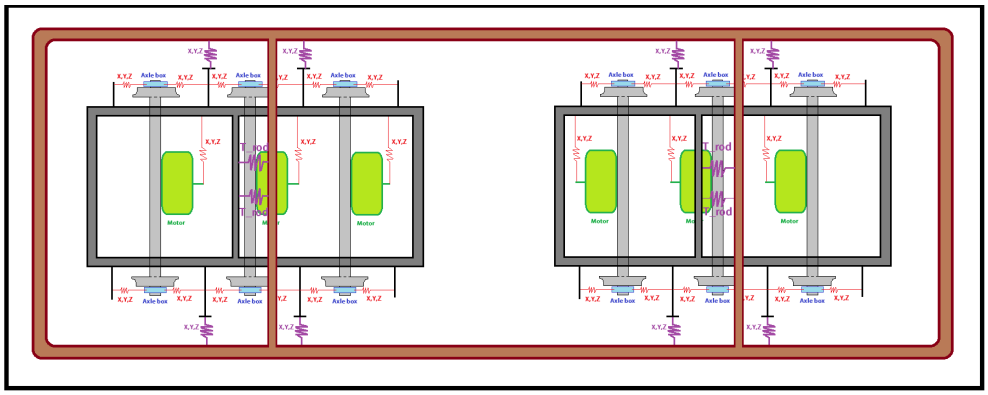

Fig. 2 The outline of the baseline model

For the passive systems, the primary stiffnesses were modified and extra mechanisms were added. The active systems used a control loop developed in Matlab. Fig. 3 shows an exemplary bogie model; the bogie with mechanical linkages.

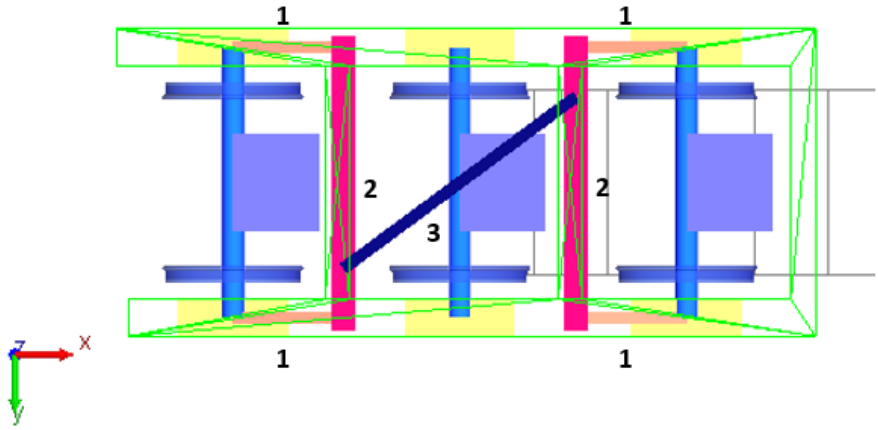

Fig. 3 The EMD bogie model in Simpack
(1- traction rod, 2- lateral beam, 3- cross link)

The traction rods are coupled on one side to the axle boxes and on the other side to the lateral beams via spherical joints, allowing the wheel to follow the track without any problems. The joints between the cross-link and lateral beams/bogie frame are rotational joints allowing one degree of freedom. For stable operation at high speeds, a primary yaw damper was added to the construction.

The different bogie models were fine-tuned to make the best possible result in the predefined worst case scenario. This is the scenario with the following attributes:

Table 2 Parameters of the worst case scenario

Friction coefficient	0.5
Curve radius	250 m
Superelevation	0.15 m
Non-compensated lateral acceleration	0.65 m/s^2
Traction	No
Irregularities	No
Curve direction	Right-hand

The wear numbers for each wheel of the leading as well as the trailing bogie are represented in Fig. 4 and Fig. 5 for this simulation using the baseline locomotive. L stands for left wheels, R for right wheels in the diagram. It can be seen that the leading wheelsets of each bogie are critical, particularly on the outer side.

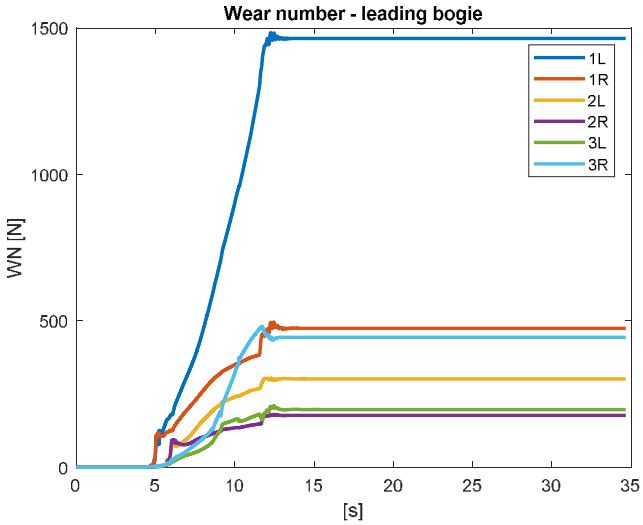

Fig. 4 Wear numbers for the worst case scenario on the leading bogie – baseline locomotive

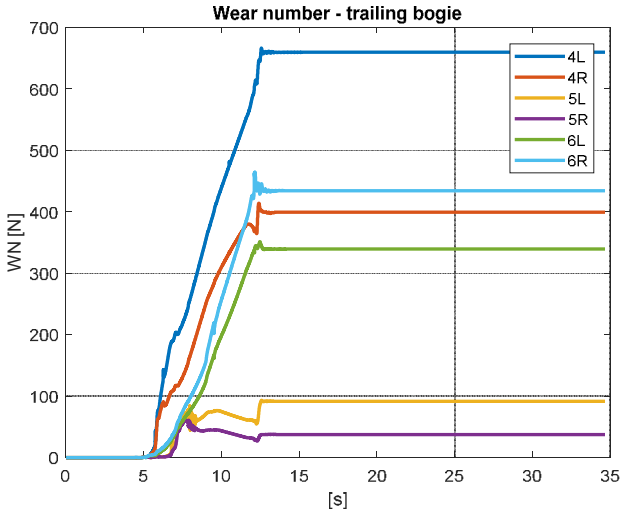

Fig. 5 Wear numbers for the worst case scenario on the trailing bogie – baseline locomotive

As far as the wear number is concerned, besides evaluating the value of this parameter for the single wheel, some other indicators were defined as proper averages of the wear numbers obtained on the single wheels. Considering that the locomotive performs bi-directional service and assuming equal probability of left-hand and right-hand curves along its path, the same amount of wear is expected on the two wheels in the same wheelset. Furthermore, when the direction of travelling is reversed, the position of the

six wheelsets is also reversed, which means e.g. the leading wheelset of the front bogie becomes the trailing wheelset of the rear bogie and so on. Therefore, assuming for the locomotive the same frequency of travelling in the two directions, the same amount of wear is expected on:

- The two external wheelsets (No. 1 and 6);
- The central wheelsets of the two bogies (No. 2 and 5);
- The two internal wheelsets (No.3 and 4).

Hence, three averaged wear indicators P1, P2 and P3 were defined as the average of the wear numbers obtained on the two wheels of the external wheelsets, central wheelsets and internal wheelsets respectively as follows:

$$P1 = \frac{WN_{1L} + WN_{1R} + WN_{6L} + WN_{6R}}{4} \quad (1)$$

$$P2 = \frac{WN_{2L} + WN_{2R} + WN_{5L} + WN_{5R}}{4} \quad (2)$$

$$P3 = \frac{WN_{3L} + WN_{3R} + WN_{4L} + WN_{4R}}{4} \quad (3)$$

With $WN_{iL/R}$ the wear number obtained for the i-th wheelset on the left or right wheel.

Table 3 shows the global wear indicators for the baseline locomotive as well as reduction for the various systems for worst-case scenario after finalizing the models.

Table 3 Global wear number reduction for the worst-case scenario

	Baseline	EMD	PHS	SYC	AHS	SS-SYC
P1	678.3	**-59.9**	**-9.7**	**-8.6**	**-91.5**	**-41.7**
P2	152.3	**-63.0**	**-4.4**	**-19.7**	**-87.0**	**-37.3**
P3	425.1	**-65.8**	**-8.3**	**-2.4**	**-97.9**	**-23.0**

From Table 3 it can be seen that the EMD and AHS solutions reduce wear significantly, while the PHS and SYC give marginally better results than the baseline locomotive. It is important to remark that the PHS modelling needs further improvement in coming projects. As expected, the SS-SYC, which combines the SYC with the EMD techniques, shows better results than the SYC.

3. SIMULATIONS

After tuning the various solutions, the modified locomotives, together with the baseline construction, were examined in various scenarios according to the standard DIN EN 14363 [1]. The parameters were chosen as input parameters to cover a wide range of

operating conditions in order to estimate the behaviour of the existing vehicle. As it is a locomotive, traction was also included in some simulation scenarios. Track irregularities were also included according to the norm. Table 4 shows the various parameters that were used in various combinations for the evaluation:

Table 4 Simulation parameters

Friction coefficient	0.25/0.4/0.5
Curve radius	250/400/600/1500 m
Superelevation*	0.15/0.1/0.07/0.02 m
Non-compensated lateral acceleration	-0.46/0/0.65 m/s^2
Traction	Maximum/No
Irregularities	Yes

*The superelevation levels and curve radius values belong together.

The focus for the evaluation was on the following quantities:

- Vertical wheel/rail forces
- Lateral wheel/rail forces
- Wear numbers
- Global wear indicators

A total of 30 simulations were carried out for each locomotive without traction, meanwhile four tests were made with maximum traction at the speed of 20 km/h. Each simulation had a length of 700 m. Fig. 6 shows exemplary results from the simulations; the global wear number P1 for the EMD locomotive at the friction level of 0.4 and the reduction with respect to the baseline locomotive. The single value of the indicators is obtained with a statistical tool; the wear numbers are averaged on every six meters and then the value is the mean of these averages.

The wear indicators decrease drastically with increasing curve radius (especially 250 m to 400 m), while they increase going from running on cant deficiency to running on cant excess. The average wear numbers on equilibrium cant and at non-compensated lateral acceleration of 0.65 m/s^2 are quite similar. It can be observed that the advantage of using the EMD solution is beneficial in the whole range of curve radii. For the equilibrium cant, the reduction peaks at the largest curves, but running with NLA= 0.65 m/s^2 shows the best results in the curve of 400 m compared to the baseline solution. The results show that even though running on cant deficiency results in higher extreme values, the average values are higher for running on cant excess.

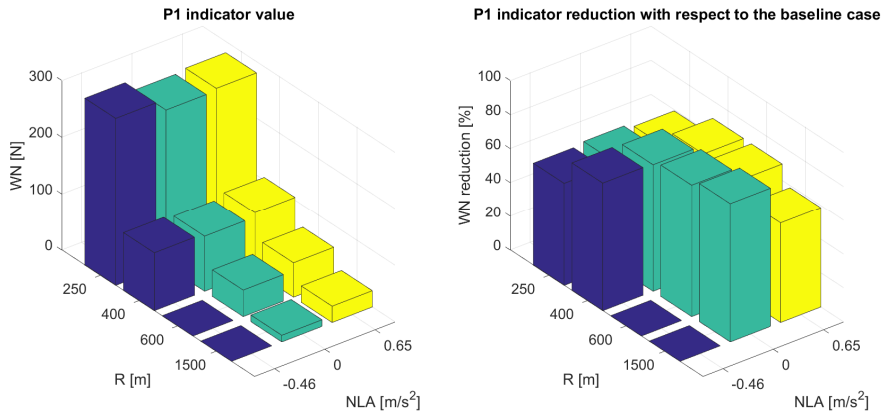

Fig. 6 Global wear indicators for the EMD simualtions

4. TRACK-FRIENDLINESS EVALUATION

The comparative assessment of track-friendliness was performed, concerning the following track-vehicle detoriation modes:

- Track component fatigue
- Track settlement
- Rail/wheel wear
- RCF accumulation

The wear and RCF were evaluated using the T-gamma method, in order to predict the track settlement, the TUM method [6] was applied. The track component fatigue was determined with the help of the UIC/Office od Research and Experiments (ORE) [7] and rail surface damage [8] models.

As a first step, 14 larger, 10 km long track layouts were built from the various shorter simulations to represent real life operation on railway lines. They include a diverse mix of straight and curved track sections and operation conditions

Then, the track damage values were calculated for every 100 m from the simulation results. Finally, contribution matrices were made from them that were then weighed using a consolidating tool according to the track layout in order to assess the chosen solutions. **Hiba! A hivatkozási forrás nem található.** summarizes the steps of the evaluation.

5. RESULTS AND CONCLUSIONS

Fig. 7 shows a relative comparison of all models concerning the four track damage mechanisms for every track layouts combined. The baseline locomotive is represented as 100% damage for all four detoriation modes.

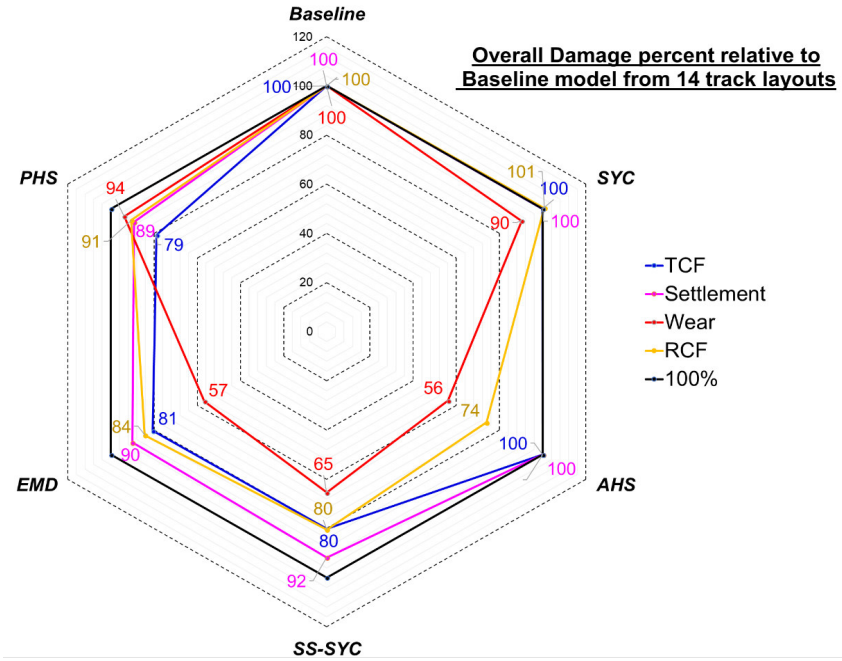

Fig. 7 Relative comparison of models with respect to track damage by different mechanisms for all track layouts

The main results obtained can be summarized as follows:

- Vehicle dynamics analysis indicate the possibility to reduce substantially wear and RCF using appropriate steering bogie concepts. The reduction of wear and RCF is higher when no traction is applied;
- The presence of traction increases the wear and RCF contributions substantially for all the five concepts. In case of full traction, the benefits provided by using steering bogies are up to 30% approximately for the most effective concepts considered in this study.
- The AHS, SS-SYC and EMD concepts are most effective in terms of reducing wear and RCF contributions but the AHS concept does not improve TCF and settlement compared to the Baseline case.
- The SS-SYC and EMD models show a better overall performance especially thanks to the reduction of TCF and settlement contributions, which are about

20% lower than the Base-line case. This is however due to the reduced stiffness of the primary suspension in these concepts.

- The SYC and PHS models are marginally better compared to the Baseline case but still provides a reduction of wear in the range of 5-10%.
- From the track layout and operating parameters studied, the sensitivity to track damage follows the trend:

Traction > Curve radius > Friction > Cant Deficiency/excess.

6. REFERENCES

[1] Norm DIN EN 14363:2016-10, Railway applications – Testing and Simulation for the acceptance of running characteristics of railway vehicles – Running Behaviour and stationary tests, 2016

[2] Dynafreight project homepage, [Online]. Available: http://www.dynafreight-rail.eu/

[3] **Simson, S**., **C. C.:** Parametric Simulation Study of Traction Curving of Three Axle Steering Bogie Designs, IAVSD 2007

[4] **Löwe**,**T. P.:** Modelling of a Passive Hydraulic Steering for Locomotives, University of Pretoria, 2014

[5] **Bruni, S. - Goodall, R. - Ward, C. - Alfi**, **S.:** Railway bogie stability control from secondary yaw actuators, Anno Academico 2013-2014

[6] **Öberg, J.:** Master of Science thesis: Track deterioration of ballasted tracks, KTH Royal Institute of Technology, Stockholm, 2006

[7] ORE, Dynamic vehicle/track Interaction phenomena from the point of view of track maintenance. Report no.3, ORE Question D161, 1988**.**

[8] **Burstow, M.:** Whole life rail model application and development for RSSB – continued development of an RCF damage parameter, AEA Technology, Derby, 2004.

NEW REGULATIONS OF THE RAIL/WHEEL CONTACT MECHANISM FOR HUNGARIAN TRAMWAYS

Róbert CSÉPKE

Doctoral School of Multidisciplinary Engineering Sciences
Széchenyi István University
H-9026 Győr, Hungary

Received: September 12, 2019

ABSTRACT

The new rules of geometric design of curves with small radii and the introduction of new test parameter are also required in Hungarian tramway tracks, which shows degree of coherence for running characteristic of the given curve and vehicle, from the aspect of infrastructure, in case of all wheelsets of bogie. This new parameter system takes into account all wheel creep values resulting from the variations (+, -) of the optimum rolling radius difference. This results the tightening of bogie design principles and for running characteristic reasons, it requires the thorough analysis of continous flange running in narrow curves.

Keywords: rail/wheel interaction, curves with small radii, new regulation, tramway track

1. INTRODUCTION

As known, Technical Specifications for Interoperability (TSIs), which regulate the running parameters, are in force for international and domestic railways. However, these are not applicable for tramways, among others. During my analysis, I suggest the introduction of system requirements, based on the mechanical conformity of rail / wheel interaction (running characteristic). This is also justified, as the normative regulation of the german tramway system (BOStrab, [1]), also applied by several infrastructure managers in Europe. The new geometric design of curves with small radii and the introduction of new test parameter are also required, which shows degree of coherence for running characteristic of the given curve and vehicle,

2. THEORETICAL BASICS

EN 15302 [5] provides a precise mathematical method for determining the equivalent conicity for non-linear tapered wheels. Wavelength of the lateral oscillation (L) is independent from the speed (v) and from the amplitude of the lateral oscillation. Only the gauge (e0), the half angle of the wheel taper (tanγ) and the radius of the wheel (r0) has an effect on its magnitude (Klingel formula) (1).

$$L = 2\pi\sqrt{\frac{r_0 e_0}{\tan\gamma}} \tag{1}$$

Frequency (f) (2) can be calculated by knowing the speed (v) as follows:

$$f = \frac{v}{2\pi}\sqrt{\frac{\tan\gamma}{r_0 e_0}} \tag{2}$$

The emerging (equivalent) conicity value, the resulting wavelength during running and wear have effect on the Wear Index of the rails and wheels. The three basic influencing

components that result from these are longitudinal, transverse and creep phenomenon [7], [8] .

3. ANALYSIS OF TRACK / VEHICLE SYSTEMS IN HUNGARY

3.1 Lack in design guidelines for tramways in Hungary

As it was already stated in the introduction, there are no technical regulations available for the infrastructure managers of tramways, that regulate the equivalent conicity in straights and running radius difference in curves for an optimal design.
The degree of wear in these narrow curves, the excessive wear of running surface of rail head and rail corrugation will increase the cost of maintenance, as known.

3.2 Mechanical / contact (running characteristic) analysis of rail / wheels in narrow curves

In the range of narrow curves, the current driven bogies with horizontaly "rigid" guided bearings, and used "wear" wheel profiles (in Budapest CAF and Siemens), result inadequate running radius differences. This has extreme impact on the tracks, resulting significant wear. On the basis of simple analyses it can be proved, that the theoretically-possible running radius difference (RRD) in wheelsets in a curve under R = 100 m radius, from the aspect of mechanical rail/wheel contact is inadequate [2], [3], [6]!
Also the lack of regulation is abnormal - which demonstrates the existence of uncertainty - in Hungary (especially in Budapest).

3.3 Practical analysis of rail-wheel interference at BKV

The lack of compatibility between the wheel profiles used at BKV Zrt. is highlighted.
The followings were under analysis:
- equivalent conicity values
- contact surface of rail / wheel interaction, contact path (for rigid material model, only in a non-computational approach)
- the maximum possible rolling radius difference
- running frequencies at 50 km/h
- in the case of "two point contact", the wheel speed difference

4. RUNNING CHARACTERISTIC PARAMETERS TO BE INTRODUCED AT DOMESTIC TRAMWAYS

The analyses carried out revealed that, in addition to interventions on rail vehicles, the professional criteria of this consistency should be put into practice from the civil engineering point of view. On the basis of the presented, the partial adaptation of the requirements of the EN 14363: 2016 standard [4] is recommend for tramway conditions.

Recommended parameters to be introduced for domestic use: there are specifications of applicable (new) wheel profile (Fig.1).

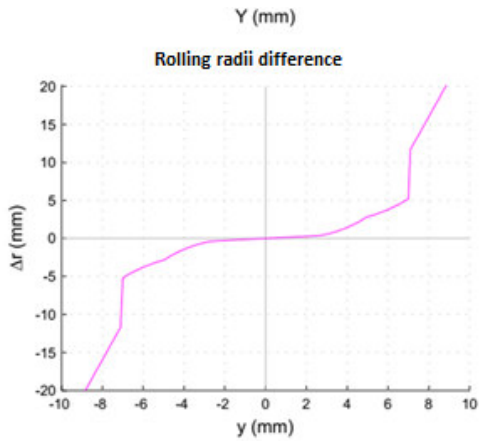

Fig. 1 An example of a favorable Δr function

Recommended parameters to be introduced for domestic use:

Specifications of applicable wheel profile:

I. A min. 120mm of wheel width should be avoided as much as possible.
II. The possibility to use 130mm wheel width, which can be a target of 135mm.
III. In narrow curves, with 1450mm track gauge and asymmetric rail inclination, the possibility of radius radius difference of Δr min.=5,5mm.
IV. In the case of 59R2 grooved rail (at 1:∞ rail inclination) and MÁV 48 vignol rail, taking into account 1:40 rail inclination, to fully comply with the parameters below (VI, VII, VIII and X).
V. In the case of other rail profiles and rail inclination combinations, to fully comply with points VI, VII. and VIII. at 1432-1450mm track gauge.

Specifications for rail/wheel contact mechanics:

VI. Equivalent conicity (tanγe, at ±3 mm y diversion and 1435 mm track gauge)
   a. max 0,4 and min 0,05 design value (new wheel and rail)
   b. max 0,5 and min 0,05 maintenance value (rails and wheel within the wear limit).
VII. Running tanγe function can only increase monotonically in the direction of the increase of ŷ lateral deflection (in the case of 1432-1450 track gauges).
VIII. In the Δr function, a "jump" greater than 2 mm is not allowed in the interval y = ± 6 mm (except in the range of ± 2 mm of the maximum side deflection).
IX. Less than 1432 mm track gauge in the track is not tolerable.
X. The upper limit of equivalent conicity (max tanγe) is max 0.6 within the total y lateral displacement range.

The introduction of the lower limit of tanγe during hunting oscillation is necessary to ensure the return force of the wheelset to the centre.

5. CONCLUSIONS

- In order to reach the optimum running parameters in narrow curves, there are suggestions for rail infrastructure and civil engineering (see Chap. 4).
- The construction of bogies of vehicles should also contribute to reducing the angle of attack.
- It is strongly recommended tram vehicles should only be designed with automatic radially steered axes and wheels. (e.g. Scheffel or other active systems,…)
- It also coincides with what is described above, but from the mechanical side, that the vehicles in the narrowest curves (~R 40m) should run on the outer wheel flange. This results the development of wheel profiles and optimisation of flange running.
- Close cooperation between professional branches is advisable to improve running on flange.

6. REFERENCES

[1] **BOStrab**, Technische Regeln für die Spurführung von Schienenbahnen nach der Verordnung über den Bau und Betrieb der Strassenbahnen (TR Sp), Ausgabe Mai 2006

[2] **Csépke, R.:** Rail/Wheel contact in curves with small radii, Proceedings of X. International Railway Bogie and Running Gear Conference, (BOGIE'16), (Ed.by Prof. I. Zobory), Department of Railway Vehicles, Scientific Society of Mechanical Engineers, Budapest, 12-15 September, 2016

[3] **Csépke, R.:** Analysis of rail/wheel contact in curves with small radii, World of Rails (Sínek Világa, in Hungarian) 2016/2., (ps. 24-28.).

[4] **EN 14363: Railway applications** - Testing for the acceptance of runningcharacteristics of railway vehicles - Testing of running behaviourand stationary tests

[5] **EN 15302:Railway applications**. Method for determining the equivalent conicity

[6] **Shevtsov, I. Y.:** Wheel/Rail Interface Optimisation, PhD Dissertation, Delft University of Technology, The Netherlands, (2008)

[7] **Zobory, I. – Gáti, B. – Kádár, L. – Hadházi, D.**: Vehicles and Mobile Machines I.,Lecture Notes, Faculty of Transportation Engineering and Vehicle Engineering, Budapest University of Technology and Economics, Budapest, 2012. (In Hungarian)

[8] **Zobory, I.:** Prediction of Wheel/Rail Profile Wear. Vehicle System Dynamics, Swets and Zwettlinger ,Vol. 28, 1997, p.221-259.

MECHATRONIC GUIDANCE FOR TRAMWAYS USING A NOVEL HALL SENSOR CONCEPT

Franz JOST and Peter GRATZFELD

Chair of Rail System Technology
Institute of Vehicle System Technology
Karlsruhe Institute of Technology
76131 Karlsruhe, Germany

Received: September 9, 2019

ABSTRACT

As tramways in cities must adapt to the street layout, tight curves cause wear and noise. An active steered wheelset can reduce both wear and noise. For an active steered wheelset, a controller using μ-synthesis is derived and tested. To measure the needed controller inputs directly on the wheelset, a new hall sensor concept is developed and verified. The sensor additionally calculates an index which represents the current measurement quality. This helps to identify erroneous measurements due to disturbances and allows a safe wheelset operation. The active steered wheelset is validated in test scenarios with a prototype of the hall sensor using a co-simulation with multi-body physics. Comparing the simulation results, a low lateral displacement showing a good running stability and curving performance is observed.

Keywords: mechatronic track guidance, active steered wheelset, control loop design, direct state measurement, hall sensor

1. INTRODUCTION

Tramways are an easy to implement and cost-efficient way to handle the increasing transportation demand in cities due to urbanization. As with given city layouts, tight curves cannot be avoided and additionally when the track is shared with other vehicles it cannot be elevated. This leads to flange contact on currently implemented wheelsets which causes wear on rail and wheel, produces noise and therefore is high in maintenance costs for operators and disturbs residents.

An active steered wheelset researched at the Karlsruhe Institute of Technology shows that flange contact can be effectively avoided by using a model-based control loop with direct measurement of the vehicle state. Direct measurement of the relative position between rail and wheel is implemented with a newly developed contactless hall sensor concept.

The focus in this paper lies in the design and evaluation of the sensor concept and the wheelset's running performance. First the active steered wheelset, the controller and the measurement concept are introduced. Secondly, the newly developed sensor and its algorithms are described. Then the sensor is verified using an automated test rig. Lastly, the active steered wheelset incorporating the sensor prototype is validated with test scenarios in a multi-body co-simulation.

1.1 Motivation

Active steered wheelsets and bogies as mechatronic systems need feedback from the system itself and from its interaction with the system environment in order to control the system's behavior in a desired way. With active track guidance the relative position of rail and wheel and the vehicle's state are possible feedback quantities [1, 2]. As a primary control goal a lateral displacement of zero is often used to avoid flange contact [3]. The technical implementation of measurement concepts to determine

(state) variables as controller inputs is difficult. So far often commercially available solutions are used. A new specialized development is often avoided. [1, 4–10]
Generally, measurement concepts can be divided into two groups: direct and indirect measurement. Indirect measurements use estimation methods to determine the needed states and input quantities for the controller and are used to reduce the overall system complexity [1]. The implementation of direct measurement however is estimated to be difficult [3, 11].
In this paper we implement and validate a new sensor concept for the direct measurement of state variables *lateral displacement* and *angle of attack*, but the sensor is not limited to this application.

2. ACTIVE STEERED WHEELSET

The mechanical structure of the Active Steered Wheelset (ASW) is shown in **Hiba! A hivatkozási forrás nem található.**. It consists of a structural frame with two independent rotating wheels attached to two steering levers. The two levers are coupled with a handlebar. This introduces a new degree of freedom, the steering angle ψ_L to the wheel-set. An actuator applies a force to the handlebar which in turn enables a controller to actively steer the wheelset. When the actuator is turned off, the wheelset is topological identical to a passive steered wheelset.

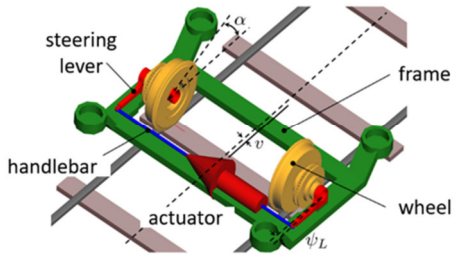

Fig. 1 Active Steered Wheelset

In the used coordinate system, the z-axis points in the direction of gravity, the y-axis in the lateral direction and the x-axis in the running direction of the wheelset. All spatial quantities are expressed in this coordinate system.

2.1 Control loop

Without a fixed coupling between the wheels, the wheelset shows no self-centreing behaviour. A mechatronic approach can stabilize the running behaviour and improve curving performance. The control goal for the closed-loop controller is a lateral displacement of or near zero. Additionally, the angle of attack should be small as well.
The measured vehicle states as controller inputs are the angle of attack α, the steering angle ψ_L and the lateral displacement v. For the angle of attack the value at either side of the wheelset can be used as the difference between right and left wheel is negligible. The lateral displacement is measured as the difference between the wheelset's center and the track center.
The closed-loop controller takes these inputs and outputs the desired force the actuator needs to apply. To consider the extended feasibility, the controller needs to further comply with the following criteria: with unknown variation of axle load (passengers), actuator uncertainties (frequency response), track disturbances (curves and track geometry errors) and sensor noise, a stable and robust track guidance without flange contact should be achieved. The actuator force should be limited to 1000 N. For the controller design a *μ-synthesis,* model-based approach is used as it fulfils the

requirements mentioned. The controller design and validation in described in detail in [10].

The controller is tested in 234 scenarios with varying vehicle mass, friction coefficient, radius and lateral acceleration in curves and vehicle speed on a straight track. For the tests the controller is implemented in a co-simulation with an ideal sensor model. The ideal sensor uses the simulation output of the vehicle state variables and applies white noise to it. The white noise characteristics were taken from a laser distance sensor. SIMPACK is used for the multi-body-simulation and MATLAB/SIMULINK for the controller and actuator models. See chapter 5 for a test scenario overview.

The control-loop using the ideal sensor model shows significant performance improvements over all test scenarios in comparison to a fixed wheelset, a wheelset with independently rotating wheels and a passive steered wheelset. Lateral displacement and wear are low while the actuator force is kept below 600 N. The active steered wheelset's potential is shown and therefore research in a technical solution for the measurement set-up and sensor concept is the next logical step. The mentioned co-simulation is also used as the basis for the new sensor development and evaluation.

2.2 Measurement set-up and sensor concept

As the steering angle can be measured easily on the wheelset frame or within the actuator, it is not further regarded. The angle of attack and lateral displacement are more difficult to measure precisely as the relative position between rail and wheel changes with the movement along the track.

Fig. *2* shows the measurement set-up used for a combined measurement of angle of attack and lateral displacement.

The set-up uses four identical sensors (S) measuring the lateral positions of the rails s_{L1}, s_{L2}, s_{R1} and s_{R2}. The sensors are mounted on the steering levers with a distance L=0.2 m to the rotation point. With these auxiliary measurements it is possible to calculate the desired vehicle states $\hat{\alpha}$ and $\hat{v}$ as per the following equations.

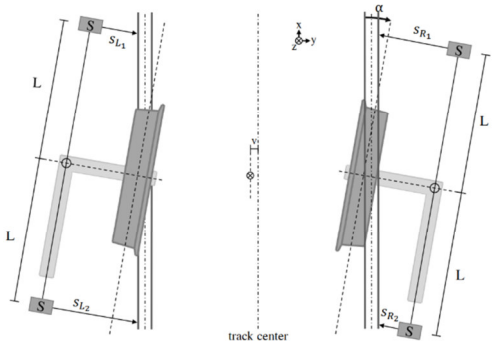

Fig. 2 Measurement set-up with four sensors

$$\hat{v} \approx \frac{1}{2}(s_{R_1} - s_{L_1}) \approx \frac{1}{2}(s_{R_2} - s_{L_2}) \qquad \hat{\alpha} \approx \tan^{-1}\frac{s_{L_2} - s_{L_1}}{2L} \approx \tan^{-1}\frac{s_{R_2} - s_{R_1}}{2L}$$

Using identical sensors reduces system complexity, development cost and time. Further, the set-up provides a level of redundancy as one sensor can fail without disturbing the measurement process.

In addition, we introduce an additional requirement for the sensor concept. The sensor must generate a *measurement quality index* for the current measurement. This index is dimensionless on the interval [0,1] where 1 indicates a measurement of high quality and 0 an inaccurate measurement. The wheelset controller can use this information to detect sensor errors. The wheelset can then be brought in a safe state.

3. SENSOR DESIGN AND VERIFICATION

For the sensor concept a contactless approach is chosen. The general idea is based on the disturbance of static magnetic fields through the ferromagnetic properties of rails. The sensors will be placed above the rail, in front and behind the wheels on each side, with a nominal air gap of 20mm. An excitation coil generates a static magnetic field and due to the ferromagnetic properties of the rail this field is disturbed. We claim that the magnetic disturbance can be used to calculate the lateral position of the rail over an air gap of 20 mm. An approach using an eddy current sensor can be found in [12].

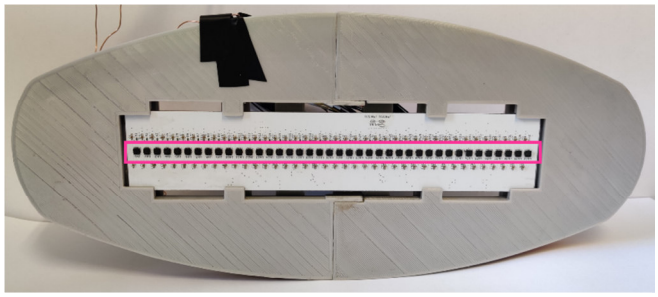

Fig. 3 Magnetic field with rectangular profile and varying air gap

Also, the sensor concept uses commercially available integrated hall elements capable of measuring all three dimensions of the magnetic field (B) with its components B_x, B_y and B_z. Forty of these hall elements are mounted on a printed circuit board (pcb) with 5 mm pitch spanning a total length of 195 mm forming a hall array. The hall array length is longer than the expected lateral position change of the rail below the sensor and ensures that the rail is always covered by the hall elements. The mechanical support structure has no magnetic properties and is 3D-printed plastic. Fig. 3 shows the sensor prototype with an oval excitation coil and a pcb with the 40 hall elements (coloured rectangle).

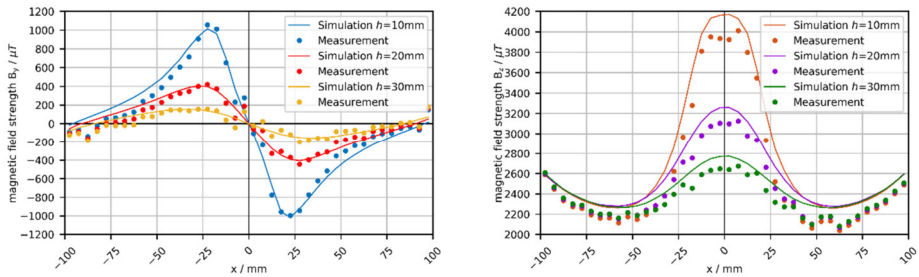

Fig. 4 Magnetic field with rectangular profile and varying air gap

Fig. 4 shows the B_y and B_z components of the magnetic field when a rectangular steel profile of 30 mm width is placed below the sensor with varying air gaps. The lateral position of the profile's center is at x=0 mm. The leftmost hall element is at position x=-97.5 mm and the rightmost at x=97.5 mm.

The figure additionally shows the expected results computed with an FEM solver as early simulations were done to ensure sensor concept feasibility.

B_x is not affected by lateral movement and therefore not considered further. In B_y the diagram shows an increase of magnetic strength with point symmetry to the origin.

The zero-crossing point indicates the lateral position of the profile. It moves accordingly when the lateral position of the profile is changed below the hall array. In B_z a maximum is formed at the lateral position of the profile. With the correlations between the magnetic components and the lateral position of the profile, an algorithm can calculate the lateral position with the measured magnetic field data as input.

4. CALCULATION OF LATERAL POSITION

The calculation of the lateral position of the rail profile below the sensor is done in four phases (see Fig. 5). In the first stage an offset correction on the hall array data is performed. As offset data, the magnetic field propagation without any rail profile below the sensor is used. Subtracting each offset in B_y and B_z the curves only represent the magnetic distortion due to the rail profile compared to the zero state. Fig. 6 shows the offset correction applied to B_y. Both components are then normalized to the outputs $\bar{B}_y$ and $\bar{B}_z$. The normalization reduces the influence of the air gap (see Fig. 7).

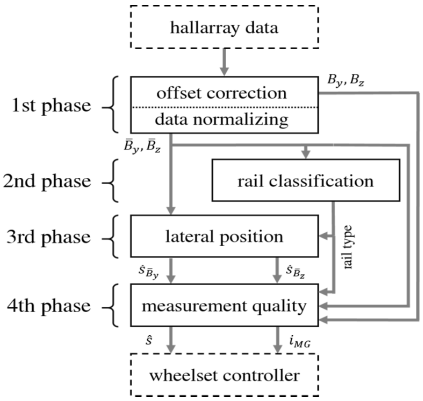

Fig. 5 Lateral position calculation procedure

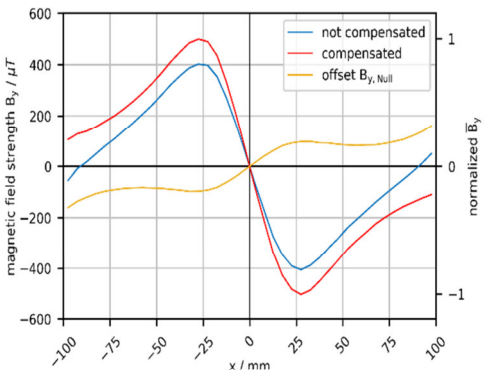

Fig. 6 Lateral position calculation procedure

The second stage uses a neural network to determine the rail profile type. Currently it can classify vignol and grooved rails. If the signal strength is not sufficient or the data is disturbed, the classifier outputs *unknown rail profile*. This information is necessary to apply the correct algorithms in the third phase or to indicate an inaccurate measurement.

The lateral position is calculated in the third phase using specialized algorithms using $\bar{B}_y$ and $\bar{B}_z$. The algorithms are optimized for one rail profile type and use linear and spline regressions as well as neural networks. In $\bar{B}_y$ the algorithmns calculate the position of the zero-crossing, in $\bar{B}_z$ they calculate the position of the maximum to determine the lateral position. In total seven algorithms were implemented and tested. In this paper we only present the results for vignol rails and the best performing algorithms. The output of the third phase are two separately calculated lateral positions $\hat{s}_{\bar{B}_y}$ and $\hat{s}_{\bar{B}_z}$.

In the fourth phase all sensor data, offset corrected and normalized, as well as the two calculated lateral positions are evaluated to a measurement quality index i_{MG} (see Fig. 8).

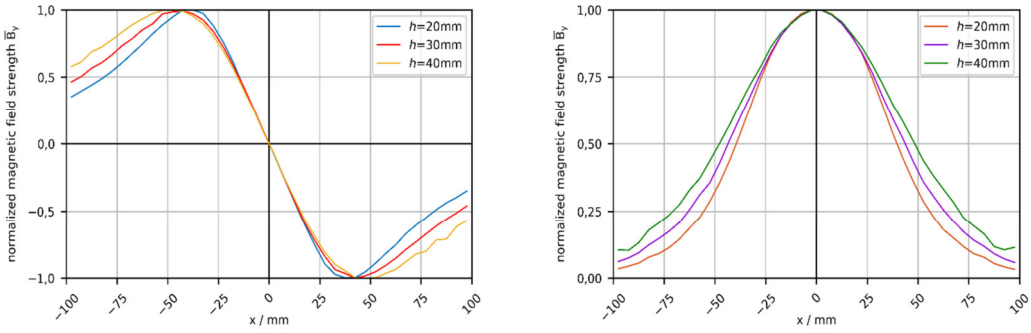

Fig. 7 Normalized magnetic components with S49 rail profile and varying air gap

The quality index first verifies three conditions. If one condition is not met, the measurement is rejected and an index of $i_{MG} = 0$ is outputed. This is also true when the rail profile could not be determined.

The first condition checks the offset corrected data for sufficient signal strength. The second condition checks the deviation between the two calculated lateral positions $\hat{s}_{\bar{B}_y}$ and $\hat{s}_{\bar{B}_z}$. If the difference between the two algorithms is too big, the measurement is rejected.

The third condition calculates two separate sub quality indexes $i_{MG,y}$ and $i_{MG,z}$. Both sub indexes must be greater than a threshold value in order to accept the measurement as valid. If all conditions are met, the quality index is calculated as the mean value of the two sub-indexes. With the application of the measurement quality index it is possible to detect stochastic events like coins, keys and cans and deterministic events like rain drains, switches and crossings on the track.

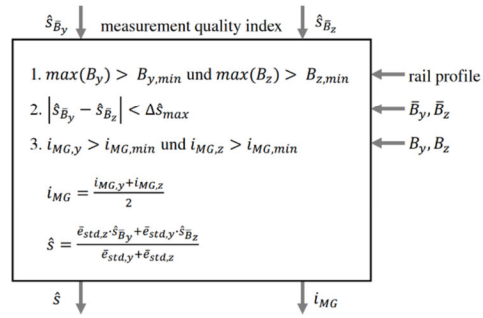

Fig. 8 Measurement quality index

	$\bar{B}_y$	$\bar{B}_z$
Max. error, $\bar{e}_{max}$ [mm]	0.61	0.92
Std. error, $\bar{e}_{std}$ [mm]	0.17	0.25

Table 1 Algorithm performance

When the measurement is considered valid, the lateral position $\hat{s}$ is calculated as the weighted sum of $\hat{s}_{\bar{B}_y}$ and $\hat{s}_{\bar{B}_z}$ with the reciprocal mean standard deviation $\bar{e}_{std}$ of the used algorithms as weights (see Table 1). The standard deviation for each algorithm is calculated over a dataset spanning different air gaps and lateral positions in a full factorial setup on an automated test rig. The next chapter shows the implementation of the algorithm used in $\bar{B}_y$.

5. RESULTS

The sensor prototype is tested on an automated test rig with a robot moving the sensor above the rail. This allows for full factorial testing of the prototype and hardware-in-the-loop-validation is also planned for further investigation. First, the sensor and its algorithms are verified. Verification ensures that the correct lateral position of the rail is measured when the sensor is moved laterally. Lastly, the sensor is validated for use in the active steered wheelset using the mentioned co-simulation, now including the sensor prototype's behaviour in a sensor look-up table.

5.1 Sensor verification

For verification, the sensor is placed above a S49 rail profile and moved laterally between -10 mm and 10 mm in 0.05 mm steps, the air gap varies between 10 mm and 30 mm in 2 mm steps. For every datapoint the lateral position is calculated using seven different algorithms, four in $\bar{B}_y$ and three in $\bar{B}_z$. The best performing algorithms in $\bar{B}_y$ and $\bar{B}_z$ are chosen using the maximal measurement error and the standard deviation of the measurement error.

The algorithm used in $\bar{B}_z$ is a neural network with 40 input neurons, 80 hidden layer neurons and 1 output neuron using a linear activation function. The network was trained on separate extended input data with an air gap of 18 mm. In $\bar{B}_y$ the algorithm shown in Fig. 9 is used. The maximum and minimal values of the sensor data closest to the x=0 y-axis are determined. Then a linear least square fit is performed on the data points contained in the green highlighted interval between the minimum and maximum. The *x*-coordinate of the intersection point (yellow) with the x-axis (y=0) is outputted as the calculated lateral position.

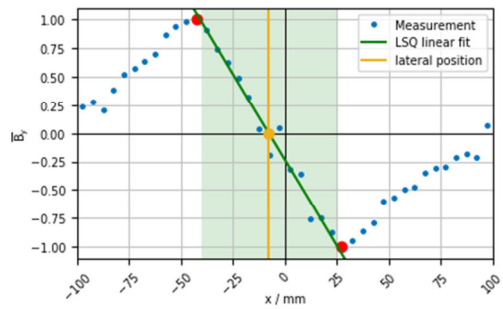

Fig. 9 Algorithm for lat. position in $\bar{B}_y$

Table 2 shows the maximal deviation $\bar{e}_{max}$ and the standard deviation of the error $\bar{e}_{std}$ of each algorithm and the combination (weighted sum calculation of $\hat{s}$, see chapter 4) over different air gaps. The measurement error is always less than 1 mm. The combination of both algorithms performs better on most data-points of the given test set. In summary, the verification shows good sensor performance and the lateral position of the rail below the sensor is measured correctly as the maximum error shows. The technical feasibility of the concept is proven

	$\bar{B}_y$		$\bar{B}_z$		combination	
air gap [mm]	$\bar{e}_{max}$ [mm]	$\bar{e}_{std}$ [mm]	$\bar{e}_{max}$ [mm]	$\bar{e}_{std}$ [mm]	$\bar{e}_{max}$ [mm]	$\bar{e}_{std}$ [mm]
10	0.31	0.13	0.92	0.53	0.19	0.08
12	0.32	0.14	0.73	0.43	0.23	0.08
14	0.35	0.14	0.56	0.35	0.24	0.08
16	0.33	0.14	0.49	0.28	0.21	0.08
18	0.42	0.16	0.45	0.23	0.23	0.09
20	0.42	0.17	0.43	0.20	0.21	0.09
22	0.42	0.17	0.38	0.18	0.28	0.10
24	0.39	0.16	0.44	0.19	0.31	0.11
26	0.43	0.16	0.29	0.11	0.26	0.10
28	0.52	0.2	0.30	0.12	0.28	0.12
30	0.61	0.25	0.27	0.11	**0.29**	**0.13**

Table 2 Comparison of algorithm

5.2 Sensor validation

To validate the sensor performance in the closed loop application of the active steered wheelset the parameter space in Fig. 10 is used. Parameters varied for all scenarios are the sensor air gap, the axle load and the friction coefficient between rail and wheel.

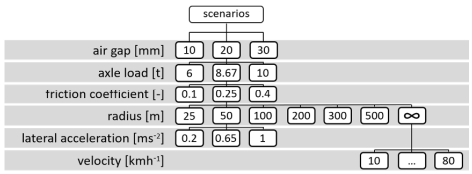

Fig. 10 Validation scenarios

Then the scenarios differ in track layout. The first scenario group is a short straight track merging in a curved track using a clothoidal transition (486 scenarios). In this group the vehicle velocity is calculated using the desired lateral acceleration in the curve. Parameters varied are the lateral acceleration and the curve radius. The second group is a straight track and the wheelset velocity is varied (216 scenarios). In total 702 scenarios all with high track irregularities are tested (ERRI B176 high).

The validation process uses the co-simulation and a sensor look-up table for the calculation of the auxiliary measurement quantities s_{L1}, s_{L2} and s_{R1}. As the measurement concept only needs three sensors to function, s_{R2} is omitted.

The look-up table is necessary as a full factorial hardware-in-the-loop simulation on the test rig is too slow to be done in an adequate time. The look-up table is calculated using the above-mentioned algorithms applied to measured data on the test rig. Additionally, white noise with the standard deviation shown in table 1 is added to the three auxiliary measurements in the simulation.

Fig. 11 and 12 show the evaluation of the test scenarios regarding the lateral displacement and actuator force. Both the maximal value and the root mean square of the quantities are shown. Fig. 11 colors the maximal values according to lateral acceleration respectively vehicle velocity. Green means low values and red means higher values. Fig. 12 colors the data points according to the air gap. An air gap of 10 mm is colored green, 20 mm light green and 30 mm red.

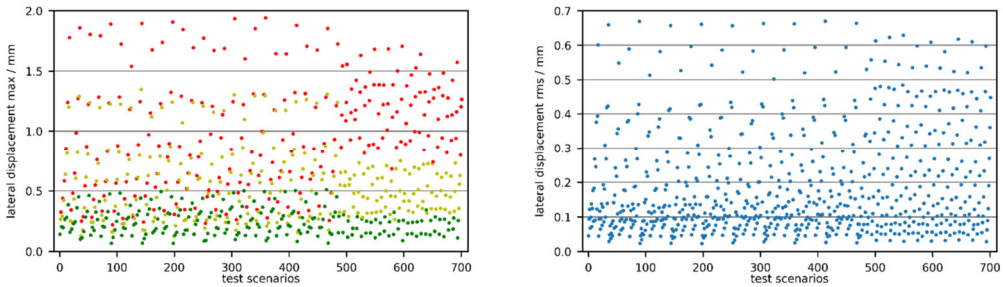

Fig. 11 Lateral displacement in test scenarios

In all test scenarios regarding the lateral displacement the active steered wheelset shows a good performance with a *rms*-value below 0.7 mm. The maximal lateral displacement of the wheelset is below 2 mm in all cases. Lower lateral accelerations and lower speeds result in a smaller lateral displacement. Points with a maximal lateral displacement >1.5 mm are tracks with high lateral acceleration in curves or high vehicle speed on the straight test track. Given the simulation results, a flange contact can be effectively avoided.

Regarding the actuator force in Fig. 12, lesser force is needed when the air gap is 20 mm or less. When the air gap reaches 30 mm, the maximal actuator force hits 1000 N. This is due to the impact of measurement quality as per table 2: the error increases with increasing air gap. Additionally, a greater air gap produces a higher

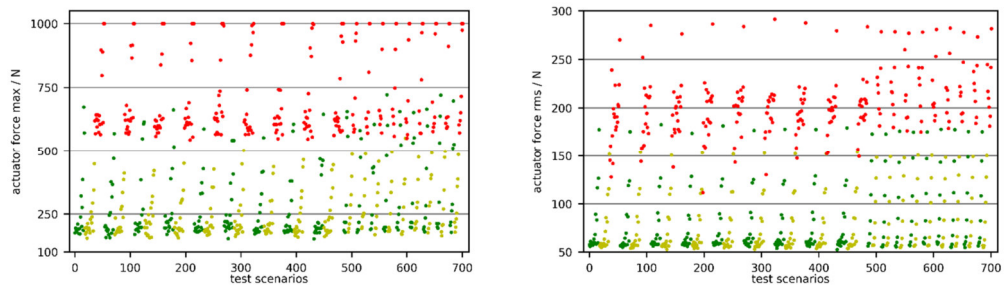

Fig. 12 Actuator force in test scenarios

frequency of error in the measurement output due to the added white noise and sensor look-up table. The controller then processes the higher frequency input and generates a high frequency output using the maximal actuator force. The simulation implements an actuator-saturation so no values above 1000 N can be reached.

Even in the test scenarios when the actuator force reaches the limit, a low lateral displacement can be observed. Thus, the closed loop track guidance is still able to center the wheelset.

6. CONCLUSION

In this paper we present a new sensor concept for the direct measurement of vehicle states on an active steered wheelset. The two states *lateral displacement* and *angle of attack* are measured using a contact-less hall sensor array. The sensor generates a static magnetic field which the ferromagnetic rail disturbs. The disturbance is measured with 40 hall elements and using this sensor data the lateral position of the rail is calculated. The measurement set-up uses four of these sensors to calculate the lateral displacement and angle of attack.

The sensor prototype is verified on an automated test rig showing low measurement errors with specially developed algorithms. A co-simulation then validates the sensor prototype in 702 test scenarios. The lateral displacement of the wheelset is kept low in all scenarios and never exceeds 2 mm while constraining the needed actuator force.

In conclusion, the proposed measurement set-up with the new designed hall sensor prototype can determine the necessary state variables on an active steered wheelset. With the implemented model-based controller an improved track-guidance in comparison with conventional wheelsets is achieved.

Further investigations will include a hardware-in-the-loop test on selected test scenarios.

7. REFERENCES

[1] **Bruni, S. - Goodall, R. - Mei, T. X. - Tsunashima, H.:** Control and monitoring for railway vehicle dynamics, *Vehicle System Dyn.*,Vol. 45, 7-8, , 2007. p. 743–779.

[2] **Kraft, D.:** *Sensoren zur elektronisch unterstützten Spurführung von Schienenfahrzeugen*. Dissertation. Düsseldorf: VDI-Verlag, 1998.
[3] **Li, H. - Goodall, R. M.:** State estimation for active steering of railway vehicles, *IFAC Proceedings Volumes*, Vol. 32, Nr. 2, p. 4359–4364., http://www. sciencedirect.com/science/article/pii/S1474667017567439, 1999.
[4] **Gretzschel, M. - Bose, L.:** A Mechatronic Approach for Active Influence on Railway Vehicle Running Behaviour, *Vehicle System Dynamics*, Jg. 33, 1999, p. 418–430.
[5] **Hermanns. M. - Dellmann, T.**: Betrachtungen zu spurführungstechnischen Rückfallebenen eines mechatronsichen Fahrwerks, *ZEVRail Glasers Annalen 131*, 11/12, 2007, p.456-466.
[6] **Mei, T. X. - Goodall, R. M.:** Recent Development in Active Steering of Railway Vehicles, *Vehicle System Dynamics*, Vol. 39, Nr. 6, 2003, p.415–436.
[7] **Powell, A. J.:** On the Dynamics of Actively Steered Railway Vehicles, *Vehicle System Dynamics*, Supplement, Nr. 29, 1998, p.506–520.
[8] **Schade, S. - Hermanns, M. - Dellmann, T.:** Mechatronische Spurführungsregelung zur aktiven Spurführung von angetriebenen Losradfahrrädern, *ZEVRail*, Jg. 134., Nr. 10, 2010, p.404–410.
[9] **Wickens A. H.:** Dynamic Stability of Articulated and Steered Railway Vehicles Guided by Lateral Displacement Feedback, *Vehicle System Dynamics*, Supplement, Nr. 23, 1994, p.541–553.
[10] **Yunfan Wei**: *Spurführungsregelung eines aktiv gelenkten Radpaars für Straßenbahnen*. Dissertation. Karlsruhe: KIT Scientific Publishing, 2014.
[11] **Kurzeck, B. - Valente, L.:** A novel mechatronic running gear: concept, simulation and scaled roller rig testing. in *9th World Congress on Railway Research*, 2011.
[12] **Aknin,P. - Placko, D. - Ayasse, J.B.:** Eddy current sensor for the measurement of a lateral displacement: Applications in the railway domain, *Sensors and Actuators A: Physical*, Jg. 31, Nr. 1, 1991, p.17–23., http://www.sciencedirect. com/science/article/pii/092442479280074D, 1992.

DYNAMIC SIMULATION TO STRUCTURAL DAMAGE

Manuel FOSSATI*, Aitor CAPELLÁN* and Aitor ZAPIRAIN**

*CAF, **TECNUN
Bogies Engineering Area, Engineering Deparment
Construcciones y Auxiliar de Ferrocarriles, CAF
J.M. Iturrioz 26, E-20200 Beasain, Spain
Tel. +34 943880100, Fax +34 943881420

Received: September 15, 2019

ABSTRACT

Fatigue analysis has always been a critical aspect when it comes to designing mechanically demanded parts. This is especially applicable to bogie frames and, in general, in all the rest of the bogie components. Even if several standards exist and are used as the base of these analyses, in most of the cases standards solely classify load cases by vehicle typology but do not take into account actual operational details. Most of the time, time-demanding track measurements are required to certify that the component performance is within its endurance limit. The methodology that is introduced along this report takes advantage of dynamic simulation tools to obtain actual forces on the components, process them in such a way that virtual endurance assessment is possible. This reduces failure risk on new designs even without constructing prototypes. An example is shown for a bogie frame for which basic vertical, lateral, twisting, roll and lozenging "factors" are derived. Those "factors" are used as inputs in simple FEA calculations where, by a rainflow analyses, obtain the cumulative damage according to Palmgren-Miner law.

Keywords: dynamical simulation, load cases, finite elements, damage hypothesis, material fatigue

1. INTRODUCTION

The main goal of this paper is to introduce a new predictive methodology which enables estimating the cumulative damage in the bogie frame by making use of dynamic simulation tools.

Simulation tools can predict the forces that act on different parts of the bogie in a particular time and track section. By performing a FEM calculation with the instantaneous forces acting on the bogie frame in different moments of time, it would be possible to obtain the number of cycles in which a particular stress range occurs along the track. This, in fact, would be sufficient to perform an endurance calculation by cumulative damage. However, this methodology would be extremely highly computationally demanding.

The alternative methodology that is presented in this document consists of separating the main input forces that act on the bogie frame in simple time dependent load functions.

1.1 Symbols and notation

The symbols and notations used in this document are defined as follows.

Parameter	Symbol	Unit
Carbody's acceleration in Z axis.	$az_{carbody}$	$\frac{\mathrm{m}}{s^2}$
Bogie's acceleration in Z axis.	az_{bogie}	$\frac{\mathrm{m}}{s^2}$
Carbody's acceleration in Y axis.	$ay_{carbody}$	$\frac{\mathrm{m}}{s^2}$

Bogie's acceleration in Y axis.	ay_{bogie}	$\frac{m}{s^2}$
Lateral elastic constant of the secondary suspension.	$K1$	$\frac{N}{mm}$
Lateral elastic constant of the lateral stop. $Stifness$	$K2$	$\frac{N}{mm}$
Secondary suspension air spring's lateral deformation.	$\delta 1$	mm
Lateral bump-stop deformation.	$\delta 2$	mm
Simulated vertical loads in the wheel. (X: Front/Rear; Y: Right/Left)	Q_{z_XY}	kN
Simulated longitudinal loads in the wheel. (X: Front/Rear; Y: Right/Left)	Q_{x_XY}	kN
Estimated vertical load in the wheel in each basic load case. (X: Front/Rear; Y: Right/Left; Z:**V**ertical/**R**oll/**T**wist)	R_{XY_Z}	kN
Estimated lateral load in the wheel in each basic load case. (X: Front/Rear; Y: Right/Left)	F_{y_XY}	kN
Estimated longitudinal load in the wheel in each basic load case. (X: Front/Rear; Y: Right/Left)	F_{x_XY}	kN

Table 1 Symbols and notations

2. METHODOLOGY

1.2 Introductory Remarks

The analysis presented in this document aimed to obtain the basic load cases from CAF's Civity UK EMU platform bogie by analyzing track simulation data from Carnforth to Preston. These hypotheses are equally applicable to other routes as long as the bogie remains invariable. For a different bogie, basic load hypotheses should be adjusted.

Disengaging the input forces on the bogie in basic loads hypotheses enables endurance calculation by cumulative damage by using the stress assessment software LIMIT. The stress state of the bogie frame in a particular moment is estimated from a combination of all these basic load hypotheses.

The resulting time dependent variables that should be estimated through dynamic simulations in order to feed the considered basic load cases are:

- $az_{carbody}$
- az_{bogie}
- $ay_{carbody}$
- ay_{bogie}
- $\delta 1$
- $\delta 2$
- Q_{z_FR}
- Q_{z_FL}
- Q_{z_RR}
- Q_{z_RL}
- Q_{x_FR}
- Q_{x_FL}
- Q_{x_RR}
- Q_{x_RL}

The following figures show the location in the model from where these variables have been obtained through simulations.

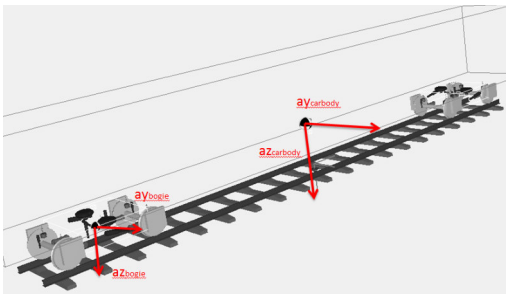

Fig. 1 Simulated variables position

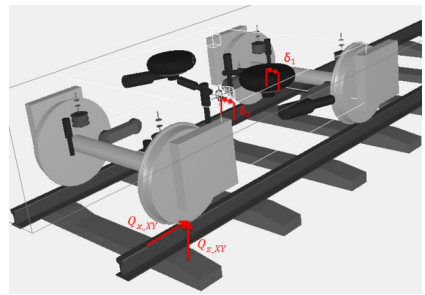

Fig. 2 - Simulated wheel load position

The theoretical values that will be obtained in each wheel from the analyzed basic load cases are:

- $R_{\_FR}$
- $R_{\_FL}$
- $R_{\_RR}$
- $R_{\_RL}$
- F_{y_FR}
- F_{y_FL}
- F_{y_RR}
- F_{y_RL}
- F_{x_FR}
- F_{x_FL}
- F_{x_RR}
- F_{x_RL}

The following figure shows the position of the theoretical wheel load variables in CAF's Civity UK EMUs platform bogie.

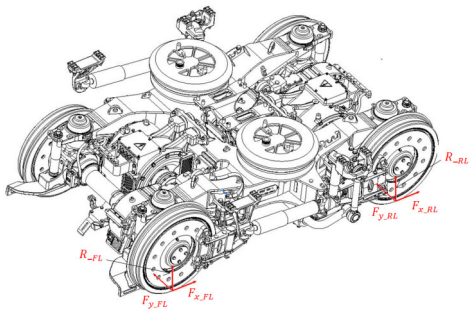

Fig. 3 Bogie wheel load variables

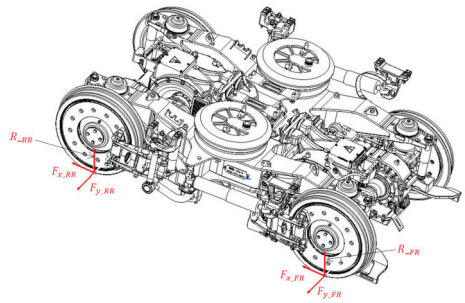

Fig. 4 Bogie wheel load variables

1.3 Basic Load Cases

1.3.1 Vertical load

The vertical reaction that is produced in each wheel by pure vertical basic load has been considered to be the same in all the wheels.

$$R_{FL\_V} = R_{FR\_V} = R_{RL\_V} = R_{RR\_V} \quad (1)$$

The vertical reaction load in the wheels per bogie has been assumed to be equal to the percentage of the mass of the car body and the bogie to the rail multiplied by its vertical acceleration.

A time dependent vertical reaction force curve was obtained for each wheel by considering the following assumption:

$$m_{carbody} * (az_{carbody} + g) + m_{bogie} * (az_{bogie} + g) = R_{FL\_V} + R_{FR\_V} + R_{RL\_V} + R_{RR\_V} = R_{V\_TOTAL} \quad (2)$$

$$m_{carbody} = m_{carbody\text{-}tare} + m_{payload} \quad (3)$$

1.3.2 Roll load

The vertical reactions in each wheel produced by pure roll basic load attend the following assumption:

$$R_{FL\_R} + R_{RL\_R} \neq R_{FR\_R} + R_{RR\_R} \quad (4)$$

In addition, the vertical reaction by pure roll load on the wheels of the same bogie side must be the same:

$$R_{FR\_R} = R_{RR\_R} \quad (5)$$

$$R_{FL\_R} = R_{RL\_R} \quad (6)$$

A time dependent vertical reaction force curve was obtained for each wheel by considering the following assumption, where Q_Z are dynamic simulation outputs.

$$R_{FL\_R} = (Q_{Z\_FL} + Q_{Z\_RL} - Q_{Z\_FR} - Q_{Z\_RR})/4 \quad (7)$$

$$R_{FR\_R} = -R_{FL\_R} \quad (8)$$

$$R_{RL\_R} = R_{FL\_R} \quad (9)$$

$$R_{RR\_R} = -R_{FL\_R} \quad (10)$$

1.3.3 Lateral load

The lateral reaction in each wheel produced by pure lateral basic load case has been considered to be the same in all the wheels.

$$F_{y\_FL} = F_{y\_FR} = F_{y\_RL} = F_{y\_RR} \quad (11)$$

Moreover, the lateral reaction load in the wheels per bogie has been considered to be equal to the percentage of the mass of the car body and the bogie to the rail multiplied by its lateral acceleration.

A time dependent lateral reaction force curve was obtained for each wheel by considering the following assumption, where a_y are dynamic simulation outputs.

$$m_{carbody} * ay_{carbody} + m_{bogie} * ay_{bogie} = F_{y\,FL} + F_{y\,FR} + F_{y\,RL} + F_{y\,RR} == F_{y\,TOTAL} \quad (12)$$

$$F_{y\,TOTAL} = F_{y\,aycarbody} + F_{y\,aybogie} \quad (13)$$

The lateral pure basic load case produces a roll effect and, consequently, a vertical reaction in the wheels. This should be considered in the total vertical reaction of the wheels in service.

1.3.4 Twist load

The vertical reactions in each wheel produced by pure twist basic load attend the following assumptions:

$$R_{FL\_T} + R_{FR\_T} = R_{RL\_T} + R_{RR\_T} \quad (14)$$

$$R_{FL\_T} \neq R_{RL\_T} \quad (15)$$

$$R_{FR\_T} \neq R_{RR\_T} \quad (16)$$

A time dependent vertical reaction force curve was obtained for each wheel, where Q_Z are dynamic simulation outputs:

$$R_{FL\_T} = (Q_{z_{FL}} + Q_{z_{RR}} - Q_{z_{FR}} - Q_{z_{RR}})/4 \quad (17)$$

$$R_{FR\_T} = -R_{FL\_T} \quad (18)$$

$$R_{RL\_T} = -R_{FL\_T} \quad (19)$$

$$R_{RR\_T} = R_{FL\_T} \quad (20)$$

1.3.5 Lozenging load

The longitudinal reactions in the wheels generated by a pure lozenging basic load case attend the following assumption:

$$F_{x\,FL} \neq F_{x\,FR} \quad (21)$$

$$F_{x\,RL} \neq F_{x\,RR} \quad (22)$$

A time dependent longitudinal reaction force curve was obtained for each wheel by considering the following assumptions, where Q_X are dynamic simulation outputs:

$$F_{x\,FL} = (Q_{x_{FL}} + Q_{x_{RL}} - Q_{x_{FR}} - Q_{x_{RR}})/4 \tag{23}$$

$$F_{x\,FR} = -F_{x\,FL} \tag{24}$$

$$F_{x\,RL} = F_{x\,FL} \tag{25}$$

$$F_{x\,RR} = -F_{x\,FL} \tag{26}$$

These longitudinal lozenging forces create lateral forces in each wheel that counterbalance the generated lozenging torque in Z axis.

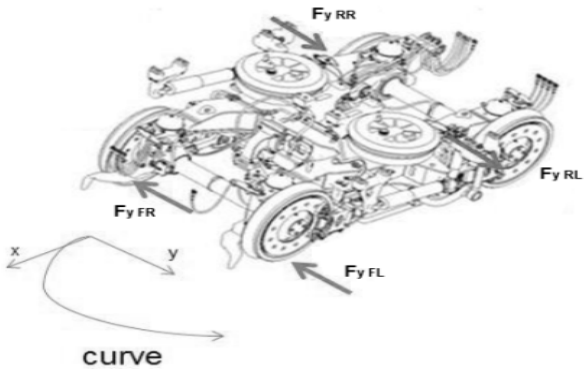

Fig. 5 Lozenging force balance

The lozenging basic load case has effect on the individual resulting lateral force per wheel. However, these lateral loads are countered if the complete bogie is considered. Therefore, the resulting lateral load in wheels per bogie to be considered in the endurance calculation would be defined with just the lateral basic load case.

1.4 Basic Load Cases Theoretical Validation

Once the input forces have been disengaged into basic load hypotheses a theoretical validation of them is necessary. Either for vertical, lateral or longitudinal reactions on the wheels it consists of comparing the sum of forces obtained from the basic load cases in each axis with the wheel reaction values obtained through simulations.

A comparison of the lateral forces on wheel is presented. As stated in 2.2.3, the lateral reaction load in the wheels per bogie is equal to the percentage of the mass of the car body and the bogie to the rail multiplied by its lateral acceleration.

As explained in the section 2.2.3 the lateral load is produced by the lateral inertia of the car body, transmitted through the lateral bump stops and the air spring to the bogie and the lateral inertia of the bogie frame.

As indicated in section 2.2.5, the lozenging case produces certain lateral reaction in wheels too. The lateral reactions produced by lozenging would be detected if a comparison in each particular wheel is made. If the complete bogie is taken into account, as the lateral forces are countered, the total wheel lateral reaction will remain unchanged.

The following figure compares the obtained the lateral force per bogie in wheels with the dynamic simulation data. The first graph takes into account only the car bodies lateral inertia, whereas the second graph takes into account the bogie lateral inertia too.

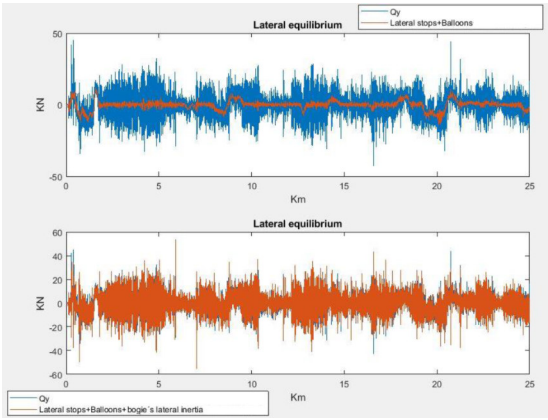

Fig. 6 Lateral equilibrium comparison

As can be checked, by considering the bogie lateral inertia, the lateral reactions are practically the same as the values obtained by dynamics simulations.

1.5 Finite Element Models

Once the main forces that act on the bogie frame and obtained from the dynamic simulations as a function of time have been divided into simple basic loads hypotheses, FE Models should be feeded with this information in order to obtain the cumulative damage. The FE Models used in this approach are the followings:

1.5.1 Vertical load case – FE Model

The vertical load curve presented in equation (2), $R_{\_VTOTAL}$, is the vertical force at wheel level of the car body and the bogie. It has been divided into the vertical load dependent on the car body inertia and the vertical load dependent on the bogie inertia. The vertical load case should be divided into two FE models for each case.

$$R_{VTOTAL} = R_{VCARBODY} + R_{VBOGIE} \tag{27}$$

$$R_{VCARBODY} = m_{carbody} * \left(az_{carbody} + g\right) \tag{28}$$

$$R_{VBOGIE} = m_{bogie} * \left(az_{bogie} + g\right) \tag{29}$$

FE model related to vertical load hypotheses from the car body is shown in the next figure.

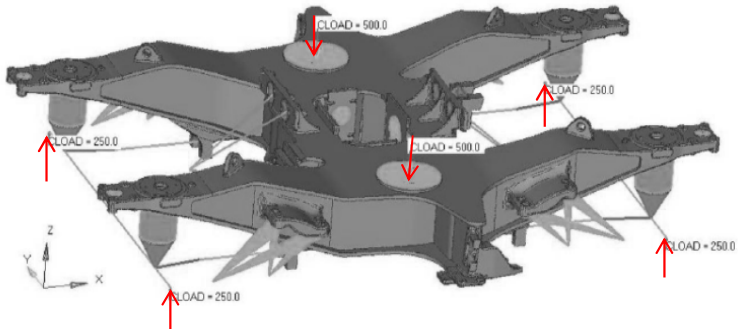

Fig. 7 Vertical load case FE Model

The vertical load hypothesis from the bogie vertical inertia is modelled separately.

1.5.2 Roll load case – FE Model

FE model related to roll load hypotheses is shown in the next figure:

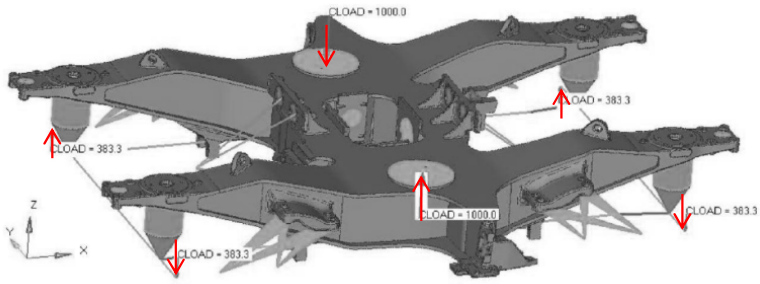

Fig. 8 Roll load case FE Model

1.5.3 Lateral load case – FE Model

FE models related to lateral load hypotheses are shown in the next figures.

The lateral load curve presented in equation (12), $F_{y\,TOTAL}$, is transmitted through the bogie by different points. Therefore, the load should be divided according to the application point.

Regarding the lateral force produced by the lateral inertia of the car body, it is transmitted from the bogie to the rail by a combination of secondary suspension air spring and lateral bump stop. It depends on the magnitude of the load and verifies the following equation:

$$F_{y\,aycarbody} = K_{spring} * \delta_{spring} + K_{bumpstop} * \delta_{bumpstop} \quad (30)$$

The part of the load from the car body inertia that is transmitted through the secondary air spring and lateral bump stop has been modelled as follows:

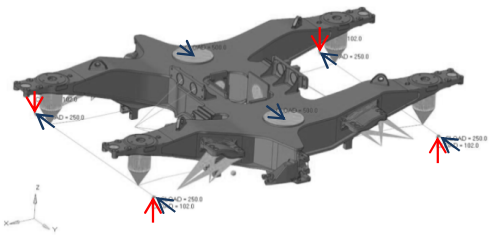

Fig. 11 Lateral - Secondary Spring FE Model

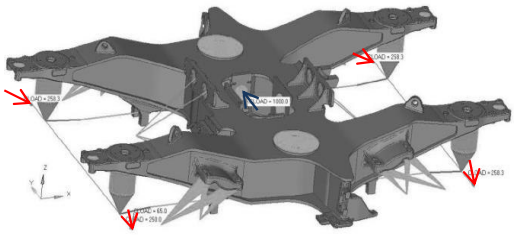

Fig. 12 Lateral–Bump stop FE Model

Regarding the lateral force produced by the lateral inertia of the bogie, it will also be transmitted through the bogie through different application points.

The main bogie elements attached to the bogie frame, motor and brake, have been treated separately. Acceleration values for these elements have been adjusted according to the mounting position in Y considering that there is a linear reduction in the accelerations from the primary suspension to half the value at the bogie centre.

The lateral force produced by the lateral inertia of the bogie results in:

$$F_{y\ aybogie} = m_{\ motor}\ ay_{\ bogie\_m} + m_{\ brake} * ay_{\ bogie_b} + m_{\ frame} * ay_{\ bogie} \quad (31)$$

The FE Models that represents the load from the lateral inertia of the motor and brake is shown in the next figures:

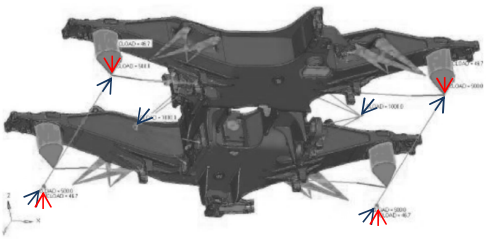

Fig. 9 Lateral – Motor Inertia FE Model

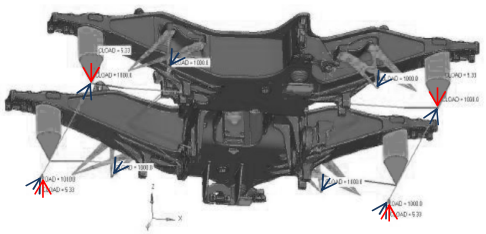

Fig. 10 Lateral - Brake Inertia FE Model

The part of the lateral load that is produced by the inertia of the rest of the bogie mass is modelled separately.

1.5.4 Twist load case – FE Model

FE model related to twist load hypotheses is shown in the next figure. Forces and momentums are equilibrated. Front wheels produce positive momentum in X axis while real wheels produce the same momentum but negative in X axis.

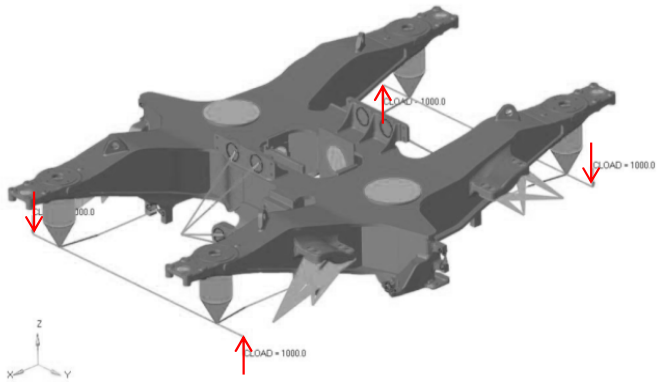

Fig. 13 Twist load FE Model

1.5.5 Lozenging load case – FE Model

FE model related to lozenging load hypotheses is shown in the next figure. Momentum in Z axis coming from longitudinal forces in wheels is compensated by lateral reactions in wheels.

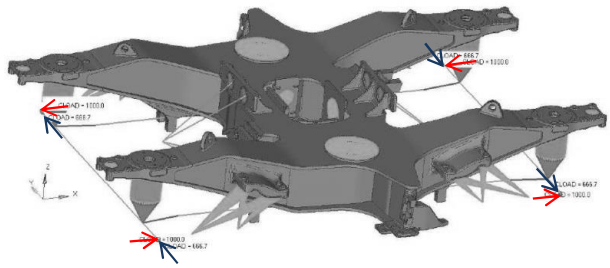

Fig. 14 Lozenging FE Model

1.6 Cumulative damage calculation

The input forces that act on the bogie have been disengaged into various basic load cases. FE Models have been created for each of these input load cases.

A FEM calculation should then be performed for each of the FE Models. FE reference results should be obtained for each FE Model.

This way, it is possible to perform a cumulative damage calculation by using the stress assessment software LIMIT. For that purpose, the basic load FE models (.inp) and the FE Reference Results (.odd) should be imported to the program.

LIMIT software allows connecting each of the FE Reference Results to its corresponding time-dependent force curve. By assuming linear stress relationship and combining the stress results obtained in each basic load case, a cumulative damage calculation is possible to be done.

3. CONCLUDING REMARKS

A new predictive methodology has been presented which enables estimating the cumulative damage in the bogie frame by making use of dynamic simulation tools.

On the basis of our theoretical investigations and numerical simulations, the following conclusions can be drawn:

- The influence of the operational details in the lifetime of mechanical parts can be quantified through this method.
- Optimized designs could be executed for each particular case instead of taking into account just vehicle typology as most standards suggest.
- In some cases, these operational details could lead to worse fatigue analysis results than most extreme loads in structural specification standards if the railway's amount of imperfections were actually high, making this method potentially significant for safety.

4. FUTURE LINES

This methodology allows performing a cumulative damage calculation by dynamic simulation track data. The input loads that act on the bogie frame have been approximated by a sum of basic load cases.

It is important mentioning that the main objective should be to reduce as much as possible the difference between the loads obtained through simulations and the loads obtained by this methodology. This implies incorporating intermediate load cases that will make the cumulative damage calculation to be as precise as possible to the real measured values. Modelling the longitudinal forces by traction and braking and performing a model of the dampers should be the next steps to follow.

For the sake of improving this methodology, a comparison should also be made between the cumulative damage results obtained by LIMIT in a simulated route with the cumulative damage results obtained in a real extensometric track test performed in the same route.

5. REFERENCES

[1] CAE-SIM-SOL, n.d. Limit 2019 Release Notes. [Online] Available at: https://www.cae-sim-sol.com/files/attachments/limit-release-notes-2019_2.pdf. [Accessed 26 April 2019].

[2] Mathworks Inc., n.d. Linear Regressions. [Online] Available at: https://es.mathworks.com/help/matlab/data_analysis/linear-regression.html [Accessed 12 March 2019].

[3] Mathworks Inc., n.d. Polynomial curve fitting. [Online] Available at: https://es.mathworks.com/help/matlab/ref/polyfit.html?lang=en [Accessed 20 March 2019].

[4] Mathworks Inc., n.d. Savitzky-Golay filtering. [Online] Available at: https://es.mathworks.com/help/signal/ref/sgolayfilt.html [Accessed 14 March 2019].

[5] **Pecora, C**.: n.d. MATLAB Central. [Online] Available at: https: //www.mathworks.com/matlabcentral/fileexchange/70402-playbar [Accessed 1 March 2019].

[6] ReliaSoft Corporation, 2007. Accelerated Life Tesing Reference, Tucso, AZ: ReliaSoft Publisihing.

[7] Signal Processing Stack Exchange, n.d. Signal Processing Stack Exchange. [Online] Available at: https://dsp.stackexchange.com/questions/38564/whats-the-pass-band-ripple-and-stop-band-attenuation-of-a-digital-filter [Accessed 16 May 2019].

[8] **Sophocles, J. O.:** Introduction to Signal Processing. Englewood Cliffs, NJ: Pretince Hall, 1996.

[9] Weibull, n.d. Miner's Rule and Cumulative Damage Models. [Online] Available at: https://www.weibull.com/hotwire/issue116/hottopics116.htm [Accessed 16 April 2019].

DATA TO THE HISTORY OF THE BOGIE-FAMILY *KALÁKA*

Istvan BÉRES[1] and József CSIBA[2]

[1]Hungarian State Railways Co.

[2]BME ITS Non-profit Plc
Business Unit for Conformity Assessment of Railway Subsystems
Budapest University of Technology and Economics
H-1111 Budapest, Hungary

Received: September 10, 2019

ABSTRACT

Numerous vehicles and major components of vehicles were born in the General Work of the Hungarian Royal State Railways (MÁV) in Dunakeszi opened in 1926 during its nearly one century-time operation. From among the famous vehicles at the first place one must mention in a quasi-chronological way the special train for transporting the *Holy Right* during the XXXIV. International Eucharistic World Congress organised in Hungary in 1938, the Governor's car transport wagon and different vehicles of service stock (for example sleeping car and musical instrument transport wagon of MÁV's Symphonic Orchestra, brake instructional car, measurement cars etc.). The bogie-family KALÁKA belongs to the head of the major components of railway vehicles. This bogie type was the running gear of a lot of carriages built or modernised or rebuilt in Dunakeszi. The tasks and the scope of duties of the Dunakeszi General Work were changed after WW2. The carriage stock of the MÁV got seriously damaged during the WW2. The passenger traffic demands were changed due to the changes in the Hungarian industrial politics. Two big tasks were assigned for the General Work, the construction of an absolutely new vehicle type for suburban traffic of the Hungarian capital Budapest and a new bogie type by using new, up-to-date construction principles, concerning for example less maintenance demands, higher operation reliability, better running quality and less loads causing track deterioration, etc. Such an advantageous bogie was needed to the new suburban vehicle type. The basic bogie type was the Ganz-Rónai bogie type from the Ganz Factory. The new Dunakeszi bogie type was designed by the three young design-engineers of the factory, namely by Tibor Kardos, Péter Lánczos and János Kalmár. This new type was named KALÁKA, the name is combined from the *two initial capitals* of the three design-engineers' family names. More variants of the basic bogie type were developed by the designing experts and engineers of the Dunakeszi General Work for numerous different purpose passenger carriages to be applied in internal traffic. The born of the bogie family, the family members and the posterities will be introduced in this paper. The guidance and damping characteristics will be described in details. The application in railway operation of bogie family KALÁKA will also be shown.

Keywords: vehicle building, bogie, bogie family, axle guiding, damping, maintenance experience

1. INTRODUCTION

The development and manufacturing of DMU-s and EMU-s took place at the Ganz & Co factory playing central role in the Hungarian railway vehicle building industry. The activity of the Ganz & Co factory gave a model for creating and manufacturing railway vehicles. The characteristic of the classic Ganz DMU was its composition from a railcar (the traction unit with passenger room) and special trailing cars connected to the former. The railcar bodies were supported on two types of bogies: on a driving bogie and on a trailing bogie. The diesel engine, and the driving system, the running gear (main coupling), the gearbox, direction-changer and the final drives were built into the driving bogie. By this technical solution there was no opportunity geometrically to build in a mechanism to ensure a connection between the bogie and the car body.

Cheap carriages of high capacity were needed due to lack of capital and the high number of passengers. In that time a significant part of the running technique experts expressed the opinion that good running quality can only be ensured by such carriages which are equipped with bogies of high weight and wide axle-base. But the MÁV's experts saw well

that the track load was higher by the above mentioned bogie parameters so light carriages were ordered from Ganz & Co factory directly prior to the beginning of WW2. The mentioned carriages were of Class Cak[1]. The bogies of the latter carriage type were named type *Ganz-Rónai*[2], their name was ordered to the vehicle Class Cak or alternatively by signalling the manufacturer firm or after the inventor personage. The bogie type can be characterized by its of V-shaped vertical axle guidance and the special bogie/carbody connection. The latter was of friction type connection. This bogie type was the basic layout achieved by the domestic bogie development after the war. After WW2 also the Dunakeszi General Work of the Hungarian State Railways (MÁV) was reorganised as a wagon factory, and the company got a new owner, the Hungarian State.

After WW2 the MÁV's vehicle stock, particularly the coaching stock was very seriously damaged, its number was reduced very significantly directly due to the war affairs and the conclusions of the Paris-peace treaty after the war[3]. There were two other factors: the available stock was very old its vehicles were mostly of 2-axle cars with car-bodies of old wood construction[4] , as well as the growing suburban traffic directed to Budapest the capital. Severe vehicle accidents with old the vehicles and the insufficient operational capacity the Budapest terminal stations were also important catalysers for the seeking the solution with respect to the vehicle side to the problems of the Hungarian railway traffic. Due to the above mentioned and shortly listed difficulties quick and efficient decisions were required both from the MÁV-Headquarters and from Hungarian railway vehicle industrial Actors.

2. THE DEVELOPMENT PHASES OF THE BOGIE FAMILY KALÁKA

Decision was made by the MÁV-Headquarters at the annular turn of 1951-1952 to design and build up-to-date, 4-axle passenger carriages for suburban traffic on the basis of carriage type Bam[5]. Concerning the decision there was a very important question: the number of doors to be open on one side of the carriage[6]. After some investigations and trials of more variants the solution was the as follows: 1+2+1 doors by vehicle sides[7].

The characteristics of the carriage type Cak were the basis to be followed during the designing work. It was obvious that an absolutely new bogie type is needed because of the experiences got during the operation of the bogie type *Ganz-Rónai* of the vehicle type Cak and the new demands of the suburban vehicles.

[1] Cak: C: Corridor Composite Third, a: vehicle with bogies, k: light construction
[2] Rónai: Rónai, Gyula Dr. Eng. main constructor of bogies in the Ganz & Co. Electrical, Machinery, Railway Carriage Works and Shipyard Ltd.
[3] 15% of the MÁV's vehicle stock were up to operate in April 1945, it means 127 locomotives, 285 passenger carriage and brake vans, 5126 freight wagons. [3]
[4] The MÁV's railway passenger carriages stock was contained by 4982 vehicles at the end of 1954. Only 788 were 4-axle ones. Mostly all of them were hauled by steam engines. [3]
[5] B: Corridor Composite Standard, a: vehicle with bogies, m: modified, it is convenient for secondary line traffic
[6] The substantially quicker passenger changing during the staying in the stations and stoops needed more doors as earlier.
[7] Numerous door variants were born between 1951 and 1956 on the engineers and the experts trestle-boards, for example: 1+2+2+1 and 2+2

A tender invitation for constructing a bogie type of a passenger carriage to be operated in suburban traffic was published in the first half-year of 1954 by the Directorate of the Ganz Waggon and Machine Factory. Four young design-engineers of the Dunakeszi Factory, János **KA**lmár, Péter **LÁ**nczos and Tibor **KA**rdos participated in the tender, too. Although their work was not the winner one, but their bogie construction was accepted. This new bogie type KALÁKA was named after the three engineers. The first carriages with bogie type KALÁKA came into manufacturing in February 1955[8].

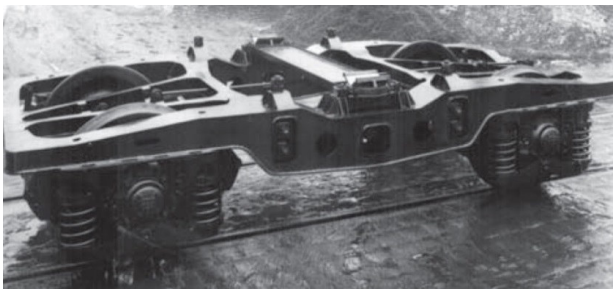

Fig. 1 Bogie type *Ganz-Rónai* as running one for passenger carriages

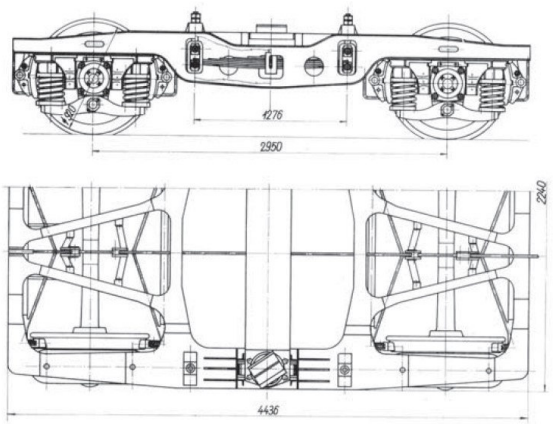

Fig. 2 The top view drawing of bogie type *Ganz-Rónai*

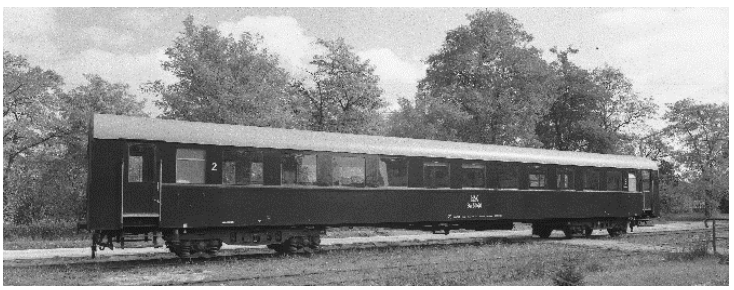

Fig. 3 The *Ganz-Rónai* bogie under carriage Class Cak

[8] This carriage type Cakmü with bogie type KALÁKA I was built for main line and secondary line traffic.

The first 4 – axle carriages for suburban traffic Class Bah[9] were built and they were up to operation in 1958 and it run in regular scheduled traffic.
The bogie family KALÁKA was manufactured until 1972. The family contains four variants. The differences among the different variants can be defined by the help of the undermentioned comparisons:

Phase A: Variants KALÁKA I. and II. In comparison to Bogie Cak:

- reducing of the axle-base from 2930 mm to 2500 mm,
- translocation of the main transverse girder to the place of the theoretical prize (centre of bogie rotatory displacement in horizontal planet) of the Bogie *Ganz-Rónai*,
- building in of central rolling plate and spring lateral support,
- straight box beam.

No changed:

- the V-shaped vertical axle-box guidance,
- the secondary leaf spring.

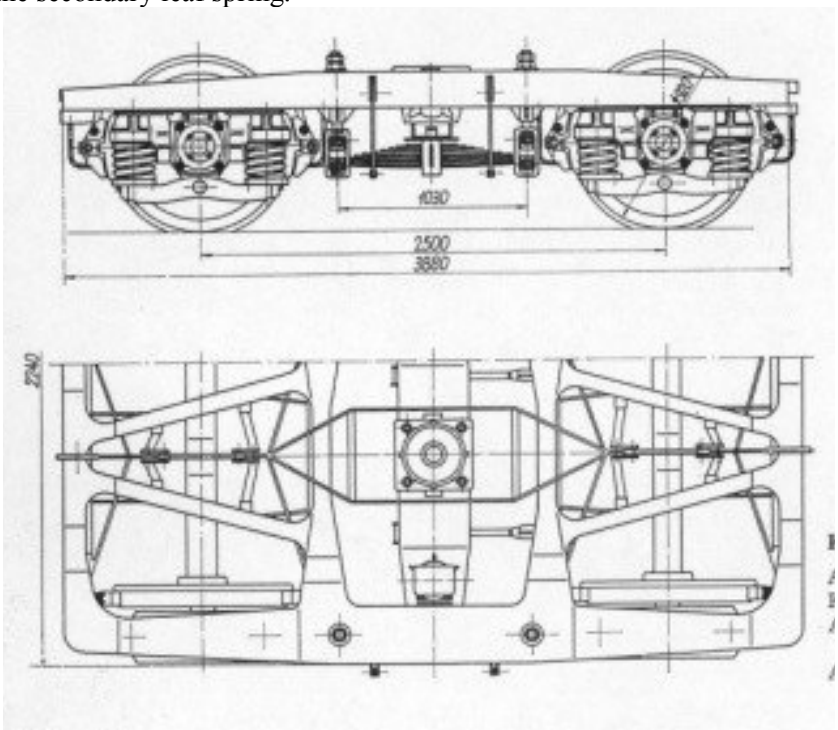

Fig. 4 Bogie type KALÁKA I. as a prototype one from 1954, manufactured in Dunakeszi for car-body type Cakmü

[9] By the end of November 1955 a vehicle Class Ha/Cah (Open Third for local/suburban traffic) with 2+2 doors on each vehicle side was completed. This carriage was already built in Dunakeszi by the documentation of the Győr Hungarian Waggon and Machine Factory. The bogie type Ganz-Rónai was given to the vehicle. There were a numerous operation difficulties during a running tests because of the unusually big the of 2950 mm theoretical pivot distance (the pivot distance in KALÁKA is 2500 mm). The unlade weight of the carriage was by about 4 tons than the planned one. The serial manufacturing of the type was cancelled.

Fig. 5 Series KALÁKA I. from 1957, 525 suburban carriages Class Bah were built until 1962 with KALÁKA I. and KALÁKA III.

Phase B: Variant KALÁKA III., the born of the type KALÁKA III :

Changes in comparison with phase A:

- helical spring instead of the leaf spring in the secondary suspension,
- application of friction damper parallel to the secondary springs, later hydraulic dampers followed,
- transforming the ball-cape-shaped central plate into flat central plate,
- application of the C-section headstocks instead of the pipe-sections.

No changed:

- the vertical V - shaped axle-box guidance.

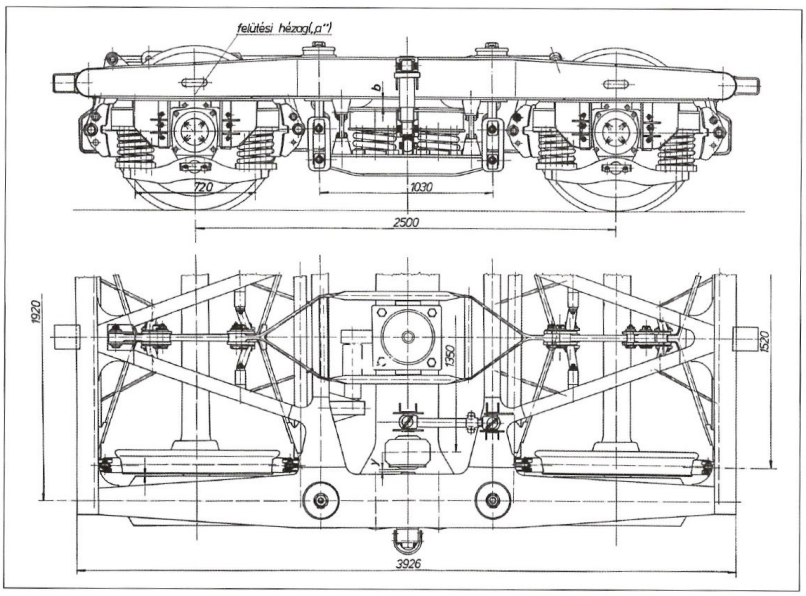

Fig. 6 The bogie type KALÁKA III., this type was manufactured in the largest number from the family

The manufacturing of the bogie type KALÁKA was taken over also by the Győr Wagon Factory in the middle of 1960s. Transition occurred to the application of the axle-box guidance system *Schlieren* for ensuring the elimination of the already mentioned manufacturing and aligning difficulties emerged with the V-shaped vertical guidance. The main advantage of this new axle-box guidance system was the common implementation of vertical guiding the primary damping. The disadvantage of this *Schlieren* system was that higher maintenance costs. This phase C of the development process can be summarized by the next way:

Phase C: KALÁKA IV, bogie type KALÁKA with axle-box guidance system *Schlieren*:

Changes in comparison with phases A and B:

- the changing of the V-shaped vertical axle-box guidance to the system *Schlieren*,
- double pendula bolster suspension,
- longitudinal bolster connecting arms, instead of bolster guidance-bolster sliding supports,
- application of cylindrical roller bearing instead of spherical roller bearing.

A big and very important changing was fulfilled in the development of the bogie family KALÁKA by the appearance of bogie types Dk 90 and Dk 91 constructed by Tibor Peták Chief of Construction in the MÁV Dunakeszi Work and László Murárik bogie designing-engineer. With types Dk 90 and Dk 91 a new bogie type was born, it is able to run at 160 km/h with very good running characteristics. In our paper this phase of the development is named phase D.

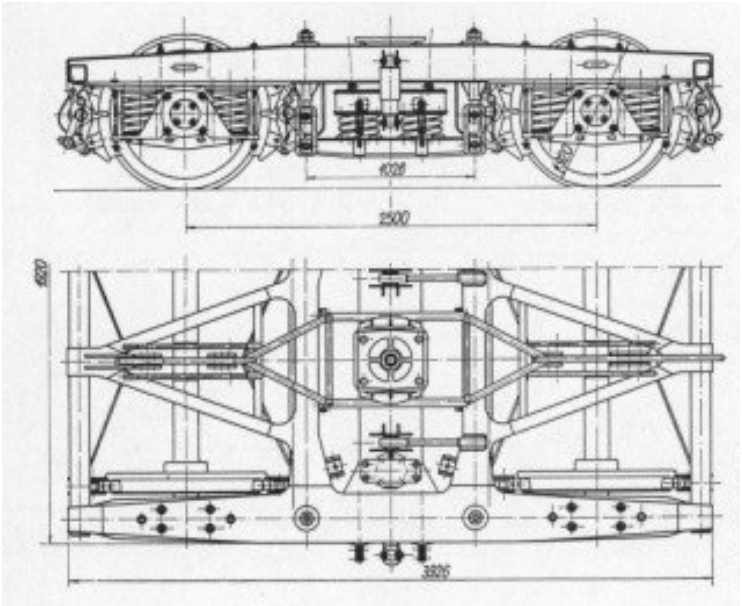

Fig. 7 The bogie type KALÁKA IV. with axle-box guidance system *Schlieren* to give a better vertical axle-box guidance and vertical damping

Phase D: Bogie types Dunakeszi (Dk) 90 and 91 changes in comparison with phases A, B and C:

- elastic axle-box guidance instead of the rigid one,
- sprung adjustable bolster suspension of long connecting arms,
- application of lateral dampers,
- introduction of bearings with cylindrical rollers

Phase E: The youngest types of the bogie family KALÁKA

From 2001 number 136 Class Bhv and number 13 Class BDt carriages were rebuilt and modernised. These renewed vehicles were mounted with significantly renewed bogies. These bogie types: KALÁKA III. 121, Dk 131[10].

Fig. 8 The modernized KALÁKA III. as bogie type Dk 131

3. THE BOGIE FAMILY *KALÁKA* UNDER THE CARRIAGES

It has been mentioned above that the KALÁKA bogie family was developed in the Dunakeszi Work. Now then it is obvious that the carriages built in this work got a certain type of this bogie family. Some modernised bogie types - for example Dk 90 and 91 - were developed from the middle of 1970 by bogie family KALÁKA. The carriage types equipped with bogies from family KALÁKA are as follows:

[10] The Ganz Hunslet Co. went shares in the mentioned suburban vehicle renewal work. Two bogie types GH 120 and GH 120-S were born as a result of this work.

For suburban traffic:

- Open Standard with steam and electric heating
- Open Standard with electric heating,
- Open Standard Brake,
- Open Standard Driving Trailer (by steam hauling engine types 324 and 424),
- Driving Open Brake Standard (by diesel hauling locomotive types M40 and M41 and for electric hauling engine types V42 and V43)[11]

Fig. 9 The original KALÁKA III. under a classical suburban carriage Class Bah with its original window construction at Budapest – East Station

For internal traffic:

- Open First,
- Corridor First,
- Open Standard,
- Buffet Standard,
- Generator Van.

More than 2000 vehicles with the bogie family KALÁKA and the bogie types Dk 90 and Dk 91 were manufactured in Dunakeszi Work between 1958 and 1982 mostly for the Hungarian State Railways. The mentioned bogie constructions operated and some of them operate as yet with a great success both in the suburban and in the internal long distance traffic.

[11] 10 driving trailer open second brake with bogie type KALÁKA and 10 open second were delivered to Greece and Vietnam from the suburban carriage family Bahv.

4. CONCLUSIONS

In the middle of the 1950s the Hungarian State Railways decided to develop the suburban traffic around the Hungarian capital Budapest. The developing and manufacturing tasks of the railway vehicle side namely the passenger carriages were given to the relatively new state owned Dunakeszi National Company. New vehicles: open standard and open standard driving trailer in a lot of variants were needed to this traffic. A new bogie type also was developed by the young engineer group of the company for these suburban vehicles. This new bogie was named KALÁKA, it is an acronym formed from the two initial capitals of the family names of the three young bogie constructers in Dunakeszi. From this absolutely new bogie construction a new bogie family was born during the approximately two – three decades by the modifications and applying new construction principles due to the experiences and the new requirements. The birth of the bogie type constructions was forced by the weak points of the ancestor solutions, and by the maintenance, repairing and operational observations, as well as by the new demands in connection with the vehicles originated in the different segments of the developing railway passenger traffic. By this process new bogie and vehicle types were resulted.

5. THE CONSTRUCTOR PERSONAGES

Two company names are very oft repeated in this study in connection with the introducing very famous and successful bogie construction. These names are only shortly: the Ganz Company and the Dunakeszi Works. Engineer generations grew up, passing on their knowledge to the new followers in these companies, the same way as it is in every railway vehicle builder company. Engineer schools were developed in connection with the different vehicle systems, subsystems, groups of components and components. There are a lot of engineers whose names one has to mention in connection with bogie developing works, designing and manufacturing activities described above. They are:

Dr.Eng. Gyula Rónai: type Cak
Mr. János Kalmár – Mr. Péter Lánczos – Mr. Tibor Kardos: type KALÁKA I,
Mr. Tibor Peták: VUKV 90/C 90/Dk 90/ 90 and KALÁKA 131.
Mr. László Murárik: 91,
Mr János Cservenák – Mr. Zsolt Baráth – Mr. Péter Sziráki: KALÁKA III.121,

6. ACKNOWLEDGEMENT

This summary has been realized by the help of my numerous colleagues, friends and rail fans. Many thanks go them for providing the authors with different documents, drawings, photos, information, comments, additions and different further data. It is compulsory to mention by name Mr. László Süveges, Mr. György Villányi, Mr. Tibor Gayer, Mr. Péter Lánczos, Mr. Gyula Zákonyi, Mr. János Cservenyák, Mr. László Murárik, Mr. Tibor J. Molnár, István Polónyi, István Szécsey, András Vizi. Warm thanks go to Prof. Dr. István Zobory for vehicle technical and grammatical helps.

The second author of this paper preserves in his memory his friend and the first author of this paper, Mr. István Béres who has unfortunately passed on in the meantime.

7. REFERENCES

[1] **Boros, B.:** Album of Railway Carriage Technical Drawings. Transportation Documentary Company, Budapest, 1967. p. 267. (In Hungarian)
[2] **Csiba, J.:** The Development of Passenger Carriages. Hungarian Railway History. 1846 – 2000. Hungarian Railways Co. Budapest, 2000, p.381-430.
[3] **Lánczos, P. – Zákonyi, Gy.:** The History of Bogie Family KALÁKA. Vasútgépészet, 2016/1, p. 3-10. (In Hungarian)
[4] **Lánczos, P.:** The History of the MÁV's Passenger Carriages Class Cak, Bam, Bah. Budapest, 2008. (In Hungarian)
[5] **Varga, K.:** The History of the Railway Vehicle Works. Hungarian State Railways Co. Budapest, 2005. p. 295. (In Hungarian)
[6] **Villányi, Gy.:** The 75 Years Old Carriage Family Class Cak/Bam. Vasútgépészet. 2017/3, p.6-11. (In Hungarian)
[7] http://www.grotius.hu/doc/pub/GTFGTG/2010_149_abelovszky_tamas_szakdolgozat.pdf
[8] http://www.kosanyo.hu/html_doc/v55a.htm

ENHANCED SAFETY CONCEPT FOR WHEEL-SET AXLES: THE PATH FROM SCIENTIFIC RESEARCH TO INNOVATION IN PRODUCT DEVELOPMENT

Martin RIEGER[1] and Franz-Josef WEBER[2]

[1]Departement of Operational Integrity and Railway Vehicles
Institute of Thermal Turbomachinery and Machine Dynamics
Graz University of Technology
A-8010 Graz, Austria
martin.rieger@tugraz.at

[2]Systems Development
Engineering Bogies
Siemens Mobility GmbH
A-8020 Graz, Austria
franz-josef.weber@siemens.com

Received: September 12, 2019

ABSTRACT

The safety of the wheelset system is based on safe design, careful production and systematic monitoring in maintenance. For each of these action fields individual standards, product requirements and instructions have been developed over the years, basing on the background of research and operational experience. The method for establishing inspection intervals will now be based on a new calculation method. This method considers short crack growth, crack retardation by overloads, and crack retardation by oxidation. In addition, the effects of residual stresses have been taken into consideration. To get these results, 35 crack propagation tests on axles in dimension 1:1 have been carried out. An optimized resonance test bench was used to carry out the test in an acceptable time. To be able to monitor crack propagation during these fatigue tests, a new device for real-time detection and measurement of cracks was developed and added to the test bench. The residual stresses acting on the crack tip have been observed by additional strain gauges in parallel. The new method opens the path for the development of new products such as axles produced by high strength steel, axles with specialized surface design or axles with extended hollow bores.

Keywords: Wheel-set axle, crack propagation, lightweight design

1. INTRODUCTION

The safety of the wheelset system is based on the interrelation of the three fields of action

- dimensioning and design
- careful production
- systematic monitoring in service and maintenance.

For each of these action fields individual standards, product requirements and instructions have been developed over the years, basing on the background of research and operational experience. These practices ensure a high safety level [1]. However to develop new products and new use of existing products the existing methods and rules had to be reassessed.

2. COMON RESEARCH

As the acceptance of a new safety-relevant method can´t be elaborated from one player in the railway sector alone, new methods were developed in joint project groups of operators, system integrators and axle manufacturers.

2.1 EBFW 1

The first project lasted from 2001 until 2004. Results after these four years of research have been the fatigue behavior of four different axle materials and partially validated load assumptions of highspeed trains. [2]

2.2 EBFW 2

The second project run from 2006 until 2009. The main result was a basic method for crack growth calculation with an analytically described stress intensity factor and fracture mechanic characterization of the materials EA4T and 34CrNiMo6. The results of the small specimens were verified in plain bending fatigue test at three axles of the material EA4T in scale 1:1 each of them with one crack. Additionally to the main result load assumptions of locomotives and regional trains were investigated. [3]

2.3 EBFW 3

The third project run from 2014 until 2019. The main result was an enhanced method for crack growth calculation taking into consideration short crack growth the influence of load sequences through plastic and oxide crack closure, and residual stresses. Fracture mechanic behavior of the materials EA4T and EA1N were characterized by small scale specimens. The transferability from small scale specimens to 1:3 scale specimens and full scale specimens has been investigated. The results of the crack growth calculations were verified at 35 full-scale axles each of them with three cracks. [4]

3. INNOVATIVE EXPERIMENTS

To carry out such an important number of experiments in an appropriate time, new experimental methods were used in the EBFW 3 project. These experiments were performed to gain a better understanding of crack propagation in wheelset axles during loading with variable load sequences. A further reason for the number of experiments was, that the models developed for the calculation of the crack propagation rate were verified with these experiments.

3.1 Fatigue crack growth model

In the course of the research project, the previously, in the predecessor project, used equation for crack propagation rates, the original NASGRO equation, was used and modified step by step. The decisive influences on crack growth were defined as short crack growth as well as sequence and overload effects. The mentioned effects were implemented as additional models in the NASGRO equation:

$$\frac{da}{dN} = C_0 \left[\left(\frac{1-f}{1-R}\right)\Delta K\right]^n \frac{\left[1-\frac{\Delta K_{th}}{\Delta K}\right]^p}{\left[1-\frac{K_{max}}{K_c}\right]^q} \quad (1)$$

For the calculation of long cracks, Newman's closure model was used. An analytical description of the implemented models can be found in [5-8]

- fatigue crack growth threshold of short cracks [5, 6]

The fatigue crack growth threshold of short cracks with increasing crack extension, the model described in [5] is used. A cyclic crack resistance curve is used and approximated by an analytical description:

$$\Delta K_{th} = \Delta K_{th,eff} + \left(\Delta K_{th,lc} - \Delta K_{th,eff}\right) \cdot \left(1 - \left(\vartheta_1 \cdot e^{\frac{\Delta a}{l_1}} + \vartheta_2 \cdot e^{\frac{\Delta a}{l_2}}\right)\right) \tag{2}$$

- plasticity-induced load sequence effects [7, 8]

The modeling of overload effects, respectively plasticity induced load sequence effects, was performed using a modified Willenborg-Gallagher model. To describe the overload effects, a plastic zone was introduced, which is defined by material parameters. In this zone, a fictive compressive residual stress intensity factor is applied, which was induced by the overload and is described as follows:

$$K_r = max\left\{0, K_{OL} \cdot K_{max,OL} \cdot \left[1 - \left(\frac{\Delta a_{OL}}{z_{OL}}\right)^{\gamma_{OL}}\right] - K_{max}\right\} \tag{3}$$

This stress intensity factor subsequently results in an effective load ratio to:

$$R_{eff} = \frac{K_{min} - K_r}{K_{max} - K_r} \tag{4}$$

and subsequently to a retarding effect in crack propagation.

- oxide-induced load sequence effects [7, 8]

Article [7] presents investigations that show the formation of an oxide layer (see Fig. *1*) when a crack is loaded with loads below its stress intensity factor threshold.

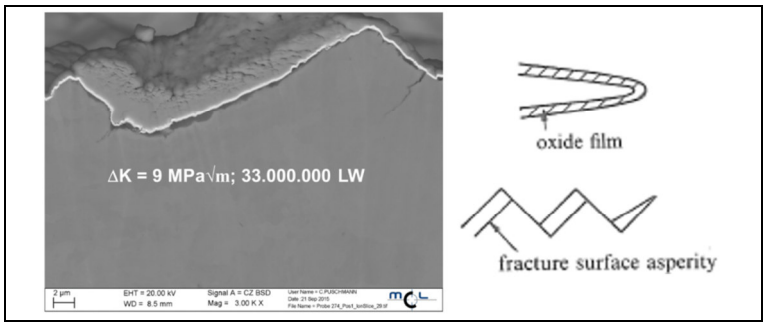

Fig. 1 Oxide layer in electron microscope .

This oxide layer which is formed by the resulting abrasion in the crack. The formation of this oxide layer causes a retardation effect. This effect was modeled using a power-law approach as follows:

$$\Delta K_{th,ox0} = \Delta K_{ox} \cdot \left(1 - R_{eff}\right)^{r_{ox}} \cdot \Delta K_{ox}^{m_{ox}} \cdot N_{ox}^{n_{ox}} \tag{5}$$

If the crack is loaded again above its threshold by lifting the loads, this oxide layer degrades again. This degradation was described with the following model:

$$\Delta K_{th,ox} = \Delta K_{th,ox0} \cdot max\left(\left[1 - \left(\frac{\Delta a_{ox}}{z_{ox}}\right)^{\gamma_{ox}}\right], 0\right) \quad (6)$$

All material parameters were determined by small sample tests.

To avoid overestimation of th crack retardation effects, the maximum crack retardation has been limited.

3.2 Optimized resonance test bench

The principle of the test bench used is that of a resonance testing machine. To optimize the test frequency and the transitions of the individual blocks in a load sequence, the masses in the test bench were reduced as far as possible. By reduction of these masses the test frequency could be increased from an average of 18 Hz to 28 Hz.A picture of the used principle and the implemented test rig is shown in *Fig. 2*

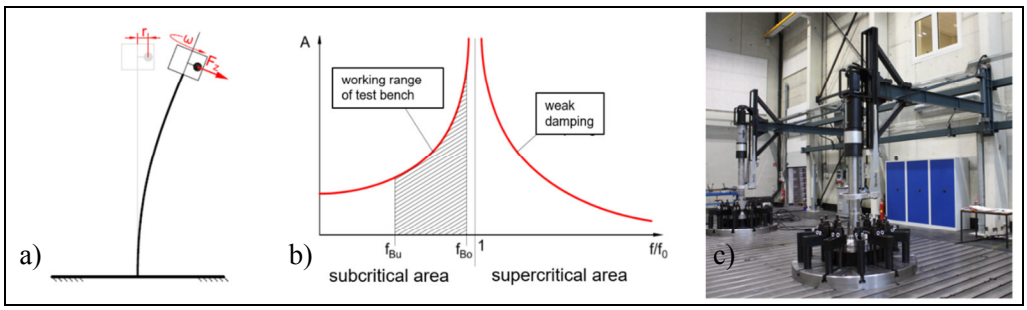

Fig. 2 Test rig principle and realized test rigs.

Fig. 2a shows the structure of the test bench principle used. The test specimen is fixed on one side and vibrated on the other side using a rotating unbalanced mass. This oscillation introduces a rotating bending moment into the test piece.

Fig. 2b shows a gain function of a weakly damped oscillating system. On the y-axis is the amplitude of the gain and on the x-axis is the frequency ratio of the current to the resonant frequency of the system. The working range of the test bench is located in the ascending section of the first bending natural frequency. To achieve the best possible performance on the test bench, the frequency ratio for a test should be in the range of f_{Bu} = 60% and f_{Bo} = 95%.

Fig. 2c shows the test benches working and realized on this principle.

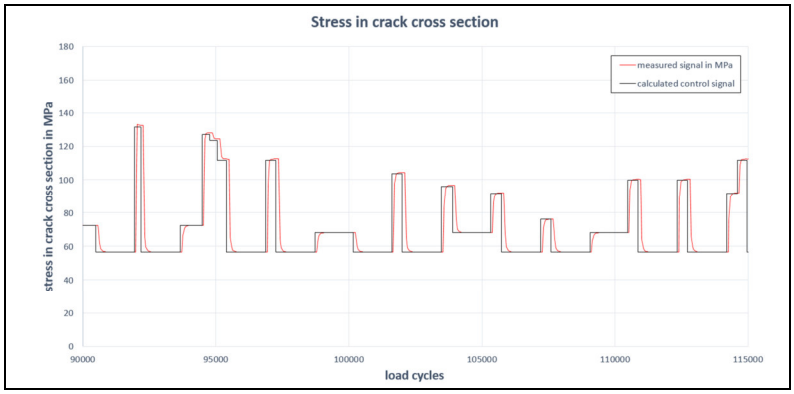

Fig. 3 Comparison of a measured test with a nominal test signal.

An exemplary section of a measured test bench signal in comparison with a control signal is shown in *Fig. 3*. Here it can be seen, that the individual blocks of a signal are only a few load cycles long. A fast transition to the next block is therefore of great interest. This requirement was very well met by the test benches implemented.

3.3 Digital image processing for real-time detection of cracks

To monitor the propagation of initiated cracks, a new device for optical real-time crack measurements was added to the test bench. All the cracks of one axle could be monitored by a digital camera with an attached telecentric objective. The image acquisition and data processing are made by a real-time system. This means that the crack length is available for post-processing in real-time. That allows the highest reliability and determinism of the overall system. A special surface treatment allows very precise detection of the crack tip. This allows accuracy of less than 50 µm to be achieved.

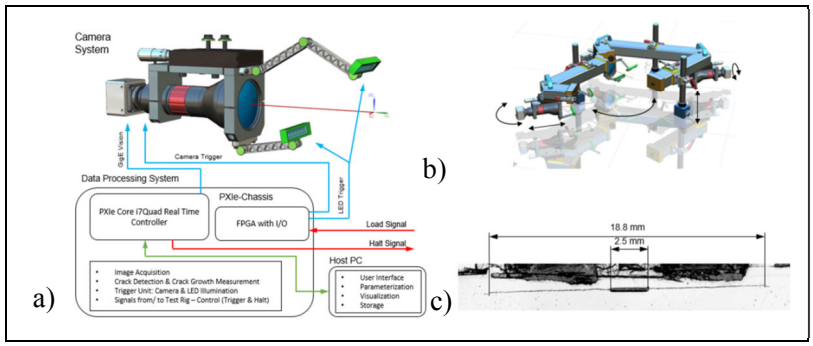

Fig. 4 Crack measurement system.

Fig. 4a shows the principle of the developed optical crack detection hardware. The suspension of all three mounted camera systems for the observation of all initiated cracks is shown in Fig. *4b*. Fig. *4c* shows a photograph with dimensions drawn.

After the first tests with these new methods, a very large scatter of the test results was found. To be able to understand this large scatter somewhat, the residual stress situation prevailing in the test specimen was examined more closely in the further course.

3.4 Measurement of residual stresses

In general, residual stresses are measured using destructive measuring methods such as cut-compliance or X-Ray depth profiles. Residual stresses, however, can vary greatly with the position of the wheelset shaft. The destructive measuring methods by principle don´t allow to measure the residual stresses exactly in the area of interest. The residual stresses might change during crack propagation test. These reasons do not allow meaningful measurement of the residual stresses before and after the test using a destructive test method. Therefore, the residual stresses were measured at the crack tip using crack tip strain gauges during crack propagation.

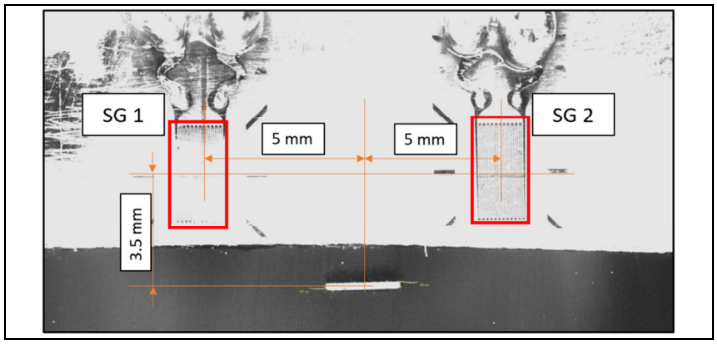

Fig. 5 Applied crack tip strain gauges

For the residual stress measurement, two strain gauges were applied to each initiated crack at a distance of 3.5 mm axially and 5 mm radially (see Fig. *5*). With these strain gauges, the strains introduced as a result of the test were continuously recorded during crack propagation.

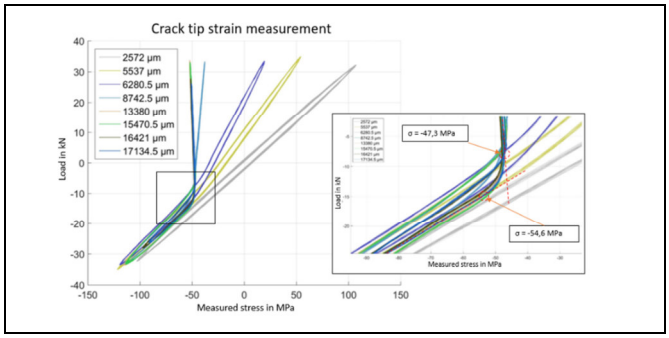

Fig. 6 Example of a crack tip strain gauge measurement signal

The stored strain signals were then converted into stresses. The applied load were plotted against the measured strains (Fig. *6*). As long as the crack does not influence the measurement, a linear relationship between the applied load and the measured strain can be seen. As soon as the crack has exceeded a certain length, a buckling point begin to evolve (Fig. *6*). If the test specimen is in a state free of residual stresses, this buckling point is close to the zero line area, in tension area, compressive stresses prevailed before

crack propagation and vice versa. After evaluation of the example shown in Fig. *6*, tensile residual stresses between 47.3 and 54.6 MPa was determined for the shown test specimen. After a closer examination of the test specimens and their residual stress condition, it was possible to explain the strong scattered results. With known residual stresses, the developed crack propagation model predicts the measured crack propagation accurately.

4. INNOVATIVE PRODUCTS BASED ON THE INNOVATIVE MEHTODS

The new models and new testing devices were used to develop better products.

4.1 Axles with special surface design

The crack propagation in axles with special surface design by cold rolling was calculated with the models developed in EBFW 3. It could be shown, that in some applications no relevant crack propagation in these axles occurs. Both the residual stresses by cold rolling and the predicted crack growth rate were verified by full scale crack propagation tests. The special surface design by cold rollinng, can be applied subsequently, even at an axle, which has been in service. As axles are a part of the wheelset, as an assembly of the axle an the wear parts wheel, brake disk and bearing, a regular change of the wear parts give the chance to improve significantly the usability of the axles.

4.2 Axles from high strength steel

Accidents with broken axles in passenger traffic are very rare. These rare accidents were in the past often in combination with the use of high strength steels. The design rules elaborated at mild steels cannot be transferred to high strength steel axleswithout additional and intensive testing. The use of the methods for material characterization and the fast testbench for fatigue testing and crack propagation testing at full scale specimens, allows intensive testing of these solutions.

4.3 Axles with extended hollow bores

The classical forges axles, do not use the method of structural lightweight construction, as forging is a method that reduces the outer diameter of a given material. The combination of tubes and joining technologies as bolting and welding gives the chance of a significant weight reduction. The new joining technologies need similar to high strength steels extensive fatigue testing and crack propagation testing at full scale specimens. As new damage mechanismens might occur e.g. fretting in the bolted connection,
The volume of the tube might be filled with compressed air. That gives the chance to use the leak-before-break assesment maybe as a permanent diagnosis and gives an enhanced safety of the system.

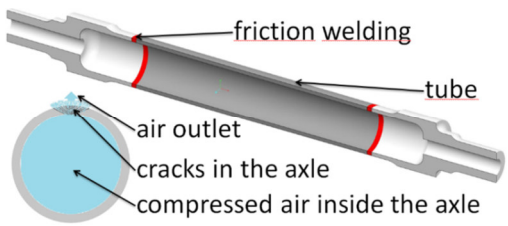

Fig. 6 Leightweight axle

5. REFERENCES

[1] **Köhler, G. / Weber, F.J.:** Die Sicherheitsphilosophie bei der Konstruktion, der Produktion und dem Betrieb von Eisenbahnradsätzen ZEVrail Glasers Annalen 135 (2011) Tagungsband SFT Graz 2011

[2] **Traupe, M. / Meinen, H. / Zenner, H.:** Sichere und wirtschaftliche Auslegung von Eisenbahnfahrwerken : Abschlussbericht / M. Traupe; H. Meinen; H. Zenner ; Bd. 1/2: Hauptteil [und Anhang] TU Clausthal, Inst. für Maschinelle Anlagentechnik und Betriebsfestigkeit, Abt. für Systemverhalten und Betriebsfestigkeit; Clausthal-Zellerfeld; 2004

[3] **Luke, M.; / Varfolomeev, I./ Lütkepohl, K./ Esderts, A.:** Fatigue crack growth in railway axles: assessment concept and validation tests; Engineering Fracture Mechanics 78/5 (2011) 714-730

[4] **Gänser H.-P. / Jenne, S. / Weber, F.J.:** Forschungsprojekt Eisenbahnfahrwerke 3 – Ergebnisse 45. Tagung „Moderne Schienenfahrzeuge“, 14.-17. April 2019, TU Graz

[5] **Maierhofer J, / Pippan R. / Gänser H.-P.:** Modified NASGRO equation for physically short cracks. International Journal of Fatigue 59 (2014)

[6] **Maierhofer J. / Pippan R. / Gänser H.-P.:** Modified NASGRO equation for short cracks and application tot he fitness for purpose assessment of surface-treated components. Procedia Material Sciences 3 (2014)

[7] **Maierhofer J. / Gänser H.-P. / Pippan R.:** Crack closure and retardation effects – experiments and modelling. Procedia Structural Integrity 4 (2017)

[8] **Gänser H.-P. / Maierhofer J.:** EBFW3 Milestone Report M3.2-3.4: Fatigue crack growth model development and parameter determination from small scale tests.

MONITORING SYSTEM OF WHEEL/RAIL CONTACT FORCE BY MEANS OF THERMAL IMAGING

Daisuke YAMAMOTO

Railway Technical Research Institute
Railway Dynamics Division, Computational Mechanics Laboratory
2-8-38, Hikari-cho Kokubunji-shi,
Tokyo, Japan

Received: September 9, 2019

ABSTRACT

This paper describes the monitoring system of wheel/rail contact using the thermal imaging, which was developed by improving the visualization method presented in the Burstow's study. It is important to understand definitely a tangential force acting between the wheel and the rail in order to know the dynamics characteristics of the railway vehicles in detail. On the other hand, it is difficult to understand the condition of wheel/rail contact during the railway vehicle running, because the sensor is not placed on a track close enough to the rail head level. To solve this problem, a new method for digitalizing the contact point of the wheel/rail by means of themal imaging was proposed in our previous study. In this paper, firstly, we review the performance of the monitoring system of wheel/rail contact by means of thermal imaging based on our proposed method. Secondly, as an application example of the monitoring system, we propose a simple inspecting method of the location of large lateral force. In order to verify the validity of our technique, the vehicle running test using the actual coach, which has a measuring wheelset of the wheel/rail contact force, is carried out on RTRI test line. As a result, it was confirmed that it is possible to estimate a occurring point of large lateral force during coach running on the test line that has curved sections and a turnout.

Keywords: wheel/rail, thermograhic camera, flash temperature, large lateral force, simple inspecting method

1. INTRODUCTION

Reducing a lateral force acting at a contact point of wheel/rail when a train runs is effective in improving a running safety or improving an efficiency of a track maintenance work. The lateral force can be measured accurately by using a vehicle equipped with a measuring wheelset that can measure wheel/rail contact force in a train running test. However, since the measuring wheelset is very expensive, and high level technical knowledge is required for a person who handle it it is difficult to conduct frequent measurements of the lateral force.

On the other hand, there are ideas that earlier detection of abnormal track condition by high-frequency inspection is more effective than precise measurement of a lateral force using measuring wheelset. It is well known that the lateral force is generated when a wheelset moves in large in lateral direction. Therefore, it is considered that a location where a large lateral force is generated can be detected easily if a measuring method of accurate motion of a wheelset in lateral direction is developed.

In the previous studies related to measuring method of motion of the wheelset in lateral direction, a visualization method of wheel/rail contact by means of thermal images proposed by Burstow et al. was presented [1]. In addition, we proposed a monitoring system of the wheel/rail contact. In the system we proposed a method for locating position of wheel/rail contact accurately during train running by improving the visualization technique proposed by Burstow et al. [2]. This measuring device based on the proposed method is called monitoring system of wheel/rail contact (hereinafter called "the monitoring system").

In this paper, firstly, the performances of the monitoring system proposed in our previous studies are reviewed. Secondly, as an application example of the monitoring system, a simple inspecting method of the location where large lateral force is generating is proposed and the result of running test conducted using an actual coach to verify the proposed technique is described.

2. DEVELOPMENT OF THE MONITORING SYSTEM

2.1 Background

In our previous studies [3][4], in order to investigate the characteristics of tangential force of the wheel/rail, a numerical analysis and an experiment were conducted. To conduct the numerical analysis and the experiment accurately, it is important to reflect an actual contact condition of the wheel/rail during train running. Figure 1 shows the difference in the view of the contact position between wheel and rail. This figure means that it is necessary for confirming the contact position of the wheel/rail to lower the view point to the rail head level. However, the camera cannot be mounted above the rail head level during train running due to the risk of its collision with the track structure. Hence, we applied the visualization method by means of the thermographic camera as the confirmation technique of the wheel/rail contact with the camera that can avoid collision with the track structure. This visualization method of the wheel/rail contact was presented by Burstow, et al. [1], and thereafter, a new technique for locating the wheel/rail contact point more precisely by improving the visualization method was proposed [2]. Specifically, in order to measure the motion of the wheelset, a method to digitize the thermal images from the relation between the metal comb-formed scale and the number of pixels was contrived, and using the obtained digital data, the contact location can be processed in detail on the computer.

On the other hand, the monitoring system cannot be used to locate the contact point stably in all environmental conditions. For example, when the surface temperature of the target object is high, or there are large temperature fluctuations, it may be

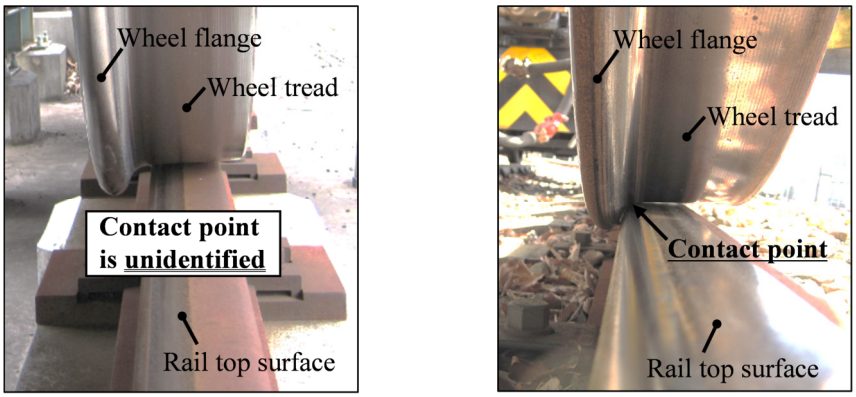

(a) From life guard height (b) From rail head height

Fig. 1 Difference of view of the contact point of wheel/rail

impossible to locate the wheel/rail point because the contrast between contact and non-contact parts of the wheel/rail is not clear. Therefore, in this study, it is a precondition to use the monitoring system under suitable environmental condition of the thermos-graphic camera.
In the case where the monitoring system is operated in the actual field, the problem mentioned above would be solved by devising the method at the time of use such as performing measurement at night when the ground temperature is relatively is low and the temperature evenness is small.

2.2 Component of the monitoring system

The monitoring system consists of the small and light thermographic camera mounted under a bogie frame of a railway vehicle, and a personal computer on a cabin of railway vehicle. In order to locate accurately the contact point of the wheel/rail, the thermographic camera is installed behind 1.34m and above 0.21m height from the contact point of wheel/rail as shown in Fig.2. In addition, the environment around the camera is a condition in which iron powder due to the flange/rail contact is scattered and dust from the railway vehicle flies when the railway vehicle is running. Therefore, in order to enhance the dust proof effect, a film that transmits infrared rays is installed in front of the thermographic camera. The major specification of the thermographic camera is shown in Table 1.

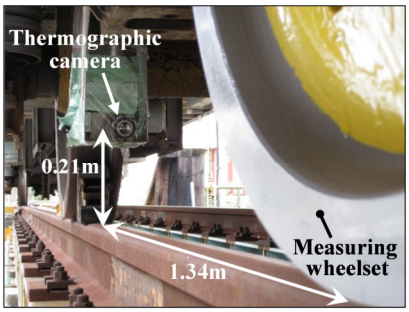

Fig. 2 Thermographic camera mounted under a bogie frame

Table 1 Major specification

Pixel resolution, pic	320×240
Thermal range of measurement, degrees C.	20～40
Accuracy, degrees C.	±0.5
Available environmental temperature, degrees C.	5～40
Weight, kg	About 0.25
Size, mm	53×81×60
Frame rate, Hz	20(Maximum)

2.3 Contact point of wheel/rail and its search areas

In this paper, the contact point of the wheel/rail is called the position at which the temperature in a searching area is the highest. The left side and the right side of the wheelset in running direction are the inside wheel/rail and the outside wheel/rail respectively because a test line in RTRI described in the Chapter 4 mainly consists of left curves and straight lines. Therefore, the inside search areas and the outside search areas are set separately for convenience. Both search areas of wheel/rail on the thermal images are shown in Fig. 3. The one search areas is on the wheel tread close to the contact point between the wheel flange and the rail gauge corner and another area is on the wheel tread on the opposite side of the wheel flange close to the contact point between the wheel tread and the rail top surface as shown in Fig. 3. The inside search areas and the outside search areas are shown in Fig. 3(a) and Fig.3(b) respectively.

Here, among the inside search areas, the contact position of wheel/rail is the position at which the flash temperature is the highest. This reasons are as follows. Under the condition of the small slip rate occurrence between the wheel and the rail such as when the vehicles run on the straight line etc., the contact position of the wheel/rail cannot be located accurately because the difference of the surface temperatures between 8 points is little. Therefore, when the temperature of search area judged having the highest temperature among the eight search areas is one degree C or more larger than the average value of the maximum temperatures of the eight search areas, it is judged as an analysis result to be correct and output it, and the results except for it output zero.

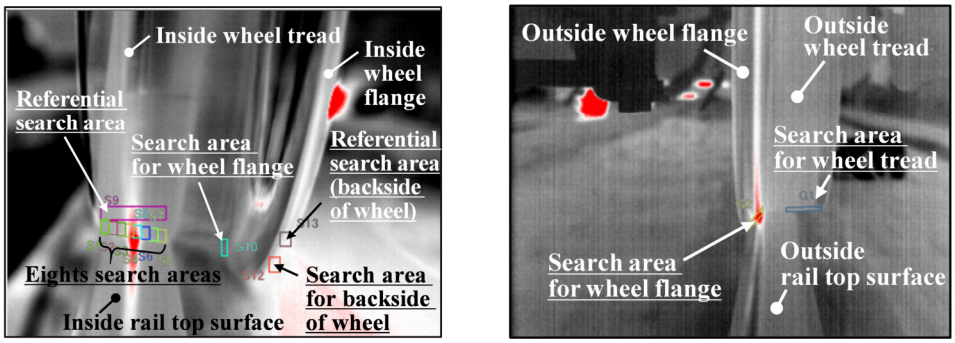

(a) The search area of inside wheel/rail (b) The search area of outside wheel/rail

Fig. 3 Search areas on the thermal imaging

3. ESTIMATION TECHNIQUE OF LOCATING POSITION GENERATING LARGE LATERAL FORCE

3.1 Theory of the Estimation Technique

The results of a contact geometry analysis calculated by a combined model of a rigid wheel and a rigid rail are shown in Fig. 4. If the wheelset moves to one side largely, the contact position of wheel/rail on the same side moves to the wheel flange side. A wheel radius at this position, which is a rolling radius, and a contact angle are large because there is a slope on the wheel tread.

In a vehicle dynamics analysis, the lateral force acting between the wheel and the rail is represented as follows;

$$Y_L = -Q_L \tan\alpha_L + F_{YL}/\cos\alpha_L \tag{3-1-1}$$

$$Y_R = Q_R \tan\alpha_R + F_{YR}/\cos\alpha_R \tag{3-1-2}$$

where, Q_L and Q_R are a wheel load, F_{YL} and F_{YR} are a lateral creep force, α_L and α_R is contact angle. Note that subscript L and R mean left and right respectively. In addition, F_{YL} and F_{YR} are determined by the product of the lateral creep coefficient and the slip ratio in lateral direction which are defined as follows;

$$S_{YL} = [(X_w + r_L\varphi_w)/vel - \psi_w] / \cos\alpha_L \quad (3\text{-}1\text{-}3)$$

$$S_{YR} = [(X_w + r_R\varphi_w)/vel - \psi_w] / \cos\alpha_R \quad (3\text{-}1\text{-}4)$$

where, r_L and r_R are the rolling radius, φ_w and ψ_w are the angle of wheelset in rolling direction and in the yawing direction respectively. vel is velocity, X_w is displacement of the wheelset in lateral direction. Thus, since the rolling radius and contact angle of the wheel become large (see Fig. 4) when the wheelset moves to one side, it is found that the lateral force becomes large based on formula (3-1-1) to formula (3-1-4). When the railway vehicle runs in the straight section with track irregularity and the curve section, the front wheelset of each truck moves to the outside rail. Therefore, if the contact position between wheel and rail of the front wheelset is located accurately by using the monitoring system, the position of large lateral force can be estimated because the movement of the wheelset can be detected qualitatively.

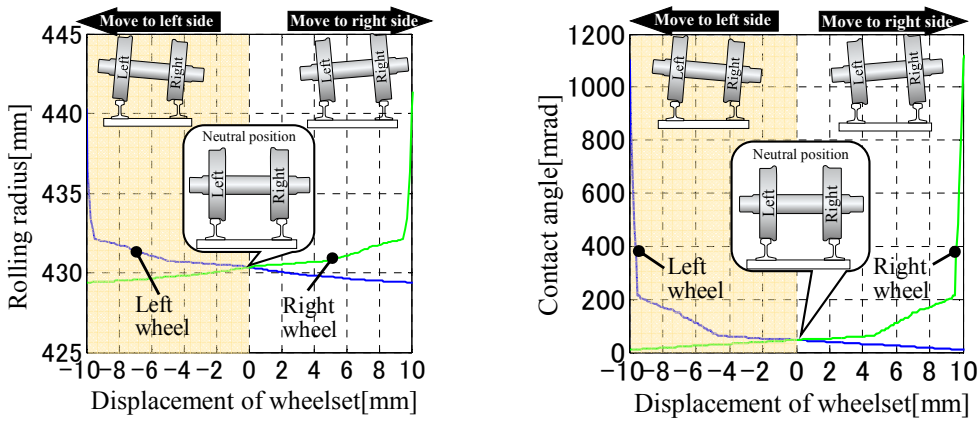

(a) Rolling radius (b) Contact angle

Fig. 4 The results of a contact geometry analysis calculated by a combined model of a rigid wheel and a rigid rail

3.2 Validation method of the estimation technique

We verify the proposed estimation technique by way of comparing the flash temperature measured by the monitoring system with the lateral force by the measuring wheelset. In order to measure the lateral force in a running test, the measuring wheelset based on a new continuous measuring method of wheel/rail contact force described in the paper [5] is fabricated. The position of strain gages and strain bridges is shown in Fig. 5(a). The linearity of the strain bridges for measuring wheel force, a lateral force and a tangential force is verified by the way to act the static load to the wheel tread using the testing device for the measuring wheelset in RTRI (see Fig. 5(b)). The merit of the new continuous measuring method of wheel/rail contact force is that the drift of zero point is small and the vertical force, the lateral force, and the tangential force can be measured continuously with designated processing unit equipped with A/D converter, low pass filter, counter, digital signal processor and D/A converter. The diameter and the back gauge of this measuring

wheelset is 821mm and 990mm respectively. The wheel tread profile is the modified arc wheel profile used in Japan Railway conventional line.

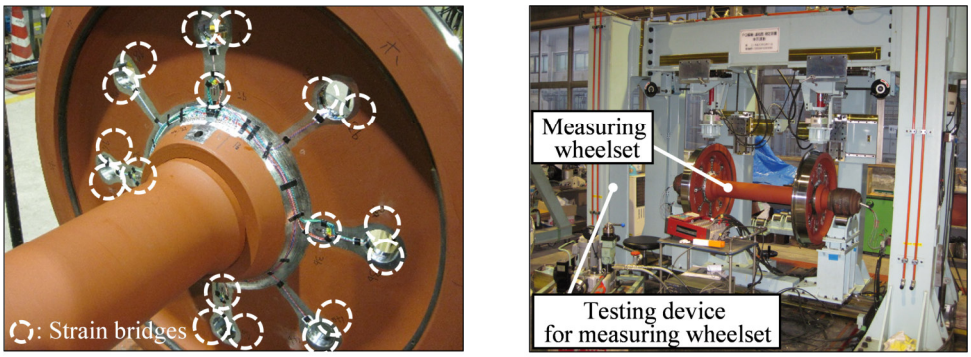

(a) Strain gages and strain bridges (b) Verification of the measuring wheelset

Fig. 5 Fabrication of the measuring wheelset

4. VERIFICATION OF THE PROPOSED ESTIMATION TECHNIQUE BY RUNNING TEST

4.1 Overview of the running test

In order to verify the proposed estimation technique, a running test in which a diesel locomotive pulls a coach is carried out in the RTRI test line under sunny or cloudy environmental conditions (see Fig. 6). The flash temperature of the wheel/rail contact of the measuring wheelset is measured by the monitoring system. At that time, the lateral force is measured by the measuring wheelset described in Section 3.2. The

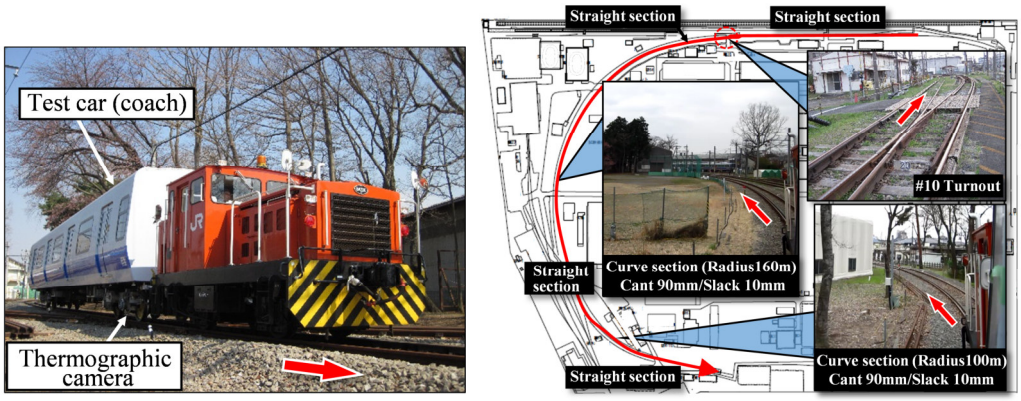

(a) Test car (coach) (b) Map of RTRI test line

Fig. 6 Running test on RTRI test line

brake device equipped with the front truck of the coach is not operated because the temperature of the wheel tread might become high due to the operation of the brake.

4.2 Relationship between flash temperature and lateral force on the inside wheel/rail

The experimental result on the inside wheel/rail is shown in Fig. 7(a). The velocity of the train is 10km/h. The black line and the gray line indicate the lateral force and flash temperature in the search area for the wheel tread relatively. The vertical axis indicates the normalized value of each running test result (Y_L is the inside lateral force and T_L is the flash temperature in the wheel tread search area as shown in Fig. 3(a).).

In the point of turnout (see point A in Fig. 7(a)), it is confirmed that both the lateral force and the flash temperature in the wheel tread search area become large suddenly. In the two curved sections with radius of 160m and 100m (see point B and C in Fig. 7(a)), the monitoring system can measure the periodically fluctuating motion in the yawing direction, and the position generating the flash temperature agrees well with that acting the lateral force. Here, the flash temperature in the wheel tread search area is approximately 22 degree C. near the rail joint at the point D in Fig. 7(a).

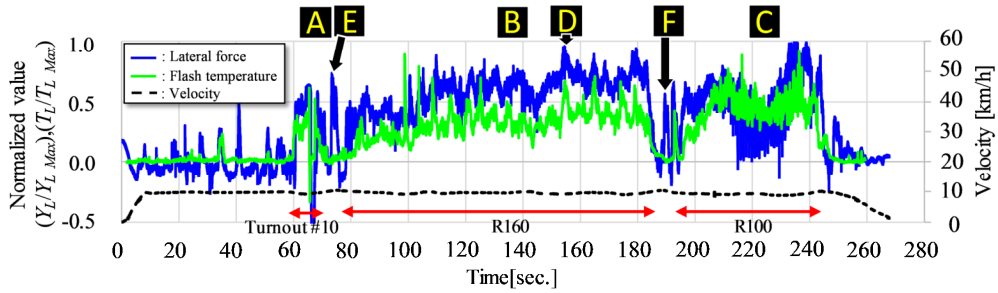

(a) Comparison between lateral force inside wheel/rail and flash temperature in search area inside wheel tread

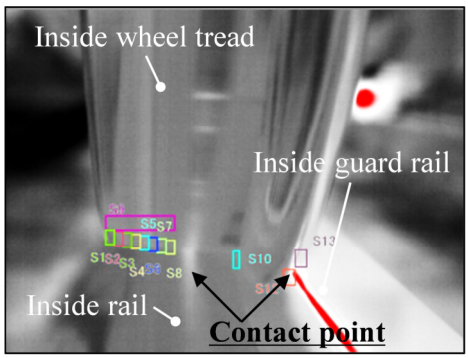

(b) Contacts at turnout

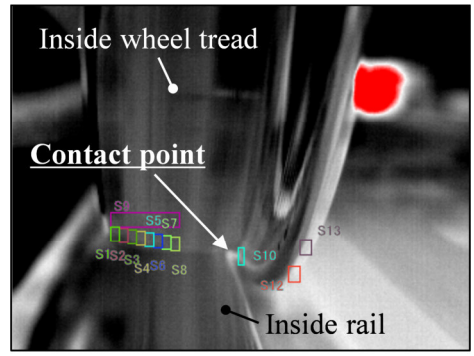

(c) Contact at point F in Fig.7(a)

Fig. 7 Experimental result on the inside wheel/rail under the velocity of 10km/h

On the other hand, although the lateral force becomes the large minus value at the crossing of the turnout (see point A in Fig. 7(a)) and the large plus value at the straight sections after curve section (see point E and F in Fig. 7(a)), flash temperatures corresponding to these lateral forces were not confirmed. The former is because the wheel

backside of the inside wheel touches the inside guard rail as shown in Fig. 7(b). The latter is because the wheelset was displaced momentarily to the inside rail, and the inside wheel flange touched the inside rail as shown in Fig. 7(c). In these cases, it is considered that the estimation of the locating point of the large lateral force is possible by confirming the flash temperatures in the search areas for the backside of inside wheel and the inside wheel flange.

4.3 Relationship between flash temperature and lateral force on the outside wheel/rail

The experimental result of the outside wheel/rail at a velocity of 10km/h is shown in Fig. 8. The black line and the gray line indicates the lateral force and flash temperature in the search area for the outside wheel flange respectively. The vertical axis indicates the normalized value of each running test result (Y_R is the outside lateral force and T_R is the flash temperature in the wheel flange search area as shown in Fig. 3(b).).

In the point of turnout (see point G in Fig. 8(a)), it was confirmed that the lateral force and the flash temperature in the wheel flange search area become large suddenly. As mensioned above, the reason is why the outside wheel runs from a tongue rail to a lead rail as shown in Fig. 8(b). At that time, the absolute value of the flash temperature in the wheel flange search area is approximately 23 degree C. In the two curved section with a radius of 160m and 100m (see point H and I in Fig. 8(a)), the periodically fluctuating lateral force synchronized with the wheelset movement in the yawing direction can be identified. The monitoring system can also measure the periodically fluctuating flash temperature in the wheel flange search area as the same as the lateral force. The position generating the flash temperature in the wheel flange search area agrees well with that generating the lateral force. Here, the flash temperature in the wheel flange search area is approximately 28 degree C near the rail joint at the point J in Fig. 8(a).

On the other hand, the flash temperature in the search area for the wheel flange cannot be confirmed at the point K and L in Fig. 8(a). This is because the wheelset moves to the inside rail, and the outside wheel flange separates from the outside rail gauge corner as shown in Fig. 8(c). In this case, it is considered that the estimation of the locating point of the large lateral force is possible by confirming the flash temperature in the search area for the outside wheel tread as shown in Fig. 8(c) and/or that for the inside wheel flange.

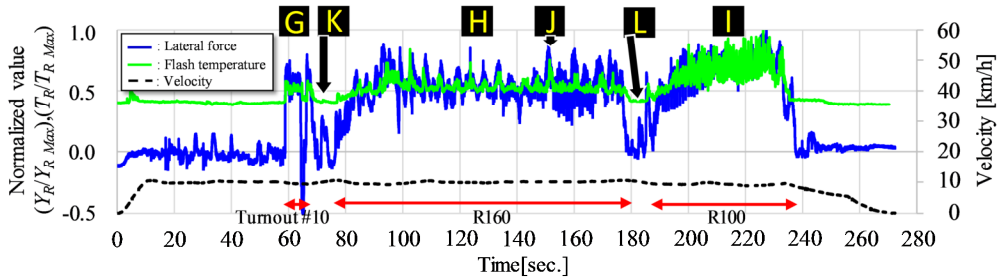

(a) Comparison between lateral force outside wheel/rail and flash temperature in search area outside wheel flange

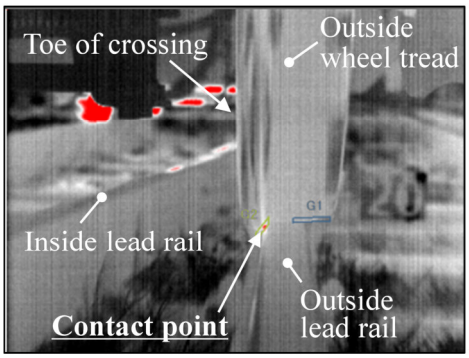

(b) Contact at turnout

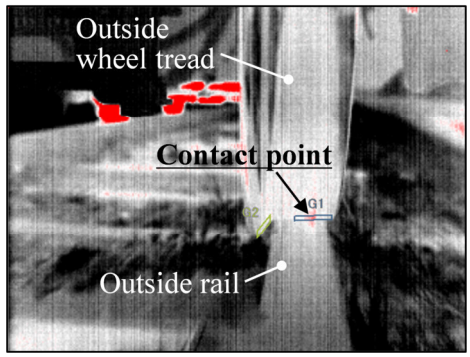

(c) Contact at point K in Fig.8(a)

Fig. 8 Experimental result on the outside wheel/rail under the velocity of 10km/h

From the experimental results described in Chapter 4.2 and Chapter 4.3, it is considered that the locating position of the large lateral force can be estimated by way of combining with the outside and the inside flash temperature, because the position of the flash temperatures agrees well with that of the lateral forces in both the inside and the outside of the wheel/rail. On the other hand, if the velocity decreases in the curved section, the difference of relation between the lateral force and the flash temperature in the all search areas on the wheel become large due to the reduction of the frictional heat at the contact point of the wheel/rail. This fact indicates that in estimating the locating position of large lateral force with the proposed monitoring system it is important to make the test train run with a constant velocity.

5. CONCLUSION

In this paper, we reviewed the performance of the monitoring system of wheel/rail contact developed by RTRI, and the simple estimation technique of the locating position generating the large lateral force was proposed. In addition, in order to verify the proposed technique, the running test was carried out using the actual coach under suitable condition for the thermographic camera. As a result, we confirmed that the peak position of the flash temperature of the wheel/rail contact agrees well with that of the lateral force under the constant velocity condition.

As an application example of the proposed technique, it is considered that if the proposed technique is applied to a simple inspecting method of the locating position acting the large lateral force in local line, the technique will contribute to the planning efficiency of the track maintenance work.

In the future, we plan to use the proposed monitoring system of the wheel/rail contact for confirming test results in order to solve the various issues related to wheel/rail contact.

6. REFERENCES

[1] **Burstow, M. - De Podesta, M. - Pearce, J.:** Understandng wheel/rail interaction with thermographic imaging. Proc. of the 22nd IAVSD-Symposium: Manchester, 2011. Paper No.105.

[2] **Yamamoto, D.:** Improvement of method for locating position of wheel/rail contact by means of thermal imaging. Quarterly Report of RTRI. Vol.60, No.1, 2019, p.65-71.

[3] **Yamamoto, D.:** Numerical analysis of wheel/rail contact characteristics based on actual wheel profiles, Quarterly Report of RTRI. Vol.52, No.3, 2011, p.129-135.

[4] **Yamamoto, D.:** Technique of reducing steady lateral force by providing micro-ribbed wheel tread profile, Proc.of the 9th International Conference on Railway Bogies and Runing Gears (BOGIE'13) (Ed. byProf. I. Zobory), BME Department of Railway Vehicles, Aircraft and Ships, Budapest, 2013, p.135-143.

[5] **Ishida, H. - Ueki, K. - Fukazawa, K. - Tezuka, K. - Matsuo, M.:** A new continuous measuring method of wheel/rail contact force, Quarterly Report of RTRI, Vol.35, No.2, 1994, p.105-111.

A DISCUSSION ON THE CONCEPT AND PERFORMANCE OF DERAILMENT DETECTOR

Hayato YONEMORI[1], Hiroto OYAMA[1], Satoshi ICHIKAWA[1], Masaki NAGAMOTO[1], Shigeki MATSUOKA[1] and Naoki KAWADA[2]

[1]Engineering & Technical Research Headquarters
Japan Transport Engineering Company
3-1 Okawa Kanazawa-ward Yokohama-city Kanagawa, Japan
[2]Department of Mechanical Engineering
Saitama Institute of Technology
1690 Fusaiji Fukaya-city Saitama, Japan

Received: September 12, 2019

ABSTRACT

Derailment accidents are one of accidents which should be prevented. But it is really difficult to eradicate these. Generally, harm of derailment accidents itself is small, but harm of secondary accidents (e.g. crash or rollover) is serious. To prevent secondary accidents, it is important to detect an accident and to notify surround trains of an accident as soon as possible. To realize that, sensor integrated derailment detector (DD) was developed. It can detect 3 types of accidents (Derailment, Rollover, Crash) by analysing acceleration data with 5 algorithm. It has 2 derailment algorithm, 1 rollover algorithm and 2 crash algorithm. As for derailment algorithm, it focused on 2 derailment phenomena. One phenomenon is falling of wheel-set from rail. The fall height of derailment is only the height of rail (e.g. 150mm in Japan). It is lower than other transportation, so it is very difficult to detect. The other is running on a rough road (e.g. sleepers and ballast). To define the threshold of each algorithm, data of regular passenger service in Greater Tokyo area had been collected. After that, many experiments were conducted to check the verification of derailment algorithm and succeeded. If 1 of 3 types of accidents is detected, it activates train protection radio (TPR) and notify a driver of an accident to prevent a secondary accident. TPR is to notify surrounding trains within a radius of 2 km of an accident. It also records x, y, z, acceleration data for 2 minutes before an accident and for 1 minute after an accident to analyse movement of a train. Culletnly, 2000 sensor integrated DDs are installed in 1000 trainsets operated by JR-EAST. It succeeded to detect 2 real accidents (SAGAMIKO derailment-crash accident and KAWASAKI crash-rollover accident). Through these accidents, the importance of DD was proved because it prevented secondary accidents. These support safe operation in Greater Tokyo area renowned for the highest density transport around the world, but it is installed in a cab only because of low cost-effectiveness of monitoring each bogie. To solve this, the DD with twin-sensor was developed in 2018. This characteristic is to divide into a mainbody and an acceleration sensor. A main body consists of a CPU and a memory. By monitoring 2 acceleration sensors with 1 CPU, it succeeded to reduce the number of CPUs. As for reliability, double system configuration for a CPU, acceleration snsor and relay was adapted to prevent malfunction.

Keywords: derailment detector, derailment, safety, condition monitoring

1. INTRODUCTION

Derailment accidents itself is hard to prevent. In recent years, the number of derailment accidents has been decreasing. But it isn't rooted out because it is difficult to identify causes of derailment. Generally, harm of a derailment accident itself isn't serious but harm of a secondary accident is serious. To prevent secondary accidents, it is important to detect derailment as soon as possible and notify surrounding trains of an accident at that time. To realize that, sensor integrated derailment detector (DD) was developed in 2008. This device can detect derailment, rollover and crash by analyzing acceleration data with 5 algorithm. The verification of algorithms was confirmed through experiments which a unused train fell from rail. As a result, it succeeded to detect 2 real accidents and prevented secondary accidents by notifing surrounding trains of each acci-

dent. Through these accidents, the importance of DD was confirmed again. Sensor integrated DD can detect accidents of each bogie by installing DD on each bogie. But it was installed in each cab only because of low cost-effectiveness. In 2018, a DD with twin sensors was developed and has been tested. This characteristic is to divide into a main unit and an acceleration sensor. As a result, by monitoring 2 accelerarion sensors with 1 main body, the cost-effectiveness was improved. This paper describes the validity and performance of DD based on the history of development and service.

2. CONCEPT OF DERAILMENT DETECTOR

2.1 Concept learnt from actual derailment accidents

Fig. 1 shows 2 actual severe accidents motivating us to develop a DD. Fig. 1 (a) shows NAKAMEGURO derailment-crash accident in 2000. In this accident, the rearmost car of an 8-car-trainset derailed due to excess of the limit value of the derailment coefficient. Since the driver didn't recognize the derailment, the derailed train continued running. After that, a secondary accident of crash against an oncoming train occurred. As a result, 5 people were killed and 63 people were injured. Through this accident, it was obvious that a driver couldn't recognize a derailment of a train. In addition to that, the importance of detection of derailment as soon as possible was proved. Fig. 1 (b) shows FUKUCHIYAMA rollover-crash accident in 2005. A 7-car-trainset came off the tracks due to excess of speed limit. The speed limit on the segment was 70 km/h. But the train was moving at 116 km/h at that point. As a result, the train turned over and crash into building. In this accident, 107 people were killed and 562 people were injured. Through this accident, it was obvious that the possibility a driver can't notify surrounding trains of an accident should be considered. In these accidents, harm of derailment was small, but harm of secondary accident (e.g. crash or rollover) was serious. A lot of effort has been made to eradicate derailment accidents so far, but it haven't realized. Because potential energy on the rail is higher than that on the sleeper when derailed. So the concept of DD became to minimize harm of

(a) NAKAMEGURO accident[5]

(b) AMAGASAKI accident[5]

Fig. 1 Severe accidents motivating us to develop a DD

accident, not prevent accident. To realize that, DD was required to detect accident and notify surrounding trains it.

2.2 Scenario analysis of wheel climb derailment accident

The NAKAMEGURO accident shown in Fig. 1-a is one of the typical wheel climb derailment accidents. Fig. 2 shows the scenario analysis of the wheel climb accident. First, a wheel climbs up a rail due to wheel load decrease, as shown in Fig. 2 (a). Second, a climbed wheelset falls onto a track, as shown in Fig. 2 (b). The fall height of wheelset equals to rail height, which is only about 150mm in Japan. Because the fall height is much smaller than that of other transportation, harm of derailment itself is very small. So, a driver is difficult to recognize a derailment of his/her train. As a result, a train sometimes continues running after derailment, as shown in Fig. 2 (c). If guide function of a derailed axis have been lost, a derailed train would deviate from track center. Finally, a derailed train will crash into infrastructure, and/or crash with an oncoming train, as shown in Fig. 2 (d). In a secondary crash accident, severe harm will be caused.

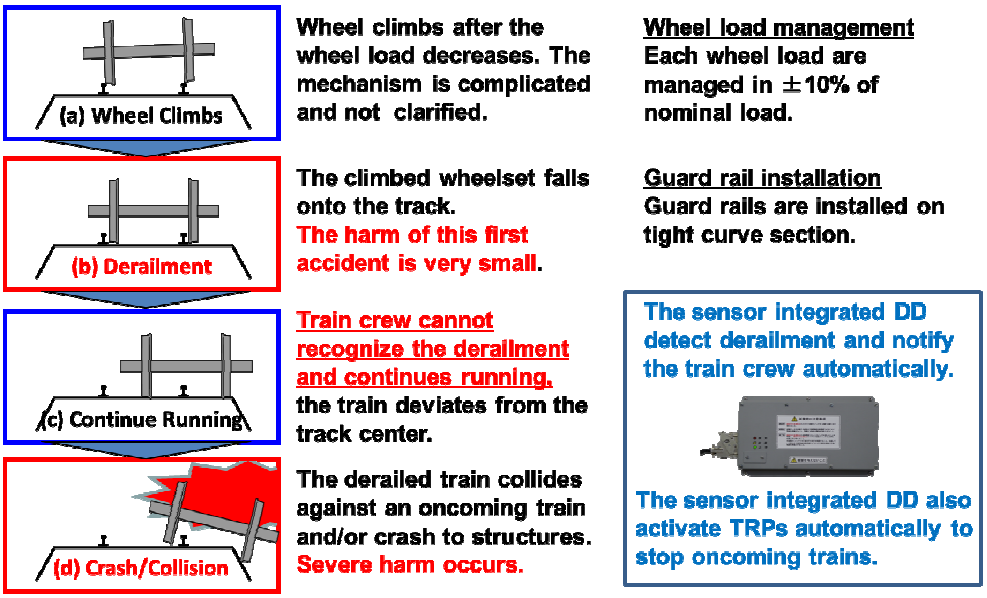

Fig. 2 Scenario Analusis on Wheel Climb Derailment[5]

3. ALGORITHMS OF DD

DD can detect not only derailment but also crash and rollover because a crash and rollover accident will lead to derailment. In this clause, DD's algorithms as shown in Table.1 to detect each accident will be introduced.

3.1 Algorithm to detect derailment

When a train derails, two stage of derailment phenomena exist. One is to detect the fall of axle from rail. The other is to detect running on a rough road (e.g. combination road with sleepers and ballast). To detect each stage, DD has two DDAs.

3.1.1 Fall of axle from rail

DDA analyses vertical acceleration (z-acceleration) at cycle of 10 milliseconds to calculate fall height of a wheelset from rail by integrating z-acceleration twice by time.

In case a fall height exceeds height of rail, the DD detect derailment. The integration is conducted under the following condition.

- Displacement and speed on z-axis is 0 at the start of integration.
- Only falling height is analyzed to separate raising height.

3.1.2 Running on a rough road

When a train runs on a rough road, a speed of train doesn't change sharply. On the other hand, vertical accerelation of a train change sharply. To detect this change, DDA analyzes vertical acceleration at cycle of 5 milliseconds. After that, DDA compares absolute value of data in 1 second with absolute value 1, 2 and 3 seconds before. If two of them exceed the threshold, DD judges that a train derailed.

Table. 1 Accident mode and applied detection algorithms[5]

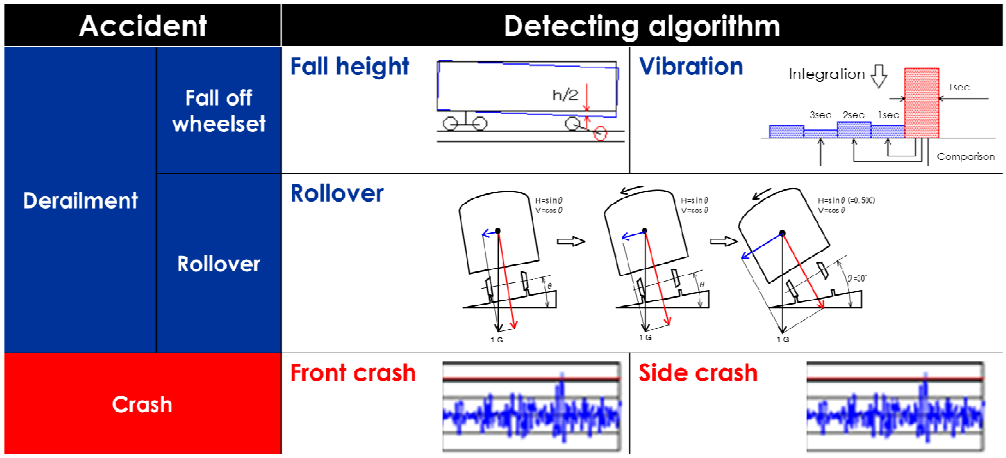

3.2 Rollover

To define threshold of rollover, an experiment was conducted by using a train whose center of gravity is lowest. We focused on decrease of z-axis of gravity acceleration at the maximum angle of incline. If the z-axis of gravity acceleration is 0G in case a train is placed vertically, the decrease is -0.1138G. By considering vibration of voltage sensitivity, the threshold of crash was defined -0.1252G. DDA of crash analyzes z-axis of gravity at cycle of 5 milliseconds. By taking into account of running data, it judges a train collides when it exceeds -0.1252G for 0.4 seconds.

3.3 Crash

To set crash algorithm, DD focused on a driver to prevent a secondary accident under a condition a driver can't activate TPR. A crash experiment was conducted by using a dummy roll with JR-East and Railway Technical Research Institute. Through the experiment, it turned out that a dummy roll fall from seat when horizontal acceleration exceed 2.7G. A dummy doll is non-resistant to shock, but human is resistant. So the threshold of crash is 3G in front-back and right-left direction.

3.4 Verification of performance of DD by experiments

By collecting and analyzing the 21000 km running data from 7 types of trains operated by JR-East, these algorithm was introduced. To prevent false detection, data at points,

rail joint and track irregularity was carefully analyzed. As for the derailment algorithm, an experiment was conducted by pushing an unused train and falling from rail as shown in Fig.3. This was held on harsh assumption which were low axle load (78 kN/axle) of derailed wheelset, low velocity (1.0 m/s) when derailed and small number of derailed axles (2 axles) and succeeded. As a result, high performance of the DD was proved.

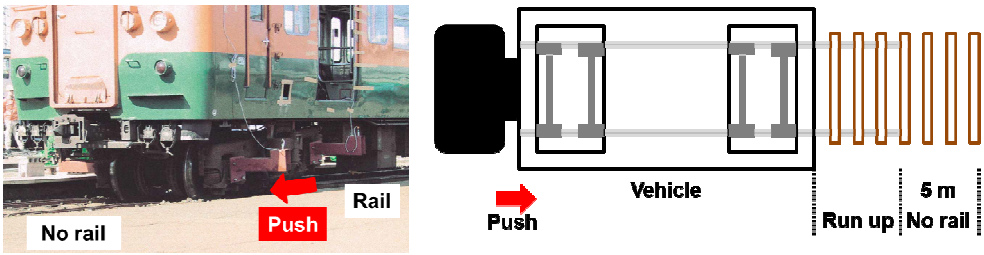

Fig. 3 Experiment[3]

4. DEVELOPMENT OF DERAILMENT DETECTOR

4.1 Sensor integrated DD

4.1.1 Facility

Table 2 shows the specification of sensor integrated DD. It consists of an acceleration sensor, a CPU and a memory for storage to record logs in accidents as shown in Fig.4 . It has 5 algorithms as discussed in clause 3 to detect 3 types of accidents. If one of 5 algorithm activates, sensor integrated DD works the following.

- Activate TPR to notify surrounding trains of an accident
- Inform a driver of an accident through a monitor
- Memorize x, y, z-acceleration data for 2 minutes before an accident and for 1 minute after an accident to analyze the movement of a train.

4.1.2 Trains installed the sensor integrated DD

Currently, about 2000 sensor integrated DDs are installed in over 1000 train-sets operated by JR-East.

Table. 2 Performance of sensor integrated DD[5]

Function	Detail
Component	3-axis acceleration sensor CPU Compact Flash memory
Dimension	250mm × 480mm × 68mm, 4.5kg
Detection	Derailment Collision Rollover
Performance	Axle load : 78kN/axle Velocity at derailment : 1m/s Derailed Axle number : 2 axles
Action	Activate train protection radio Notify a driver of an accident Record acceleration data

This is only installed in each cab to notify surrounding trains of an accident when a driver can't activate TPR due to an accident. It is possible to detect an accident of each bogie by installing in each side of a car, but it isn't realized due to cost-effectiveness.

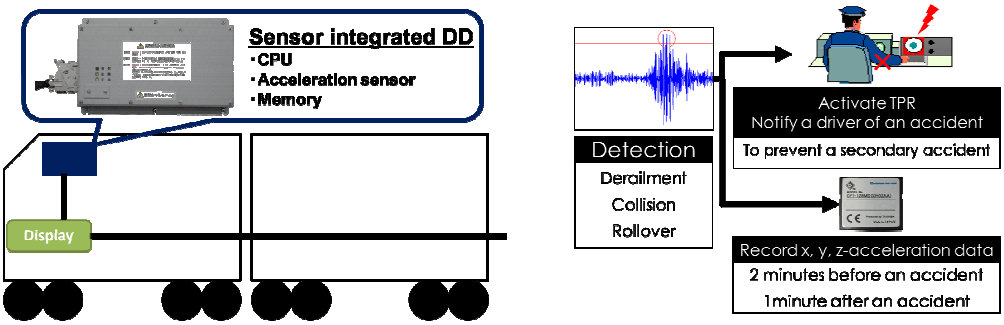

Fig. 4 Sensor integrated DD[5]

4.2 DD with Twin-Sensor

4.2.1 Concept and facility of DD with Twin-Sensor

Fig 5 shows DD with Twin-sensor. It was developed based on the know-how of sensor integrated DD. As for sensor integrated DD, a sensor and a CPU and memory were put in one container, so the device needs too large space to fit on a car. And if two devices are installed in each car to check each bogie, cost effectiveness is low due to 2 CPUs and 2 memories in each car.

To maximize the cost-effectiveness of monitoring each bogie, DD with Twin-sensor was developed. This characteristic is to divide into a main control unit and an acceleration sensor as shown in Fig. 5. A main control unit consists of a CPU and a memory for storage, etc. By monitoring 2 sensors with 1 main control unit, cost-effectiveness to detect accidents in each bogie was improved as shown in Fig 6. The algorithm is based on the conventional device, and the detectable accidents are derailment and rollover. In addition, while the conventional DD has single system configuration, the new DD has double system configuration for each acceleration sensor, a CPU and relay to prevent false detection, false alarm, malfunction and so on.

4.2.2 Specification of derailment detector with Twin-sensor

This DD has a removable recording device. It is possible to copy recorded data from 2 sensors into a PC through a communication connector. It is also equipped with a second communication connector to update software. When accidents occur, a main control unit indicates output signal and information on the type of an accident, power supply status, monitoring status and self-diagnosis failure. These signals are excited by a relay circuit in the interface unit of a vehicle control system. At the same time, information is sent to a central unit in a vehicle control system and displayed on a cab monitors. After detection, it is possible to reset a device by turning on the reset switch button in the cab.

4.2.3 Trains installed DD with Twin-sensor

DDs with Twin-sensor are under examination to check the function and compatibility with 13000 series trainsets operated by Tokyo Metro Co., Ltd. It was temporarily installed only

in two cars; the first and fourth car. Since bases to mount acceleration sensors weren't installed in the cars, a hammering test was conducted to confirm that temporary installation was equivalent condition to real installation. As a result, there was no resonance below 200 Hz. Through test run after regular service operation, data on vibration of running vehicles was collected. As a result, no abnormal acceleration or noise was confirmed. So it was confirmed that the DD with Twin-sensor has no problem with the functional aspect. Therefore, appropriate threshold value will be set by analyzing the collected data of long-term monitoring run. DD with Twin-sensor will start operation from 2019.

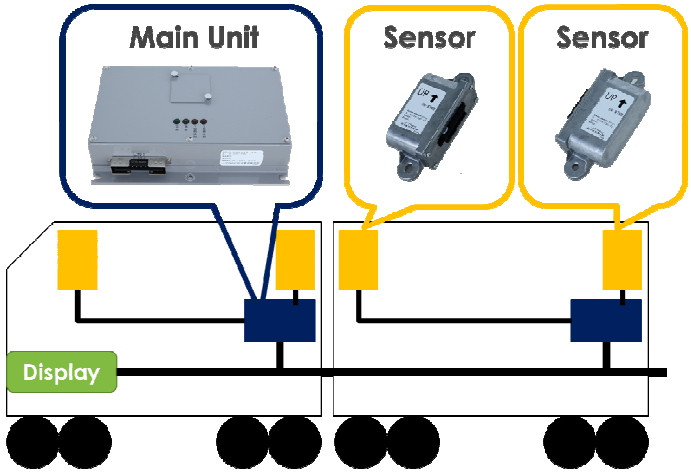

Fig. 5 DD with Twin sensor[1]

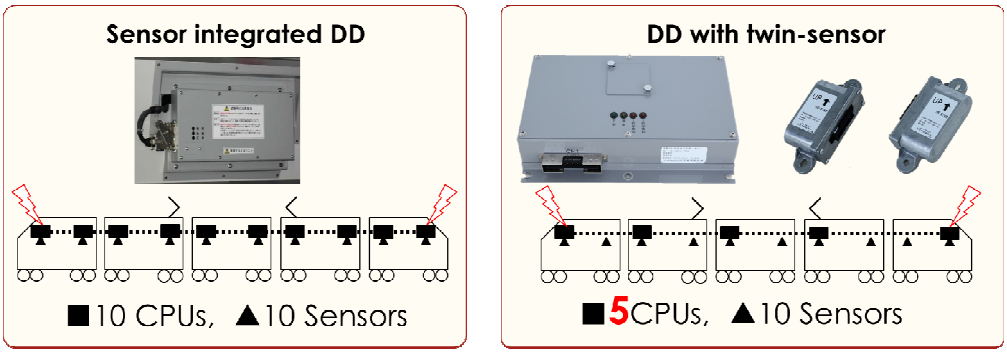

Fig. 6 DD with Twin sensor

5. DISCUSSION

5.1 Two actual accidents detected by DD

Fig. 7 show two actual accidents detected by DD. Fig.7-a shows SAGAMIKO derailment-crash accident in 2013. Leading two axles of a rearmost vehicle of 10-car-trainset derailed. When DD detected derailment, the train stops by an emergency brake and the DD also activated TPR to notify the surrounding trains of the accident to prevent sec-

ondary accident. The train attacked the platform due to derailment but no one was injured fortunately.
In this accident, DDA (Running on a rough road) worked. It was difficult condition to detect derailment due to the following conditions.

- The number of derailed axles was 2.
- The velocity when derailed was 10 km/h.
- The axle load of derailed wheelset was 6t.

The derailed train had a DD in the cab only. DD isn't designed to detect an accident at opposite side of a car. But DD could detect because of the transmission of vibration. Through this accident, the effectiveness of algorithm was confirmed again. And it was proved that the concept of DD was appropriate because it detected the accident prior to driver's recognition and also prevented a secondary accident by activating TPR.

(a) Sagamiko derailment accident[5]

(b) Kawasaki crash-rollover accident[5]

Fig. 7 Actual accidents detected by the DD

Fig. 7-b shows KAWASAKI crash-rollover accident in 2014. An out of service train operated after regular service operation crashed with a vehicle for maintenance. After that, the foremost vehicle of 10-car-trainset overturned and the other cars derailed. In this accident, one driver and one crew are injured. When DD detected crash, DD activated TPR. Through the inspection, it was obvious that the train collide with the vehicle at 64 km/h and the driver fall from the seat. As a result, it is presumed that the horizontal acceleration was more than 3G. The front damaged entirely, but DD worked properly because it was installed on the celling which is hardly damaged. Through this accident, the validity of DD was proved because DD prevented secondary accidents in case a driver couldn't activate TPR.

6. CONCLUSION

DD can detect derailment, crash and rollover. As for derailment, the validity of algorithum was proved by the experiments and the detection of the actutual derailment accident in SAGAMIKO. As a result, it was proved that 3 parameters (axle load of derailed wheelset, velocity when derailed and the number of derailed wheelset) defined in experiment were appropriate to specify the performance of DD. As for crash, the validication of algorithum was proved by the actutual derailment in KAWASAKI be-

cause DD succeeded to detect the crash which the driver fell from a seat and didn't activate TPR because of injury. Through both accidents, DD is expected to contribute to further safety of railway system because it also succceded to prevend a secondary accident. Cullently, a DD with Twin-sensor which has same algorithms with a sensor integrated DD is under examination. This improved low cost-effectiveness to monitor each bogie. In addition to that, this has double system configuration for each acceleration sensor, a CPU and relay failure to prevent false detection, false alarm, malfunction and so on. Through these improvements, it achieved high accuracy in detection, high reliability, space saving and cost-effectiveness. Therefore, it will be widely adapeted by many railway operators around the world due to magnificiently contribution to improvement of railway safety.

7. REFERENCES

[1] **Oyama, H. – Nagamoto, M. – Matsuoka, S. – Yano, K. – Maeda, T.**: Development of Derailment Detector with Twin Sensor: Proceedings of J-RAIL 2018, 2018. (In Japanese)

[2] **Kino, J. – Terada, K. – Ishige, T.**: Development of Safety Research Laboratory Type System for Automatic Transmission of Train Protection Radio Signals: JR East Technical Review, No.11, 2007.

[3] **Hirabayashi, K. – Kawada, N. – Ohno, M. – Kaminaga, T. – Eguchi, F.**: Development of derailment detector with road service: Tokyu Car Technical Review, No.51, 2001.

[4] **Saito, K. – Misu, Y. – Yoshida Y.**: Development of derailment detector: JR East Technical Review, No.2, 2003. (In Japanese)

[5] **Matsuoka, S. – Ishikami, K. – Nagamoto, M.**: Development of the Derailment-Rollover-Crash (DRC) Detector and its Derailment Detection in Actual Accidents: Proceedings of the Third International Conference on Railway Technology, 2016.

[6] Railway Accident Investigation Commission (2000) Derailment at the Teito Rapid Transit Authority's Naka-Meguro Station on the Hibiya Line: The Ministry of Transport of Japan, 2000. (In Japanese)

[7] Railway Accident Investigation Report- Train Derailment Accident between Tsukaguchi and Amagasaki Stations of the Fukuchiyama Line of the West Japan Railway Company: Aircraft and Railway Accident Investigation Commission, 2007. (In Japanese)

[8] Railway Accident Investigation Report- Train Derailment Accident at Sagamiko Station of Chuo Line of East Japan Railway Company: Japan Transport Safety Board, 2015. (In Japanese)

[9] Railway Accident Investigation Report- Train Derailment Accident at Kawasaki Station of Keihin-Tohoku Line of East Japan Railway Company: Japan Transport Safety Board, 2015. (In Japanese)

FAULT DETECTION AND IDENTIFICATION IN THE SUSPENSION COMPONENTS OF RAIL VEHICLES BASED ON ACCELERATION MEASUREMENTS

Stefano ALFI, Binbin LIU and Stefano BRUNI

Departimento di Meccanica
Politecnico di Milano
I-21036 Milano, Italy

Received: September 11, 2019

ABSTRACT

This paper proposes a methodology for fault detection and identification in suspension components of rail vehicles based on acceleration measurements. The methodology consists of three stages corresponding to parameter estimation, fault detection and finally fault identification. The estimation of the interested parameters is realized by a least square-based algorithm, then the estimates are fed to a procedure for outlier detection based on the evaluation of Mahalanobis squared distance (MSD) to detect the fault. Moreover, the fault can be identified by further elaborating various subspaces of the MSDs. Numerical experiments have been performed to demonstrate the proposed methodology.

Keywords: parameter estimation, fault detection and identification, condition monitoring, vehicle dynamics, least square, Mahalanobis squared distance

1. INTRODUCTION

Condition monitoring and predictive maintenance are seen as major means to increase safety, reliability and availability of railway bogies and to optimize life cycle costs. To this end, various fault-detection and identification (FDI) techniques have been developed as a means to provide an early warning of a fault or component degradation, allowing to substantially reduce the in-service failures and to switch from time-based to event-driven maintenance. The FDI techniques are generally classified into two basic categories: model-based methods and data-driven techniques.
The aim of this work is to detect and possibly isolate the faults occurring in the primary suspension components based on on-board acceleration measurements.

2. METHODOLOGY

The methodology consists of three stages namely parameter estimation, fault detection and fault isolation. The parameters to be estimated in this work are the stiffness and damping coefficients of the suspension components of a rail vehicle.
A conventional passenger rail vehicle with two bogies is considered, see Fig. 1. Each bogie consists of two stages of suspension. The primary suspension consists of a spring seating on the axle-box (green box in Fig. 1) and a vertical damper (cyan cylinder in Fig. 1) mounted on one end of the axle-box swing arm. The other end of the axle-box swing arm is connected to the bogie frame (yellow frame in Fig. 1) with a bushing element.
Numerical experiments are used to assess the performances of the proposed methodology in terms of fault detection and fault isolation. To this aim, a multi-body system (MBS) model of the vehicle is developed in SIMPACK, which is used both as the baseline and the faulty case, after faults with different severity are injected in the model.

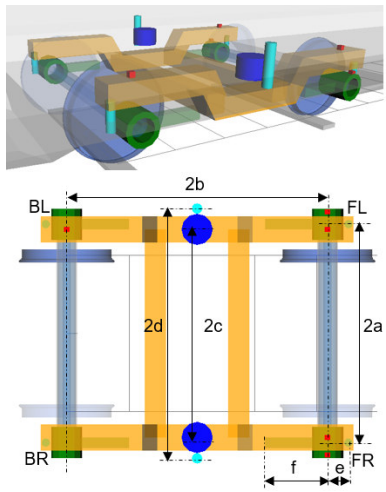

Fig. 1 Layout of accelerometers on the bogie

The equation used for suspension parameter estimation is the one describing the vertical motion of the bogie under the action of forces coming from primary and secondary suspensions and is as follows:

$$M_f \ddot{Z}_f(i) = \sum_{i=1}^{4} C_{pi} V_{pi}(t) + \sum_{i=1}^{4} K_{pi} D_{pi}(t) + \sum_{j=1}^{2} C_{sej} V_{sej}(t) + \sum_{j=1}^{2} K_{skj} D_{skj}(t) + F_{exZ} \quad (1)$$

where $\ddot{Z}_f$ is the vertical acceleration of the bogie frame; M_f is the mass of the bogie frame; C_{pi} is the primary damping coefficient; V_{pi} is the velocity of the primary damper; K_{pi} is the primary stiffness; D_{pi} is the deflection of the primary spring; C_{si} is the secondary damping coefficient of the bogie; V_{si} is the derivative of deflection of the secondary vertical damper; K_{si} is the secondary stiffness of one bogie; D_{si} is the deflection of the secondary spring; F_{exZ} is the external force regarded as the modelling error. Subscript i=1…4 denotes the front right, front left, back right and back left corner of the bogie frame, while j=1…2 represents the left and right side of the bogie.

The direct use of Equation (1) requires a double integration of the acceleration measurements which introduces cumulative numerical errors. Therefore, the method is implemented using the following derived form of Equation (1):

$$M_f \ddot{Z}_f(t) = \sum_{i=1}^{4} C_{pi} A_{pi}(t) + \sum_{i=1}^{4} K_{pi} V_{pi}(t) + \sum_{i=1}^{2} C_{sei} A_{sei}(t) + \sum_{i=1}^{2} K_{ski} V_{ski}(t) \quad (2)$$

In this form, the method requires the differentiation of the bogie acceleration to obtain the vertical jerk of the bogie frame and the single integration of the primary and secondary suspension accelerations to obtain the corresponding velocities. Before applying the parameter estimation algorithm, the acceleration signals are filtered in the 2-10 Hz frequency range to select the portion of the signals most related to the forces generated in primary suspension components.

The equation of motion expressed in Equation (2) shows that the parameter estimation of this system can be considered as a data fitting process where the required signals are determined in the way presented above. The most commonly used data-fitting technique is least squares fitting. The recursive least square (RLS) algorithm was implement in [1] for parameter estimation of the suspension of a rail vehicle and the same algorithm is also used here. As an alternative, we introduce another type of least square-based algorithm called damped least square (DLS) which refers to the Levenberg-Marquardt algorithm used in least squares curve fitting [2]. This method estimates the coefficients using a minimum number of data values which depends on the number of variables whose value is to be identified. With the increase of time, the width of the window containing the data to be analyzed is increased. The initial guess is updated with the previous estimation to speed up the calculation. The difference between RLS and DLS methods in this application is marginal, but the computational efficiency of the RLS method is higher. However, it was also found that the convergence speed of the DLS method is faster than that of the RLS method when the standard equation of motion (see Equation (1)) is used.

If the parameters of the system under investigation could be estimated with a high accuracy, then the fault detection and identification would become straightforward. However, this is not the case in practice when the physical system is complex, and the number of channels of measurement is limited.

The aim of the parameter estimation in the proposed methodology is to capture the abnormal variations of the components under monitoring rather than to precisely estimate the parameters themselves. Therefore, a simple and fast while less accurate estimation algorithm is preferable for the proposed methodology. The parameter estimation is followed by a procedure for outlier detection based on the evaluation of Mahalanobis squared distance (MSD) [3, 4].

The MSD outlier detection works first on the healthy population of estimated parameters, considering a vector with the complete set of suspension parameters or a sub-set of these. The different vectors obtained from the different simulations of healthy cases are treated statistically, to obtain the mean value vector and the covariance matrix.

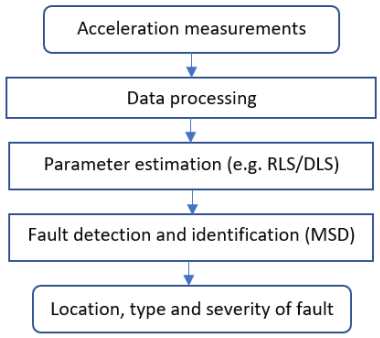

Fig. 2 Flowchart of the methodology

To this end, a set of training data shall be created defined as the healthy dataset of the vehicle under monitoring. Then the calculated MSDs of current estimated parameters

with respect to the heathy cases are used to detect the fault with a properly assigned threshold and the identification is accomplished by further elaborating various subspaces of the MSDs. The flowchart of the proposed methodology is shown in Fig. 2.

3. RESULTS AND DISCUSSIONS

3.1 Parameter estimation

Two case studies are considered in this section corresponding to the healthy vehicle and a vehicle with a 50% reduction in the vertical stiffness and damping of the primary suspension, respectively, at the front right (FR) corner of the leading bogie.

The estimated results for the healthy vehicle by the RLS/DLS method are shown in Figs. 3 and 4 for the primary spring and damper, respectively. The nominal values of the parameters used in the MBS simulation are also shown by a horizontal dashed line for comparison. In the following figures, FR, FL, BR, and BL stand for the front right, front left, back right and back left corner of the bogie, PS represents the primary suspension, Kz and Cz stand for vertical stiffness and damping, respectively and Error is defined as follows:

$$Error = \frac{Estimated\ value - Nominal\ value}{Nominal\ value} \times 100\ \% \tag{3}$$

where the estimated value is evaluated as an average of last 5s in the simulation, while the nominal value is the one used in the MBS simulation.

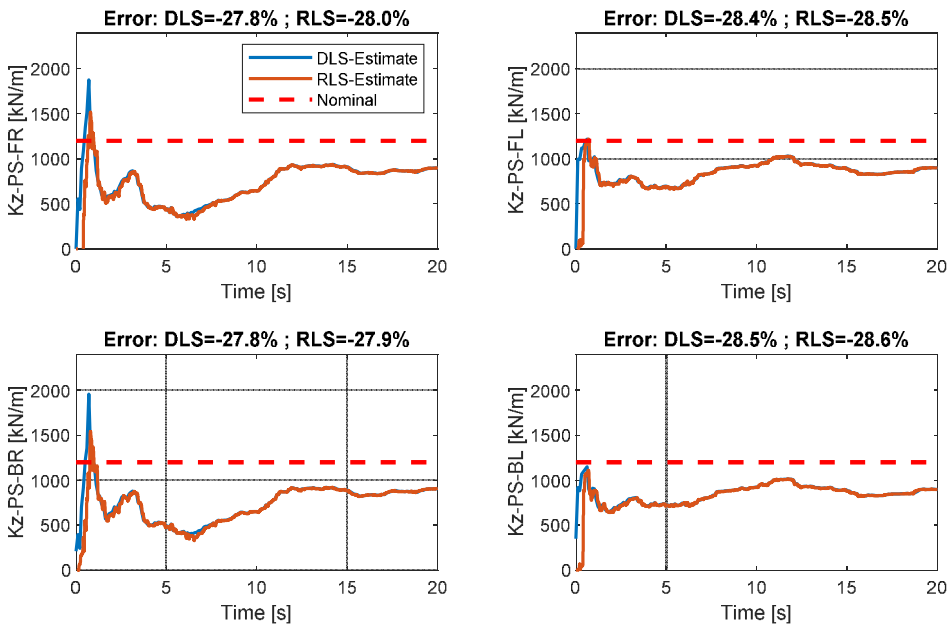

Fig. 3 Parameters of the primary spring at four corners of the bogie

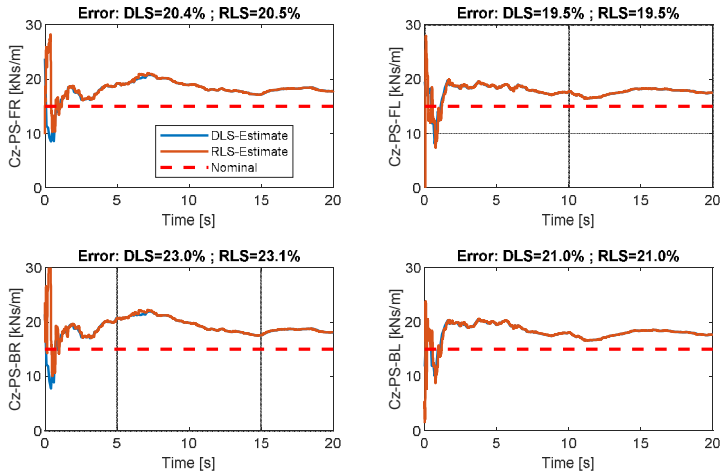

Fig. 4 Parameters of the primary damper at four corners of the bogie

Parameter estimation errors obtained in the healthy condition range from 20% to 30% approximately. In this case, the stiffness parameters are underestimated in all corners about 28%, whereas the damping coefficients are overestimated in the range of 20-23%. The results obtained with both RLS and DLS are almost the same.

The results for the faulty cases are reported in Table 1 compared to the estimation of the parameters with the vehicle in healthy condition. Since the estimated results from RLS and DLS are almost the same, only the results obtained from DLS are reported in the table.

Table 1: Estimated parameters with DLS method

Type	Bogie corner	Healthy case Value [kN/m] or [kNs/m]	50% reduction in stiffness Value [kN/m] or [kNs/m]	50% reduction in stiffness Variation [%]	50% reduction in damping Value [kN/m] or [kNs/m]	50% reduction in damping Variation [%]
Spring	**FR**	**866.09**	**185.46**	**-78.59**	805.69	-7.0
	FL	859.12	777.43	-9.5	805.79	-6.2
	BR	866.20	831.32	-4.0	754.03	-12.9
	BL	857.50	784.26	-8.5	816.04	-4.8
Damper	**FR**	**18.06**	17.96	-0.5	**10.82**	**-40.09**
	FL	17.93	17.85	-0.1	15.61	-12.9
	BR	18.46	20.81	12.7	19.72	6.8
	BL	18.16	18.10	-0.3	16.11	-11.3

As for the results obtained in Table 1, the method detects the maximum variation of the parameters in the actual faulty element of the suspension. For the faulty spring case the variation is overestimated with a variation detected of 78% against an actual variation of 50%. Although the detected reduction is not precise, a clear indication is obtained of the change occurring in the condition of the spring. The estimated variation of the parameters in the healthy components is limited to 10% for the springs and 12% for the

dampers. In the case of the faulty damper, the variation of the damping coefficient is estimated at 40% against an actual variation of 50%. In the healthy components, the variation of the parameter estimation is limited to 13% for both springs and dampers.
It can be concluded that the RLS/DLS method is able to estimate the changes in both stiffness and damping of the primary suspension to a degree of accuracy which makes it possible to establish a fault detection scheme based on changes of the estimated parameters in combination with an outlier detection scheme as it will be shown in the next section.

3.2 Fault detection and identification

A multi-dimensional space is formed considering the different parameters estimated by RLS/DLS method to detect and identify the faults, the dimension of the space being up to 8, which is the total number of suspension parameters being estimated (4 stiffness values and 4 damping values, one for each bogie corner).

Table 2: Healthy cases

Simulation case	Velocity [km/h]	Irregularity type	Irregularity factor
1	130	Irr_type_1	1
2	140	Irr_type_1	1
3	145	Irr_type_1	1
4	150	Irr_type_1	1
5	155	Irr_type_1	1
6	160	Irr_type_1	1
7	150	Irr_type_1	0.9
8	150	Irr_type_1	0.8
9	150	Irr_type_2	1
10	150	Irr_type_2	0.9
11	150	Irr_type_2	0.8

A population of healthy individuals is created, representing different conditions (e.g. slightly different vehicle speeds, different track irregularities) for the vehicle in healthy/nominal condition. This forms a base set towards which any next estimation of suspension parameters is tested by the outlier detector to find a deviation from the trend of healthy parameters, eventually enabling to point out a deviation from the healthy condition. This scheme can be applied using different sub-sets of estimated parameters, i.e. besides an 8D space considering all estimated parameters, two 4D spaces considering only stiffness parameters and only damping parameters, or sub-sets representing the values estimated for the left/right side or front/rear end of the bogie. This enables the isolation of faults, i.e. besides pointing the occurrence of a fault (so-called “fault detection”) the classification of the fault as one happening in a spring or damper and possibly also the corner in the bogie where the fault is happening.

A series of simulations was performed with the baseline vehicle to define the "healthy" condition of the vehicle by considering the variations in the vehicle's velocity, the type and the quality level of the track irregularity. The selected healthy cases are summarized in Table 2.

The calculated MSDs for the healthy cases in the full 8D-space (consisting of four stiffness Kpi i=1-4 and four damping parameters Cpi i=1-4) of primary suspension parameters are shown in Fig. 5.

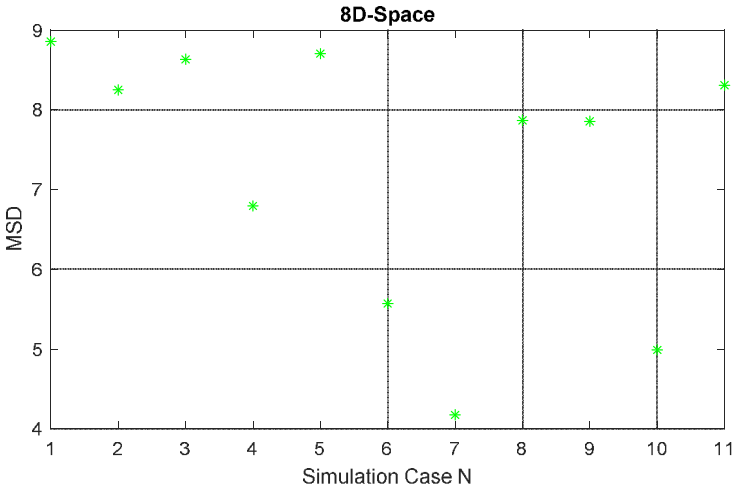

Fig. 5 The MSDs for the healthy cases in the full 8D-space

It can be seen from Fig. 5 that the variation of the MSDs for the healthy cases in the full 8D-space is bounded in the range of 4-9 which is mainly due to the changes in the running conditions of the vehicle and the quality of the track.

To test the performance of the proposed methodology, simulations were performed injecting faults of different severity in the model where a degradation from 20% to 100% of the nominal value for both stiffness and damping coefficient in the primary suspension was considered. For each case, the eight parameters characterizing the primary suspension were estimated using the RLS/DLS method. Then the MSDs were computed considering different spaces.

The results for the full 8D space are shown in Fig. 6 and Fig. 7. It can be observed that the method is able to detect the presence of faults. The value of the MSD is increasing with the severity of fault in the case of faulty dampers and also for the faults in springs except when the fault occurs in the FR corner. Even in the case when the MSD is not monotonically increasing with fault severity, the values obtained for faulty conditions are at least two orders of magnitude greater than for the any healthy case, so that fault detection is still possible. It can be noted that in this case the fault in the damper is easier to be detected than the spring since the values of MSD for the cases with faults in dampers are generally higher under the same degree of fault severity.

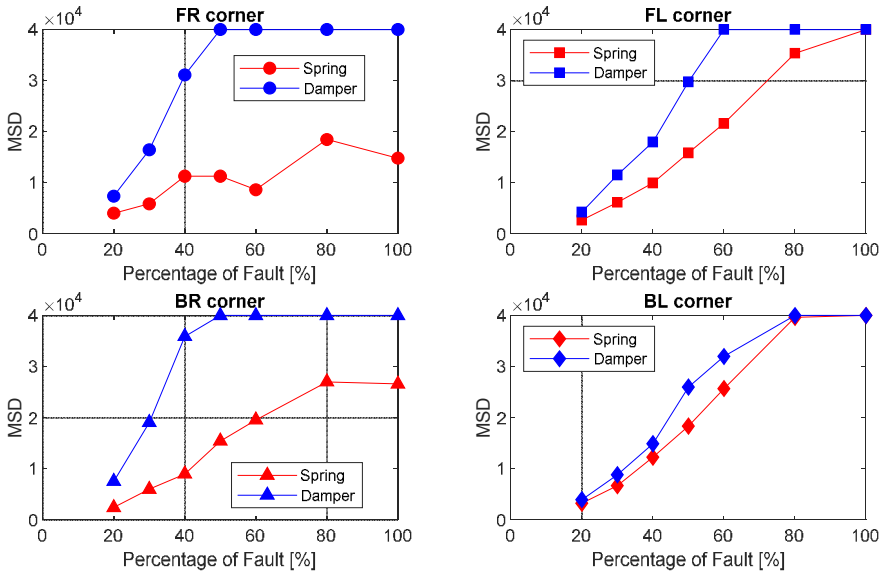

Fig. 6 Reduced set layout: the MSDs for the faulty conditions in 8D space

Fig. 7 compares all the faulty cases with the healthy ones, showing the possibility to set a threshold at about MSD=10^3 allowing to distinguish all the faulty cases from the healthy conditions. In this figure, and in the next two ones, green starred points denote cases representing a healthy condition of the bogie, red-colour points represent faults happening in one spring, the position of the spring being represented by a different shape of the point, and points in blue colour denote faults occurring in one damper. The severity of faults increases from left to right.

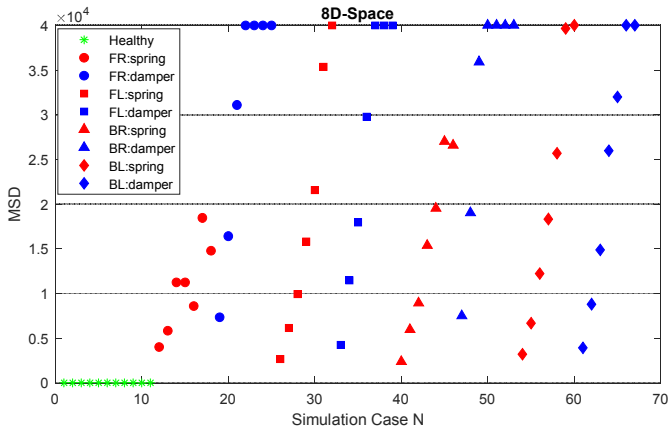

Fig. 7 The MSDs as a function of the number of the simulation cases in 8D-space

The isolation of the faulty element can be achieved considering both the isolation of spring versus damper fault and the isolation of the position of the fault among the four corners of the bogie. For the sake of brevity, only results from the 4D subspace of spring/damper are reported in Fig. 8 and Fig. 9. It is observed that a fault occurring in a damper always leads to a value of the MSD computed for the 4D subspace springs below MSD=600, whilst a fault happening in a spring leads to a MSD exceeding 1000 even in all cases when the severity of the fault is higher than 30%. Conversely, when the MSD is computed for the 4D subspace only including damper parameters, even large faults occurring in one spring lead only to a moderate increase of the MSD whilst damper faults with severity of at least 30-40% lead to much higher variations of the MSD.

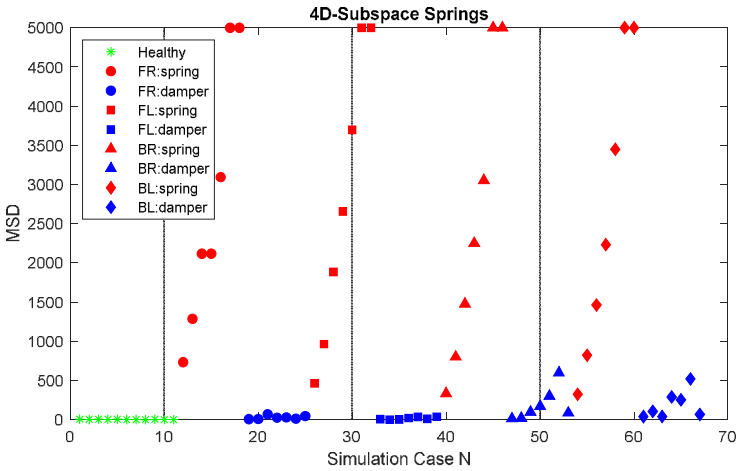

Fig. 8 The MSDs as a function of the number of the simulation cases in 4D-spring

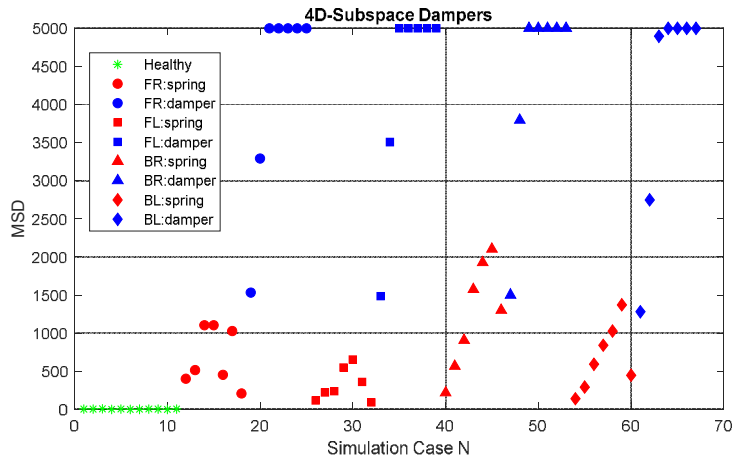

Fig. 9 The MSDs as a function of the number of the simulation cases in 4D-damper

In conclusion, the RLS/DLS combined with MSD method is able to detect the presence of faults in the suspensions. The use of different parameter subsets allows to achieve isolation of the faults (i.e. spring fault vs damper fault). Similar results can be obtained considering 4D-subpace front/rear and 4D-Subpace left/right (not shown for the sake of brevity) allowing the possibility to distinguish the presence of a faulty element in a particular corner of the bogie. The relationship between the MSD and the severity of faults could be further explored with the help of machine learning techniques to also achieve fault classification according to the severity of faults.

4. CONCLUDING REMARKS

In conclusion, the results obtained show that detection and isolation of faults happening in primary suspension components are possible using least square-based identification of suspension parameters in combination with a proper set of MSD-based indicators, e.g.:the MSD computed in the 8D space formed by all suspension parameters; the MSD computed in the 4D space formed by stiffness parameters; the MSD computed in the 4D space formed by damping parameters; the four MSDs computed in the 4D space formed by parameters for only the left/right side and for only the front/rear edge of the bogie. Using the method presented in the paper, it is possible not only to detect the occurrence of a fault, but also to identify whether the fault is happening in a spring or damper and to find the corner of the bogie where the fault has occurred.

5. ACKNOWLEDGEMENTS

The work presented in this paper has received funding from the Shift2Rail Joint Undertaking under the European Union's Horizon 2020 research and innovation programme under grant agreement no. 777564. The contents of this publication only reflect the authors' view and the Joint Undertaking is not responsible for any use that may be made of the information contained in the paper.

6. REFERENCES

[1] **Liu, X. – Alfi, S. – Bruni, S.**: An efficient recursive least square-based condition monitoring approach for a rail vehicle suspension system, Vehicle System Dynamics, vol. 54, no. 6, 2016, p.814-830.

[2] **Levenberg, K.**: A Method for the Solution of Certain Non-Linear Problems in Least Squares, Quarterly of Applied Mathematics, vol. 2, no. 2, 1944, p.164-168.

[3] **De Maesschalck, R. – Jouan-Rimbaud, D. – Massart, D.L.**: Tutorial The Mahalanobis distance, Chemometrics and Intelligent Laboratory Systems 50, 2000, p.1–18.

[4] **Ekiz, M. – Ekiz, OU.:** Outlier detection with Mahalanobis square distance: incorporating small sample correction factor. J Appl Stat; 44(13), 2017, p.2444–2457.

INVESTIGATION INTO IMPACTS OF BOGIE SECONDARY SUSPENSION SYSTEM ANOMALIES ON WHEEL WEAR PROPAGATION

Péter FERENCZ

Budapest University of Technology and Economics
Faculty of Transportation Engineering and Vehicle Engineering
Group of Railway Vehicles and Vehicle System Analysis
H-1521 Budapest, Hungary, ferencz.ptr@gmail.com

Received: 12 September, 2019

ABSTRACT

This paper describes the investigation aim into the impacts of bogie secondary suspension system anomalies on wheel wear propagation on basis of a past issue of an electric locomotive bogie design flaw. The results of the past study derived to a general correlation study between the origin of such anomalies ad and the resultant in unexpected wheel wear phenomena. The hereby written line of thoughts covers the procedure of extension of current available simulation method to handle vertical, pitching and tilting parasite movements in order to establish the possibility to evaluate the influence on the running stability and wear propagation process.

Keywords: Bogie suspension system anomaly, unexpected wheel wear propagation, dynamics of vertical bogie suspension system, wear propagation simulation

1. INTRODUCTION

This paper describes the investigation aim into the impacts of bogie secondary suspension system anomalies on wheel wear propagation on basis of a past issue of an electric locomotive bogie design flaw. The results of the past study derived to a general correlation study between the origin of such anomalies ad and the resultant in unexpected wheel wear phenomena. The object of the past case-study, the certain effected series suffered from dramatically fast wheel-wear propagation after overhauls from the year 2001, the question of this study was how to eliminate this problem. The investigation that time had the aim and method into the impacts of bogie secondary suspension system anomalies on wheel wear propagation on basis of the issue of a bogie re-design flaw happened via a modernization procedure. The results of the past study derived to a general correlation between the origin of such anomalies and the resultant in an unexpected wheel wear phenomena. The hereby written line of thoughts covers the procedure of extension of current available simulation method to handle vertical, pitching and tilting parasite movements in order to establish the possibility to evaluate the influence on the running stability and wear propagation process.

2. CASE STUDY BASIS

The basis case-study was dealing with the MÁV V43 (now No. 431) series electric locomotives, which series suffered from dramatically quick wheel-wear propagation after bogie and wheelset overhauls had been carried out. In several cases during the years 2000-2006 more than 3 mm difference measured between the two flange thickness values of certain wheel-sets performed about only approximately 80 000 km mileage (Fig.1). In the year 2000 this anomaly occurred 2-3 times a year, afterwards it started to occur more frequent. In 2006, 2-3 cases were registered per month. Consid-

ering the highly increased expenditures in warranty period after overhauls caused by this unwanted phenomena, a crucial necessity turned up to solve the problem.

Fig. 1 Asymmetric profile wear (picture of left and right wheel of one wheelset)

The phenomena appeared in an absolutely random way, in different combinations: it could not be stated that the phenomena occurred on regularly one or the other side wheelsets. Fig.2 chart shows sample measurements, (on loco No. V43 1245) suffered from dramatically large asymmetric flange wear.

With an implementation of a modernization purpose design change of the bogie - loco-body connection, rubber springs have been put in operation, since 1998. The renewal of these spring units became necessary in large amount from Year 2003 during the overhaul of the bogies. After more than hundreds of measurements it has turned out that the stiffness parameters of these springs can show a grate standard deviation.

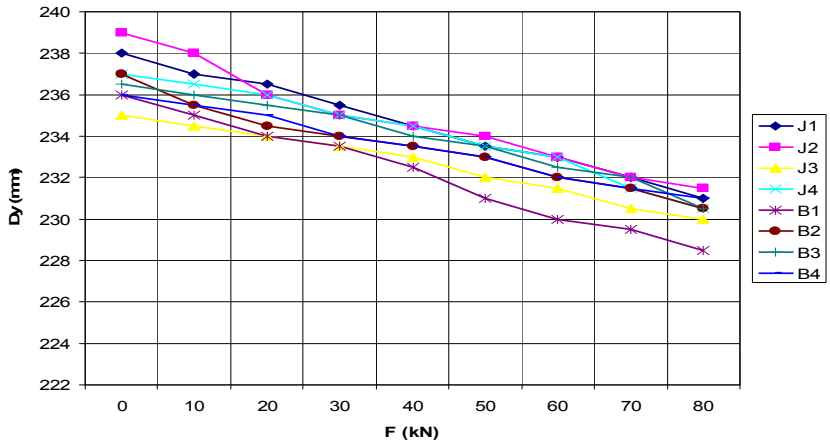

Fig. 2 Sample data of vertical spring force characteristic

To eliminate this problem, a digital wheel-profile wear simulation method and software (developed by at BME, Department of Railway Vehicles) was suitable to give acceptable solution. Dealing with several elastic components of the bogie construction, it was necessary to use non-linear models built in the wear simulation method (named ELDACW). The method contains a lateral dynamic model of a rail vehicle with 4 wheel-sets, with 30 degrees of freedom. Simulation processes focused on wear propagation on wheels each by each.

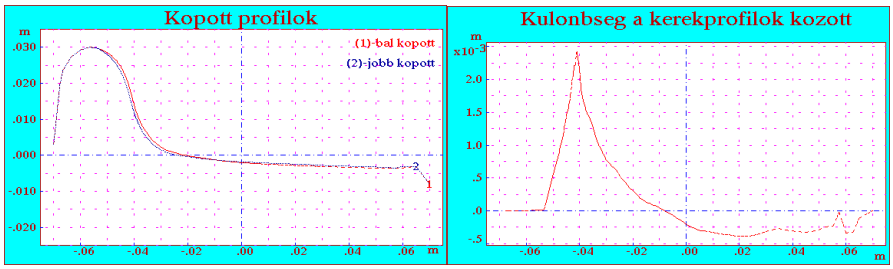

Fig. 3 Difference between right and left worn wheel profile features

Adaptation of the V43 series locomotive was a complex procedure. To build up the dynamical models, to create the input data pool (mass element, moments of inertia, interface spring stiffness and damping features). Then the most critical point was to determine the bogie/loco-body connection features. The spring characteristics tests revealed that the probable randomly mounted springs can have great stiffness differences that lead to a special effect which was realized in simulation procedure as a remained horizontal retentive torque in the bogie - loco-body connection. After composing a complete set of the effective parameters, 15 complete wear simulation processes were carried out, sample simulation result figures are showed on Fig. 3. and Fig 4. [5]

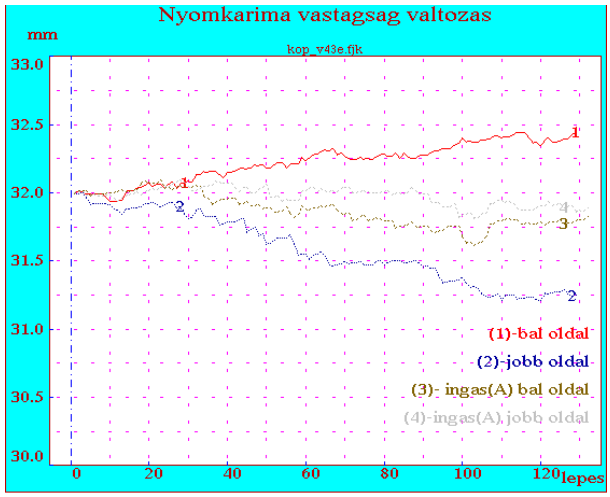

Fig. 4 Propagation of each wheel flange thickness change over increment of simulation steps

It had turned out that the developed lateral and vertical dynamical models of the locomotive could show and reveal the real behavior of the locomotives. It was proved that differences in characteristics of the secondary springs applied caused the heaviest influence of this kind of abnormal wear process, the asymmetric wheel flange wear. As an edification of the study it was real necessity of emphasized control of the secondary suspension characteristics of the applied springs, rubber-to-metal elements. On the basis of the studies carried out, several modifications were realized according to the results of the examinations (i.e. secondary suspension design was modified; maintenance and overhaul technology was modified). After the modifications the mentioned kind of abnormal wheel wear phenomena disappeared on the locos put up in use, no cases were recorded after the year 2007.

3. CONCERNING THE FUNCTION OF WEAR OPERATOR

As goal of study can be specified to *create better vehicle parameter features* with focusing on the application of diagnostic processes in maintenance, as the above described case study calls for its need. Concerning the vehicle as collection of general system characteristic space of parameters shown on Fig. 5. for general treatment of system deterioration describes the stochastic process of system deterioration. Parameter space 'P' is set of parameter vectors varying with time t:

$$\mathbf{p}(t) \tag{1}$$

where sub-vectors may contain the masses, moments of inertia, stiffness, damping and certain operational features. Determining the actual technical configuration of dynamical system is the goal to settle, considering the time dependent state vector as of: **Y**, described as

$$\mathbf{Y}(t); \tag{2}$$

The continuous slow deterioration in technical state is time-dependent and reflected so in the variation with time of the parameter vector **p**(t).

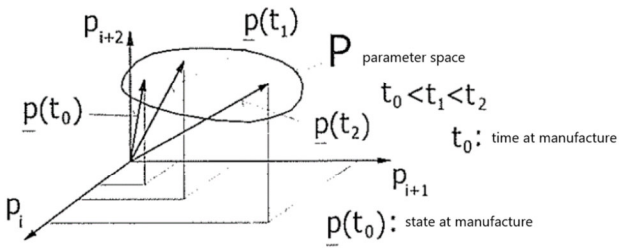

Fig. 5 Characteristic space of parameters [1]

With application of above designations, the change procedure of technical features (i.e. sub-system feature of wheel profile alteration) can be represented by the following expression.

$$\mathbf{p}(t) = \mathcal{W}_t\, \mathbf{Y}(0) \tag{3}$$

Here, $\mathcal{W}_t$ represents the technical state deterioration (it can be identified as *the* profile wear) operator (on the basis of description [2] p.255).

Within computation results of wear simulation worn profiles, the optimal profile selection is connected with the applied simulation method of using wear coefficient control. Possible, determined allocation of control function (Fig. 6.) gives the opportunity to implement the influence of the material properties that can be derived from measurement characteristics (on basis of description [2] p.256).

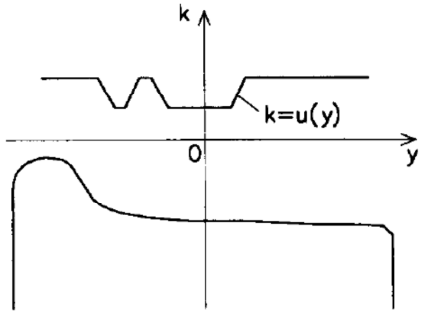

Fig. 6 Possible form and allocation of wear coefficient control function ([2] p.256.)

As the case had solved, the derived system parameter anomaly issue is worth to have a wider look at, in order to set basis for general statements. So as the current task defined, it is important to identify the most efficient impact features, the content behind the Wear operator.

4. IDENTIFICATION AND METHOD OF PARAMETER IMPORTANCE SORTING

The available 15 simulation results from the past case study provided the pool of input and output parameters for the further development, and re-check for parameter sensitivity and effectiveness behind the function of the wear, the work of the Wear operator.
As for the simulation, as well in the past and the re-run issues, a certain distribution of track types was given to have all simulation runs on the same basis. Considering simulation processes limits to end a calculation, wear propagation was of maximum nominal section wear limited as of 2 mm besides the minimum of flange thickness limited as of 29 mm, when simulations stopped.

4.1 Introduction of varied system features

Concerning this pool, sorting of features needed to be considered to evaluate importance of the varied system features. Importance considered as method of sensitivity control, in which pool three parameter groups as important factors have been defined. The case-applied set of parameters needed to have been sorted out, and picked to create the most effective basis of wear propagation influencers. The MIMO – multiple input, multiple output system defined with groups shown on Fig.7.
The parameter groups defined as of:

gj Right rail features input
gb Left rail features input
z Vector of vertical displacements
y Vector of lateral displacements
c Vector of rotational movements

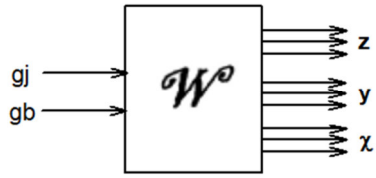

Fig. 7 MIMO system classification for the Wear operator

4.2 Vertical dynamical model application

Development of the basis case study used vertical dynamics model has been utilized to evaluate vertical force result changes depending on the secondary suspension stiffness deviation of each side. Evaluation carried out as classic linear, simplified model with 6 degrees of freedom, vertical movements and relevant rotations as shown on Fig.8.

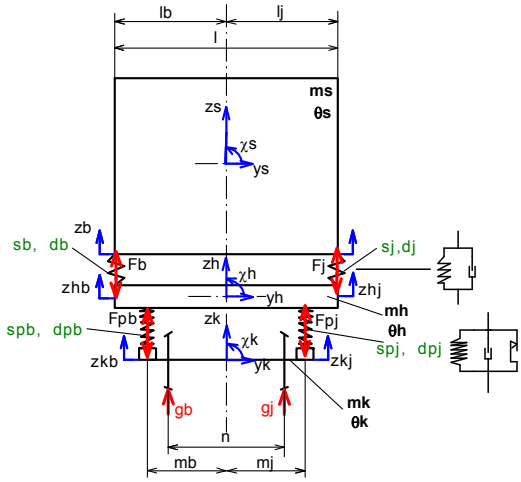

Fig. 8 Vertical dynamical model features

Equations of motion and connections are calculated as the below listed descriptions.

$$F_b + F_j = m_s \cdot z''_s \tag{4}$$

$$F_j \cdot l_j - F_b \cdot l_b = \Theta_s \cdot \chi''_s \tag{5}$$

$$F_{pb} + F_{pj} - F_b - F_j = m_h \cdot z''_h \tag{6}$$

$$F_b \cdot l_b - F_j \cdot l_j - F_{pb} \cdot m_b + F_{pj} \cdot m_j = \Theta_h \cdot \chi''_h \tag{7}$$

$$g_b + g_j - F_{pb} - F_{pj} = m_k \cdot z''_k \tag{8}$$

$$F_{pb} \cdot m_b - F_{pj} \cdot m_j - g_b \cdot \frac{n}{2} + g_j \cdot \frac{n}{2} = \Theta_k \cdot \chi''_k \tag{9}$$

$$F_b = s_b \cdot (z_{hb} - z_b) + d_b \cdot (z'_{hb} - z'_b) \tag{10}$$

$$F_j = s_j \cdot (z_{hj} - z_j) + d_j \cdot (z'_{hj} - z'_j) \tag{11}$$

$$F_{pb} = s_{pb} \cdot (z_{kb} - z_{hb}) + d_{pb} \cdot (z'_{kb} - z'_{hb}) \tag{12}$$

$$F_{pj} = s_{pj} \cdot (z_{kj} - z_{hj}) + d_{pj} \cdot (z'_{kj} - z'_{hj}) \tag{13}$$

The evaluation of vertical force result changes from the vertical dynamics depending on the secondary suspension stiffness deviation portion in percentage on each (derived from measurement results of case study [5]) side for sensitivity control calculated and shown in vectors named $\boldsymbol{\tau_b}$ and $\boldsymbol{\tau_j}$ of Fig.9.

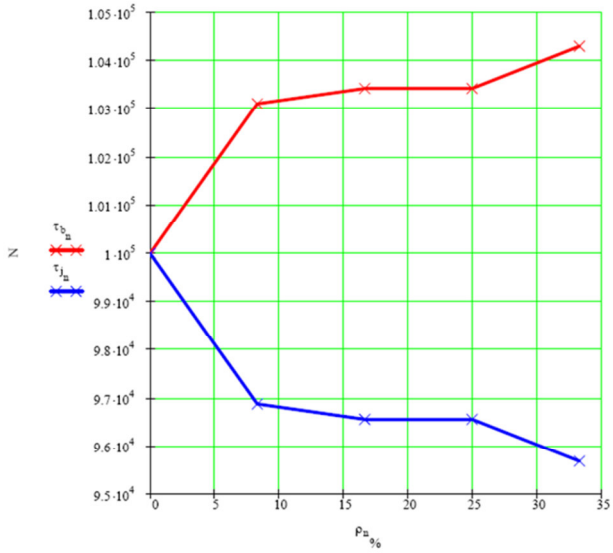

$$\tau_b = \begin{pmatrix} 1 \times 10^5 \\ 1.031 \times 10^5 \\ 1.034 \times 10^5 \\ 1.034 \times 10^5 \\ 1.043 \times 10^5 \end{pmatrix} \text{ (N)} \qquad \tau_j = \begin{pmatrix} 1 \times 10^5 \\ 9.688 \times 10^4 \\ 9.657 \times 10^4 \\ 9.657 \times 10^4 \\ 9.569 \times 10^4 \end{pmatrix} \text{ (N)} \tag{14), (15}$$

Fig. 9 Vertical dynamics – results of force deviation values over stiffness deviation on each side

As result the check on vertical dynamics carried out to calculate output figures as function of certain variation of input parameters, the deviation of secondary system applied stiffness values. The implementation in wear simulation of these results applied as pre-determined measure of the described **remained horizontal retentive torque**.

Further computation resulted from withdrawal of sensitivity check by the relative deviation method on the vertical force differences coming from static equations of the model. The in-simulation applicant vales of differences of each side force transmission capabilities are listed in a sample of portion vector **ε.**

$$\varepsilon = \begin{pmatrix} 0 \\ 6.043 \\ 6.64 \\ 7.364 \\ 8.262 \end{pmatrix} (\%) \tag{16}$$

These values are applied as direct impact of **deviation** caused **vertical forces**.

4.3 Utilization of wear coefficient control

On basis of the case study measurements, great standard deviation was detected also among wheel tread material (rim ring) surface hardness values. This feature is to be implemented in simulation method via the utilization of the already described (Chapter No.3) function of the **k** = **u**(y).

The wear coefficient control function, determined alongside above the wheel tread profile as function could give the flexibility to realize the measured **distribution of surface hardness** feature measurement values over the profile curve.

5. APPLICATION AND EVALUATION OF SIMULATION RESULTS

Application of above criteria provided an opportunity to evaluate the simulation results on comparison to a reference simulation run base. This reference was chosen with the past results indicated as 'A' simulation run, showing the features of an ideal dynamics, system of no deviation, and no impact of the above mentioned three main influencers.

5.1 Asymmetric secondary suspension system, retentive torque

Examination of impact of the deviation in secondary suspension system, the deviation applied by the bogie – carbody interface remained horizontal retentive torque, 10% - simulation 'C'; 33% - simulation 'D'. Results are shown on Fig.10. and Table 1.

Simulation Run ID	"n" left (mm)	"n" right (mm)	Calculated Mileage (km)	Portion to reference	Calculated wear propagation speed on "n" left (10^{-6} mm/km)	Calculated wear propagation speed on "n" right (10^{-6} mm/km)
A	31,83	31,89	27 557,00	1,00	6,31	3,88
C	31,83	31,87	27 283,00	0,99	6,08	4,76
D	30,11	30,87	59 080,54	2,14	31,94	19,16

Table 1. Simulation results 'C' and 'D'

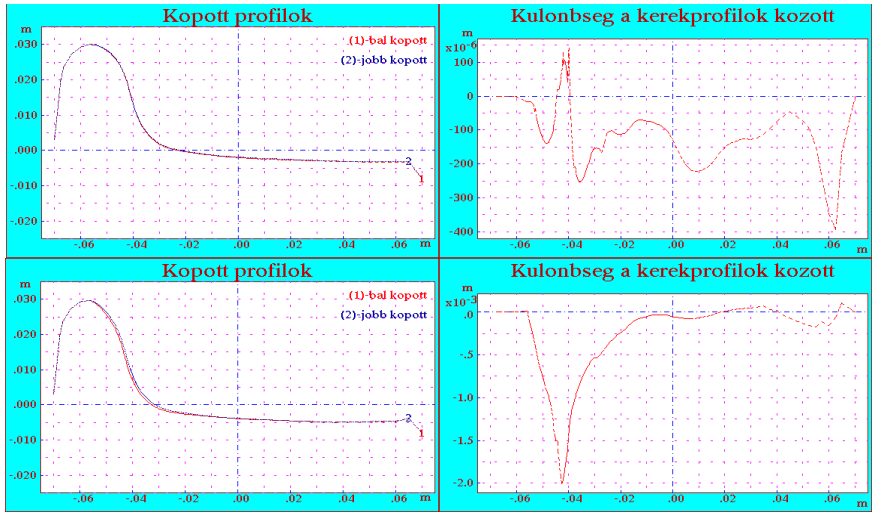

Fig. 10 Worn wheel profiles and difference between the two profiles realization simulations ’C’ and ’D’

The wear propagation speed significantly increased by the increase of the impact of the deviation sourced interface remained horizontal retentive torque.

5.2 Direct impact of applied vertical wheel force

Examination of direct impact of the deviation in vertical forces applied on wheels within the simulation run, determined by the static examination of the vertical system features, resultant from 4000 kg mass difference loaded on each side (simulation run ‘F’). Results are shown on Fig.11, 12. and Table 2.

Simulation Run ID	"n" left (mm)	"n" right (mm)	Calculated Mileage (km)	Portion to reference	Calculated wear propagation speed on "n" left (10^{-6} mm/km)	Calculated wear propagation speed on "n" right (10^{-6} mm/km)
A	31,83	31,89	27 557,00	1,00	6,31	3,88
F	30,91	32,11	29 115,00	1,06	37,30	-3,71

Table 2. Simulation results ’F’

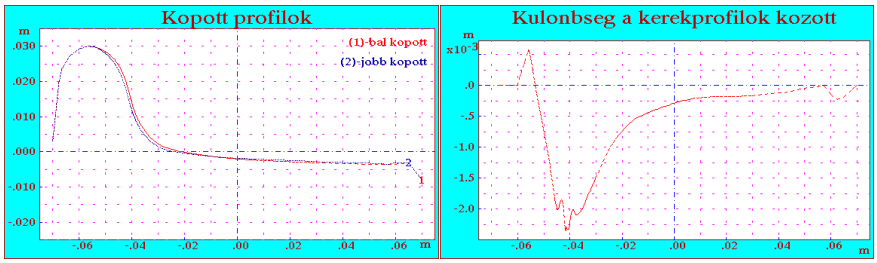

Fig. 11 Worn wheel profiles and difference between the two profiles realization simulation ’F’

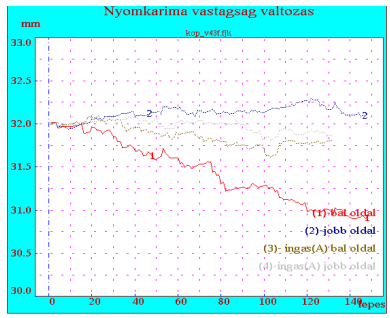

Fig. 12 Wheel flange thickness alteration over steps in simulation 'F'

The wear propagation speed value is within the same scale as the impact of the retentive horizontal torque.

5.2 Impact of wheel surface hardness deviation

Examination of impact of the deviation in wheel surface hardness deviation application, as utilization of the wear control coefficient function within the simulation run, 20% alongside the entire wheel profile - simulation run 'G', and 50% in simulation run 'J'. Results are shown on Fig.13, and Table 3.

Simulation Run ID	"n" left (mm)	"n" right (mm)	Calculated Mileage (km)	Portion to reference	Calculated wear propagation speed on "n" left (10^{-6} mm/km)	Calculated wear propagation speed on "n" right (10^{-6} mm/km)
A	31,83	31,89	27 557,00	1,00	6,31	3,88
G	31,24	31,26	24 133,00	0,88	31,49	30,83
J	31,69	31,85	18 527,00	0,67	16,95	8,04

Table 3. Simulation results 'G' and 'J'

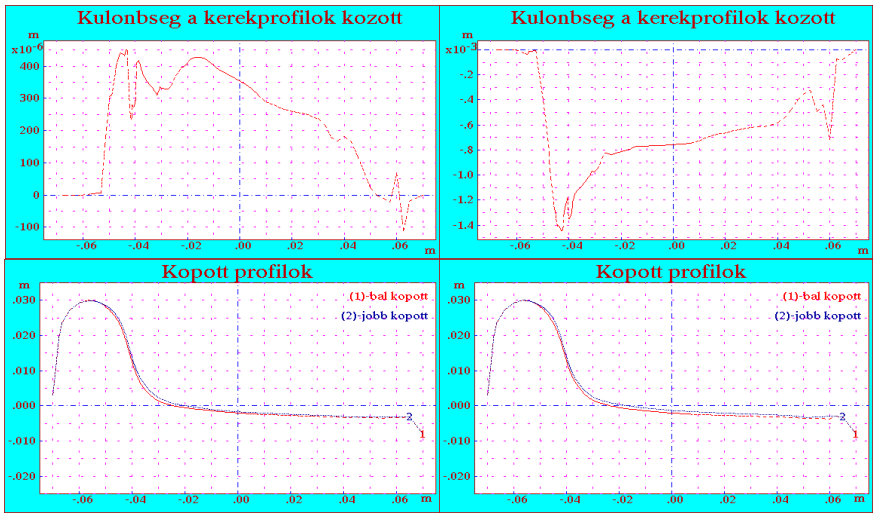

Fig. 13 Worn wheel profiles and difference between the two profiles realization simulations 'G' and 'J'

The impact of surface hardness deviation can reach a value of wear propagation speed only in un-realistic case. It can be stated, that this influencer parameter is effective, but much less compared to the impact efficiency of the secondary interface feature deviations.

5.2 Superposition case of interface feature asymmetricity and wear control coefficient

Examination of impact of the superposition of two influencers as of the interface feature deviation, with same value as in simulation 'D', and impact of surface hardness deviation as of 20% - simulation run 'H1'. Results are shown on Fig.14, and Table 4.

Simulation Run ID	"n" left (mm)	"n" right (mm)	Calculated Mileage (km)	Portion to reference	Calculated wear propagation speed on "n" left (10^{-6} mm/km)	Calculated wear propagation speed on "n" right (10^{-6} mm/km)
A	31,83	31,89	27 557,00	1,00	6,31	3,88
H1	31,41	32,08	23 925,00	0,87	24,49	-3,34

Table 4. Simulation results 'H1'

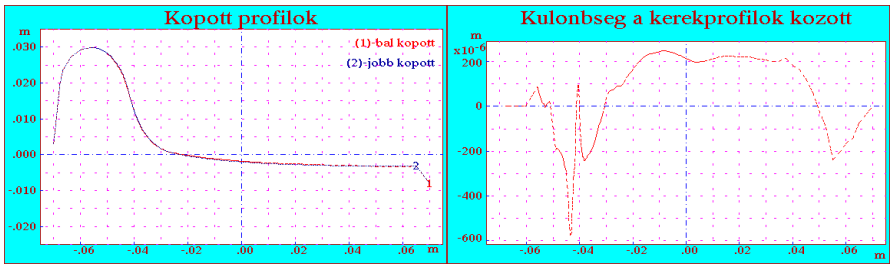

Fig. 14 Worn wheel profiles and difference between the two profiles realization simulations 'H1'

This run showed the possibility of superposition of the above described two influencers, with dominant effect of interface feature deviation. The two influence effects the same way, resultant in enlarged propagation of wear, this case can lead to a more intensity of wear, higher speed of propagation.

5.3 Superposition case of interface feature asymmetricity and wear control coefficient - counter productivity

Examination of impact of the superposition of two influencers as of the interface feature deviation, with same value as in simulation 'D', and impact of surface hardness deviation as of 20% but, on opposite sites - simulation run 'H2'. Results are shown on Fig.15, and Table 5.

Simulation Run ID	"n" left (mm)	"n" right (mm)	Calculated Mileage (km)	Portion to reference	Calculated wear propagation speed on "n" left (10^{-6} mm/km)	Calculated wear propagation speed on "n" right (10^{-6} mm/km)
A	31,83	31,89	27 557,00	1,00	6,31	3,88
H2	31,39	31,71	26 321,00	0,96	23,25	10,90

Table 5. Simulation results 'H2'

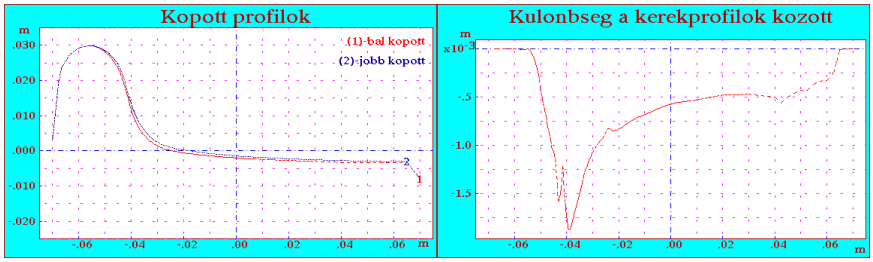

Fig. 15 Worn wheel profiles and difference between the two profiles realization simulations 'H2'

These results provided evidence to the case that the two examined influencer features can have counterproductive impact. This means although the dominant deviation enforces the wear propagation, the simulated wheel surface hardness deviation via the wear coefficient function can decrease the speed of it.

4. CONCLUSIONS

- The case study showed that the lateral and the vertical dynamical models of certain locomotive simulated the real behavior of the structure. It proved that differences in characteristic features of the secondary suspension elements have effective cause of asymmetric wheel wear. As an edification of the study it is a real necessity to provide emphasized control of force transmission elements.
- The past investigations into an asymmetric wheel flange wear phenomena proved that differences in characteristics of the secondary suspension elements applied caused the heaviest influence of this kind of abnormal wear process, the asymmetric wheel flange wear.
- On present basis of development of certain case study, the investigation into impacts of secondary suspension system anomalies settled;
- Important parameters checked, applied with simple sensitivity control methods;
- Currently independent dynamic models are developed to carry out the control on vertical and lateral dynamics. The lateral dynamic system gives the basis of the well-known „ELDACW" algorithm system, which is serving as crucial tool of this study;
- Identification of most efficient influencer parameters carried out under the umbrella of concerning the general profile wear operator;

- Goal of study achieved: possibility opened to create better vehicle features with application of the simulation method;
- On further thoughts shall be concerned the usage and merging of dynamic models, especially in frame of time. Long termination of process – impact of vertical dynamics' changes can be questioned, in short time: impact of changes is sudden.

5. REFERENCES

[1] **Zobory, I. - Benedek, T. – Győri, J.:** Vehicle Diagnostics – lecture notes, BME Department of Railway Vehicles, Budapest, 2004 (In Hungarian)

[2] **Zobory, I.:** Prediciton of Wheel/Rail Profile Wear, Vehicle System Dynamics, Vol.28, 1997, p.221-259

[3] **Szabó, A.:** Determination of the Lateral Running Dynamical and Wheel-Wear Processes by Means of Digital Simulation. (Vasúti járművek keresztirányú dinamikai és kerékkopási folyamatainak meghatározása digitalis szimulációval); PhD Thesis (Kandidátusi értekezés), Budapest, 1993 (In Hungarian);

[4] VM14 Treating Guide. Part: Vehicle Structure. Ganz-MÁVAG Budapest, 1985. (In Hungarian)

[5] **Ferencz, P.:** Investigation into Wheel Profile Wear Processes Influenced by Parameter Anomalies in Suspension Characteristics of Electro-Locomotive Bogies, Proceedings of BOGIE'10. (Ed. by Prof. I. Zobory), SSME, Budapest, 2017, p.201-211.

[6] **Hamby, D. M.:** A Review of Techniques for Parameter Sensitivity Analysis of Environmental Models, Westinghouse Savannah River Company, SC 29808, U.S.A.

TECHNOLOGIES FOR ACHIEVING BOTH RELIABILITY IMPROVEMENT AND WEIGHT REDUCTION OF N700S SHINKANSEN BOGIE

Seiji KANAMORI, Tomohiro OTSUKA, Masahito ADACHI and Kei SAKANOUE

Central Japan Railway Company
1545-33, Oyama, Komaki, Aichi, Japan

Received: September 12, 2019

ABSTRACT

In designing Shinkansen, it is necessary to constantly improve reliability, and it is also important to consider weight reduction. In particular, weight saving of the bogie strongly affects the running safety, the bogie hunting, the ride quality and the ground vibration. For this reason, it is important to achieve both high reliability and weight reduction while giving priority to safety when we design the rolling stock. In this research, we focused on bogie frame which accounts for 20% of the bogie weight. We aimed at reducing bogie frame weight by 75kg and reducing welded points of bogie frame while improving reliability by changing its structure, which had no major design change since 300 series Shinkansen. Further, we developed the light weight and compact traction motor. Since the weight of bogie frame and traction motor was reduced, it became possible to use a more reliable double helical gear device, a brake device with increased the plate thickness, and full-active suspension improving the ride quality. We confirmed the basic performance of the new bogie through bench tests and running tests in commercial line in 2017 and we are planning to install it on N700S in 2020.

Keywords: Reliability, Weight reduction, Welded bogie frame, Doble helical gear, Full active control

1. INTRODUCTION

The Tokaido-Shinkansen marked its 50th anniversary in 2014 since commencing operations in October 1964. Tokaido-Shinkansen runs between Tokyo ana Osaka, and it is the most important infrastructure in Japan. It's operation area covers about 24% of the whole country, and about 60% of Japanese population is concentrated in this area and its GDP accout for 64% of the country's whole GDP.

JR Central has been pursuing the utmost safety, and has been improving its operation by increasing the maximum speed, the number of trains in operation and enhancing quality of services. Maximum operation speed was 210km/h when it started operation in 1964, and was increased to 270km/h with the introduction of "Nozomi" in the spring of 1992 and further to 285km/h in 2013. In order to increase the speed, it is important to reduce the weight of the vehicle. Also, the bogie weight reduction has been achieved by various means such as downsizing of parts and structural changes. Weight saving of the bogie affects running safety, bogie hunting, and ride quality. On the other hand, the bogie has the role of supporting car body to run stably on rails. Therefore, weight saving of the bogie may affect running safety, bogie hunting, and ride quality. For this reason, giving top priority to safety, it is important to achieve both high reliability and weight reduction when designing the bogie.

2. EVOLUTION OF TOKAIDO-SHINKANSEN BOGIE

Shinkansen is adopted the bolsteress bogie since 300 series as shown in Fig.1. The wheelset accounts for about 50% of the whole bogie weight, the bogie frame follows at about 20%, the motor attachment at about 10%, and the car body suspension and the axle box assembly follow them. Therefore, in order to reduce car weight, first items to consider are the wheelset and the bogie frame. Since all of them are primary components, it is important to reduce weight while maintaining or improving reliability.

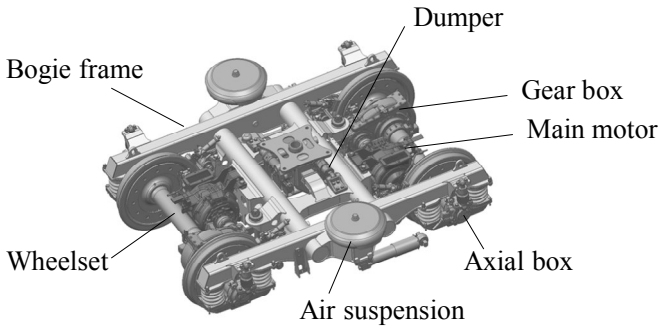

Fig. 1 Bolsterless bogie for Tokaido-Shinkansen (N700S)

In the past, the 300 series achieved significant weight reduction in the Shinkansen bogie. In order to achieve a maximum speed of 270 km/h, we incorporated bolsterless bogie in 300 series. In addition, significant weight reduction has been achieved by adopting hollow axle, induction motor, floating caliper brake device, axle box and gearbox made of aluminum. As a result, the 300 series bogie became about 30% lighter than the 100 series. This bolsterless bogie has become standard in high-speed vehicles, and has been widely adopted in Japan and overseas.

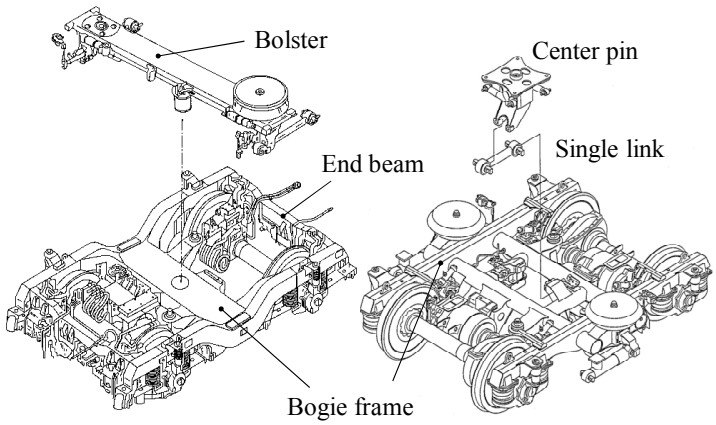

Fig. 2 Progeress from 0series to 300series

N700A has adopted a new type brake disc and brake pad. The purpose of these is to improve the braking disntance upon earthquake hit. In emergency as earthquake, we have to make shinkansen stop quickly as possible as we can by using the mechanical braking system. To enhance brake performance, brake disc and pad has been redesigned so that they contact with each other more uniformly and evenly. Because there are so many earthquakes, it is important to take measures against earthquakes in Japan.
Another feature to note is that the mass per one wheelset is significantly reduced by changing the disk shape. As described above, the development of the Tokaido Shinkansen is characterized by always pursuing safety, reliability, and weight reduction[1] .

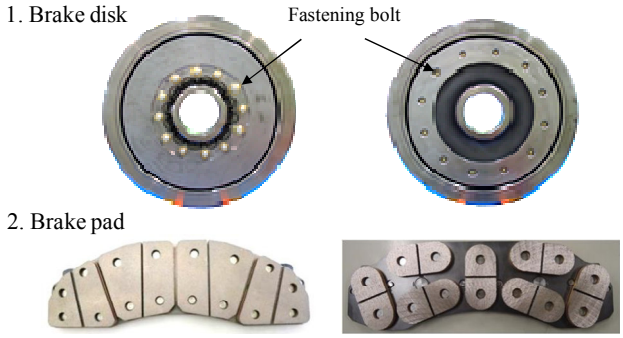

Fig. 3 Characteristics of brake disk and pad in N700A

3. DEVELOPTMENT OF BOGIE FRAME FOR N700S

3.1 Improved reliability and weight reduction of the bogie frame [2]

The bogie frame is the most important component that supports the car body and transfers its load to the wheels. The bogie frame consists of two side beams and two cross beams (Fig.4). In order to prevent the generation of uneven stress in the bogie frame due to the load from the body, the side beams have a shape capable of distributing the force while enduring the car body weight.

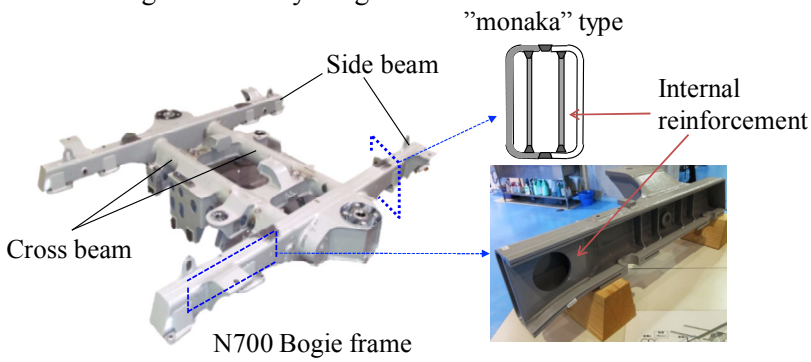

Fig. 4 Bogie frame of the conventional type

The side beams are structured to connect with a large number of members, and there are various welded joints. At the time of manufacture, it is important to conduct welding without defect such as penetration lack and verify the condition by nondestructive inspection as UT, MT, PT.

We focused on bogie frame which accounts for 20% of the weight of the bogie. We aimed at reducing bogie frame weight while improving reliability by changing its structure. Bogie frame structure is called ”monaka” type (Fig.5(a)) in conventional model where two U-shaped components with 8mm thickness facing each other are welded together. By placing reinforcing plates inside (=Internaol reinforcement), the stiffness requirement for side beams is satisfied. We have knowledge on which part of the bogies needs more strength than other through past field tests and bench tests. We confirmed that the suitable structure of the bogie frame to achieve the objective is hat-type. Hat type structure is the one where a U-shaped component is welded to a single lower plate from above (Fig.5 (b), Fig.6). By incorporating a hat type structure, it is possible to freely change the thickness of the lower plate of the bogie frame. We reduced the thickness of parts that do not require much strength and increased thickness for ones where strength margin was small. As a result, the internal reinforcement was no longer required due to the improvement the side beam’s toughness and reduction in weight was achieved. The weight was reduced by about 75 kg per bogie frame and vertical stiffness was improved by about 15%. This change of side beam lower plate is the result of successful collaboration between design and manufacture. Furthermore, hat type structure requires less welding of the bogie frame and this improves reliability while saving weight of the bogie frame.

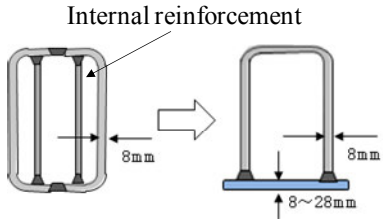

(a) Conventional type (”monaka” type) (b) Developed type (”hat” type)

Fig.5 Cross section of side beams

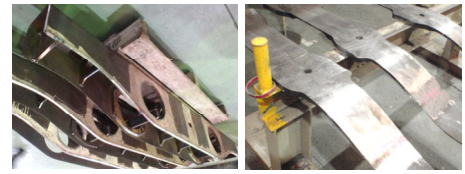

(a) U-shaped component (b) Lower plate

Fig.6 Structure of hat-type side beams

3.2 Utilization of the bogie frame as an air reservoir

The N700S utilizes a hat-type structure to create a closed section in the side beams to function as an air reservoir. As shown in Fig. 7, the reservoir was constructed by making the central part of the side beams a completely enclosed space. As a result of making the bogie frame into a tank, the soundness of the welded bogie frame can be secured by air leakage confirmation. The auxiliary reservoir for air suspension tank

in N700A was configured in cross beams. In N700S, since the side beams closer to the air spring is used as the auxiliary reservoir for air suspension, the cross beams can be made into the main air reservoir. As a result, it became possible to eliminate part of the main air reservoir installed in the car body, making the vehicle body lighter and creating new space.

As described above, the main feature of our approach in reducing bogie weight is to consider utilizing bogie frame on other application and therefore eliminating some components on car body.

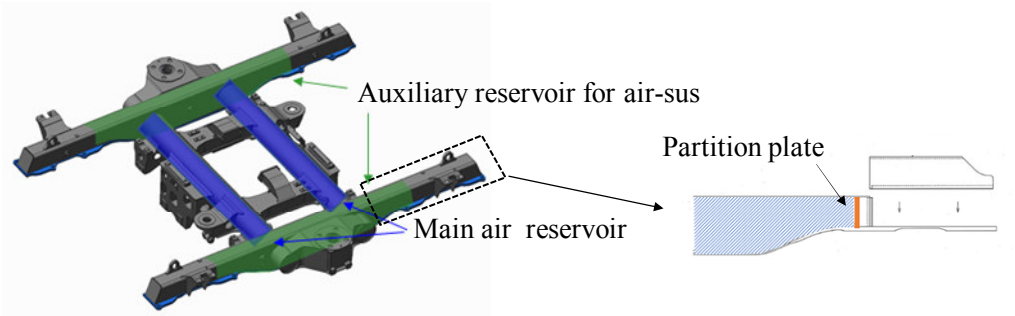

Fig.7 Utilization of the bogie frame as an air reservoir

3.3 Performance verification of developed bogie

When a new bogie is developed, it is necessary to confirm that there are no problems in both running stability and strength aspects. In especially, the most unfavorable bogie behavior which needs to be avoided is the hunting motion. There are forced hunting motion and one by the self-induced vibration. The latter is of particular importance, and it is important to design the bogie to keep the speed at which the self-induced vibration occurs sufficiently high with respect to the operating speed. We use the rolling stock field test simulator in our research center to confirm that hunting motion does not occur (Fig.8).

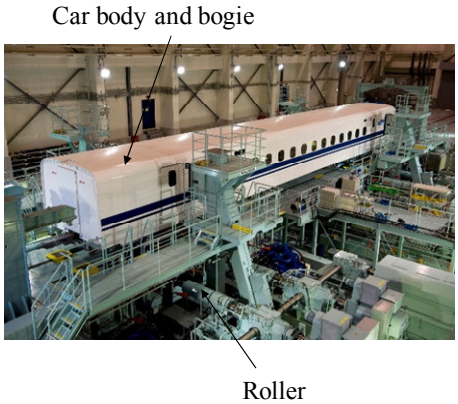

Fig.8 Rolling stock field test simulator

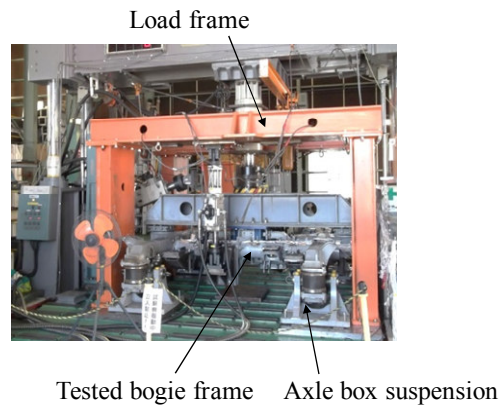

ig.9 Statistic and dynamic testing machine

Static load tests and fatigue tests were carried out to verify the strength of the bogie frame (Fig.9). In the static load test, extremely severe load conditions were set, and it was confirmed that the bogie frame stress was below the tolerance limit at any point. In the fatigue test, a cumulative load of 20 years was applied to the bogie frame, and it was confirmed that no cracks were generated from any welded parts.

4. IMPROVED RELIABILITY AND RIDE COMFORT

In the developed bogie, induction motors has been miniaturized and its length is reduced by about 70mm in the axle direction. The gear unit, the induction motor, and the brake device were put on the cross beams of the N700A's bogie frame and there was no extra space in the axial direction. Induced space and weight created as a result of induction motor downsizing for N700S's bogie is utilized for the purpose of improving reliability of the gear device, ride quality, and extending the life of brake pad.

4.1 Improved gear unit [3]

Helical gears are incorporated on the gear unit from 0 series to N700 series Shinkansen. In the helical gear, gears are machined in a diagonal direction with respect to the shaft. When the gear and the pinion mesh, several faces are designed to mesh simultaneously. Vibration and noise are reduced by increasing the meshing number. The bearing for supporting the rotation of the helical gear is a tapered roller bearing, which allows the rotation while bearing the axial force generated by the driving torque. Therefore, clearance adjustment is very important in maintenance (Fig.10). If this clearance is too small, the contact in the bearing will be excessive and seizure will occur by a sharp rise in temperature, and if too large, it will lead to the partial peeling due to exceeding allowable surface pressure. Currently, this clearance adjustment is performed carefully in maintenance for all gear units.

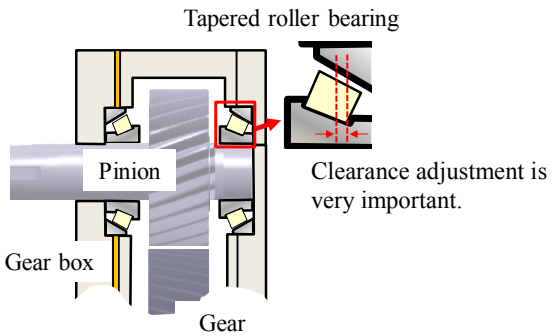

Fig.10 Construction of herical gear unit (from 0 to N700 series)

In N700S series, cylindrical roller bearings were adopted for gear device. Cylindrical roller bearings do not require as severe clearance adjustment as tapered roller bearings. By this application, the clearance adjustment task can be eliminated from maintenance

and improving reliability. However, since cylindrical roller bearings need to receive an axial force at the flanges of the inner and outer rings, it is necessary to reduce the axial force generated by the driving torque as much as possible.

We decided to use a double helical gear unit for the N700S bogie. Since the double helical gear is formed by facing two helical gears, the axial force generated by the driving torque is canceled by them (Fig.11). On the other hunds, the double helical gear requires more space than the helical gear. But the extra space created by the miniaturization of the induction motor is utilized for additional space needed for double helical gear. Since meshing area are simultaneously increased by adoption of double helical gear, it is also noted that vibration and noise at high speed rotation are reduced.

We optimized the module and twist angle, as a result, the meshing area is increased, and the gear noise and vibration were reduced. The unsprung mass was reduced by reducing the machine groove (Fig.11). By renewing the manufacturing equipment, we were able to create gears with small mechanical grooves.

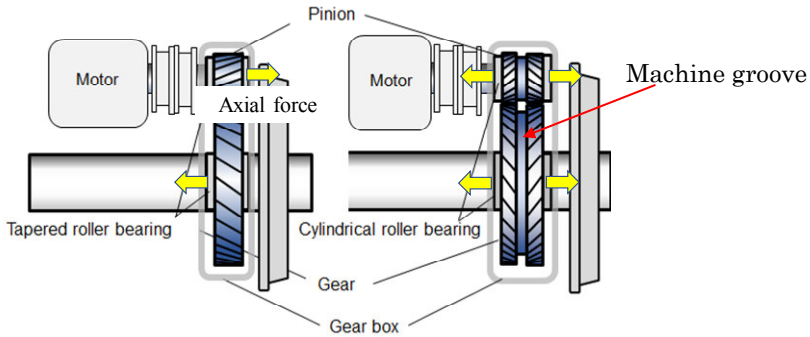

Fig.11 Cancel of the driving torque by double herical gear

We confirmed that the temperature, vibration, and noise performance of the double helical gear has been improved in bench tests (Fig.12). This is because the double helical gear reduced the axial force and the meshing rate increased. Reduced temperature improves lubricant life, and the reduction of vibration and noise not only improves service but also reduces the load on bearings.

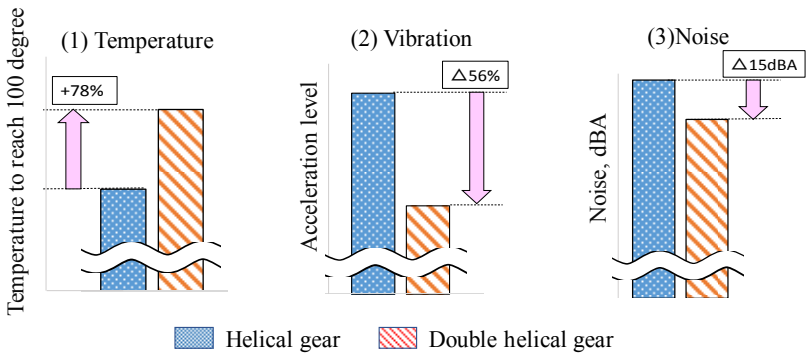

Fig.12 Characteristic of double helical gear

4.2 Improvement of ride comfort [4]

Improving ride comfort is an esssetial techonology for the passenger's perspective. In Tokaido Shinkansen, we developed the control technologies such as a car body tilting system inclination to reduce steady lateral acceleration in the curve. In addition , in order to improve the lateral acceleration, the semi-active suspension system was installed in a part of cars for 700 series. In the Series N700, which started operation in 2007, we developed an improved semi-active suspension system with further improved performance and installed it on all cars. Improvement of ride comfort levels are shown in Fig.13.

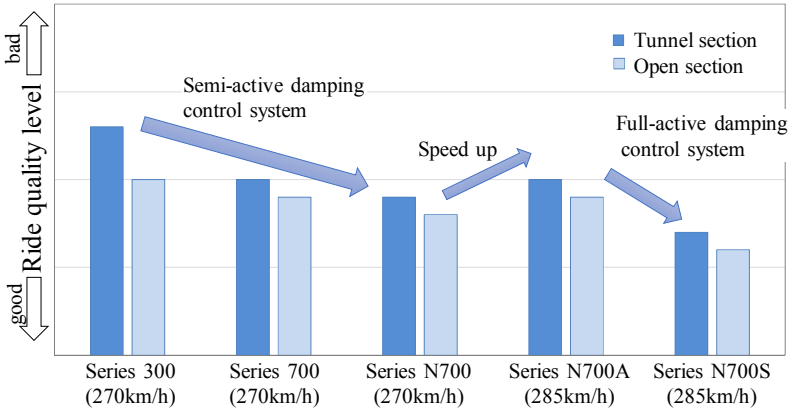

Fig.13 Ride comfort of Tokaido Shinkansen (Lateral direction)

In improving ride comfort, it is important to reduce steady lateral acceleration and vibration acceleration level. In N700S, in particular, in order to reduce the lateral acceleration during tunnel running, a full active suspension system was installed.
Both the full-active suspension system and the semi-active suspension system control the force of the device mounted between the car body and the bogie so as to minimize the vibration of the car body. Based on the signal of the acceleration sensor attached to the car body, it is always calculated how much and in which direction force should be generated.

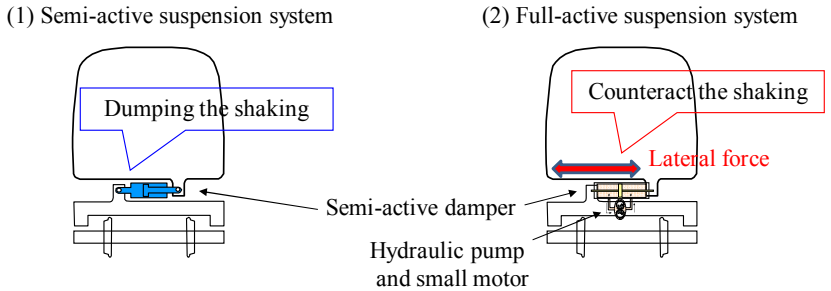

Fig.14 Ride comfort of Tokaido Shinkansen (Lateral direction)

The conventional semi-active suspension system changes the strength of the damper to damp the vibration of the car body, but in the full-active suspension system, the hydraulic pump is rotated to generate motive power, so, it cancels the vibration of the car body (Fig.14).

There are electric and hydraulic power types for full active suspension. We selected the latter, which has been proven in semi-active suspension of N700S. It has a compact structure with a small driving motor and hydraulic pump attached to the conventional semi-active suspension (Fig.15). Semi-active suspension will operate as a back-up to ensure ride comfort of N700A even when full-active suspension fails. AC100V was adopted for the inverter power supply for driving a small motor, which has been a major issue, thereby reducing the size and weight of the system.

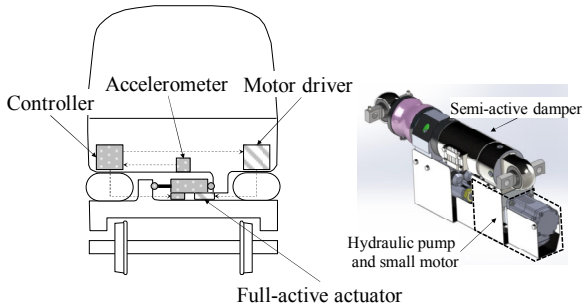

Fig.15 Overall structure of Full-active suspension system for Tokado-shinkansen

Running test in commercial line was carried out by converting the semi-active suspension system of the pantograph car and the last car of the N700S test car into a full-active suspension system. In the open section, the ride quality level of the pantograph car has improved by 1.5dB, and the leading car has improved by 5.7dB. In the tunnel section, the ride quality level of the pantograph car has improved by 8.3dB, and the leading car has improved by 6.2dB (Fig.16).

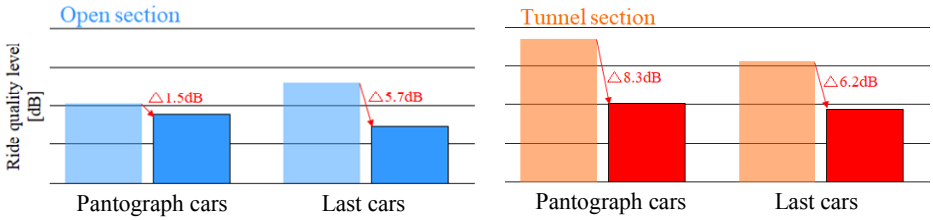

Fig.16 Confirmation of ride comfort in commercial line

5. CONCLUDING REMARKS

Since the weight of bogie frame and the size of induction motor was reduced, it became possible to use a more reliable doubole helical gear device and a full-active suspension in the developed N700S bogie. The developed bogie weight about 160kg less

than conventional bogie, which leads to more than 5 tons of weight reduction for Shinkansen as a whole. In terms of reliability, the change in the bogie frame structure greatly reduced the welding line. The load on the cylindrical roller bearing was greatly reduced by the double helical gear device. It is the first time that the double helical gear device is used in high-speed commercial vehicles.
The developed bogie is already incorporated in the latest-type Shinkansen N700S, which started running test for confirmation in March 2018. We are planning to put the new bogie into service in 2020.

6. REFERENCES

[1] **Kanamori, S. - Kobayashi**, G.: "Development of high performance brake system for passenger's safety upon earthquake hit", The Third International Conference on Railway Technology 2016.
[2] **Kanamori, S. - Otsuka, T. - Adachi, M. – Sakanoue, K.:** "Technologies for achieving both reliability improvement and weight reduction of Shinkansen bogie", WCRR2019
[3] **Kamiya, M. - Asano, J. - Kanamori, S. - Adachi, M. – Yamaoka, K.:** "Development of double helical gear for Shinkansen", J-Rail2018
[4] **Okada, Y. - Adachi, M. - Kato, H. - Aoya, T. – Okada, N.:** "Efforts to improve riding comfort of the Tokaido Shikansen", WCRR2019

ANALYSIS OF THE SAFETY AGAINST DERAILMENT OF NARROW-GAUGE RAILWAY VEHICLES MOVING IN CURVES OF SMALL RADII

András SZABÓ and István ZOBORY

Budapest University of Technology and Economics
Faculty of Transportation Engineering and Vehicle Engineering
Group of Railway Vehicles and Vehicle System Analysis

H-1521 Budapest, Hungary

Received: September 12, 2019

ABSTRACT

The paper investigates the safety against derailment of vehicles operating on 760 mm narrow-gauge railway tracks. The purpose of the paper is to determine the extent of change in safety against derailment as curve radius decreases (less than 60 m). The investigation included several vehicle parameters on the one hand and several track parameters on the other. Thus, five different vehicles were included: a lighter and a heavier four-axle passenger car, a two-axle passenger car as well as a two-axle and a four-axle Diesel locomotive. As regards the track side, the presence of vertical track deviations and the type of sleeper (concrete or wooden sleepers) were used as variable parameters. The extent of lateral profile wear was included in the parameter set both for the wheel flanges and for the rail heads. The risk of derailment will be evaluated for several parameter combinations by means of numerical simulation of the wheel/rail dynamical system.

Keywords: railway vehicle/track system, curved track, safety against derailment, safety rail.

1. INTRODUCTION

Safety against derailment is very important for narrow gauge railways. For the construction of 760 mm narrow-gauge railway tracks, where the radius of curvature is less than 60 m, a „third" rail, or safety rail is prescribed. The question is: what are the differences in safety against derailment at track radii less than 60 m under different operation conditions?

The goal of this investigation is to compare the safety against derailment of different vehicles running on curved tracks of radii smaller than 60 m. The reference case is running on curve of 65 m radius (this radius is greater than 60 m), and the analysed cases are running on curves of radius: 60, 50 and 40 m.

The method used was to simulate the motions of the wheel and the rail while the vehicle runs on curved tracks of different radii. We had a simple computer program developed earlier for analysing the derailment-process of a wheel moving along the rail. This simple and fast simulation program allowed carrying out several simulations with different vehicle and track parameters. In Fig.1 the flowchart of the simulation procedure is shown.

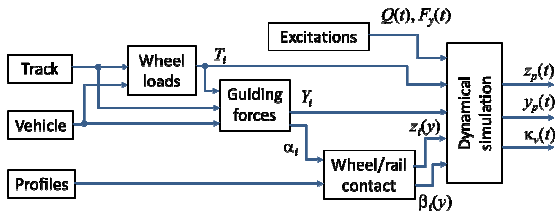

Fig. 1 The flow-chart of the simulation

In Fig. 1 is seen, that for the simulation there are two types of input data: on one hand the vehicle-, track- and profile parameters, and on the other the "excitations", which are time dependent variations in the vertical and horizontal forces acting on the wheel. The outputs of the simple simulation are the vertical and horizontal motions of the rail ($z_p(t)$, $y_p(t)$), and the "*risk of derailment*" ($\kappa_v(t)$). The latter is defined by formula (1) below:

$$\kappa_v = \frac{\text{The lifting of the wheel from the rail}}{\text{The maximum lifting possibility to the top of the rail}} . \quad (1)$$

From the results of the simulation the "*static running safety*" is also determined by formula (2) below:

$$S = \frac{\text{The value of the vertical wheel force (wheel load)}}{\text{The minimum vertical wheel force required for a given guiding force}} . \quad (2)$$

The simulation program allows analysing not only the "static" running safety, but also the process of *dynamical derailment*. That latter possibility means that in case of a situation of risk of derailment, there is sufficient time for the full derailment process to take place.

The simplicity and speed of the simulation program allows for analysing several simulation results with different vehicle and track parameters. In this investigation 640 simulation cases are analysed.

2. THE SIMULATION PROGRAM AND THE DYNAMICAL MODEL

Dynamical simulation was based upon a previously developed computation method [1], [2]. Fig. 2 shows the model of the wheel flange/rail contact. The rail is connected to the environment at rest by vertical and lateral elastic and dissipative force connections.

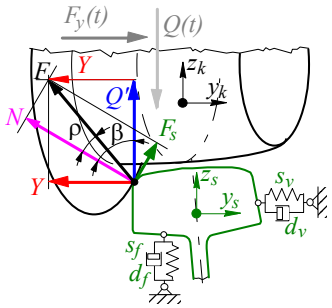

Fig. 2 Dynamical model of the wheel/rail connection

As it is seen in Figs. 1 and 2 the lateral and vertical forces in the wheel-rail connection are the two main effects, which basically determine the running safety. The necessary vertical force depends on the wheel load, which can change due to the following reasons:

- The wheel loads are not balanced:
- The wheel-rail contacts don't emerge in a common horizontal plane due to the presence of track irregularities or to the change in super-elevation.
- The stiffnesses of the vertical suspension springs are not identical.

- One or more vertical spring(s) is(are) broken.
- The load of the vehicle may be asymmetric.

In this simulation changes in wheel load equivalent to that due to a 5 mm vertical track irregularity under a single wheel are considered. To determine the necessary vertical forces in the wheel-rail contact the static balance of the vertical forces must be determined. In the general case, if the wheel positions-, springs parameters- and vehicle loads are given, the vertical forces arising between the elements of a four axle vehicle are shown in Fig.3.

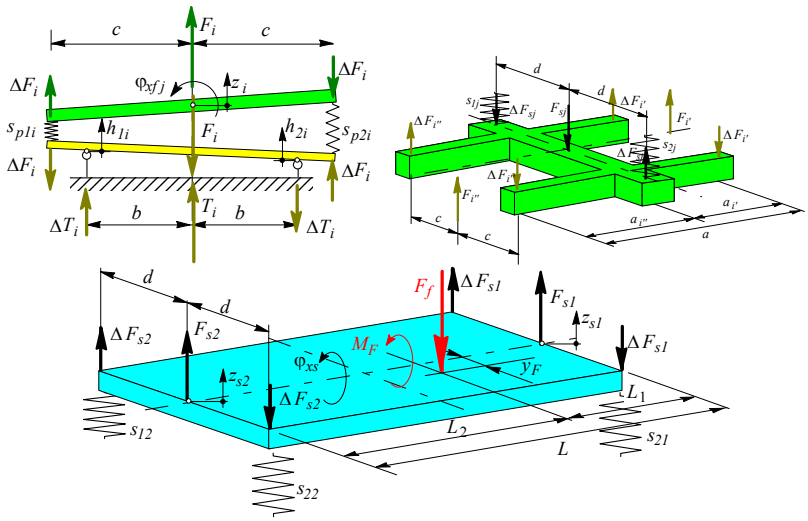

Fig. 3 Balance of the vertical forces

Force and torque equations for static equilibrium can be established, but it appears there are too many unknowns. So it is necessary to taken into consideration the relationships between the restoring forces and the vertical positions of the wheelsets, bogies and the vehicle body. After this the equilibrium of the system is described by a system of 29 linear equations for the 29 unknowns (displacements, forces and torques). The outputs are: the 8 wheel loads acting on the 8 wheel-rail contacts: (designated by T_i in Fig.1).

Further important forces are the necessary lateral guiding forces Y_i arising at the wheel-rail contact. To determine the latter forces the first step is the determination of the position of the vehicle in the given curved track. In Fig. 4 the lateral position of a four-axle vehicle in a curved track is shown.

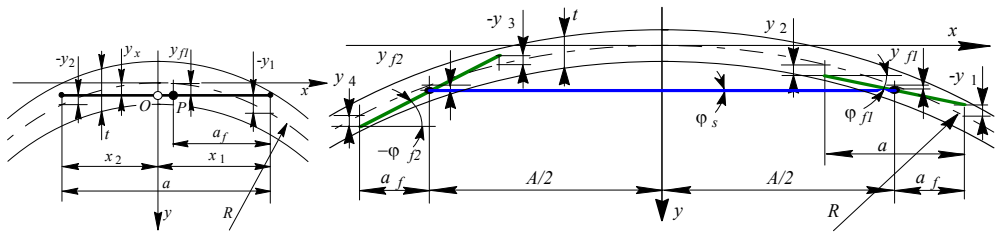

Fig. 4 Position of the vehicle in curved track laying in a horizontal plane

If the position is known, then the lateral forces and necessary torques between the elements of the vehicle can be calculated, and the necessary lateral forces in the wheel-rail contacts are found by the static balance equations of the bogies and vehicle car-body (Fig. 5).

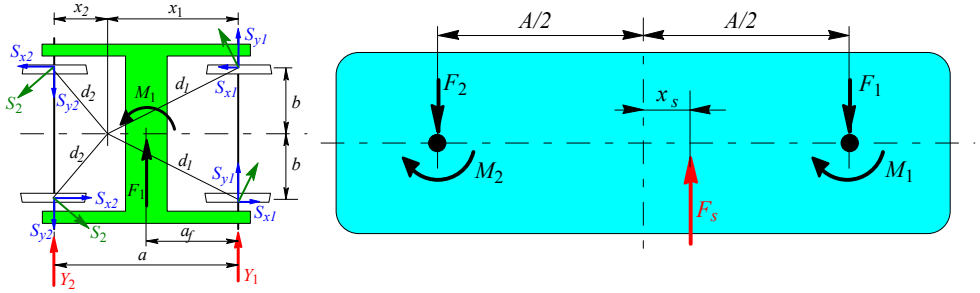

Fig. 5 Lateral forces and torques acting on the bogie and vehicle car-body

The results may not satisfy compatibility, because the guiding force in the wheel-rail contact may not be compatible with the wheel-rail relative position: namely the guiding force must be zero, if there is no flange-contact between the wheel and rail (the displacement of the wheel directed to the rail is smaller than the half of the gauge-clearance $t/2$). Thus an iterative procedure is necessary, for which a flow-chart is shown in Fig. 6.

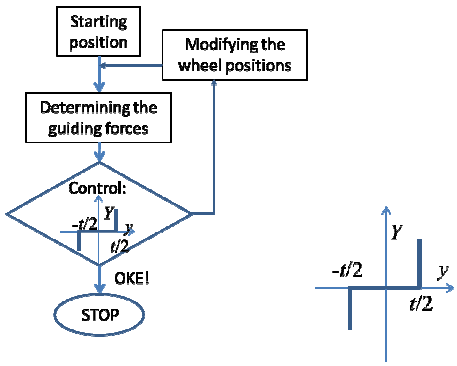

Fig. 6 Iteration procedure for determining the guiding forces

In the iterative procedure the vehicle position is initially computed and the necessary guiding forces determined from this position are controlled. If the results are not in accordance with the criterion mentioned above, then the vehicle position is adjusted. The necessary guiding forces in each wheel-rail contact are the outputs of this procedure. The guiding forces depend on: the nominal gauge-clearance, the actual gauge extension, as well as on the worn wheel and rail profiles.

The next important question is the treatment of the wheel-rail contact. In this program arbitrary wheel and rail profiles, given by their profile co-ordinate pairs can be taken into consideration. Continuous wheel-rail contact is assumed, thus there is no loss of contact (disunion) in the connection. The wheel and rail are rigid, the connection occurs in a single point, in the contact point.

For the sake of determining the position of the wheel and rail contact point some coordinate transformation is necessary. The relative position between the wheel and rail is given by the relative lateral displacement Δy and the relative angle of attack α of the two profiles, as can be seen in Fig. 7. In the procedure the wheel profile is turned round the vertical coordinate axis by the angle of attack α, and the rail profile is turned around the longitudinal coordinate axis by the inclination angle δ, and the Δy relative lateral position is adjusted. Results of this procedure are the angle of the contact plane from the horizontal plane $\beta(\Delta y)$, and the lifting of the wheel $z(\Delta y)$ as the function of the lateral relative position (see Fig.7).

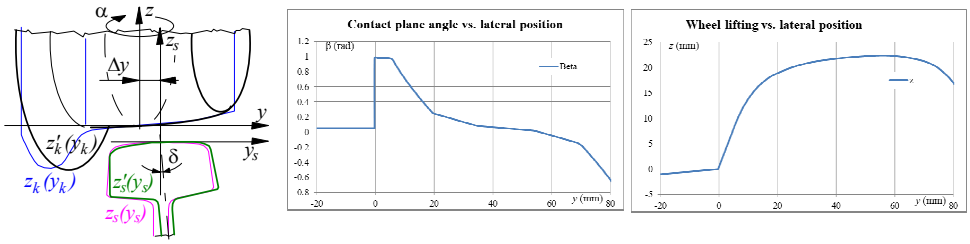

Fig. 7 Wheel-Rail contact

The dynamical model consists of two lumped masses: the wheel-mass and the rail-mass under the wheel.

The wheel and rail masses are in continuous contact on the contact patch of the wheel flange surface in the presence of sliding frictional force. The model includes the vertical and lateral displacement coordinates of the wheel mass and the associated rail mass, taking into account the relation between them by formula (3) due to the continuous contact:

$$\dot{z}_k \cos\beta - \dot{y}_k \sin\beta = \dot{z}_p \cos\beta - \dot{y}_p \sin\beta. \tag{3}$$

The excitation of the model comes from the time-dependent wheel load $Q(t)$ and the lateral force $F_y(t)$ acting on the wheel. Both of the time dependent excitation forces are considered as sinusoidal with different angular frequencies and phase angles, as follows:

$$Q(t) = Q_0 + Q_A \sin(\omega_Q + \varepsilon_Q) \quad F(t) = F_0 + F_A \sin(\omega_F + \varepsilon_F) \tag{4}$$

The motion equations are established in accordance with Newton's second law:

$$Q' - Q = m_{kf}\ddot{z}_k \ , F_y - Y = m_{kv}\ddot{y}_k \ , Y - s_v y_p - d_v \dot{y}_p = m_{pv}\ddot{y}_p \ , -Q' - s_f z_p - d_f \dot{z}_p = m_{pf}\ddot{z}_p \ , \tag{5}$$

and the well-known *Nadal*-formula is also used:

$$\frac{Y}{Q'} = tg(\beta - \rho) = \frac{\mathrm{tg}\beta - \mathrm{tg}\rho}{1 + \mathrm{tg}\beta\,\mathrm{tg}\rho} = \frac{\mathrm{tg}\beta - \mu}{1 + \mu\,\mathrm{tg}\beta} \tag{6}$$

The time dependent motions and forces are resulted by the solution of the above formulated system differential equations. The *risk of derailment* $\kappa_v(t)$ (see formula (1)) also becomes known, so the process of the dynamical derailment can be analysed.

3. THE SIMULATION PROCEDURE

The simulation procedure consists of the following steps (see Fig.1):

1. *Determination of wheel loads*: Determination of the vertical force on each wheel taking into account vertical track irregularity.
2. *Determination of guiding forces*: Determination of the geometry of the vehicle in a given curve, of the evolving guiding forces, of the evolving angles of attack of the wheels, taking into account the curved track and the track gauge clearance. From the point of view of safety against derailment, the most unfavourable wheel should be selected from among all the wheels of the vehicle considered.
3. *Determination of wheel/rail contact characteristics*: after the profile transformations, determination of geometrical properties of contact, depending on the relative lateral position of wheel and rail: β is the angle of the contact plane measured from the horizontal, and *z* degree of wheel elevation. (see Fig. 7).
4. *Determination of static running safety* (2): determination of running safety by the *Nadal* formula according to equation (6).
5. *Dynamic derailment simulation*: Determination by simulation of the wheel and rail motion using time dependent vertical wheel load $Q(t)$ and lateral force $F_y(t)$.

In dynamic simulation, the amplitude of the vertical wheel load $Q(t)$ is the change in wheel load within the limit of static running safety, and its frequency is the same as the vertical eigen-frequency of the vehicle. The amplitude of the lateral force $F_y(t)$ was 10% of the deflection force and its frequency was 10, 5, 3 and 1 Hz, respectively.

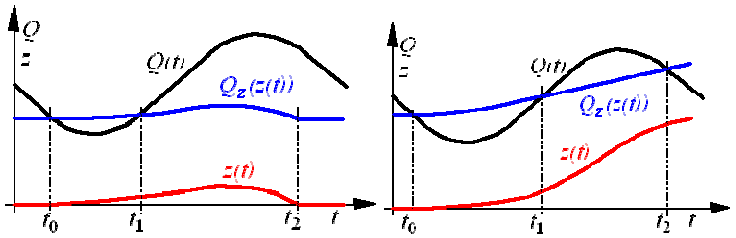

Fig. 8 Wheel-Rail contact

In Fig. 8 the process of dynamical derailment is illustrated. There are variations in the vertical force $Q(t)$, and when it is smaller than the necessary vertical force $Q_z(z(t))$ (t_0 in Fig.), the wheel starts to climb ($z(t)$). In the left hand side figure the time interval $[t_0,t_1]$ is shorter than in the right hand figure, so the increase in vertical force $Q(t)$ restores the wheel position. At the right hand figure the higher vertical force acts for a short time $[t_1,t_2]$ and too late, so the wheel elevation is not restored. Derailment can only occur if there is sufficient time for the flange to climb to the top of the rail.

3. THE SIMULATION RESULTS

In this investigation the Budapest "Children's" narrow-gauge railway system is analysed. There are 5 vehicle types: 3 passenger cars and 2 types of locomotives. The track includes 4 different radii of curvature and 2 types of sleepers: concrete (marked as B) and wooden (marked as F). The parameter disturbance has four combinations: Nominal values (marked as N), wheel and rail flange/side wear: total 5 mm (marked as J), decrease in vertical wheel load (track settlement 5 mm) (marked as P) and decrease in both wear and wheel load (marked as M).

The disturbance forces are present both in vertical and in lateral direction. The amplitude of the vertical force is maximum, when there is no static derailment, and its frequency is the near the vertical eigen-frequency of the vehicle. The amplitude of the horizontal force is 10 % of the nominal value, and the frequency of this horizontal force has four cases: 10 Hz (without mark), 5, 3 and 1 Hz (marked as 5Hz, 3Hz, 1Hz). In Fig. 9 the special wheel profile for narrow-gauge vehicles and the rail profile type *MÁV 48.5.r* are shown.

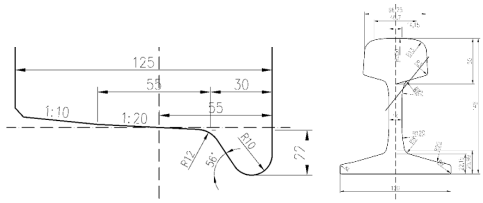

Fig. 9 The wheel and rail profiles.

As regards the track radii of curvature, the reference radius is the 65 m, and the investigated radii are 60, 50 and 40 m. The total number of simulation cases is 640 of which only some can be presented in the following. For each vehicle type the dynamical process of minimum frequency, with no derailment and maximum frequency, with dynamical derailment, is presented, for both concrete and wooden sleepers.

The dynamical simulation results are plotted versus *time*. The following quantities are shown: the wheel load Q; the lateral force F_y appearing as Y , the lateral and vertical displacements y_p, z_p of the track mass; and the risk of derailment κ_v from (1). (see Fig.1)

Results 1: 4-axle passenger car with „Szarajevo" type bogie (marked as BaxS)

In this case dynamical derailment did not occur at normal parameter values and in cases when the wheel and rail wears are considered only, and the radii are larger than 40 m.

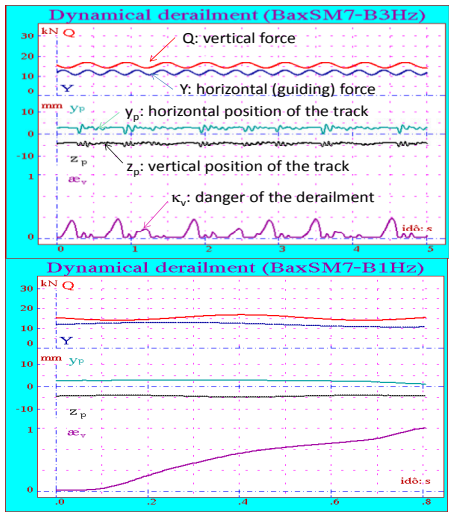

Track + Profile, Sleeper: Concrete

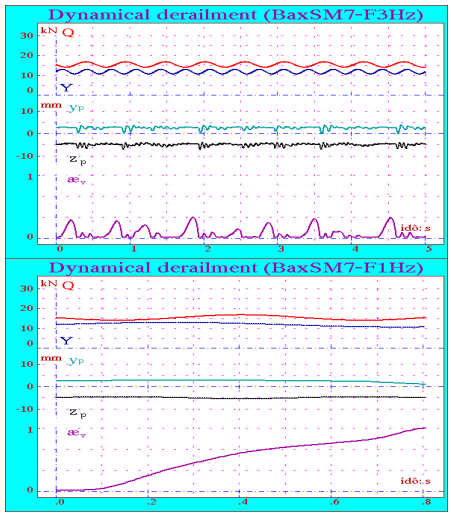

Track + Profile, Sleeper: Wooden

Fig. 10 4-axle passenger car with bogie „Szarajevo": R = 65 m

In a curve of 40 m track radius dynamical derailment occurred at a frequency of 1 Hz with normal parameters and worn profiles, and at 3 Hz with wheel unloading. The change in static running safety: 1-1.2 % to the reference radius, and there is no difference between the cases of the concrete and wooden sleepers. Fig.10 shows the dynamical processes in case of running on a curve of radius 65 m with wear to both profiles and wheel unloading. For a lateral force frequency of 3 Hz frequency there is systematic wheel lifting, but derailment did not occur, while for 1 Hz frequency the derailment limit is reached after only 0.8 s.

Results 2: 4-axle passenger car with bogie „Diamon" (marked as BaxD)

In this case the car-body mass is less, but the bogie is more rigid. If wheel unloading is present, dynamical derailments occur at all radii and also at the highest frequency investigated. For a curve of radius 40 m, with nominal parameters, dynamical derailment occurred only at the lowest frequency investigated. The change in static running safety was 1-1.2 %.

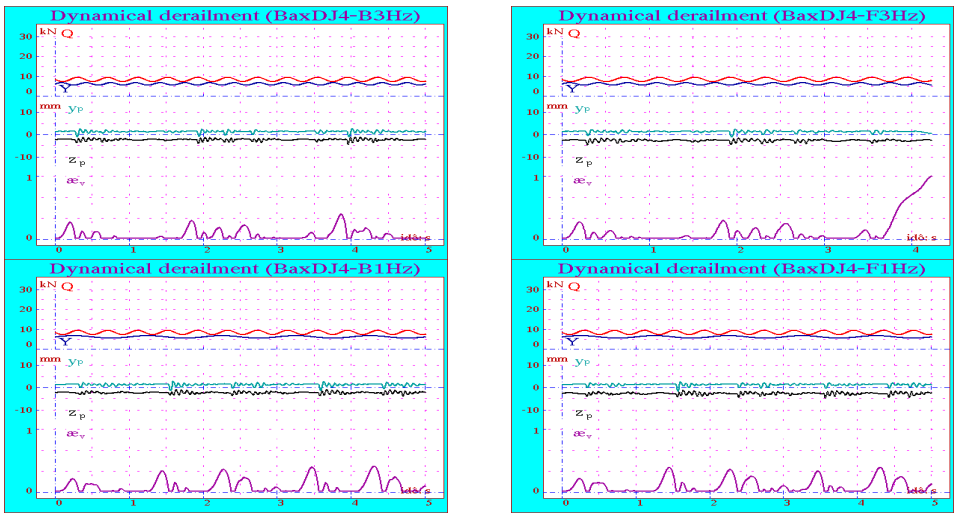

Profile wear, Sleeper: Concrete Profile wear, Sleeper: Wooden

Fig. 11 4-axle passenger car with bogie „Diamond": R = 40 m

The time dependent processes of the dynamical derailment are shown in Fig.11 in case of a curve of radius 40 m, and with worn profiles. It is very interesting, that in case of wooden sleepers the dynamical derailment occurred after 4 s time for the higher frequency (3 Hz) force variation, while at the lower frequency only systematic wheel lifting can be observed, without any derailment. It shows the random character of the derailment process and the role of coincidence in the derailment.

Results 3: 2-axle passenger car (marked as Bak2)

In this case in the range of lateral force frequency investigated, dynamical derailments occurred only on the smallest curve radius and if wheel unloading is present. There is no change in static running safety relative to the reference radii.

The dynamical derailment is shown in Fig.12. The derailment occurred only in case of concrete sleepers and when the frequency of the lateral force variation was 3 Hz.

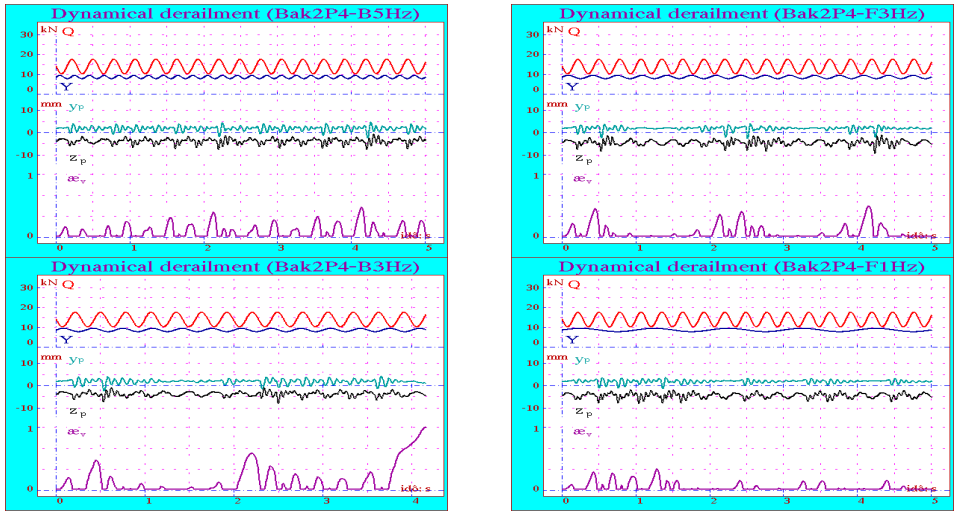

Track 5 mm, Sleeper: Concrete — Track 5 mm, Sleeper: Wooden

Fig. 12 Results of dynamic derailment analysis: 2-axle passenger car R = 40 m

Results 4: 4-axle locomotive (marked as Mk48)

In most cases the decrease in running safety did not change, but sometimes it was 1.5-1.8 %. The limit lateral force frequency, when the dynamical derailments can be observed is between 1-5 Hz. Fig.13 shows the situation, when wheel unloading is present (track settlement is 5 mm) and the locomotive runs in a curve of radius 50 m. Derailment occurs after a series of flange climbing occurrences followed by a return to tread contact.

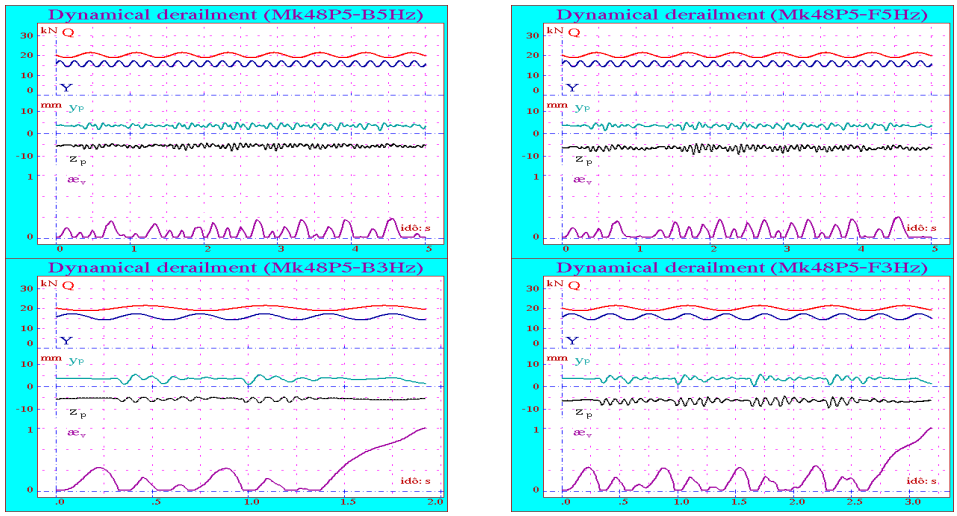

Track 5 mm, Sleeper: Concrete — Track 5 mm, Sleeper: Wooden

Fig. 13 Results of dynamic derailment analysis: 4-axle locomotive R = 50 m

Results 3: 2-axle locomotive (marked as C50)

In this case the vehicle has high vertical eigen-frequency. The static derailments occurred with wheel unloading. The dynamical processes are shown in Fig.14.

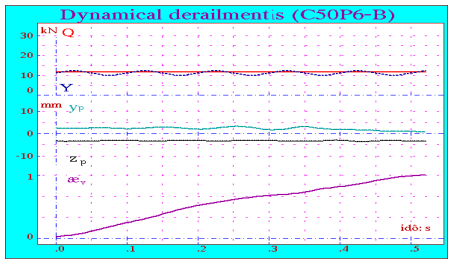

Track 5 mm, Sleeper: Concrete

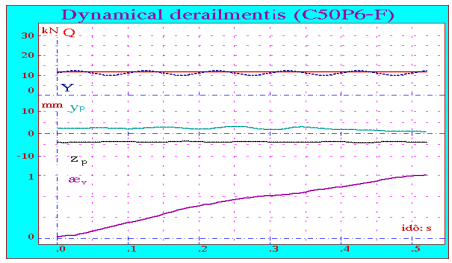

Track 5 mm, Sleeper: Wooden

Fig. 14 Results of dynamic derailment analysis: 2-axle locomotive R = 60 m

As it can be seen in Fig. 14 in case of static derailment, half a second is enough for the derailment process.

8. CONCLUSIONS

During the research, we investigated the running safety behaviour of 5 different narrow-gauge vehicles as they travel in small-radius curves. In addition to determining the static running safety, we also monitored the process of dynamic derailment, i.e. wheel and rail motions with varying vertical wheel loads and lateral thrust. The conditions in a 65 m radius arc were considered as a reference,

Simulations covered 4 track radii (65, 60, 50, 40 m), and 2 sleeper types (concrete and wooden), 5 vehicles (3 cars and 2 locomotives), 5 mm track vertical deviation - to induce wheel unloading , 5mm profile wear and a combination of both.

Based on the simulation results, the following statements can be made:

- The change in static running safety is within the range 1-1.8 % of the value in the reference curve.
- In the presence of a 5 mm track error, static derailment occurs for all curve radii for one of the four-axle coaches and the two-axle locomotive. This is due to the increase in the frictional momentum of the frictional torque between the bogie and the car-body at low wheel load, and in the case of the locomotive, the short wheelbase and high stiffness of the suspension.
- Under the profile and curve conditions studied, the degree of wheel wear does not significantly influence running safety and dynamic derailment.
- Lightweight wooden sleepers are less favourable for dynamic derailment.
- The most critical parameter for dynamic derailment and running safety is the presence and extent of track damage.
- Dynamic derailment in 40 or 50 m radius curves is typically faster (at higher deflection frequency) than in 60-65 m radius curves.

9. REFERENCES

[1] **Szabó, A**. (topic leader): Investigation into the hidden causes of derailments by dynamical method with regard to the increase in train speeds and accident prevention. Research report, (Ordered by the MÁV Co.), Part I. BME Department of Railway Vehicles, Budapest,1993, (p.50) (in Hungarian)

[2] **Szabó, A**. (topic leader): Investigation into the hidden causes of derailments by dynamical method with regard to the increase in train speeds and accident prevention. Research report, (Ordered by the MÁV Co.), Part II., BME Department of Railway Vehicles, Budapest,1994, (p:32) (in Hungarian)

IMPROVING BOGIES DESIGNS FOR NARROW GAUGE RAILWAYS

Sergii S. MIAMLIN

Dnipropetrovsk National University of Railway Transport
named after Academician V. Lazaryan, Ukraine
49010, Ukraine, Dnipropetrovsk, ac. Lazaryana str, 22/112,
sergeymyamlin91@gmail.com
phone: +38-097-135-68-84

Received: June 30, 2019

EXTENDED ABSTRACT

1. INTRODUCTION

The development of railway transport is accompanied, as a rule, by the introduction of modern structures of rolling stock and infrastructure elements. Along with traditional rail transport, narrow-gauge railways are also relevant, which are used not only as technological means of transport, but also as regional and interregional means of transport. As it is known, rolling stock running gears are largely decisive in the formation of dynamic road performance of rail vehicles, therefore, improving the design of rolling stock bogies for narrow-gauge railways is a relevant research area. The paper discusses options for improving the design of bogies for freight and passenger cars that are used on narrow-gauge railways in the mountainous regions of Ukraine and the nearest European countries. This type of rolling stock has an important advantage over bogies of traditional railways, since it does not require rearrangement of wheel sets and change of the gauge when crossing the border between countries that have a narrow-gauge infrastructure.

2. DESIGN OF PASSENGER CAR BOGIE

The author carried out research, as a result of which constructive schemes, design models and technical solutions for narrow-gauge freight and passenger cars bogies, considering the peculiarities of operation in mountain sections of railways, were obtained. At the first stage of these studies, the author developed technical solutions for narrow gauge rolling stock bogies. Which take into account not only the features of operation of this type of rolling stock, but also allow to significantly improve its dynamic characteristics. Fig. 1 shows the design of the proposed two-axle passenger car bogie. This bogie is a frame structure, which is made of profile metal so that the distribution of stresses in the bearing parts allows you to evenly distribute the forces between the elements. The design feature of this bogie is that the spring suspension parameters are selected according to the results of vector optimization, taking into account the main indicators of dynamics and wear. As a result of mathematical modeling of spatial oscillations of a narrow-gauge passenger car and determining the interaction forces of the car and the bogie, the parameters of the three spring suspension stages of the carriage were determined: elastic side bearings, center suspension, axle box suspension.

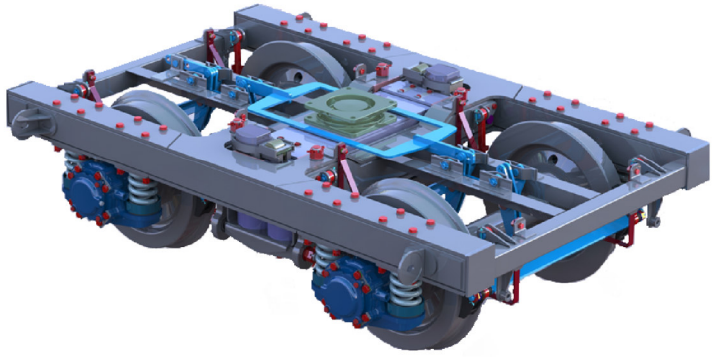

Fig. 1 Passenger car bogie for track gauge 1000 mm and 750 mm

3. DESIGN OF FREIGHT CAR BOGIE

Similar studies have been conducted for several types of freight cars, as a result of which rational characteristics of a universal two-axle bogie for freight cars (Fig. 2) of various types have been obtained. The features of this bogie design also include a set of spring suspension parameters consisting of elastic side bearings, a central spring suspension and an axle box suspension. As elastic elements, both traditional cylindrical springs and special elastomeric elements are used.

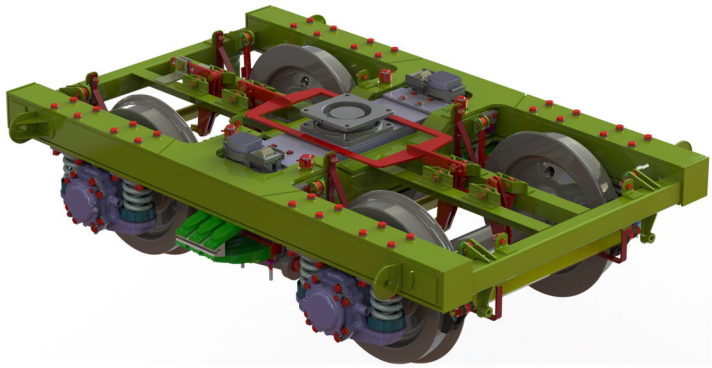

Fig. 2 Passenger car bogie for track gauge 1000 mm and 750 mm

4. CONCLUSIONS

The features of the proposed designs of bogies include the determination of the optimal parameters of all stages of suspension using the methods of vector optimization. Practical recommendations on the parameters of spring suspension elements, which are implemented in real structures, are obtained. Thus, as a result of the implementation of an experimental design complex development, theoretical and experimental research, technical solutions have been obtained for the designs of bogies for narrow-gauge freight and passenger cars for use in mountain sections of railways.

5. REFERENCES

[1] **Myamlin, S. S. - Bosyi, D. - Sablin, O. - Khomenko, I. - Kosariev, Y. – Kebal, I.**: Intelligent technologies for efficient power supply in transport systems. Transport Problems. Volume 12, 2017, p.57-70.

[2] **Prihodko, V. - Pshinko, A. - Myamlin, S. – Duzik, V.:** Modern coach construction. Proceedings of the 11th MINI Conference on Vehicle System Dynamics Identification and Anomalies, VSDIA 2008, (Ed. by Prof. I. Zobory) BME Department of Railvay Vehicles, Budapest, Budapest, 2008, p.309–313.

[3] **Kebal, I. - Kolesnykov, S. - Romaniukha, R.:** Wheelset axle with the cavity of uniform cross section. Science and Transport Progress. Bulletin of Dnipropetrovsk National University of Railway Transport.– N 5(53). – 2014, p.119-125.

[4] **Dailydka, S. - Lingaitis, L. P. - Myamlin, S. – Prichodko, V.:** Mathematical model of spatial fluctuations of passenger wagon. Eksploatacja i niezawodnosc. – № 4. 2008, p.4–8.

[5] **Dailydka, S. - Lingaitis, L. P. - Myamlin, S. – Prichodko, V.:** Modeling the interaction between railway wheel and rail. Transport / Vilnius Gediminas Tech. Univ., Lithuanian Acad. of Sciences.– № 23. – 2008, p.236–239.

CREEP CONTROL IN BRAKE OPERATION TO AVOID WHEEL SLIDING AND WHEEL FLATTENING

István ZOBORY[1] and Dezső NAGY[2]
Budapest University of Technology and Economics,
[1] Faculty of Transportation Engineering and Vehicle Engineering,
[2] Faculty of Electric Engineering and Informatics
H-1111 Budapest, Műegyetem rkp. 3. Hungary

Received: 7 September, 2019

ABSTRACT

The creep control procedure is elaborated to avoid the macroscopic sliding in the rail/wheel contact due to the too intensive braking torque application. If macroscopic sliding takes place it can lead to wheel flattening and to a considerable decrease in the force level that can be transmitted from the rail to the wheel, in short: the braking force is also decreased. In the present study, the extension of the model elaborated for VSDIA 2016 will be described. The first item of the extension is the elaboration of the vertical springing and damping connections of the rigid bodies in the vehicle model. Due to this extension, the excitation effect of the vertical track irregularities has been introduced into the dynamical system through the linearized vertical contact spring/damper (the Hertzean spring and damper) elements. The other item of the extension gives further innovative feature to the study. It is the precise modelling of the asinchronoeus motor working in brake mode of action, and detailed modelling of the disc brake unit of controlled friction torque. The delimited modelling of the braking torque exetring items gives a flexibile character to the simulation procedure and prepares the real applicatios. The control itself refers for the longitudinale creepages, i.e. the creepages are held in the close neighbourhood of a prescribed creepage-value. The control system ensures such variation of the braking torques acting on the wheelsets, that the time function of the creepages at every wheel in case of certain disturbances always returns to the prescribed creepőage value, i.e. the resultant control process is asimptotically stable.

Keywords: feed-back control, creepage, rolling contact, vehicle dynamics, track excitation, simulation, noisy measurement, optimum gain

1. INTRODUCTION

When developing brake gears it is important to improve the anti-skid devices for avoiding the macroscopic wheel sliding under pour adhesion conditions. In most approaches it is crucial to have information on the creep-dependent *force connection coefficient* (*fcc*) defined by the ratio: $\mu = F_t/F_n$, i.e. *the ratio of the tangential F_t and normal F_n forces acting upon the wheel/rail contact surface* either in a deterministic or a stochastic scheme. From among the possible control strategies in our approach the measure of braking torque exertion is determined on the basis of the measured longitudinal acceleration and velocity, as well as measured angular acceleration and angular velocity of the wheels for selecting the appropriate compensating torque acted upon the wheel. Furthermore the measured values of the relative displacement and speed of the wheel and the bogie-frame are needed. The principle **„***inverse dynamics*" is used which method *does not need* the *fcc* function, still, it is apt to ensure the *always stable recurrence* to the pre-scribed creepage in the presence of disturbing effects. This method is called a *„creep control"* procedure, and it was introduced in our VSDIA 2016 paper for a four-axle locomotive/train model. In this study the former dynamical model has been developed by including the *track excitation* and the *vertical a pitching vibration responses of the wheels, bogies and the loco superstructure*. Furthermore all measured quantities determining the controlled variable have been disturbed by measurement noise processes.

2. CREEP-CONTROL

The longitudinal creepage arising in the course of rolling contact is in a changeable stochastic connection with the force transmitting fcc property of the rolling wheel. If in the course of braking a small and constant creepage can be maintained, then it can be anticipated that the macroscopic sliding and the wheel flattening can be avoided. The principle of „Inverse Dynamics" will be introduced, in the course of which an always stable linear creep-control system is achieved, and *the method does not require the explicit knowledge of the fcc*. First for an elementary system of 3 DF will be treated by creep-control, then the method will be applied for all the four braked wheel-sets of a *vertically sprung* locomotive pulling a non-braked train. The extended dynamical system is *excited by the controlled braking force and by the vertical track uneven-nesses* (*track irregularities*). The motion equations of the excited dynamical system will be numerically solved in the time domain for pointing out the stability of the control process under the effect of the *track excitation and measurement noise.*

3. SIMPLIFIED ELEMENTARY MODEL

Dynamical model of one braked wheel-set with its longitudinal elastic/dissipative guidance and a mass is attached to the connection for modelling the bogie. Equations of motion:

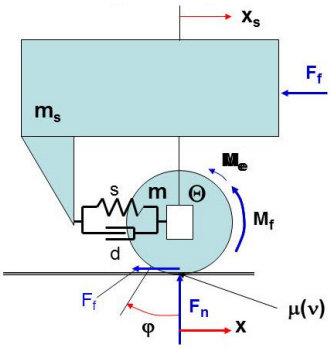

Fig. 1 Elementary model of the barked wheel-set

1. Wheel-set rotation:

$$\theta\ddot{\varphi} = -F_n\mu(v)R - M_e(\dot{\varphi}) - M_f(t)$$

2. Wheel-set translation:

$$m\ddot{x} = F_n\mu(v) + s(x_s - x) + d(\dot{x}_s - \dot{x})$$

3. Bogie translation:

$$m_s\ddot{x}_s = -s(x_s - x) - d(\dot{x}_s - \dot{x}) - C\dot{x}_s^2$$

In explicit form:

$$\ddot{\varphi} = \frac{1}{\theta}(-F_n\mu(v)R - M_e(\dot{\varphi}) - M_f(t))$$

$$\ddot{x} = \frac{1}{m}(F_n\mu(v) + s(x_s - x) + d(\dot{x}_s - \dot{x}))$$

$$\ddot{x}_s = \frac{1}{m_s}(-s(x_s - x) - d(\dot{x}_s - \dot{x}) - C\dot{x}_s^2)$$

For non-zero velocities ($\dot{x} \neq 0$) the *longitudinal creepage* ν is defined as follows:

$$v = \frac{R\omega - \dot{x}}{\dot{x}} \ .$$

The ***force connection coefficient*** (*fcc*) is defined as the ratio of the wheel-tread creep-force $F_f < 0$ when braking, and the wheel load $F_n > 0$:

$$\mu = \frac{F_f}{F_n} \ .$$

In accordance with the theory and experiences, the force connection coefficient μ is *creep-dependent* and when braking, the sign of μ is negative:

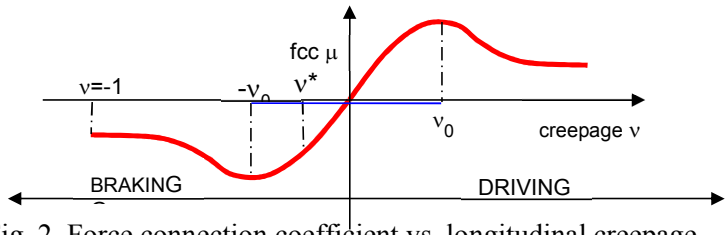

Fig. 2 Force connection coefficient vs. longitudinal creepage

As it can be seen the maximum driving effect can be exerted at ν_0, whilst the maximum braking effect can be exerted at $-\nu_0$. The creepage span $[-\nu_0, \nu_0]$ is called the interval of *micro sliding* on the wheel/rail contact spot. Our following intent is to maintain the prescribed creepage $\nu^* < 0$ by the *creep control process*.

2. CREEP-CONTROL

2.1 Introductory remarks

The longitudinal creepage arising in the course of rolling contact is *in a changeable stochastic connection* with the force transmitting property *ffc* of the rolling wheel. If in the course of braking a small and constant creepage can be maintained, then it can be anticipated that the macroscopic sliding and the wheel flattening can be avoided. The principle of „Inverse Dynamics" will be introduced, in the course of which an always stable linear creep-control system is achieved, and the method does not require the explicit knowledge of the *ffc*. First, for an elementary system of 3 DF will be treated by creep-control, then the method will be applied for all the four braked wheel-sets of a vertically sprung locomotive, pulling a non-braked train. The extended dynamical system excited by the controlled braking force and by the vertical track unevennesses (irregularities).The motion equations of the excited dynamical system will be numerically solved in the time domain for pointing out the stability of the control process under track excitation and in the continuous present of measurement noise in the feed-backs.

The objective of the creep-control is to maintain the prescribed *constant creepage value* ν^* in the course of a stop braking, thus the task is to determine the appropriate variation with time of the braking torque $M_f(t)$ to be exerted.

In order of determine the appropriate $M_f(t)$ function, consider first the *deviation* $\Delta\nu(t)$ of the actual creepage $\nu(t)$ from the prescribed ν^* value, in formula: $\Delta\nu(t) = \nu(t) - \nu^*$.

For achieving the objective of the control, consider the time derivative of *creep deviation* function $\Delta\nu(t)$ with respect to time, taking into consideration, that ν^* is constant, thus:

$$\frac{d}{dt}\Delta\nu(t) = \dot{\nu}(t) = \frac{d}{dt}\left(\frac{R\dot{\varphi} - \dot{x}}{\dot{x}}\right) = \frac{(R\ddot{\varphi} - \ddot{x})\dot{x} - (R\dot{\varphi} - \dot{x})\ddot{x}}{\dot{x}^2} = \frac{R\ddot{\varphi}}{\dot{x}} - \frac{R\dot{\varphi}}{\dot{x}^2}\ddot{x}$$

From motion equation No 2, written for the wheel translator motion, the *longitudinal force* F_f arising on the wheel/rail contact area (the braking force) when braking torque $M_b(t)$ is applied on the wheel can easily be expressed:

$$F_f = F_n \mu(v) = m\ddot{x} - s(x_s - x) - d(\dot{x}_s - \dot{x})$$

From the last equation it can be read off that knowing $\ddot{x}, \dot{x}, x, \dot{x}_s \; and \; x_s$ the braking force can be determined *without knowing the explicit value of the creep dependent fcc function* μ(ν). In other words it turns out that the *value of the fcc is reflected in the motion characterising quantities of the system*, thus it is *not necessary to get direct information on the fcc* for realising the control process if the motion state characteristic quantities $\ddot{x}, \dot{x}, x, \dot{x}_s \; and \; x_s$ can continuously be measured. It is a direct consequence of the above train of thoughts that in equation No 1 concerning the rotatory motion of the wheel the presence of the *fcc* can be eliminated by substituting the known motion state characteristic values. The first step is to express the angular acceleration of the wheel in form:

$$\ddot{\varphi} = \frac{1}{\Theta}\left[\left(-m\ddot{x} + s(x_s - x) + d(\dot{x}_s - \dot{x})\right)R - M_e(\varphi) - M_f(t)\right].$$

If one substitutes the above expression of the angular acceleration into the formula of the creep-derivative, then one can recognise the proper time variation of the braking torque $M_f(t)$which ensures a stable control of the longitudinal creepage, by which the prescribed creepage ν^* can always be maintained in a stable way also in those cases as well, when outer disturbances temporarily forces to deviate the longitudinal creepage from the prescribed (commanded) value ν^*. The creep-derivative deducted above now takes the following form [2]:

$$\frac{d\nu}{dt} = \frac{R\ddot{\varphi}}{\dot{x}} - \frac{R\dot{\varphi}}{\dot{x}^2}\ddot{x} = \frac{R}{\Theta\dot{x}}\left[\left(-m\ddot{x} + s(x_s - x) + d(\dot{x}_s - \dot{x})\right)R - M_e(\varphi) - M_f(t)\right] - \frac{R\dot{\varphi}}{\dot{x}^2}\ddot{x}.$$

With certain phantasy it can be recognised that if the braking torque has the variation with time

$$M_f(t) = \frac{\dot{x}\theta K}{R}\Delta v - M_e(\dot{\varphi}) - \left(R + \frac{\theta\dot{\varphi}}{m\dot{x}}\right)\ddot{x} + sR(x_s - x) + d(\dot{x}_s - \dot{x}),$$

then, the whole right hand side part of the expression got for the creep-derivative takes the following very simple and useful form [2]:

$$\frac{d\Delta\nu(t)}{dt} \equiv -K\Delta\nu(t) \;\text{ or }\; \frac{d\Delta\nu(t)}{dt} + K\Delta\nu(t) \equiv 0, for\ any\ t \in I.$$

Here *I* stands for the time interval of the analysis. Since the initial value problem of the resulted first order ordinary differential equation can always be solved under any initial value being not too far from the origin, and the solution is always stable, the appropriate brake torque variation $M_f(t)$ on the basis of the time dependent and measured motion state characteristics $\ddot{x}, \dot{x}, x, \dot{x}_s \; and \; x_s$ the intended stopping brake process with constant deceleration can be realised in a successful way. The logical flow-chart of the control process concerning a single wheel-set One of the four braked wheel-sets) is plotted in Fig. 3.

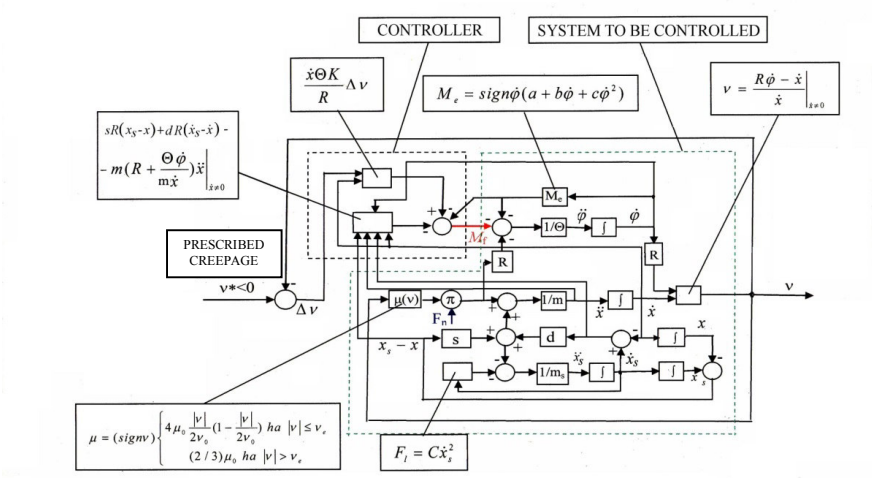

Fig. 3 Flow-chart of the control process concerning a single wheel-set

3. SYSTEM MODEL FOR THE TRAIN CONTROL ANALISES

3.1 The original model version for longitudinal dynamics

The original vehicle system model is plotted in Fig. 4, which models only the longitudinal dynamics [2]. The total number of degrees of freedom of the model is 11+1=12.

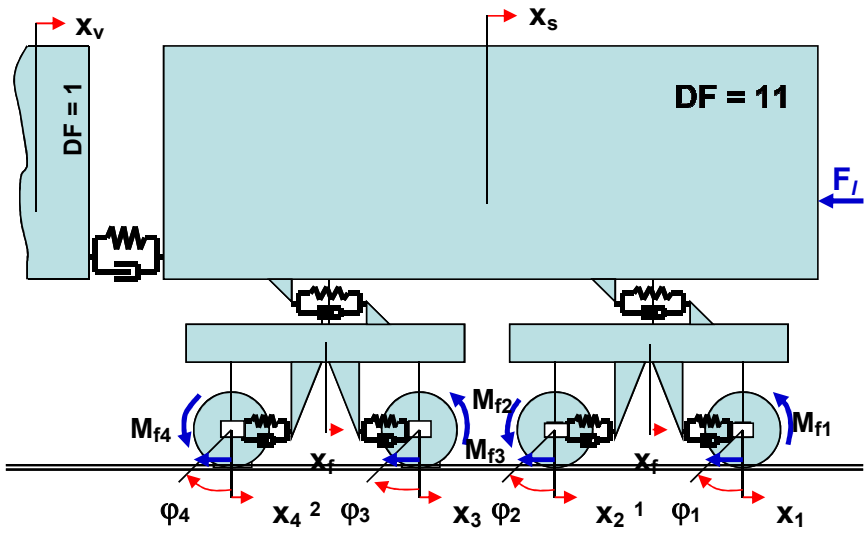

Fig. 4 The original vehicle system model for longitudinal dynamics

3.1 The extended model for longitudinal, vertical and pitching dynamics

The developed model is plotted in Fig. 5. Two characteristic changes can be identified with this developed model, namely the vertical linear elastic and dissipative *Hertzean*-contact at the wheel/rail contact spots, and the vertical linear elastic and dissipative primary suspensions, which connect the axle boxes and the bogie frames, as well as the vertical linear elastic and dissipative secondary suspension elements at the which connect the bogies and the locomotive-body. Thus, the number of the free coordinates

– degree of freedom of the system - has increased in comparison with the original version, its value is DF = 21+1 = 22.

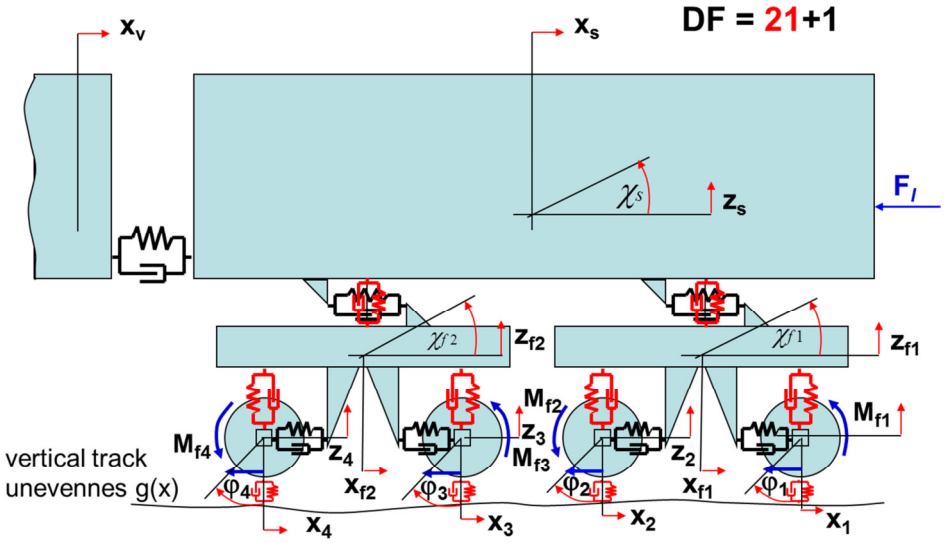

Fig. 5 The developed model to be controlled for constant creepage at the wheel/rail contact when stop braking of the train is to be carried out in the presence of a prescribed constant deceleration and disturbances due to the track unevennesses

3.3 Disturbances of the control process due to track excitation of the system

It is obvious that due to the elastic and dissipative suspension elements both the bogies and the locomotive-body as rigid bodies can undergo both vertical and pitching motions (vibrations) in the vertical plane. The vertical motion of the wheel-sets and the vertical and pitching motion of the bogies and the locomotive-body are excited by the rail surface irregularities emerging at the wheel/rail contact spots in the course of the motion of the train system. The effect of the geometric irregularity excitation is given by the rail profile function $g(x)$. The lower point of the *Hertzea*n spring/damper elements at the wheel/rail contact spots follow the track profile in the course of the whole braking process. It is a consequence of the track unevenness excitation that the vertical wheel supporting forces transmitted by the *Hertzean* elements will vary in the course of the braking process, which obviously *disturbs* also the rotating motion of the wheel-sets and gives *disturbances* for the control process. All the same, each wheel-set of the locomotive is controlled by its own braking moment exertion $M_{fi}(t)$, i=1,2,3,4 determined by applying the same control process shown in Fig. 3. The prescribed (commanded) creepage ν^* is the same for all the four wheel-sets.

3.4 Disturbances of the control process due to measurement noise in the feedbacks

this In study we intended to get information on the system behaviour also in the presence of certain disturbances contained by the measured quantities to be fed back to the controller when generating the controlled brake torque. To this end the all the fed back components to be realized by measurements in the real control system should be loaded certain disturbing signal. For the first approach of the problem, took constant frequency sine-form signals of small amplitude, and they were added to all the fed back

quantities at that cross section of the flow chart which is situated prior to entering the controller. More exactly, the small amplitude of the disturbances was selected as x% of the actual values in the actual time dependent quantities "flowing" in the fed back branches. The value of disturbance percentages were selected for 2,5% and 5%. The frequency of the sine form signal disturbing the fed back quantities was selected uniformly $f = 7\ Hz$, and the *phase angles* were random values from interval $[-\pi, \pi]$. Some results of the simulated time functions of the decisive for the control system will be shown in diagrams in Chapter 5.

4. THE SYSTEM EQUATIONS

The strongly non-linear *implicit* set of the system equations, which take into consideration the non-linearities of the wheel/rail contacts (the non-linear *fcc*), the journal friction torques, the air drag and the fed back motion state dependent braking torques can be formulated for the unknown motion state vector $\boldsymbol{x}(t)$ as follows:

$$\boldsymbol{F}(\dot{\boldsymbol{x}}(t), \boldsymbol{x}(t)) \equiv 0, for\ any\ t \in I,$$

where in accordance with Fig. 5, the motion state vector $\boldsymbol{x}$ of *44*-dimension has the following co-ordinates:

$$\boldsymbol{x} = [\dot{x}_{k1}, \dot{x}_{k2}, \dot{x}_{k3}, \dot{x}_{k4}, \dot{x}_{f1}, \dot{x}_{f2}, \dot{x}_s, \dot{x}_v, \dot{z}_{k1}, \dot{z}_{k2}, \dot{z}_{k3}, \dot{z}_{k4}, \dot{z}_{f1}, \dot{z}_{f2}, \dot{z}_s, \dot{\varphi}_{k1}, \dot{\varphi}_{k2}, \dot{\varphi}_{k3}, \dot{\varphi}_{k4}, \dot{\chi}_{f1}, \dot{\chi}_{f2}, \dot{\chi}_s,$$
$$x_{k1}, x_{k2}, x_{k3}, x_{k4}, x_{f1}, x_{f2}, x_s, x_v, z_{k1}, z_{k2}, z_{k3}, z_{k4}, z_{f1}, z_{f2}, z_s, \varphi_{k1}, \varphi_{k2}, \varphi_{k3}, \varphi_{k4}, \chi_{f1}, \chi_{f2}, \chi_s] \in R^{44}$$

For a prescribed initial time instant t_0 the state vector should take a prescribed vector value: $\boldsymbol{x}(t_0)=\boldsymbol{x}_0 \in R^{44}$. The initial-value problem formulated was solved numerically. The actual structure of function $\boldsymbol{F}$ is determined by the motion equations written for the number *22* moving masses, and contains also the rule of the feedbacks, formulated above in the form of the motion-state dependent braking torques. The relative difficulty of treating the formulated initial value-problem concerning the implicit differential equation system is avoided by an *approximating method.* The motion state dependent braking torque entering the set of motion equations at time instant t_i is computed by using the motion state values belonging to the previous time instant t_{i-1} of the simulation. In case of very small time steps in the simulation this approximation proved to be proper. Thus, the numerical solution procedure is working in a *two tact operation mode*:

1. Computation of $\boldsymbol{M}_\mathrm{f}$ at t_{i-1}, let's designate it by $\boldsymbol{M}_\mathrm{f}(t_{i-1})$,
2. Computation of all the accelerations at t_i **using** $\boldsymbol{M}_\mathrm{f}(t_{i-1})$ **.**

5. SIMULATION RESULTS

The differential equation system of the train model consisting of 22 free co-ordinates was solved numerically by using the approximation. The train runs on vertically periodic rail surfaces of 6 m wavelength and 1mm amplitude. The creep-controlled *stop braking process* was analysed with an initial velocity of $v_0 = 30$ km/h. The mass of the loco was 80 t and that of the trailer vehicle was 25 t. Only the loco was braked. The intended train deceleration was $a_v = -1\ m/s^2$. The *prescribed creepage* was computed on the basis of the anticipated deceleration: $\nu^* = -0.0026$. The simulation program was written in MATLAB.

5.1 The controlled braking torques applied on the wheel-sets

The controlled braking torques acting on the four wheel-sets for the stop braking process in case of gain factor K = 10000 are shown in Fig. 6.

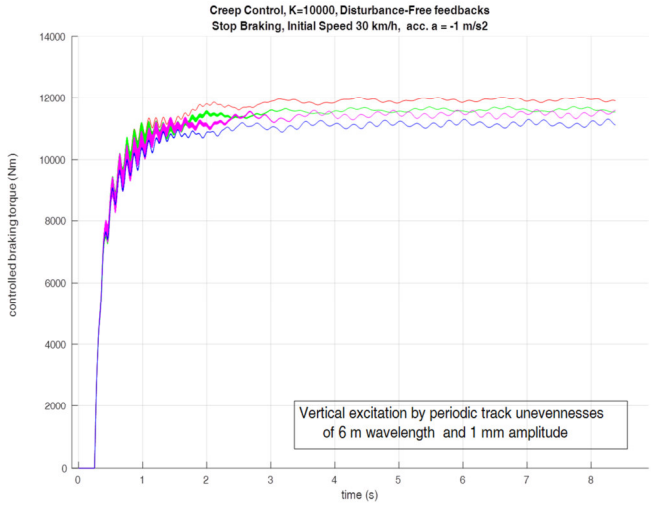

Fig. 6 The controlled braking torques vs. time
applied on the wheel-sets in case of gain factor K = 10000

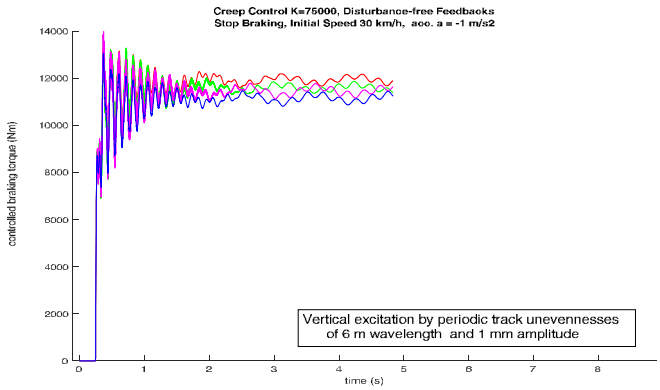

Fig. 7 The controlled braking torques vs. time
to be applied on the wheel-sets, at gain factor K = 75000

The controlled braking torques acting on the four wheel-sets process in case of gain factor K = 75000 are shown in Fig. 7. The increased gain factor is disadvantageous, because the harmonic content in the transition interval shows higher amplitudes. In Fig. 8 the controlled creepages vs. time functions are shown in case of gain factor K = 10000. In Fig 9 the controlled creepages vs. time function is plotted, for the case of gain factor K=75000. It is straightforward that in this case the control target achieved in a fast way, which is in accordance with the expectations.

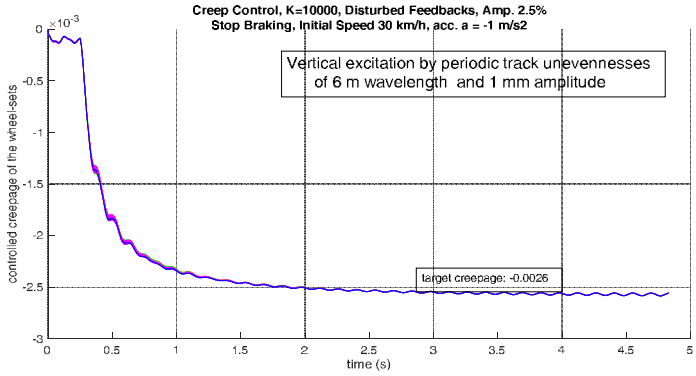

Fig. 8 The controlled creepages vs. time in case of gain factor K = 10000

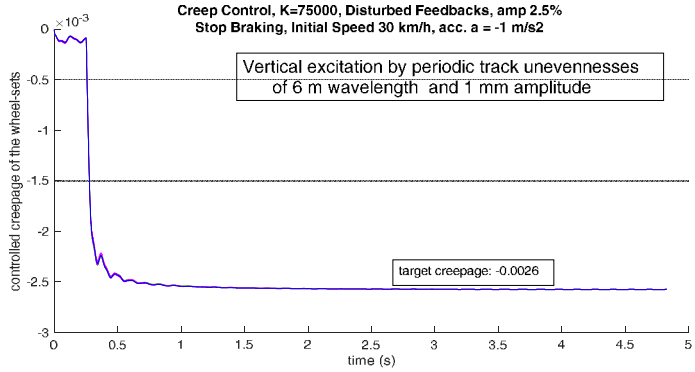

Fig. 9 The controlled creepages vs. time in case of gain factor K = 75000

In Figs. 10 and 11 the diagrams received for the case when parallel to the track excitation also those feed-backs were sinusoidally disturbed by 5% amplitudes of the actual motion characteristics values which the controlled brake torques depend on.

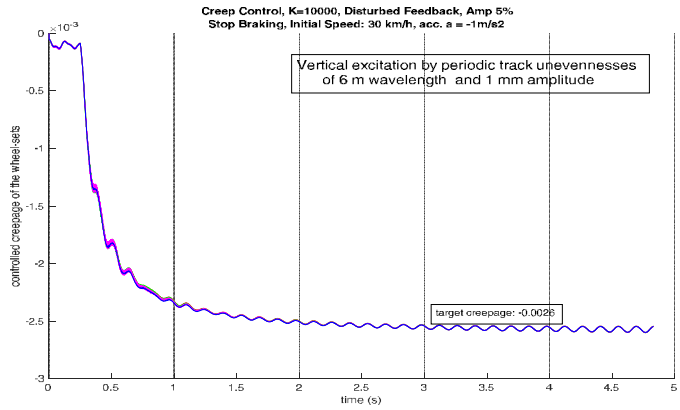

Fig. 10 The controlled creepages, K=10000
with *disturbed feed-backs* were sinusoidal inaccuracy functions
with frequency 7 Hz and amplitude, 5 % of the actual accurate values

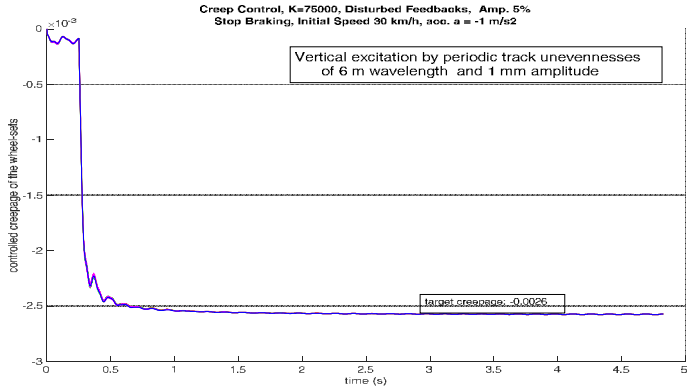

Fig. 11 The controlled creepages, K=75000
with disturbed feed-backs which were sinusoidal inaccuracy functions
with frequency 7 Hz and amplitude, 5 % of the actual accurate values

6. CONCLUSIONS

On the basis of the investigations introduced above the following conclusions can be drawn:

- The creep-control elaborated on the basis of the principle of „inverse dynamics" gives the stable solution to the stop braking with constant deceleration, gives steps towards the development of a ***novel antiskid-device***.
- The elaborated dynamical model with the Hertz springs and dampers works reliably also on tracks loaded with vertical irregularities, thus the vertical and pitching vibrations excited by the track unevennesses don't bother the operation of the creep control system
- The parameter sensitivity analysis concerning the gain factor K pointed out, that the smooth operation needs lower values, while the fast reaction requires higher values. A medium solution K=50000 could balance the contradictory demands,
- The parameter sensitivity analysis concerning the measurement failures and noise pointed out, that even if all the five feedbacks in the control processes are loaded by a sinusoidal signal failure of 5% amplitude bandwidth concerning the ever instantaneous signal levels the control system did not lose its stability,
- Further research target is the elaboration system models for the braking torque exerting machines both in electric and frictional versions,
- The sensor system to be used in a real control system also needs detailed research activities.

7. REFERENCES

[1] **Ariyur, K.B. – Krstič, M.:** Real-Time Optimization by Extremum Seeking Control. Wiley&Sons, Inc. New-York, 2003.

[2] **Zobory, I. – Nagy, D.:** Dynamical Analysis of a Special Anti-Skid-System for Railway Cars and Traction Units. Proceedings of the 15th MINI Conference on Vehicle System Dynamics, Identification and Anomalies (VSDIA 2016). (Ed. by Prof. I. Zobory). BME ITS non-profit ZRt. Budapest, 2017. p.149-162. ISBN: 9789633132661

[3] **Gáspár, P. – Szabó, Z. – Bokor, J.:** An Estimation Method For The Wheel-Rail Friction Coefficient. Proceedings of the 10th MINI Conference on Vehicle System Dynamics, Identification and Anomalies (VSDIA 2006). (Ed. by Prof. I. Zobory). BME, Department of Railway Vehicles, Budapest, 2007, p.237-244. ISBN: 9789634209683

THE QUESTION OF LIFETIME: EXTENSION POSSIBILITIES OF BOGIE FORCE TRANSMISSION ELEMENTS ON THE BASIS OF CONDITION TEST RESULTS

Péter FERENCZ

Department of Railway Vehicles, Aircraft and Ships
Faculty of Transportation Engineering and Vehicle Engineering
Budapest University of Technology and Economics
H-1521 Budapest, Műegyetem rkp.3., Hungary

Received: November 7, 2018

ABSTRACT

The actual railway vehicle maintenance issues have changed compared to the last century. Market participants can also provide a satisfactory response to repair functions. Of course, it is unchanged that each operator works with different circumstances, environmental impacts may be different, and the mileage is greatly influenced by these. Market players therefore offer customized repair services. Customization is done on the basis of test results, especially the various ratings of the force transfer elements are the subject of consideration when, for example, the overhaul of the bogie is due. The line of thought described here covers the method by which a good estimate of the service life of a component can be given, depending on the size of the railway fleet operated.

Keywords: bogie revision, tailor made products, part lifetime determination, deterioration curve, fleet size, risk maintenance strategy, component lifetime extension, customized repair technical content, service fleet size dependent repair

1. INTRODUCTION

More and more emphasis is placed on the development of state-of-the-art testing systems that create modern railway vehicle maintenance strategies. Operators are increasingly looking for sustainable, reliable, low-cost solutions. The Original Equipment Manufacturer already determines the revision cycle time of the running gears and bogies at the time of manufacture, but of course, as new products, the technical content and cycle time of the revision may differ depending on the operating conditions. This train of thoughts provides a comprehensive analysis of possible data collection methods for related operations, possible ways and principles for determining the continued usability of individual components.

By way of example, mention is made of rubber-metal elements used in both primary and secondary suspension elements, parts of longitudinal force transfer elements, rubber-metal elements, which may remain in the function of even one revision cycle, up to an additional one million running kilometers. Based on the test parameters of each component, test procedures can be developed and, in the light of the test results, if the component has the option of continued usability, additional simple technological steps may be taken, including the involvement of component manufacturers to determine the features and criteria of a component for further usability, or just need to be replaced. For each parameter, further usability criterion values are determined, which results in a diagnostic database for a series of tests and their results. In addition to rubber-metal elements, the subject of the study, including the rating of wheel-mounted brake discs, and the comparability of parameters of the same type of system components operated by several other operators, is also included.

2. PURPOSE OF TESTS

The purpose of the state-of-the-art vehicle maintenance philosophy is to monitor the operation of individual components as individuals and keep them in operation until certain parameters reach their operational limit values or exceed the criteria.
The basic goal of study can be specified as to create better vehicle parameter features with focusing on the application and the application of diagnostic processes in maintenance. The characteristic space of parameters shown in Fig. 1 for general treatment of system deterioration describes the stochastic process of system deterioration. Parameter space P is set of parameter vectors **p**. It is obvious that in the course of operation the parameter vector of a vehicle does not remain constant, but due to the unavoidable deterioration process it will show certain time dependence:

$$\mathbf{p} = \mathbf{p}(t) , \tag{1}$$

where the components of **p** (the sub-vectors) may contain the masses, moments of inertia, stiffness, damping and unique operational features.
Determining the actual technical configuration of the vehicle dynamical system and designating the motion state of the latter by **Y**, the goal is to establish a relationship between the time dependent motion state, described as

$$\mathbf{Y}(t) \tag{2}$$

and the time-dependent parameter vector **p**(t), which describes the *slow but continuous deterioration* in technical state of the vehicle system.

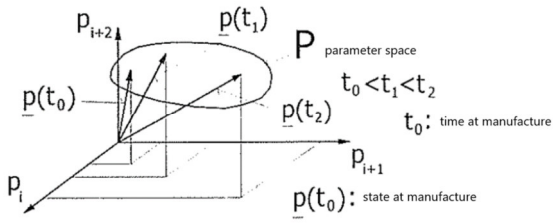

Fig. 1 Characteristic space of parameters [1]

With application of above designations, the change of technical change (i.e. sub-system feature of wheel profile alteration) can be represented by the following mapping:

$$\mathbf{p}(t) = \mathcal{W}_t \, \mathbf{Y}(t) \tag{3}$$

Here, the $\mathcal{W}_t$ represents the technical state deterioration (can be the wear) operator (on the basis of description [2] p.255).
On the basis of the above described principle, the original manufacturers of bogies and their components provide life expectancy and replacement cycle data. The individual tests may be carried out by the manufacturers of the components or by another independent company, respectively. Uniform test results are classified into three simple categories. The purpose of such a simple classification is to determine whether a given part can be used without restriction, for further use, or, where appropriate, for no longer to be used.
It is necessary to distinguish “special” damages from the process of damage due to normal operational failure. These are exceptional issues that need to be treated as out-

liers when evaluating results as a statistical population. Of course, these component parts fall into a clearly unavailable category, but they do not form part of a large number of outages due to operational wear.
Consequently, the results of these tests provide the basis for further usability classification. For example, components that were previously considered mandatory by the previous manufacturer's specifications for revision, and the results of the tests may indicate that they may serve as a further revision cycle time, result in significant cost reductions. These have an impact on future computable costs, on their distribution and on the realization of the total life cycle cost. Certain technological steps, maintenance and repair tasks of the maintenance can be reworded or rescheduled.
The following can be reported along the lines of traditional maintenance strategy. The physical process of normal damage, the process of destruction, deterioration, is controlled by test tasks. The regularity of tasks defined for each subspace group gives a cycle. Compared to the status-based strategy, the Critical Criteria for specific tests must be designed to exit traditional task lists as compared to the standard tasks. The task list defined for a specific component group at a given time is made as a technical content depending on the inspection and test results. The age of vehicles is also a determining factor. If we want to define the first technical (approx. 1 million km) or second revision technical data for certain group of components like bogies from production, the vehicle fleet size and age matters. The Life Cycle Cost (LCC) of a given component group is assessed and determined by the method of determining the life of the parts assigned to the product. Production (design) data is possible by reconsidering data from certain substructures, such as component level lifetime extensions. Usually, this process should be adapted to the individual number of individuals in the fleet.
The following method can be considered as the deterioration of the natural state of the components and the classic description of the statistical evaluation of the process of system degradation. Fig. 2 illustrates the progress of the process over time, for example, the process of natural wear propagation. The curve consists of three main sections divided by two inflection points, so the derivative of the first section is negative, the middle and the third are positive. The rate of change of function (1) is described by the following expression, which gives the following velocity.

$$v_z = (z_2 - z_1) / (t_2 - t_1) = dz/dt \tag{4}$$

The second inflection point of the quasi-linear portion of the function (Fig. 2) gives the lifetime measure.

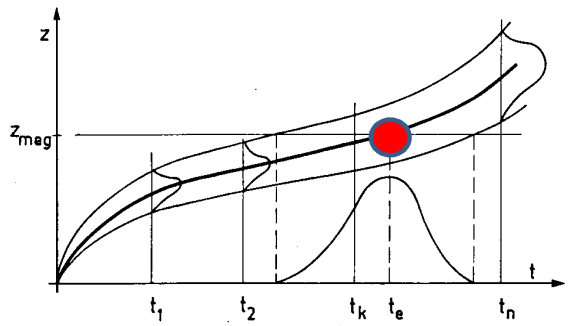

Fig. 2 Deterioration function of part

Examination of a sample group consisting of parts of the same type gives the bunches of individual curves assigned to each sample, and the batch expected value process as a function can be used to determine the purpose of the test, the reference point of which is the red point.
The permissible component life (2) can be expressed as:

$$t_e = z_{meg}/v_z; \tag{5}$$

As used in (2), "z_{meg}" means the maximum allowable limit, such as the limit of a wear process.

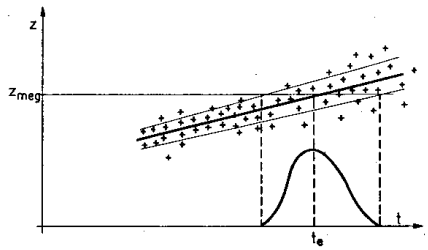

Fig. 3 Statistic results of limit [5]

Thus, the determination of the limit value for a group of samples is the purpose of the statistical evaluation. The deterioration criterion for the maximum or allowable state is at the intersection point of the expected value function of the quasi-linear scale limit values and the expected value of the plurality of inflection points.
This leads to an optimization process, the results of which are the "lifetime" action parameters on basis of MINIMUM RISK! and MAXIMUM QUALITY!
The basic question is, on the basis of a test at a given moment, is it possible to establish that each component or group of parts can be used for another revision cycle?
How does the reliability and safety of the components change, so does the structure, and the system?
Optimization boundary conditions, such as safety, warranty liability, original manufacturer specifications, operating conditions, method of determining original lifetime cost, and implementation of the bogie review process must be taken into account.

3. COMPONENT GROUPS THAT SHALL BE CONSIDERED

The full range of power transfer elements, rods, rubber-metal elements, bushings, silent blocks, longitudinal and transverse force transmission components can be considered as test subjects. Particularly important for rubber-metal elements, where static load-performance tests are performed repeatedly to provide primary results. The measured characteristics of the spring are to be compared with the original values of the original factory characteristic and the spreading range. The results of the comparison, the difference and the degree of agreement give the input information of the mentioned usability categorization.

There are rubber-metal element units that can be considered as generally usable after the results of the tests, and then a new test method, such as a special visual inspection of the element in question, or a comparison with a “picture-catalog”, is a normal new technology for the eventual revision. This makes it possible to judge a necessary exchange. Suspension system elements must always be subjected to a characteristic test. The testing of the primary spring elements, mostly steel coil springs, is based on a comparison method and the stiffness parameter of the test is carried out in the range defined in the nominal working point (s). Damper units need to be qualified based on their full operating characteristics.

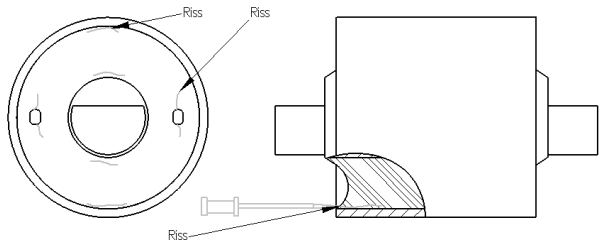

Fig. 4 Example of features to be checked on axle guide bearing bush [4]

Both axle bearings and brake discs provide a broad base for testing and creating a diagnostic database. There are two main categories between the parts and parts that can be tested. All types of rubber-metal elements and dampers are considered to be "**rather uncertain**" because the mapping, modeling and measurement of the deterioration process is more complex. Wheel discs, brake disc wear rings, axle bearings are “easy-to-test” materials, these can be labeled as "**less uncertain**" because of their definite limitations on their usability, such as wear propagation limits.

3. TEST RESULTS AND APPLICATION

In the simple category described, a method associated with the test results of the bogie components is ranked and evaluated. Generally, the sample size is so low that the certainty of the result is low in that the "true" value is calculated based on the "deterioration" function described above, with simple expected value defined. The result is as follows. "Test revisions” carried out for each type of component groups, even bogies in the certain fleet. By replacing these certain parts, a complete condition examination is performed on the dismantled parts. Assessing the state of deterioration by positioning it on the "deterioration curve”, then examining original components by specialist OEMs or independent experts follow. The primary question is whether the fault found or the picture of the situation is abnormal, so outlier, or the normal condition is deterioration faced? In the event that the “normal” deterioration condition is identified, the criteria for continued usability are determined by the safety criteria. What is a reliable test method for a particular part? What is the result? Should a decision be made in addition to a low sample number, and even if that "result point" is located in the quasi-linear phase of the damage process?

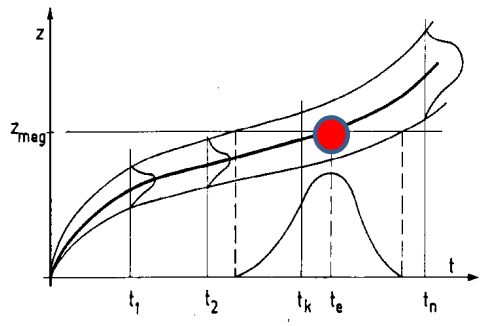

Fig. 5 Worst and the best fit case

In addition to the test results, the available operating data for the “more certain” result is to be taken into account. These are usually the results of vehicle maintenance inspection tasks, which can be collected as preliminary data for repairing or revising bogies or parts. After the test revision, the operator, the original manufacturer and the suppliers shall be informed of the results. The results can be feedback, the technical content of the maintenance or the repair can be changed, which can be considered as a lifetime change. Thus, the test results of the components described above are evaluated in two different ways.

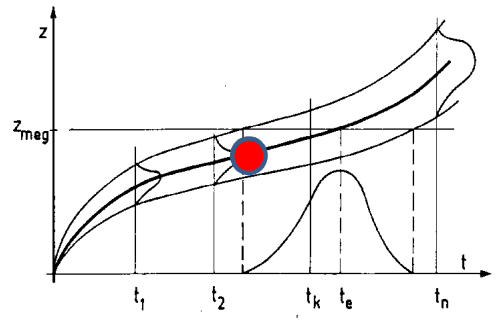

Fig. 6 Worst and the best fit case

The uncertainty arises from the fact that the position on the result curve is not known at which point of the quasi-linear phase situated. It may be in the immediate vicinity of an inflection point. Depending on the characteristics of the component group, the so-called "**more uncertain**" and "**less uncertain**" categories are derived. The theory is expanded to include the additional attribute applied to the categories, the “**worst-case**” and the “**best-fit**” categories.

Fig. 5 illustrates the "worst case" case, so the result is considered to be still in good condition and replaced at the end of its usability. Fig. 6 illustrates the "best fit" case, the test results are considered good, and the degree of continued usability can reach or exceed the next revision cycle time. Fig. 6 illustrates the "best fit" case, the test results

are considered good, and the degree of continued usability can reach or exceed the next revision cycle time.

4. CONTRADICTION OF RESULTS APPLY IN MIRROR OF FLEET SIZE

The size of the operating fleet is a very important factor. Take an example of a fleet of 100 train units, in which a train consists of 2 driven and 4 running bogies. In addition to this "big" fleet operator, also at a "small" fleet operator company shall be compared to with i.e. 5 same train units, but contracted for 100% availability performance. Which parameters are used and how the decision parameter criteria for above described test procedure to be defined? Examining the reliability of each bogie element by type can be generalized, which is highly dependent on the size of the fleet. Of course, for a small fleet, one of the elements of the 10 bogies of the 5 trains can be tested with greater reliability than the whole of the 100 trains. The reliability of the test results ultimately affects the extent to which the original manufacturer's specifications can be deviated from and the reliability of the technical content of the revision ahead.
A "small" operator with 5 train units is more likely not to have spare bogie units, so the loss of an unexpected operation of a part, even for the entire train, is much more costly, even in terms of lifetime cost. The company operating the "small" fleet is at greater risk with the continued operation of "old" parts.

The following simple example illustrates the effect of fleet size.

Sample brake down analysis of a „SMALL" OPERATOR FLEET

Quantity of the operated trainsets is: 5
Bogie type distribution in trainset:
Driven bogie 2 units,
Jacobs trailer 3 units
Sum:
Driven bogie 10 units
Jacobs trailer 15 units

The most important RISK of the certain type of fleet is:
brake down of 1 trainset has strong influence on fleet availability.

Yearly mileage performance of the fleet is : 450 000 – 600 000 km
Auxiliary fleet float conditions are:
No or low amount of spare sub-systems or components, or bogies;
Strong sensitivity on process LEAD time shall be considered.
Sensitivity on COST reduction is high, keeping trains at 100% availability.
Resultant fleet availability sensitivity:

$$AS = 1 / 5 = 20\% \quad (6)$$

The „Less uncertain" items are considered to be exchanged in case no possibility to reach the next revision cycle period.

For the „Rather uncertain" items the application of „**WORST or BEST FIT CASE** abstraction" applied depending mainly on experiences with certain part usage in other applications.
Despite the simple reliability factor of i.e. tested axle guide bearing units case for driven bogies is:

$$R = 4 / 10*4 = 0,1 \text{ -> } 10\% \quad (7)$$

Besides on increment sensitivity of the parameter is:

$$S = 1 / 10*4 = 2,5\% \quad (8)$$

Sample break down analysis of a „BIG" OPERATOR FLEET

Quantity Operated trainsets is: 105
Bogie type distribution in trainset:
Driven bogie 2 units
Jacobs trailer 3 units
Sum:
Driven bogie 210 units
Jacobs trailer 315 units

The most important RISK of the certain type of fleet is:
The unexpected brake down or malfunction of a component in higher amount.

Yearly mileage performance is: 180 000 – 250 000 km
Auxiliary fleet float conditions are:
Significant amount of spare sub-systems or components, or bogies.
Sensitivity on process LEAD time lower then small fleet operator
Sensitivity on COST reduction with keeping items on further usage.
Resultant fleet availability sensitivity:

$$AS = 1 / 105 = 0,95\% \quad (9)$$

The „Less uncertain" items are considered to be further used even in case no possibility to reach the next revision cycle period but a certain further mileage.

For the „Rather uncertain" items of Application of „**BEST FIT CASE** abstraction" applied relying on maintenance check and higher certainty, less sensitivity.
Despite the simple reliability factor of i.e. tested axle guide bearing units case for driven bogies is:

$$R = 4 / 210*4 = 0,0047 \text{ -> } 0,47\% \quad (10)$$

Besides on increment sensitivity of the parameter is:

$$S = 1 / 210*4 = 0,12\% \quad (11)$$

5. TO ENSURE THE DECISIONS

On basis of the above described data flow, the „small fleet operator" decision point are influenced by other risks comparing to the „big fleet operator". The dependency of on „AS" sensitivity value is high at a small fleet. Thus even the „less uncertain" parts and groups, even in case of existing possibility of further usage are considered to be ex-

changed, i.e. the wheels or brake discs, in order to not to stop any of the train out of the fleet.
The „big fleet operator" decides strongly relying on the size and features of the available exchange float of parts, even a higher quantity of complete spare bogie units. Therefore, the risk is considered more depending on a certain part failure in a high quantity. The „less uncertain" type of items is always considered to be further used. The technical content of revision process can be adjusted in accordance with the test results.
So the application and evaluation in general can be described as simple question. Where is a certain result located on the lifetime – technical state deterioration curve? The decision shall be ensured with a process based on the statistical evaluation of test results. Reference distribution (i.e. designed, simulated, on recent tests carried out feature) shall be considered to compare the evaluated empirical distribution (refer to [3] p. 13). The degree of similarity between distributions to be used to indicate the degree of sensitivity between the references, expected values, and measured by values. The *Kolmogorov-Smirnov* test statistics measured here directly the greatest vertical distance between the two distribution functions, shown on same graph (see Fig. No.7). The test statistics can be calculated using:

$$T_1 = \sup | S_1(x) - S_2(x) | \quad , \tag{12}$$

where with supremum indication the equation represents the greatest absolute difference between the distributions.

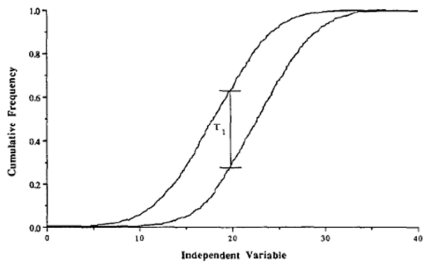

Fig. 7 Example of the determination of K-S statistics [3]

To end up the analysis method, certain maximum limit of T_1 to be defined in an evaluation of a certain parameter that features the deterioration of system. This parameter T_1 provides the criteria of decision described in the above chapters and ensures the stability (boundary conditions) of optimization.

5. CONCLUDING REMARKS

- Bogie force transmission elements as defined groups have possibility for further usage comparing to OEM determined revision cycle, lifetime extension, this possibility provides identification of decision points within overhaul, diagnostic technologies;
- The optimization has the main goal of risk minimization besides cost minimization;

- The remained „effective" lifetime is depending on the optimization boundary conditions;
- The fleet size has contradiction feature in decision making of components further usability;
- Part-group dependent decision making method is settled;
- The decision shall be ensured, for this the proposal of usage parameter sensitivity test of *Kolmogorov-Smirnov* method implemented;
- On basis of thoughts unique, customized revision technical content can be provided on each unit of bogies, or even vehicles.

6. REFERENCES

[1] **Zobory, I. – Benedek, T. – Győri, J.:** Vehicle Diagnostics. Lecture Notes. BME Budapest, 2004. (in Hungarian);

[2] **Zobory, I.:** Prediciton of Wheel/Rail Profile Wear, Vehicle System Dynamics, Vol.28 (1997), p.221-259.

[3] **Hamby, D. M.:** A review of techniques for parameter sensitivity analysis of environmental models, Westinghouse Savannah River Company, SC 29808, U.S.A.

[4] **Ferencz, P.:** Lifetime extension possibilities of Stadler bogie force transmission elements on the basis of test results, Proceedings of the 10th International Conference on Railway Bogies (BOGIE'16), (Ed. by Prof. I. Zobory), Scientific Society of Mechanical Engineers (SSME/GTE), Budapest, 2017, p.357-366.

[5] **Sólyomvári, K. – Ferencz, P.:** Maintenance and Repair of Railway Vehicles c. course lecture notes, BME Department of Railway Vehicles, Aircraft and Ships Budapest, 2007 – 2018.

TOOLS AND PROFESSIONAL ACTIVITIES OF THE RESEARCH AND TESTING INSTITUTE IN PILSEN ON THE FIELD OF DEVELOPMENT AND QUALITY INCREASING OF RAILWAY STOCKS AND THEIR COMPONENTS

Jan CHVOJAN

Dynamic Testing Laboratory, Research and Testing Institute in Pilsen
CZ-30100 Plzen, Czech Republic

Received: June 28, 2019

ABSTRACT

The paper presents professional, technical and methodical tools and possibilities of the company, which has been engaged for more than 110 years in research, development and experimental support of engineering products especially in the field of power engineering and transport technology, including components of rail vehicles. The support of rolling stock products of the Research and Testing Institute can take place in three levels: firstly, in the theoretical using modern computational tools in the field of virtual design by multi-point simulations, strength calculations and evaluation by FEM tools, noise and vibration prediction. Other activities of the first plane include internal and external flow calculations and their theoretical description for all relevant operating conditions. The second pillar of technical support by our institute lies in the experimental verification of computational models and real constructions in the field of mechanical properties, noise and vibration, vibration resistance and static and fatigue strength of the product. This support includes accredited testing following TSI certification. For this purpose, the laboratories are equipped with unique loading and measuring systems and technology and accredited testing procedures. The third level of support of engineering products consists in verification of driving properties of complex dynamically loaded structures under operating conditions, their evaluation and prediction of their fatigue life. In addition to these activities, VZU Plzen is engaged in research and development in the field of thermal spraying coating, custom manufacturing and refurbishing parts by different types of thermal spray technologies which can be used in railway stocks industry. This paper demonstrates and illustrates examples of the research institute's research, development and testing capabilities to support rolling stock.

Keywords: reseach and testing, railway vehicle tests, fatigue, crash, noise, vibration, material testing

1. INTRODUCTION

The lifetime and operational reliability of structures is a unique combination of technical and economic knowledge, knowledge and experience, whose successful mastery and ability to continually modernize them significantly contributes to a substantial increase in critical safety parameters including health and property protection, optimization of production costs and significantly increases the competitiveness of individual industries and, as a result, the whole economy.

Unique technical competence, the necessary long-term experience, international references and the appropriate technical background are indispensable prerequisites for active activity in the field of life testing especially in the field of large structures.

1.1 Introductory remarks

The Research and Testing Institute Pilsen s.r.o. (hereinafter referred to as VZU Plzen), has been operating in the field of durability assessment of large structures and industrial structures since its foundation in 1907. Since 1981, when the unique workplace of the Dynamic Testing Room has been opened, which has a unique electro-hydraulic loading and clamping system by means of which conducts experimental research and testing of large-scale structures in the field of transport engineering, power engineer-

ing, construction, chemical and mining industries for domestic and foreign customers in Europe, Australia, Asia and North and South America.
Current mathematical methods and tools allow the theoretical solution of dimensioning problems. However, the results are very sensitive to the correct estimate of the input parameters of the calculations and the suitability of the calculation methods and models used and can be affected by significant errors. Objective sizing procedures are based on the systematic linking of mathematical modeling methods to experiments prior to industrial application. This process is technically very demanding and requires a base capable of analyzing the actual operating load of the structure and then simulating this time-varying load in laboratory conditions.

For example, proper strength verification of structures often requires a complex spatial loading that models all major operating forces. With increasing pressure to reduce the weight of the structures, the weight optimization requirements of these structures are growing enormously. In the experimental research of fatigue properties of real large-scale constructions and finished products, which is provided by VZU Plzen, there is currently a great qualitative leap. Complex spatial simulations of the main operating forces are already inadequate, with the progressive weight optimization increasing the strength potential of structural material to limit values. The structural failure, such as fatigue fracture, is also due to secondary operating stresses, such as in the case of load-bearing vehicles from shock absorbers, stabilizers, braking systems and other elements that are subject to the dynamic effects of time-varying loads when operating the structure. Their force effects were previously either neglected or estimated by computational models for static simulations. With decreasing weight of structures and their load-bearing components, these secondary loads can also cause fatal failure with an impact on major material damage and passenger lives.

Comprehensive support for research and development of complex engineering products requires a summary of both theoretical and experimental activities, knowledge, skills, experience and theoretic-experimental background that VZU Plzen has and can offer to manufacturers in many areas.

2. STRENGTH, FATIGUE AND CRASH CALCULATIONS OF VEHICLES AND THEIR PARTS

An essential and very important tool for the development of a new engineering product is computational support for the prototype design, which initially assesses the most important factors that are design in its operating conditions and which it must withstand. These activities are solved in the VZU Plzen in the Department of Applied Mechanics, which has a massive software arsenal, which allows the developed product to assess in the field of strength, simulation of fast processes and crashes, simulations of dynamic rigid and flexible systems and heat transfer by finite volume method and thermodynamic calculations including an internal an external aerodynamics, see Fig. 1 and 2. Applied Mechanics Department is interested in technical tasks from a wide range of engineering practices, research and subsequent development of computational modules and methods to specific customer requirements.

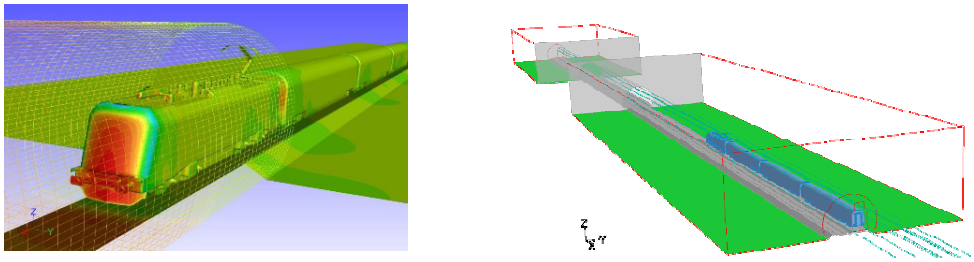

Fig. 1 Entering and passage through a tunnel

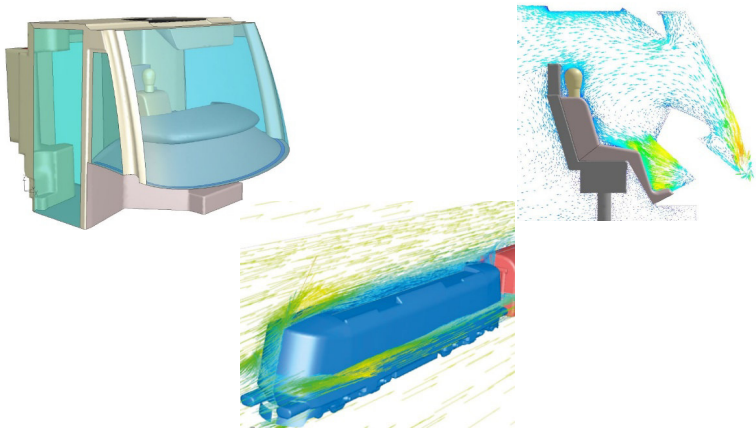

Fig. 2 Internal and external flow, aerodynamic drag of rolling

3. MEASUREMENT, ANALYSIS AND REDUCTION OF VEHICLE NOISE AND VIBRATION

Measurement of noise and vibrations, identification of noise and vibration sources, proposals for reduction of vibrations and anti-noise measures are provided in the Laboratory of Noise and Vibration of VZU Plzen. They are also technically very well equiped for performing experimental modal analysis and doing telemetric mesasurements of stresses, temperatures and other physical quantities on rotating parts and generally accredited and non-accredited noise and vibration testing of equipment in transport industry. The examples are shown in Fig. 3.

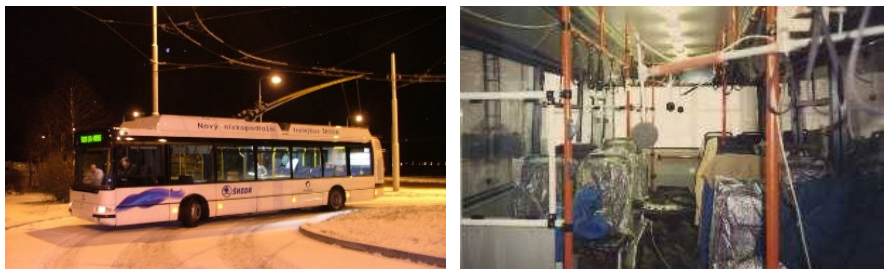

Fig. 3 Measurement of an infra noise and internal processes

4. MATERIAL TESTING

The Mechanical Testing Department deals with the detection of mechanical properties of metals, alloys, plastics, welded joints, etc. They accredited to static and impact load tests, hardness testing of metallic materials and plastic, breakthrough breaking test with brittle fracture, low and high cycle fatigue tests and measurements of crack growth rate during cyclic loading, see Fig. 4.

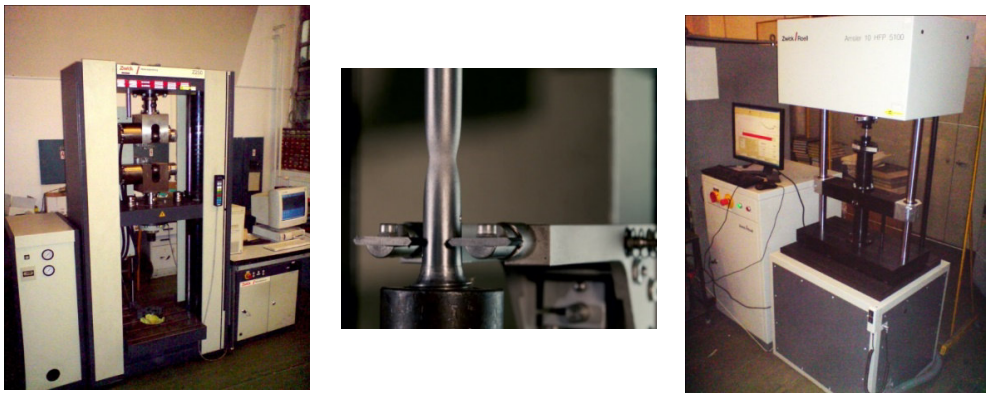

Fig. 4 Evaluation of material mechanical

5. STRENGTH AND FATIGUE TESTS OF VEHICLES AND THEIR PARTS

One of the most active and also the largest departments of VZU Plzen in the area of supporting the development of rolling stocks is the Dynamic Testing Laboratory. This workplace is equipped with a unique electrohydraulic loading system to simulate the load on structures and assess their resistance to operating conditions and their compliance with regulations, standards and laws. It focuses on accredited testing of strength and fatigue life of vehicles (Fig. 5), locomotives, wagons, trams, trolly buses, cars and their components.

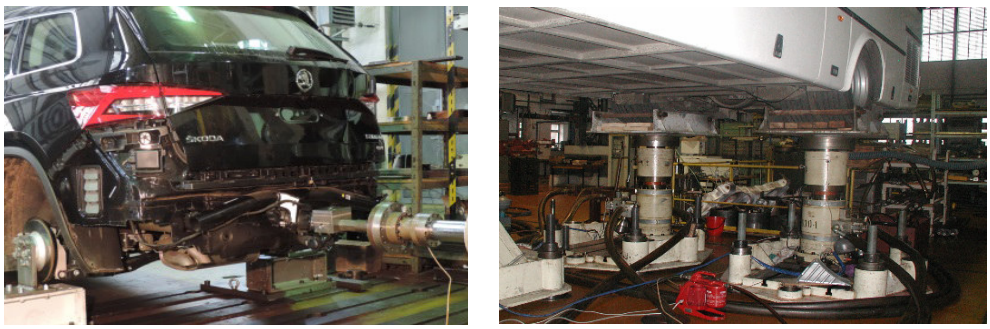

Fig. 5 Evaluation of tests of vehicles and transport systems

The most important tests are testing of the bogie frames of rolling stocks. The laboratory has all accreditation certificates for this activity according to Czech, European and

world norms and standars, it has excelent technical equipment and expert knowledge and skils of specialists, which perform these tests for customers all over the world including Australia and North and South America, see Fig. 6.

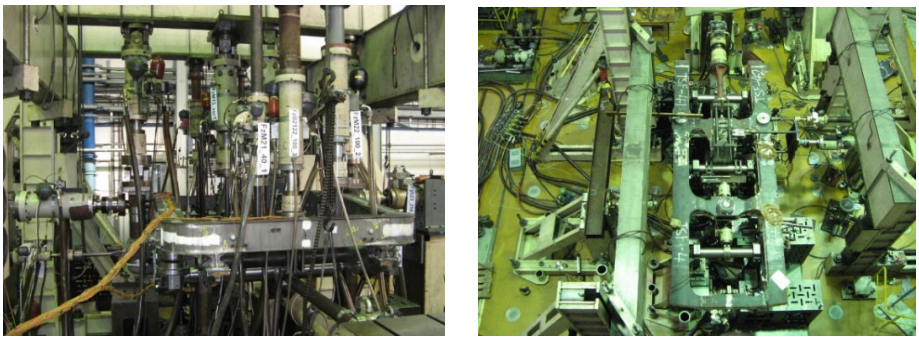

Fig. 6 Fatigue tests of bogie

The dynamic testing laboratory also performs tests of vibration resistance of rolling stock equipment (Fig. 7 and 8), laboratory strain gauge measurements of uniaxial and plane stresses, strain gauge measurements under operational conditions including measurements on rotating parts in magnetic field, corrosive atmosphere, fatigue tests of structural materials at diferent temperatures and measurements of technological and residual stresses.

Fig. 7 Vibration tests of rolling stocks components

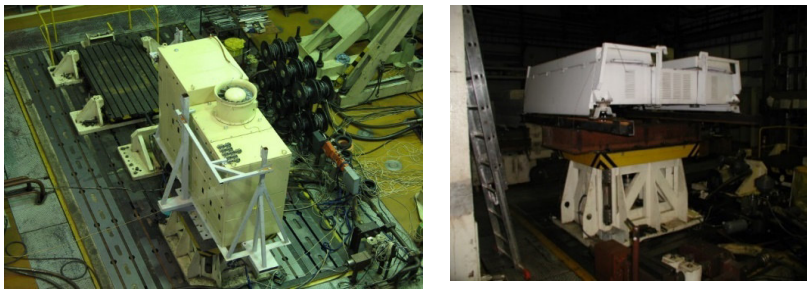

Fig. 8 Vibration tests of rolling stocks components

6. THERMAL SPRAYING COATING

An application of protective coatings using thermal spraying methods is a very useful tool for refurbishment and repair of damaged parts by creating new surface resistant to wear, abrasion, erosion, corrosion, high temperation, etc. based on metal, alloy, super-alloy, cermet and ceramic materials, see Fig. 9.

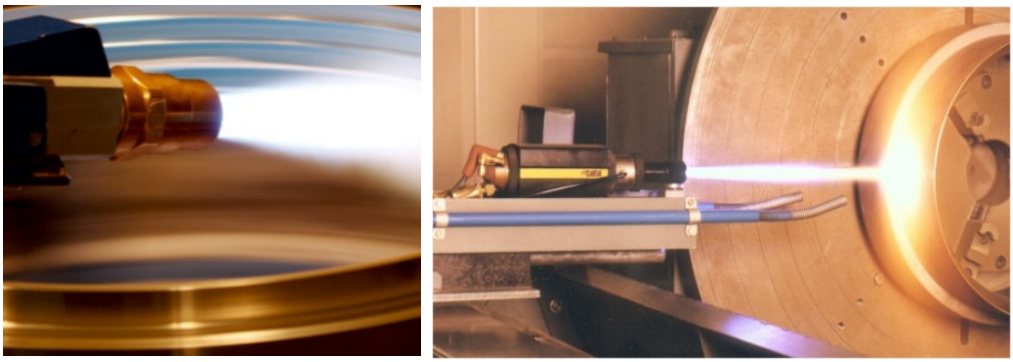

Fig. 9 Thermal spraying based on metals, alloys, superalloys, cermet and ceramics

A large amount of money was invested in the last year to build a new Research Center of Surfaces of VZU Plzen with state-of-the-art technology to investigate and apply quality and durable thermal and plasma spraying. It is demonstrated on Fig. 10.

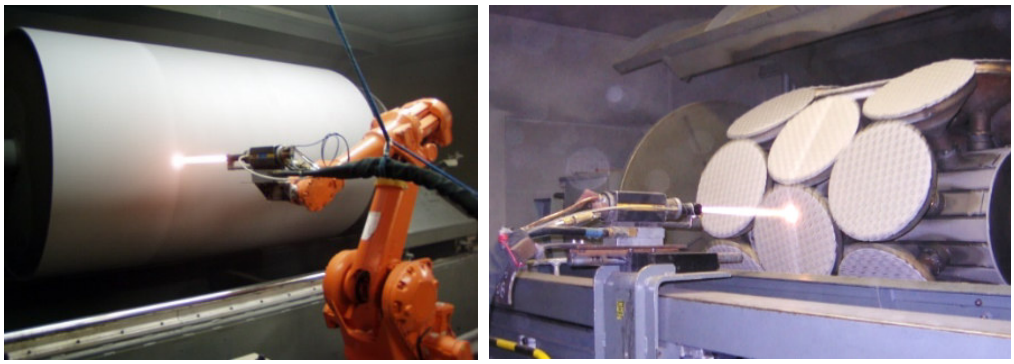

Fig. 10 Plasma spraying of the heavy fusible materials

7. CONCLUSIONS

This paper shows tools and professional activities of the Research and Testing Institute in Plzen on the field of delelopment and quality increasing of railway stocks and their components. It presents individual fields and scientific disciplines in which the Institute and its experts have high knowledge, skills and experience. Its advantage is a combination of theoretical mathematical approaches and procedures and a highly sophisticated experimental base that is able to simulate complex operating conditions and thus optimize computational models and refine their real outputs and results. In the field of thermal spraying, modern methods of coating surfaces based on metals, alloys,

super alloys, cermets and ceramics, which are resistant to abrasion, abrasion, erosion, corrosion and high temperatures, are described. It is suitable to use these resources for repairs and reconstructions of parts of rail vehicles.

7. ACKNOWLEDGMENT

This paper was also created and supported by Institutional support for long-term strategic development research organization for the years 2018-2022 in the frame of the decision No. 12/2018 provided by the Ministry of Industry and Trade of the Czech Republic.

ADVERTISEMENTS

NIPPON STEEL

Rolling Stock Parts

-Solid rolled wheels
-Wheels & axle
-Driving gear units
-Flexible couplings
-Couplers
-Draft gears
-Air Springs
-Bogie
-Active suspensions
-Pneumatic spring tilting system

<Steering Bogie>

Commuter train & Subway

Excellent curving performance

- Less derailment risk
- Silent curving

Linear Metro

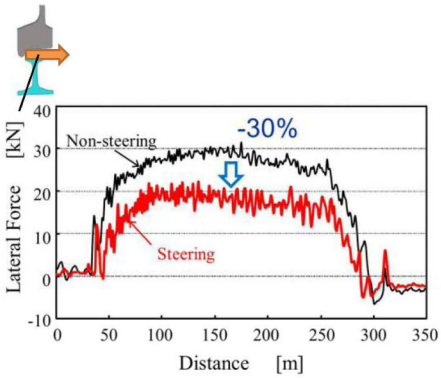

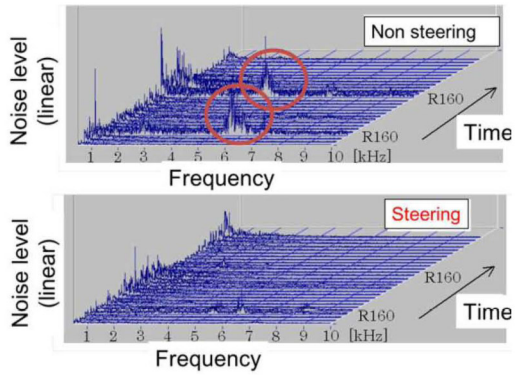

Head office 2-6-1 Marunouchi, Chiyoda-ku, Tokyo 100-8071, Japan
Phone +81-3-6867-6902
Fax +81-3-6867-4958
http://www.nipponsteel.com

NIPPON STEEL CORPORATION

KNORR-BREMSE

Wheel slide protection system MGS3

Optimized WSP control for shorter stopping distances even in extreme weather conditions

Decades of experience and ongoing technical improvement enable Knorr-Bremse to offer state-of-the-art wheel slide protection.

Additional features of high performance MGS3

- Multi-mode switch over WSP control between low and extremly low adhesion for shorter stopping distances
- Higher pneumatic performance for shorter ventilation times
- One system for all markets: easier homologation of trains
- eNozzle functionality: electronic adaption to different brake cylinder volumes for less commissioning efforts
- Improved system control and diagnostic by pressure sensor integration

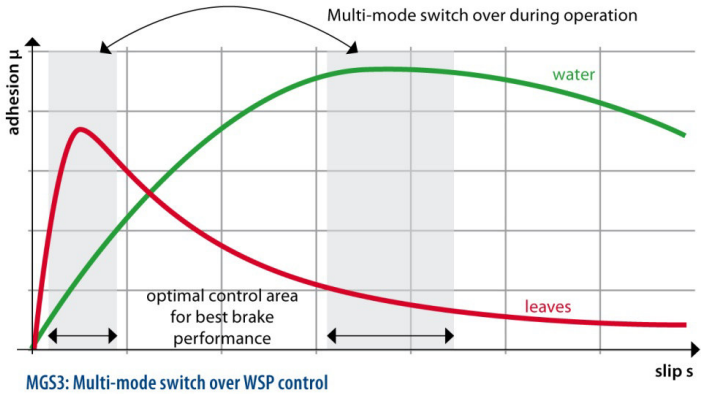

MGS3: Multi-mode switch over WSP control for different track conditions

Multisensor

- One multifunctional sensor for WSP and COMORAN system
- Measuring speed, acceleration and temperature
- Output signal: Rectangular current signal, polarity reversal protected, permanently shortcircuit protected
- Temperature range:
  – 40 °C ≤ T ≤ + 100 °C
  (optionally extended to cover low temperature requirements)

High Performance Anti-Skid Valve

- One valve for all market requirements
- Integrated pressure sensor
- Operating pressure: max. 6.5 bar
- Temperature range:
  – 40 °C ≤ T ≤ + 70 °C
  (optionally extended to cover low temperature requirements)

Application example: MGS3 integrated in ESRA Evolution Control Unit

- Interface to typical train network systems such as MVB, CANopen, RS485 HDLC, Ethernet protocol variants etc.)
- Service and maintenance interface (Ethernet)
- Data Log function with large storage volume
- Temperature range: – 40 °C ≤ T ≤ + 70 °C (optionally extended to cover low temperature requirements)
- Additional integrated functions such as:
  - Control for electromagnetic track brake and sanding
  - Speed signal output
  - Distance counter


STADLER
KULKUVUOKAT
H-START
415 062
MAKING
RAIL TRAVEL FUN
www.stadlerrail.com

In an ever-changing market, flexibility is essential to success. With this in mind, we've created Vectron, a locomotive that delivers both quality technology and flexibility for freight and passenger transportation.

The Vectron platform is based on our many years of experience, and takes into account the needs of our customers. It has been designed so that it can be adapted specifically to meet the needs and requirements of European rail traffic. Modular retrofitting provides the greatest flexibility for cross-border traffic, and keeps conversion costs low if requirements change. In an industry where locomotives are usually made-to-order to specific customer preferences, Vectron offers a ground-breaking, truly international transport solution.

With optimum flexibility, adaptability and tailored service packages to ensure peak performance, you can trust Vectron to be a sturdy investment in an unpredictable future.

Hungarian Transport Association

Professional Association of Hungarian Local Public Transport Operators was founded in 1998. It was renamed in 2011 as Hungarian Transport Association. The Association represents numerous transport professional issues and brings together undertakings working in local public transport, takes part in legislation preparations and represents the common interests of its members. Presently, its main objective is to take part in preparation of launching operation of vehicles with different alternative tractions. Its president is Dr. Gyula Várszegi. Number of members is growing, it includes now 9 major transport undertakings:

Budapest Transport Privately Held Corporation

BKV carries 1.4 billion passengers a year and operates 5 branches (bus, tram, metro, suburban railway, trolleybus) in an integrated system. Beyond these, it operates other modes primarily of touristic importance, like cogwheel railway, funicular, chairlift and river boat services. BKV preserves the heritage from its own history and from its predecessors by maintaining two museums as well as by operating nostalgic transport services.

BKV Railway Vehicle Repair and Service Ltd.

The company was established in 1997 and deals with repair and production of main parts and other special components of tram, suburban railway and metro vehicles. Its activity has been extended in recent years by production of railway switches as well as overall modernisation of buses and trolleybuses. Regular vocational trainings have been carried out at the company's premises since its founding.

INTER TAN-KER Closed Public Limited Company

The legal predecessor of our company, INTER TAN-KER Kft., was founded in 2002. Today, the company's core business is in the field of transport, in turn carrying out the operator's activities. INTER TAN-KER Zrt. regards it as its mission to help the work of the government and local governments as well as multinational, small and medium-sized enterprises in the field of transport with comprehensive solutions. In order to further develop transport in Hungary, we are open to understanding and supporting the goals of our partners by involving our own and external resources. We would like to maintain our key role by meeting the various needs of Hungarian and international transport and introducing innovative solutions. During our activities, it is our guiding principle to satisfy our partners' needs beyond their expectations and to further facilitate their work and make it more effective.

Szeged Transport Company Ltd.

Public transport of Szeged is currently provided by two operators (the municipality owned Szeged Transport Company and the state owned Tisza Volán Share Holding Company). Szeged Transport Company operates trams and trolleybuses, furthermore it runs pay parking system and an automated parking house.

GRAMPET DEBRECENI VAGONGYÁR KFT.
H-4034 DEBRECEN, HÉT VEZÉR U. 24/B.
WWW.VAGONGYAR.HU ☎+36 52 889 100 FAX: +36 52 889 199 INFO@VAGONGYAR.HU

TÜVRheinland® CERT ISO 9001

Wheelset workshop

- Maintenance of spare parts (e.g. buffing and draw gear, mechanical brakes, springs)
- Overhaul wheelsets IL, IS1, IS2 and IS3
- Assembly of new wheelsets
- Manufacturing welding constructions

OUR COSTUMERS ARE FROM:

- Hungary
- Germany
- Austria
- Switzerland
- France
- Romania

Rebuilduing Hbbills

CERTIFICATES, AUTHORIZATIONS:

- ECM Maintenance delivery function
- ISO 9001:2008
- VPI
- DIN EN ISO 3834-2
- EN 15085-2
- DIN EN 27201-7
- AD 2000 – Merkblatt HP0
- RID 6.8.2.1.23
- AFER (Zaes 68 m3, Eaos, Uagps 562, Uagps 535, Habis, Habfis)

Building Ro-La

NOTES: